

UNIVERSITÉ LILLE 2 DROIT ET SANTÉ (FRANCE)
en cotutelle avec
**UNIVERSITÉ DES SCIENCES MÉDICALES
DE HÔ CHI MINH VILLE (VIET NAM)**

ÉCOLE DOCTORALE BIOLOGIE-SANTÉ DE LILLE (ED 446)

Thèse de doctorat

Spécialité: Sciences du médicament

Conception, synthèse et développement de nouveaux composés antituberculeux selon une approche par fragments

présentée et soutenue publiquement le 26 juin 2015 à Lille
par **TRẦN Ngọc Châu**

devant le jury composé de:

M. Benoît DÉPREZ Professeur à l'Université Lille 2 Droit et Santé	Membre invité
Mme. Line BOUREL-BONNET Professeur à l'Université de Strasbourg	Rapporteur
M. Pierre VERHAEGHE Professeur à l'Université Toulouse III Paul Sabatier	Rapporteur
M. Nicolas WILLAND Professeur à l'Université Lille 2 Droit et Santé	Directeur de thèse
M. LÊ Minh Trí Professeur à l'Université des Sciences Médicales de Ho Chi Minh-ville	Co-directeur de thèse

POUR UN MONDE SANS

TUBERCULOSE

“Vision de la stratégie Halte à la tuberculose - Organisation Mondiale de la Santé”

À la mémoire de mon père

Trần Đức Chấn

[Cette page a été intentionnellement laissée blanche]

Remerciements

Je tiens dans un premier temps à exprimer ma profonde gratitude à Monsieur le Professeur Benoît Déprez, vice président de l'Université Lille 2 et directeur de l'Unité U1177 qui m'a accueilli chaleureusement au sein de son équipe de recherche très dynamique et m'a permis de profiter d'excellentes conditions de travail pour réaliser ma thèse. Je vous remercie aussi de votre lecture attentive et vos corrections considérables concernant mon manuscrit.

Mes plus vifs remerciements reviennent à Monsieur le Professeur Nicolas Willand, sans qui cette thèse ne serait pas ce qu'elle est. Sincèrement, je vous remercie de m'avoir toujours supportée dans mes démarches de recherche ainsi que lors de mon séjour en France, et d'avoir consacré du temps, malgré votre emploi du temps très chargé, à corriger cette thèse. J'ai appris chez vous la patience, le dynamisme et l'énergie infatigable. Franchement, j'ai la chance d'avoir bénéficié de votre encadrement.

Je voudrais remercier Madame Line Bourel-Bonnet, Professeur à l'Université de Strasbourg et Monsieur Pierre Verhaeghe, Professeur à l'Université Toulouse III Paul Sabatier. Je vous suis très reconnaissant d'avoir bien voulu porter à ce travail en acceptant d'en être les rapporteurs. Votre présence au sein de ce jury est pour moi un honneur.

J'exprime ma reconnaissance à Monsieur le Professeur Võ Tấn Sơn, Président de l'Université des Sciences Médicales de Ho Chi Minh ville (Viet Nam), à Monsieur le Professeur Lê Quan Nghiêp, Vice-Président et à Monsieur le Professeur Trần Hùng, Doyen de la Faculté de Pharmacie qui ont signé les décisions pour me permettre de réaliser ce travail en France.

Je tiens également à remercier Monsieur le Professeur Lê Minh Trí, responsable du département de Chimie thérapeutique-Faculté de Pharmacie de Ho Chi Minh ville (VietNam) où je travaille. Je vous remercie d'avoir suivi tous mes pas depuis ma 5^{ème} année en pharmacie jusqu'à votre présence pour cette thèse en tant que co-directeur en cotutelle.

Ce projet m'amène à interagir avec de nombreuses personnes au sein du laboratoire mais aussi à l'extérieur. Je souhaiterais aujourd'hui exprimer toute ma reconnaissance à ces personnes qui ont contribué de près ou loin à ce travail.

Je tiens à remercier Docteur Marion Flipo qui m'a été d'une grande aide lors de mes débuts au laboratoire. Merci d'avoir travaillé à mes côtés sur le projet d'inhibiteurs de MabA.

Je remercie tout particulièrement Madame Catherine Piveteau, ingénieur d'étude à la plateforme ADMET, pour votre aide à déterminer des propriétés physico-chimiques et pharmacocinétiques des inhibiteurs d'EthR et la spectrométrie de masse en haute résolution et surtout votre gentillesse. Je vous remercie aussi pour m'avoir formé à la détermination de la solubilité des fragments.

Je voudrais remercier Docteur Alain Baulard, directeur de recherche et Docteur Martin Moune, post-doctorant à l'unité INSERM U1019 et tous les collaborateurs au Centre d'Infection et d'Immunité de Lille qui nous aider à déterminer les activités biologiques.

J'adresse un remerciement à Mme. le Professeur Nathalie Azaroual, M. Vincent Ultré et M. Pierre Larzilliere et toutes les personnes du service commun de RMN pour leur sympathie et leur aide précieuse.

Je tiens également à remercier Docteur Laurence Goossens et son doctorant Omar pour m'avoir permis d'utiliser la spectrométrie d'infrarouge.

J'exprime également mes sincères remerciements à tous les membres de l'unité U1177: Mme. le Professeur Rébecca Déprez-Poulain, Mme. le Professeur Hélène Gras-Masse, M. le professeur André Tartar, M. le Professeur Jean-Claude Gesquière, Docteur Julie Charton, Docteur Terence Beghyn, Mme. Nathalie Dekeyne, Mme. Carole Desruelle, Mme. Sylvie Leroy, Mme. Renelde Leroy, Mme. Sandrine Dassonneville qu'ils soient assurés que j'ai trouvé entre vous une ambiance amicale et chaleureuse dont je garderai un excellent souvenir.

Je tiens à remercier l'ensemble des post-doctorants, des doctorants et des stagiaires de l'unité U1177 (U761) que j'ai croisé tout au long de ces années et qui m'ont fait partager leurs expériences, leurs points de vue et leurs connaissances. Merci à Dr. Aurélia Dinut, Dr. Artur Pinto, Dr. Marilyne Bourotte, Dr. Sylvain Picon, Dr. Damien Bosc, Dr. Rajaa Boulahjar, Dr. Jouda Jakhlal, Dr. Nicolas Probst, Dr. Cyril Ronco, Dr. Tristan Verdelet, Dr. Ronan Gealageas, Dr. Catalin Pintilia, Antoine Henninot, Manuel Lasalle, Arnaud Mathieu, Gonzague Berthe, Paul Hermant, Vanessa Hoguet, Hugues Prevet, Hélène Lapière, Hasina Tolojamahary, Camille Moreau, Abdallah Jeoual, Dimitri Milville, Kaotar El Manyani, Thomas De Vliegère, Zhao Feng, Heleen Dhondt, Eva Bannerman, Marion Prieri, Aurélie Beghin, Ingrid Ciliberti et tous ceux que j'ai pu oublier pour m'avoir encouragé et partagé mes joies et mes peines tout au long de la réalisation de ce travail. Un merci particulier pour Dr. Baptiste Villemagne qui m'a fait l'honneur de relire attentivement ce manuscrit. Bon courage et bonne continuation à vous tous.

Je voudrais remercier mes collègues au département de Chimie Thérapeutique (Ho Chi Minh ville, Viet Nam): Assoc. Prof. Trương Phương, Assoc. Prof. Huỳnh Thị Ngọc Phương, Assoc. Prof. Trần Thành Đạo, Assoc. Prof. Thái Khắc Minh, MSc. Nguyễn Thị Thu Hà, Dr. Võ Thị Cẩm Vân, MSc. Huỳnh Nguyễn Hoài Phương d'avoir partagé mes charges d'enseignement pendant mon travail de thèse. Je tiens à remercier à toutes les techniciennes du laboratoire de Chimie thérapeutique: chị Hồng Chi, chị Hồng Diệp, bạn Kiều Khương và cô Ngọc Thảo.

Je remercie l'Agence Universitaire de la Francophonie (AUF) pour m'avoir aidé un financièrement me permettant ainsi d'avoir les conditions matérielles et administratives nécessaires pour réaliser ce travail.

Je tiens également à remercier le Service de Relation International de l'Université Lille 2, spécialement Monsieur Philippe Cordonnier et Madame Mathilde Modaine pour tous les soutiens qu'ils m'ont apportés pendant mon séjour en France.

Je souhaite également exprimer ma reconnaissance à Monsieur le professeur Bernard Sablonnière, directeur de l'Ecole Doctorale Biologie-Santé Lille (EDBSL), à Madame Laurence Fofana, secrétaire et à toutes les personnes de l'EDBSL de m'avoir aidé pour tous mes dossiers administratives lors de ces trois années.

Un grand merci à tous les membres de la communauté Salésiennes et la paroisse Saint-Luc Lille-sud, à mes amis Vietnamiens et Français à Lille qui m'ont aidé beaucoup dans la vie quotidienne et m'ont donné des moments amicaux et agréables pendant tout le temps où j'étais loin de ma famille. Même si je ne vous ai pas tous cités, sachez que je pense à vous.

J'adresse enfin mes plus profonds sentiments (en ma langue maternelle) à ma mère, à mes beaux-parents, à mon épouse, et à toute ma grande famille qui m'ont toujours accompagné pendant ces années de thèse malgré cette grande distance.

“Con cảm ơn Bố Mẹ đã sinh ra con và nuôi con khôn lớn đến ngày hôm nay, con cảm ơn Mẹ đã luôn thay mặt Bố trong thời gian qua để động viên con theo đuổi ước mơ của mình.”

“Con cảm ơn bố Hiền và mẹ Nhàn, đã luôn động viên và luôn âm thầm cầu nguyện cho con.”

“Anh cảm ơn Một, em đã vất vả lo lắng mọi việc trong gia đình trong thời gian anh đi học và luôn động viên anh có thể làm được điều này ngay những khi anh không còn tin ở bản thân mình”

“Em cảm ơn gia đình anh Tí, gia đình chị Ty, anh cảm ơn chú Điền...”

...vì sự động viên và những lời cầu nguyện của mọi người”

Lille, 15 mai 2015

Trần Ngọc Châu

[Cette page a été intentionnellement laissée blanche]

Avant-propos

Les travaux présentés dans cette thèse ont été majoritairement réalisés à l'unité INSERM U1177 (précédemment U761): «Médicaments et Molécules pour Agir sur les Systèmes Vivants - M2SV» dans le cadre d'une thèse en cotutelle pendant trois ans (2012-2015) entre l'Université Lille 2 Droit et Santé, France (7 mois par an) et l'Université des Sciences Médicales de Ho Chi Minh-ville, Vietnam (3 mois par an) avec l'aide financière de l'Agence Universitaire de la Francophonie (AUF).

Ce travail a été réalisé en collaboration avec plusieurs équipes de chimistes, de biologistes et d'analystes :

- Toutes les réactions de la synthèse ont été réalisées par moi-même à l'unité U1177
- Le test TSA sur EthR et MabA ont été réalisés par le Dr. Martin Moune (Unité INSERM U1019)
- L'évaluation des composés sur *M. tuberculosis* et macrophages infectés a été réalisée par les équipes des Dr. Alain Baulard et Dr. Priscille Brodin (Unité INSERM U1019)
- Le criblage enzymatique sur MabA a été développé et réalisé par Dr. Marion Flipo (U1177)
- Le criblage *in silico* et l'étude de modalisation moléculaire ont été réalisés par moi-même au département de chimie thérapeutique, faculté de Pharmacie –Université des Sciences Médicales de Hồ Chí Minh ville.
- La mesure des paramètres physico-chimiques et pharmacocinétiques des composés a été effectuée par la plateforme ADME de l'unité U1177 (Florence Leroux, Catherine Piveteau et Sandrine Dassonneville)
- La mesure de la solubilité des fragments 3-D a été effectuée par moi-même à la plateforme ADME de l'unité U1177
- Les analyses de spectrométrie de masse haute résolution ont été réalisées par Mme. Catherine Piveteau, l'ingénieur d'étude de la plateforme ADME
- Les analyses RMN ont été réalisées au Laboratoire d'Application RMN de l'Université de Lille 2.
- Les analyses IR ont été réalisées par moi-même à l'Institut de chimie pharmaceutique Albert Lespagnol - Lille

Ce manuscrit est écrit en anglais et accompagné d'un résumé en français.

Bonne lecture.

[Cette page a été intentionnellement laissée blanche]



COLLEGE DOCTORAL

École Doctorale
BIOLOGIE SANTÉ



Lille 2 University of Law and Health (France)

in collaboration with

University of Medicine and Pharmacy, Ho Chi Minh city (Viet Nam)

DOCTORAL SCHOOL OF BIOLOGY AND HEALTH - LILLE (ED 446)

Thesis submitted to attain the degree of

Doctor of Philosophy (Ph.D.)

in Pharmaceutical Science

Design, synthesis and development of novel antituberculosis agents by fragment-based approach

presented by **TRẦN Ngọc Châu**

on June 26th, 2015 in Lille

The thesis defense committee is composed of:

Invited member:

Prof. Benoît DÉPREZ, Lille 2 University of Law and Health

Examiners:

Prof. Line BOUREL-BONNET, University of Strasbourg

Prof. Pierre VERHAEGHE, Paul Sabatier Toulouse III University

Thesis advisors:

Prof. Nicolas WILLAND, Lille 2 University of Law and Health

Prof. LÊ Minh Trí, University of Medicine and Pharmacy, Ho Chi Minh City, Vietnam

This page intentionally left blank

LIST OF PUBLICATIONS AND CONTRIBUTIONS

PUBLICATION

Ngoc Chau Tran, Heleen Dhondt, Marion Flipo, Benoit Deprez and Nicolas Willand. "Synthesis of functionalized 2-isoxazolines as three-dimensional fragments for fragment-based drug discovery" *Tetrahedron Letters*, 2015, volume 56, issue 27, p. 4119-4123. (doi: 10.1016/j.tetlet.2015.05.035)

CONTRIBUTIONS TO SCIENTIFIC CONFERENCES

1. **Tran Ngoc Chau**, Dhondt Heleen, Deprez Benoit, Flipo Marion, Willand Nicolas. "Synthesis and functionalization of C-sp³ enriched isoxazoline scaffold as 3-D fragments for fragment-based drug discovery"
22nd Young Research Fellow Meeting of the SCT, Paris, France, 4th-6th February, **2015**
(poster presentation)
2. **Baptiste Villemagne**, **Ngoc Chau Tran**, Marion Flipo, Catherine Piveteau, Alexandre Wohlkönig, René Wintjens, Adrien Herledan, Vincent Delorme, Pricille Drodin, Martin Moune, Alain Baulard, Benoit Deprez, Nicolas Willand. "Pharmacokinetic profile optimization of EthR inhibitors derived from fragment-based approaches"
22nd Young Research Fellow Meeting of the SCT, Paris, France, 4th-6th February, **2015**
(poster presentation)
3. **Ngoc Chau Tran**, Martin Moune, Alain Baulard, Benoit Deprez, Marion Flipo and Nicolas Willand. "Integrating Fragment-screening and Fragment-based drug design for the discovery of *Mycobacterium tuberculosis* MabA inhibitors"
14th Journée André Verbert, Ecole doctorale Biologie Santé de Lille, France, 11th Sep, **2014**
(poster presentation)
4. **Ngoc Chau Tran**, Martin Moune, Alain Baulard, Benoit Deprez, Marion Flipo and Nicolas Willand. "Integrating Fragment-screening and Fragment-based drug design for the discovery of *Mycobacterium tuberculosis* MabA inhibitors"
Rencontres de la Chimie, de la Biologie et de la Physique du PRIM, Lille, France, 26th June, **2014**
(poster presentation)
5. **Ngoc Chau Tran**, Martin Moune, Alain Baulard, Benoit Deprez, Marion Flipo and Nicolas Willand. "Integrating Fragment-screening and Fragment-based drug design for the discovery of *Mycobacterium tuberculosis* MabA inhibitors"
21st Young Research Fellow Meeting of the SCT, Montpellier, France, 24th-25th March, **2014**
(poster presentation)

This page intentionally left blank

TABLE OF CONTENT

Introduction	1
Chapter I. Tuberculosis and fragment-based approach	3
Part A. A literature review on tuberculosis	3
1. A history of tuberculosis	3
2. Epidemiology	3
3. Tuberculosis and <i>Mycobacterium tuberculosis</i>	7
4. Pathogenesis of tuberculosis	12
5. Symptoms	13
6. Diagnosis of tuberculosis	14
7. TB vaccines and immunizations	17
8. Antitubercular chemotherapy	21
Part B. Tuberculosis and fragment-based drug discovery.....	41
1. Introduction to fragment based drug discovery.....	41
2. Application of FBDD in TB drug development	43
Chapter II. Development of novel EthR inhibitors with improved pharmacokinetic properties	47
Part A. EthR—a validated target for ethionamide potentiation	47
1. Role of EthR in ethionamide bio-activation	47
2. Structure of EthR.....	48
3. Validation of EthR as therapeutic target	49
Part B. EthR inhibitors and ETH boosting effect	50
1. Development of EthR inhibitors by ligand-based approach.....	50
2. Development of EthR inhibitors by rational drug design	51
3. Development of EthR inhibitors by high-throughput screening	53
4. Development of EthR inhibitors by fragment-based approach.....	53
5. Conclusion and outlook	55
Part C. Improving the microsomal stability of EthR inhibitors	56
1. Metabolism study of the potent EthR inhibitor BDM43266	56
2. Development of novel EthR inhibitors with improved pharmacokinetic and physicochemical properties.....	58
3. Molecular docking modelling of novel inhibitors in EthR structures	64
4. Conclusions and outlook.....	66

Table of content

Chapter III. Design and synthesis of MabA inhibitors	69
Part A. MabA.....	69
1. MabA– a forgotten target in FAS-II pathway.....	69
2. MabA enzyme – a validated target of <i>M. tuberculosis</i>	71
3. Conclusion.....	84
Part B. Identification of potential compounds targeting MabA by virtual screening	84
1. Compound library preparation	85
2. Protein structure preparation.....	85
3. Virtual screening	86
4. Testing hits in MabA enzymatic assay	90
Part C. Design and synthesis of novel MabA inhibitors by fragment-based approach.....	90
1. Fragments screening methods	91
2. Primary screening of U1177 fragment library on MabA	95
3. Validation of the 12 hits using a functional assay	98
4. Validation of the hits in a functional enzymatic assay.....	105
5. Synthesis of amino uracil analogs.....	107
Chapter IV. Design and synthesis of novel 3D-fragments for fragment-based drug discovery	111
Part A. An overview on actual fragment libraries.....	111
1. Fragment library design	111
2. Actual fragment libraries in literature	119
3. Analysis of some commercial fragment libraries.....	125
4. Analysis of the fragment library in research group U1177.....	125
5. Conclusion.....	127
Part B. Synthesis of functionalized 2-isoxazolines as 3D fragments for fragment-based drug discovery	128
1. Synthesis of novel 2-isoxazoline fragments.....	128
2. Analysis of synthesized fragments.....	137
3. Conclusion and outlooks.....	141
General conclusion	143
Experimental section	147
Annexes	235
Bibliography.....	241

Introduction

Tuberculosis (TB) is an infectious disease caused by the bacteria *Mycobacterium tuberculosis*. Despite the variable protective efficacy of the bacillus Calmette-Guérin (BCG) vaccine in TB prevention¹, this disease is curable by chemotherapy. In fact, combination of the first-line TB drugs can help drug-susceptible TB patients to completely recover in six months.² However, the principal problem in TB control is the long and complex drug regimen which can result in non-adherence and consequently leads to undesired response (e.g. failure and relapse). This may also allow the development of more problematic forms of TB, e.g. drug-resistant (DR) strains. Treatment of DR-TB is more challenging and requires second-line TB drugs. These medications are often more expensive and are responsible for severe and frequent side effects.³ Moreover, the World Health Organization (WHO) estimated that one third of the world's population is infected by latent TB bacteria, which can reactivate as an airborne and transmittable disease.⁴

HIV/AIDS pandemic provoked the re-emergence of TB from middle 1980s. In 1993, WHO declared TB as a global public health emergency. This alarm has stimulated many efforts in order to decrease and eliminate this disease worldwide. In fact, global TB control has been placed in the Millennium Development Goals. Importantly, WHO developed the directly observed treatment short-course (DOTS), a multidrug therapy program which is actually considered as the most efficient weapons against the global TB epidemic.³ However, this infectious disease remains a major public health problem until now despite the significant progress in the fight against TB worldwide over 20 years. WHO estimates that 9 million people contracted the disease in 2013 and 1.5 million died in that year. TB is still a leading cause of death from an infectious disease in many countries.⁵

For that reason, the need of new antitubercular drugs is very urgent. Recently, two new compounds, bedaquiline and delamanid were approved in combination to the actual MDR-TB chemotherapy.^{6,7} Nevertheless, there is always the possibility that the tubercle bacillus can quickly develop resistance related to the mechanism of action of these new drugs. Therefore, the actual therapeutic arsenal must be strengthened by other TB drugs. These new antituberculosis compounds are inspected to be able to shorten the treatment time, improve patient safety and/or overcome drug resistance issues.

Among many strategies that are actually used in the drug development, fragment-based drug discovery (FBDD) approach has emerged as a promising strategy which is resulting in the quality, rather than the quantity, of hits and leads. This method relies on the screening of small chemical entities that can probe biological targets more effectively than drug-like molecules. Identified hits are then rapidly optimized using rational design to lead-like compounds.⁸ We believe that compounds developed from FBDD could be carefully controlled in molecular size. Therefore, these new molecules with tuned physico-chemical properties can easily penetrate the waxy and lipid-rich cell wall of *M. tuberculosis* in order to reach to the intracellular targets.

These promising advantages have encouraged us to apply FBDD in our TB projects.

Outline of the thesis:

This thesis comprises 4 chapters and an experimental section. The outline of the manuscript is organized as follows:

In **chapter I**, we present an overview on TB disease and application of FBDD method in drug development. Concerning the TB, we describe the epidemiology of TB, physiology and pathogenesis of *M. tuberculosis*. Furthermore, we discuss on the actual diagnosis, vaccination and chemotherapy which are currently used in TB management and their development tendency in future. In this chapter, we also summarize the main principle of the FBDD approach and their application especially in TB drugs development.

In **chapter II**, we report the first application of FBDD in development of new EthR inhibitors. The work described in this chapter is a continuation of the research project which was started during the thesis of Baptiste Villemagne.⁹ This work aims to develop compounds that can boost the activity of ethionamide, a second-line drug used to treat MDR-TB. The transcriptional repressor EthR has been validated as a key element in the bioactivation of ethionamide. EthR inhibitors were identified using a fragment-based approach and were optimized to potentiate the activity of ethionamide *in vitro*. However, the low microsomal stability of the lead compound has limited its use *in vivo*.⁹ The metabolism study of the lead compound and key structural modifications allowed a development of new potent EthR inhibitors having acceptable pharmacokinetic and physico-chemical properties for *in vivo* testing.

In **chapter III**, fragment-based approach is applied for the development of MabA inhibitors. MabA is a mycobacterial β -ketoacyl-ACP reductase involved in the synthesis of long-chain fatty acids, precursors of mycolic acids, which are major constituents of the mycobacterial cell wall. This enzyme has been shown to be essential for the survival of the bacteria but until now no inhibitor has been identified.¹⁰ In this chapter we present how we can use a small fragment library in combination with several screening methods to discover and develop new MabA inhibitors with activity in the micromolar range. In addition, we also present in this chapter an *in silico* screening that was also developed to try to identify MabA inhibitors.

In **chapter IV**, a design and synthesis of new fragments is described. The aim of this project is to build a collection of original fragments showing a 3D-structure scaffold amenable for rapid derivatization. Synthesis of new fragments that contain an original 2-isoxazoline scaffold is presented. Furthermore, the conformational analysis of these structures and their experimental solubility were also measured and are reported in this chapter. These new fragments are suitable for the screening against new biological targets to help kick-start new hit discovery programs.

Finally, the experimental section illustrates in detail all synthetic reactions and biological procedures related to the works presented in chapter II, III and IV.

Chapter I. Tuberculosis and fragment-based approach

Part A. A literature review on tuberculosis

1. A history of tuberculosis

Tuberculosis (TB) is one of the oldest human diseases, but not a disease of the past.³ The evidence of tuberculosis has been found in many ancient civilizations over the world. Indeed, signs of the disease have been found in Egyptian mummies, in ancient eastern civilization (e.g. China and India), in Africa and even in South American area as early as many thousand years ago. The disease has gone by several names, e.g. phthisis (an archaic name originated from classical Greece); consumption (because of the severe weight loss and the way this disease appeared to “consume” the patient); the great white plague or the white death (because of the extreme anemic pallor of those affected) and so on. In 1839, Johann Lukas Schönlein used the name “tuberculosis” for this disease. This ancient disease has been a scourge throughout human history and may have killed more persons than any other microbial pathogen.¹¹

Understanding of the tuberculosis pathogenesis began from the beginning of the 19th century with the contribution of many researchers. These studies have led to the identification of the tubercle bacillus by Robert Koch on March 24th 1882. For that reason, the 24th of March each year has been chosen as the World Tuberculosis Day until now. The discovery of *Mycobacterium tuberculosis* as the etiologic agent of tuberculosis has accelerated research and development of treatment and prevention of this disease. In 1921, the TB vaccine bacillus Calmette-Guerin (BCG) was firstly used in clinics. After the discovery of streptomycin as the first antituberculosis drug in 1944, many other antituberculosis drugs were then developed, e.g. isoniazid, rifampicin, ethambutol and pyrazinamide. Consequently, quadri-therapy regimen have been started for the treatment of TB in 1967.¹¹

The development of TB vaccines and effective TB drugs has led to a remarkably rapid decrease of TB cases over the world. TB became curable and for that reason many people have believed that this disease could almost be defeated. However, in the mid-80s, with the epidemic of acquired immune deficiency syndrome (AIDS), TB has returned as one of the most dangerous infectious diseases.¹² Therefore, the World Health Organization (WHO) declared TB as a global emergency from 1993. Today, TB remains one of the leading infectious disease killers around the world. Unfortunately, TB that we face today is not exactly the same as fifty years ago. Decades of widespread and uncontrolled application of antibiotics in clinical has resulted in the emergence of drug resistant strains of *M. tuberculosis*.^{3,13}

2. Epidemiology

2.1. Global situation

Understanding of the TB epidemiology is critical for an effective control. According to the recent Global Tuberculosis Report in 2014, there were an estimated 9.0 million incident cases of TB globally, equivalent to 126 cases per 100 000 population. Among these new TB

cases, an estimated 1.1 million (13%) were HIV-positive in 2013. Interestingly, this ratio revealed that HIV/AIDS until now is not the main cause for the re-emergency of TB worldwide.⁵

In addition, WHO also evaluated the global trends of TB from the period 1990-2014 (Figure 1). The data show a decrease of TB incidence at an average rate of about 1.5% per year between 2000 and 2013. In addition, the TB mortality rate fell by an estimated 45% between 1990 and 2013 and the TB prevalence rate fell by 41% during the same period. TB is slowly declining each year. WHO estimates that 37 million lives worldwide were saved between 2000 and 2013 through effective diagnosis and appropriate treatment. The world and all of WHO's six regions are on track to achieve the Millennium Development Goal target that TB incidence rates should be falling by 2015.⁵

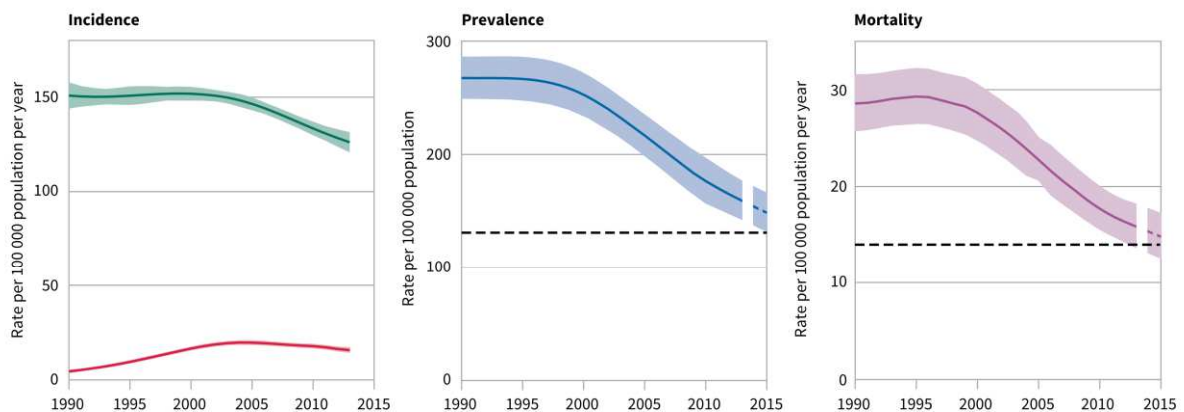


Figure 1: Global trends in estimated rates of TB incidence, prevalence and mortality in the period 1990–2015
(adapted with permission from WHO for ref.⁵)

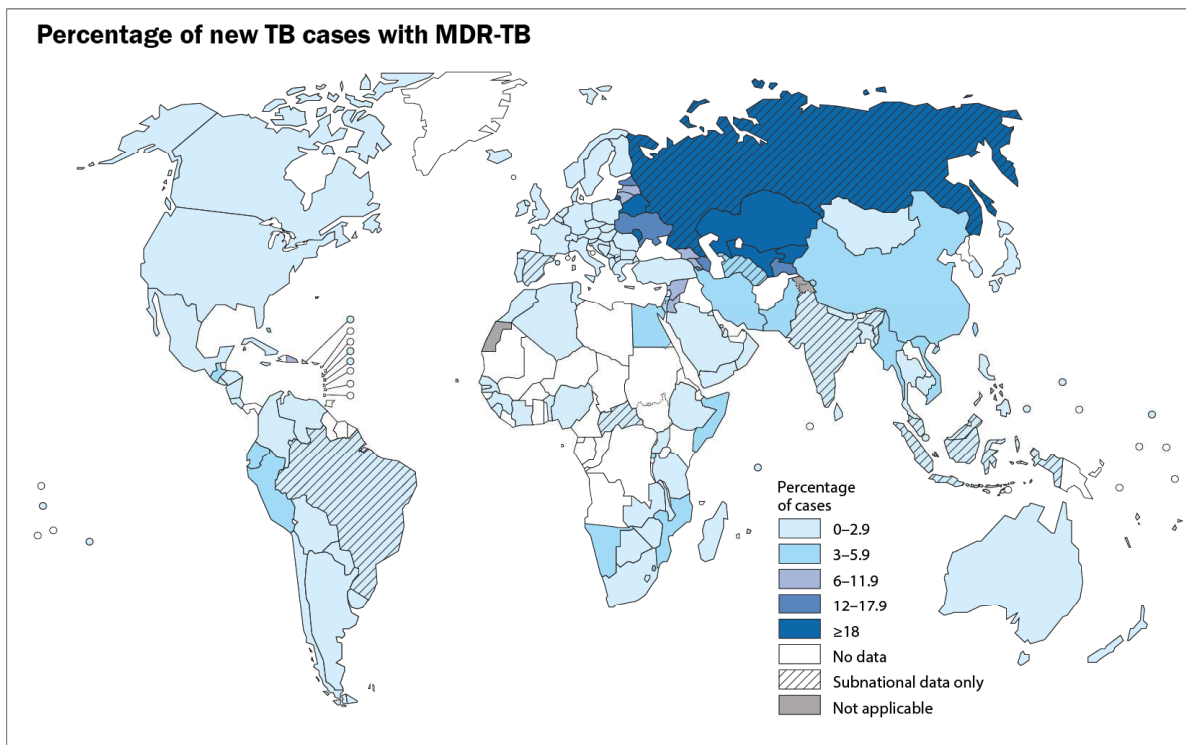


Figure 2: Percentage of new TB cases with multidrug-resistant tuberculosis worldwide (WHO, 2014)
(adapted with permission from WHO for ref.⁵)

Despite a decline in mortality of TB each year from 2000 until now, the death toll from the TB disease is still unacceptably high. In fact, WHO estimates that 1.5 million died from

TB in 2013 (1.1 million deaths among people who were HIV-negative and 360 000 among people who were HIV-positive).⁵

Among these TB deaths, there were an estimated 210 000 cases from multidrug-resistant tuberculosis (MDR-TB), a relatively high ratio (44%) in comparison with 480 000 total incident cases of MDR-TB. Globally, 3.5 % of new TB cases are estimated to have MDR-TB. According to the MDR-TB distribution world map (see Figure 2), MDR-TB has been reported in nearly every country all over the world with substantial differences in the frequency from one country to another. Especially, this proportion is highest in Eastern Europe. Moreover, extensively drug-resistant TB (XDR-TB, defined as MDR-TB plus resistance to any fluoroquinolones and any second-line injectable drug) has been reported by more than 100 countries by the end of 2013.⁵

In addition, several TB strains that showed *in-vitro* resistance to all first and second line drugs tested have been recently reported in some country (e.g. Italy¹⁴, India¹⁵, South Africa¹⁶ and Iran^{17,18}). Some authors have named these strains as extremely drug resistant TB (XXDR-TB) or totally drug resistant TB (TDR-TB). However, these terms have not yet been recognized by the WHO until now.

2.2. Tuberculosis in France

In France, the number of notified TB cases and mortality ratio has been decreasing for several decades (see Figure 3).¹⁹ With less than 10 new TB cases per 100 000 population since 2004, France is now considered as a low incidence country according to WHO.²⁰ In the recent Global TB report, WHO estimates that the prevalence rate of TB is 11 and the incidence rate is about 8.8 per 100 000 population. The mortality of TB in France is very low (about 0.52 per 100 000 population). However, 4939 TB cases were reported in this country in 2013. Among the notified pulmonary TB cases, 15 patents were identified as MDR-TB.⁵ In fact, France is also affected by the drug resistant TB as many others countries. Recently, a surge of drug resistant TB have been observed in France.^{21,22}

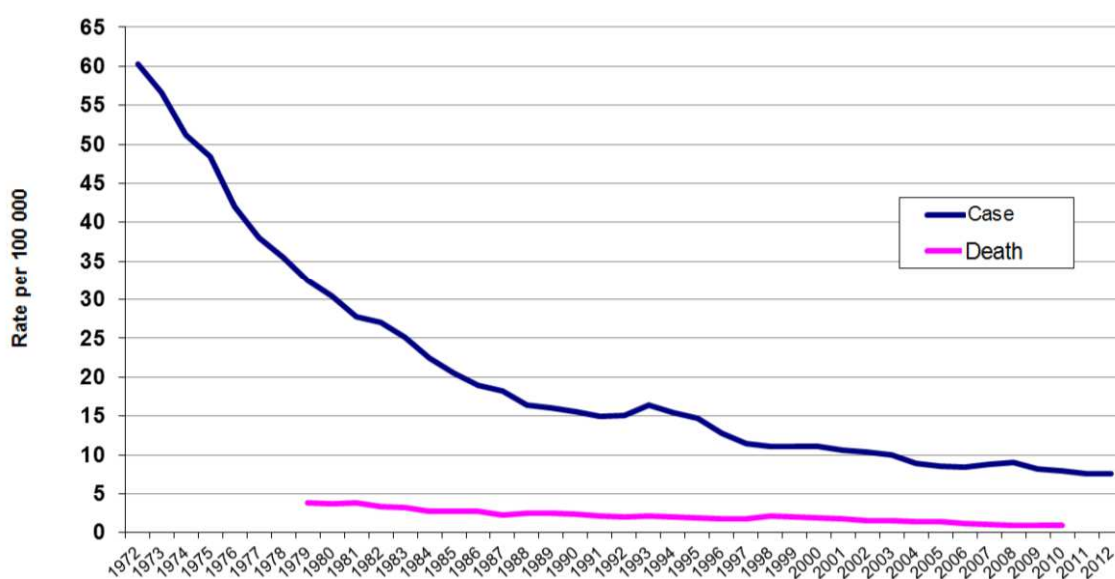


Figure 3: Trends in estimated rates of TB prevalence and mortality in France (adapted with permission from l'Institut de veille sanitaire InVS for ref.¹⁹)

2.3. Tuberculosis in Viet Nam

Viet Nam is a country in South East Asia. The estimated total population of Viet Nam was about 92 million in 2013. The current Viet Nam National Tuberculosis Control Programme (NTP) is adopted from the principles of the DOTS strategy recommended by WHO. The objective of the NTP in Viet Nam is to reduce TB morbidity, mortality and transmission and to prevent emerging of TB drug resistance. Two years after the declaration of WHO on TB re-emergence, Vietnamese government has announced TB control as a national priority in 1995.²³ With many efforts from government policy in combination with supports from WHO, TB prevalence, incidence and mortality in Viet Nam has decreased from 1990 until now (see Figure 4).⁵

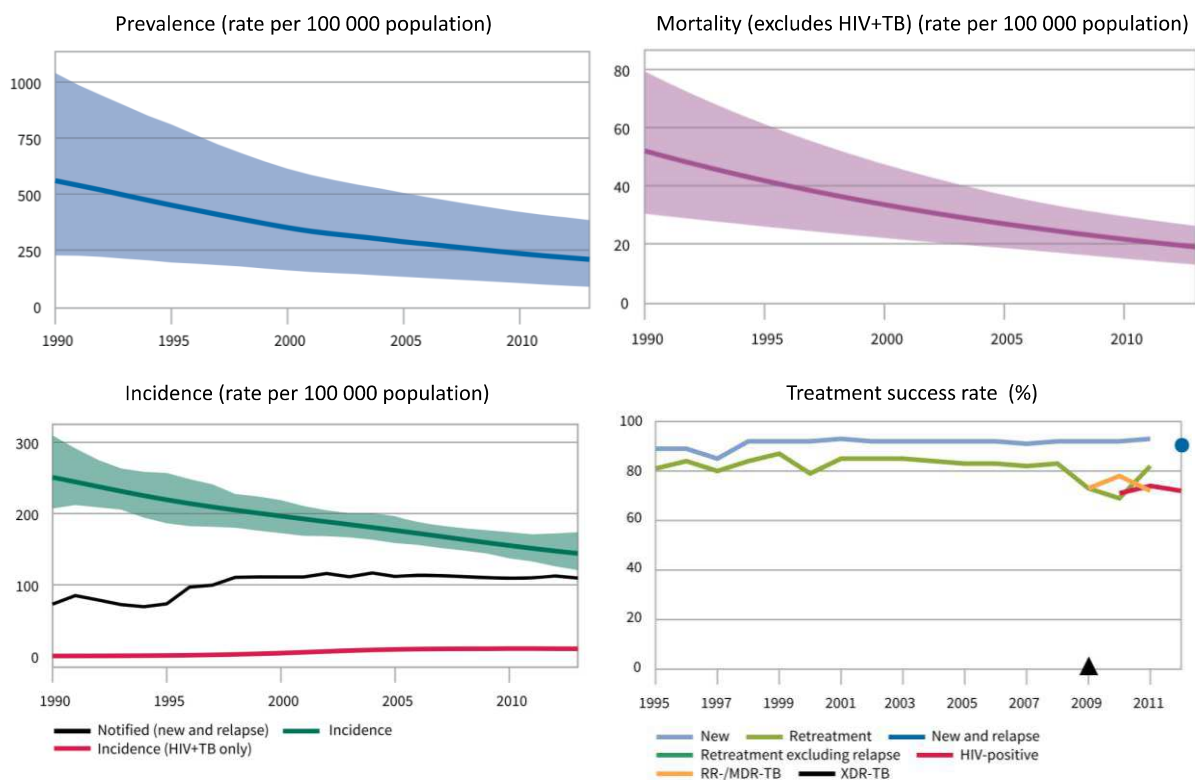


Figure 4: Estimated TB trends in Viet Nam during 1990-2013 (WHO, 2014)
(adapted with permission from WHO for ref.⁵)

However, TB in Vietnam remains a serious concern. Indeed, WHO estimated that the prevalence rate of TB is 209 TB cases per 100 000 population. The incidence rate is 144 cases per 100 000 population while mortality is still high with 19 cases per 100 000 population. According to WHO, Viet Nam is among the 22 high TB burden countries in the world and is also listed in 27 high burden countries for MDR-TB. The incidence rate of MDR-TB is 4% regarding new cases and 23% regarding re-treatment cases.⁵ Recently, Vietnamese government has approved the National Strategy for TB control to 2020 in order to accelerate the TB control program with a vision to 2030. This strategy is disseminated to all localities and TB control facilities nationwide. The principal objective of this national strategy is to reduce the prevalence rate in community to less than 131 cases per 100 000 population in 2020 and to less than 20 in 2030. Moreover, this strategy has also aimed to decrease the MDR-TB rate to less than 5% among new TB cases in 2015.²⁴

3. Tuberculosis and *Mycobacterium tuberculosis*

3.1. The genus *Mycobacterium*

Mycobacterium tuberculosis is the main cause of TB. Moreover, there are also some others species can cause TB in human which are classified in *Mycobacterium tuberculosis* complex (MTBC). MTBC consists of *M. tuberculosis*, *M. bovis*, *M. africanum*, *M. microti*, *M. canettii*, *M. caprae* and *M. pinnipedii*. *M. bovis* is the pathogen of tuberculosis in cattle (known as bovine TB). This species can also cause tuberculosis in human *via* the contaminated cattle's milk. However, tuberculosis caused by *M. bovis* in developed countries has largely been eliminated nowadays because of the introduction of pasteurized milk. Other species in MTBC are not common worldwide. *M. africanum* is the most important TB cause in some West African countries. *M. canettii* is rare and seems to be limited to the Horn of Africa. *M. caprae* is a pathogen which has been recognized mainly in central Europe.^{25,26}

M. tuberculosis and other species in MTBC belong to the genus *Mycobacterium*, a family of small rod-shaped bacilli, which also comprise others pathogenic bacteria. Notably, there are *M. leprae* and *M. lepromatosis* which cause leprosy (Hansen's disease) and some others species which cause neither TB nor leprosy, but can cause pulmonary diseases resembling tuberculosis, lymphadenitis, skin disease, or disseminated disease. These species are known as nontuberculous mycobacteria (NTM).^{27,28}

3.2. Characteristics of *Mycobacterium tuberculosis*

3.2.1. General properties

M. tuberculosis is a bacillus which have a rod-shaped with 0.3-0.5 μm in diameter and between 2-4 μm in length.²⁶

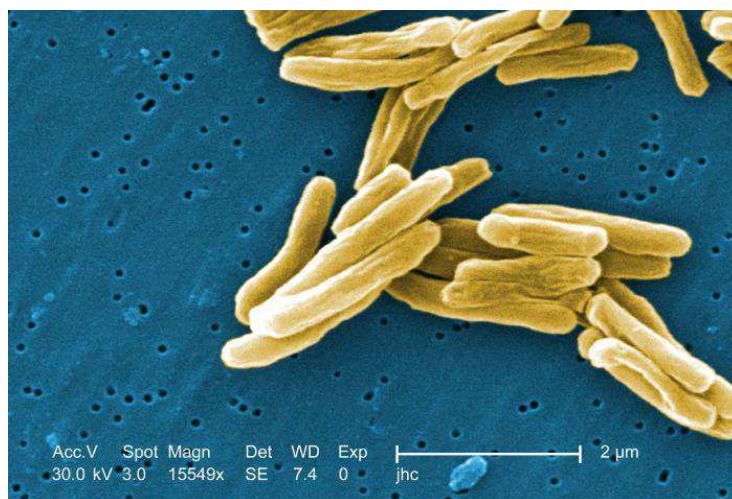


Figure 5: A group of *M. tuberculosis* depicted by digitally-colored scanning electron micrograph
(image courtesy of Janice Haney Carr and Ray Butler, CDC)

M. tuberculosis is an aerobic bacterium which requires high levels of oxygen to grow. This bacillus can be cultured in nutrient-rich environments as Löwenstein-Jensen medium. *M. tuberculosis* grows slowly with an average replication time of 22-24 hours. This division time is extremely slow in comparison with other bacteria. The optimum for *M. tuberculosis* growing is pH 6.8–7.2 at temperature 37–38°C. Besides, *M. tuberculosis* also tends to switch

to a state of dormancy or steady-state when exposed to highly stress environments in the host. This pathogenic bacillus is common and dangerous because of its ability to shirk the defense mechanisms of host and adapt to unfavorable environments. However, under the influence of direct sunlight and ultraviolet rays, *M. tuberculosis* is killed within a few minutes, and it is also destroyed by boiling during 45 minutes.²⁶



Figure 6: A close-up of *Mycobacterium tuberculosis* culture
(image courtesy of Dr. George Kubica, CDC)

One special characteristic of *M. tuberculosis* is its unusual cell wall with high lipid content. Because of the presence of mycolic acid, *M. tuberculosis* has a waxy coating on the cell surface, which makes the cells impenetrable to Gram staining. Therefore, the Ziehl-Neelsen staining, or acid-fast staining, is alternatively used. Acid fastness is a physical property by which mycobacteria resist decolorization by mild acid or ethanol after staining with Ziehl-Neelsen dye making it visible as bright red rods against blue background. Two special characteristics of *M. tuberculosis* are its cell envelope and persistence.²⁶

3.2.2. Composition of the mycobacterial cell wall

M. tuberculosis has a lipid-rich cell envelope which is distinctive and associated with its pathogenicity. The cell wall is extremely thick and multi-layered with varied hydrophobicity, posing an effective obstacle for the entry of most chemical compounds and protects the tubercle bacillus from human immune system.²⁹ A simple visual representation of the *M. tuberculosis* cell wall is depicted in Figure 7. In detail, the cell wall is mainly composed of three different covalently linked structures (e.g. peptidoglycan, arabinogalactan and mycolic acids). The mycolic acids layer is hydrophobic with extremely low fluidity. This layer is also named as the mycomembrane. The outer part of the mycomembrane contains various free lipids. Most of these lipids are specific for mycobacteria. They include phenolic glycolipids, phthiocerol dimycocerosates, cord factor or dimycolyltrehalose, sulpholipids and phosphatidylinositol mannosides. These components are intercalated with the mycolic acids. The outer layer, which is generally called the capsule, mainly contains polysaccharides (glucan and arabinomannan).³⁰ Mycolic acids are the major constituents of the mycobacterial protective layer.³¹

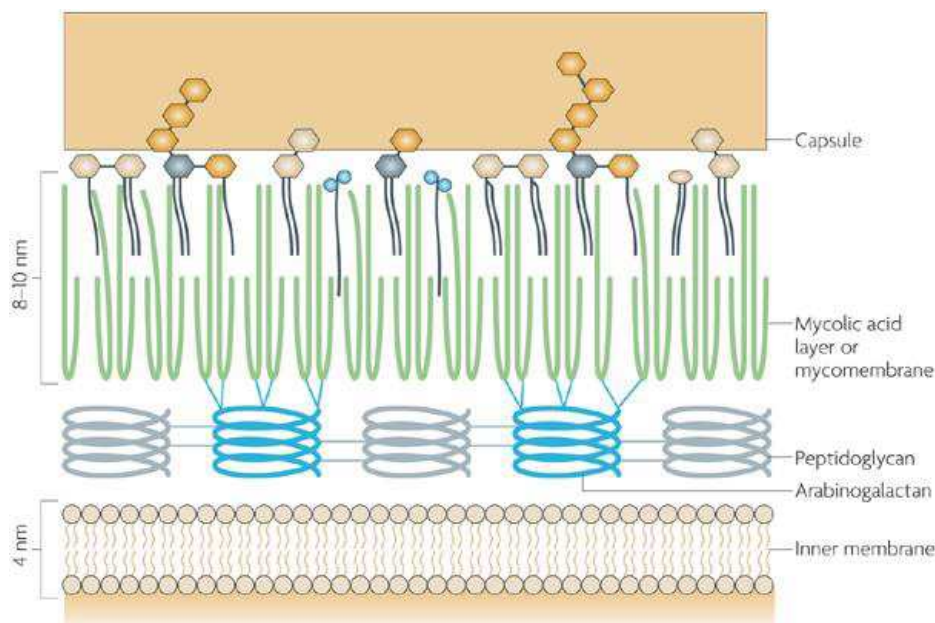


Figure 7: Schematic representation of the cell envelope of *M. tuberculosis*
(adapted with permission from Nature Publishing Group for ref.³⁰)

3.2.3. Mycolic acids

As defined by Asselineau and Lederer³², mycolic acids are homologous series of C₆₀-C₉₀ long-chain alpha-alkyl, beta-hydroxy fatty acids. The chemical formula of these mycolic acids usually differ by 28 Da (a two-carbon unit). In *M. tuberculosis*, mycolic acids are characterized by very hydrophobic C₅₄ to C₆₃ fatty acids with C₂₂ to C₂₄ alpha side chains. The alpha-chain is functionalized by cyclopropyl, alpha-methyl ketone, or alpha-methyl methyl ethers groups. There are three distinct structural classes of mycolic acids. They are comprised of alpha-mycolic acids, methoxy-mycolic acids and keto-mycolic acids, as shown in Figure 8.

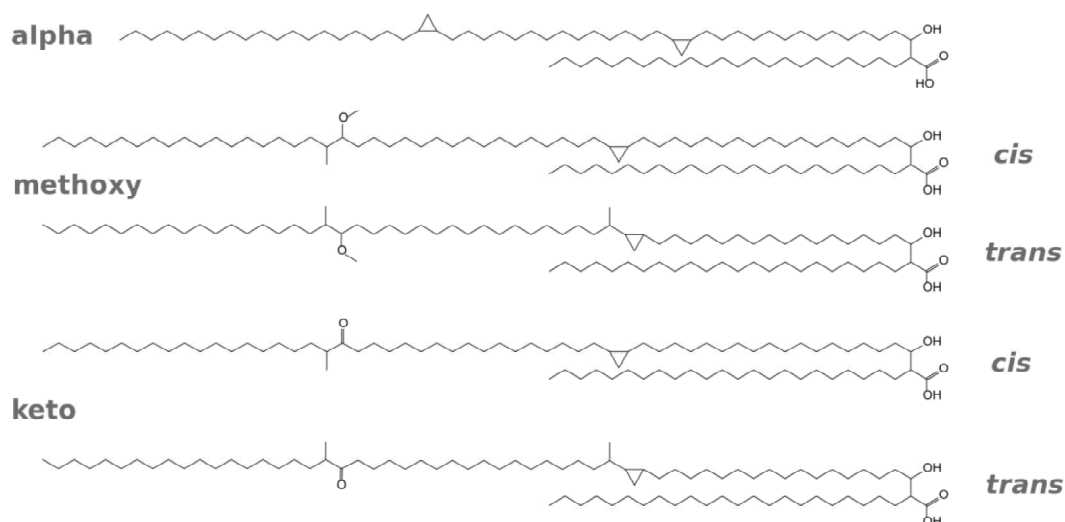


Figure 8: Chemical structures of mycolic acids from *M. tuberculosis*

Alpha-mycolic acid is the major form. The alpha-mycolic acid is a cis, cis-dicyclopropyl fatty acid. There are two structural variations of this mycolic acid, depending on the source. The variations appear in the length of the terminal alkyl group and the number

of methylene groups between the cyclopropane rings and the carboxyl group. Both methoxy- and keto-mycolic acids are found either in cis- or trans-configurations.³¹

Mycolic acids possess unique characteristics essential for their physiological roles in maintaining the cell wall structure of mycobacteria. The importance of the mycolic acids in the formation of the cell wall permeability barrier was known long ago. Mycobacteria are extremely impermeable to hydrophilic molecules, including antibiotics and nutrients such as glucose and glycerol. This low permeability was correlated with the extremely hydrophobic surface attributed mainly to the high amounts of mycolic acids in the cell wall (see Figure 7). Mycolic acids can also be found in the form of arabinogalactan esters as well in the form of trehalose-dimycolate (TDM). Arabinogalactan-mycolate is covalently linked to the cell wall peptidoglycan *via* a phosphodiester bond located on the inner leaflet of the outer membrane. TDM (formerly known as “cord factor”) is the principal biologically active lipid of mycobacteria which has been proven to protect the bacilli within macrophages by reducing antibiotic effectiveness and inhibiting the stimulation of protective immune responses.^{33,34} Moreover, mycolic acids have been found to constitute a scaffold for mycobacterial lipid antigens stimulating CD1-restricted T cells, making these lipid antigens active players in the immune recognition of this pathogen.³⁵

3.2.4. Biosynthetic pathway of mycolic acids

The overall process of mycolic acid biosynthetic pathway is illustrated in the Figure 9 and has been proposed to involve five distinct stages^{33,34}:

- 1) synthesis of C₂₄ to C₂₆ straight-chain saturated fatty acids for alpha-alkyl branch³³
- 2) synthesis of the meromycolic acid chain to provide the main carbon backbone³³
- 3) modification of this backbone to introduce other functional groups³³
- 4) the final Claisen-type condensation step followed by reduction³³
- 5) various mycolyltransferase processes to cellular lipids³³

In this procedure, it has been noticed that mycolic acids are synthesized by at least two discrete elongation systems in Mycobacteria - the type I and type II fatty acid synthases (FAS-I and FAS-II, respectively). Firstly, FAS-I produces fatty acids with a bimodal distribution, C₁₆–C₁₈ and C₂₄–C₂₆ acids, with the latter corresponding to the “alpha branch” in mycolic acids. Mycobacteria have a single FAS-I-encoding gene (*fas*, *Rv2524c*). The mycobacterial FAS-I protein displays the seven distinct domains corresponding to the catalytic activities required for the synthesis cycle. The fatty acids produced by FAS-I are long-chain acyl-CoAs that subsequently participate, after carboxylation by ACCase, in mycolic acids biosynthesis (see Figure 9). Secondly, the bacterial-like dissociated FAS-II composed of a series of discrete soluble enzymes. FAS-II is responsible for the elongation of fatty acids at the origin of the very long meromycolic chains. These two FAS system in *M. tuberculosis* share similar reaction sequences with an iterative series of reactions built on successive additions of a two-carbon unit from malonyl coenzyme A (malonyl-CoA) to a nascent acyl group. Malonyl-CoA is produced by the carboxylation of acetyl-CoA, catalyzed by the acetyl-CoA carboxylase, a key enzyme in most living organisms.^{31,33,36}

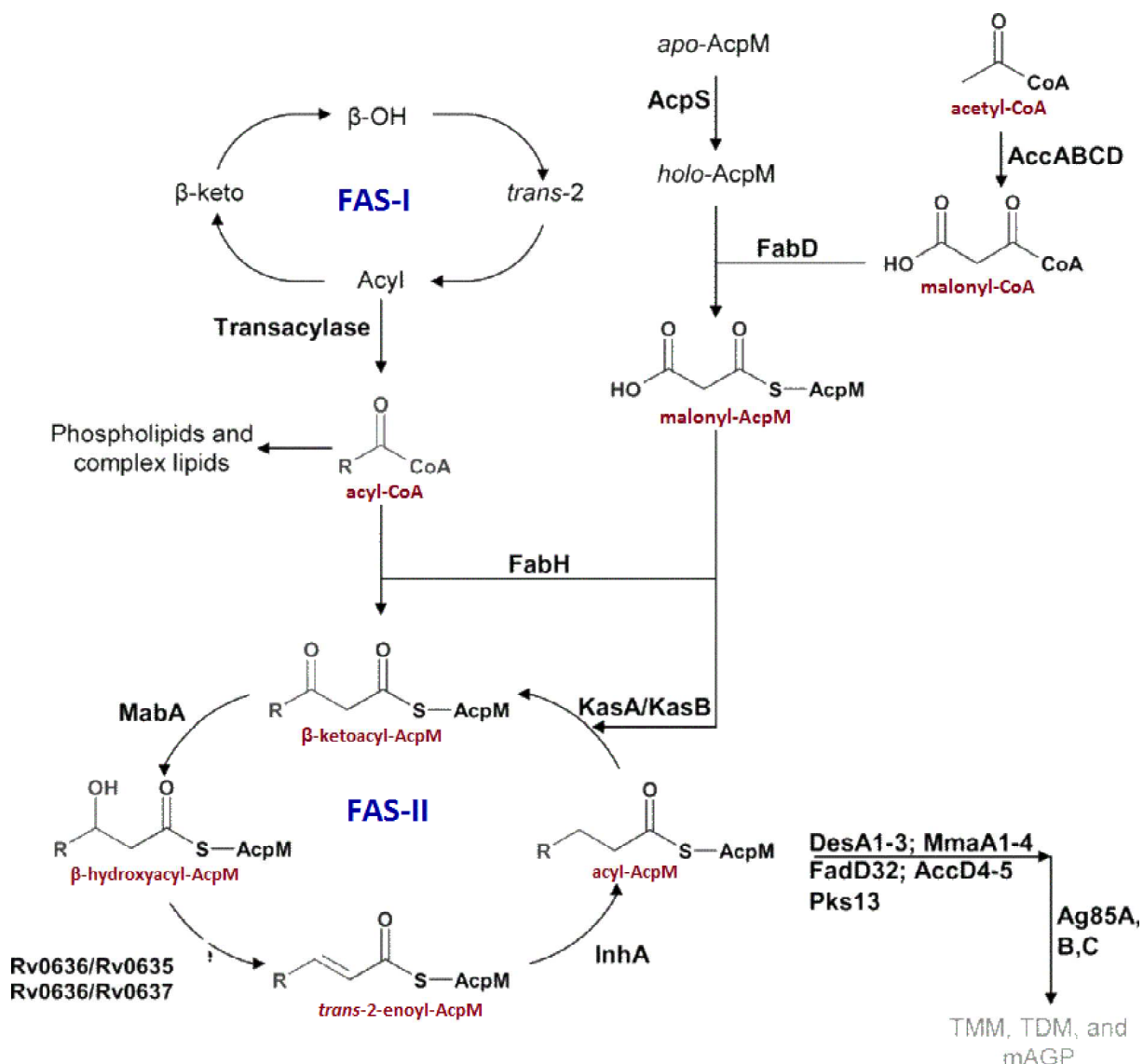


Figure 9: Biosynthesis, inhibition, and regulation of mycobacterial mycolic acids (adapted with permission from the Biochemical Society for ref.³⁶)

The *M. tuberculosis* FAS-II system has a different property to other bacterial FAS-II systems. In fact, it could not conduct *de novo* synthesis. Instead, mycobacterial FAS-II elongates C₁₂–C₁₆ acyl-CoA primers generated by FAS-I to a mixture of homologous fatty acids of longer chain lengths (meromycolic acids). The synthesis proceeds through the elongation of enzyme-bound intermediates, covalently linked to mycobacterial acyl carrier protein (AcpM, *Rv2244*), by several iterative cycles, each comprising four steps. In the first step, the malonate group is transferred to ACP by malonyl CoA-acyl carrier protein transacylase (MtFabD, *Rv2243*) to form malonyl-ACP. Then, FAS-II is initiated by the Claisen condensation of malonyl-ACP with acyl-CoA, catalyzed by MtFabH to form beta-ketoacyl-ACP. Next, there are 4 enzymes that catalyze each stage of elongation: the β -keto group is reduced by the nicotinamide adenine dinucleotide phosphate (NADP)-dependent β -ketoacyl-ACP reductase (MabA, *Rv1483*), and the resulting β -hydroxyl intermediate is dehydrated by the heterodimer β -hydroxyacyl-ACP dehydratases (HadAB and HadBC, *Rv0635-Rv0636* and *Rv0636-Rv0637*, respectively) to an enoyl-ACP. The reduction of the enoyl chain by the nicotinamide adenine dinucleotide hydrogen (NADH)-dependent trans-2-enoyl-ACP reductase (InhA, *Rv1484*) produces an acyl-ACP. Additional cycles of elongation

are initiated by the β -ketoacyl-ACP synthase (KasA or KasB, *Rv2245* or *Rv2246*) that elongates the acyl-ACP by two carbons to form a β -ketoacyl-ACP.^{33,36}

Elongation finishes when the acyl-ACP attains the chain length required for the meromycolic acids chain modification or condensation.³³ The mycolic acids synthesis involves, in addition to FAS-I and FAS-II, a condensation reaction between two activated fatty acids, a key step leading to the formation of the “mycolic motif”. The formation of a new carbon-carbon bond by a Claisen condensation is a reaction shared by both fatty acid and polyketide synthase biosyntheses and is catalyzed by condensing enzymes. The final stages in the synthesis of the cell wall of *M. tuberculosis* are transport and attachment of newly synthesized mycolic acids to the peptidoglycan-arabinogalactan complex of the cell wall and the formation of TDM (trehalose dimycolate).^{31,33,34}

Mycolic acids biosynthesis has been described as a target for many antitubercular drugs e.g. INH, ETH. In addition, pyrazinamide was shown to inhibit fatty acid synthase type I.³⁷

3.3. The complete genome of *M. tuberculosis* H37Rv

Recently, genomics has provided a valuable drug discovery resource by catalyzing genetic manipulation in order to characterize many key enzymes participating in mycolic acids biosynthesis. The outcomes allow an understanding of their role in the physiology of the mycobacteria, and might lead to the identification of new drug targets.³⁸

In 1998, the complete genome sequence of *Mycobacterium tuberculosis*, H37Rv, has been determined and analyzed. This genome comprises 4,411,529 base pairs, contains around 4,000 genes, and has a very high guanine and cytosine content. These results helped to improve the understanding of this pathogen biology and contribute to the development of new therapeutic interventions.³⁹ In 2008, the Tuberculosis Database (TBDB) was established. This is an integrated database providing access to TB genomic data and resources, relevant to the discovery and development of TB drugs, vaccines and biomarkers.⁴⁰

4. Pathogenesis of tuberculosis

Following environmental exposure with *M. tuberculosis*, about 30% of individuals are infected. In these cases, *M. tuberculosis* is transmitted into the lungs *via* aerosol. After entering the lungs, the tuberculosis bacilli stagnate on bronchial and alveoli (often near the pleura) where they will be taken up by alveolar macrophages once they reach the lung. Macrophages will absorb the tubercle bacilli and destroy or inhibit the majority of them, but some will survive and multiply inside the cell. The activation of macrophages and dendritic cells induce an immune response which is initiated by secretion of cytokines and chemokines that attract neutrophils, monocytes, T cells, B cells and other alveolar macrophages, finally leading to the formation of cellular structures called granulomas.^{4,41}

If the multiplication of *M. tuberculosis* is not controlled, the spread of bacilli will enter to local lymph nodes. This tends to lymphadenopathy, a characteristic expression of primary tuberculosis. Five to ten percent of the cases immediately develop active disease called primary tuberculosis. On the contrary, 90-95% are considered latently infected and do not

present any clinical symptoms. This latent TB infection can be reactivated later when there is an imbalance between host immunity and bacterial virulence (see Figure 10).^{4,42}

The risk of tuberculosis reactivation is about 10% for healthy adults, 20% for children aged < 5 years, 30% for people with HIV infection and 40% for children aged < 2 years. In addition, various other high-risk clinical situations (such as administration of biologic agents or steroids, chronic renal failure, diabetes, and so on) could disrupt the balance between host immunity and bacterial virulence, thus increasing the bacterial multiplication.⁴

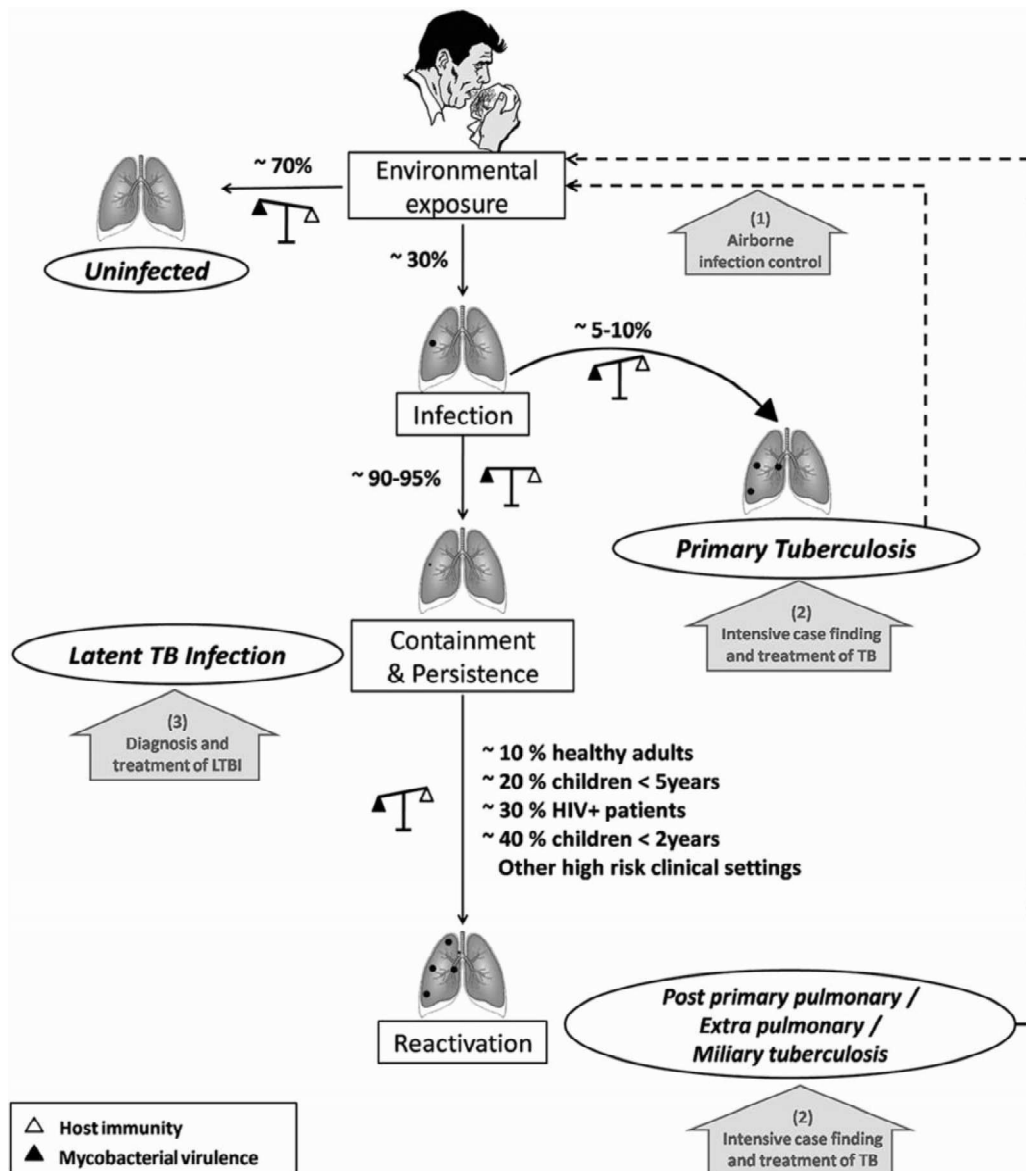


Figure 10: Outcomes following exposure to *M. tuberculosis* in an individual (adapted with permission from American College of Chest Physicians for ref.⁴)

5. Symptoms

In general, symptoms in tuberculosis disease are fever (known as the most common symptom), lack of appetite, weight loss, weakness, fatigue, or rarely sweating at night. In addition, the symptoms of tuberculosis also depend on where the tubercle bacillus is located. In fact, tuberculosis disease may have many forms, e.g. pulmonary tuberculosis, extrapulmonary tuberculosis, or miliary tuberculosis. Among the forms mentioned above,

pulmonary tuberculosis is the most common and poses a significantly infectious risk to the community.^{42,43}

Pulmonary tuberculosis

This is the tuberculosis infection that affects the lungs. Therefore, the additional symptoms may contain a heavy cough that lasts more than three weeks. The initial cough may be accompanied by yellow or green sputum that can rapidly become bloody. In addition, patient may have breathlessness plus chest pain (pleuritic or retrosternal pain).⁴³

Extrapulmonary tuberculosis

The tuberculosis may have spread from the lung through the blood to any parts of the body. Extrapulmonary tuberculosis is a type of tuberculosis that involves many organs of the body outside the lungs, such as: kidneys, lymph nodes, bone, the membranes (brain, abdominal cavity, and pericardium). Extrapulmonary tuberculosis is less common than tuberculosis in lung. Because this tuberculosis type is related to many organs of body, symptoms of extrapulmonary tuberculosis are varied and vague. The additional symptoms may be: swollen glands, pain, abscess, loss of movement in an affected bone or joint, headache, seizures and so on.^{42,43}

Miliary tuberculosis is a life-threatening type of tuberculosis that was caused by the spread of tubercle bacillus in the host bloodstream.^{42,43}

Latent tuberculosis

Patient with latent tuberculosis may usually have no specific symptom.⁴⁴

6. Diagnosis of tuberculosis

Diagnosis of active TB (including pulmonary and extra-pulmonary TB) is usually based on several methods, e.g. clinical suspicion, diagnostic imaging, smears for acid-fast bacilli (AFB), solid and liquid culture and molecular-based detection of tubercular nucleic acid in clinical specimens.⁴⁵ On the other hand, tuberculin skin test and interferon-gamma release assay are widely used in diagnosis of latent TB infection.⁴⁶ Until now, many reviews on TB diagnostic methods were published.^{45,47,48} In this section, we will point out a brief outline on principal TB diagnostic methods.

6.1. Diagnostic imaging

The conventional chest X-ray is still now the most commonly imaging method. This method is used for screening, diagnosis and following up of treatment responses in patients with pulmonary tuberculosis and other pulmonary disease. Chest radiography can identify calcified lesions in the parenchyma of the lungs indicating a granuloma. Furthermore, chest computerized tomography scan (CT) is more sensitive than conventional chest X-ray to identify early parenchymal lesions or mediastinal lymph node enlargements and to determine disease activity in tuberculosis.⁴⁷ Recently, serial pulmonary [¹⁸F]-2-fluoro-deoxy-D-glucose positron emission tomography (FDG-PET) has been investigated as a promising non-invasive method to monitor disease activity and responses to anti-tuberculosis chemotherapy.⁴⁹

Although highly expensive, this technique could be useful and even be cost-effective for the management of patients with MDR and XDR tuberculosis in some cases.⁴⁷

6.2. Microbiological diagnosis

A definitive diagnosis of tuberculosis can be only made by identification of *M. tuberculosis* in a specimen from the patient. The most common specimen is sputum. However, in patients who are incapable of producing a sputum sample, other alternative specimens can be used (e.g. gastric washings, laryngeal swab, bronchoscopy and others). The specimen is then examined by several methods including sputum smear examination by microscopy, culture examination, and/or several recent molecular tests.⁵⁰

6.2.1. Sputum smear examination by microscopy

Microscopic examination of acid fast-stained sputum, with Ziehl-Neelsen (ZN) is one of the easiest, inexpensive and rapid methods used in many developing countries. The recent development in conventional tuberculosis microscopy is fluorescent microscopy.⁴⁷ Recent reviews have confirmed the importance of specimen processing and fluorescence microscopy in achieving optimal sensitivity for smear microscopy. On the other hand, concentration of sputum (by centrifugation) increases the sensitivity of smear microscopy by 18%, while fluorescence microscopy is on average 10% more sensitive than standard microscopy.⁵⁰

6.2.2. Culture examination

Culture examination is a phenotypic method. Tuberculosis culture usually requires a sputum decontamination step in order to prevent cultures from being overgrown by contaminating others bacteria and fungi. The culture also allows species-specific identification in order to distinguish between active TB and nontuberculous mycobacteria (NTM). Culture of *M. tuberculosis* in clinical specimens is substantially more sensitive than smear microscopy. This method is considered as the gold standard for TB diagnosis until now. However, this method often requires a long time to confirm the results. Recently, a modification of this technique is the liquid media. A systematic review demonstrates that liquid cultures are more rapid and sensitive than solid medium cultures. Thus, WHO endorsed the use of liquid tuberculosis culture and drug susceptibility testing for *M. tuberculosis*. However, culture results are still frequently received too late to have an impact on clinical management. The currently available culture methods are technically demanding and require implementation of biosafety practices and equipment to prevent infection of laboratory staff.^{47,50,51}

6.2.3. Molecular methods

Recently, many genotypic methods have been developed in order to determine and confirm the presence of *M. tuberculosis* in the specimens.

The first genotypic method developed is Nucleic Acid Amplification Techniques (NAAT). This method relies on the specific detection of *M. tuberculosis* DNA or RNA in specimen. NAAT results can be available to the clinician within one day and can have important implication for the management of TB patients. Furthermore, an advantage of

NAAT is that this method can amplify regions specific to *M. tuberculosis* which are potentially highly sensitive and may allow for rapid detection of mutations associated with drug resistance. In patients with positive AFB sputum smears, the sensitivity of NAAT to detect *M. tuberculosis* nucleic acid on these specimens is greater than 95%. In contrast, in individuals with negative AFB sputum smears, the estimated sensitivity of NAAT for the diagnosis of active tuberculosis is highly heterogeneous and is not consistently accurate enough to be routinely recommended for the diagnosis of tuberculosis.⁵⁰

Recently, GeneXpert MTB/RIF system has been developed and has been rapidly considered as a major advance in TB diagnosis. This system is a fully automated sputum-processing, DNA extraction and real-time PCR-based detection platform for TB which is able to simultaneously detect the presence of TB in a sample and determine susceptibility to rifampicin. It uses hemi-nested real-time PCR assay to amplify a specific sequence of the *rpoB* gene, which is then probed with molecular beacons for mutations within the rifampin-resistance determining region. Result can be obtained within only two hours. This method has a detection of 100% of smear-positive and 72% of smear-negative cases and high specificity. A large multicenter evaluation study is ongoing. The major advantage of this system is the need for minimal operator training, suitability for decentralized models of TB diagnosis and ability to rapidly detect both the presence of TB and rifampicin resistance.^{50,52}

Despite the rapid development of molecular-based tests in TB diagnosis, these methods could not replace microscopy and culture method until now. Alternatively, they are rather used to confirm the presence of *M. tuberculosis* in positive sputum and non-sputum smears.⁴⁵

6.3. Immunological diagnosis

The tuberculin skin test (TST) and interferon- γ release assays (IGRA) evaluate *in vivo* (TST) or *ex vivo* (IGRA) the presence of persistent mycobacteria-specific T cell responses. These two methods are performed on peripheral blood of patient. However, they cannot distinguish between individuals with LTBI, active tuberculosis or infect tuberculosis in the past.

6.3.1. Mantoux tuberculin skin test (TST)

In 1934, a purification method of tuberculin was investigated and a protein precipitate of antigens from metabolically active *M. tuberculosis*, namely purified protein derivatives (PPD) was developed. Currently, PPD is used intradermally in the Mantoux technique to diagnose TB. This method has remained the established screening method to identify persons with LTBI. Moreover, TST is also frequently used in children as an adjunctive test to support a diagnosis of active TB disease. However, TST is an imperfect marker for TB exposure as the test reagent, purified protein derivative (PPD), is cross reactive and contains antigens present in BCG vaccine and non-tuberculous mycobacteria. This leads to decrease of test specificity and cause false-positive results. Most importantly, the sensitivity of TST is reduced in individuals with advanced TB disease, malnutrition or HIV infection, leading to false-negative results.⁵⁰

6.3.2. Interferon-gamma release assays

Interferon-gamma release assays (IGRAs) are a new set of diagnostics using *M. tuberculosis*-specific antigens and reduce the risk of false positive due to cross-reaction with other mycobacterial strains and BCG vaccine. This method detects the presence of circulating T cells sensitized to TB-specific antigens by the release of IFN- γ . The growing evidence supports the use of IGRAs for the diagnosis of LTBI in adults. Studies have shown that IGRAs have a reasonably high sensitivity for TB disease and correlate better with *M. tuberculosis* exposure than TST. The only drawback of IGRAs is their inability to distinguish between active and latent TB infection.⁵⁰

Currently, two IGRAs formats have been officially approved worldwide: QuantiFERON-TB Gold[®] assay (Cellestis Limited, Victoria, Australia) and T-SPOT.TB[®] test (Oxford Immunotec, Oxford, UK). Both systems rely on host reaction to infection by measuring interferon- γ produced by T-cell responses to the *M. tuberculosis*-specific antigens. IGRAs have several important advantages over the TST. The testing requires only one visit to the diagnostic centre and since the assay is *ex vivo*, there is no boosting effect when tested again like TST. Also, results can be obtained within one day. IGRAs are now approved for use in several countries.^{50,51}

6.4. TB diagnosis in the future

In summary, all of the actual diagnostic methods presented above have some limitation in TB diagnosis. Therefore, other biomarkers for tuberculosis disease status and diagnosis should be discovered and developed. Moreover, the rise of many drug-resistant-TB types has drawn attention to the need for rapid drug susceptibility testing for TB. Delay in diagnosis is associated with unfavorable outcomes and an increased opportunity for transmission of tubercular resistant strains.⁵⁰

7. TB vaccines and immunizations

Nowadays, vaccination has been considered as the most effective method for preventing individuals from infectious diseases. In the case of tuberculosis, TB vaccine works by stimulating the human immune system to develop adaptive immunity to tubercle bacilli in order to prevent or ameliorate morbidity. Until now, the only approved vaccine against TB is bacillus Calmette–Guérin (BCG). This vaccine can reduce the risk of getting TB in human.⁵³ However, BCG vaccine has also several limitations, and research to develop other new TB vaccines is ongoing.

7.1. Bacillus Calmette–Guérin vaccine

The current vaccine bacillus Calmette–Guérin (BCG) was developed by Albert Calmette and Camille Guérin at the Pasteur institute in Lille, France. This vaccine is a live attenuated strain of *Mycobacterium bovis*, obtained through many *in vitro* passages over 13 years-study period. It was firstly administered as oral vaccine to an infant in 1921 and until now it is still the only vaccine licensed to prevent TB.⁴²

BCG is a pre-exposure vaccine which only reliably protects against tuberculosis in newborn children but the protective efficacy of BCG against pulmonary TB and other

mycobacterial diseases in adults is inconsistent.⁵⁴ Several studies showed that BCG vaccination has efficacy against childhood tubercular meningitis and miliary tuberculosis.^{53,55,56} However, the major controversial aspect of BCG vaccination is the variable efficacy which have been found in different clinical trials. Some systematic reviews showed that vaccination with BCG significantly reduces the risk of tuberculosis by an average of 50%,⁵⁷⁻⁵⁹ while the result from other meta-analysis study indicated that the protective effect against miliary or meningeal TB ranges from 75% (in case control studies) to 86% (in randomized controlled trials).⁵⁵ Nevertheless, a recent systematic review and meta-analysis on the vaccinated and unvaccinated children under age 16 with known recent exposure to patients with pulmonary tuberculosis indicated that the BCG vaccine reduced infection by 19-27% and reduced progression to active TB by 71%.⁵³ Some possible hypothesis for the variable efficacy of BCG has been proposed. Firstly, it has been observed that there are many different BCG vaccines produced around the world. Although all currently used vaccines were derived from the original *M. bovis* strain, they differ in their characteristics when grown in culture, for that reason they may not be bacteriologically identical, due to the biological variability of the strains, with different genotypic and phenotypic characteristics. As a result, depending on the strain, they have different viability, immunogenicity, and residual virulence. Moreover, several other reasons should be cited such as genetic differences among human populations, interference by environmental mycobacteria, and exposure to other bacterial infections. But none of them have been proven.

In addition, the protection provided by BCG vaccine has been proven to decrease with time since vaccination.⁶⁰⁻⁶² The protective duration of BCG are inconsistent in many different studies.⁶¹ There is good evidence that BCG vaccination protection declines with time and that protection can last for up to 10 years.⁶⁰ While a study conducted by Medical Research Council in Great Britain revealed that protection decreased from 84% in the first five years to 59% between 10 and 15 years.⁶² Interestingly, a study⁶³ on the American Indians and Alaska Natives who participated in a placebo-controlled BCG vaccine trial during 1935-1938 have demonstrated that BCG vaccine efficacy persisted for 50 to 60 years. However, further studies are required to exactly determine the duration of protection by BCG vaccination.⁶³ Moreover, there is some evidence that a second dose of BCG vaccine does not increase its protective efficacy.^{64,65}

BCG is generally a safe vaccine in healthy infants. However this vaccination has reported to cause TB infection in immune-compromised individuals. Different studies revealed a risk of disseminated BCG disease in HIV- infected children, even if asymptomatic at time of vaccination.⁶⁶ This has led to changes in policy from the WHO Global Advisory Committee on Vaccine Safety, recommending that BCG should not be used in HIV-positive children.^{5,67} Another concern BCG vaccination is that this vaccine may cause a false positive reaction to a Tuberculin Skin Test (TST). A positive reaction to a TB skin test may be due to infection with TB bacteria but also due to the BCG vaccine itself.

Nowadays, BCG vaccine was eventually accepted by 157 countries around the world⁶⁸, especially in TB endemic countries (see Figure 11). It is routinely administered to newborn children in many countries worldwide and provides significant protection against TB, mostly

disseminating and meningeal forms. Moreover, BCG is recommended by WHO as part of tuberculosis control and now in the WHO's List of Essential Medicines. However, there remains about 23 countries have either stopped BCG vaccination due to a reduction in TB incidence, or never recommended BCG immunization programme.⁶⁸ The use of BCG vaccine has been limited in these countries because of its variable efficacy in TB prevention, or may be the low and declining prevalence of disease in these countries and the strategic choice to treat latent tuberculosis infection. Alternatively, their policy focuses on selective vaccination of TB 'at risk' groups.⁶⁸

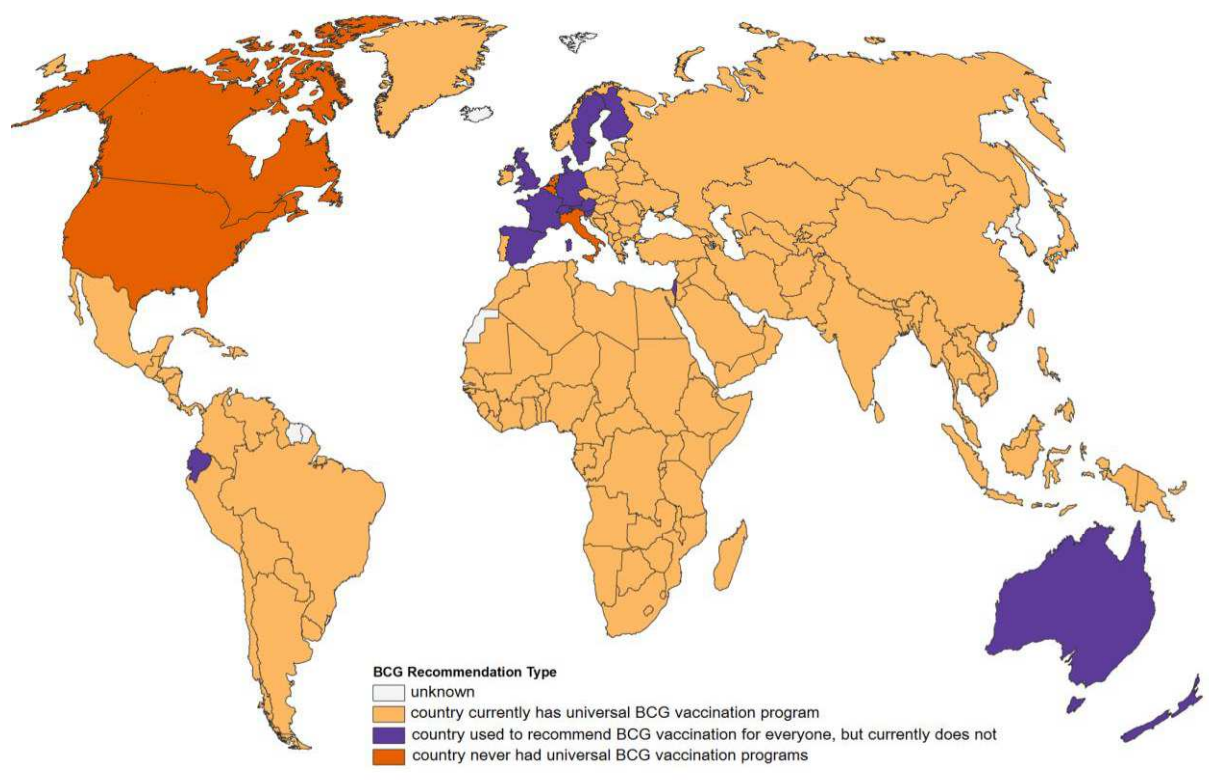


Figure 11: Map displaying BCG vaccination policy by country
(adapted with permission from PLOS under Creative Commons Attribution License, ref.⁶⁸)

Despite nearly a century of use, BCG vaccine is clearly insufficient for worldwide TB control. Due to its limited efficacy, this vaccine has not successfully eliminated the resurgence of tuberculosis observed in the last decade of this century. For that reason, there is a strong need to develop novel TB vaccines that not only have a superior ability to induce protective immunity against TB, but also have a better safety profile compared to BCG. Specifically, new vaccines that prevent adolescents and adults from developing tuberculosis disease would be the greatest advance of the global TB control.

7.2. Novel vaccination strategies against tuberculosis

A significant progress in TB vaccine development has been observed after the declaration of tuberculosis as a global health emergency by the World Health Organization in 1993. In fact, from a pipeline nearly empty of new TB vaccine candidates in the early 1990s, the global pipeline of TB vaccine candidates in clinical trials is more robust than at any previous period in history. There are currently 15 vaccine candidates in clinical trials (Figure

12) which were developed by number of pharmaceutical companies and academic research groups over the world.^{67,69,70}

Phase I	Phase IIa	Phase IIb	Phase III
Ad5 Ag85A McMaster University, Can Sino	Crucell Ad35 / Aeras402 Crucell, Aeras (formerly PhIIb)	MVA85A /Aeras-485 UOXF, AERAS	M. Indicus pranii IT Dpt of Biotechn (Govt of India), Cadila
ID93 + GLA-SE IDRI, Aeras	VPM1002 MPIIB, VPM, TBVI, SII	M72 + ASO1E GSK, Aeras	M. vaccae IT An Hui Longcom
MTBVAC UniZaragoza, Biofabri, TBVI	RUTI Archivel Pharma		
DAR-901 Dartmouth University, Aeras	H I + IC31 SSI, TBVI, Intercell, EDCTP		
ChAdOx1.85A UOXF	H56 : IC31 SSI, Intercell, Aeras		P priming vaccine B boosting vaccine IT therapeutic vaccines
Crucell Ad35 – MVA85A prime-boost B UOXF, Aeras, Crucell	H4 : IC31 SSI, SP, Aeras		

Figure 12: Global clinical TB vaccine candidate pipeline until April 2015
(used with permission of Stop TB Partnership, ref.⁷¹)

TB vaccines under development are generally designed by many different strategies.⁶⁷ Firstly, novel vaccines can boost the initial effects of BCG (i.e. boosting vaccine). The aim of boosting vaccines is to enhance the immune response of BCG vaccine. The combination between these novel vaccines with BCG is also called the prime-boost strategy. Second, another strategy was also developed which are known as priming vaccine. This strategy aims to replace BCG with a safer and more long-lasting vaccine. These vaccines can be a recombinant BCG strain or genetically attenuated *M. tuberculosis*. Two classes of TB vaccine above are also known as pre-infection vaccine which prevent human from TB infection. In addition, a post-infection vaccine strategy is suggested in order to prevent the reactivation of TB in latent infection individuals. On the other hand, a therapeutic vaccine strategy can improve the response to chemotherapy and reduce duration of TB therapy.⁶⁷

Despite an impressive progress, TB vaccine development has to face many significant obstacles like other vaccine development. In fact, it has proven challenging to develop vaccines against pathogens whose control depends on the cellular immune response. With many other infectious diseases, scientists can rely on protective markers in the blood known as correlates of protection to predict whether a vaccine will work. But in case of TB, the mechanisms of protection against TB has not fully discovered. Therefore, no biomarker of protection has been determined to predict whether these TB vaccines will have protective efficacy in humans.⁶⁷ As a result, clinical trials of TB vaccine likely need several years for evaluation of its efficacy.^{72,73}

Recently, the most potential TB vaccine candidate MVA85A with promising immunogenic results in animal models and humans has failed to show effectiveness in a phase IIb of clinical study in 2013. The results from this trial, involving 2 797 HIV-negative infants previously vaccinated with BCG, showed that differences between the rates of TB in infants vaccinated with MVA85A and in the placebo group were not statistically significant. It means that that MVA85A was not effective in prevention of BCG-vaccinated infants from TB.⁷⁴ Despite the inadequate results, this trial could help researchers to learn more about the mechanism on how the human immune response to TB and to determine biological markers that predict risk of developing TB disease or protective ability of vaccine. Researchers believe that the lessons learned from this study hopefully can be applied to improve the entire global portfolio of TB vaccine candidates in future.

8. Antitubercular chemotherapy

TB is curable by chemotherapy. Many TB drugs have been developed and actually used in TB management. However, the current TB regimen also has some limitations. In order to improve the actual TB chemotherapy, it is important to understand the efficiency, mechanisms of action of TB-drugs and mechanism of drugs resistance in *M. tuberculosis*.

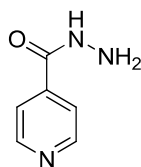
8.1. Current antituberculosis drugs

There are more than twenty drugs that are currently used for the treatment of TB in which only 14 TB-drugs were approved by the U.S. Food and Drug Administration (FDA). According to WHO, anti-tuberculosis drugs are generally categorized into 5 groups based on evidence of efficacy, potency, drug class and experience of use (Table 1).^{75,76}

8.1.1. First-line TB drugs (group 1)

Essential first-line anti-tuberculosis agents (also named as front-line TB drugs) are the most effective agents in TB management. This group comprises isoniazid (INH), rifampicin (RIF), ethambutol (EMB), pyrazinamide (PZA) and streptomycin (SM). These drugs are used in the initial treatment of drug-susceptible TB (DS-TB). We present herein an overview of these drugs with their mechanism of action and resistance in *M. tuberculosis*.

8.1.1.1. Isoniazid



isoniazid

Isoniazid (INH) is the most commonly used anti-tuberculosis drug since recognition of its clinical activity in 1952. INH belongs to the nicotinamide family and appears to penetrate host cells readily and diffuses across the *M. tuberculosis* membrane. This is a pro-drug, requiring oxidative activation by the *M. tuberculosis* catalase-peroxidase enzyme KatG leading to an INH-NAD adduct. This active adduct then binds to enzymes of the Fatty acid synthesis type II cycle. The exact target of INH is still a contentious issue with evidence

suggesting involvement of InhA, the enoyl-ACP reductase and KasA, the beta-ketoacyl synthase. Consequently, INH blocks mycolic acid synthesis at meromycolic chain elongation step. This leads to accumulation of C₂₄/C₂₆ fatty acids, drastic changes in the cell wall envelope followed by cell lysis. INH is the most potent mycobactericidal drug with an MIC of 0.2 µg/ml. Because of its significant bactericidal activity, it has become a critical component of the first-line antituberculosis regimens.^{2,54}

Table 1: Classification of drugs in treatment of tuberculosis according to WHO⁷⁵⁻⁷⁷

	Groups	Drug (year of discovery)	Drug target (action)
FIRST-LINE	Group 1 (first-line oral agents)	isoniazid (1952) [@] pyrazinamide (1954) [@] ethambutol (1962) [@] rifampicin (1963) [@] <i>rifapentine (1965)[@]</i> <i>rifabutin (1975)</i>	InhA (inhibition of mycolic acid biosynthesis) ribosomal protein S1 (unclear effect) arabinosyl transferases (inhibit arabinogalactan biosynthesis) RNA polymerase (inhibition of transcription) RNA polymerase (inhibition of transcription) RNA polymerase (inhibition of transcription)
SECOND-LINE	Group 2 (injectable agents)	<i>streptomycin (1944)[@]</i> kanamycin (1957) amikacin (1972) capreomycin (1963) [@] viomycin (1971)	30S ribosomal subunit (inhibition of protein synthesis) 30S ribosomal subunit (inhibition of protein synthesis) 30S ribosomal subunit (inhibition of protein synthesis) 30S+50S ribosomal subunit (inhibition of protein synthesis) 30S+50S ribosomal subunit (inhibition of protein synthesis)
	Group 3 (fluoroquinolones)	ofloxacin (1980) levofloxacin (1992) moxifloxacin (1999) gatifloxacin (1999)	Target for all drugs in this group: DNA gyrase and topoisomerase (inhibition of the relaxation of DNA supercoiling)
	Group 4 (oral bacteriostatic second-line agents)	ethionamide (1961) [@] prothionamide [@] cycloserine (1955) [@] terizidone [@] <i>p</i> -aminosalicylic acid (1948) [@]	InhA (inhibit mycolic acid biosynthesis) InhA (inhibit mycolic acid biosynthesis) <i>D</i> -Ala racemase and ligase (Inh of peptidoglycan synthesis) <i>D</i> -Ala racemase and ligase (Inh of peptidoglycan synthesis) Dihydropteroate synthase (Inhibition of folate biosynthesis)
THIRD-LINE	Group 5 (agents with unclear role in DR-TB treatment)	clofazimine (1954) linezolid (1996) amoxicillin + clavulanate (1978) thioacetazone (1980) imipenem + cilastatin high-dose of isoniazid clarithromycin (1970) meropenem	Guanine bases (inhibition of replication) Inhibition of protein synthesis Inhibition of peptidoglycan synthesis /β-lactamase cyclopropane mycolic acid synthases Inhibition of peptidoglycan synthesis /β-lactamase - Large ribosomal subunit (inhibition of protein synthesis) Inhibition of peptidoglycan synthesis
	un-classified group	bedaquiline (2012) [@] delamanid (2014)	ATP synthase Inhibition of mycolic acid biosynthesis

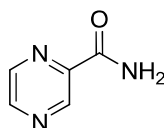
@ : approved by FDA ; Three *drugs in italic* are classified in these groups for specific reasons as described in the main text.

Because INH is the most commonly used antitubercular drug, resistance to INH occurs more frequently among clinical drug-resistant strains. Mutations in INH-resistant clinical isolates are most commonly detected in the *katG* gene, occurring in 50–80% of cases, thus reducing the ability of the catalase-peroxidase to activate the INH pro-drug. Depending on the

type of mutation, and the degree to which function of the KatG enzyme is preserved, the MIC of isoniazid may change. Point mutations in *katG* are more commonly observed than other types of mutations, and a single point mutation resulting in substitution of a threonine for a serine at residue 315 (S315T) accounts for the majority of INH resistance among clinical isolates. The S315T mutation results in a significant diminution in catalase and peroxidase activity, and is associated with high-level of INH resistance (MIC = 5-10 $\mu\text{g/mL}$).⁵⁴

In addition, INH resistance may also arise from mutations in *inhA* gene, resulting in reduced affinity of the enzyme for NADH without affecting its enoyl reductase activity or in the promoter region of the *mabA-inhA* operon resulting in overexpression of the wild-type enzyme. Generally, mutations in *inhA* or in the promoter region of its operon usually confer low-level resistance (MIC=0.2–1 mg/L). Importantly, mutations in *inhA* also cause resistance to the structurally related second-line drug ethionamide. Furthermore, mutations in the *ndh* gene, which encodes a NADH dehydrogenase, conferring resistance to INH and ethionamide have been also detected in INH-resistant *M. tuberculosis* clinical isolates. Defective NADH dehydrogenase could lead to an increased ratio of NADH/NAD⁺, thereby interfering with KatG-mediated peroxidation of INH, or by displacing the INH-NAD⁺ adduct from the InhA active site. Furthermore, mutations in *kasA* and *ahpC* genes have been associated with INH resistance.⁵⁴

8.1.1.2. Pyrazinamide



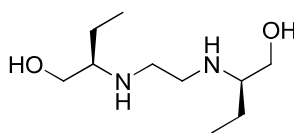
pyrazinamide

Nowadays, the mechanism of action of PZA remains poorly understood. This drug has a high bactericidal activity *in vivo* while *in vitro* activity requires acidic pH and or hypoxia. This suggests activity against semi-dormant bacteria located inside cells and in anoxic or hypoxic lesions in the lung. PZA is a prodrug which needs activation by the tubercular protein PncA, a pyrazinamidase (PZase). Pyrazinamide activity is dependent on pyrazinoic acid release, which causes intake of proton and dysfunction of the pH balance of the mycobacteria. It has been recently shown that pyrazinoic acid targets the ribosomal protein S1, an essential protein involved in the ribosome-sparing process of translation. There has been no clear resolution of its mechanism of action since resistant mutants mostly carry mutations in the activating PncA gene. Pyrazinamide (PZA) was approved as a potential TB drug in 1954. Its introduction in the TB treatment in the 1980s was a great success as it allowed to shorten the duration of the TB therapy from 9-12 months to 6-9 months.⁵⁴

PZA resistance has been attributed primarily to mutations in the *pncA* gene encoding PZase. Most mutations, including point mutations, deletions, and insertions, have been reported in a 561-bp region of the open reading frame or in an 82-bp region of its putative promoter. The relatively high degree of diversity in *pncA* mutations among PZA-resistant clinical isolates has complicated the development of molecular assays for the rapid and economical detection of PZA resistance. A small percentage of isolates with high-level PZA

resistance contain no mutations in *pncA* or its promoter, suggesting alternative mechanisms of resistance such as deficient uptake, enhanced efflux, or altered *pncA* regulation. The high specificity of PZA for *M. tuberculosis*, with little or no activity against *M. bovis* and other mycobacteria, is attributable to *pncA* mutations, which render PZase inactive in the latter mycobacterial species.⁵⁴

8.1.1.3. Ethambutol



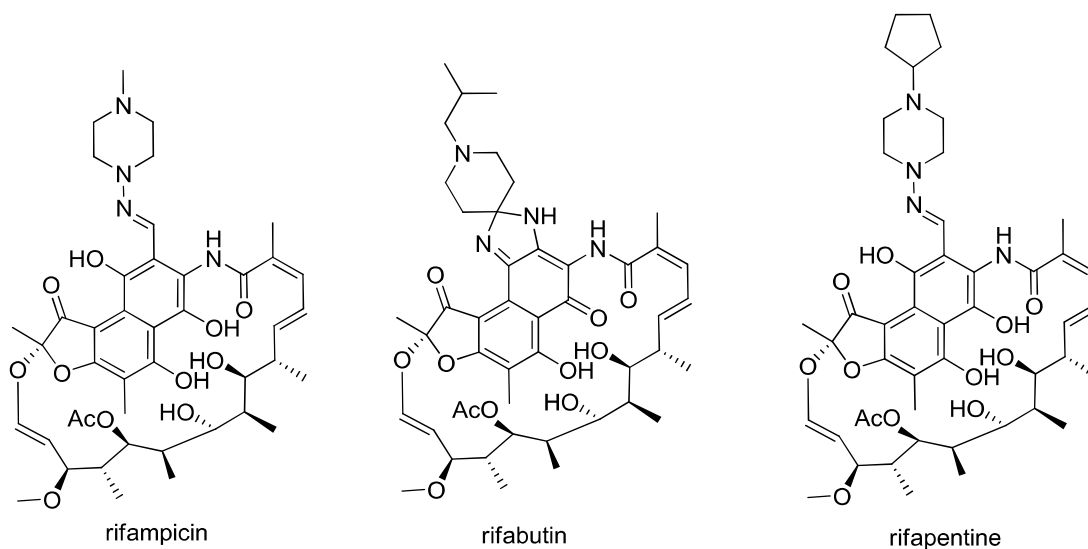
ethambutol

Ethambutol belongs to the family of diamine analogues. This drug interferes with cell wall synthesis as shown by the almost immediate destabilization of the cell envelope. Detailed radiolabeling studies indicated that arabinogalactan synthesis was impaired at the level of arabinosyl transferases. These enzymes were confirmed as the target of ethambutol.⁵⁴

Resistance to ethambutol in *M. tuberculosis* is usually associated with point mutations in the *embCAB* operon encoding for arabinosyl transferases. As the majority of ethambutol-resistant clinical isolates contain mutations in the *embB* gene, *EmbB* is considered to be the main target of ethambutol. More recently, the most commonly observed mutations in *embB* codon 306 have been reported to be associated with variable degrees of ethambutol-resistance, indicating that such mutations may be necessary but not sufficient for high-level of resistance. Other potential mutations involved in ethambutol resistance include a Gln379Arg substitution in *M. tuberculosis embR*, as well as mutations in the *rmlD*, *rmlA2*, and *Rv0340* genes.⁵⁴

8.1.1.4. Rifampicin and other rifamycins

The rifamycins are a group of natural products which were first isolated in 1957 from *Amycolatopsis mediterranei* as part of an Italian antibiotic screening program. All rifamycins contain an aromatic nucleus linked on both sides by an aliphatic bridge. The rifamycins easily diffuse across the *M. tuberculosis* cell membrane due to their lipophilic profile and are potent inhibitors of the mycobacterial activity.⁵⁴



Rifampicin (or rifampin), a semi synthetic analogue of rifamycin B, is a broad-spectrum antibiotic. This drug has been the most widely used to treat TB since 1963. It inhibits RNA synthesis by binding to the beta-subunit of the prokaryotic DNA-dependent RNA polymerase. This specific binding also prevents any toxic side effect on host cells because eukaryotic RNA polymerases are inhibited only at concentrations about 10^4 fold above the MIC of rifampicin. The incorporation of rifampicin in standard anti-tuberculosis regimen allowed reduction of the duration of the treatment from 18 to 9 months. Nowadays, rifampicin is a key component of first line drug treatment for TB. The main drawback of rifampicin is its inductive effect on cytochrome P450 enzymes leading to rapid metabolism of certain AIDS drugs reducing efficiency of anti-retroviral treatment in HIV co-infected individuals.⁵⁴

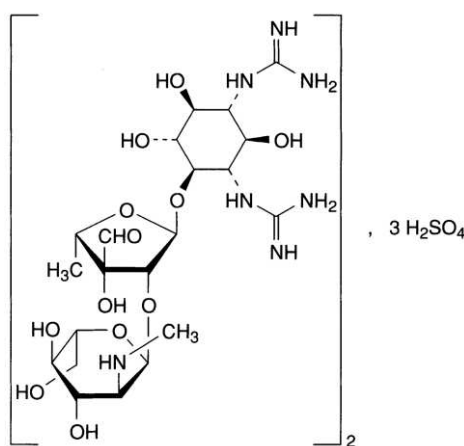
Recently, some novel rifamycin analogs (e.g. rifabutin and rifapentine) have also been considered as first-line drugs in special situations. Rifapentine stays in the body longer than rifampicin and therefore may have the potential to shorten the treatment of active TB. A clinical study showed that rifapentine can shorten latent TB treatment from nine months of daily isoniazid to just 12 once-weekly doses combination of isoniazid and rifapentine. This result can reduce the treatment time for TB patients. For active DS-TB, rifapentine is attractive as a possible TB drug for shortening treatment, and for intermittent TB drug treatment. Clinical trials are under way to confirm this hypothesis. Rifapentine has been shown to allow for once (when given with moxifloxacin) or twice-weekly dosing in the continuation phase of DS-TB treatment.⁷⁵

The use of rifabutin is preferred in combination with HIV medicines, since it has fewer drug-drug interactions than rifampicin. Rifabutin was approved for use in preventing *M. avium* complex disease in patients with HIV infection. But this drug has not yet been approved for TB disease. It is useful for treating TB disease in patients concurrently taking drugs that interact with rifampicin (e.g., certain antiretroviral drugs). However, rifabutin is not included in the WHO TB drug list because for most developing countries, it is impractically expensive.⁷⁵

In *M. tuberculosis*, resistance to rifampicin (RMP) occurs at a frequency of 10^{-7} to 10^{-8} . Mutations in the *rpoB* gene coding for the RNA polymerase mostly confer resistance to rifamycin groups. Mutations in a defined region of the 81 base pair (bp) region of the *rpoB* are found in about 96% of RMP-resistant *M. tuberculosis* isolates. Mutations at positions 531, 526 and 516 are among the most frequent mutations in RMP-resistant strains. Mutations in *rpoB* generally result in high-level resistance (MIC > 32 $\mu\text{g/ml}$) and cross-resistance to all rifamycins. However, specific mutations in codons 511, 516, 518 and 522 are associated with lower-level resistance to RMP and rifapentine, but retain susceptibility to rifabutin and rifalazil.⁷⁸

8.1.1.5. Streptomycin

In 1944, streptomycin was the first compound used to treat TB. However, an increasing prevalence of resistance to streptomycin in many regions of the world has decreased its overall usefulness. Nowadays, this drug is no longer considered as a first line TB drug because of the high rate of resistance.⁵⁴



Streptomycin sulfate

Streptomycin is a natural product which was first isolated from *Streptomyces griseus*. The poor oral absorption of streptomycin led to an administration of this drug in form of sulfate salt by a parenteral route. This amino-glycoside antibiotic is a protein synthesis inhibitor. It binds to the small 30S subunit of the bacterial ribosome, interfering with the binding of formyl-methionyl-tRNA to the 30S subunit. This leads to codon misreading, eventual inhibition of protein synthesis and ultimately death of microbial cells. Streptomycin is an antibiotic that inhibits both Gram-(+) and Gram-(-) bacteria and is therefore a useful broad-spectrum antibiotic including *M. tuberculosis*.⁵⁴

Resistance to streptomycin and the other aminoglycosides in *M. tuberculosis* usually develops by mutation of the ribosome target binding sites. Mutations in the *rpsL* gene, which encodes the ribosomal protein S12, account for approximately half of all streptomycin-resistant clinical isolates with the K43R mutation predominating. In about 20% of streptomycin-resistant *M. tuberculosis* clinical isolates, such resistance is associated with mutations in the *rrs* gene. Generally, mutations in the *rpsL* and *rrs* genes confer high-level (MIC>1000 mg/L) or intermediate-level (MIC=64–512 mg/L) of resistance to streptomycin. On the other hand, mechanisms of low-level resistance to streptomycin (MIC=4–32 mg/L) remain largely undefined but may be attributable to changes in the cell envelope permeability or diminished drug uptake. More recently, it has been shown that mutations in *gidB*, which encodes a conserved S-adenosyl methionine-dependent 16S rRNA methyltransferase, can confer low-level resistance to streptomycin.⁵⁴

8.1.1.6. Conclusion

All the medicine in the first-line group were discovered during the 1950's and the 60's. Until now, these drugs stills remain the main components of the drug-susceptible TB treatment. Despite the efficiency of the drugs alone, a significant improvement of the treatment was obtained with combined therapy in order to limit the apparition of resistant strains. The current regimen is the result from a comprehensive series of trials which was conducted over 20 years that has led to a quadri-therapy in 6-months. This regimen consist of a 2 month "intensive" treatment phase with rifampicin, isoniazid, pyrazinamide, and ethambutol given daily and followed by a 4 month "continuation" phase with rifampicin and

isoniazid. Until now, no new drug classes have succeeded in reducing the current regimen to a shorter one.⁷⁹

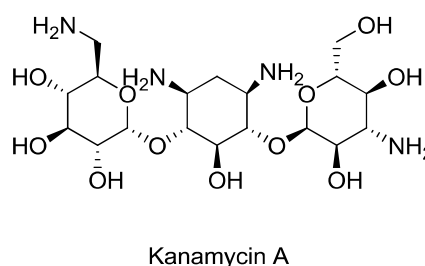
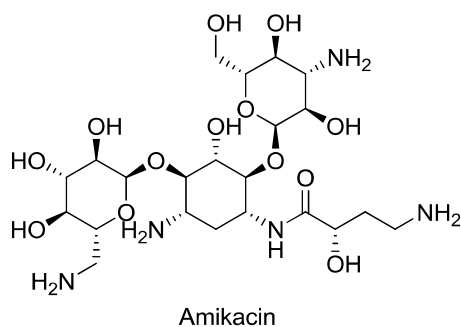
On the other hand, tubercle bacteria rapidly developed many mechanism of resistance to all TB front-line drugs. Many lethal drug-resistant-TBs (DR-TBs) were observed. Multidrug-resistant TB (MDR-TB) are TB strains which resist to at least isoniazid and rifampicin, two cornerstones in the first-line group. Furthermore, when the tubercle bacilli is resistant to isoniazid and rifampicin, plus any fluoroquinolone and at least one of three injectable second-line drugs (i.e., amikacin, kanamycin, or capreomycin), it becomes extensively drug-resistant (XDR-TB). In these cases, treatment of DR-TBs is more challenging and requires the use of second-line drugs and/or “third-line” drugs.

8.1.2. Second-line and “third-line” groups

WHO categorized these drugs in 4 groups (2,3,4 and 5).

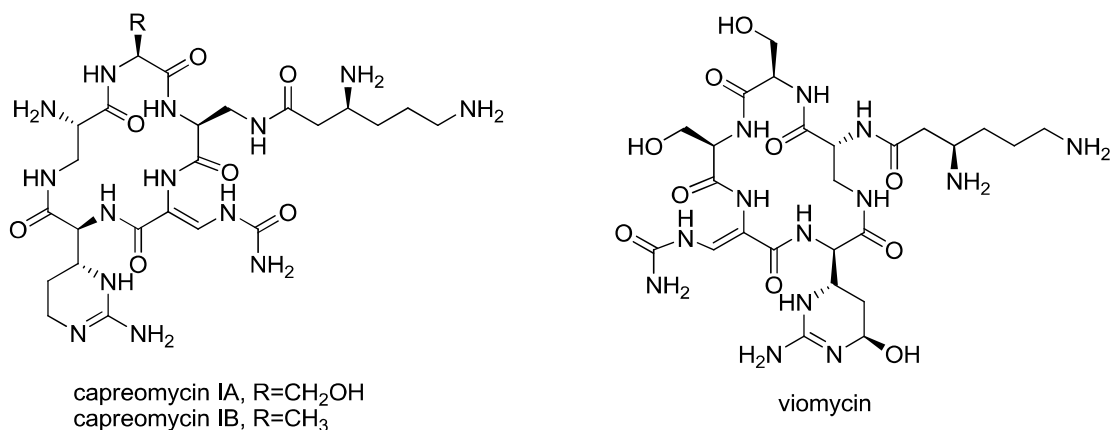
8.1.2.1. Group 2 (injectable agents)

TB drugs in group 2 consist of the aminoglycosides analogues (kanamycin, amikacin) and polypeptides (viomycin, capreomycin). These drugs are delivered by injection. Although belonging to two different antibiotic families, these drugs target the tubercle bacillus at the level of protein translation. In fact, aminoglycosides (kanamycin and amikacin) target the small subunit 30S of the ribosome and inhibit the protein synthesis as streptomycin. However, amikacin and kanamycin are not approved by the FDA for the treatment of TB and can only be used in treatment of TB disease caused by drug-resistant strain. On the other hand, cyclic peptides (capreomycin and viomycin) target the ribosome machinery by binding to the interface between the subunits. These drugs have the same side-effect in renal toxicity. Therefore, regular monitoring of hearing and renal function is recommended during treatment.^{48,54}



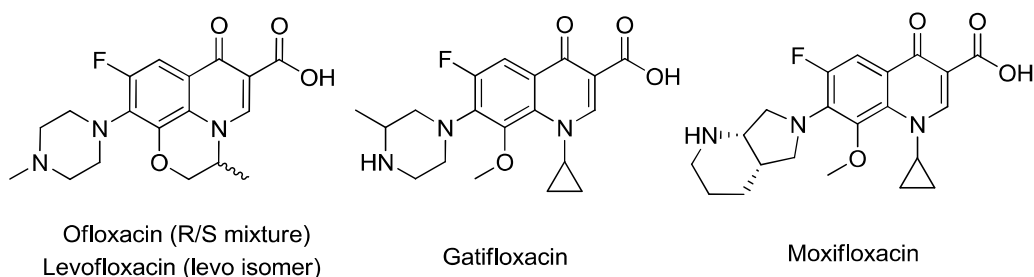
Amikacin and kanamycin are aminoglycosides that have a high level of cross-resistance. Capreomycin is structurally unrelated to the aminoglycosides and can be used if resistance to aminoglycosides is suspected. Resistance to these drugs is associated with changes in the 16S rRNA (*rrs*). Several *rrs* mutations were observed, e.g. A1401G, C1402T, and G1484T. Moreover, a kanamycin resistance TB strain has been identified with mutations in the promoter region of the *eis* gene encoding aminoglycosides acetyltransferase, the enhanced intracellular survival protein, Eis. Furthermore, resistance to capreomycin has also been associated with mutations in *tlyA* gene which encodes a putative 2'-O-methyltransferase

(TlyA) that has been suggested to methylate nucleotide C1402 in helix 44 of 16S rRNA and nucleotide C2158 in helix 69 of 23S rRNA in *M. tuberculosis*.^{48,54}



8.1.2.2. Group 3 (fluoroquinolones)

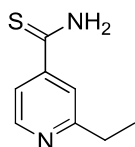
Fluoroquinolones were introduced into clinical practice in the 1980s. Characterized by broad-spectrum antimicrobial activity, they are recommended and widely used for the treatment of bacterial infection of the respiratory, gastrointestinal and urinary tracts. In mycobacteria, fluoroquinolones target the DNA gyrase (or Topoisomerase II) which maintains DNA supercoils necessary for DNA replication. Resistance to fluoroquinolones is attributed to stepwise mutations in the quinolone resistance determining region of GyrA and GyrB genes which encode topoisomerases.^{75,80}



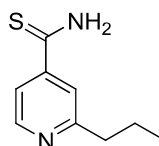
Although not approved by the FDA for TB treatment, fluoroquinolones have been also found to have activity against *M. tuberculosis* and are currently part of the recommended regimen as second-line drugs in the treatment of drug-resistant TB and are now also under clinical study as first-line agents. Levofloxacin, moxifloxacin, and gatifloxacin are all active *in vitro* and in a mouse model, resulting in the ability to shorten treatment to 4 months. Phase II trial results with fluoroquinolones have been inconsistent, but larger ongoing studies will better define the contribution of this class of drugs. Fluoroquinolones do not have significant drug-drug interactions with antiretroviral drugs, although adverse effects limit their use in children and pregnant women. Moxifloxacin may also have overlapping toxicity with regard to prolongation of the QT interval. Several studies with fluoroquinolones are ongoing.^{80,81}

8.1.2.3. Group 4

These drugs are used in the treatment of MDR-TB. Although they do not have strong TB-killing activity, they can prevent the development of resistance to other drugs used in the regimen.

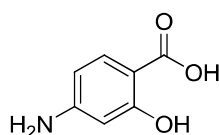
Thioamide analogues

ethionamide

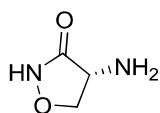


prothionamide

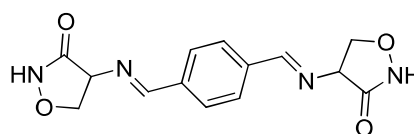
Ethionamide and prothionamide are isoniazid analogues. As isoniazid, they are prodrugs and are bioactivated by EthA to lead to the formation of a NAD adduct that inhibits mycolic acids biosynthesis through the inhibition of InhA. Two independent studies show that EthA, a FAD containing monooxygenase, and its repressor EthR play an important role in its activation and binding to InhA thus affecting mycolic acid synthesis.⁵⁴ This will be further detailed in chapter II.

***p*-Amino salicylic acid***p*-aminosalicylic acid

The mechanism by which *p*-amino salicylic acid inhibits *M. tuberculosis* growth is not well understood even though thymidylate kinase and mycobactin synthesis pathways seems to be implicated. The target of *p*-aminosalicylic acid is still the subject of investigations.⁵⁴

Cycloserine and terizidone

cycloserine



terizidone

D-cycloserine, another cell wall inhibitor, was discovered in 1969. This drug competitively inhibits two necessary enzymes (alanine racemase and alanine ligase) that incorporate alanine into an alanyl-alanine dipeptide, an essential component of the mycobacterial cell wall. Cycloserine is the most significant TB drug associated with central nervous system (CNS) toxicity. Terizidone is a combination of two molecules of cycloserine. Some clinicians found that the side effects associated with terizidone are less severe.⁴⁸

8.1.2.4. Group 5

Group 5 comprise all pharmaceutical agents whose very few clinical trials have been carried out to evaluate their activity against drug resistant TB. In some case, this group was also considered as the “third-line” TB drugs. The medications in this group are not recommended by WHO for routine use in drug-resistant TB treatment because of their unclear efficacy. They can be only used in cases where it is impossible to design adequate regimens with the medicines from Groups 1–4, such as in patients with XXDR-TB or TDR-TB.⁷⁶

8.1.3. Directly observed standardized short-course chemotherapy (DOTS)

In 1990s, a new multidrug therapy program was developed by WHO. This regimen is centralized around the direct supervision of drug intake by patients and was labeled as “Directly observed standardized short-course chemotherapy” (DOTS). A key element of this strategy was the supervision of drug intake. DOTS comprises five elements that constituted a framework for effective TB control:³

- 1) Generating government commitment to mobilize sufficient resources for TB control.³
- 2) Case detection using sputum smear microscopy in patients with respiratory symptoms.³
- 3) Treatment using standard short-course chemotherapy regimens containing rifampicin, administered under direct observation for at least the first 2 months of treatment.³
- 4) Securing a regular supply of essential anti-TB drugs.³
- 5) Establishing a reliable monitoring, recording and reporting system for supervision.³

DOTS became rapidly one of the most efficient weapon against the global TB epidemic. This strategy is an effective treatment for drug susceptible tuberculosis disease with a cure rate of up to 95%. However, DOTS alone may not work in areas where there is high incidence of MDR-TB, where its cure rate is as low as 50%. In such situations, WHO recommends the use of DOTS-Plus, which is DOTS plus second-line TB drugs for the treatment of MDR-TB. However, treatment of MDR-TB with DOTS-Plus takes up to 30 months and is not only costly but also has significant toxicity.^{82,83}

8.1.4. Drawbacks of the current TB treatment

Although DOTS can cure TB in most cases, some serious problems still remain. Firstly, the treatment duration for TB is long in comparison with that of other infectious diseases. A 6-9 months treatment of DS-TB makes patient compliance very difficult. Moreover, treatment regimen for MDR-TB or XDR-TB can last up to 30 months and consists of many drugs in the second-line groups (including injectable agents) which usually have significant side effects. This limitation of current regimen can result in non-adherence to treatment and consequently leads to suboptimal response (e.g. failure and relapse), continuous spread of the disease and the emergence of resistance.⁵⁴ Many researchers have tried to find out the answer for why is TB treatment so long and complex. They proposed that this persistence of *M. tuberculosis* might be due to the physiologic heterogeneity of the bacteria in the tissues. Four different populations of *M. tuberculosis* were found in the lesions^{54,81} :

- 1) Actively growing bacilli which can be killed by INH, EMB and RIF^{54,81}
- 2) Bacilli with spurts of metabolism which can be killed by RIF^{54,81}
- 3) Bacilli with low metabolic activity (in acidic pH) which can be killed by PZA^{54,81}
- 4) Dormant bacilli which could not be killed by any existing drug/regimen.^{54,81}

The actively multiplying bacilli are killed in the first 2 days. However, the remaining dormant bacilli are sterilized very slowly by the existing anti-TB drugs and therefore the treatment period need to be extended. Furthermore, the incapability of the host immune

system to eliminate tubercle bacilli in the lesions could be another factor that leads to the persistence of TB. Thus, development of new anti-TB drugs targeting non-replicating (or dormant) bacteria is a main requirement to shorten the current therapy.^{54,81}

The second reason for the urgent need of new TB-drugs development is a rapid and lethal spread of drug-resistant TB. In fact, the first TB drug, streptomycin, was used in clinical to treat TB in 1944 and shortly after that, streptomycin resistant strains of *M. tuberculosis* were found. The following years showed tremendous promise in TB chemotherapy, each time to be let down by the occurrence of drugs-resistant TB strains. Nowadays, mutations have been found for almost every current TB drugs. Tubercle bacillus has an extraordinary ability to survive the long periods of treatment. This together with the problem of low patient compliance has led to the emergence of multiple drug resistant strains. Recently, the totally drug-resistant (TDR-TB) is a generic term for tuberculosis strains that are resistant to a wider range of TB-drugs.^{15,17,18} The increase of drug-resistant TB strains has led to a crucial need for new TB drugs that have a new mechanism of action. Thus, it becomes more difficult for the tubercle bacilli to develop a resistance mechanism.

Last but not least, another major difficulty is the high prevalence of TB amongst HIV patients. It has been showed that many anti-TB drugs have clinical interactions with anti-HIV drugs. For that reason, novel TB drugs is required not to be antagonistic to current anti-HIV drugs.^{54,81}

8.2. Development of novel antituberculosis drugs

The drawbacks of actual TB regimen described above have led to an urgent need for research on new TB drugs. Nowadays, development of more effective drug regimens against TB becomes a major public health emergency. In general, an ideal new TB drug should have the following considerable characteristics:

- ✓ A safety profile would reduce side effects and increase compliance in treatment
- ✓ Adequate and pharmacokinetic properties would shorten and simplify treatment
- ✓ A more potent activity than existing drugs on *M. tuberculosis*
- ✓ No drug interactions (with actual drugs used in treatment of HIV and TB)
- ✓ A potent activity on drug-resistant tuberculosis strains

Nowadays, there are 4 strategies which are routinely used in order to improve the actual complex regimen and/or develop new drugs to treat the drugs-resistant TB strains (Figure 13).

First, new analogues of actual TB drugs could be developed with improved pharmacokinetic properties and/or antimycobacterial activity. Second, other antibacterial drug classes which are currently used in treatment of other infectious disease could be reconsidered to be used in TB treatment. Third, a new booster agent could be developed to target the resistance mechanism of *M. tuberculosis* in order to reactivate current antibiotics or TB drugs.

Finally, new chemical scaffolds with new mechanisms of action could be developed in order to target the drug resistant strains.

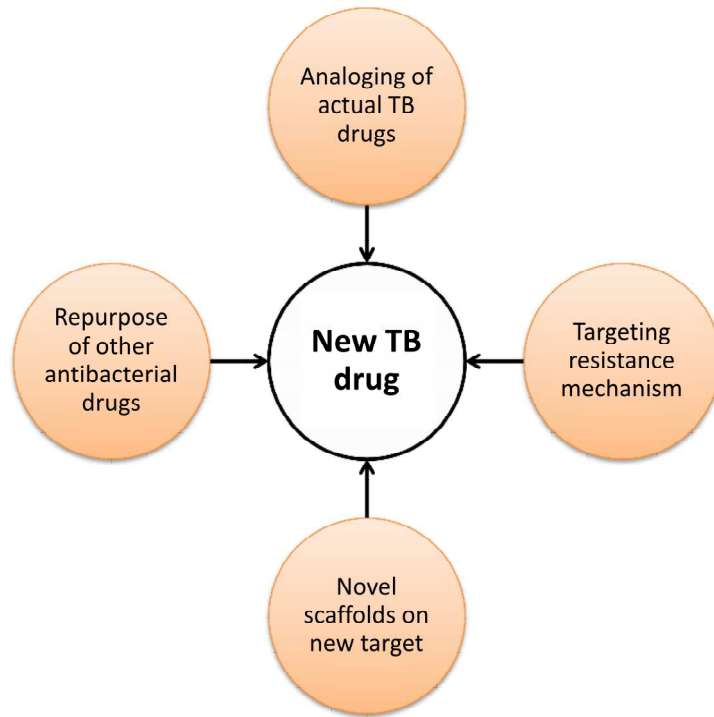


Figure 13: Current strategies in the development of new TB drugs

In addition, it has been observed that TB treatment always require multiple drugs due to the resilient nature of *M. tuberculosis*. However, actual strategy in TB drug development always requires that each new drug candidate need to be tested and approved separately, and then be substituted into the combination with TB drugs. This process need to repeat until the drugs in the existing regimen are replaced. It seems to be a very long paradigm in development of new TB regimen. For that reason, some authors have suggested a new model where the promising TB drug candidates can be tested together in clinical trial (Figure 14). This combination strategy could accelerate the TB drug development in the future and rapidly lead to a discovery of novel regimen.⁸⁴

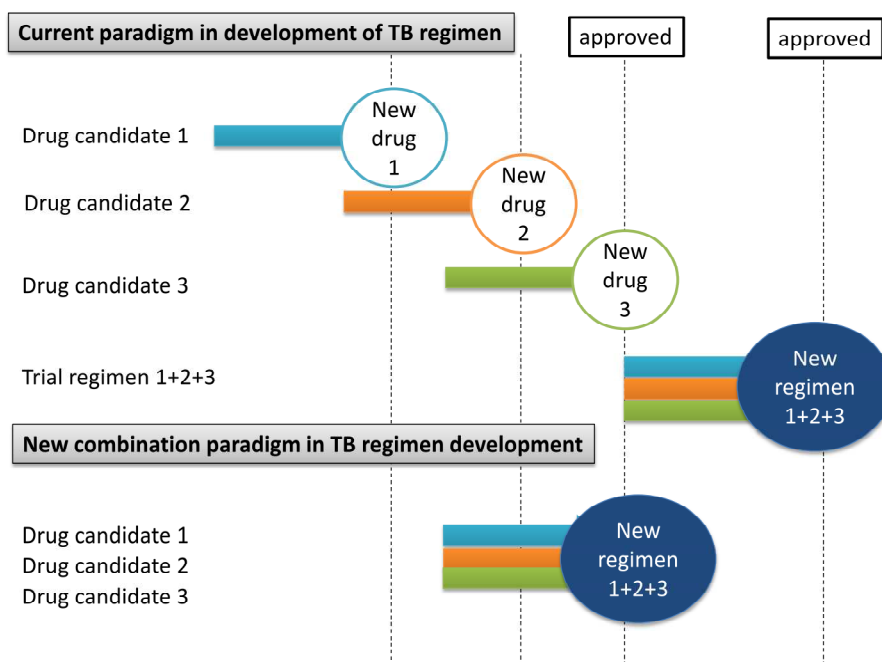


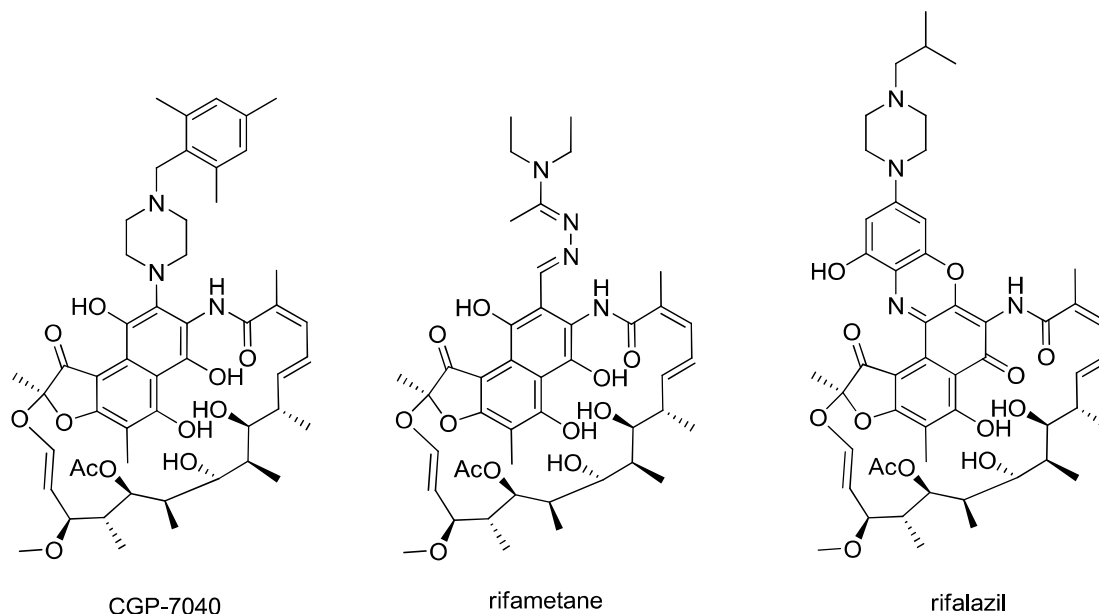
Figure 14: New combination strategy in development of TB regimen

8.2.1. Novel analogues of actual TB drugs with improved properties

This strategy is used to shorten and simplify the actual TB regimen. Many derivatives of existing TB drugs were developed in order to improve the antitubercular activity and/or pharmacokinetic properties.^{81,85}

Rifamycin derivatives

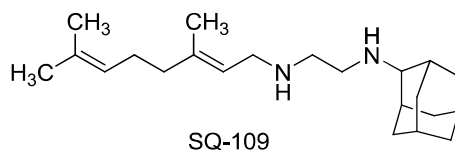
Rifampicin is actually considered as the most potent TB drug. This drug generally is well tolerated in human. However, some adverse effects were also reported. Rifampicin potently induces cytochrome P450 in liver and can cause a discoloration of body fluids. In actual regimen for DS-TB, rifampicin must be given once daily in combination with other TB drugs. For these reasons, many rifamycin derivatives have been synthesized to improve antimycobacterial activity and pharmaco-kinetic properties. Rifapentine and rifabutin are two semi synthetic rifamycin have been used in clinical with some specific indications. Rifapentine is more lipophilic and has a serum half life about five times longer than rifampicin with $t_{1/2}$ = 10-15 hours (versus 2-3 hours for rifampicin). This allows once-weekly dosing of rifapentine in TB treatment. While rifabutin is a less potent inducer of CYPs and can be used in tuberculosis-infected HIV patients treated concurrently with protease inhibitors. Nowadays, these two analogues are under clinical trial for some other indication in TB treatment.^{83,86}



Furthermore, others rifamycin derivatives, e.g. CGP-7040, rifametane (SPA-S-565) and rifalazil (RLZ, KRM1648 or benzoxazinorifamycin) are also developed. Rifametane has been found with a more favorable pharmacokinetic profile than rifampicin, while rifalazil have proven to be more active than rifampicin against *M. tuberculosis*. This compound was progressed into clinical trials. A preliminary safety study in humans showed that although RLZ at doses of 10 mg and 25 mg was safe, a dose of >100 mg produced flu-like symptoms and a transient dose-dependent decrease in white blood cell and platelet counts, and did not show better efficacy than RIF. For that reason, the clinical trial of RLZ for the treatment of

mycobacterial infections has been interrupted. Furthermore, RIF-resistant strains confer cross-resistance to all rifamycins, including RLZ, limiting the use of RLZ and other rifamycin derivatives in the treatment of RIF-resistant TB.^{86,87}

Ethambutol derivatives



An effort to develop second-generation analogues of ethambutol was conducted in order to increase antimycobacterial activity of this first line TB-drug. By screening a combinatorial library based on the pharmacophore of ethambutol, diamine SQ-109 has been identified. When tested in mice using a low-dose infection model of TB, SQ-109 at 1 mg/kg was as effective as ethambutol at 100mg/kg. However SQ-109 did not show improved effectiveness at higher doses (10mg/kg; 25mg/kg) and was clearly less effective than isoniazid. Interestingly, SQ-109 has been found to be effective against drug-resistant strains of *M. tuberculosis*, including those that are ethambutol-resistant, and that it targets different intracellular pathways. For this reason it can be considered as a new TB drug and not simply as an ethambutol analogue. Further study showed that this compound inhibits the trehalose monophosphate transferase, a different target with ethambutol.⁸¹

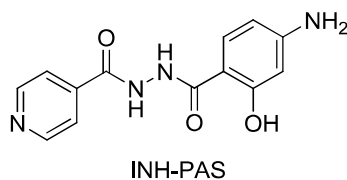
Pyrazinamide analogues

Several pyrazinoic prodrugs with increased lipophilic properties have demonstrated potent activity against *M. tuberculosis*. Some substituted pyrazinoic esters demonstrated a better activity than pyrazinamide against *M. tuberculosis* with a higher plasma stability. Other pyrazinoic and quinoxaline esters derivatives were prepared and evaluated against *M. tuberculosis*. The compounds 4-acetoxy-benzyl esters of pyrazinoic acid and 4'-acetoxybenzyl-2-quinoxalinecarboxylate demonstrated MIC values of 1 - 6.25 $\mu\text{g/mL}$. The use of the prodrug approach in order to obtain new esters prodrugs as pyrazinamide analogues seems to be an important strategy for discovery of new drugs with improved pharmacokinetic and pharmacodynamic properties.⁸⁵

Isoniazid

In order to decrease the toxicity and prolong half-life of isoniazid, some micellar systems of polyethyleneglycol-poly (aspartic acid) copolymer and N-methylene phosphonic chitosan were used as carrier to obtain isoniazid prodrugs. The micellar prodrugs demonstrated activity against *M. tuberculosis*.⁸⁵

Another prodrug approach was by combining para-amino-salicylic acid (PAS), a second line drug, with isoniazid. This association has a purpose to reduce gastrointestinal toxicity and the extensive metabolism of PAS, reduce intestinal acetylation of isoniazid and increase the duration of actions of both drugs.⁸⁵



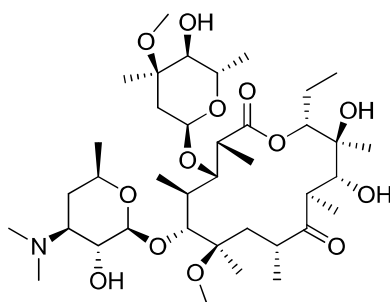
In summary, many derivatives of actual TB-drugs have been developed. Modification of existing TB drugs in order to improve the half-life, bioavailability, or drug delivery has led to some application in TB treatment. However, these new compounds usually target the same cellular processes as drugs currently in use. For that reason, this approach may have a cross-resistance problem.⁸¹

8.2.2. Repurposing of current antibacterial drug classes

Many antibiotics which are routinely used in other bacterial infections have never undergone to clinical trials for TB treatment. These abandoned drugs should be repurposed in more effective ways in TB treatment, at least in cases of drug-resistant TB treatment where the first-line drugs are inactive. Nowadays, this approach has led to some antibiotics classes which are now used as second-line TB drugs (e.g., aminoglycosides, fluoroquinolones, and polypeptides) and identified other candidates for clinical trials. Furthermore, concerns over toxicity and low therapeutic indexes might be overcome through chemical modifications.

Macrolides

Macrolides are important antibiotics group which inhibit bacterial protein synthesis by binding to the 50S ribosomal subunit. Clarithromycin, a medication in this group, appear to kill TB bacteria in laboratory settings. Several preclinical results have demonstrated that this drug may reduce mortality associated with TB infection. However, no clinical studies evaluating the efficacy of clarithromycin for the treatment of tuberculosis have been reported to date. For that reason, clarithromycin is now in group 5 of TB drug list and can only be used as off-label for DR-TB when few other treatment options remain.^{75,88}



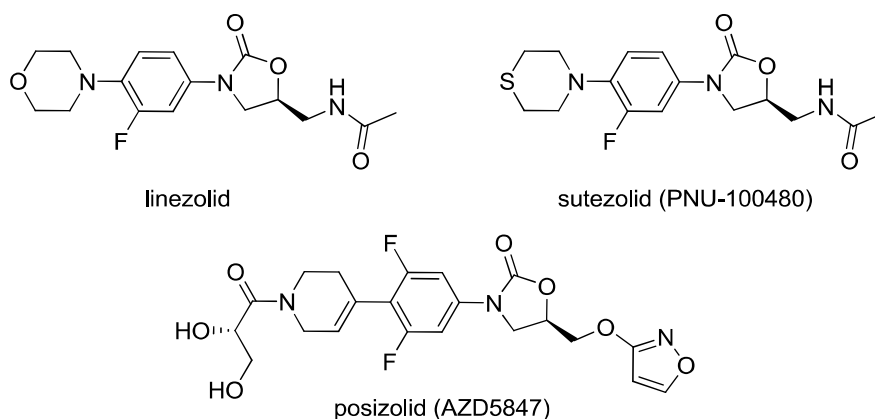
clarithromycin

Other drug candidates from the macrolide class are in preclinical testing. Recently, a study on the optimisation of anti-TB activity of the macrolide antibiotics through the synthesis of additional chemically modified derivatives of erythromycin was conducted. More than 200 derivatives have been synthesized and three series were identified with potent antituberculosis activity superior to that of clarithromycin. This study can lead to some promising results. However, a resistance mechanism of *M. tuberculosis* to currently available macrolides was observed. The tubercle bacilli can rapidly induce resistance due to

methylation of 23S rRNA by the *erm37* gene product, which prevents macrolide binding to the ribosome. This main constrain can limit the repurposing of macrolides as significant potential drugs for DR-TB.^{75,88}

Oxazolidinones

Oxazolidinones is a group of compounds with broad spectrum antimicrobial activity. Some of them are currently used in clinic for the treatment of serious infections caused by resistant gram-positive bacteria. The oxazolidinones antibiotics are protein synthesis inhibitors. They disrupt the translation of mRNA into proteins in the ribosome and consequently stop the growth and reproduction of the bacteria. The rate of emergence of resistant strain with this group is low. Many studied showed that oxazolidinones are active on *M. tuberculosis*. This class which includes linezolid, sutezolid (PNU100480) and posizolid (AZD5847) are currently under clinical trials in patients with multidrug-resistant and extensively drug-resistant TB. Nowadays, linezolid is listed in group 5 of WHO-TB drug categories and should be used as off-label in the treatment of some DR-TB cases.²

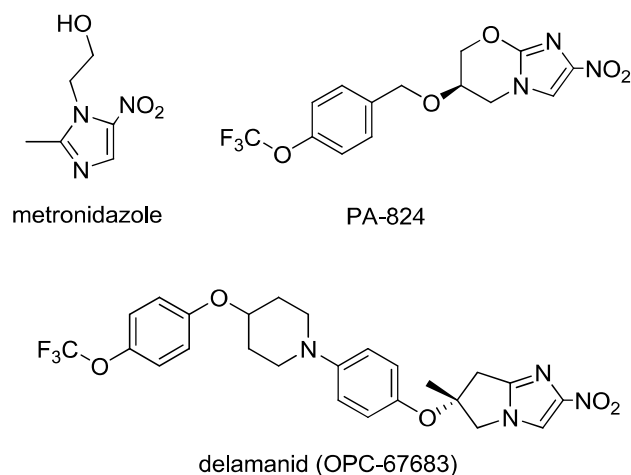


Nitroimidazoles

Nitroimidazoles is a drug class which is used to treat anaerobic bacteria and parasitic infections. The representative medication of this class is metronidazole. An interesting feature of nitroimidazoles relates to their original mechanism of action. These compounds inhibit host defence strategies by producing microbicidal molecules, such as nitric oxide and other reactive nitrogen intermediates. These intermediates will then damage multiple targets including respiratory chain cytochrome oxidases. The target specificity of such a mechanism of action is achieved through bioactivation of these prodrugs by flavin-dependent nitroreductases, which are absent in mammalian cells but present other species including *M. tuberculosis*. Therefore, several synthetic modifications have been introduced to this scaffold in order to reduce the side-toxic effects and increase their antimycobacterial potential. Nowadays, two candidates from this group, PA-824 and delamanid (OPC-67683), are under clinical trial and should potentially shorten treatment duration.^{2,89}

PA-824 is a bicyclic nitroimidazofuran analogue which is bioreduced intracellular. This compound is active against tubercle bacillus in both aerobic and hypoxic conditions. Until now, two mechanism actions of PA-824 are separately proposed. The first suggests that PA-

824 can inhibit the biosynthesis of mycolic acid. The second mechanism lies on the formation of the desnitro metabolite and concomitant release of NO in anaerobic conditions. This drug candidate is now in phase II of clinical trial.⁹⁰ Another clinical candidate in this group is delamanid (OPC-67683). This is a structurally analogue of PA-824 that shares the same mechanism of action.⁹⁰ Recently, delamanid has obtained a conditional authorization from European Medicines Agency (EMA) in treatment of multidrug-resistant pulmonary tuberculosis.⁷



8.2.3. Potentiation of current antibiotics by targeting resistance

M. tuberculosis has some intrinsic resistance mechanism to many antibiotics. In addition, this special bacterium can also develop many acquired resistance mechanism to TB drugs. Consequently, some antibiotics and TB-drugs have been underused or even abandoned in TB treatment. For that reason, some authors tried to develop new compound that could inhibit the known resistance mechanisms. These new compounds are able to decline the growth of *M. tuberculosis* in the presence of sub-active doses of known antituberculosis drugs. This will potentiate or restore the activity of abandoned drugs against TB and lower their toxicity. These compounds are named as boosters or potentiators (Figure 15).^{91,92}

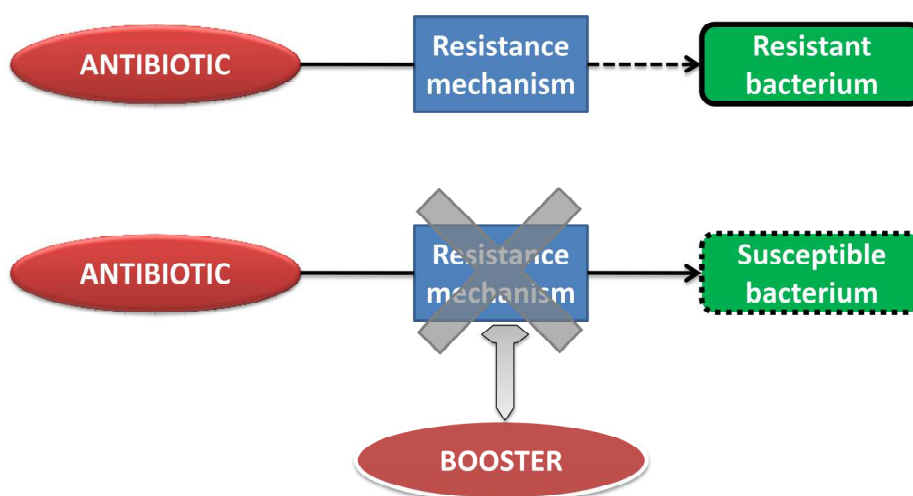


Figure 15: Concept of drug potentiation by targeting resistance mechanism

β -lactams and β -lactamase inhibitors

A typical example demonstrating the effectiveness of this method is the use of β -lactamase inhibitors to reactivate the activity of β -lactams antibiotic in clinical practice. This approach has extended the application of β -lactams in many years.⁹¹

In *M. tuberculosis*, a BlaC-like β -lactamase was also discovered. A genetic knockout study of *blaC* gene resulted in an improved sensitivity of the tubercle bacteria to β -lactams, particularly carbapenems. The β -lactam/ β -lactamase inhibitor combinations now become a TB treatment option in groups 5 of TB drugs list and should be used only in case of DR-TB. These combinations consist of “amoxicilline+clavulanate”, “imipemen+cilastatin” (synergistic effect in this case), and “meropenem+clavulanate”. Moreover, the combination of meropenem and clavulanate effectively kills drug resistant *M. tuberculosis* strains as well as the tubercle bacillus growing in anaerobic conditions. This suggests that a drug combination may also be useful for treatment of latent TB. Furthermore, availability of structural and mechanistic knowledge around BlaC will help researchers in designing more potent and *M. tuberculosis* specific inhibitors to be used in combination with classical β -lactam antibiotics. In addition, the expression of BlaC is inducible by β -lactams and tightly regulated by the transcriptional regulator BlaI. So BlaI regulator and related protein might be interesting targets for the design of new booster of β -lactam.^{89,91-93}

Ethionamide and EthR inhibitors

Targeting resistance mechanisms can also be used to boost the anti-TB activity of actual anti-TB drugs. For example, ethionamide is used as a second-line TB antibiotic to treat MDR-TB strains that are resistant to first-line drugs such as isoniazid or rifampicin. Ethionamide is a prodrug that requires enzymatic activation in the cytoplasm of *M. tuberculosis* by EthA, an intrinsic monooxygenase that converts ethionamide to ETH-NAD adduct. Unfortunately, the expression of EthA is repressed by a transcriptional regulator, EthR, thus limiting the anti-TB activity of ethionamide. Consequently, ethionamide must be used with high-dose in clinical which can cause many serious side effects and limit its clinical application. Recent studies demonstrate that EthR could be chemically inhibited by a specific ligand resulting in an over-expression of EthA and then the re-activation of ethionamide. The synthesized EthR inhibitors could be then used in association with lower doses of ethionamide in a regimen of higher tolerance and improved efficacy.^{90,92,93} We were interested in this strategy in order to improve the therapeutic index of ethionamide. A study on the development and optimization of drug-like inhibitors of EthR is described in the chapter II of this thesis.

Sulfonamide and potentiators

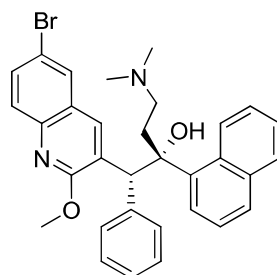
Co-trimoxazole (sulfamethoxazole+trimethoprim) is the antifolate combination which is based on the concept of potentiation. Sulfamethoxazole, which targets dihydropteroate synthase (DHPS) in *de novo* folate biosynthesis, is synergized by trimethoprim that inhibits dihydrofolate reductase (DHFR) required for the reduction of dihydrofolate. Antifolates were regarded as promising anti-TB drugs many years ago. Indeed, early experiments using animal models proved that sulfonamides are effective in curing TB. However this antibiotic group has been forgotten due to the discovery of streptomycin and other more potent TB drugs.

Recently, urgent need in the development of MDR-TB led to reconsider the synergy of trimethoprim–sulfonamides in *M. tuberculosis*. However, it remains unknown why trimethoprim does not work against *M. tuberculosis*. The result suggested that DHFR might not be the major reductase responsible for the reduction of dihydrofolate to tetrahydrofolate in *M. tuberculosis*. A recent paper reported the role of 5,10-methenyltetrahydrofolate synthase (MTHFS) Further studies should be conducted to identify the unknown reductases which is responsible for this essential reaction, followed by the development of inhibitors and testing their sulfonamides-potentiating activity. Moreover, recent studies showed that folate synthesis is also targeted by other TB drugs like INH, ETH and PAS. Therefore, development of novel cocktails regimen consist of sulfonamides and folate-targeting TB drugs such as INH, ETH and PAS might hold exciting future discoveries.^{91,93}

8.2.4. New drug candidate and new targets in *M. tuberculosis*

Due to the increase of drug-resistant tuberculosis, it is important to develop new TB drugs with new chemical scaffolds that inhibit novel targets of *M. tuberculosis*. In this scenario, these novel compounds have the capacity to retain activity against the resistant TB strains and may provide an important treatment option for drug-resistant TB patients. Nowadays, this strategy is considered as the most potent approach in TB drug development.

The typical example of new TB drug which was successfully developed from a phenotypic-based approach is bedaquiline (TMC207). It has a diarylquinoline scaffold. Interestingly, this bactericidal TB drug is active against *M. tuberculosis* by a new mechanism of action.⁹⁰



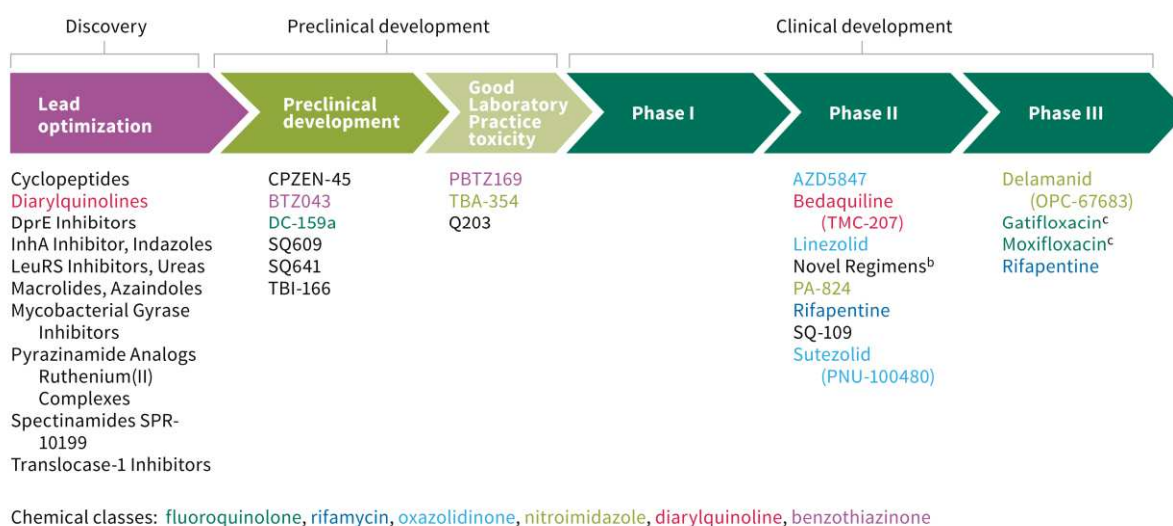
bedaquiline

In fact, bedaquiline inhibits the proton transfer chain of the mycobacterial ATP synthase and depletes cellular energy stores. Fortunately, this action does not impact on human mitochondrial ATP synthase. The antimycobacterial activity of bedaquiline was successively evaluated *in vitro*, *in vivo* efficacy in mice and in clinical studies.⁹⁰ In 2012, bedaquiline was approved by FDA for the treatment of MDR-TB under an accelerated-approval regulation for serious or life-threatening conditions although this drug candidate has not yet completed clinical trials. Currently, bedaquiline is in phase III of clinical trials (ID:NCT02333799) to assess the safety and efficacy of this drug in combination with PA-824 and linezolid. This study is estimated to be completed in 2018.⁹⁴

8.2.5. Current pipeline of new antituberculosis drugs

The TB drug development pipeline has begun to increase during the past decades. Nowadays, the TB drug pipeline is being enriched with a range of novel drugs in preclinical development and many drug candidates being assessed at all stages of clinical trials (Figure 16). Development of the tuberculosis drugs portfolio is being achieved using many strategies, e.g. repurposing of old antibiotics, re-engineering of existing TB-drug structures, targeting resistance mechanism and discovery of new scaffolds.

The development pipeline for new TB drugs, August 2014^a



- ^a Details for projects listed can be found at <http://www.newtbdrugs.org/pipeline.php> and ongoing projects without a lead compound series identified can be viewed at <http://www.newtbdrugs.org/pipeline-discovery.php>
- ^b Combination regimens: NC-001-(J-M-Pa-Z), Phase IIa, NCT01215851; NC-002-(M-Pa-Z), Phase IIb, NCT01498419; NC-003-(C-J-Pa-Z), Phase IIa, NCT01691534; PanACEA-MAMS-TB-01-(H-R-Z-E-Q-M), Phase IIb, NCT01785186
- ^c These trials have been completed and results published. See chapter text for further details.

Figure 16: Current global pipeline of new tuberculosis drugs
(adapted with permission from WHO for ref.⁵)

8.3. Conclusion and outlooks

Current TB treatments still have major drawbacks. In addition, the emergence of drug-resistance TB strains stresses the need to find new alternatives. The increased number of candidates reaching clinical phases is a positive response to this situation. However it will take some time before some of these compounds are approved. Hope arisen recently with the conditional approval by the FDA and EMA of the 2 new TB drugs, i.e. SirturoTM (bedaquiline) and DelybaTM (delamanid).^{6,7} However, we are still far away from a global solution for the treatment of all TB-patients as these two drugs have been granted exclusively for the treatment of lung infections due to multidrug-resistant tuberculosis when alternative treatments cannot be used due to resistance or intolerance. In conclusion, active compounds that can be used safely, in combinations with first and second line drugs are still highly required.

Part B. Tuberculosis and fragment-based drug discovery

1. Introduction to fragment based drug discovery

The concept of fragment-based drug discovery (FBDD) was first introduced by Abbott Laboratories in 1996.⁹⁵ Nowadays, this approach has become a remarkably efficient alternative approach to high-throughput screening (HTS) in drug discovery. In fact, this approach has been validated recently with the introduction of candidates in clinical trials from various programs and the approval of Zelboraf[®] (vemurafenib) by FDA in 2011⁹⁶ which is considered as the first approved drug discovered using a fragment-based approach.⁹⁷

In general, chemical space grows by increasing the content of heavy atoms. Therefore, fragments occupy a smaller region of chemical space in comparison to conventional HTS compounds because of their small size. However, FBDD has emerged as a promising and focused strategy which is based on the quality, rather than the quantity, of hits and leads.^{8,98,99} The main advantages of FBDD is that hits can be identified from a relatively small screening fragment-library at the difference with HTS screening where larger libraries are used.^{100,101} In practical, the maximum size of a fragment-library does not exceed 10 000 molecules. However, the main constraint of this approach is the requirement of a suitable screening method that can reliably detect the weak binding and strategies for evolving the fragments into larger lead compounds.¹⁰²

The fragment-based approach in drug discovery and development (as illustrated in Figure 17) consists of three steps^{96,101}:

Step 1: Design of a fragment screening library

Step 2: Identification and validation of fragment hit by suitable screening methods

Step 3: Elaboration of the fragment hit into drug-like lead compound

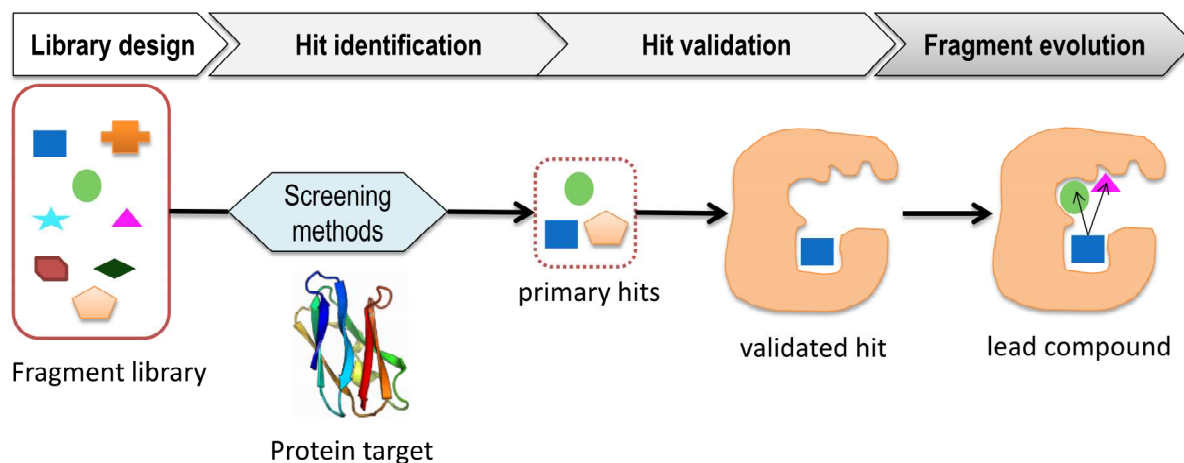


Figure 17: The principle components of a fragment-based approach in drug discovery

In the first stage, the constitution of a suitable fragment library is performed. The fragment library may range from a focused set of about hundreds fragments to much more substantial generic screening sets of around thousands fragments. Fragments, e.g. small entities, have low potency for most targets, and therefore need to be screened at high

concentrations. For that reason, it is very important that they are soluble and free from inappropriate toxicities. To ensure that objective, fragments should be designed to comply with “Rule of 3” (Ro3) proposed by Congreve *et al.* These authors suggested that fragments should have molecular weights of less than 300, a ClogP less than 3, and contain no more than 3 hydrogen bond (H-bond) donors and 3 H-bond acceptors.¹⁰³ Furthermore, fragment libraries may provide a good diversity with a relatively small number of compounds.¹⁰⁴ Library design is the first stage and has been also considered as the most important component of the FBDD process.¹⁰⁵ (In this thesis, we discuss in detail in chapter IV how to improve the quality of such fragments especially by incorporating 3D-structures).

Once a fragment library has been assembled, a screening method must be implemented. Owing to their small size, fragments usually have a low chemical complexity. Therefore, these small pieces only have a weak binding affinity to protein and consequently a low activity (100 μ M- 10mM). On the contrary, the fragments exhibit a high potency. Indeed, when we consider the degree of binding affinity or activity per heavy atoms, fragments will display a higher efficiency than larger elaborated drug-like ligands.¹⁰⁶ In general, fragment screening techniques have some specific features in comparison to conventional HTS assays. (In this thesis, analysis on the screening methods used to screen fragments is presented in chapter III).

In the final step, fragment hits are then optimized with the aim of obtaining a highly potent drug-like substance.¹⁰¹ Practically, there are several strategies for the optimization to a lead compound starting from fragment hits (Figure 18):^{101,107}

- (1) **Fragment growing:** initial fragments are expanded to larger and more complex molecules that can bind the active site of the protein with additional interactions and consequently increase the potency (affinity and activity). The main advantage of this strategy is that the increase of molecule size can be carefully controlled.¹⁰⁷
- (2) **Fragment linking:** two or more fragments are identified at separate binding sites of the target but are close enough to be linked together by a chemical linker. This strategy always results in a larger molecule with higher-affinity and activity.¹⁰⁷
- (3) **Fragment merging:** incorporation of structural portions of overlapping molecules into a final product, using structural information of other fragments, substrates, and known ligands in complex with the protein. Trends in potency from different series can be used to identify important binding motifs and interactions, and this information can be used to produce a hybrid series.¹⁰⁷
- (4) **Fragment self-assembly:** two fragments connect to each other thanks to a chemical reaction that uses the targeted protein as a catalyst (e.g. “click chemistry”).¹⁰⁷

In practice, there tends to be an overlap between these methods; for example, fragment linking may also involve an element of fragment merging. In the chapter II of this thesis, we describe how these strategies were applied in our laboratory to develop new fragment-based inhibitors of EthR.

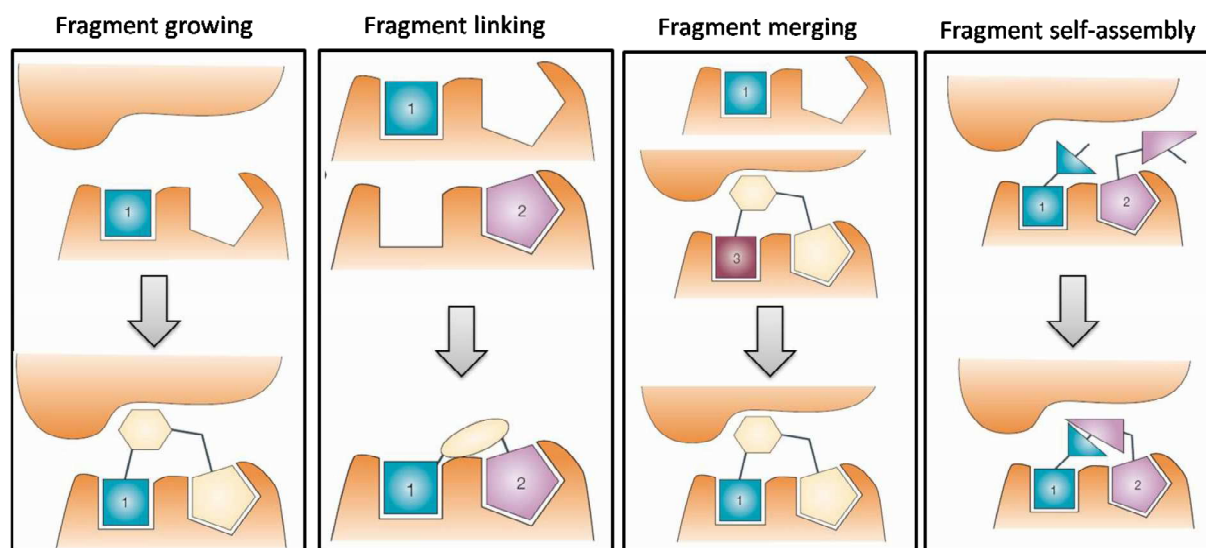


Figure 18: Different strategies to be used for fragment evolution
(modified with permission from Nature Publishing Group, Ref. ¹⁰⁷)

2. Application of FBDD in TB drug development

Fragment-based approach is now applied to a wide range of targets, including essential proteins of *M. tuberculosis*. Until now, many success studies in tuberculosis drug discovery starting from fragment have been reported. A summary of all these studies are presented in Table 2.

In fact, the first application of fragment-based approach for the discovery of anti-TB compounds was conducted by Manger *et al* in 2005.¹⁰⁸ These authors used fragments in combination with natural substances to identify new inhibitors of *M. tuberculosis* protein tyrosine phosphatase A (MptpA). This enzyme is a secreted virulence factor that act on macrophage signaling pathways to promote tubercle bacillus survival in the infected host. Moreover, MptpA inhibitors were also developed by Rawls and his co-workers in 2009 by using a similar strategy. Inhibition activity was evaluated by enzymatic assay.¹⁰⁹ In addition, these authors also used this approach for the development of several inhibitors of MptpB, an analogue of MptpA.¹¹⁰

Moreover, FBDD was also used to identify inhibitors of pantothenate synthetase. This enzyme catalyzes the magnesium adenosine triphosphate (ATP) dependent condensation of pantoate with β -alanine to form pantothenate. This is an important component for the survival of *M. tuberculosis*. In this study, Hung *et al* have used several screening techniques (e.g. thermal shift assay (TSA), WaterLOGSY-NMR, isothermal calorimetry (ITC), X-ray crystallography and *in silico* docking) in combination with two fragment evolution strategies (growing and linking) to develop a new low-molecular weight inhibitor of pantothenate synthetase from a library of 1300 fragments.¹¹¹

In 2010, Scheich *et al* have conducted a study on the development of new Ag85C inhibitors. In *M. tuberculosis*, the Ag85 mycolyltransferases family is a promising target. They catalyze the transfer of mycolates between trehalose monomycolate (TMM) and trehalose dimycolate (TDM or cord factor). These authors started from a library of 5000 synthetic fragments. A protein-based NMR screening technique followed by a phenotypic

assay on *M. smegmatis* allowed identifying fragment hits. Then, a growing strategy was applied to improve the interaction and affinity of fragment hits. New Ag85C inhibitors were also active on MDR-TB.¹¹²

Table 2: Application of fragment-based approach in TB drug development

Target	Fragment Library	Screening method	Fragment Elaboration	Ref
MptpA	20 000 compounds from ChemBioNet	Spectroscopically enzymatic assay	-	108
MptpA	21 phenyl difluoro-methylphosphonic acid	Spectroscopically enzymatic assay	growing (analoging)	109
MPTpB	Library of 140 O-aryl phosphates	Spectroscopically enzymatic assay	growing, merging and isostere replacement	110
pantothenate synthetase	1300 fragments	TSA; WaterLOGSY-NMR, ITC and X-ray crystallography; <i>in silico</i> docking	growing and linking	111
<i>Mtb</i> Ag85C	a diverse library of 5000 synthetic fragments in pools of 16 compounds each	¹⁵ N-HSQC NMR and whole cell <i>M. smegmatis</i> antibacterial testing; then testing on <i>Mtb</i> -H37 and MDR- <i>Mtb</i> .	growing	112
<i>Mtb</i> CYP121	library of 665 commercial fragments	TSA, ligand-observed NMR, ITC and X-ray crystallography	merging	113,114
InhA	NCI library	virtual screening,	-	115
dehydroquinase Type II	13 aryl-based fragments	<i>in silico</i> screening, enzymatic assay	growing	116
EthR	1250 fragments	TSA, SPR, X-ray	structural analogue and linking	117
EthR	1040 fragments	TSA, X-ray	growing, merging and linking	118

Another fragment-based study on new TB drug focused on cytochrome P450 CYP121. This enzyme has been shown to catalyze an unusual intramolecular reaction between the ortho-positions of two tyrosines in cyclodityrosine (cYY) to form mycocyclosin. These compounds are believed to play important roles in *M. tuberculosis* infection, growth and persistence. The researchers at University of Cambridge have screened a library of 665 commercial fragments with different methods, including TSA, ligand-observed NMR, ITC and X-ray crystallography. Then, the hits were merged together to afford a triazolylphenol analogue which inhibits CYP121.¹¹³ Interestingly, the limitation of merging strategy have been analyzed in this study. In addition, these authors have conducted further stepwise structure modifications to overcome the conformational limitation of merged fragments in order to obtain more potent CYP121 inhibitors.¹¹⁴

More recently, Tran *et al.* used *in silico* docking to design new fragment-based inhibitors of type II dehydroquinase. These aromatic compounds were then optimized and finally shown to inhibit the growth of *M. tuberculosis* in the low-micromolar range.¹¹⁶

Surade *et al.* also used a structure-guided fragment linking strategy to discover new inhibitors of mycobacterial transcription repressor EthR.¹¹⁷ At the same time, fragment-based approach was also implemented in our laboratory to develop new EthR inhibitors.¹¹⁸ These results are presented in more detail in chapter II of this thesis.

In summary, there is a significant increase of fragment-based studies in new TB drug development. This trend can be explained by the major advantages of low molecular weight compounds obtained from this approach. In fact, these small size compounds exhibit better physicochemical properties, especially solubility, than HTS drug-like compounds. In case of an intracellular pathogen like *M. tuberculosis*, these particular properties will help fragment-based compounds to more easily penetrate the phagosomes of macrophages and even to go through the waxy and thick cell wall of tubercle bacillus in order to bind to their target.

This page intentionally left blank

Chapter II. Development of novel EthR inhibitors with improved pharmacokinetic properties

Part A. EthR—a validated target for ethionamide potentiation

1. Role of EthR in ethionamide bio-activation

Ethionamide (ETH), a thionamide analogue of isoniazid (INH), is used as a second line antituberculosis drug. These two agents are known to target InhA, an important enzyme involved in mycolic acids biosynthesis in *M. tuberculosis*.^{119–121} However, only small cross-resistance ratio between INH and ETH was observed among clinical isolates.¹²² Indeed, many INH-resistant *M. tuberculosis* strains have been found to be sensitive to ETH, whereas some other strains which were reported to resist ETH can be treated by INH. These observations suggested a different bioactivation mechanism between INH and ETH. In 2000, a KatG-independent bioactivation of ETH was discovered simultaneously by two research groups.^{123,124} The authors found that over-expression of *ethA* in *M. smegmatis* resulted in substantially increased ETH sensitivity. This evidence suggested that the mycobacterial mono-oxygenase EthA has an important role in the activation of the prodrug ETH in mycobacteria.¹²³ Subsequently, the understanding of the mechanism by which ETH is bioactivated by EthA has attracted many researchers.^{124–127} The results showed that ETH was firstly transformed by EthA to reactive intermediates which are then combined with nicotinamide adenine dinucleotide (NAD⁺) to form ETH-NAD adduct. This active adduct can bind to InhA and consequently inhibit the mycolic acid biosynthesis (Figure 19).^{127,128}

In addition, a neighboring open reading frame of *ethA* which is named *ethR* was also determined. EthR protein was found homologous to transcriptional repressors of the TetR family and controls the expression of *ethA* by binding to the *ethA* promoter located within the intergenic region between *ethR* and *ethA*, thus preventing its transcription. Over-expression of this gene led to ETH resistance, whereas chromosomal inactivation of this gene by transposition led to ETH hypersensitivity. These data strongly suggested that EthR negatively regulates the production of EthA and then control the bioactivation of prodrug ETH.^{123,124}

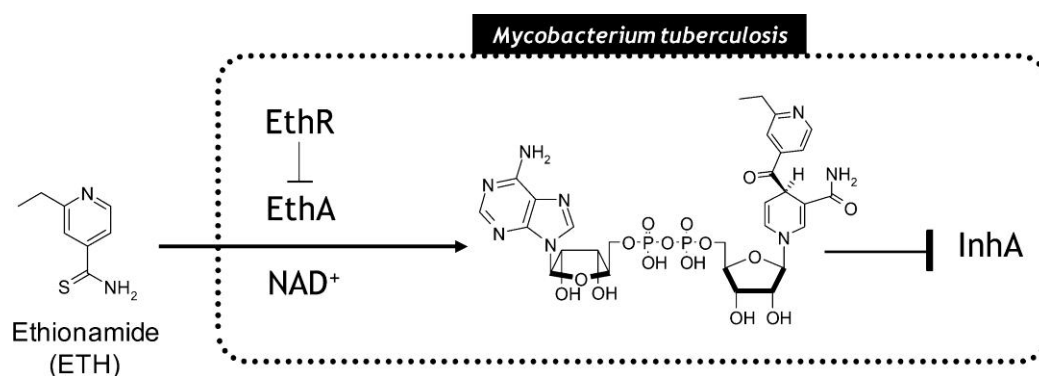


Figure 19: Transcriptional regulator EthR control the bioactivation of ETH in *M. tuberculosis* (adapted with permission from the American Chemical Society for ref.¹²⁸)

2. Structure of EthR

Two distinct crystal structures of EthR^{129,130} were obtained in 2004. These structures confirmed that EthR shares the same scaffold with other members of the TetR family of proteins.¹³¹ The overall EthR structure is a homodimer (see Figure 20). Each EthR monomer is entirely helical with 9 α helices organized in two domains.¹³² The first three helices of each EthR monomer form a three-helix bundle DNA binding domain. The classical helix-turn-helix (HTH)-DNA binding motifs are represented in blue in the figure which contains $\alpha 2$ and $\alpha 3$, stabilized by $\alpha 1$. Meanwhile, the C-terminal domain of EthR (displayed in red) is composed of six α helices and is involved in the dimerization of EthR. Dimerization occurs by coupling one pair of α helices of each monomer of EthR to form a four-helix bundle composed of helices of $\alpha 8$, $\alpha 9$ of the first, and $\alpha 8'$, $\alpha 9'$ of the second monomer. This interaction buries 1562 \AA^2 of surface area.^{130,132}

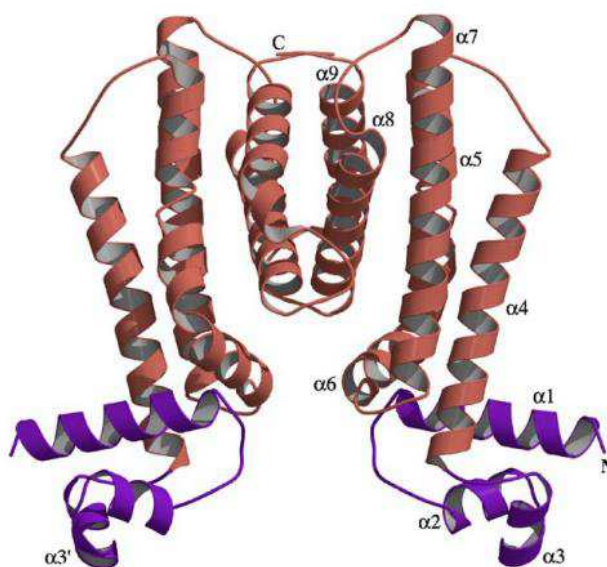


Figure 20: Overall structure of the EthR homodimer

(adapted with permission from Elsevier for ref.¹³²)

Helix-turn-helix (HTH) domain: a classical helix-turn-helix motif which also named as DNA binding domain. This domain has an important role in the interaction between EthR and DNA strand. Indeed, the double-stranded DNA was expected to bridge the two DNA-binding domains of the dimer with the HTH-motif inserted into the major groove.¹²⁹ Unlike other TetR/CamR members, which typically bind 15 bp operators, EthR recognizes an exceptionally long 55 bp region suggesting multimerization of the repressor on its operator. Furthermore, surface plasmon resonance analyses showed that eight EthR molecules bind cooperatively to the 55 bp operator, which represents a novel repression mechanism for a TetR/ CamR member.^{133,134}

Regulation domain: this domain contains a narrow tunnel-like cavity formed by helices 4, 5, 7, and 8 that opens to the bottom of the molecule. The tunnel measures about 20 \AA in length and is lined predominantly by aromatic residues, with helices 5 and 7 constituting the majority of side chains. The loop connecting helices 4 and 5 restricts the opening of the hydrophobic tunnel, and the electron density in this loop is only poorly defined, indicating a

certain degree of structural flexibility in the loop. This cavity may serve as the binding site for a ligand.¹³³ The two holo-structures of EthR were obtained with co-crystallized ligands. One structure was characterized in the presence of hexadecyl octanoate in the core domain of each monomer of EthR (PDB: 1U9N)¹³⁰, thus revealing the long linear ligand binding pocket of this protein. The other revealed the presence of two dioxane molecules in the ligand binding pocket of each monomer (PDB: 1T56)¹²⁹. Analysis of the EthR holo-form indicates that the DNA recognition helices $\alpha 3$ and $\alpha 3'$ are separated by 52 Å. This distance between the two HTH domains is incompatible with the binding of the repressor on its operator, since it is 18 Å longer for binding to two successive major grooves of the DNA double helix (with 34 Å repeat distance).¹³⁰

3. Validation of EthR as therapeutic target

In *M. tuberculosis*, ETH action is limited due to a bioactivation requirement. This process is controlled by EthR.^{123,124} Therefore, ETH has an unfavorable therapeutic index, as the high dose necessary to kill *M. tuberculosis* generally causes serious adverse effects. Administration of ETH at its recommended therapeutic dosage (750 mg/day) is frequently associated to gastrointestinal side effects.¹³⁵ Because most of the side effects of ethionamide are dose-related¹³⁵, it has been hypothesized that enhancement of bacterial bioactivation would decrease ETH body circulating doses and then limit the dose-related toxicity.⁹¹

Results obtained from the mycobacterial ETH bioactivation study have suggested two possible strategies to boost ETH activity. Firstly, stimulation of EthA expression could be used to enhance the bioactivation of ETH and its activity in *M. tuberculosis*. In fact, it has been shown that over-expression of EthA led to higher susceptibility to ETH and deficient mycolic acid synthesis in *M. smegmatis*.¹²³ In the second strategy, inhibition of the transcriptional repressor EthR activity should reactivate the EthA enzyme and consequently increase ETH bioactivation.

EthR has been shown to impair the sensitivity of *M. tuberculosis* to ETH.¹²³ Indeed, over-expression of *ethR* leads to reduced levels of intracellular EthA and specifically induces ETH resistance.¹²³ On the contrary, a knockout genetic technique was applied to remove *ethR* gene in *M. bovis BCG*. The resulting strain was found to be extremely sensitive to ETH. This result confirmed that a knock-out of *ethR* is able to increase bioactivation of ETH *via* overproduction of EthA. Thus, any physiological condition down-regulating *ethR* or any agent with the ability to block EthR may favor the production of EthA and lead to the activation of substantial amounts of ETH. Consequently, the sensitivity of the tubercle bacilli to ETH will increase.¹²³ (Figure 21)

Interestingly, analysis of EthR holo-structures (PDB codes: 1U9N, 1T56)^{129,130} suggested that the presence of either hexadecyl octanoate or dioxane is translated in structural modifications of the DNA binding heads which keep these repressor in a configuration incompatible with DNA binding. The structures of these ligands were considered as templates to develop novel drug-like EthR inhibitors which can be also applied therapeutically as ETH potentiators (or ETH boosters). The aim of this strategy was to decrease the ETH therapeutic dose, consequently lower the side-effects and improve its therapeutic index.

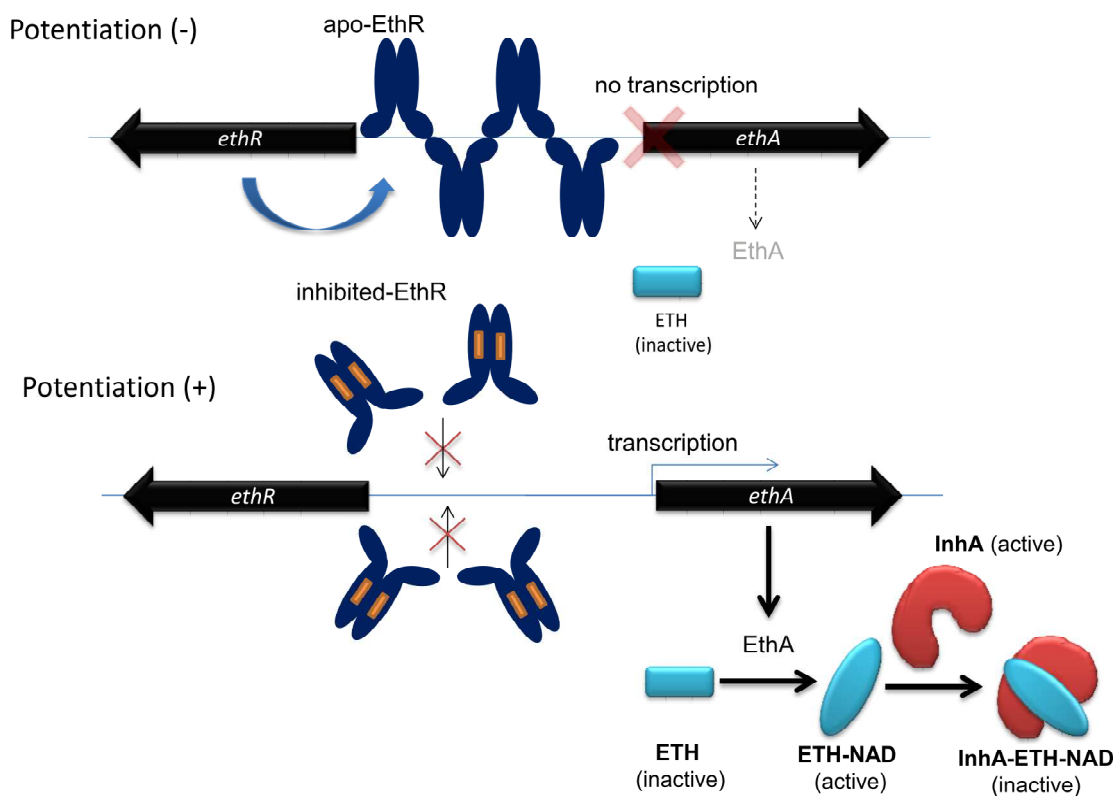


Figure 21: Potentiation of ethionamide by targeting EthR

Part B. EthR inhibitors and ETH boosting effect

Since the starting of our work on the validation of EthR as a drug target to boost the activity of ethionamide, several research groups worldwide have also developed research programs in this field. Until now, many series of EthR inhibitors were designed and synthesized by scientists from BioVersys, a Swiss biotech company and also from academic research groups at the University of Cambridge (UK).

1. Development of EthR inhibitors by ligand-based approach

In 2008, Weber *et al*¹³⁶ applied a ligand-based approach to develop novel EthR inhibitors. These authors supposed that esters which are known to be the main products of EthA-catalyzed Baeyer–Villiger oxydation can inhibit EthR by a negative feedback-controlled mechanism. This mechanism can be found frequently in nature.¹³⁷ For that reason, a library of hexadecyl-octanoate analogues was synthesized. With the integration of EthR into a synthetic mammalian gene network, these authors have been able to identify 2-phenylethyl-butyrates (Figure 22) as a potent inhibitor of EthR in *M. tuberculosis* which increases the sensitivity of this pathogen to ETH.^{136,138,139} This promising result has attracted attention from a Swiss biotech company BioVersys. In this context, many amide and thioamide analogues of 2-phenylethyl-butyrates have been synthesized and tested *in vitro*.¹⁴⁰

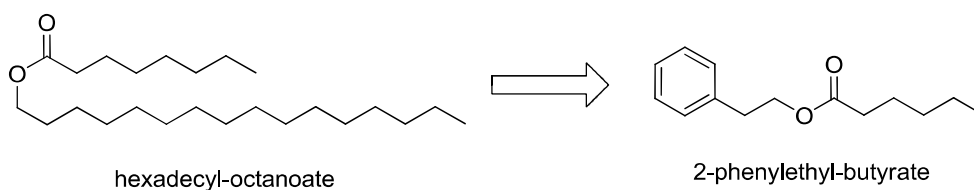


Figure 22: EthR inhibitor 2-phenylethyl-butyrates developed by ligand-based approach

2. Development of EthR inhibitors by rational drug design

At the same time, a project aiming at discovering new EthR inhibitors was started at the Pasteur institute of Lille in collaboration with the School of Pharmacy. A target-based drug design approach was used to identify starting hits.

2.1. From pharmacophore model to hit identification

As mentioned earlier, structure analysis of two liganded-EthR crystals (PDB codes: 1U9N, 1T56) showed that holo-protein conformations are unable to bind to DNA and thus to repress transcription of ethA.^{129,130} The chemical structure of the ligands identified in these holo-structures and physicochemical properties of the EthR ligand binding site inspired the construction of a pharmacophore model. The putative EthR ligands were supposed to be a low-molecular weight compound ($MW < 500 \text{ g}\cdot\text{mol}^{-1}$) bearing two hydrophobic ends (H) connected by a 4-6 Å linkers (L), with hydrogen-bonding capabilities set to interact with Asn176 and Asn179 (see Figure 23).¹⁴¹

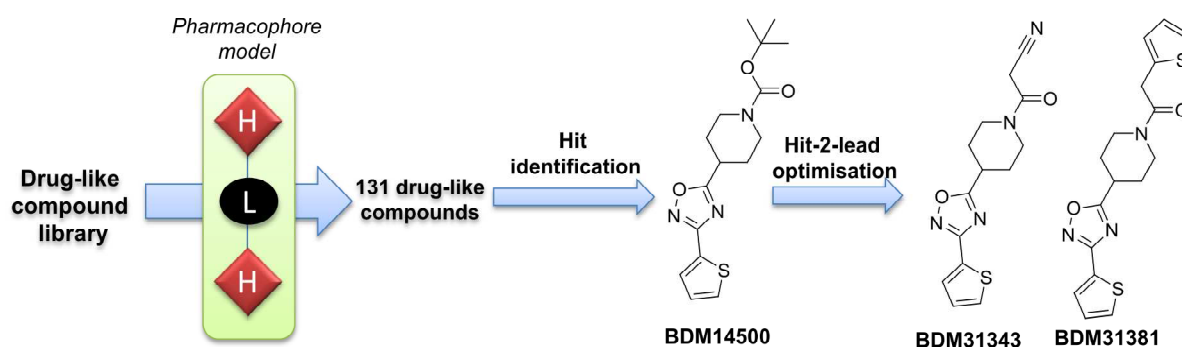


Figure 23: Development of EthR inhibitors by rational drug design

In the next step, 131 compounds which are complying with the above pharmacophore model were selected from the in-house library of drug-like molecules. The ability of these ligands to inhibit the DNA-binding function of EthR was measured by surface plasmon resonance (SPR). The screening led to the identification of a thiophen-2-yl-1,2,4-oxadiazole family of inhibitors which was represented by BDM14500. The binding of this hit to the ligand binding domain of EthR was confirmed by X-ray studies and the ETH boosting effect of this compound was validated *in vitro* on agar plates.¹⁴¹

2.2. Hit to lead optimization process

Preliminary hit optimization led to the identification of two 1,2,4-oxadiazole analogues (BDM31343 and BDM31381).^{141,142} BDM31381 was the most potent booster of ethionamide bioactivation *in vitro* but was rapidly cleared in mice resulting in a low systemic exposure. In contrast, BDM31343 was a less active compound *in vitro*, but showed a more favorable pharmacokinetic profile. Both compounds were evaluated in *M. tuberculosis* infected mice. The result revealed that daily IP treatment with BDM31343 at 50 mg/kg was able to triple the activity of ethionamide in the mice model of TB infection.^{141,143}

2.3. Lead optimization to preclinical candidate

During the hit-to-lead optimisation process, X-ray crystallography of EthR liganded by the potent inhibitor BDM31381 demonstrated a new orientation in the ligand binding domain

in comparison to the initial hit. This observation stimulated Willand and his colleagues to optimize new EthR inhibitors via a protein-templated *in situ* click chemistry approach. Unfortunately, the novel compounds developed from this approach could not improve the EthR inhibition activity and ETH boosting effect of lead compound. However, the results has led to a much better understanding of the target and the flexibility of the ligand binding pocket of EthR.¹⁴⁴

Alternatively, these authors applied a structure-based approach to optimize lead-compound BDM31343 in order to yield a candidate for preclinical trial.^{128,145,146} Firstly, a series of thiophen-2-yl-1,2,4-oxadiazole analogues was synthesized in order to optimize BDM31343 structure by exploring the replacement of its piperidine core and cyanoacetyl group.¹²⁸ Consequently, SAR study was performed by replacing either the thiophene or the oxadiazole in *N*-(4,4,4-trifluorobutyryl)-piperidine series (Figure 24).¹⁴⁵

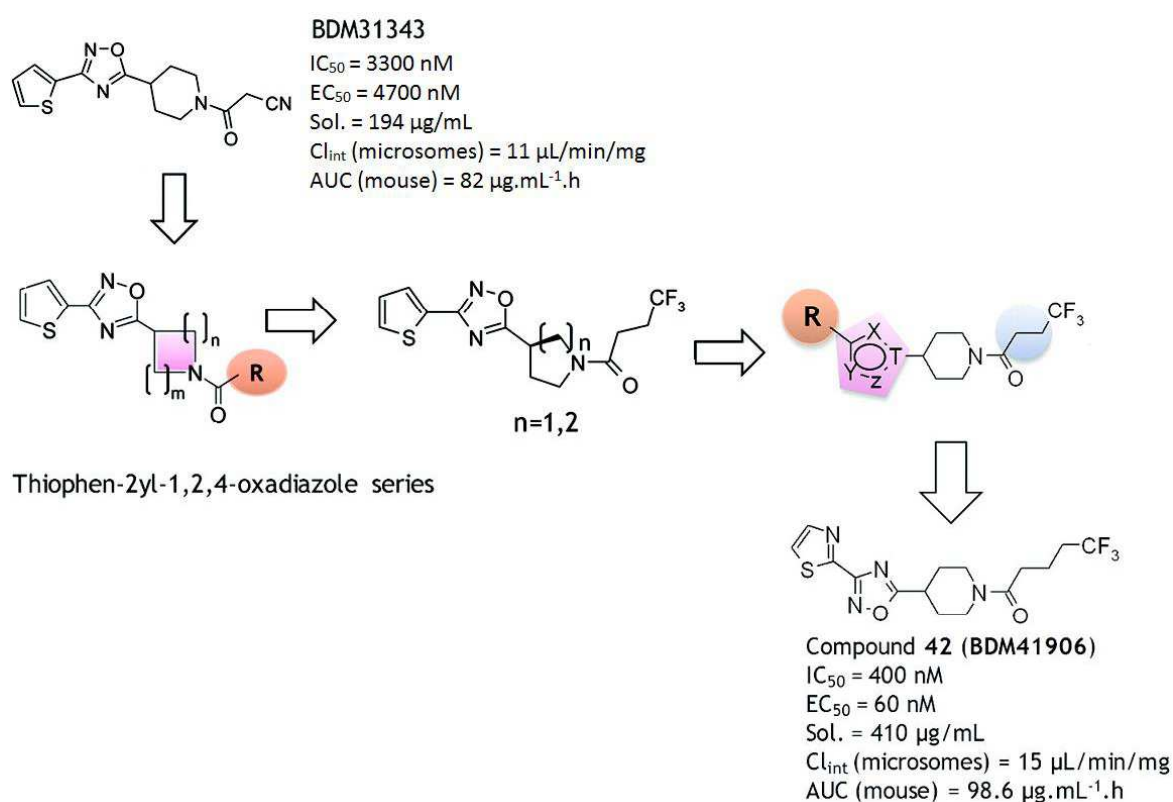


Figure 24: Optimisation of lead compound BDM31343 by a SAR study
(modified with permission from American Chemical Society for ref.^{128,145})

This modification led to the discovery of compound BDM41906 that revealed optimal physicochemical and pharmacokinetic properties. Furthermore, this lead compound was able to boost 10-fold ethionamide activity on *M. tuberculosis* infected macrophages at nanomolar concentration ($EC_{50} = 60 \text{ nM}$). Notably, this compound revealed good systemic exposure following oral administration at 20 mg/kg ($AUC = 98.6 \text{ } \mu\text{g}\cdot\text{mL}^{-1}\cdot\text{h}$).¹⁴⁵ Encouraged by potent pharmacodynamic and pharmacokinetic properties, BDM41906 was then evaluated in a model of *M. tuberculosis* infection in mice. Results showed that, as BDM31343, an equivalent boosting effect on the ETH activity is obtained with compound BDM41906 given orally once per day, at 20 mg/kg , using beta-cyclodextrine as vehicle.¹⁴⁷ Until now,

BDM41906 is considered as the best ETH booster candidate for preclinical assay. This result opens new perspectives for the use of such combinations in humans.

3. Development of EthR inhibitors by high-throughput screening

A back-up series of EthR inhibitors was also developed based on a phenotypic high-throughput screening. This approach is believed to reveal new chemotypes that show both the capacity to bind to EthR target and also to cross the complex mycobacterial envelope (Figure 25).

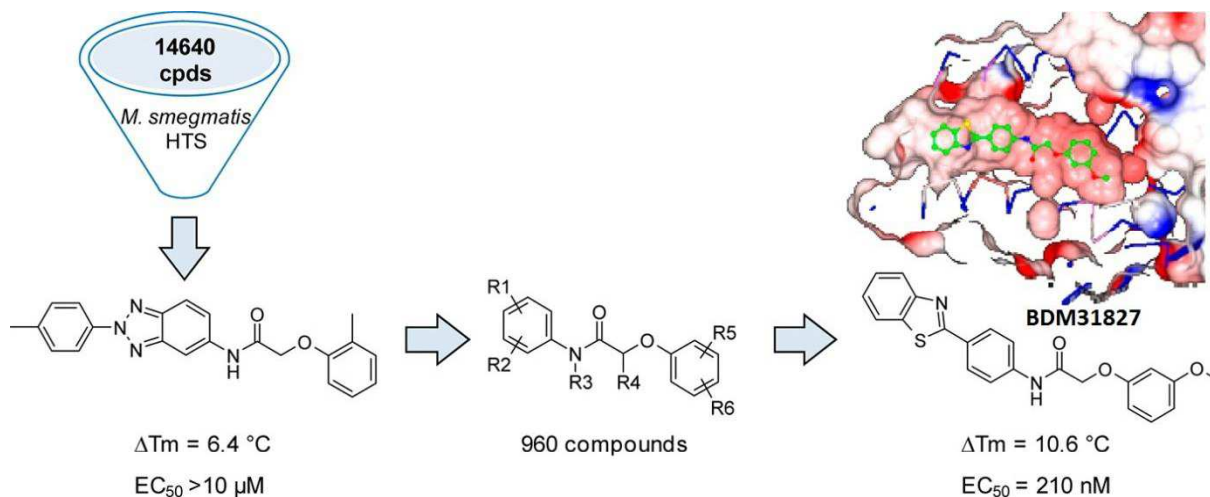


Figure 25: Development of EthR inhibitors by high throughput screening
(adapted with permission from American Chemical Society for ref. ¹⁴⁸)

Firstly, a screening of a chemical library of drug-like molecules (14640 compounds) was performed using a whole mycobacterial phenotypic assay on *M. smegmatis*. This led to the discovery of an *N*-phenylphenoxyacetamide family. The optimization of this series was driven by the synthesis of a 960-member focused library that was screened on EthR using a rapid thermal shift assay. The best compounds were synthesized on a larger scale and confirmed as potent ethionamide boosters on *M. tuberculosis*-infected macrophages. Finally, the cocrystallization of the best optimized analogue BDM31827 with EthR revealed an unexpected reorientation of the ligand in the binding pocket.¹⁴⁸

4. Development of EthR inhibitors by fragment-based approach

In order to increase the chances of finding new low-molecular-weight EthR inhibitors with suitable physicochemical properties that penetrate into the mycobacteria and bind to the EthR target, a fragment-based approach was applied by two independent research groups in order to investigate the design of novel fragment-based EthR inhibitors.

Recently, the scientists at the University of Cambridge conducted a structure-guided fragment-based approach to develop allosteric inhibitors targeting the lipophilic binding site of EthR (Figure 26). From a fragment library containing 1250 molecules, they have identified the fragment [1] as hit compound *via* a screening process comprising thermal-shift assay (TSA), surface plasmon resonance (SPR) and X-ray crystallography. The replacement of the cyclopentyl by phenyl led to compound [5] with a similar activity. A fragment-linking approach was then applied successfully to yield compound [9] with an improved inhibition activity. In fact, it is worth noting that the IC_{50} of compound [9] is approximately 280-fold

that of fragment **[1]** (Figure 26). However, the ethionamide MIC boosting activity of compound **[9]** is similar to fragment **[1]** in the REMA (resazurin reduction microplate assay). The reduction of the disulfide bond was hypothesized to explain this result.¹¹⁷

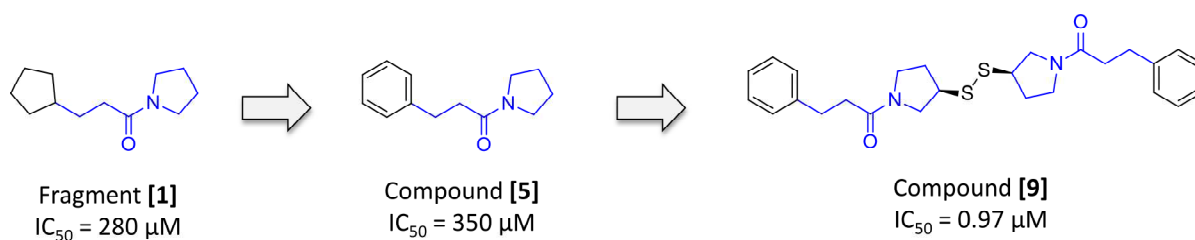
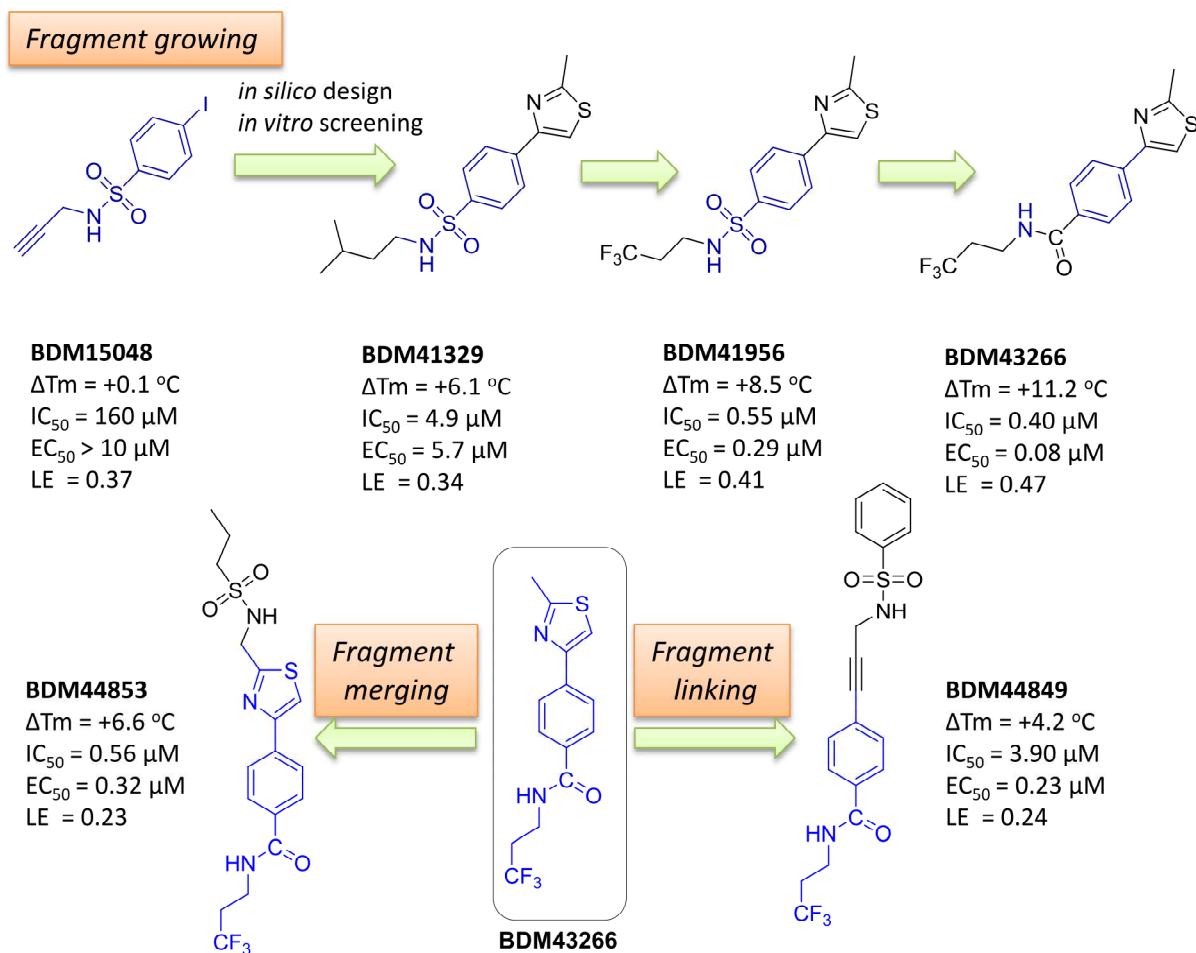


Figure 26: EthR inhibitors developed by a fragment-linking approach¹¹⁷

In parallel, a fragment-based strategy was simultaneously conducted in our research group.^{9,118} This study was started with the fragment BDM15048 which was identified as a weak EthR ligand ($\Delta T_m = +0.1$ °C, IC₅₀ = 160 μM and EC₅₀ >10 μM). Through three fragment-based approaches, e.g. fragment growing, fragment linking and fragment merging strategies, we optimized this fragment into potent ligands of EthR and ETH boosting activity (Figure 27).

Firstly, the growing approach was started by an *in silico* screening of 976 sulfonamides analogues to identify 10 hits. These hits were then tested *in vitro* to cellular assays and results have pointed out BDM41329 as the most potent compound in this series. Interestingly, a substitution of the isopentyl chain (BDM41329) by trifluoropropyl chain (BDM41956) increased significantly the affinity ($\Delta T_m = +8.5$ °C) and by 20-fold the efficacy (EC₅₀ = 0.29 μM, LE = 0.41). Furthermore, an optimization of the potency was obtained when replaced the sulfonamide function by an amide linker. The BDM43266 showed gains in all activities ($\Delta T_m = +11.2$ °C and EC₅₀ = 80 nM) while keeping equal solubility (14.7 μg/mL). Secondly, a fragment linking and fragment merging approaches were also used in order to optimize the more potent ligand which can completely fit to EthR binding pocket. This led to potent EthR inhibitors BDM44849 and BDM44853. However, a decrease of ligand efficiency and solubility was observed in these compounds.

In summary, the “growing” strategy was particularly successful in this case leading to an increase of the ligand efficiency. This increase is not usually observed in fragment-based design. Compound BDM43266 was identified as the best candidate in this series with high affinity to EthR ($\Delta T_m = +11.2$ °C), a potency in boosting ethionamide activity in the low nanomolar range (EC₅₀ = 0.08 μM).¹¹⁸ However, BDM43266 showed a poor *in vitro* metabolic stability in mouse liver microsomes with $t_{1/2} = 10$ minutes and Cl_{int} = 144 μL/min/mg.⁹ This compound was therefore not suitable to start *in vivo* assays. For that reason, further optimization was performed in the course of my thesis.

Figure 27: EthR inhibitors developed by fragment growing, linking and merging strategies¹¹⁸

5. Conclusion and outlook

In the context of Tuberculosis Drug Boost project at INSERM-U1177, many drug-design approaches were applied to find drug-like EthR inhibitors (eg. click chemistry¹⁴⁴, high-throughput screening¹⁴⁸, rational drug design^{128,141,145} and fragment-based drug design¹¹⁸). This procedure eventually led to the identification potent drug-like EthR ligands that boost *in vitro* and *in vivo* ethionamide activity. We ended up with a family of compounds bearing an acylated 1,2,4-oxadiazolylpiperidinyl scaffold which was developed by a structure-based design approach. BDM41906, a representative of this series, has shown to be able to boost ETH 4 times in an intravenously infected TB mice model and can be considered as the most potent EthR inhibitor for preclinical assay. In addition, two distinct families as back-up series were also developed. One serie contains *N*-phenylphenoxyacetamide motif (BDM31827) developed by HTS approach and the other serie bearing a thiazole benzamide scaffold (BDM43266) obtained from FBDD. However, the lead compound in fragment-based serie, BDM43266, displays limited pharmacokinetic properties. Thus, further optimization was considered.

Part C. Improving the microsomal stability of EthR inhibitors

In this context, we decided to develop novel EthR inhibitors based on the scaffold of lead compound developed starting from fragment-based screening.¹¹⁸ Firstly, a study on the metabolism of the most active compound BDM43266 was performed to determine the influence of structural components on its stability in microsomes. Then, we performed key structural modifications to improve microsomal stability of active analogues. These novel EthR inhibitors are believed to have suitable pharmacokinetic properties for *in vivo* experiments.

1. Metabolism study of the potent EthR inhibitor BDM43266

Our first hypothesis to explain the microsomal instability of BDM43266 was a possible oxidation of the methyl group connected to the thiazole ring. We thought that this methyl group could be oxidized by liver microsomes to an alcohol and then a carboxylic acid derivative (Figure 28). For that reason, we synthesized these two hypothetical metabolites.

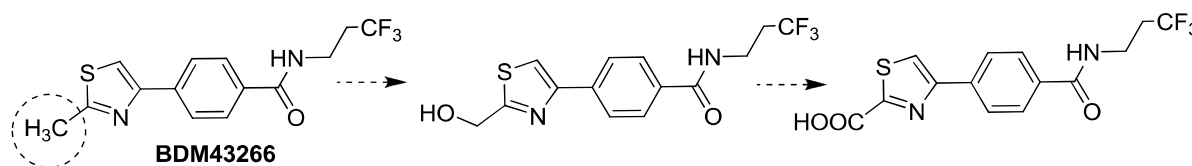
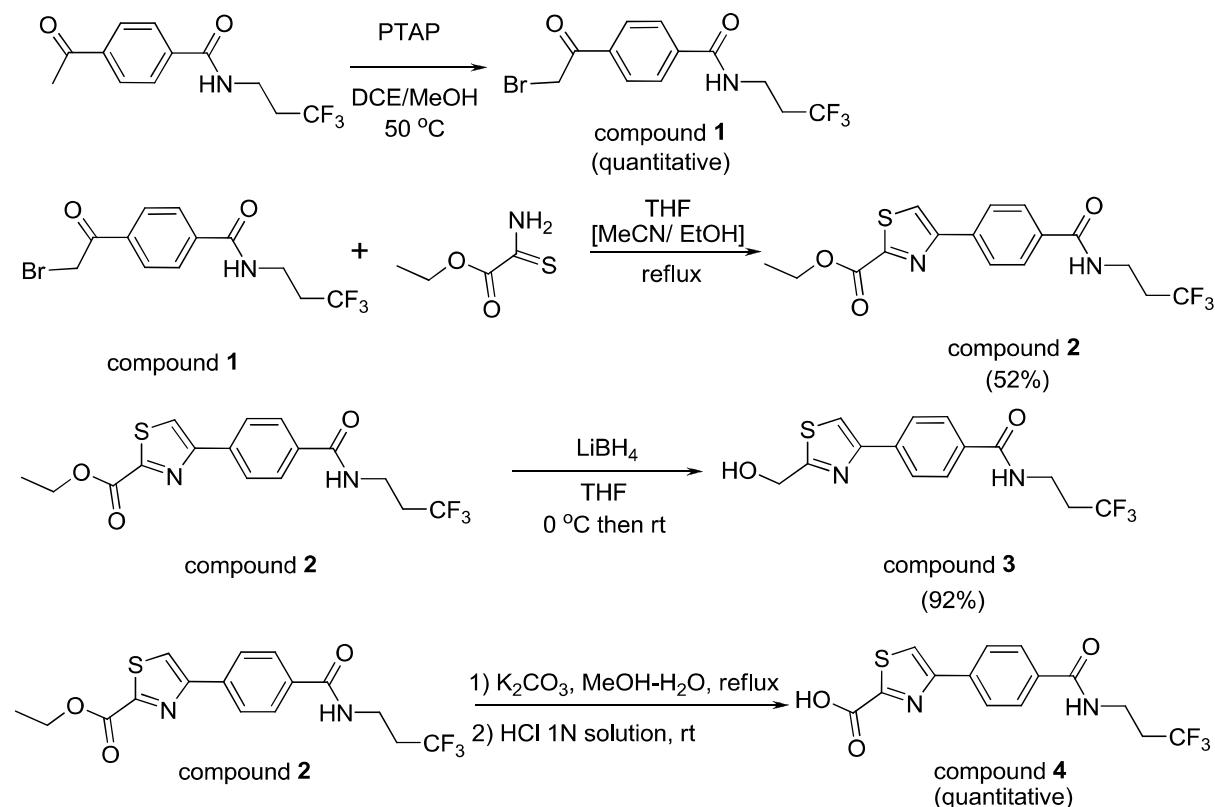


Figure 28: Hypothetic metabolism of EthR inhibitor BDM43266

1.1. Synthesis of two hypothetical metabolites of compound BDM43266

The synthetic pathway of the two compounds is summarized in Scheme 1.

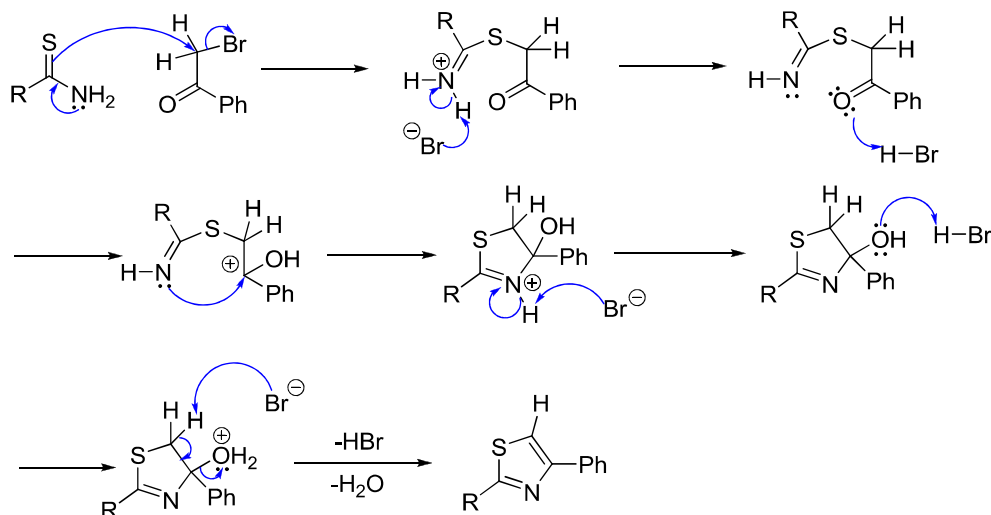


Scheme 1: Synthesis pathway of two hypothetical metabolites of BDM43266

The first reaction is a bromination of 4-acetyl-*N*-ethyl-*N*-[3,3,3-tris(fluoryl)propyl]-benzamide using phenyl trimethyl ammonium tribromide (PTAP) in a mixture solvent of

dichloroethane and methanol (DCE/MeOH). This reaction afforded the desired compound **1** in quantitative yield.

In the next step, the brominated compound **1** was then reacted with ethyl 2-amino-2-thioacetate in a Hantzsch reaction to yield the desired thiazole **2**. The mechanism of this reaction is illustrated in Scheme 2.



Scheme 2: Mechanism of the Hantzsch thiazole synthesis

The thioamide is considered as a nucleophile reagent with its sulfur atom. The first step is the substitution of the bromine atom of the bromoketone by the sulfur atom. The nitrogen then reacts on the carbonyl group, activated through protonation. The intramolecular arrangement leads to the formation of thiazoline. The reaction conditions then promote the elimination of a water molecule that allows the formation of the expected thiazole. This reaction was firstly conducted in tetrahydrofuran (THF) to give the thiazole with an average yield (52%). However, we observed a by-product which was confirmed to be the debrominated ketone (yield 11%). Unfortunately, by using different solvents (e.g. EtOH and MeCN) we could not improve the yield of this reaction.

In the next step, the ester group was then reduced in alcohol **3** using LiBH_4 with an excellent yield (92%). On the other hand, the ester **2** was also saponified using K_2CO_3 to give the carboxylic acid derivative **4** in a quantitative yield. It was noted that the carboxylic derivative was unstable as we observed a partial decarboxylation of this compound during purification by flash chromatography.

1.2. Metabolism study of BDM43266 in liver microsomes

Two synthesized derivative of BDM43266, the alcohol (compound **3**) and the carboxylic acid (compound **4**), were then used as references in the microsomal stability assay. Compound BDM43266 was mixed with liver female mouse microsomes in buffer at pH 7.4. The mixture was then incubated at 37°C for 180 minutes. After that, microsomes were denatured by acetonitrile. The mixture was then analyzed by LC-MS/MS in order to identify the metabolites. Peaks attributed to metabolites were compared to the peaks of the two hypothetical metabolites which were synthesized in section 1.1. The results confirmed our hypothesis that the alcohol derivative (compound **3**) was one of BDM43266 metabolites.

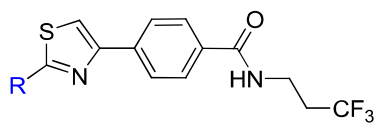
However, no peak corresponding to carboxylic derivative (compound **4**) was observed. The detail results are presented in experimental section.

1.3. Biological activities of synthesized hypothetic metabolites of BDM43266

As commonly observed in drug discovery, an active metabolite could be also used as a drug.¹⁴⁹ We then decided to test these two derivatives *in vitro*. The assay was performed with *M. tuberculosis* in the presence of subactive concentrations of ethionamide (0.1 µg/ mL of ethionamide = MIC/10), which allows determination of a compound's efficacy to boost ethionamide activity (EC₅₀).

However, the results in Table 3 showed that there is a loss of boosting effect with these two metabolites. In fact, alcohol derivative (compound **3**) is 5-times less active than BDM43266 with an EC₅₀ is 0.73 µM and carboxylic acid (compound **4**) have almost no boosting effect with EC₅₀ > 2.5 µM. As a result, these metabolites could not be used as EthR inhibitors and other novel EthR inhibitors should be developed.

Table 3: Biological activities of two hypothetic metabolites of BDM43266



	R	EC ₅₀ (µM)	HA ^c	MW (Da)	LE ^d
BDM43266	-CH ₃	0.10	21	314	0.45
compound 3	-CH ₂ OH	0.73	22	330	0.39
compound 4	-COOH	> 2.5	23	344	-

EC₅₀ represents the concentration of ligand that allows ethionamide at 0.1 µg/mL (normal MIC/10) to inhibit 50% of *M. tuberculosis* growth ; MW = molecular weight
HA = number of non-hydrogen atoms ; LE = -1.37log(EC₅₀)

2. Development of novel EthR inhibitors with improved pharmacokinetic and physicochemical properties

2.1. Enhancement of microsomal stability

The microsomal study in the previous section confirmed that BDM43266 was oxidized at the methyl group. Therefore, we tried to modify firstly the BDM43266 structure at this position in order to limit the oxidation. The substituent group should have similar properties (polarity, shape, etc.). In literature, a replacement of an oxidizable C-H bond by a C-F bond has been reported to increase metabolic stability of the molecule.^{150,151} Furthermore, fluorine atom can also change the basicity of compound and in some case can increase the affinity of compound to the target.¹⁵⁰ For that reason, we synthesized a fluorinated analogue of compound BDM43266 by replacing the methyl group with a trifluoromethyl.

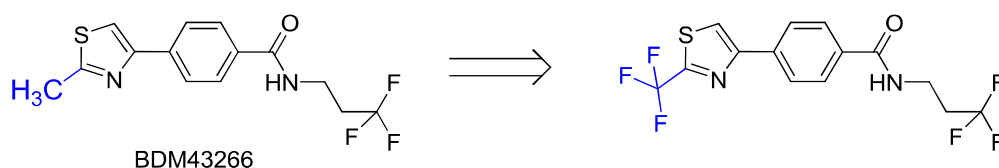
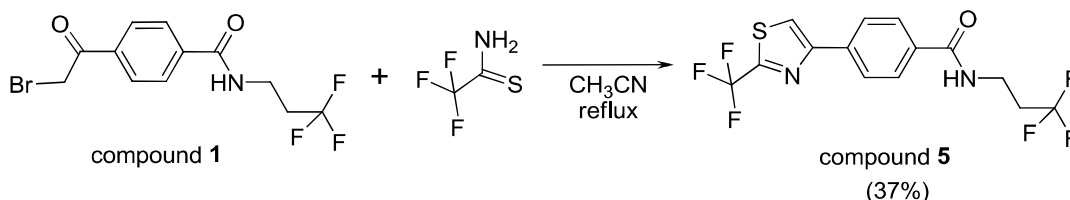


Figure 29: Strategy to improve the microsomal stability by a fluorinated analogue

The analogue was synthesized by reacting alpha-bromo ketone (compound **1**) with 2,2,2-trifluorothioacetamide to afford the desired trifluorinated thiazole analogue (compound **5**) in a poor yield (37%), which can be explained by the decrease of the reactivity of the nucleophile due to the electron withdrawing effect of the CF₃ group. This also led to an increase in reaction time (81 hours at reflux in CH₃CN). In addition, the debrominated by-product was also obtained in 29% yield.



Scheme 3: Synthesis of fluorinated derivative **5**

When we substituted the methyl group in BDM43266 by a trifluoromethyl, the biological activity on *M. tuberculosis* and affinity to EthR were unchanged (EC_{50} = 0.10 μ M, ΔT_m = 9.9 °C). As supposed, this modification led to an increase of the microsomal stability. Indeed, $t_{1/2}$ of the compound **5** is almost 2-fold better than that of BDM43266 (19 minutes versus 10 minutes) and its clearance is also improved. However, we observed a decrease of solubility with the fluorinated analogue. In fact, solubility of compound **5** is decreased to 8.2 μ g/mL versus 14.7 μ g/mL for BDM43266. Therefore, a second modification was conducted in order to enhance the physico-chemical properties while keeping the ETH boosting activity and pharmacokinetic properties unchanged.

Table 4: Pharmacodynamic, pharmacokinetic and physico-chemical properties of compound **5**

	R	ΔT_m (°C)	EC_{50} (μ M)	HA	MW (Da)	LE	$t_{1/2}$ (min)	CL_{int} (μ L/min/mg)	Solubility (μ g/mL)	logD
BDM43266	CH ₃	10.6	0.10	21	314.33	0.46	10	144	14.7	2.8
compound 5	CF ₃	9.9	0.10	24	368.30	0.40	19	62	8.2	3.6

ΔT_m = T_m (holo-protein)- T_m (apo-protein) in TSA ; EC_{50} represents the concentration of ligand that allows ethionamide at 0.1 μ g/mL (normal MIC/10) to inhibit 50% of *M. tuberculosis* growth ; HA = number of non-hydrogen atoms ; MW = molecular weight ; $LE = -1.37 \log(EC_{50})$; $t_{1/2}$ = half-life of compound in microsomes ; CL_{int} = Clearance.

2.2. Enhancement of physico-chemical properties by pyridine replacement

In the second strategy, a less lipophilic analogue was designed by replacing the benzene ring in compound **5** with a pyridine ring.

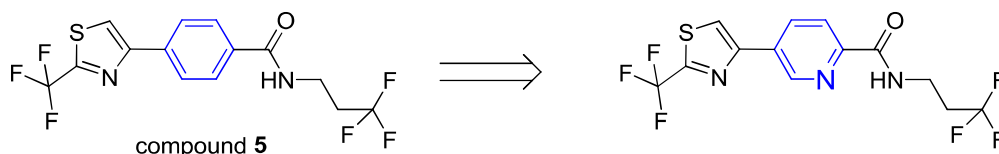
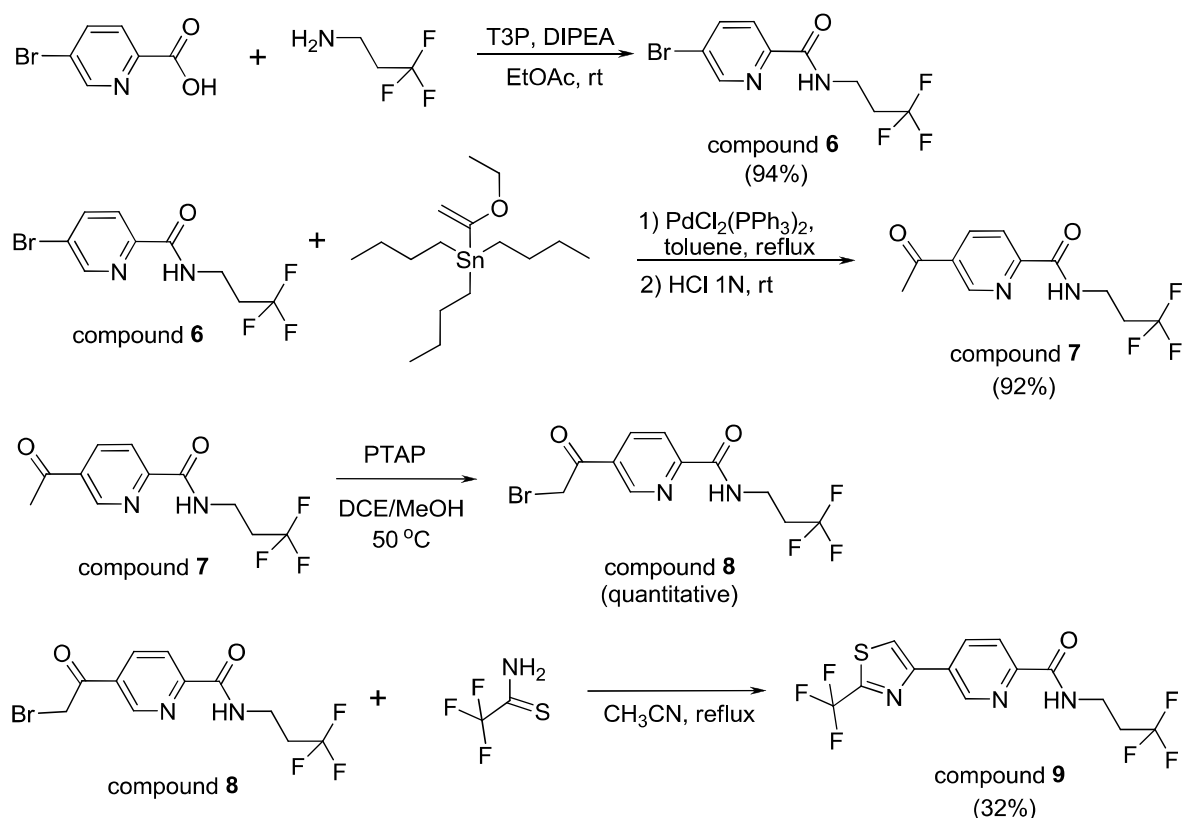


Figure 30: Strategy to improve the solubility by a pyridine analogue

This compound was obtained after a 4-step-synthesis which is summarized in Scheme 4. In the first step, amide bond was formed with an excellent yield by activating the carboxylic

function using propylphosphonic anhydride (T3P[®]) in the presence of diisopropylethylamine (DIPEA). This reaction was carried out in ethyl acetate (EtOAc) at room temperature.



Scheme 4: Synthesis of fluorinated pyridine containing derivative 9

T3P[®], a cyclic phosphonic anhydride, is widely known as a coupling reagent in peptide synthesis. Recently, this reagent was also used in the formation of nitriles, amides, isonitriles or other heterocyclic rings.¹⁵² This compound is less toxic than other amide coupling reagents (e.g. SOCl₂, PCl₃). Furthermore, T3P is water soluble and generate little epimerization. The mechanism of activation and coupling with amine is presented in Figure 31.

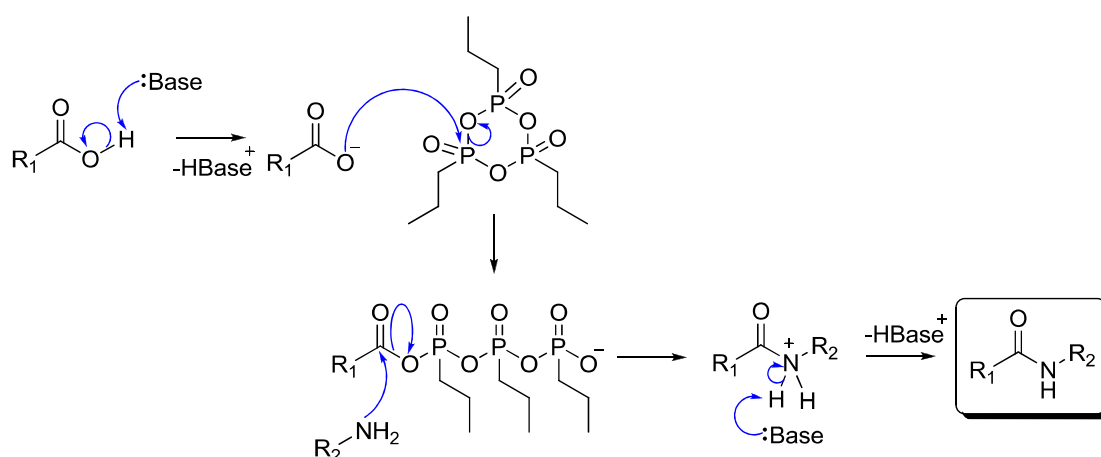


Figure 31: Mechanism of amide formation catalyzed by T3P[®]

Firstly, the carboxylic acid is deprotonated in the presence of a base. The resulting carboxylate then attack T3P[®] and lead to the formation of a mixed anhydride. This mixed anhydride then reacts with amine (or other nucleophile compounds). Finally, a second

equivalent of base will allow the deprotonation of the intermediate to yield the corresponding amide **6**.

In the second step, the substitution of bromine atom by a methyl-ketone function was then obtained using a Stille cross-coupling reaction.¹⁵³

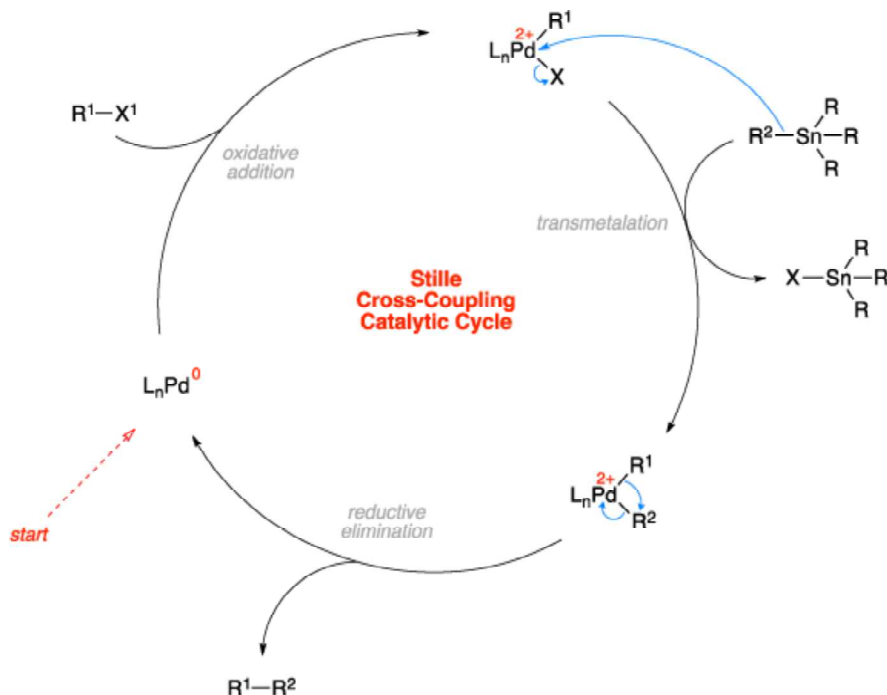
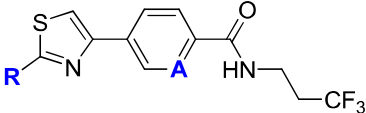


Figure 32: Catalytic cycle of Stille cross-coupling reaction

In this reaction, the brominated derivative **6** was refluxed with tributyl-(1-ethoxyvinyl)tin and $\text{PdCl}_2(\text{PPh}_3)_2$ in toluene. The basic catalytic cycle of Stille reaction is shown in Figure 32. The first step is the oxidative addition of the halide derivative to palladium catalyst. In the transmetalation step, the tin atom bonded to allyl group (R_2), can coordinate to the palladium via the double bond, then R_2 group is exchanged with the halogen atom (X). Next, reductive elimination step leads to the desired compound ($\text{R}_1\text{-R}_2$) and regenerate the palladium catalyst. Finally, acid hydrolysis of the reaction mixture resulted in the recovery of the methyl ketone **7** with a yield of 92%. In step 3, the resulting methyl ketone **7** was then brominated using PTAP in quantitative yield. In step 4, the desired thiazole **9** was formed *via* Hantzsch reaction between the corresponding alpha-bromo ketone **8** with the 2,2,2-trifluorothioacetamide. Similar to other Hantzsch reactions described in this chapter, a debrominated by-product was also obtained (22%) that led to a poor yield (32%) in thiazole formation.

We also measured all biological activities, pharmacokinetic and physico-chemical properties of compound **9** and compared to other thiazole analogues. Results are displayed in Table 5. We noticed that the replacement of benzene ring by a pyridine did not impact the ETH boosting activity. Compound **9** is still active ($\text{EC}_{50} = 0.098 \mu\text{M}$ and $\Delta\text{Tm} = 9.5 \text{ }^\circ\text{C}$). However, the microsomal stability was slightly decreased ($t_{1/2} = 16 \text{ min}$) in comparison with compound **5** ($t_{1/2} = 19 \text{ min}$) but still better than for BDM42366. On the contrary, we obtained an increase in the solubility ($17.2 \mu\text{g/mL}$).

Table 5: Pharmacodynamic, pharmacokinetic and physico-chemical properties of 3 thiazole analogues



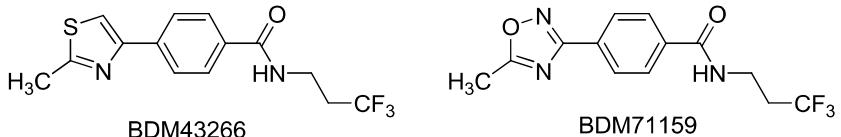
	R	A	ΔT_m ($^{\circ}C$)	EC_{50} (μM)	HA	MW (Da)	LE	$t_{1/2}$ (min)	CL_{int} ($\mu L/min/mg$)	Solubility ($\mu g/mL$)	logD
BDM43266	CH ₃	C	10.6	0.10	21	314.33	0.46	10	144	14.7	2.8
compound 5	CF ₃	C	9.9	0.10	24	368.30	0.40	19	62	8.2	3.6
compound 9	CF ₃	N	9.5	0.098	24	369.29	0.40	16	79	17.2	3.3

ΔT_m = $T_m(\text{holo-protein}) - T_m(\text{apo-protein})$ in TSA ; EC_{50} represents the concentration of ligand that allows ethionamide at 0.1 $\mu g/mL$ (normal MIC/10) to inhibit 50% of *M. tuberculosis* growth ; HA = number of non-hydrogen atoms ; MW = molecular weight ; $LE = -1.37 \log(EC_{50})$; $t_{1/2}$ = half-life of compound in microsomes ; CL_{int} = Clearance.

2.3. Optimisation of an 1,2,4-oxadiazole analogue

The result of fragment-based EthR inhibitors development in our group also demonstrated that the replacement of thiazole in BDM43266 by a 1,2,4-oxadiazole ring is not detrimental for the ETH boosting activity.⁹ Indeed, compound BDM71159 (in Table 6) revealed a potent ETH boosting activity in comparison with BDM43266 (thiazole analogue). However, these two compounds share the same methyl group connected to heterocyclic ring. This can explain in similar way the microsomal instability of BDM71159 ($t_{1/2} = 7$ min).

Table 6: Biological and physico-chemical properties of 2 lead compounds in FBDD



	ΔT_m ($^{\circ}C$)	EC_{50} (μM)	HA	MW (Da)	LE	$t_{1/2}$ (min)	CL_{int} ($\mu L/min/mg$)	Solubility ($\mu g/mL$)	logD
BDM43266	10.6	0.10	21	314.33	0.46	10	144	14.7	2.8
BDM71159	9.3	0.082	21	299.25	0.46	7	172	21.8	2.3

Therefore, we decided to carry out two structural modifications as described above in order to improve the microsomal stability and solubility of compound BDM71159.

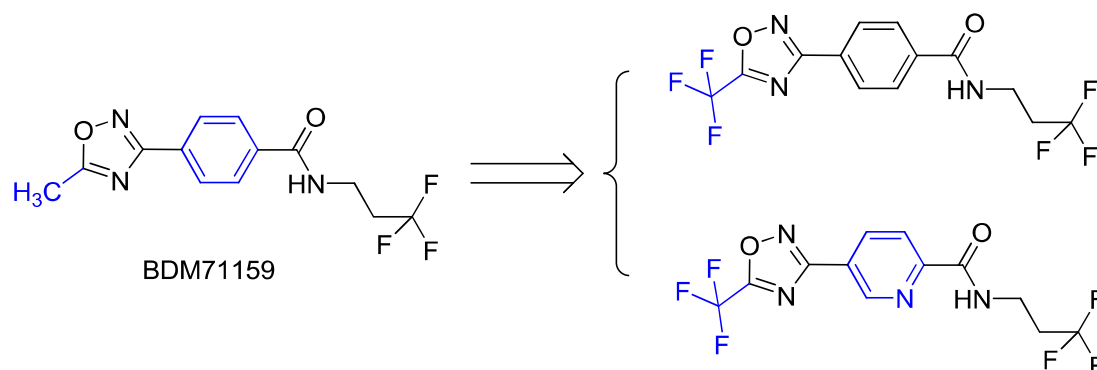
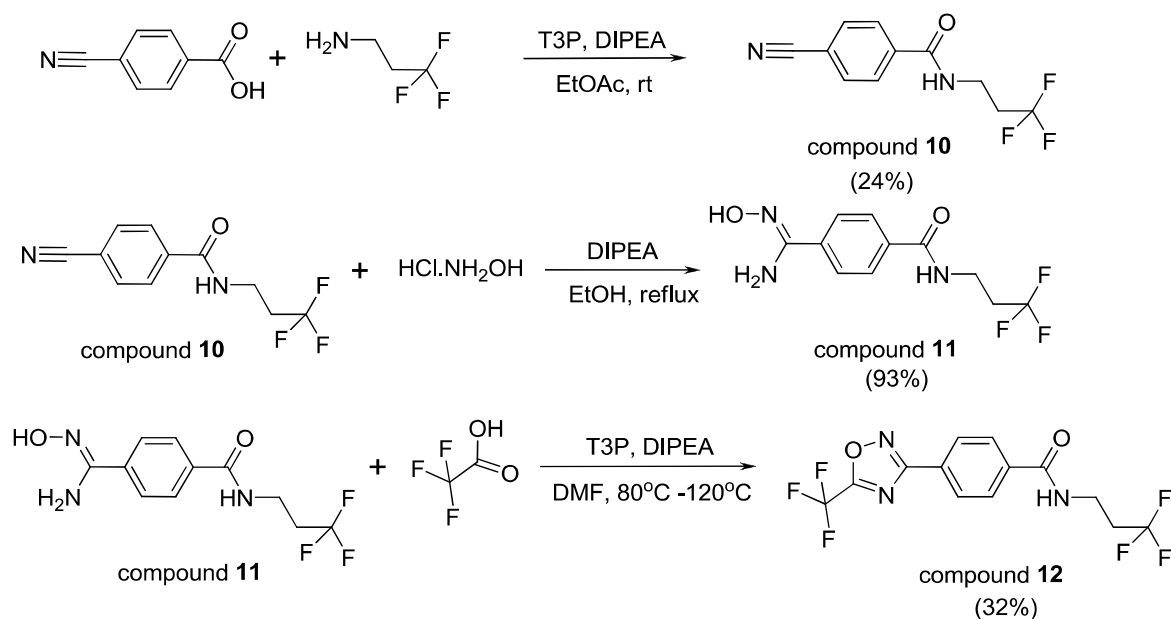


Figure 33 : Strategy to improve pharmacokinetic properties and solubility of BDM71159

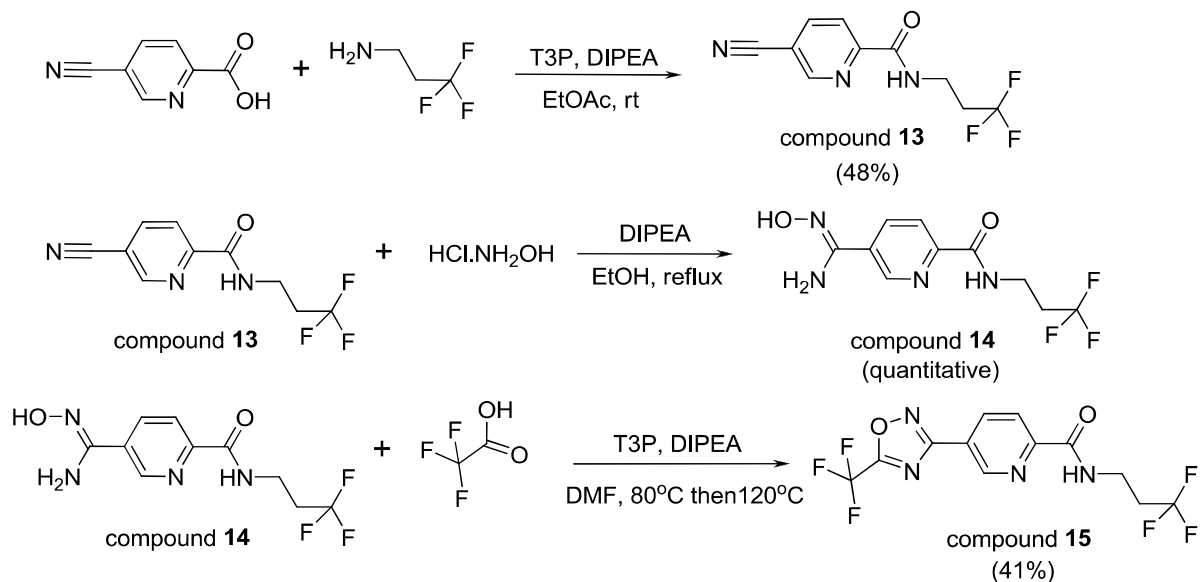
The synthesis of the fluorinated analogue **12** is presented in Scheme 5. Firstly, 4-cyano-benzoic acid was coupled to 3,3,3-trifluoropropylamine using propylphosphonic anhydride (T3P) in the presence of diisopropyl-ethylamine to yield the corresponding amide **10** in a poor

yield (24%). Then, the nitrile group of compound **10** was then converted into amidoxime by using hydroxylamine under basic condition in excellent yield (93%).



Scheme 5: Synthesis of fluorinated 1,2,4-oxadiazole derivative **12**

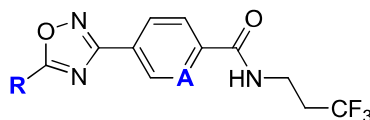
Finally, the amidoxime **11** was coupled with trifluoroacetic acid in the presence of T3P[®] and DIPEA and then cyclized to yield the corresponding 1,2,4-oxadiazole derivative (compound **12**). The final step was conducted in *N,N*-dimethylformamide (DMF) which allowed to heat the mixture to 120 °C. We obtained the desired oxadiazole analogue with a 32% yield. The same synthetic pathway was used for the synthesis of pyridinyl derivative **15** starting from 5-cyano-2-pyridin carboxylic acid (Scheme 6).



Scheme 6: Synthesis of fluorinated 1,2,4-oxadiazole derivative **15**

These two analogues of BDM71159 (compound **12** and **15**) were then tested. Results (in Table 7) showed that the replacement of the methyl by a trifluoromethyl group once again improved the microsomal stability. In fact, compound **12** has a half-life ($t_{1/2}$ =22 min), 3-fold longer than BDM71159.

Table 7: Potency, physico-chemical properties and microsomal stability of BDM71159 analogues



	R	A	ΔT_m ($^{\circ}C$)	EC_{50} (μM)	HA	MW (Da)	LE	$t_{1/2}$ (min)	CL_{int} ($\mu L/min/mg$)	Solubility ($\mu g/mL$)	logD
BDM71159	CH ₃	C	9.3	0.082	21	299.25	0.46	7	172	21.8	2.3
compound 12	CF ₃	C	10.2	0.073	24	353.22	0.41	22	34	2.4	3.5
compound 15	CF ₃	N	7.3	0.39	24	354.21	0.37	17	73	16.8	3.0

ΔT_m = T_m (holo-protein)- T_m (apo-protein) in TSA ; EC_{50} represents the concentration of ligand that allows ethionamide at 0.1 $\mu g/mL$ (normal MIC/10) to inhibit 50% of *M. tuberculosis* growth ; HA = number of non-hydrogen atoms ; MW = molecular weight ; LE = $-1.37 \log(EC_{50})$; $t_{1/2}$ = half-life of compound in microsomes ; CL_{int} = Clearance.

Interestingly, the ETH boosting activity and affinity for EthR were also improved (EC_{50} = 0.073 μM and ΔT_m = +10.2 $^{\circ}C$). However, a decrease in solubility was observed with one of these two fluorinated analogues. In fact, solubility of compound **12** is 9-fold lower than that of BDM71159 (2.4 versus 21.8 $\mu g/mL$). By replacing the benzene ring by a pyridine (compound **15**), we could recover an acceptable solubility (16.8 $\mu g/mL$). However, this modification has led to a decrease in ETH boosting activity. In fact, compound **15** was 5-fold less active than the reference compound BDM71159 (EC_{50} = 0.39 and 0.082 μM , respectively).

3. Molecular docking modelling of novel inhibitors in EthR structures

3.1. Co-crystallized structure of BDM43266-EthR

BDM43266 was co-crystallized with EthR. The structure of this complex was obtained at a resolution of 2.0 \AA (PDB ID 4M3B). The result shows that this ligand can be stabilized in the EthR pocket by hydrogen bonding with Asn179 and Asn176 at the same time (see Figure 34). These interactions can explain the high affinity of BDM43266 to EthR and consequently its high potency in ETH boosting effect.

Until now, we have not yet obtained the co-crystallized structures of the newly synthesized compounds in complex with EthR. Therefore we docked these compounds into the ligand binding domain of EthR, in order to predict the interactions between the four analogues with the residues in the binding pocket of EthR. The results were used to build a correlation between the antitubercular activity of these compounds and their EthR binding ability.

3.2. *In silico* docking of 4 synthesized analogues

For the two thiazole analogues compound **5** and compound **9**, the best docking poses obtained *in silico* are presented in Figure 35. The interaction modes between these thiazole analogues are similar to BDM43266. Indeed, the amide group in these structures are H-

bonded to the two asparagine residues Asn176 and Asn179. These results are in agreement with the good activities of these compounds.

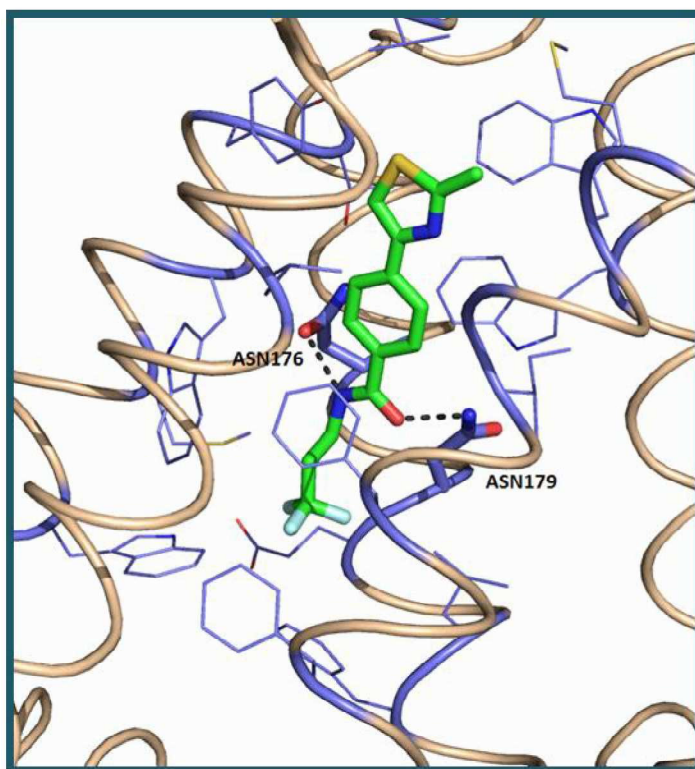


Figure 34: Interaction between BDM42366 and EthR binding pocket residues (PDB ID 4M3B)¹¹⁸

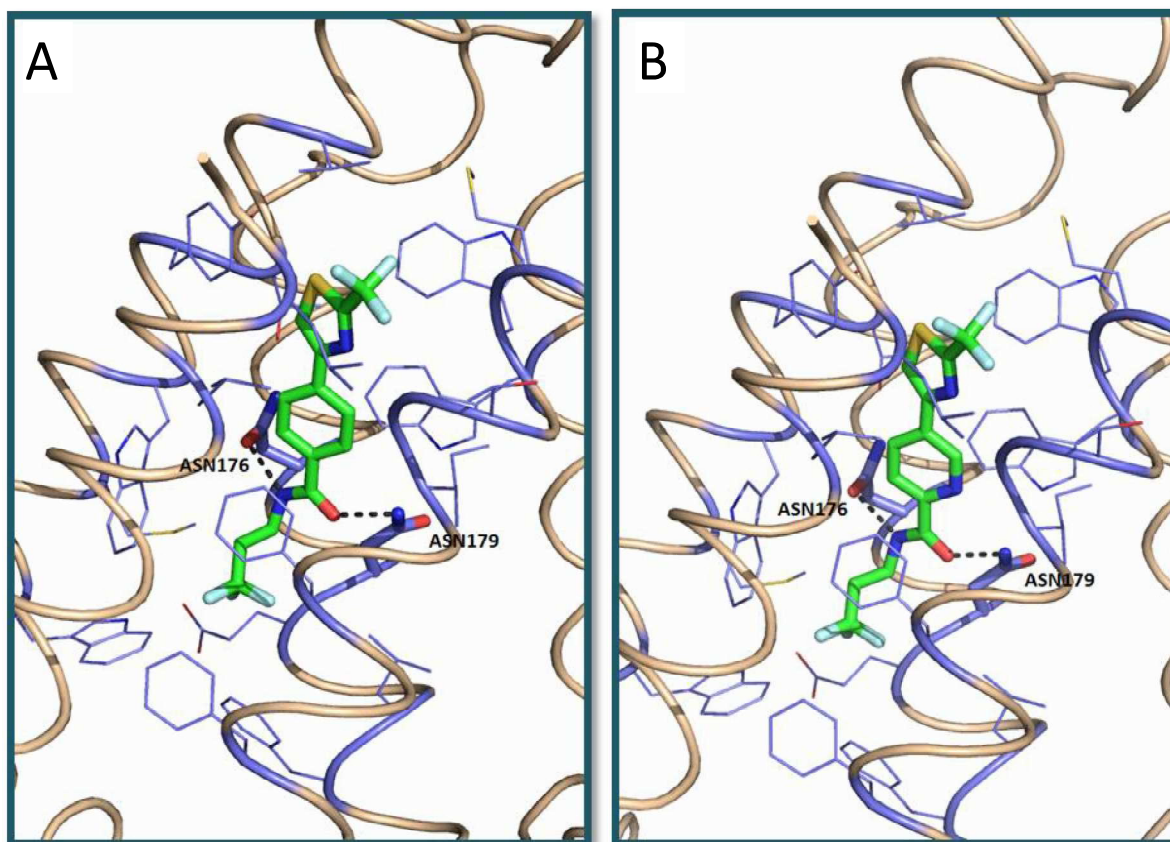


Figure 35: The best docking pose of compound 5 (A) and compound 9 (B) in the EthR binding pocket
Colors legend: blue (protein) and green (compound) = carbon, dark blue = nitrogen, red = oxygen, yellow = sulfur, cyan = fluoro. Black dashed lines indicate the hydrogen bond interaction. Images were generated with Pymol.

Docking poses of the two oxadiazole analogues to EthR are shown in Figure 36. We noted that replacement of the thiazole ring by an oxadiazole motif did not change the binding mode of compound **12**. This compound can also form hydrogen bonds with Asn176 and Asn179. This result is also in agreement with its potent *in vitro* activity.

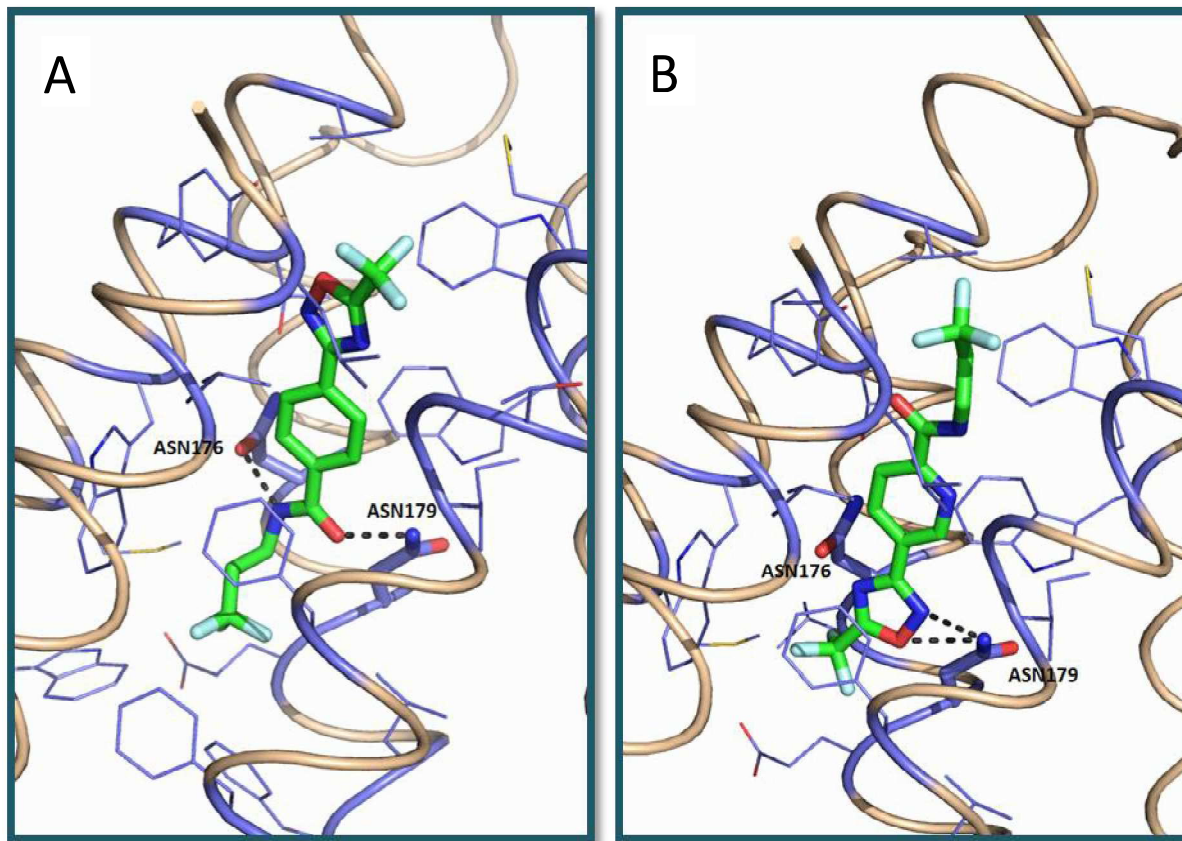


Figure 36: Docking pose of compound **12** (A) and compound **15** (B) in EthR binding pocket

However, the docking study of compound **15** was informative. The best docking of this compound in the EthR binding pocket is different to those of other analogues (Figure 36B). The compound has flipped by 180° inside the cavity; the oxadiazole ring is only H-bonded to asparagine Asn179 *via* only one nitrogen atom. No interaction with Asn176 was observed.

Therefore, the replacement of the benzene ring by pyridine in this case may affect the binding of this compound in the EthR binding pocket. This predicted binding pose may explain the loss in activity observed with compound **15**. The latter result also suggests that the trifluoropropyl chain can also interact with EthR in a hydrophobic cavity formed by aromatic residues Trp145, Phe110, Phe114, Trp138 and Phe184.

4. Conclusions and outlook

In the first part of this thesis, a study on the metabolism of the potent fragment-based EthR inhibitor (BDM43266) was realized. The results confirmed our hypothesis that oxidation proceeds on the methyl group and leads to the hydroxyl derivative. In order to increase the microsomal stability of these EthR inhibitors, we introduced fluorine atoms at the point of metabolism. Moreover, we decreased the lipophilicity of these analogues by introducing a pyridine ring at position of benzene in order to improve the aqueous solubility

and logD. These compounds were successfully synthesized and we measured their potency to boost sub-active doses of ethionamide on *M. tuberculosis*. The results confirmed our hypothesis on the effect of the trifluoromethyl group in preventing these compounds from being oxidized on that particular position. Indeed, we observed an enhancement of the microsomal stability. Interestingly, the replacement of methyl group with trifluoromethyl did not impact the activity. In addition, molecular docking modelling was built in order to illustrate the interactions between these compounds and the residues in the EthR binding site. A correlation between the binding affinity in EthR and biological boosting effect in *M. tuberculosis* was investigated. Compounds **5** and **9**, which showed the best compromise between activity, microsomal stability and solubility, will be further evaluated in an *in vivo* model of tuberculosis.

This page intentionally left blank

Chapter III. Design and synthesis of MabA inhibitors

In the previous chapter, we described our first strategy to boost the bioactivity of thioamide drugs. The drug-like EthR inhibitors could then be used in association with lower doses of ethionamide in a regimen of higher tolerance and improved efficacy. However, novel TB drugs that are developed will not only active against drug resistant bacteria but also, more importantly, can kill persistent bacteria and shorten the duration of treatment.⁸⁷ In the second strategy, we tried to develop new antitubercular compounds with a direct inhibitory effect on the growth of the tubercle bacillus.

In fact, it has been noted that all actual TB drugs target only a small number of essential functions in *M. tuberculosis*. Therefore, the identification of further pathways in bacterial growth should furnish novel targets for the rational design of novel TB drugs.¹⁵⁴ Moreover, the complete genome sequencing of *M. tuberculosis*³⁹ has provided an opportunity for identification of new antitubercular targets. In recent years, a number of new mycobacterial genes and their encoded-protein have been identified.¹⁵⁵ These proteins that control vital aspects of mycobacterial physiology (e.g., metabolism, persistence, virulence, signal transduction and cell wall synthesis, etc.) would be attractive targets for new drugs.^{83,156-160} In the second part of this thesis, we will focus on MabA (also named FabG1) as a new target for TB drug development.

Part A. MabA

1. MabA— a forgotten target in FAS-II pathway

As absent in human, the type II fatty acid synthase (FAS-II) which is composed of condensing enzymes represent a pool of valuable drug targets for TB drug development. Nowadays, many drug-design projects focus on the development of novel inhibitors which target these FAS-II enzymes. FAS-II system comprises four enzymes which act successively and repeatedly to ensure fatty acid elongation, ultimately leading to meromycolic acid synthesis. These enzymes are the condensing enzymes KasA and KasB, the β -keto-reductase MabA, dehydratases HadABC, and the enoyl-reductase InhA.^{33,161}

Firstly, thiolactomycin (TLM), a natural molecule produced by *Nocardia* was found to disrupt the activity of the mycobacterial KasA and KasB enzymes. TLM was shown to inhibit mycolic acids biosynthesis *in vitro* while retaining good antimycobacterial activity *in vivo*. Recent efforts are being directed toward improving the affinity of TLM for KasA and developing chemical tools to investigate the substrate binding and catalytic mechanism of KasA through design and synthesis of substituted TLM-derivatives.^{33,161}

The enoyl-ACP reductase InhA has been demonstrated to be the target of both isoniazid (INH) and thionamide (ETH), validating it as a remarkable antitubercular drug target. INH, one of the oldest known anti-TB and structurally simplest drugs, was found to have a bactericidal activity against *M. tuberculosis* more than 50 years ago. INH is activated by the catalase-peroxidase KatG to form an adduct with nicotinamide adenine dinucleotide (NAD) that is responsible for the inhibition of InhA. Likewise, ETH is a prodrug and is activated in *M. tuberculosis* by EthA, a flavin monooxygenase, to form a covalent ETH-NAD adduct that

inhibits InhA. Expectedly, inhibition of InhA leads to inhibition of mycolic acids biosynthesis, accumulation of long-chain fatty acids and ultimately to cell death. Nowadays, the search for novel compounds that directly target InhA without the activation step represents a promising approach to circumvent this resistance mechanism. In this context, the broad-spectrum antimicrobial triclosan (TRC) and a natural product pyridomycin (PYR) have been proven to inhibit InhA without requesting activation. The results open promising avenues for the treatment of INH-resistant tubercle bacilli.³³

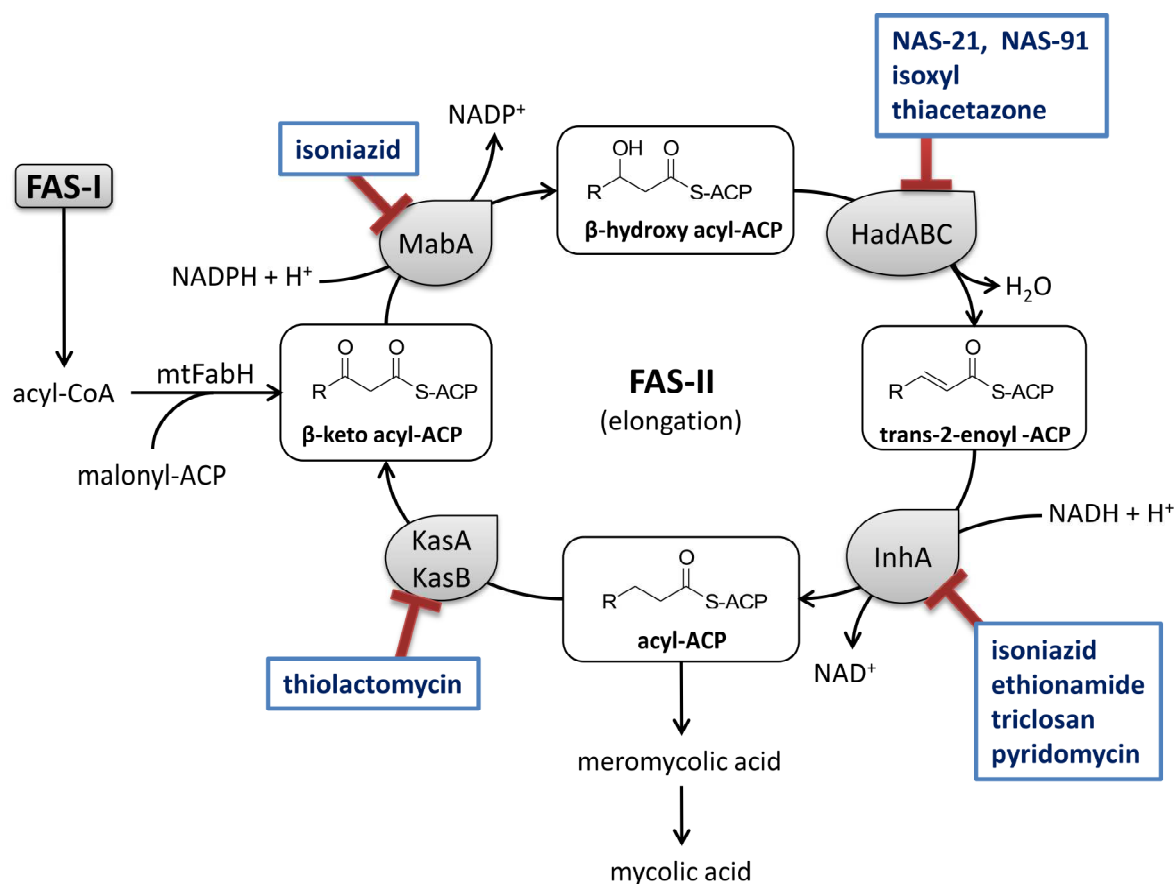


Figure 37: Mycolic acid biosynthesis pathway and inhibitors

Furthermore, isoxyl (ISO) and thiacetazone (TAC), two other TB-prodrugs, have been identified to interrupt the dehydratase step, catalyzed by the β-hydroxyacyl-ACP dehydratases (encoded by the hadABC genes). Both compounds are the first clinically used anti-TB drugs reported to act at the dehydration step. They have dramatic effects on mycolic acids biosynthesis, consistent with both drugs inhibiting an early and essential step of the pathway. Moreover, the antimalarial phenylsulfanylmethyl-[1,4]-naphthoquinones NAS-21 and NAS-91, first identified as inhibitors of the β-hydroxyacyl-ACP dehydratase FabZ of *P. falciparum* were found to exhibit potent antimycobacterial activity. Synthesis of NAS analogs and evaluation of their whole-cell activity against *M. bovis* BCG allowed for determination of their activity against FAS-II but not FAS-I synthesis *in vitro*, implicating in particular *Rv0636* (HadB) as the candidate target of these inhibitors.³³

Concerning MabA, there is only one study conducted by Ducasse-Cabanot and his colleagues in which these authors have reported an *in vitro* inhibition of MabA by isoniazid-NADP adduct.¹⁶² The inhibitory mechanism is similar to that of isoniazid-NAD adduct.

Indeed, antitubercular prodrug isoniazid (INH) is normally bioactivated by the catalase peroxidase KatG to form an INH-NAD adduct. In this study, these authors involved the formation of a covalent adduct between Mn^{III}-activated INH and cofactor NADP⁺. The interaction between MabA and this adduct was observed. MabA activity was shown to be inhibited by this adduct. The IC₅₀ of the INH-NADP⁺ adduct for MabA has the same order of magnitude as the IC₅₀ for InhA (2.2 μM and 1-2 μM, respectively). Furthermore, fluorospectrometry assay showed that the adduct binds to the MabA active site.¹⁶² Besides this promising result, no drug-like MabA inhibitors have been discovered until now.

In summary, inhibitors of majority enzymes of the FAS-II system are known.¹⁶³ Thus, these compounds were showed to inhibit three of the four enzymes of the mycobacterial FAS II (KasAB, InhA and HadABC).³³ However, no drug-like low-molecular-weight inhibitors of MabA have yet been reported until now although this enzyme has been shown to be essential for *M. tuberculosis* survival. For that reason, the design and synthesis of novel MabA inhibitors should be a promising approach in the development of new agents against mycobacteria.

2. MabA enzyme – a validated target of *M. tuberculosis*

2.1. MabA gene position in *M. tuberculosis* genome

In 1994, while conducting a study on the *inhA* gene as target for INH and ETH¹²¹, Banerjee and his colleagues have surprisingly found that the *inhA* operon consists of two continuous open reading frames (ORFs), respectively designated as *orf1* and *inhA*, which may participate in fatty acid biosynthesis. The protein encoding by the *orf1* gene located immediately upstream of *inhA* in tested mycobacterial. This gene exhibits sequence similarity with β-ketoacyl-ACP reductases (KARs) or FabG in others bacteria.¹²¹ FabG is the common name of beta ketoacyl reductase. This gene was later renamed as *mabA* (mycolic acid biosynthesis A) because of its probable involvement in mycolic acid biosynthesis.¹⁶⁴ Despite the same operon sharing by *mabA* and *inhA* in *M. tuberculosis* genome, it has been noted that no mutations have been mapped to the MabA ORF in the INH-ETH-resistant *M. tuberculosis* clinical isolates. In fact, genetic dissection showed that these drugs resistance phenotype is encoded only by *inhA*.¹⁶⁵

In 1998, Banerjee *et al.* conducted an analysis¹⁶⁵ of the DNA sequence of the *mabA* gene from *M. tuberculosis* H37Rv. The result showed that the length of this gene is about 741 base pairs which correspond to a protein comprising 247 amino acids. The authors have also found that DNA sequence of the *mabA* gene is highly conserved between different mycobacteria. In fact, this gene of *M. tuberculosis* is identical to that of *M. bovis* BCG and is stronger homology to *M. avium* MabA than the *M. smegmatis* protein. With a similarity score about 88-90%, the amino acid residues are conserved between the different MabA proteins, These results indicate that MabA is likely to be essential in mycobacteria, like InhA.¹⁶⁵

The sequence of the *mabA* gene from *M. tuberculosis* has been now reported on the GenBank/EMBL with the accession number U66801.¹⁶⁶ This gene can also be accessed in the *Mycobacterium tuberculosis* H37Rv genome with the code Rv1483.^{38,39} Another name of this

gene is *fabG1* which is called after the encoding product 3-oxoacyl-[acyl-carrier protein] reductase, FabG1.¹⁰

In addition, analysis of the complete sequence of the *M. tuberculosis* genome³⁹ show the presence of five FabG genes, but only two, FabG1 (Rv1483) and FabG4 (Rv0242c), are conserved among the mycobacterial species.¹⁶⁷ FabG1 as described above is associated with the FAS-II system in the mycolic acids biosynthetic pathway whereas FabG4 belongs to an operon possibly involved in a non-conventional processing of fatty acids. Furthermore, FabG4 belongs to the HMwFabG group (high-molecular-weight FabG). FabG1, in contrast, belongs to the LMwFabG (low-molecular-weight FabG). Recently, many reports have made FabG4 a new attractive target as FabG1 to fight tuberculosis.^{168,169}

2.2. Purification methods and enzymatic activity of MabA

A total soluble protein extract of *E. coli* expressing *mabA* was tested for KAR activity.¹⁶⁵ The extracts were tested in the presence of either NADH or NADPH. Acetoacetyl coenzyme A was used as the substrate in this reaction. The conversion of NADH or NADPH respectively to NAD⁺ or NADP⁺ was measured by spectrophotometry at 340 nm. The extracts from the induced cells were found to have considerable KAR activity with specificity for NADPH. This preference for NADPH is in accordance with the presence of an NADP-binding motif in MabA protein sequence.¹⁶⁵

Four years later, Marrakchi and his colleagues developed a method¹⁰ for the purification of MabA. The *mabA* gene was cloned in *E. coli*, in an expression vector. The N-terminal His-tagged MabA protein (H-MabA) was produced at high levels and purified by chromatography over a Ni-NTA agarose column. Purity of the H-MabA was analyzed by denaturing electrophoresis (SDS-PAGE) after staining by Coomassie blue and/or silver nitrate. The result indicated the homogeneity of the MabA protein with purity greater than 96%. Unfortunately, verification of the primary sequence has detected the loss of the first methionine of the poly-His tag MabA protein. This precise mass of MabA was also confirmed by electrospray ionization mass spectroscopy (ESI-MS).¹⁰

In an attempt to increase the recovery of homogeneous MabA, a different protocol was developed.¹⁰ This improved method permitted the enzyme to be successfully purified to homogeneity by a two-step purification (FPLC Q-Sepharose Fast Flow column then Sephacryl S-200 column)¹⁷⁰ or three-chromatographic steps protocol (FPLC HT-Blue column → Sephacryl S-200 column → Mono-S cation exchange column).¹⁷¹ MabA was successfully purified, in an active form, as indicated by a single band on SDS-PAGE having the expected molecular weight. The significant advantage of this method is that MabA enzyme is not His-tagged. ESI-MS analysis demonstrated that the recombinant enzyme has a subunit molecular weight of 25.563 Da. The predicted molecular weight based on its amino acid sequence is 25.697 Da, while the predicted molecular weight with the first methionine removed is 25.566 Da, and N-terminal amino acid sequence analysis confirmed that the initiator methionine had also been completely removed. However, the loss of the first methionine residue and the presence of an N-terminal poly histidine tag do not seem to affect the enzymatic activity of MabA. Experimental data is in agreement with this hypothesis.¹⁷⁰⁻¹⁷²

The reduction of β -ketoacyl derivatives by the recombinant purified H-MabA protein was monitored by spectrophotometry method as described above.¹⁶⁵ The assay was also conducted with acetoacetyl-CoA as substrate and the authors showed that pure MabA or H-MabA is active in the simultaneous presence of acetoacetyl-CoA (C_4 substrate) and NADPH. This result was also confirmed by MALDI-TOF/MS with the reduction of acetoacetyl-CoA to hydroxybutyryl-CoA displaying by an increase of m/z . However, this activity was not detected when NADPH was replaced by NADH, indicating that the enzyme is specifically NADPH-dependent. The overall scheme of the reduce reaction in the assay catalyzed by MabA was designed in the Figure 38.

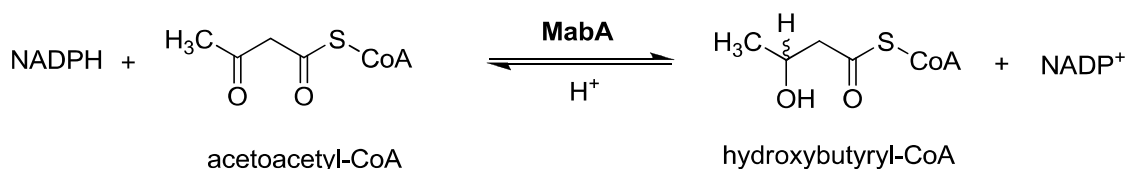


Figure 38: Reaction scheme for the reduction of acetoacetyl-CoA substrates by MabA protein

Moreover, a study on the parameters affecting the activity of the MabA protein was conducted. Firstly, the effect of the pH on the enzymatic activity of MabA was evaluated. The result showed that the optimum activity of MabA is obtained at pH 5.5. This is probably linked to a protonated form involved in the binding of the substrates or in the catalysis. This relate to two histidine residues (H46 and H247) in the active site of MabA. Moreover, another study on the pH dependence of k_{cat} confirmed that pH acid is essential for catalysis. In fact, the pH dependence of $k_{\text{cat}}/K_{\text{NADPH}}$ revealed the importance of the ionization state of the 2'-phosphate moiety of NADPH.¹⁷⁰ However, experimental showed that NADPH is unstable at pH acid and is oxidized spontaneously, which leads to a variation in absorbance over time in the absence of MabA. For that reason, the pH of the experiment was then changed to the physiological pH 7. On the other hand, the dilution of MabA has been found to influence the catalytic activity. In fact, the enzymatic activity decreases rapidly when the concentration of the enzyme is below $1\mu\text{M}$.^{10,172}

Furthermore, the kinetic parameters of MabA enzyme were also determined. In order to examine the substrate specificity of the protein, longer-chain β -ketoacyl-CoAs (C_8 - C_{20}) were synthesized. Steady-state kinetic experiments gave a K_m value of MabA for each substrates (e.g., NADPH, acetoacetyl-CoA and others β -ketoacyl-CoAs ranging from C_8 to C_{20}). These results showed that MabA has a predilection for long-chain substrates, especially for C_{12} - C_{16} substrates.^{10,172} The affinity of MabA for the long chain hydrocarbon substrates is compatible with the size and hydrophobic nature of the substrate-binding pocket. This affinity was also observed in InhA enzyme with a slightly different for longer C_{16} - C_{24} substrates. The enzymatic activity of MabA and InhA, in particular their specificity for medium to long chain substrates, have once again confirmed the hypothesis that these enzyme belongs to the same mycobacterial fatty acids elongation system, FAS-II, which is known to be specific for long chain substrates.³³

A study has suggested a chemical mechanisms for the MabA-catalyzed reaction as described in Figure 39 on the basis of the experimental data.¹⁷⁰

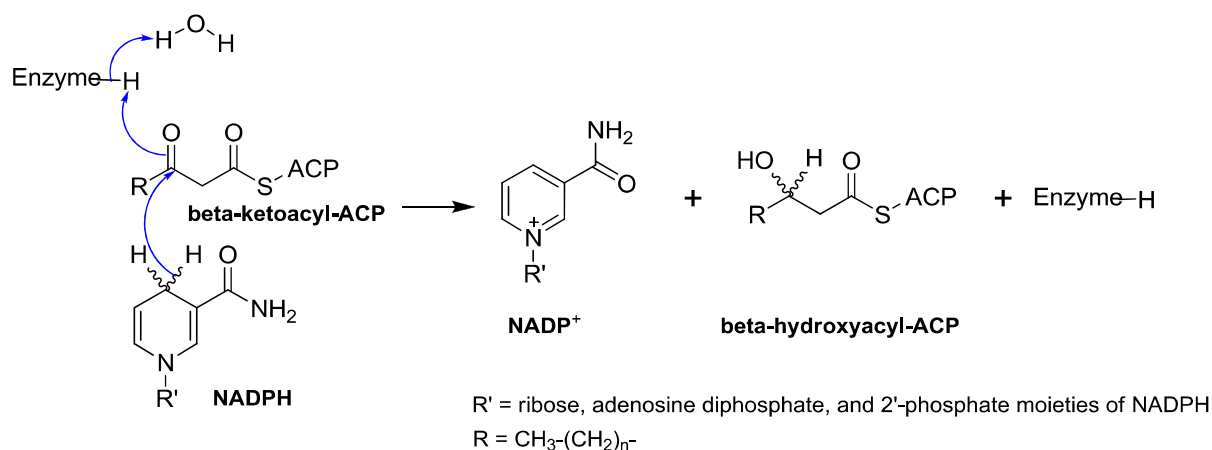


Figure 39: Proposed chemical mechanism for the β -ketoacyl-ACP-reductase-catalyzed reaction¹⁷⁰

2.3. Structure of MabA protein

2.3.1. Primary and secondary structure of MabA

The *mabA* gene of *M. tuberculosis* produces a protein which contains an amino acid sequence similar to β -ketoacyl-ACP reductases. This putative sequence with 247 amino acids was firstly published by Banerjee *et al.* in 1998.¹⁶⁵ In addition, these authors showed that a total soluble protein extract of *Escherichia coli* expressing *mabA* had an *in vitro* KAR activity (see 2.2). This hypothetical sequence of MabA protein was then confirmed by others studies^{10,173,174} in comparing with that of KARs (FabG) from others bacteria. Moreover, MabA secondary structures (α -helices, β -strands) were also assigned by homology and were used as additional restraints in the following modeling step (see Figure 40). The result showed that the N-terminal is not preserved; this region “floats” to the outside of the protein structure and does not correspond to a defined secondary structure. This suggests that this domain of the protein can tolerate variations and that it is not important for the function of the protein.

In addition, a search for the protein with peptide sequences similar to that of MabA in data banks^{10,173,174} was carried out in order to build a three-dimensional model of the MabA protein by molecular modeling. Firstly, MabA sequence is highly conserved among mycobacteria¹⁶⁵ as described above in section MabA gene (see Part A.2.1) while identity scores with other KARs from various others bacteria and plants, including those from *Escherichia coli* (KARec) and from *Brassica napus* (KARbn) ranged from 29 to 43% over the whole sequence about 240 amino acids. Most residues essential for cofactor binding and catalysis are well conserved in MabA sequence(see Figure 40).¹⁰

The search for related three dimensional structures indicated that MabA is similar with the KARs. This group of enzyme belong to a SDR enzyme family.¹⁷⁵ InhA is also an enzyme in SDR family and have many crystallized structure. However, MabA and InhA share only 20% sequence despite the similarity of their ligands. In contrast, the result showed that the closest structure to MabA is the PDB1EDO, with 40% identity. For that reason, the crystal structure of KAR from *Brassica napus* in complex with NADPH (PDB1EDO) was chosen as the template to build a three-dimensional model of *M. tuberculosis* MabA structure.¹⁰

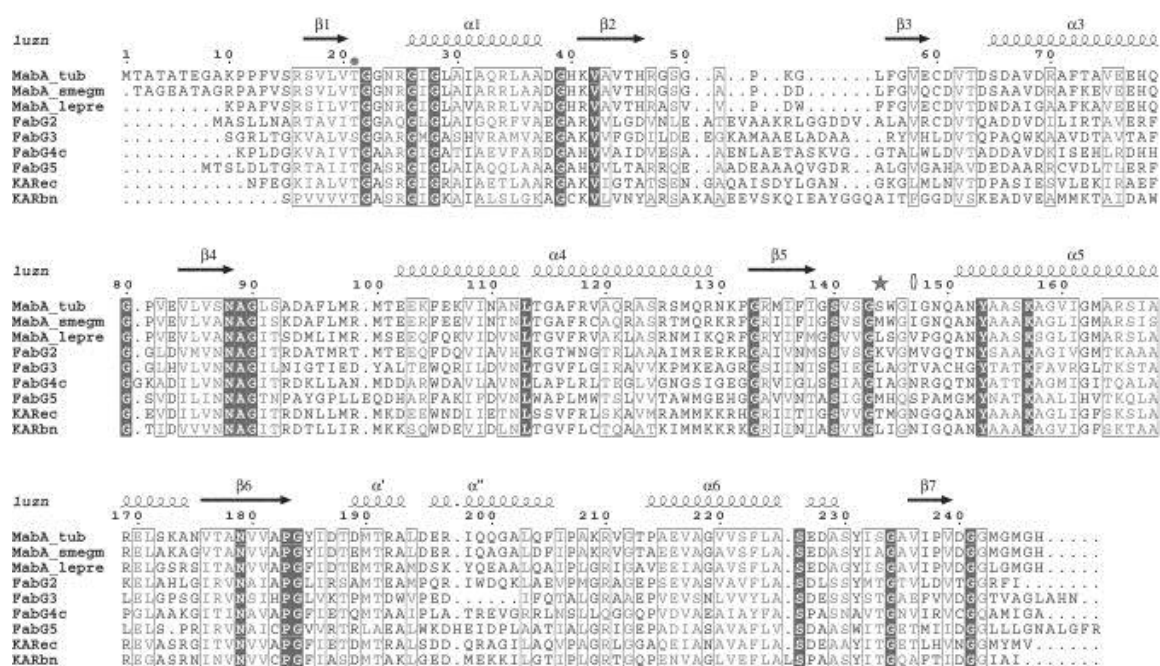


Figure 40: Sequences alignment of the tubercular MabA with others bacterial KARs¹⁷⁴
(adapted with permission from John Wiley and Sons publisher for ref. ¹⁷⁴)

This figure presents the sequences alignment of the MabA (FabG1) from *M. tuberculosis* with others bacterial KARs (MabA_tub: MabA from *M. tuberculosis*; MabA_smegm: MabA from *M. smegmatis*; MabA_lepre: MabA from *M. leprae*; FabG2, FabG3 (or PDB1NFG), FabG4c and FabG5: sequence of the four paralogs annotated in the *M. tuberculosis* genome; KARbn (or PDB1EDO): KAR from *B. napus*; KARec (or PDB1Q7B): KAR from *E. coli*. Secondary structure elements assigned from the crystal structure of MabA_C60V/S144L (PDB1UZU) are drawn on the top of the alignment.¹⁷⁴

Moreover, MabA has been proven to be a beta-ketoacyl-ACP reductase that catalyzes the NADPH-dependent reduction of beta-ketoacyl-acyl carrier protein to generate beta-hydroxyacyl-acyl carrier protein and NADP⁺. It means that this enzyme requires a cofactor (NADPH) for the catalytic action.¹⁰ So the tertiary structure of MabA like other SDR structures can be found in two forms: apo-enzyme and holo-enzyme.¹⁷⁵ The terminology ‘apo-form’ is used for the protein structure without the cofactor; this form is inactive and also called ‘closed-form’. In contrast, the name ‘holo-form’ or ‘open-form’ is used for the enzyme in complex with cofactors and/or its substrates as ligands.

2.3.2. 3D-structures of apo-MabA and the MabA-NADPH complex

In this context, the X-ray crystallography structure of MabA in apo-form was obtained at a 2.03 Å resolution.¹⁷³ The result confirmed the homology model of MabA which was built by molecular modelling.¹⁰ In fact, MabA tertiary apo-structure is similar to Rossmann folding that is usually found in dinucleotide-binding protein (see Figure 41). The central is hydrophobic which comprise seven stranded β -sheets (β 1 to β 7) in parallel. The β -sheet is flanked by helices α 1 and α 6 on one side and by helices α 3, α 4 and α 5 on the other side.¹⁷³

It has been noted that MabA protein has two specific features in 3D-structure. Firstly, the helix α 2 is not observed in MabA structure. Secondly, there are two others helices α' and α'' at the β 6- α 6 loop. However, the lack of helix α 2 and two additional helices have only small effect on the remaining structure of the protein and does not change the total conformation of Rossmann type in this enzyme.¹⁷³

In the apo-form of MabA, several residues are not visible in the electron density suggesting that these regions are highly flexible. They comprise of the N-terminal extension (residues 1-14), the residues in the $\beta 4/\alpha 4$ loop (residues 94-99) and $\beta 5/\alpha 5$ loop (residues 142-149).¹⁷³

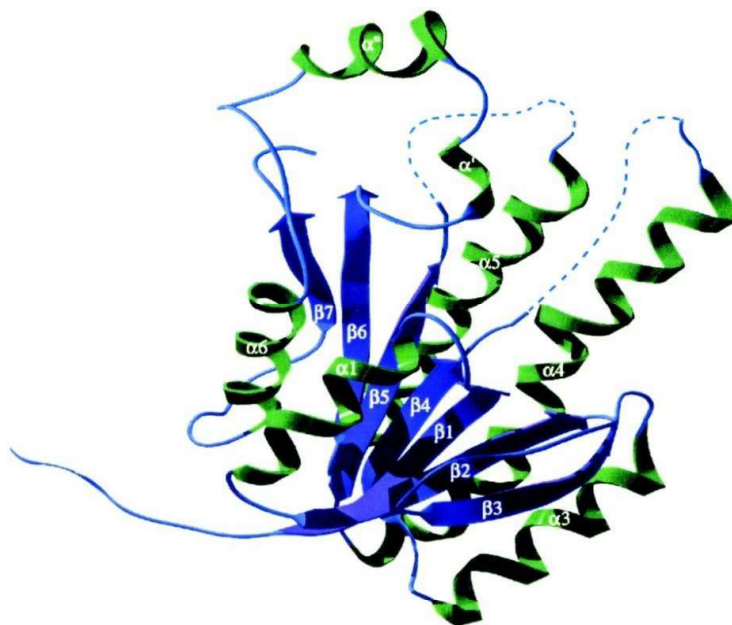


Figure 41: Global fold and topology of the crystal structure of MabA
(adapted with permission from Elsevier for ref.¹⁷³)

On the other hand, many efforts to co-crystallize MabA in complex with cofactor NADPH and/or its substrate have failed. For that reason, the structure of MabA holo-form was first modelled based on two templates (e.g. apo-MabA and holo-KARbn (PDB-1EDO) in binary complex with NADPH). The result showed that the conformational changes induced upon cofactor and/or substrate binding seemed to be located in the active site rather than involving the overall structure of MabA.^{173,176}

The active site in holo-form of the MabA protein was found to comprise three distinct parts. The first part is the binding site of NADPH cofactor which is found in an extended conformation resting on the C-terminal ends of the $\beta 1$ - $\beta 5$ strands. The $\beta 2$ strand contains a sequence specific to NADP(H)-dependent enzyme which is in the agreement with the enzymatic data showing the strict specificity of MabA for NADPH and indicates that the additional phosphate is probably important for the stabilization of the cofactor in satisfactory orientation for the catalysis. Moreover, the nicotinamide part of NADPH, involved in the ion exchanges, is oriented towards the bottom of the cavity. Secondly, the binding cavity of the substrate of MabA is probably delimited by the C-terminal ends of the strands $\beta 4$, $\beta 5$, $\beta 6$, $\beta 7$ and the helices $\alpha 4$, $\alpha 5$, $\alpha 6$ (including α' and α''). It has been noted that the bottom of the substrate-binding pocket appeared mainly hydrophobic in comparison to other KARs. These specific structural features can be explained by the specificity of MabA for long chain substrates. The third part of the active site is the catalytic triad including three residues Ser140-Tyr153-Lys157 which are conserved among short-chain dehydrogenase reductase members. This catalytic triad is surrounding by a patch of polar residues and a mainly hydrophobic region in face.^{172,173} (see Figure 42)

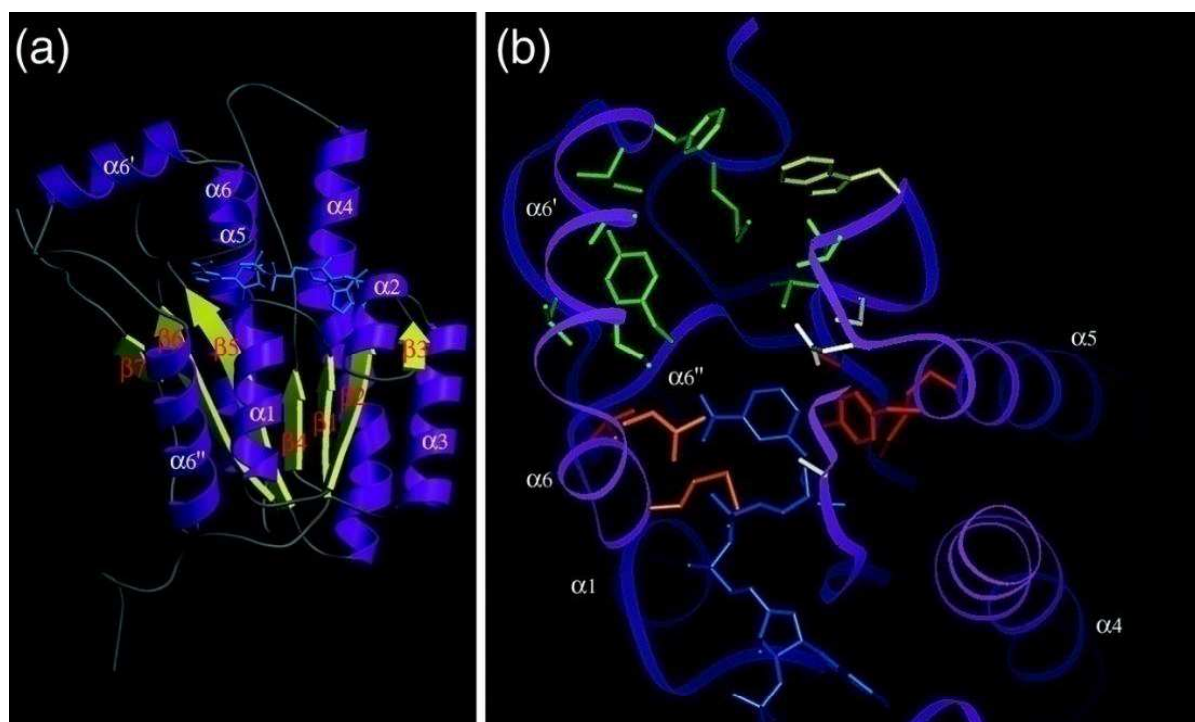


Figure 42: Ternary model of a MabA subunit complexed with one NADPH molecule

(adapted with permission Society for General Microbiology for ref.¹⁰)

(a): Complete view of the subunit MabA produced by using the MolScript program. α -Helices are colored in blue and β -strands in yellow; the trace of the amino acid chain is displayed as a ribbon. Secondary-structure elements are labelled. NADPH is drawn as blue sticks. **(b):** top view of the predicted active site of MabA designed by using the InsightII program (MSI). A rotation of 90° compared to the view in (a) was performed. The trace of the amino acid chain is colored in blue. The side chains of selected amino acid residues are shown including the hydrophobic residues at the bottom of the substrate-binding pocket are colored in green except for W145, which is in yellow. The catalytic triad is colored in red (S140, Y153, K157), polar residues surrounding the triad are in white and hydrophobic residues facing the triad are in orange.¹⁰

Another effort to yield the crystalline structure of MabA in holo-form was carried out with a double-mutant protein, MabA-C60V/S144L.¹⁷⁴ This activity of this mutant protein is equal to 84% of the wild-type activity. Moreover, affinity of NADP to this protein is similar to wild-type MabA. However, this double-mutant protein is more stable during purification (C60V) and stabilizes the catalytic loop in the holo-form (S144L). The structure of this mutant protein in co-crystallized with oxidized cofactor (NADP⁺) was solved at a 1.91 Å resolution and displayed an “open” form (see Figure 43). We observed that the region between β_6 and α_6 displayed a little change in comparison with apo-MabA. However, the β_4/α_4 loop, β_5/α_5 loop and the very end of the C-terminus (245–247) in both monomers are not visible in electron density like in structure of apo-MabA. In addition, the NADP⁺ is partial invisible. In fact, the adenosine part and the three phosphate groups are visible, the nicotinamide moiety and the corresponding ribose appeared disordered. The visible part of the cofactor is stabilized by various interactions including a highly conserved hydrogen-bonding network. These residues comprise the aspartate D61, the glycine-rich loop β_4 – α_4 , and asparagine N88. The additional 3-phosphate group interacts with the side chains of two arginines R25 and R47. Furthermore, the hydrophobic side chain of residue leucine L144 is in close contact with isoleucine I161 and also surrounded by two hydrophobic side chains alanine A158 and valine V236 while lying in the vicinity of the C-terminal histidine H247 from a second monomer. These interactions are in agreement with previous modelling studies.¹⁷⁴

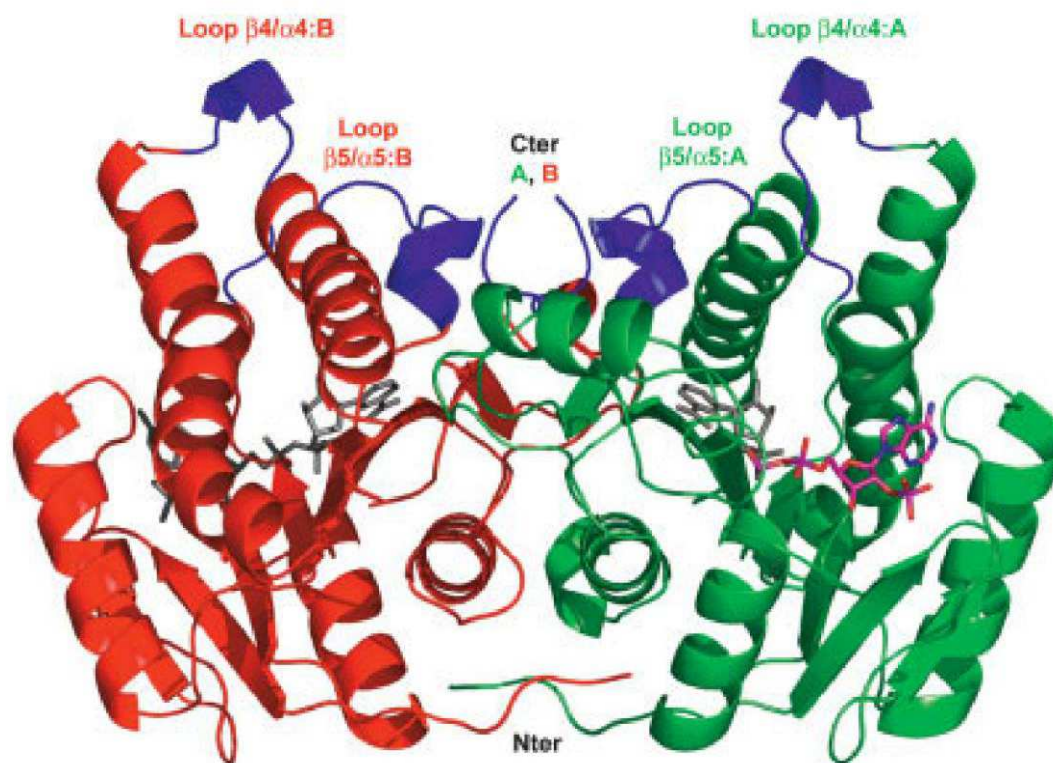


Figure 43: Overview of the crystallographic dimer of holo-form MabA_C60V/S144L

(adapted with permission from John Wiley and Sons publisher for ref. ¹⁷⁴)

The monomer named A is colored in green and the monomer named B in red. In monomer A, the visible part of the NADP (the adenosine and the three phosphates) is represented in pink, orange, and blue. The nonvisible nicotinamide moiety and the corresponding ribose in A and the entire NADP⁺ in B were modeled and are shown in gray. The presence of the NADP⁺ leads to some conformational changes in and around the catalytic site. Consequently, the loops $\beta 4/\alpha 4$, $\beta 5/\alpha 5$ and the C-terminus of both monomers are structured. These regions of the protein are shown in blue. This figure was produced using PyMol.

2.3.3. Quaternary structure of MabA

Quaternary structure of MabA was firstly developed base on the known structures of others SDR proteins. In literature, all the described SDR structures are dimeric or tetrameric.¹⁷⁵ Similarly, results from gel filtration chromatography and sedimentation equilibrium experiments both showed that MabA are in form of a tetrameric structure. The result also suggested that there is an equilibrium between the dimeric and tetrameric forms of MabA in solution.¹⁰ In addition, another study by analytical ultracentrifugation method suggested that the MabA enzyme was presented as a dimer in solution at concentration of 8 μM .¹⁷⁰

The tetrameric structure of MabA was also analyzed.¹⁷³ There are two interfaces in tetrameric structure. The first is the C-terminal region corresponding to the $\alpha 6$ - $\beta 7$ loop and the $\beta 7$ strand which has a very high similarity with the equivalent region of the known tetrameric KARs. These structural components have an important role in stabilizing the asymmetric unit. The second dimer interface is composed of the two helices $\alpha 4$ and $\alpha 5$. These residues in these two interfaces are hydrophobic.^{172,173} An illustration of the quaternary structure of MabA is presented in Figure 44.

A study on the switch from the “closed” to the “open” conformation of MabA was conducted by Cohen-Gonsaud and his colleagues.¹⁷⁴ These authors have pointed out different

properties between the tetrameric structure of holo-form and apo-form MabA. The overall structure of MabA protein the tetrameric structure is well conserved in both the “open” and “closed” conformations.¹⁷⁴

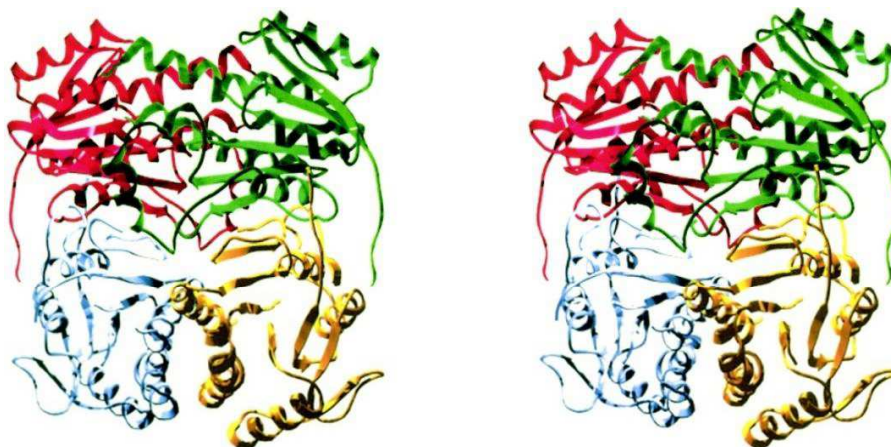


Figure 44: Stereo drawing of the tertiary structure and quaternary structure of MabA
(adapted with permission from Elsevier for ref.¹⁷⁵)

Each individual subunit of the tetramer is colored differently. The two types of interfaces are shown. The α 4- α 5 interface (helix bundle) is observed between the blue and yellow monomers. The β 7 interface is observed between the blue and red monomers. The figure was produced using Swiss-PDB Viewer and POV-Ray.

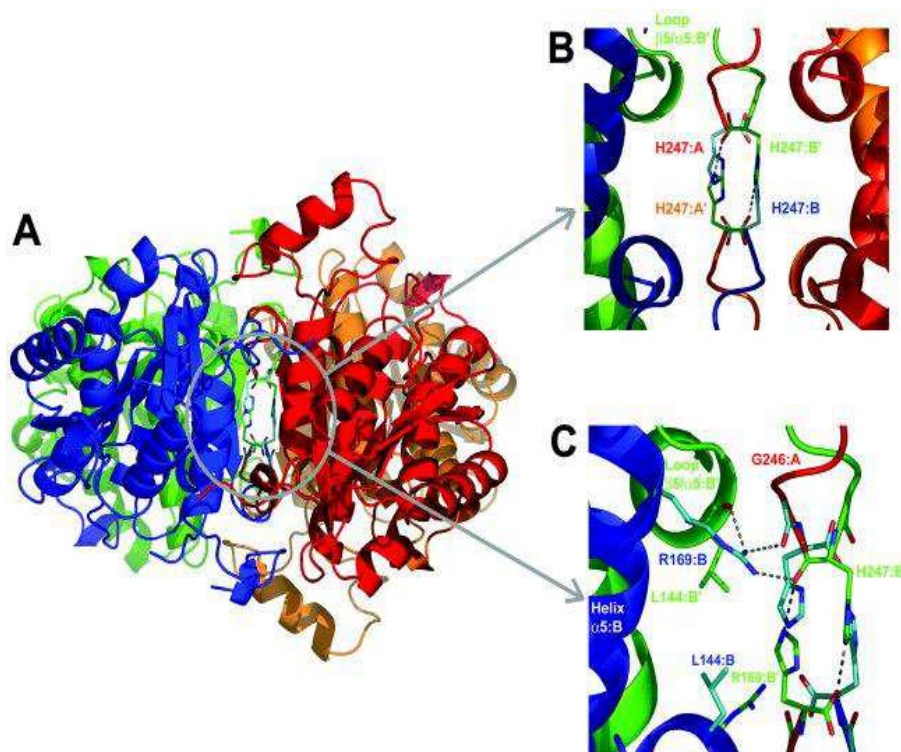


Figure 45: Quaternary structure of the holo- MabA tetramer induced by NADPH
(adapted with permission from John Wiley and Sons publisher for ref.¹⁷⁴)

(A) Overview of the “open-form” of the MabA tetramer. The monomers were named A (in red), B (in blue), and the crystallographic symmetric named A’ (in orange) and B’ (in green). The four C-terminus (motif: “GGMGMGH”) of each monomer lay down at the common buried interface of the tetramer. (B) Detail of the common buried interface of the tetramer. The histidine H247 side chains from a monomer points at hydrogen-bonding distance toward the main-chain carboxyl group of the histidine of the crystallographic symmetric monomer. The region is surrounded by the loop β 5/ α 5 of the four monomers. (C) Element of the hydrogen-bond network between the C-terminus, the loops β 5/ α 5, helix α 5, water molecules (not showed) of the four monomers created by the binding of the cofactor, the loop β 5/ α 5, and the C-terminus.

When the cofactor binds to MabA, the conformational changes seem to be restricted to the active site and the neighboring C-terminus. The authors observed only a stabilization of the segments $\beta 5$ – $\alpha 5$ and the C-terminus in the holo-form of MabA. In fact, the two C-terminal residues (glycine G246 and histidine H247) clearly appeared in the electron density of the “open” conformation of both the double mutant (C60V/S144L) and the wild-type enzymes. In the apo-conformation, these two amino acids are not visible.¹⁷⁴

The tetrameric structure of MabA is stabilized by the C-terminus of MabA (motif “GGMGMGH”) which is buried at the tetrameric interface. In fact, the four C-terminal segments are in close contacts. The histidine H247 side chain from one monomer forms a H-bond with the main-chain carboxyl group of a histidine of another monomer. This conformation is also stabilized by favorable interactions with neighboring residues including arginine R169. Each arginine R169 side chain formed a H-bond with the carbonyl of residue at position 144 of the related monomer.¹⁷⁴

2.4. Relation between structure and function of MabA

The three-dimensional structure of MabA in previous section reveals a serine-tyrosine-lysine (S140-Y153-K157) catalytic triad¹⁷³ which is conserved among short-chain dehydrogenase reductase members.¹⁷⁵ For that reason, these amino acids have been believed to play an important role in the enzymatic activity of MabA. Indeed, serine S140 was shown to have an indirect role in NADPH binding and in catalysis. In the “closed” apo-form of MabA, several rearrangements impact on the structure of the active site in comparison to the “open” holo-forms. When “closed” conformation switches the “open”, the phenol ring of the catalytic tyrosine Y153 rotates by 90° that are induced by the hydroxyl group of “catalytic” serine S140. Furthermore, the catalytic serine S140 and valine V141 have been found moving by 5 and 8 Å, respectively. This particular rearrangement prevents entrance of the ribose and the nicotinamide ring of NADP. Therefore, the movement of the catalytic residues (S140 and Y153 in this case) seems to activate the enzyme (see Figure 46).

Moreover, a study of Rosado and coworkers¹⁷⁷ on site-directed mutagenesis of MabA enzyme at position serine S140 confirmed that two mutant proteins, MabA_S140T and MabA_S140A, have no enzymatic activity. Although the S140T protein showed affinity with cofactor NADPH. The results suggest that the main role of S140 residue is in MabA activity. The S140 side chain has been suggested to play an indirect role in NADPH binding. Interestingly, NADPH titration curves shifted from sigmoidal for wild-type MabA to hyperbolic for S140A, suggesting that the S140 residue may play a role in displacing the pre-existing equilibrium between two forms of MabA in solution.¹⁷⁷ Therefore, a compound which is able to block MabA in its inactive conformation (apo-form) by binding to the catalytic residues (e.g. S140, Y153 and K157) was believed to be able to inhibit the MabA enzymatic activity.¹⁷⁷

On the contrary, several mutant assays on MabA protein have been observed to induce just a partial loss of MabA enzymatic activity. In MabA, the cysteine C60 residues located at the C-terminus of strand $\beta 3$ which cause a rapid formation of an inter-chain disulphide bridge in MabA_wt purification step. For that reason, MabA_wt enzyme is not stable in the crystallographic condition. A site-directed mutagenesis was then performed to substitute this

unique cysteine residue by a valine residue. The MabA_C60V mutant appeared to be more stable. However, this mutant MabA_C60V displayed a lower activity than the wild-type enzyme (only 60% of wild type activity) and a slightly decreased affinity for the cofactor as shown by spectrofluorimetry. Comparisons of the two structures revealed no significant changes in the vicinity of the mutation. Thus, the partial loss of activity of MabA_C60V can be related to change in an overall dynamic of the NADPH-binding site.¹⁷³

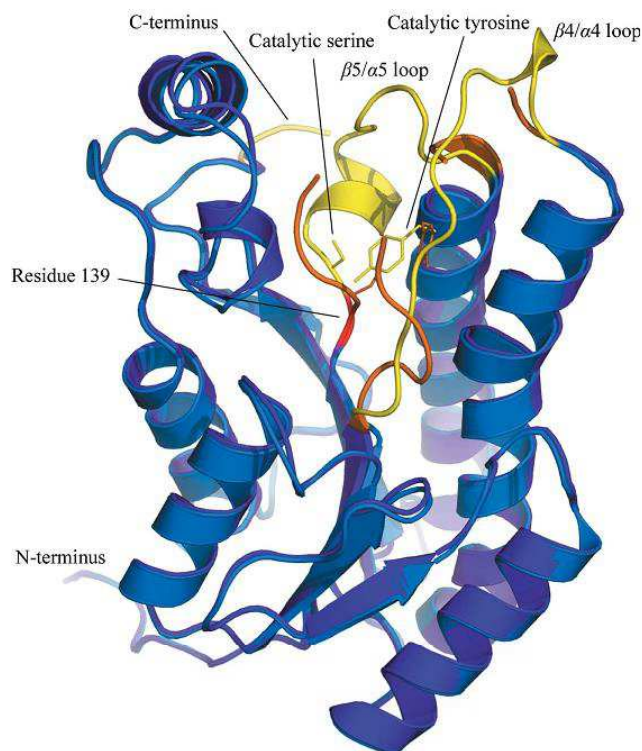


Figure 46: Superposition of the closed form (in light blue) and the open form (in dark blue) of MabA

(adapted with permission from the International Union of Crystallography for ref. ¹⁷⁸)

The catalytic S140 and Y153 are shown in stick representation. The rearranged regions of the protein are represented in yellow for the open form and orange for the closed form. Residue 139 is colored red.

In another study conducted by Cohen-Gonsaud and coworkers¹⁷⁴, a design and the crystal structures of a double-mutant protein, MabA_C60V/S144L in the presence and the absence of a cofactor was carried out. In the predicted structure of holo-MabA, the serine S144 would be surrounded by three apolar residues (I161, A180, and P238). This serine residue S144 in MabA would be located at the C-terminus of a helical conserved turn in the connecting loop $\beta 5$ - $\alpha 5$ of the SDRs. In this study, the authors predicted that the presence of a leucine has a stabilizing effect by an enhancement of the hydrophobicity. Also, a leucine residue is expected to stabilize the predicted α -helical conformation. In steady-state kinetic experiments, this mutant enzyme retained 84% of the wild-type enzyme activity, and has an affinity for the cofactor similar to that of the wild type.¹⁷⁴

Moreover, another study was conducted in order to identify a mutation that would stabilize the complex of MabA with both the cofactor and a ligand, a substitution of glycine G139 by alanine was thus predicted to decrease the conformational dynamics observed in the apo-form of the wild-type enzyme. This triple mutant MabA_C60V/G139A/S144L bearing an alanine instead of a glycine at position 139 was generated and has been found to be totally

inactive in the steady-state kinetic experiments in the presence of acetoacetyl-CoA and NADPH. This result opens new perspectives for drug-design studies by finding a noncompetitive inhibitor that locks the protein in its closed and ‘inactive’ state.¹⁷⁸

On the other hand, a study conducted by Veyron-Churlet and coworkers¹⁷⁹ showed that MabA was efficiently phosphorylated *in vitro* by several *M. tuberculosis* serine/threonine protein kinases, including PknB, as well as *in vivo* in mycobacteria. Mass spectrometric analyses using LC-ESI/MS/MS and site-directed mutagenesis identified three phosphothreonines (T21, T114 and T191) in which threonine T191 has been proven to be the primary phosphor-acceptor. Further assay with MabA_T191A and MabA_T191D mutant was designed to mimic constitutive phosphorylation, exhibited markedly decreased ketoacyl reductase activity compared with the wild-type protein, as well as impaired binding of the NADPH cofactor, as demonstrated by fluorescence spectroscopy. In fact, the activity of MabA_T191A and MabA_T191D was around 22% and 10% of MabA_wt, respectively. These results clearly indicate that T191 plays a critical role in the catalysis, as supported by its strategic location on the MabA three-dimensional structure. Replacement of T191 by an alanine residue may possibly prevent formation of a hydrogen bond between residue 191 and the MabA substrate and/or NADPH, resulting in reduced KAR activity. Besides, this inhibitory effect on KAR activity was even more pronounced for MabA_T191D than for MabA_T191A presumably due to the negative charge carried by the Asp residue. Previous studies have shown that acidic residues such as asparagine or glutamate qualitatively mimic the effect of phosphorylation with regard to functional activity. Indeed, introducing a negative charge, for example, *via* a phosphate group, may destabilize α helix and prevent correct binding of both substrate and NADPH. Therefore, by adding a phosphate group to T191, *M. tuberculosis* has developed an original and powerful strategy by weakening the activity of MabA, subsequently leading to partial inhibition of mycolic acid production.¹⁷⁹

Moreover, the isoleucine residue I147 in MabA could be responsible for the recognition of substrates with longer acyl chains. In order to test this hypothesis, a substitution of this isoleucine residue by asparagine at position 147 in MabA was performed. While this mutant protein MabA_I147N appeared less stable, a partial functional characterization could be performed by fluorescence. The affinity constant for short and medium-length substrates, C₄ and C₁₂, were measured for the I147N mutant and the wild-type purified proteins and the result agreed with the proposed model of the substrate-binding site, and the role that I147 may play in the specificity of MabA. In addition, the lower degree of stability of the I147N mutant protein observed during the purification step suggested that the mutated residue could be involved in the stabilization of the active-site loop and/or interaction with surrounding hydrophobic residues such as tryptophan W145.¹⁷³

Furthermore, tryptophan W145 and isoleucine I147 in MabA structure are brought into the substrate-binding site. A significant change of the tryptophan W145 environment upon cofactor and ligand binding was reported.¹⁰ In the “open” form, the tryptophan W145 side chain is sandwiched by the side chains of methionine M243 and arginine R169. The hydrophobic environment in the active site cavity made up by the tryptophan indol ring and

the neighboring methionine M243, and isoleucine I147 might correlate with the unusual specificity of MabA for long-chain substrates.¹⁷⁴

In a study on the inhibition of INH-NADP adduct on the activity of MabA enzyme¹⁶², these authors suggested that a hydrophobic interaction with the isonicotinoyl moiety of INH-NADP could readily make a π - π stacking with the tyrosine residue Y185 that faces serine S140. Alignment of the MabA sequence with that of KARs of 16 other organisms (bacteria or plants) revealed that the position equivalent to Y185 most often corresponds to a phenylalanine residue. In one case only over 16 KARs, it corresponds to a leucine. To investigate the potential involvement of Y185 in the binding of the INH-NADP adduct to MabA, the residue was changed to leucine by directed mutagenesis, and the mutated protein was purified. The MabA_Y185L mutant protein was crystallized under conditions similar to those used for the MabA_wt protein. The crystal structure of the mutant enzyme revealed that the Y185L mutation did not induce any significant changes in the overall structure of the protein. The enzymatic activity of MabA_Y185L is about 70% compared to that of the MabA_wt protein under identical experimental conditions. Indeed, the strong conservation of an aromatic residue at position 185 among the known KARs suggested that it is important for enzymatic activity. The observed loss of activity upon replacement of tyrosine by another hydrophobic residue (leucine) is in agreement with its location within the active site. Moreover, the IC₅₀ of the INH-NADP adducts measured for MabA_Y185L appeared to be three times greater than that for the MabA_wt protein. These results showed that the interaction of MabA with a substrate or a cofactor derivative such as the INH-NADP adduct, but not with the cofactor, was significantly affected by the Y185L mutation. This result confirmed the above hypothesis of the MabA-adduct complex suggesting that the stabilization of isonicotinoyl-NADP in the MabA active site is partly based on the interaction between the isonicotinoyl moiety and the aromatic ring of residue Y185.¹⁶²

2.5. Validation of MabA as a target for antitubercular drugs

In 2007, Parish and coworkers¹⁸⁰ have conducted a study to determine whether the FAS II complex, especially *mabA* gene, is essential for *M. tuberculosis*. The results demonstrated that this gene can be deleted from the *M. tuberculosis* chromosome only in the presence of another functional copy. This can be considered as a formal genetic proof that *mabA* is indeed an essential gene under culture conditions. FabG1 activity can be replaced by the corresponding enzyme from the closely related species *M. smegmatis* but not from *Escherichia coli*. Furthermore, *M. tuberculosis* carrying FabG from *M. smegmatis* showed no phenotypic changes, and both the mycolic acids and cell wall permeability were unchanged. These authors concluded that *M. tuberculosis* and *M. smegmatis* FAS-II enzymes are interchangeable and do not control the lengths and types of mycolic acids synthesized.¹⁸⁰

Moreover, a study¹⁷⁹ on the mutant of MabA in threonine T191 residue showed that the decrease in KAR activity of MabA_T191D mutant is relevant *in vivo* in mycobacteria was subsequently demonstrated by: (i) impaired mycobacterial growth of an *M. bovis* BCG strain transformed with a multicopy vector carrying the *mabA_T191D* allele and (ii) inhibition of *de novo* biosynthesis of mycolic acids following conditional expression of the phosphomimetic MabA_T191D in this strain. Thus, this result suggested that complete inhibition, leading to

mycolic acid cessation and cell death, is likely to occur in the context where endogenous MabA protein would be missing. These above results suggested that the MabA (FabG1) protein from *Mycobacterium tuberculosis* could be a validated drug target for the design and development of novel antitubercular agents.¹⁷⁹

Furthermore, the *fabG* gene is also predicted to be essential in others species e.g. *E. coli*¹⁸¹ and *M. smegmatis*¹⁶⁵. Therefore some author suggested that KARs could be used as targets for broad-spectrum antimicrobials. However several studies have previously shown that the MabA has specific functional and structural properties compared to those of the homologous bacterial KAR. In fact, this enzyme has a large hydrophobic substrate binding pocket, which correlates with its preference for long-chain substrates. Therefore, MabA could be considered as a specific target for the design new TB drugs.

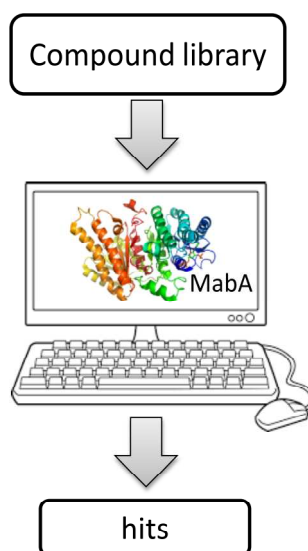
3. Conclusion

The above review on MabA has shown that this mycobacterial enzyme is a key component of FAS-II in *M. tuberculosis*. Inhibition of this enzyme will block the biosynthetic pathway of mycolic acids and consequently inhibit the growth of *M. tuberculosis*.^{10,180} In addition, no drug-like inhibitors of MabA enzyme were reported until now. Therefore, MabA was considered as a target of choice to start a new antitubercular drug discovery program.

Part B. Identification of potential compounds targeting MabA by virtual screening

Firstly, we applied a virtual screening method to identify MabA inhibitors. In general, there are two fundamental approaches for virtual screening, e.g. ligand-based approach and receptor-based approach. The ligand-based virtual screening aims to identify molecules with physical and chemical properties similarity to some known ligands of the target. This approach comprises the pharmacophore based and molecular descriptor-based virtual screening. On the other hand, receptor-based virtual screening uses the 3-D structure of the binding site in protein to impose a structure-based filter. Then a chemical database will be screened to select potential hits that would interact with the residues in the binding site of protein.¹⁸²

Until now, there is only the INH-NADP adduct which was reported as MabA inhibitor.¹⁶² So it seems more challenging if we apply the ligand-based approach for virtual screening. In contrast, the complex structure of the cofactor NADP and MabA was co-crystallized (PDB-ID: 1UZN). For that reason, we decided to develop an *in silico* screening by using a structure-based approach.

Figure 47: Principle of structure-based *in silico* screening

1. Compound library preparation

The virtual compound database ZINC was used in this study. This library contains 35 million commercially available compounds that are usable for structure based virtual screening. Compounds are provided in ready-to-dock, 3D formats.¹⁸³ We conducted a combination search in order to filter the drug-like compounds (conformed to Lipinski's rule).

Table 8: Predefined subset criteria for drug-like compound library

Predifined subset	Criteria
Structure	containing isoniazid scaffold
molecular weight (p.mwt)	$150 \leq \text{p.mwt} \leq 500$
XlogP (p.xlogp)	$-4 \leq \text{p.xlogp} \leq 5$
rotatable bond (p.rb)	$0 \leq \text{p.rb} \leq 7$
Polar surface area (p.psa)	$0 < \text{p.psa} < 150$
H-bond donors (p.n_h_donors)	$\text{p.n}_h_donors \leq 5$
H-bond acceptors (p.n_h_acceptors)	$\text{p.n}_h_acceptors \leq 10$

After the combination filtering in ZINC database and due to limitation in the calculation, we selected 4081 drug-like compounds.

2. Protein structure preparation

The MabA structure was obtained from PDB. The chosen protein structure was 1UZN in which MabA is binding NADP.¹⁸⁴ The MabA-NADP complex structure was then analyzed by CLC Drug Discovery Workbench 1.0.2 to predict the binding pocket (Figure 48). For docking study in CLC program, the protein structure was optimized in this software before screening. The results showed that 1UZN is a homo-dimer with two chains A and B. There are 271 water molecules in this structure (displayed by red point in Figure 48). There are two cesium atoms binding two each chain. A partial structure of NADP cofactor was found in a binding pocket of chain A. This structural position was then chosen as binding pocket for virtual screening.

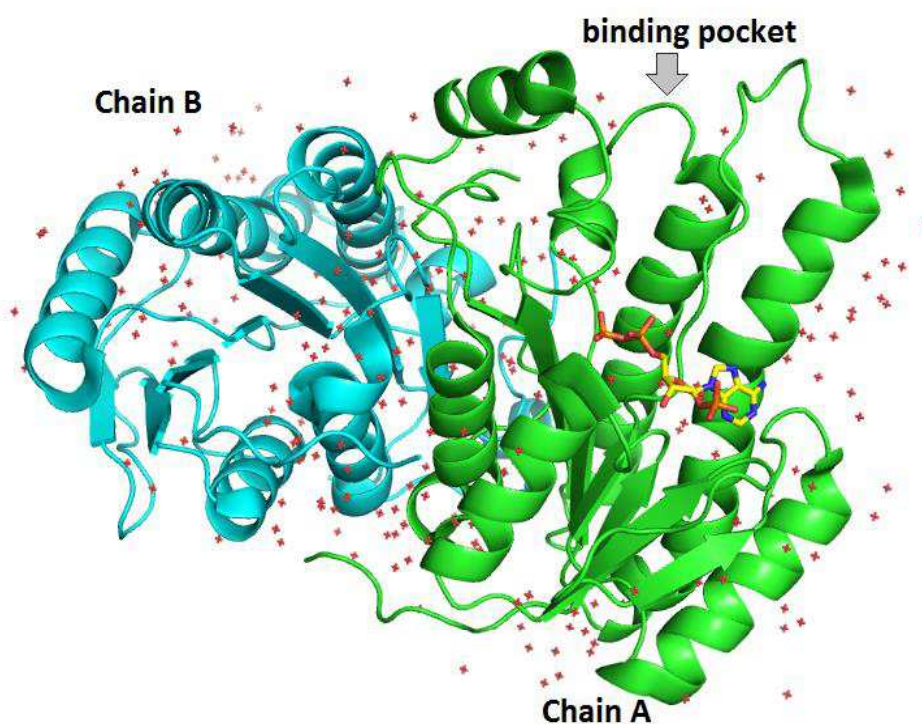


Figure 48: Analysis of MabA X-ray structure PDB-ID:1UZN

3. Virtual screening

In the first screening step using CLC Drug Discovery Workbench 1.0.2, the docking target was setup with following parameters: the binding site was centered by the predicted binding pocket that contains the NADP in 1UZN (volume = 1437.76 \AA^3) with the radius about 13 \AA . This binding site is located on the chain A of this protein. All glutamic acids, aspartic acids and histidine residues in this binding site were either deprotonated or protonated at pH 7. The cofactors and water molecules were removed. The docking score used in the Drug Discovery Workbench is the PLANTSPLP score.¹⁸⁵ This scoring algorithm mimics the potential energy change, when the protein and ligand come together. It scores the interaction affinity between target and ligand by rewarding and punishing different types of heavy atom contacts (inter atom distance below $\sim 5.5 \text{ \AA}$) including: H-bond interactions, lone-pair-metal ion interactions, non-polar interactions, non-polar-polar contacts and repulsive contacts. In this scoring function, a more negative score corresponds to a strong binding and a less negative or even positive score corresponds to a weak or non-existing binding. The CLC screening of the chemical compound library (4081 compounds) predicted the top 10%. The grid scores of these compounds were estimated to be below the threshold of -52 kJ/mol .

The top 409 compounds obtained from the first step could bind to the active site of MabA with a high affinity. However, the active site is so large (1437.76 \AA^3) that the compound could not block all surface of this pocket. For that reason, we suggested that the compound which can bind to the catalytic triad of this active site have more chance to inhibit the enzymatic activity of MabA.

In the second step, we applied the AutodockVina docking algorithm in PyRx program, which performs receptor–ligand docking to explore flexible ligand conformations and allows partial receptor flexibility. In PyRx platform, the chosen macromolecule needs to be

optimized for virtual screening preparation. The macromolecule was cleaned from solvents and cofactor molecule and Cs atoms by using Chimera (version 1.9).¹⁸⁶ The hydrogens were then added. This structure need to be optimized by AutoDockTools in MGLTools 1.5.4 and Gasteiger partial charges and AutoDock force field were applied.

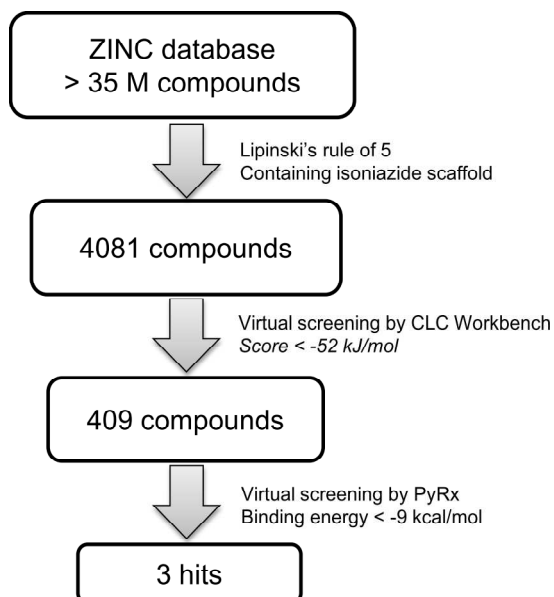


Figure 49: Virtual screening procedure

In the first step, we tried to redock the full structure of NADP cofactor to MabA. The result showed that NADP can bind to the binding site of MabA with an affinity = -10.5 kcal/mol (see Figure 50).

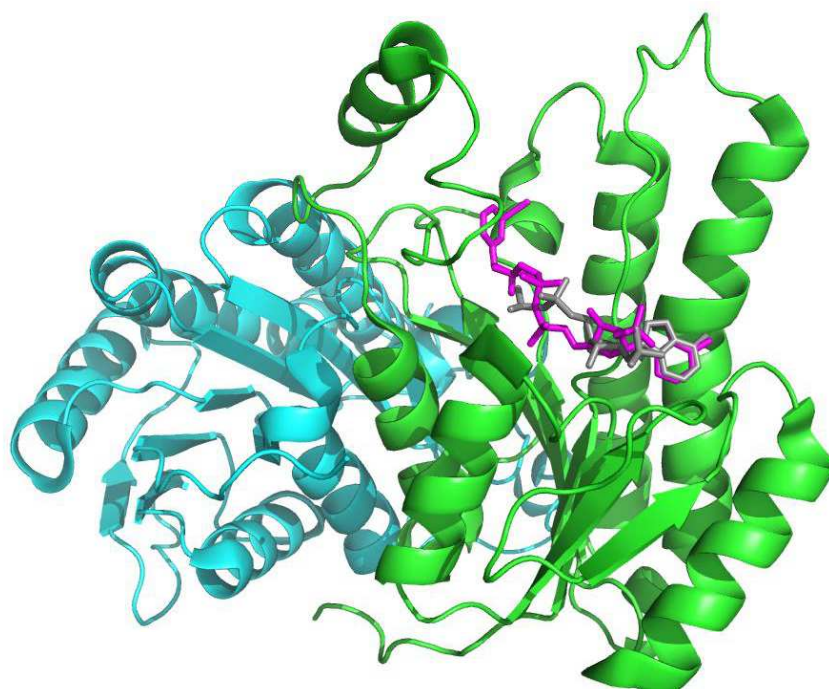


Figure 50: Superimpose between partial NADP co-crystallized (grey) and re-docked NADP (rose)

Using the 409 compounds identified from the first step, virtual screening was done using AutodockVina in PyRx software. Grid parameters were centered at this position: center_x = -0.149, center_y = 12.902, center_z = 8.971 with size_x = 18.0, size_y = 18.0, size_z = 18.0. This position is surrounded by serine-tyrosine-lysine catalytic triad (S140-Y153-K157).

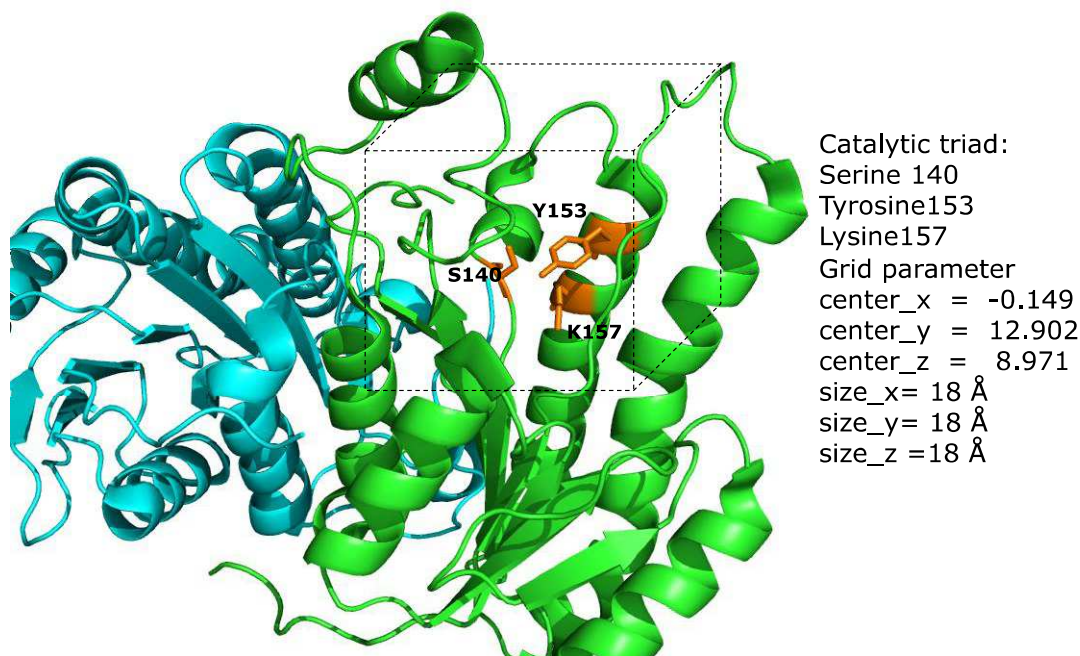
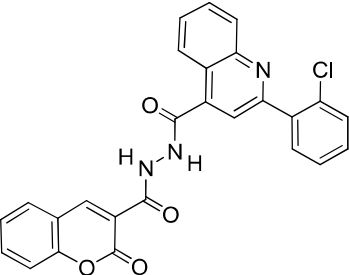
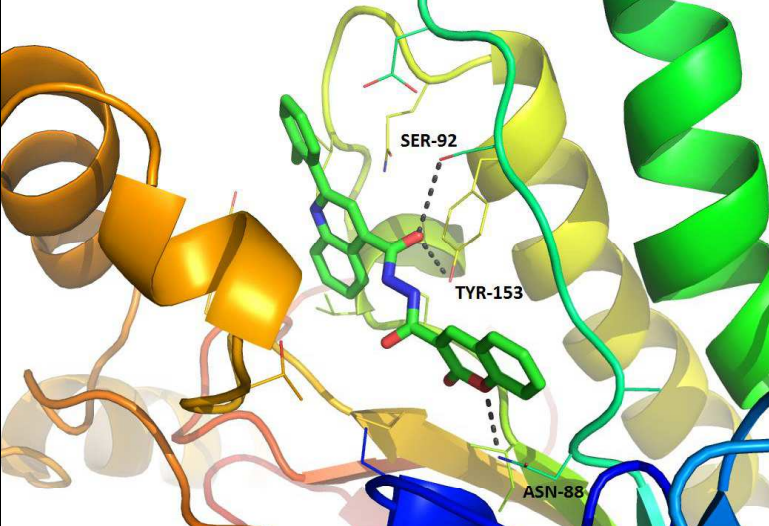
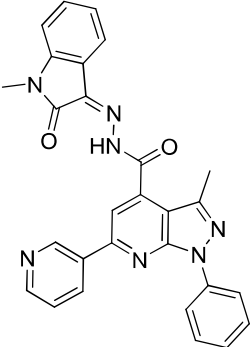
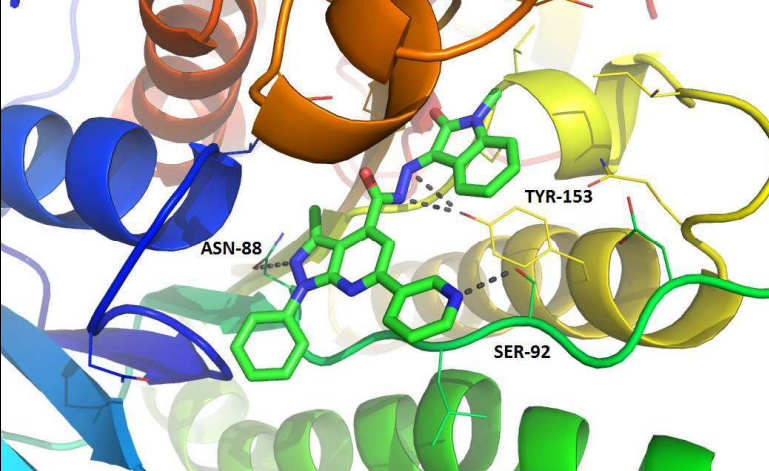
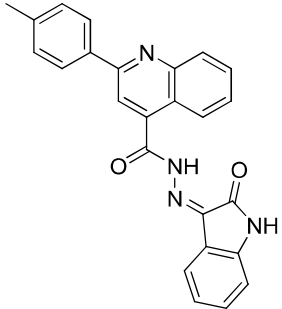
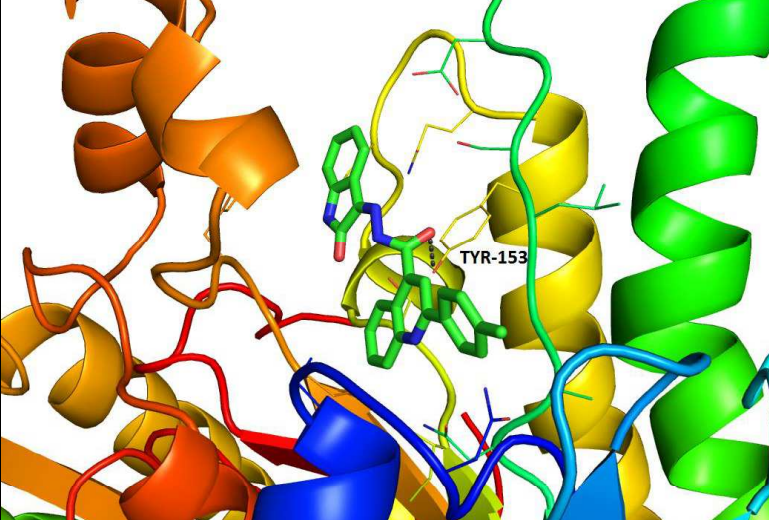


Figure 51: Grid parameter in Autodock (PyRx) screening

The AutodockVina program evaluates the calculated results of the protein-chemical compound hydrogen bonding energy, the van-der-Waals contact energy, and the torsion energy to determine binding energy between the protein and ligand. The result were presented in binding energy and top 3 ranking compounds with binding energy threshold below -9.0 kcal/mol were considered as hits. (Table 9)

The best docking pose of these hits in MabA were analyzed using Pymol software (Schrodinger, Inc.). The H-bond between these ligands and residues at binding site were also identified (Table 9). We observed the role of tyrosine-153, serine-92 and asparagine-88 in forming the H-bond (dash-lines) with the 3 hits. As a result, these ligands could prevent the interaction between residues of the catalytic triad and substrate. Consequently, the enzymatic activity of MabA would be inhibited

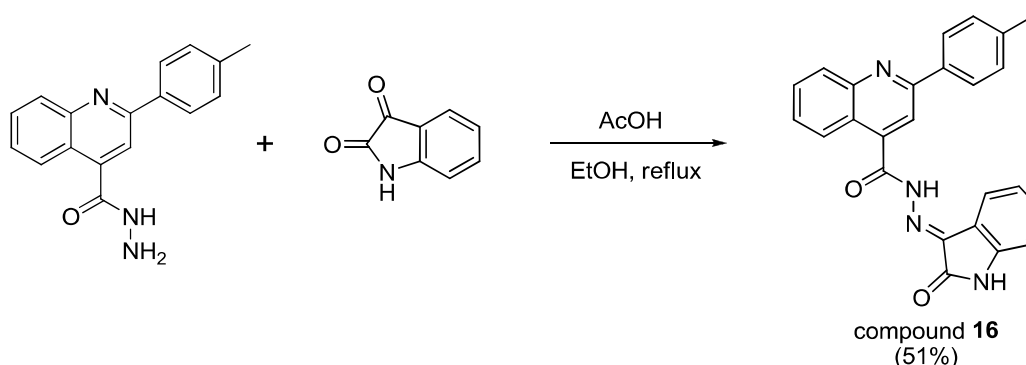
Table 9: Top 3 hits from PyRx-Autodockvina screening

Structure and docking score	Interaction with residues in MabA
 <p>ZINC-03375877 -9.5 kcal/mol</p>	 <p>SER-92 TYR-153 ASN-88</p>
 <p>ZINC-03264375 -9.3 kcal/mol</p>	 <p>TYR-153 ASN-88 SER-92</p>
 <p>ZINC-05601203 -9.1 kcal/mol</p>	 <p>TYR-153</p>

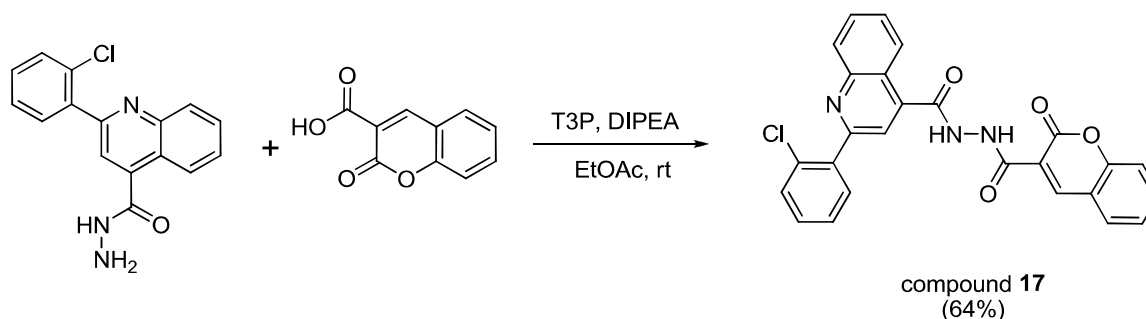
Colors legend for ligand: green = carbon, dark blue = nitrogen, red = oxygen, yellow = sulfur. Black dashed lines indicate the hydrogen bond interactions of the ligand with the backbone residues. Images were generated with Pymol.

4. Testing hits in MabA enzymatic assay

Two hits (ZINC-05601203 and ZINC-03375877) were synthesized from commercial building blocks. These reactions are presented respectively in Scheme 7 and Scheme 8. Compound ZINC-03264375 was purchased from Enamine.



Scheme 7: Synthesis of *in silico* hit ZINC05601203



Scheme 8: Synthesis of *in silico* hit ZINC03375877

The three *in silico* hits were then tested in an enzymatic assay. However, the three compounds did not show any inhibitory activity even at the highest tested concentration. This disappointing result may be partly explained by the lack of solubility encountered with the three hits, which did not allow us to achieve active concentrations. Finally, this result prompted us to work with more soluble molecules such as fragments to identify MabA inhibitors.

Part C. Design and synthesis of novel MabA inhibitors by fragment-based approach

These advantages of fragment-based drug discovery have encouraged us to apply this approach for the screening of MabA. In fact, the probability that a ligand binds to an active site of a protein is inversely proportional to its size. Since drug-like ligands in HTS are more specific in binding and therefore have less chance to fit any given active site, fragments with smaller size have more chance to bind to targets. Moreover, these small bioactive compounds can easily penetrate mycobacterial cell wall to bind to MabA.

In practical terms, a fragment-based approach starts with a screening. Then the identified and validated hits are optimized by rational design to drug-like molecules. In a first paragraph, we will describe an overview of several methods that can be used for the screening

of fragments. Then we will present the results of the different screenings we performed on MabA for the identification of hits.

1. Fragments screening methods

In general, there are two different types of screening techniques used in fragment-based approaches: function-based methods and affinity-based methods. First, function-based screening can measure the small variation of target activity induced by specific binding of a fragment. However, screening conditions must be usually optimized for each target showing different functions. Several affinity-based screening methods have also been developed. These techniques must be very sensitive to detect the weak interactions between fragments and targets. In consequence, fragment concentration during such a screening is usually high (100 μ M to 10 mM).¹⁰¹ All fragment screening methods are summarized in Table 10 and several relevant techniques were described in detail herein.

1.1. Thermal shift assay

One of the biophysical technique used to screen fragments is the fluorescence-based thermal shift assay (TSA) also called differential screening fluorimetry (DSF). This method is based on the thermal-denaturation of a protein that is recorded using a fluorescent probes. Upon binding of the sensitive fluorescent dye to hydrophobic pockets, an increase of fluorescence is recorded. The inflection point of the protein unfolding curve is defined as the melting temperature (T_m). Compounds that stabilize the native protein in a more stable conformation will increase the melting temperature. Hits are therefore identified by measuring the difference of this T_m value for protein in presence or absence of the tested molecule. It has been reported that this temperature shift (ΔT_m) is proportional to both ligand concentration and binding affinity.¹⁸⁷ This technique is particularly useful as it is a cost-effective method and readily applicable in high-throughput.^{104,188} However, this method does not discriminate between compounds that bind to the active site of the targeted protein and those that will only stabilize the protein without having any functional activity.¹⁸⁹

1.2. Nuclear magnetic resonance

Nuclear magnetic resonance (NMR) is the first FBDD screening method developed at Abbott Laboratories in the 1990s. This technique is also named as structure activity relationship (SAR) by NMR.⁹⁵ Nowadays, two principal strategies have been developed: protein-observed NMR and ligand-observed NMR.

Protein-observed NMR monitors changes in isotopically labeled (either ^{13}C or ^{15}N) protein in the presence of ligands. Chemical shifts of the target in the presence and absence of the ligand are observed and compared in two-dimensional (2D) hetero-nuclear single-quantum coherence (HSQC) spectra. This method provides the structural information about interaction of the ligand at the binding site. However, there is limit on protein size to approximately 40 kDa. These requirements severely restrict the range of proteins that could be targeted by this method.^{104,190}

In an effort to expand the application of NMR screening to other targets, a number of ligand-based NMR methods were introduced that detect binding via changes in the spectrum

of the ligand. Two notable ligand-based NMR methods are Water-Ligand Observed via Gradient Spectroscopy (WaterLOGSY) and saturation transfer difference (STD). WaterLOGSY detects fragment binding by magnetization transfer from bulk water to fragments, via stable bound water molecules in the protein-fragment complex. STD exploits a magnetization transfer process directly from the protein to the bound fragment. Furthermore, many other NMR-based fragment screening methods have been developed, notably Target Immobilized NMR Screening (TINS) and Labeled Ligand Displacement (LLD).¹⁰⁴

All ligand-detected NMR experiments can be used in competition with a known ligand to the target. Competition screening lowers the false positive rate and allows focusing on a particular binding site on the target. An advantage of this approach is that the target is not isotopically labeled. However, a limitation of the ligand-observed NMR experiments is that no information of the binding site is obtained. Like other screening methods at high concentration, fragment libraries for NMR-based detection technique also need to be composed of very soluble fragments.^{104,191,192}

1.3. X-ray crystallography

X-ray crystallography is a useful technique for determining protein structures. In FBDD, this method is very important as it provides direct validation of the fragment binding. Moreover, it can be routinely used to generate high-resolution structural information to direct chemical elaboration during hit-to-lead and lead optimization. However, fragment screening using X-ray crystallography is sometimes technically challenging. First, a major drawback is the finding of suitable experimental conditions to obtain crystal structures of the protein; then the crystal system must have an accessible binding site and be capable of withstanding soakings of fragments at high concentrations. Data must be collected for each soaked crystal and the resultant electron density maps need to be interpreted to determine whether or not fragment binding has occurred. This is an extremely time consuming and laborious process. Therefore, X-ray crystallography is often used to confirm and characterize hits obtained from other screening techniques.^{104,190}

1.4. Mass spectrometry

In normal mass spectrometry (MS), biomolecule (protein) are usually denatured in vacuum under high electric field. However, native MS is a modified method from electrospray ionization ESI-MS which allow maintaining protein and even fragment-protein complex in their native state. Analysis of the protein-ligand complexes then allows for determination of both binding stoichiometry and dissociation constants (K_d). This method consumes a very small amount of protein. However, the stability of the fragment-protein complexes in native MS is not correlated with the solution phase affinity. This can be explained by the variation of polar and hydrophobic interaction when solution transform directly to gas phase.^{101,190,193,194}

1.5. Surface plasmon resonance

Surface plasmon resonance (SPR) can be used to measure affinity of a ligand and kinetic parameters of ligand-protein interactions in a fluidics-based system. Typically, using

SPR fragment binding affinity is measured in real time based upon changes in the local index of refraction at the surface of a sensor chip where the target protein is immobilized.¹⁸⁹

This is a label-free method. The sensitivity and throughput of the latest generation of SPR instruments facilitate the detection of interactions between fragments and proteins at low-affinity. The screening can be realized with a large fragment library. Rapid screening of entire fragment libraries by SPR is now possible within a few weeks. For example, the Biacore 4000 (GEHealthcare) benefits from rapid assay development and low-target consumption (typically consuming as little as 25–50 µg of protein for an entire SPR screening campaign).¹⁰¹ However, the high concentration required to detect weak-affinity fragments limits the use of SPR to sufficiently soluble fragments.

1.6. Weak affinity chromatography

The principle of this technique is based on weak affinity separations of small fragment. Protein must be immobilized on a silica column. When the mobile phase pass through the column, the different affinity of fragment are demonstrated by different retention time. In order to increase throughput, this method can be coupled with MS detection.¹⁹⁵

1.7. Ultrafiltration

Ultrafiltration is used to separate between unbound and bound fragments. In fact, a compound library was incubated with the protein target. Filtration of the mixture through a membrane will retain large molecule (protein and fragment-protein complex) but allows small molecules (unbound fragments) to traverse. Composition of the filtrate and initial mixture is compared to identify which fragments bind to target. Moreover, the bound fragments can be released from the complex by a competitive ligand. Following ultrafiltration, the filtrates were analyzed by HPLC/MS method.¹⁹⁶

1.8. Virtual screening method

Recently, several *in silico* screening techniques have also been applied in fragment hit selection. Firstly, molecular docking can be used as a complementary method to predict the binding mode for a validated hit in the absence of X-ray structural information. On the other hand, the virtual method can also be used as part of an *in silico* primary screening, the hits selected from this virtual screening should be then validated by other biophysical methods. This method can be applied with a large number fragment library including the virtual fragments. However, virtual screening still plays a minor role in fragment screening until now.¹⁰¹

Table 10: Screening methods in fragment-based approach^{101,190}

Method	Principles	Advantages	Disadvantages
Function-based assay	Level of substrate or cofactor or product can be measured by a suitable method (absorbance, fluorescence or MS)	function-based method ; average throughput	Requires biochemical function (usually enzyme) ; high concentration of fragment
Thermal shift assay	Measure the thermal stability shift of protein upon binding with fragments	a small quantity of protein require ; high-throughput	difficult to detect weak interaction; solubility of protein must be considered
Protein-based NMR	Determination of interaction effects on NMR spectra of labelled protein	3D-structure information at the binding site ; low false positive rate	High protein consuming ; protein must be labeled ; low throughput
Ligand-based NMR	Observation effects of ligand and protein interactions on ¹ H or ¹⁹ F NMR spectra of fragment	moderate to low protein consumption ; average throughput ; no labeled require	moderate protein consuming ; moderate throughput
X-ray crystallography	Measure the electron density of protein with bound fragments	3-D structure information ;	High protein consumption ; low throughput ; high false negative
Tethering	Fragment form S-S with cysteine residue, detect mass of covalent complex	Target to a specific site of target based on cysteine mutation position.	Fragment must contain SH ; mutant protein.
Mass spectra	Fragment-protein complex was analyzed by MS under careful conditions	Low protein consumption ; average to high throughput	Fragment-protein affinity in solution and gas phase are not correlated
Surface plasmon resonance	Detect of changes in optical properties of surface containing protein with ligand	Low protein consumption ; moderate to high throughput	Require protein immobilization (on Au surface)
Isothermal titration calorimetry	Measure thermal changes upon fragment-protein binding	Free-label, solution-based method	Low throughput
capillary electrophoresis	Interaction fragment-target is display by reduce in mobility shift of probe ligand	Free-label; solution-based method; low protein consumption	Require a probe ligand of target
Affinity chromatography	Measure retention time of fragments on a column	Free-label protein;	Require immobilization of protein
Ultrafiltration	Separation of bound and unbound fragments through a membrane	Free-label; high throughput	
Biolayer interferometry	Optical analysis of the white light reflected from biolayer upon fragment binding	Label-free ; interactions are measured in real-time	Require immobilization of protein
In silico method	Docking fragments to protein and ranking by a scoring function	High throughput; no protein and fragment consumption	Results need to be confirm by others method

1.9. Conclusion

Nowadays, many screening techniques have been developed for fragment screening. Each method presents advantages and drawbacks. For some screening methods, as the protein consumption level can be high, the production of the protein in large quantities should be possible. Moreover, for some cases protein needs to be immobilized (SPR, affinity chromatography) and/or labeled (protein-observed NMR) or mutated (tethering) prior screening. In addition, most of screening methods are usually conducted at high concentration requiring a high aqueous solubility for the tested fragments. Some techniques require fragments to incorporate specific atoms or functions such as fluorine atoms for ^{19}F -NMR or thiol function for tethering.

In order to select a suitable technique for a screening process, many criteria need to be considered but an important advantage of biophysical screening methods listed above is that they can measure the special weak interactions between fragment and targets. Last but not least, the throughput of screening methods is also an important point to consider when starting a screening.

2. Primary screening of U1177 fragment library on MabA

2.1. The first version of U1177 fragment library

The first version of our in house fragment library contained 1040 molecules coming from commercial suppliers or from in-house library of building blocks. This library was assembled with compounds that respect the commonly accepted "Rule-of-Three" and other physicochemical and structural properties.¹⁰³ Compounds were selected using filters: molecular weight (MW <300), number of H-bond donors ≤ 3 , number of H-bond acceptors ≤ 3 , hydrophobicity (cLogP <3), and calculated aqueous solubility (pSw < 5). Compounds containing reactive functional groups were discarded. The detailed properties of this library are analyzed in the chapter IV of this thesis. The set of 1040 fragments was formatted in barcoded 96-microplates ready for screening.

2.2. Fragment screening by thermal shift assay

In our laboratory, thermal shift assay (TSA) has already been used to measure the affinity of drug-like and fragment-like compounds to the mycobacterial transcriptional regulator EthR.^{118,128,145} We decided to apply this method for the screening of our fragments on MabA. The principle of the thermal shift assay, as described in previous section, lies on the monitoring of the thermal unfolding of the protein using a conformation-sensitive dye, SYPRO Orange, in which fluorescence is quenched in aqueous solution but enhanced in a nonpolar environment, such as the hydrophobic domain of unfolded protein.

The assay is carried out on standard Q-PCR instruments in 96-well plates. Results are produced as graphs (Figure 52) showing the fluorescence intensity of SYPRO Orange as a function of temperature. The inflection of the sigmoid curve indicates the melting temperature (T_m) of the protein. The variation of the melting temperatures between holo-MabA and apo-MabA (ΔT_m) demonstrate capacity of fragments to stabilize the MabA protein in a liganded conformation. This value is directly correlated to the affinity of the fragments to MabA.

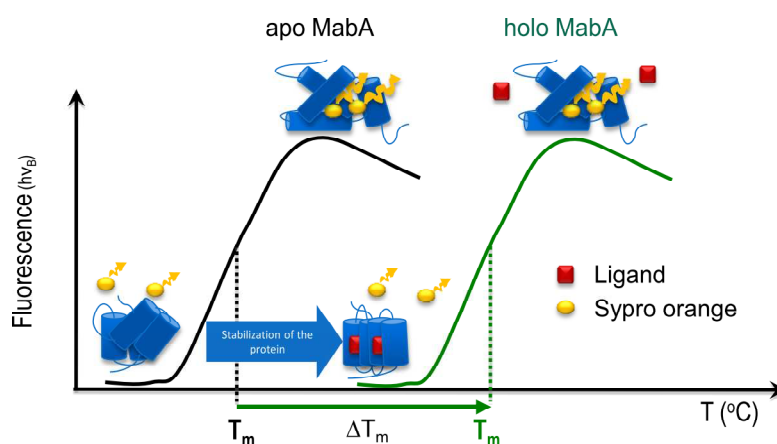


Figure 52: Principle of thermal shift assay

The experimental conditions were optimized to allow the screening of fragments at 1 mM. The apo-MabA protein showed a reproducible melting temperature of $41.9^{\circ}\text{C} \pm 0.1^{\circ}\text{C}$. NADPH cofactor was used as positive control in this assay and the holo-protein, e.g. liganded with NADPH, showed a higher melting temperature ($T_m = 48.3^{\circ}\text{C} \pm 0.2^{\circ}\text{C}$), which corresponds to $\Delta T_m = 6.4^{\circ}\text{C}$. With these conditions in hands, we then screened the entire fragments library (1040 fragments) and the results are presented in Figure 53.

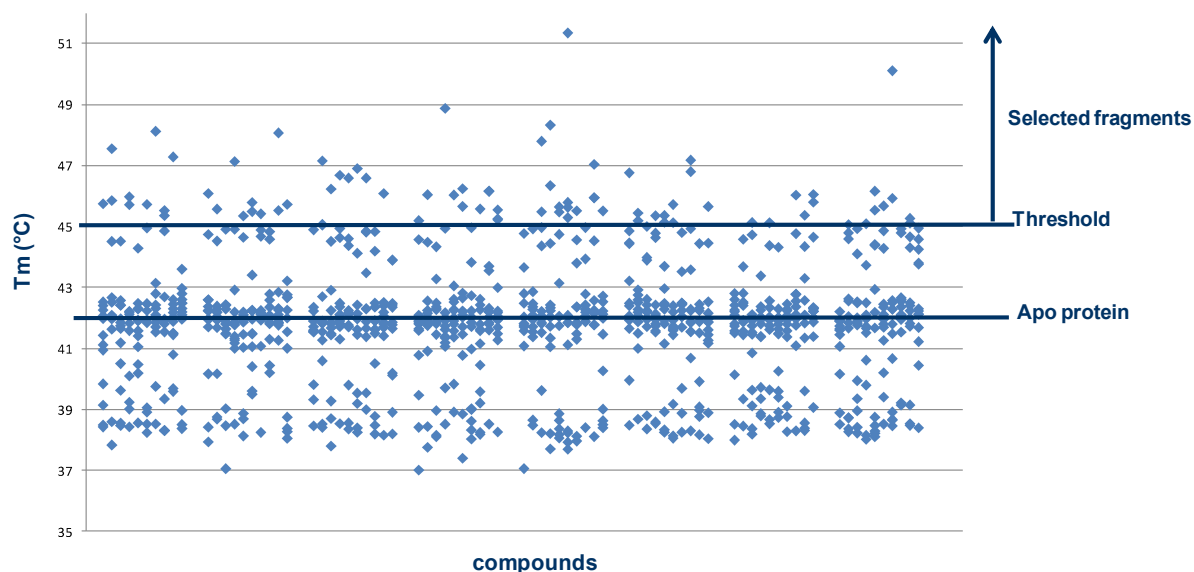


Figure 53: T_m distribution of MabA in complex with the 1040 fragments

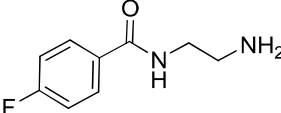
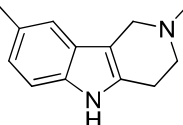
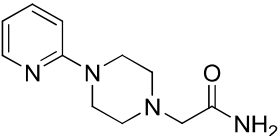
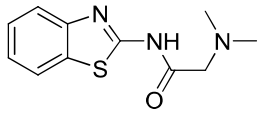
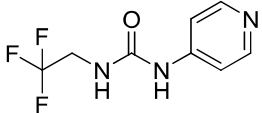
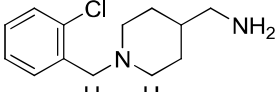
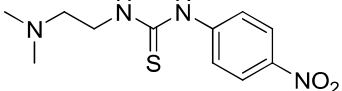
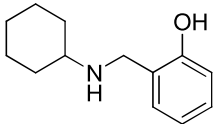
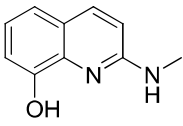
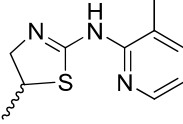
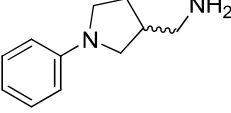
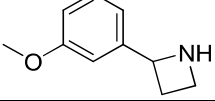
We decided to select fragments having a T_m greater than 45°C ($\Delta T_m > 3^{\circ}\text{C}$). Thus, 82 fragments were conformed to this criteria (hit rate = 7.8 %). These fragments were then confirmed in a dose response experiments.

2.3. Selection of candidates for further optimization

In order to select hits to be further optimized, we tested the 82 fragments using a HCS phenotypic assay where the growth of *M. tuberculosis* in infected macrophages is monitored. In this assay, Raw264.7 macrophages harboring GFP-expressing *M. tuberculosis* H37Rv were used. The growth of intra-macrophage bacteria was measured in the presence and absence of fragments. Results are presented in percentage of inhibition of *M. tuberculosis* growth.

Compounds were tested at 1 mM in a buffer containing 1% DMSO. 100% inhibition was obtained using isoniazid at 0.1 μ g/mL. From the 82 fragments displaying a ΔT_m higher than 3 $^{\circ}$ C, 12 fragments were confirmed to be bactericidal at 1 mM (%inhibition > 80%) without showing any toxicity on macrophage. The structure of these 12 fragments and their activities are presented in Table 11.

Table 11: List of selected fragments from TSA and HCS

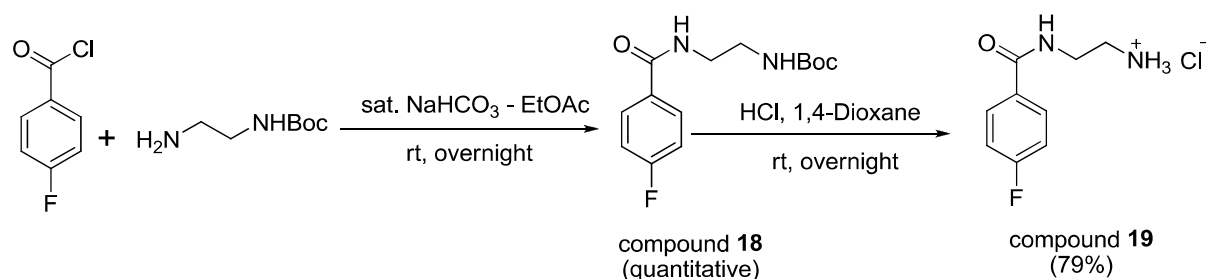
Fragment ID	Structure	ΔT_m	% inhibition
1		3.1	> 95
2		3.7	> 95
3		3.7	> 95
4		3.8	> 95
5		4.1	> 95
6		5.4	80
7		3.1	> 95
8		3.3	82
9		4.8	> 95
10		3.7	> 95
11		3.9	> 95
12		3.8	> 95

3. Validation of the 12 hits using a functional assay

In order to clearly validate that the bactericidal activity identified for the 12 hits could be associated to an inhibition of MabA, we developed a functional assay. In parallel, the resynthesis of the hits was performed.

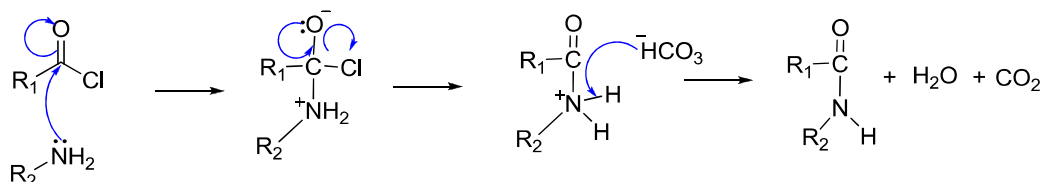
3.1. Synthesis of fragment ID-9098328

The fragment hit ID-9098328 was obtained from fluorobenzoyl chloride in two steps. In the first reaction, 4-fluorobenzoyl chloride was coupled with *N*-Boc-ethylenediamine in a mixture of water and EtOAc.¹⁹⁷ This reaction was carried out in basic condition, using saturated NaHCO₃ solution to afford the amide **18** in quantitative yield (Scheme 9).



Scheme 9: Synthesis of fragment hit ID-9098328 (compound 19)

The mechanism of this nucleophilic addition–elimination is illustrated in Scheme 10. First, the carbon in carbonyl group of acyl chloride is attacked by the nucleophilic amine, nitrogen atom acting as an electron pair donor. Simultaneously, the π electron pair of the C=O double bond moves onto the oxygen atom to give it a full negative charge. Second, the C-Cl bond pair moves onto the chlorine atom and leaves a chloride anion. In the same time, one of electron pair from the negative oxygen shift to reform the C=O bond. Finally, a base (in this case is NaHCO₃) will remove a proton to yield the desired amide.

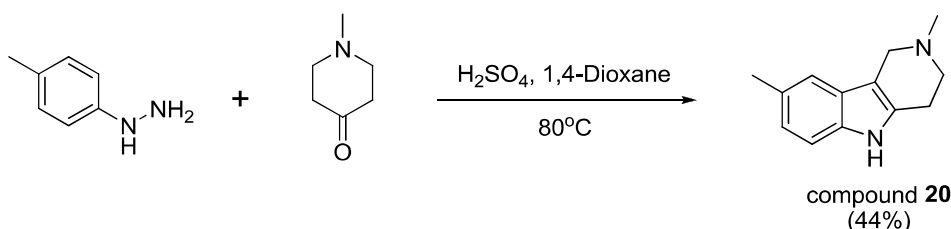


Scheme 10: Mechanism of amide formation from acyl chloride

The Boc-protecting group of amide **18** was then removed under acidic condition¹⁹⁸ to give the desired compound **19** in a good yield (79%).

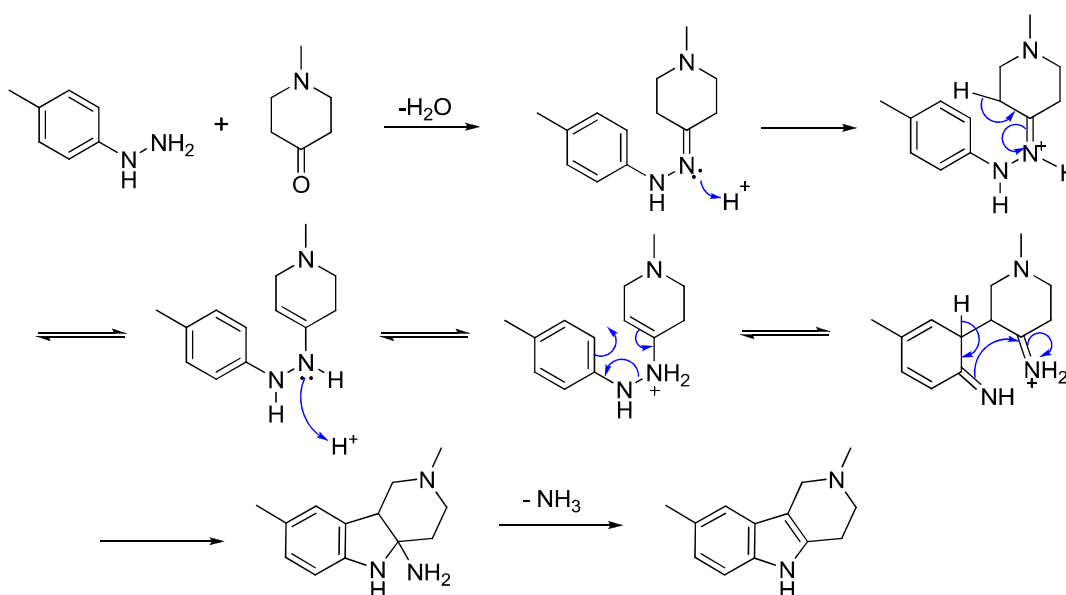
3.2. Synthesis of fragment ID-5161544

The fragment ID-5161544 was synthesized using a Fischer indole reaction between *p*-tolylhydrazine and 1-methyl-4-piperidone.¹⁹⁹ This reaction was catalyzed by sulfuric acid in 1,4-dioxane to afford the desired aromatic indole **20** in 44% yield.



Scheme 11: Synthesis of fragment hit ID-5161544 (compound 20)

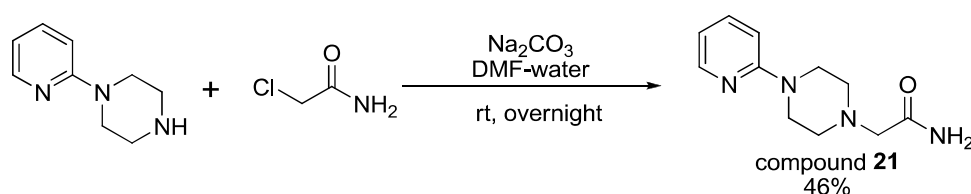
The mechanism of Fischer indole synthesis is described in Scheme 12. *N*-aryl hydrazone is converted into indoles under Brønsted acid (H_2SO_4) catalysis with loss of ammonia. Firstly, hydrazone tautomerized to an enhydrazine which by a [3,3] sigmatropic rearrangement, establishes a C-C bond in the ortho-position of the arene (diaza-cope rearrangement). The resulting di-imine was then converted into 2-amino-1,2-dihydroindole. This intermediate finally cyclized to give indole with elimination of NH_3 .



Scheme 12: Mechanism of Fischer Indole synthesis

3.3. Synthesis of fragment ID-9055294

The hit ID-9055294 was synthesized by alkylation of 1-(2-pyridyl)piperazine using 2-chloro-acetamide (Scheme 13).²⁰⁰ This reaction was conducted in a mixture of water and DMF under basic condition. After purification by flash chromatography, the desired compound **21** was obtained as white solid in 46% yield.



Scheme 13: Synthesis of fragment hit ID 9055294 (compound 21)

3.4. Synthesis of fragment ID-9052337

Hit ID-9052337 was obtained thanks to the coupling 2-benzo-thiazolamine with *N,N*-dimethylglycine using T3P as activating reagent.²⁰¹ DIPEA was used to deprotonate the

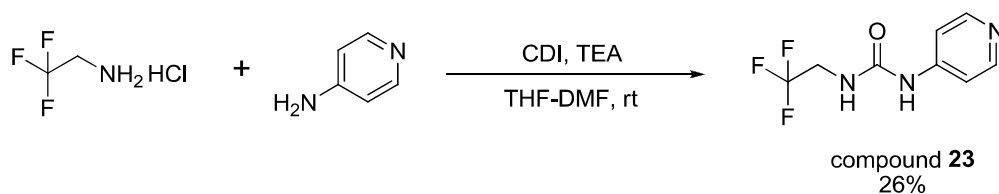
carboxylic acid. Purification by flash chromatography allowed isolating the desired amide **22** in 55% yield.



Scheme 14: Synthesis of fragment hit ID-9052337

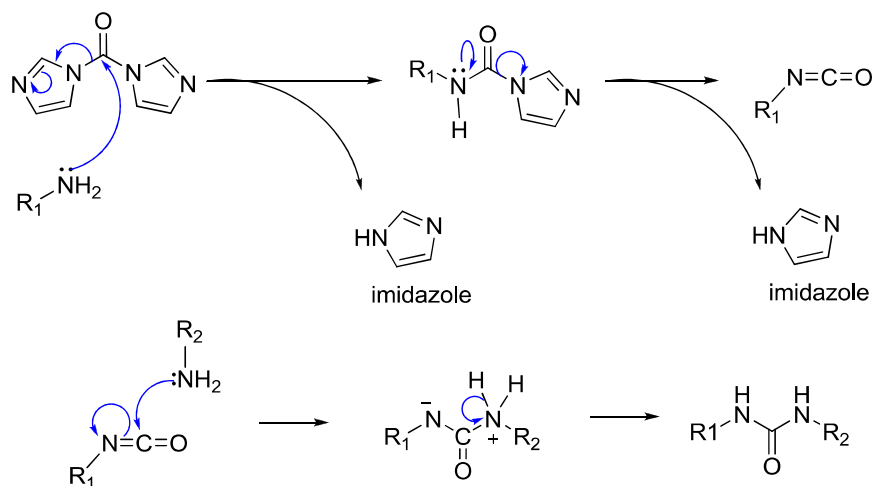
3.5. Synthesis of fragment ID-7930121

The urea ID-7930121 was synthesized from 4-amino-pyridine and 2,2,2-trifluoroethylamine by using carbonyldiimidazole (CDI) as electrophilic reagent.



Scheme 15: Synthesis of fragment hit ID-7930121

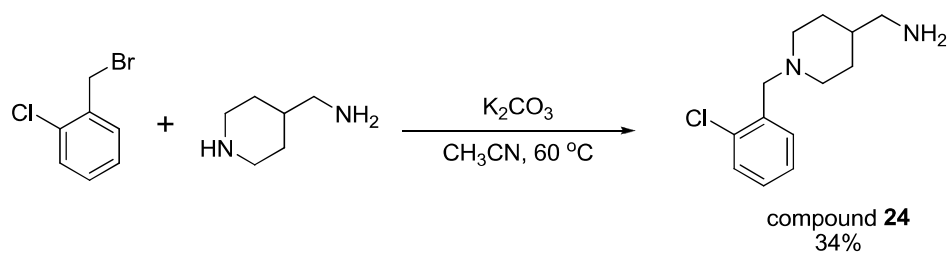
The reaction proceeds in two steps, 4-amino-pyridine was converted into the corresponding isocyanate by reacting with CDI. This reactive intermediate was then coupled with 2,2,2-trifluoroethylamine to form the corresponding urea (Scheme 16). TEA was used to avoid the protonation of primary amine. After purification by flash chromatography, the desired urea **23** was isolated as white solid in 26 % yield.



Scheme 16: Mechanism of urea synthesis using CDI

3.6. Synthesis of fragment ID-7976697

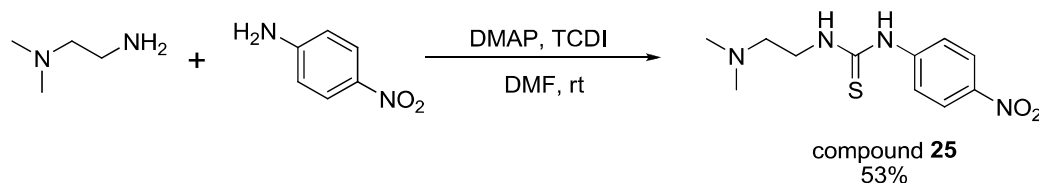
Fragment ID-7976697 was obtained through the alkylation of 4-(aminomethyl)-piperidine using 2-chlorobenzyl bromide.²⁰² This reaction was conducted in acetonitrile at 60 °C to afford the desired amine **24** in 34% yield.



Scheme 17: Synthesis of fragment hit ID-7976697

3.7. Synthesis of fragment ID-7805186

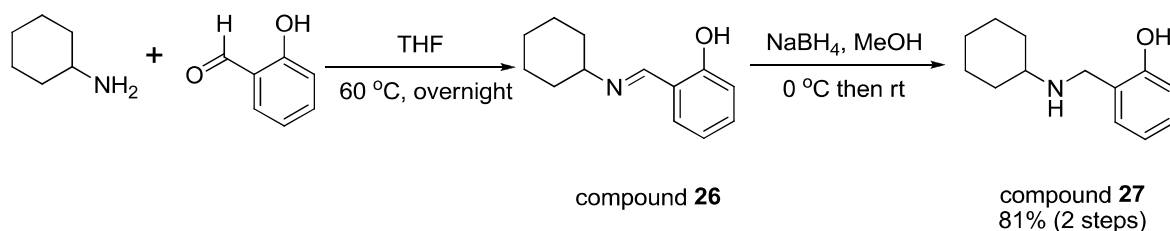
The thiourea ID-7805186 was obtained from *N,N*-dimethylethylenediamine and 4-nitro anilin using 1,1'-thiocarbonyldiimidazole (TCDI) as a thiocarbonyl transfer reagent.²⁰³ This reaction was conducted in DMF at room temperature and 4-dimethyl-aminopyridine (DMAP) was used as a base. The thiourea **25** was isolated from flash chromatography with a yield of 53%.



Scheme 18: Synthesis of fragment hit ID-7805186

3.8. Synthesis of fragment ID-5847719

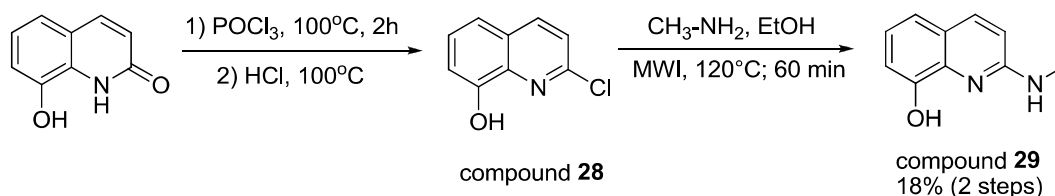
Fragment ID-5847719 was obtained in a 2-steps synthesis. Firstly, the imine **26** was synthesized from cyclohexylamine and salicylaldehyde under heating at 60°C in THF.²⁰⁴ This Schiff base was then reduced by sodium borohydride (NaBH₄) in methanol²⁰⁵ to afford the desired amine **27**. The final product was obtained in a good yield (81%, over 2 steps).



Scheme 19: Synthesis of fragment hit ID-5847719

3.9. Synthesis of fragment ID-5175081

The fragment ID-5175081 was obtained from 8-hydroxyquinolin-2(1*H*)-one in two steps. The first reaction is a chlorination using phosphorus oxychloride (POCl₃)²⁰⁶ to afford the 2-chloro-8-hydroxy-quinolin **28**. This intermediate was then substituted by methyl amine under microwave irradiation.²⁰⁷ The desired compound **29** was obtained in 18% over 2 steps.

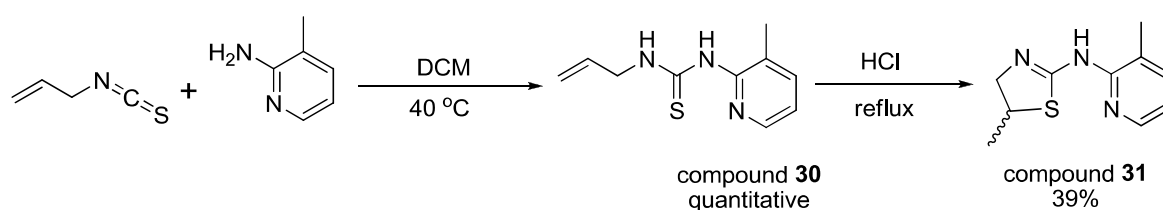


Scheme 20: Synthesis of fragment hit ID-5175081

3.10. Synthesis of fragment ID-7937388

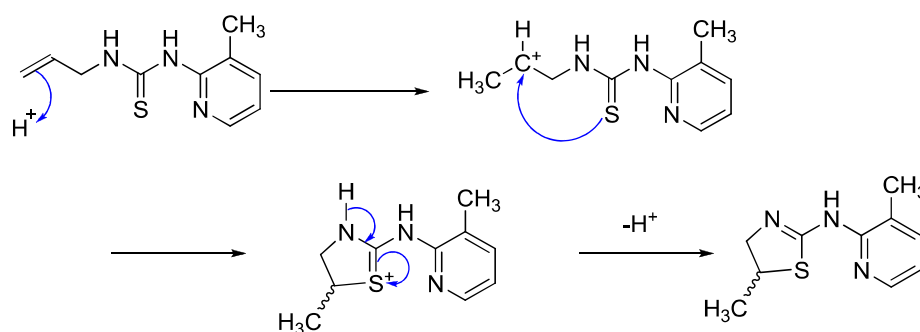
The fragment ID-7937388 was obtained using a 2-steps synthesis. The first reaction is a thiourea formation from 2-amino-3-picoline and allyl isothiocyanate.²⁰⁸ We observed that this reaction was influenced by solvent. In a polar protic solvent (e.g. anhydrous ethanol), we did not obtain a total conversion although many conditions have been applied (room temperature, reflux by classical heating method or in microwave condition). Furthermore, we observed formation of by-products. Conversely, in dichloromethane (a polar aprotic solvent) the thiourea **30** was obtained in quantitative yield.

The second step is a cyclization to form dihydro-1,3-thiazol derivative **31**. The acidic condition of this intramolecular cyclization was adapted from a protocol found in literature.²⁰⁹ We obtained a total conversion. However, difficulty in flash purification allowed us to isolate the pure compound **31** in 39% yield.



Scheme 21: Synthesis of fragment hit ID-7937388

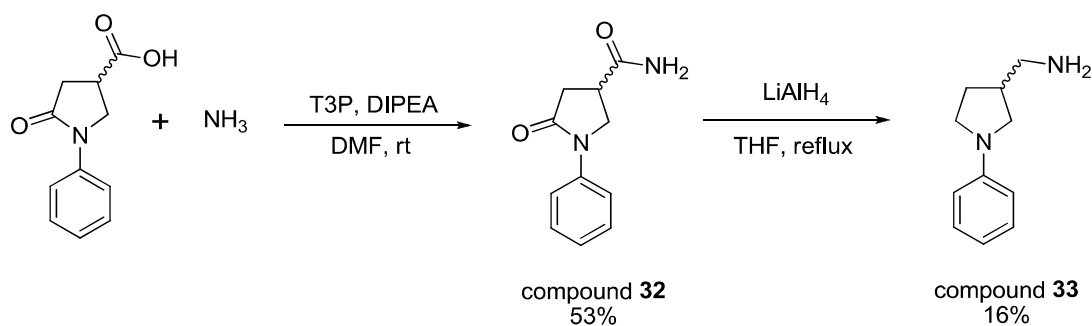
In Scheme 22, we present a proposed mechanism for this cyclization. The alkene group may be protonated under acidic conditions. Then nucleophilic sulfur atom of thiourea will bind to the carbocation that leads to cyclization into dihydro-1,3-thiazole. Finally, intramolecular rearrangement affords the desired product **31**.



Scheme 22: Proposed mechanism for the cyclization that allow the formation of compound 31

3.11. Synthesis of fragment ID-4003805

The fragment ID-4003805 was synthesized from 5-oxo-1-phenylpyrrolidine-3-carboxylic acid in 2 steps. The first reaction is the carboxamide formation using ammonia. This carboxylic acid was activated by T3P in DMF. Amide **32** was obtained in 53% yield. This intermediate was then reduced using lithium aluminium hydride LiAlH_4 .²¹⁰ Purification by preparative HPLC afforded amine **33** in poor yield (16%).



Scheme 23: Synthesis of fragment hit ID-4003805

3.12. Synthesis of fragment ID-4019055

The fragment ID-9098329 was synthesized from *m*-anisaldehyde in 3 steps (Figure 54).

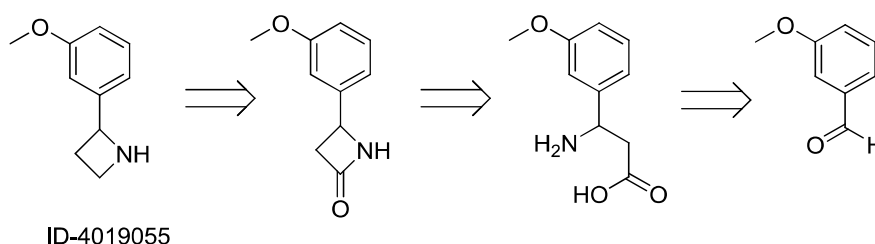
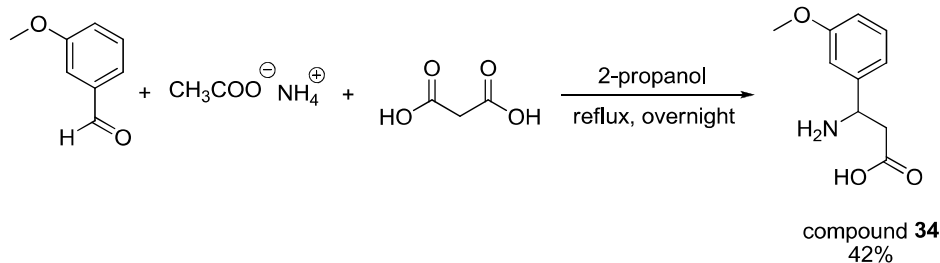


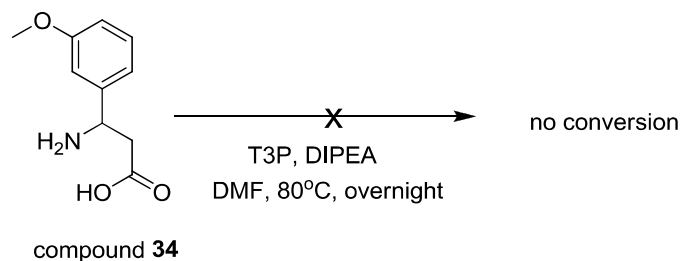
Figure 54: Retrosynthesis of fragment ID-4019055

First of all, beta amino acid **34** was synthesized according to a described protocol.²¹¹ The mixture of starting materials (e.g. *m*-anisaldehyde, malonic acid and ammonium acetate) was refluxed in 2-propanol. Compound **34** was obtained in average yield (42%) as white solid.

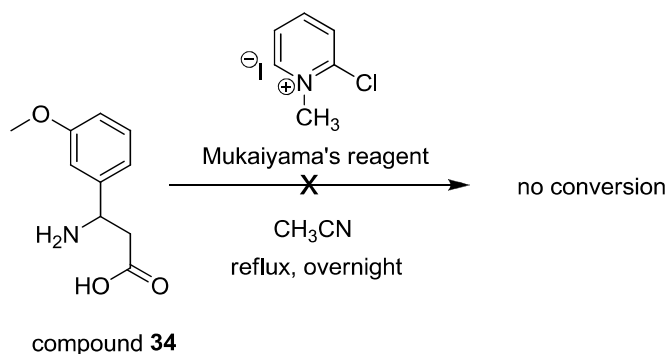


Scheme 24: Synthesis of compound 32

The second step is a lactamization to afford the azetidinone. Different conditions have been tried for the coupling of amino group with carboxylic acid group. Firstly, we have tried T3P as activator for beta-lactam formation but there was no conversion. Secondly, Mukaiyama reagent was used as activating agent for carboxylic group. Unfortunately, the reaction did not occur (Scheme 25, Scheme 26).

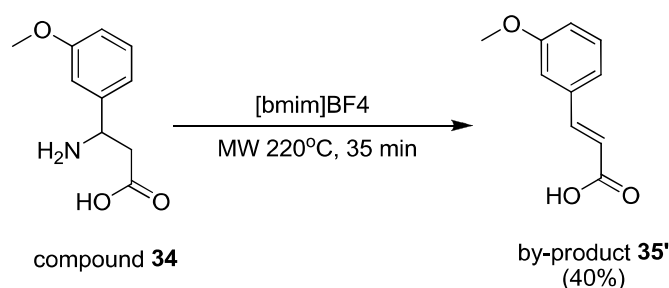


Scheme 25: Unsuccessful conditions in beta-lactam formation



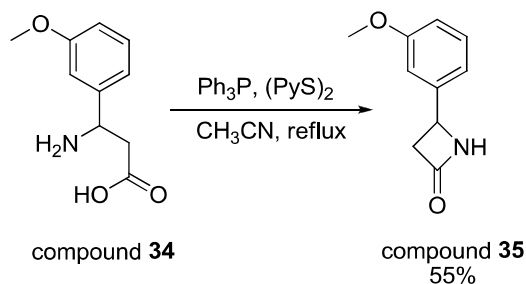
Scheme 26: Unsuccessful beta-lactam formation with Mukaiyama reagent

In addition, ionic liquid (e.g. 1-butyl-3-methylimidazolium tetrafluoroborate, [Bmim]BF₄) was also described in literature as reagent for lactam formation from lactone.²¹² However, application of this protocol in this case led to an elimination of the starting material (compound **34**). We obtained the undesired-product **35'** in 40% yield (Scheme 27).

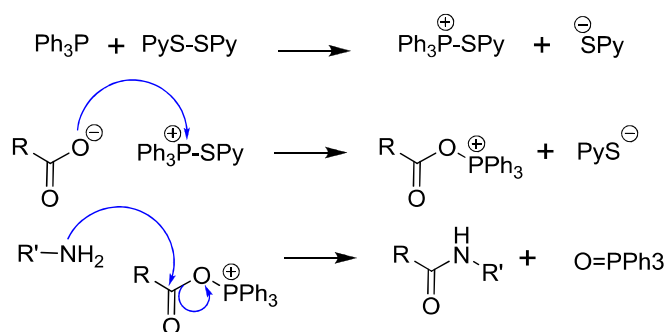


Scheme 27: Undesired-product formation in ionic liquid

Finally, a second Mukaiyama's reagent was used. This reagent was formed in the presence of triphenylphosphine (PPh₃) and di(2-pyridyl)disulfide (PyS-SPy).²¹³ The reaction in reflux acetonitrile afforded the beta lactam **35** in 55% yield (Scheme 28).

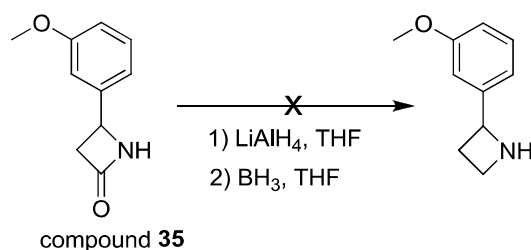
Scheme 28: Synthesis of beta-lactam **35**

The proposed mechanism of this reaction is described in Scheme 29.

Scheme 29: Proposed mechanism of lactam formation by Ph₃P and (PyS)₂

In the first step, triphenylphosphine is oxidized and (PyS)₂ is reduced. An active phosphonium intermediate is formed. Then carboxylate attacks the phosphorus atom of the phosphonium salt and the “activated ester” then reacts with amine to form an amide bond and triphenylphosphine oxide.²¹⁴

In step 3, the beta lactam was reduced using several conditions (LiAlH₄ in THF or BH₃ in THF). A formation of the desired product was verified on LC-MS. However, this product was not stable under purification conditions.



Scheme 30: Reduction of beta lactam **35**

3.13. Conclusion

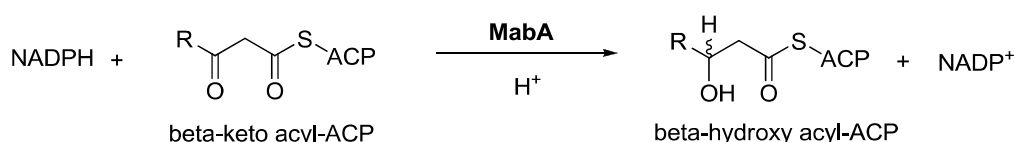
In summary, 11/12 fragment hits from the primary screening (based on TSA and HCS) have been successfully synthesized. However, we could not obtain the fragment ID-9098329 due to the challenging reduction in final step. Instead, the intermediate compound **35** was used as alternative fragment.

4. Validation of the hits in a functional enzymatic assay

4.1. Principle

It has been described that MabA catalyzes the reduction of beta-keto-acyl-ACP to afford the beta hydroxyl-acyl-ACP in *M. tuberculosis*. The first enzymatic assay on MabA was developed by Marrakchi and his colleagues in 2002.¹⁰ The authors replaced the native substrate by acetoacetyl-CoA that is commercially available. NADPH was used as cofactor for this reaction (Figure 55). In general, this reaction can be followed by two methods. The first one lies on the monitoring of the decrease of cofactor concentration (NADPH). Oxidation of NADPH is followed spectrophotometrically by measuring the decrease in absorbance at the wavelength of 340 nm. This method was used to evaluate the inhibitory activity of INH-NADP adduct.¹⁶²

in *M.tuberculosis*



in enzymatic assay

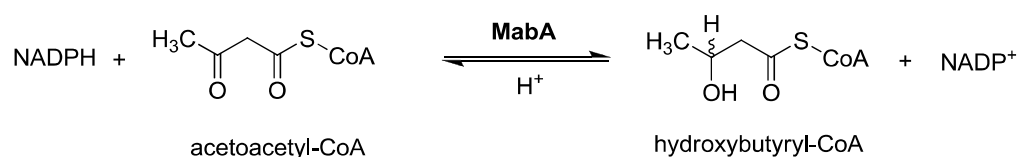


Figure 55: MabA enzyme catalyze the reduction of beta-keto acyl derivative

The second method that we have developed lies on the detection of hydroxybutyryl-CoA, product of the enzymatic reaction. We used LC-MS/MS analysis to measure quantitatively the formation of hydroxybutyryl-CoA (unpublished data).

4.2. MabA activity inhibition of the primary hits

Following the development of the enzymatic assay and its validation with INH-NADP adduct, we screened the 12 resynthesized fragments to evaluate their ability to inhibit the activity of MabA. These fragments were screened at 1mM. Unfortunately, none of them showed any activity at that concentration. This result allowed us to draw two conclusions:

1. Binding of fragments to MabA, observed under the conditions of TSA experiment, does not seem to have any impact on the enzymatic activity of MabA. Therefore, this assay may not be predictive for the detection of true inhibitors of MabA.
2. The activity of the fragments measured in the whole cell bacteria assay may not be attributed to the inhibition of MabA and will be investigated as part of this project.

For these reasons, we decided to rescreen our set of fragments using our high throughput enzymatic assay.

4.3. Reformatting of the fragment library and identification of new hit

At the same time, our fragment library was completed with the addition of new fragments (e.g. halogen fragments and 3-D fragments). These modifications which are fully described in chapter IV of this thesis have helped to increase the number of fragments to 1280. The screening of this library firstly conducted at concentration 1mM for fragments. Then, 50 fragments having the % inhibition superior to 30% were tested in a dose response experiment at 8 different concentrations (1 mM to 0.45 μ M). The final results led to the identification of 12 hits in 9 families of new inhibitors with IC_{50} ranging from 30 to 300 μ M.

As part of the selection, 5-amino uracil derivative BDM72261 was selected for further studies. This fragment inhibits 100% of the enzymatic activity of MabA at 1mM. Furthermore, a dose–response experiment showed a half maximal inhibitory concentration (IC_{50}) equal to 98 μ M (Figure 56).

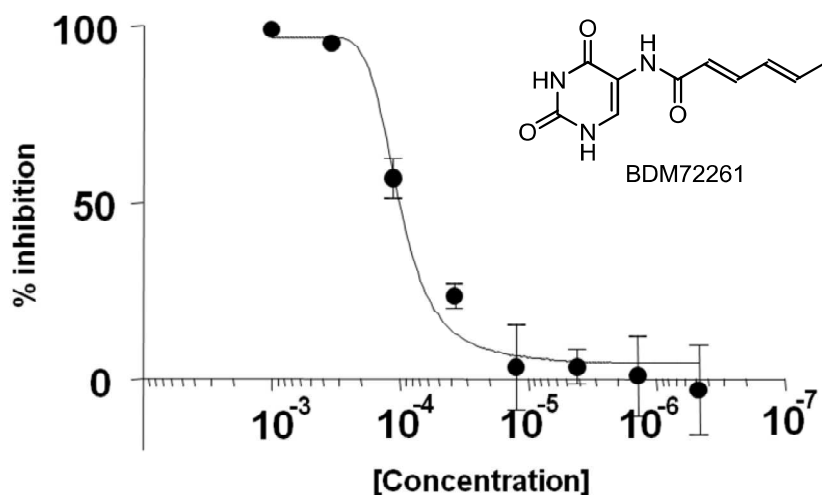


Figure 56: Dose – Response Curve (DRC) obtained with BDM72261

5. Synthesis of amino uracil analogs

In order to improve the activity of the starting hit, we started to modify the nature of the aliphatic chain linked to the 5-aminouracil motif thanks to an amide bond (Figure 57).

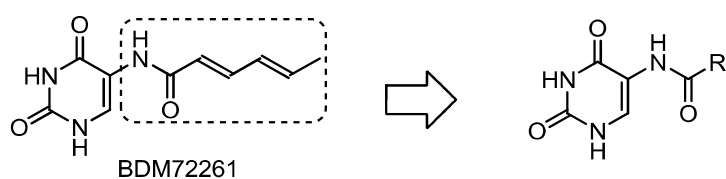
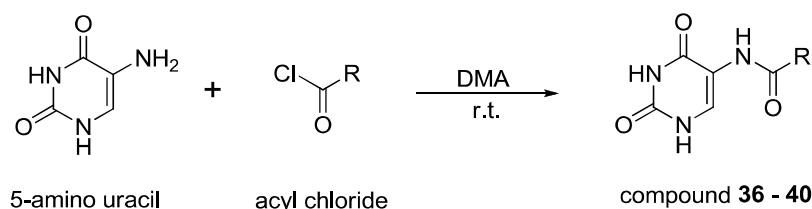


Figure 57: Structural modification of fragment hit BDM72261

In the first effort, we tried to replace the unsaturated chain in BDM72261 by a saturated aliphatic chain with the same size (compound **36**), or a shorter chain (compound **37**), or a longer chain (compound **38**). We also tried to substitute with a cycloalkyl or aryl group in order to inspect the impact of these modifications on MabA activity.

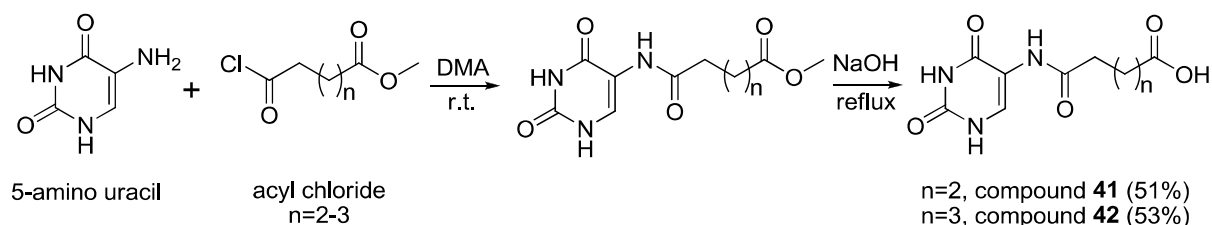
Amide couplings were conducted between commercially available 5-aminouracil and corresponding acyl chlorides at room temperature in *N,N*-dimethyl acetamide (DMA).



Scheme 31: Synthesis of amide analogues of uracil 36-40

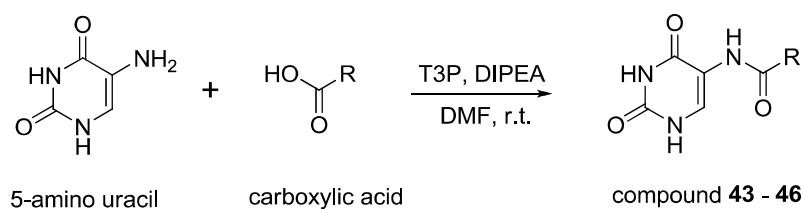
This protocol was applied to afford five amides **36-40** in good to excellent yield (69%-91%). The structures of these analogues with their corresponding yields are presented in Table 12.

In addition, compounds **41** and **42** were synthesized and obtained in a 2-steps synthesis in order to determine the impact of acidic functions on the activity of analogues. The second step, which is the saponification of esters obtained in the first step allowed the isolation of the desired carboxylic acid derivatives.



Scheme 32: Synthesis of uracil analogues 41-42

Furthermore, 5-aminouracil was then coupled with several carboxylic acids in DMF at room temperature to afford 4 others amides **43-46**. In this protocol, T3P was used as activating reagents in the presence of DIPEA. In this case we tried to modify the alkyl chain by adding a phenyl group (compound **43**), phenoxy group (compound **44**), trifluoromethyl group (compound **45**), or an amide group (compound **46**) at one end of the alkyl chain.



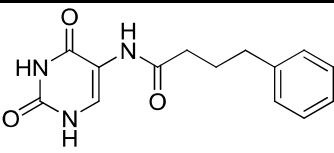
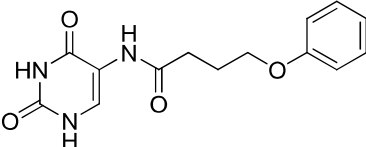
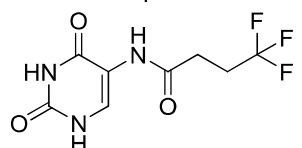
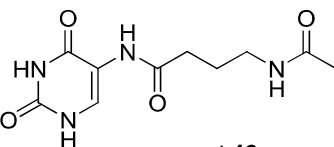
Scheme 33: Synthesis of amide analogues of uracil 43-46

These amides **43-46** were successfully synthesized. In Table 13, we present the structure of these compound with their corresponding yields.

Table 12: Structure of amide analogues of uracil 36-40 and isolated yield

Entry	Structure	Yield
1	<p style="text-align: center;">compound 36</p>	84%
2	<p style="text-align: center;">compound 37</p>	72%
3	<p style="text-align: center;">compound 38</p>	86%
4	<p style="text-align: center;">compound 39</p>	91%
5	<p style="text-align: center;">compound 40</p>	69%

Table 13: Structure of uracil analogues 43-46 and isolated yields

Entry	Structure	Yield
1	 compound 43	63%
2	 compound 44	71%
3	 compound 45	47%
4	 compound 46	33%

The 11 synthesized analogues (compounds **36-46**) will be further tested in enzymatic assay to start drawing structure-activity relationships in this series.

This page intentionally left blank

Chapter IV. Design and synthesis of novel 3D-fragments for fragment-based drug discovery

Part A. An overview on actual fragment libraries

1. Fragment library design

The quality of the fragment library has been endorsed as a pivotal element which influences on the success rate of FBDD. In this section, we will summarize all available sources for fragments selection and point out some principles which are useful for the design of a fragment library.

1.1. Sources for fragments

Fragments are low molecular weight (<300Da) organic molecules having a weak affinity to the target. In order to design a typical fragment screening library, a key question is how to obtain a library with a small number of fragments suitable for screening against various biological targets and sample an extremely large chemical space. There are many possible fragment sources that can be used as primary scaffolds in designing a fragment collection e.g. known drugs or bioactive compounds, natural products and novel scaffolds which are depicted in Figure 58.

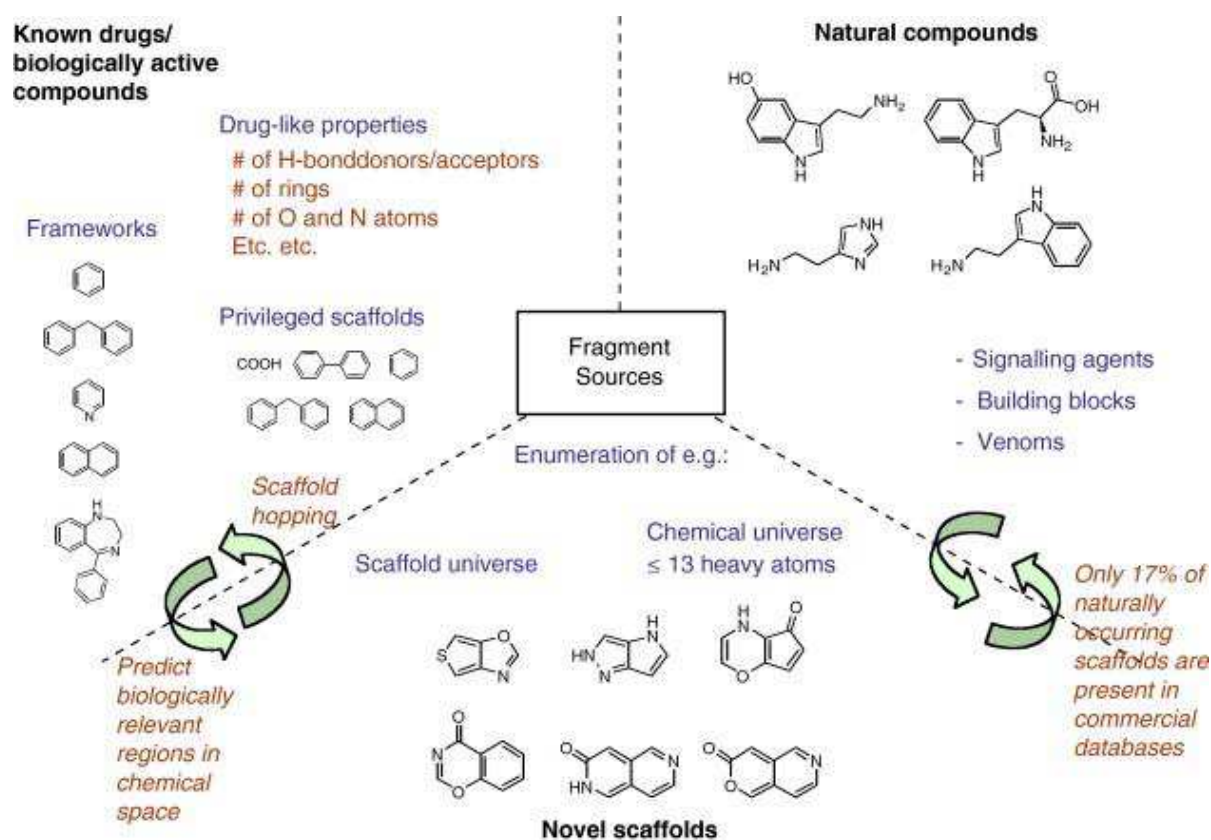


Figure 58: Overview of possible fragment sources (adapted with permission from Elsevier for ref.²¹⁵)

1.1.1. Known drugs or biologically active compounds

Sir James Black, winner of the 1988 Nobel Prize in Physiology or Medicine, said that “the most fruitful basis for the discovery of a new drug is to start with an old drug”.²¹⁶ This concept has opened a new approach in drug discovery using an old drug as a starting point for the discovery of a new one. Similarly, this strategy can be also applied in design of fragment screening library.

By comparing the structures of all drugs, these studies have been established how many times one scaffold occurred as a substructure within the marketed drug. These results allowed the identification of some suitably fragmented drugs to be included in fragment libraries or used as templates to search for commercially available analogues. The descriptors or criteria derived from these analyses of known drugs were also used to select fragments.²¹⁷

This concept was exemplified by the SHAPES library of Vertex. This library is based on molecular frameworks and side chains of known drugs.²¹⁸ On the other hand, an alternative fragmentation approach (RECAP) based on retrosynthetic rules has been developed.²¹⁹ In most cases, databases of drugs and/or bioactive molecules in development are analyzed in order to identify interesting chemical scaffolds that can be used for library design.

In general, databases that were used for fragment library design comprise some commercial drug databases, e.g. Comprehensive Medicinal Chemistry CMC (Elsevier MDL), MDL Drug Data Report (Elsevier MDL) and World Drug Index (Thomson Scientific), Dictionary of Drugs (CHEMnetBASE). Some other drug databases are freely available on the internet for academic purpose such as DrugBank²²⁰, the NCI Drug Dictionary²²¹ and Supper Drug DataBase²²² developed by Institute of Molecular Biology and Bioinformatics in Germany. Moreover, when expanding to the bioactive molecules or clinical compounds in development, the list can be enlarged with Med Chem Database (Daylight Inc.), PubChem project²²³ of US National Center for Biotechnology Information and ChEMBL database²²⁴ (developed by European Bioinformatics Institute). Recently, ligands found in Protein Data Bank¹⁸⁴ have also been considered as source of fragments. In fact, protein-ligand interaction data in PDB could allow enlarging information on important recognition elements.

The positive point of this fragment source is that privileged scaffolds from drug are known to bind to a specific target protein, so these fragments could enrich fragment libraries for biological activity. However, when applying this strategy, one must be aware of the fact that this is a retrospective analysis and that the evolution of the fragments from this approach may lead to an already known structure.^{190,215}

1.1.2. Natural compounds

Natural products have always been a source for drug discovery. These compounds are produced in nature and may have some biological activities and then become candidates for drug development.²²⁵ By definition, natural product should have a biological function, and many will exhibit affinity to several receptors. Natural scaffolds offer a good starting point for building a fragment library. Furthermore, the large amount of uncovered druggable protein targets suggests that more diversity is needed than the skeletons presented in current drugs. While a high amount of natural diversity is still not covered in commercial databases.²²⁶

Natural products are rich in stereo centers and comprised of many scaffolds in chemical space typically not occupied by synthetic molecules and actual drugs. An analysis of natural product structures allows establishing the criteria for fragment likeness. These filtering criteria were then used to select natural-product-derived fragments with a high degree of three-dimensionality. Accessibility to and use of such fragments with suitable functional groups for derivatization would provide a novel opportunity to synthesize natural-product-inspired compound libraries and to overcome the main drawbacks of natural products in drug discovery because of a lack of accessibility and synthetic intractability.²²⁷

The natural products database which is often used for library design is a dictionary of Natural Products developed by CHEMnetBASE. Many other natural databases were listed in a general survey developed by researchers at Institute of Biochemistry in Berlin (Germany).²²⁸

The Fragments of Life (FOL) developed by Emerald Biostructures is an example of fragment library from natural products. This library contains natural small molecule metabolites, metabolite-like compounds and their bioisosteres.²²⁹ Recently, a natural-product-derived fragments library has been designed by Waldmann and his colleagues at Max-Planck Institute of Molecular Physiology in Germany. This library was designed with a high degree of three-dimensionality in comparison with the published fragments.²²⁷

1.1.3. Novel scaffolds

Whereas the known chemical space including public databases and corporate collections probably contains on the order 100 million molecules, it has been estimated that the Lipinski virtual chemical space might contain as many as 10^{60} compounds of less than 30 heavy atoms when considering only basic structural rules or a more modest 10^{20} – 10^{24} molecules if combination of known fragments are considered.^{230,231} Fragment space is smaller than the drug space. However it is still huge.

An interesting approach to achieve novel chemical scaffold is the enumeration of chemical space, following by extensive analysis of physicochemical, fragment-like and structural properties. Prediction of novel bioactive scaffolds could be guided by focusing on the area of ring systems. Reymond and his colleagues conducted a comprehensive study in which they enumerated all possible organic molecules up to 11 heavy atoms, containing C, N, O and F. Filters were applied for chemical stability and synthetic feasibility. This allows careful inspection of currently occupied chemical space, while also extending the boundaries of applicable synthetic chemical space.²³² The algorithm has been then optimized in 2009 so that enumeration up to 13 heavy atoms is possible, creating a library of 970 million compounds²³³ (named as Generated Databases GDB-13). Recently, the enumeration has been scaled up to 17 heavy atoms (GDB-17).²³⁴

For fragment library design, a structure with 13 heavy atoms is an interesting size. Based on the GDB-13 database, the research group at Abbott Healthcare Products has designed a diverse, high-efficiency, unique fragment collection based on molecular graph theory. This fragment collection navigates a chemical space not previously populated by others commercial fragment libraries. Chemical matter was carefully selected by applying classical Ro3 filters and chemical tractability, diversity, scaffold complexity, and non-

commercial criteria. This work resulted in the ultimate 1357 fragments set, here referred to as the high fragment efficiency from the total approximately 970 million C/N/O/S/Cl-containing compounds in GDB-13.²³⁵

1.1.4. Authentic fragments *versus* virtual fragments

In practical terms, the fragments are usually designed based on a fragmentation algorithm of drug-like molecule (drugs, bioactive molecule, and natural products) or selected from novel designed scaffolds. Some fragments are commercially available which are named as ‘commercial fragments’. However, other fragments are not always available from commercial suppliers. In this case, the pharmaceutical company and/or academic research group must find a suitable method for their synthesis. Therefore, these fragments are known as ‘in-house fragments’.

Some authors have developed virtual screenings for the finding of hits in fragment-based approaches. A large fragment library which is virtually designed is screened on X-ray structure of the target. These fragments can be named as virtual fragments in this case. The selected hits from *in silico* screening will then be synthesized and validated by classical fragment screening methods. Based on this approach, these authors believed to find more noteworthy chemotypes by increasing the fragment library. This approach has been validated by Chen and his coworkers for the development of beta-lactamase inhibitors from a library of 300 000 virtual fragments.²³⁶ The concept of virtual fragment is now gently accepted.²³⁷

1.2. Principles in fragment library design

In any screening process, the quality of the hits is clearly influenced by the quality of the screened library. The screening of fragments has several additional constraints, including the fact that fragments need to be screened at high concentrations and that we need to find appropriate synthetic routes to evolve the fragment hits into lead compounds. Fragment libraries differ from drug-like and lead-like. First, they comprise compounds with a significantly lower molecular weight (MW), typically in the 140–300 Da range. Second, rigorous quality control is required for validating the fragment library. The good selection step will help to improve the success rates of the fragment library.²³⁸

1.2.1. Fragment selection criteria

A well-chosen set of fragments should be able to cover a large chemical space using a small number of compounds. Since fragments tend to be smaller than most drugs, clinical candidates, leads, or high-throughput screening (HTS) hits, they are able to make fewer interactions and tend to have lower affinities to their protein targets. Affinities are often observed in the high micromolar to millimolar range. Therefore the fragments must have a very good solubility in order to be tested at high concentrations in the goal of detecting low affinity for the target of interest.¹⁰¹

In addition, drug-like molecules are usually defined by the Lipinski rules (“Ro5”). This “rule of five” tries to summarize properties to be met to achieve oral availability which is essential for an active substance as prospective candidate for clinical trials.²³⁹ Congreve and coworkers introduced a similar rule for fragments and became popular as the Astex “rules of

three” (Ro3).¹⁰³ In particular, the molecular weight is < 300 g/mol, the number of hydrogen bond donors (HBD) and acceptors (HBA) is ≤ 3 , ClogP is ≤ 3 , the number of rotatable bonds (NROT) is ≤ 3 and the polar surface area (PSA) is ≤ 60 Å. These criteria are not only used to assure the aqueous solubility, but also to ensure that compounds resulting from the elaboration of fragment hits conform to the “Ro5”.¹⁰³

Consequently, fragment libraries assembled and offered commercially by many providers over the last few years are usually in agreement with Astex “Ro3”. However, the value of using the Ro3 in FBDD is being challenged as many useful fragment hits do not adhere to its restrictions. Recently, a study of Gerhard Klebe’s group at Philipps University Marburg has demonstrated the success of lead developed from fragment hit which is not entirely conformed to the Ro3. Furthermore, Klebe and his colleagues assembled a library of 364 fragments in which the average properties of the fragments were within Ro3 guidelines but there were some outliers. They then performed a fluorescence-based competition screen against the model endothiapepsin protein. The results showed that only 4 of the 11 hits are consistent with the rule of 3. Restriction to this rule would limited the fragment hits to a strongly reduced variety of chemotypes. In this context, the authors wanted to critically ask whether Ro3 are too strict for a fragment library holding candidates that leave sufficient room for subsequent chemical modifications.^{240,241}

Table 14: Comparison between Ro3 and 3D Fragment Consortium’s rules

“Ro3” in 2003	“Ro3” in 2013	3DFrag
MW < 300 Da	HAC < 17	$9 < \text{HAC} \leq 18$
HBA ≤ 3	HBA ≤ 3	HBA < 6
HBD ≤ 3	HBD ≤ 3	HBD < 4
cLogP ≤ 3	cLogP ≤ 3	$-3 \leq \text{clogP} \leq 3$
NRot ≤ 3 (optional)	NRot ≤ 3 (optional)	NRot ≤ 3
TPSA ≤ 60 (optional)	TPSA ≤ 60 (optional)	TPSA ≤ 100
-	-	$-\text{clogS} \leq 3$

MW: molecular weight; HAC: heavy (non-H) atom count ;
 HBA: hydrogen bond acceptors; HBD: hydrogen bond donors;
 NRot: number of rotatable bonds; TPSA: topological polar surface area;

Recently, this rule has been reviewed by the researchers at Astex company after nearly 10 years of apparition.²⁴² Congreve and his colleagues have always believed that the Ro3 concept has limitations and like other rules related to desirable physicochemical properties, such as the ‘rule of five’ guidelines, it is simply a guideline that should not be overemphasized. Nevertheless, the authors believed that Ro3 has been useful in limiting the molecular complexity in fragment libraries which presents substantial technical challenges for detection of low-potency fragment hits. In this review, these authors also proposed that non-hydrogen atom count (< 17) may be more suitable to measure the molecular size for fragments than molecular weight, as this is more tolerant with halogen atoms. Moreover, the

limits on the number of rotatable bonds (NRot) and topological polar surface area (TPSA) are suggested to be optional.

Besides the Ro3 which becomes the most popular selection criteria in the fragment based approach, many others companies and academic research groups have tried to define their in-house selection criteria.^{243,244} Recently, a more flexible rule was suggested by the 3D Fragment Consortium in United Kingdom.²⁴⁵ In this filtering concept, Heavy Atom Count was limited to 18, hydrogen bond donors (HBD) < 4, hydrogen bond acceptors (HBA) < 6, Polar surface area $\leq 100\text{\AA}^2$, cLogP value from -3 to 3 and a predictable solubility criteria was added with $-\text{clogS} \leq 3$

Besides the physicochemical properties for fragment selection which were defined in the Astex Ro3, there are many other appropriate physicochemical properties that are pertinent to the design of fragment libraries and the success rate of the fragments screening procedure. These properties will be described in this following section.

1.2.2. Fragments solubility

The water solubility of fragments is very important when building a screening library¹⁰⁴ since most of the biophysical detecting methods used to screen fragment usually in aqueous buffer. Moreover, solubility is an issue that needs to be addressed carefully when selecting compounds for screening at high concentration. Aqueous solubility greater than 2 mM has been proposed which can allow selecting soluble fragments amenable for screening by using many different methods.²⁴⁶

It is often advisable to measure experimentally solubility of fragments at conditions appropriate for the screening method. For example, nuclear magnetic resonance (NMR)-based screening is usually performed at low temperatures in order to enhance fragment binding.²⁴⁷ However, these low temperatures could also affect the solubility of certain fragments. Solubility is also important when using X-ray crystallography to confirm the fragment-protein interaction. Protein crystals contain approximately 50% solvent and the fragments need to be able to diffuse to the binding site through solvent channels when conducting soaking experiments. It is also necessary to design fragment libraries with high solubility in order to avoid aggregation that could generate a lot of false positives.¹⁰⁴

Alternatively, fragments solubility can be estimated computationally *via* a number of algorithms. However, prediction of aqueous solubility *in silico* remains a computational challenge because both the crystal and solution state of the compound must be considered. Therefore, in place of using a solubility descriptor such as logS to filter these fragments where the margin of error in the calculation is usually at least a log unit, considerable success has been reported with the use of more reliable computational descriptors such as cLogP in combination with hydrogen- bond donor/acceptor counts. Low lipophilicity and the presence of ionizable groups usually enhance the aqueous solubility.¹⁹⁰ Because solubility is such a critical requirement, the presence of ionizable groups within the fragments becomes an important consideration. Based upon their analysis that ~25% of marketed drugs contain an ionizable group, the researchers at Pfizer has selected fragment that contain the ionizable groups which are fairly represented in their library.²⁴⁸

1.2.3. Ligand efficiency

Ligand efficiency (LE) is a term first applied by Pfizer scientists to describe the average Gibbs free energy of binding per heavy atom (HA).²⁴⁹ Variants of LE include group efficiency (GE), which extends the LE definition to cover a functional group contribution to binding and ligand-lipophilic efficiency (LLE), which takes lipophilicity into account. In some case, K_d can be replaced by IC_{50} .²¹⁵

$$LE = \frac{\Delta G}{HA} = \frac{-RT \times \ln K_d}{HA}$$

$$GE = \frac{\Delta \Delta G}{\Delta HA} = \frac{-RT \times \ln(K_{d,B} - K_{d,A})}{HA_B - HA_A}$$

$$LLE = pIC_{50} - clogP$$

GE represent the affinity gained by molecule B, through the introduction of additional group having ΔHA non-hydrogen atoms to molecule A, this value is expressed as the difference of the free energies of binding ($\Delta \Delta G$). In LLE, $clogP$ is an abbreviation of the ‘computed logP’, which is a measure of differential solubility or rather hydrophobicity by the octanol/water partition coefficient.¹⁰⁶

LE is usually used during lead optimization projects. A typical lead with molecular weight equal to 500 Da would need to have $LE > 0.3$ to achieve potency $< 10nM$. In FBDD, the relative LE values of fragments can be used as a criteria in fragment selection. In fact, LE cutoff is considered as a guide for the identification of useful and efficient fragments which can be suitably optimized to a “lead”. In order to stay Ro5 compliant during fragment evolution, it is beneficial to start with fragments displaying high LE because in most cases LE decreases during optimization. In fact, there are very few examples in the literature of fragment-based study where LE could be maintained or even increased. Therefore, a highly efficient fragment hit is usually a good starting point to optimize the fragment into a drug-like compound.^{106,215}

1.2.4. Synthetic considerations

During the library design process, synthetic accessibility of fragments needs to be considered. Fragments should not only be readily synthesizable themselves, but should contain suitable synthetic anchors to allow future elaboration. It means that fragments should be selected to enable linking or merging to other chemical moieties found or predicted to be useful for binding complementary regions of the binding site of interest, or to enable hit fragments to be grown into additional regions of the binding site.^{104,215}

However, some synthetic chemical functional group may interact directly with the protein site and further elaboration would be expected to negatively impact binding. To avoid use of fragments with this potential issue, it has been proposed to use masked fragments, whereby the synthetic handle is protected prior to the initial fragment screen. The presence of masked linker groups ensures that chemical tractability for future fragment elaboration is

feasible, whereas limiting exposure to reactive functionalities which could aggregate or react under screening conditions, particularly when mixture of many fragments are screened simultaneously.^{104,250}

Alternatively, fragments can be selected which do not contain functional groups. But the hetero cycle in structure and other substituents (e.g. halogen) will involve the ligand-protein interaction. In all cases, these structural consideration could considerably impact on the physicochemical properties of the fragments.¹⁰⁴

1.2.5. Diversity

For general screening purpose, the fragment library should ideally be diverse. The concept of diversity within a library can be understood in many aspects of the design. In fact, diversity approaches can build in diversity on the basis of physicochemical properties, molecular structure or shape, or indeed any combination of the aspects. Several physicochemical descriptors were investigated to quantify molecular diversity. Based on the 2D or 3D topological similarity of molecules, the relationship between physicochemical metrics and biological activity was studied to find valid descriptors. Diversity was suggested to be more important for diverse screening library than in case of targeted library.^{251,252}

1.2.6. Complexity

In fragment library design, the complexity should be as low as possible. Chemical space can be more efficiently represented by the assembly of simple fragments than by a set of complex larger structures. In addition, lower complexity increases the chance of a fragment binding to receptor binding sites. However, too low complexity will decrease the chance of a detectable binding and increases the probability to find multiple and non-specific binding modes. Recent studies have shown that often several binding modes can be obtained for fragments. Fragment optimization changes in binding modes which can make fragment growing/linking more difficult, especially when structural information is unclear. Therefore, an explicit binding mode is preferable where the specific interactions with the receptor should be made. In this case, the presence of H-bond donors/acceptors and other functional groups are therefore essential. From this respect, low molecular weight fragment dense with heteroatom and are substituted by some functional groups would furnish an interesting fragment library. These polar scaffolds which can form specific hydrogen bonds are considered to be good starting points for further optimization.²¹⁵

1.2.7. Influence of screening method on fragment library design

Despite their low potency to targets, fragments are also considered as bioactive compounds. Therefore, biological screening is ideal method for fragment-hit identification. However, applicable biological assays could not always be developed. For that reason, more generally suitable biophysical screening methods were alternately used. In general, the actual size and properties of fragment library depend on the screening method because each technique has its own practical limits in terms of the number of compounds that can be screened. In general, fragment libraries that are to be used with these techniques at high concentration in order to detect their weak affinity with protein. Therefore, the aqueous

solubility of fragment library should be carefully verified. In addition, some usual detection methods and their influence on the fragment selection criteria will be discussed herein.¹⁹⁰

In NMR screening methods, the low hit rate of protein-observed NMR demands a rather large fragment library (typically more than 15,000 compounds). While ligand-based approaches generally have 5–10-fold higher hit rates. Therefore, the library size can be reduced in these techniques.¹⁰⁴ In some ligand-observed NMR methods, the fragments must be labeled by an isotope to facilitate detection output, e.g. the use of ¹⁹F-labelled fragments has particular advantages of sensitivity and throughput in competition screening or ¹³C-labelled fragments were used in LLD.¹⁰⁴

X-ray crystallography can be used to screen fragment-like libraries, but is typically limited to less than 1000 compounds. Furthermore, the fragments for X-ray screening must be soluble at high concentration in organic solvents. In practical, stock solutions typically range from 100 to 500mM in dimethyl sulfoxide (DMSO) in order to facilitate soaking at sufficiently high concentrations to fully saturate the potential binding site(s) in the crystal.^{104,190}

Tethering, through disulfide trapping of fragments to the target, has proven a powerful method of developing leads for soluble targets. However, an obvious limitation of tethering method is the requirement that all compounds in the fragment library must contain an accessible SH group.¹⁰⁴

In SPR, the high concentration required to detect weak-affinity limits the use of SPR. In addition, a clean screen is necessary to remove compounds from the fragment library that can bind to the unmodified chip surface in the absence of protein prior screening.¹⁰⁴

2. Actual fragment libraries in literature

An increasing number of commercial companies are now offering well defined ready-made fragments libraries. Some companies have assembled general screening fragment sets using their in-house compounds while others have created fragment library from entirely commercial sources. Moreover, some have created fragment sets highly focused toward specific target classes. A common point of all libraries is that they contain small fragments which are highly soluble in aqueous solution, and appropriate for the detection methods intended to be used in fragment screening.

2.1. Classification of fragment library

Depending on the application purpose, the fragment library is further divided into 3 types:

- (a) General screening library (also called diverse library) is a collection of fragments with many different chemical structures. The chemical diversity is very important for this type of library.
- (b) Protein-targeted library (or focused library) is a collection of fragments that generally contain a known pharmacophore, i.e., a set of structural features responsible for a specific biological activity. They may also contain structural scaffolds that interact with a variety of molecular targets, commonly called privileged scaffolds.

- (c) Screening method-based library in which the fragments are designed for a specific screening method.

2.2. Fragment library for general screening purposes

Recently, Boyd and his colleagues have analyzed some commercially available fragment libraries.^{104,215} Nowadays, not only big pharmaceutical companies, who have put considerable effort into design and selection of in-house fragment screening libraries, but many small companies and academic research group have also tried to develop their own fragment library. Here, we describe some libraries in order to exemplify the various strategies and principles used.

The Vertex SHAPES library was designed and applied before the apparition of Ro3. However, several filtering principles were used in the same intent. The library was based on common structural scaffolds in known drugs. Other selection criteria included commercial availability, lack of aggregation in water at 1 mM, isomeric purity, and lack of reactive species. Finally, 132 fragments were selected with a MW between 68 and 341 Da (average 194 Da), containing 6–22 heavy atoms with cLogP between –2.2 and 5.5. The SHAPES library has been implemented in several fragment-based screening projects at Vertex with successful results.¹⁰⁴

The GFSL05 library was designed by researchers at AstraZeneca for generic screening both in target and detection methods. A set of in-house computer programs using fingerprint-based measures of molecular similarity allowed the design of this fragment library. Selected compounds in this library have up to 21 non-hydrogen atoms, with good solubility. They also contained a good representation of ionizable groups, and were available in solid form of at least 100 mg. In addition to similarity-based selection, molecular shape indexing was used as a secondary tool in order to select compounds with small structural modifications but with different conformational preferences. Experimental solubility was measured for selected compounds with cLogP greater than 2.2 and poorly soluble compounds were removed. The resulting GFSL05 library consisted of 20,000 fragments in which 70% of the compounds had at least one structurally analog, for which at least 10 mg was available in-house as a single sample enabling fast follow-up screening.¹⁰⁴

A similar general multipurpose fragment library named as Global Fragment Initiative (GFI) was recently developed by researchers from Pfizer. This library was designed to have a suitable complexity for binding and to cover a diverse set of pharmacophore and structural functionality within the constraints of good molecular properties. The fragments in this library are also chemically suitable for fragment elaboration step. Compounds from multiple sources including both in-house collections and commercial vendors were filtered to remove reactive or otherwise undesirable moieties. The physicochemical property filters applied in the first step included a more stringent requirement than the common Ro3 criteria (e.g. $100 < MW \leq 250$ and $cLogP \leq 2.0$) but a less stringent cutoff for the polar surface area ($\leq 110 \text{ \AA}^2$). In the end, approximately 15% of selected fragments were removed based on solubility issues. Interestingly, a large number of cationic and anionic molecules were included, based on the observation that many approved drugs are charged. Also, roughly a quarter of the compounds contained at least one chiral center. The final library consisted of 2885 compounds, with 25%

containing one or more chiral centers, having between one or three rings and having almost as many basic and acidic compounds as neutral compounds. Most of these fragments came from commercial or in-house collections, but 293 were synthesized in-house. This library has successfully been screened using ligand-detected NMR experiments and had a hit rate range from 2.8% to 13% for 13 different targets. A number of unique hits were found for each target and interestingly also for the four different kinase proteins included among the targets.¹⁰⁴

Another fragment library was constructed by researchers at Vernalis by a different approach in order to maximally represent chemical available space. This is an interesting method for companies lacking an extensive in-house compound source. In fact, compounds from various vendors were filtered to remove duplicates, salts, and unwanted functionality and then separated into a fragment set and a non-fragment set by Ro3. The fragment set was then categorized by using similarity methods to select out the fragments that maximally represent the chemical space of the compounds in the non-fragment group. Therefore, the fragment hits have an increased probability that nearest-neighbor compounds will be available from commercial sources for subsequent fragment evolution.¹⁰⁴

The researchers at Emerald Biostructures have developed a totally different method in order to build their general purpose library. This library was assembled from compounds that are known to target protein structure and are divided into one of three categories: natural metabolites, including molecules known to be presented in living cells; derivatives of metabolites, such as isosteres or heteroatom derivatives of natural metabolites; and synthetic biaryl molecules, whose energy-minimized structures tend to mimic peptidic α -, β -, and γ -turns. Thus, 1500 fragments were selected in the resulting library. They are divided in 192 cocktails with eight fragments in each group, sorted for diversity in order to simplify crystallographic screening method. Interestingly, these fragments are stored as 50 mM stock solutions in methanol instead of DMSO. The authors believed that methanol can completely evaporated in the crystallization well, leaving only the dry compound that simplifies the soaking of the compound into the crystal. This will eliminate the influence of organic solvent on the crystallization.¹⁰⁴

In addition, other pharmaceutical companies have tried to develop their in-house fragment libraries, e.g. Astex²⁵³, deCode²²⁹, Novartis²⁵⁰, Plexxicon²⁵⁴, Roche²⁵⁵, Schering-Plough²⁵⁶ and ZoBio/Pyxis.¹⁹⁰ These in-house general libraries have been analyzed in the recent review on fragment library design.²¹⁵ Many others diverse fragment libraries are commercially available by supplier e.g. Key Organics²⁵⁷, Enamine²⁵⁸, Vitas M. Lab²⁵⁹, Chembridge²⁶⁰, Life Chemicals²⁶¹, Maybridge²⁶², and so on.

2.3. Fragment library focused on a specific target

2.3.1. Kinases

Many fragment libraries are developed specifically for kinase protein. The KINACoreTM library is a computationally selected library of more than 6,000 fragments from ChemBridge's CORE Library. This fragment library is composed of two groups: compounds selected using the same methods in selecting KINASet, a drug-like kinase focused library, and compounds selected using pharmacophore generated from known kinase actives. With more

than 60 core scaffolds are represented, this fragment library has already yielded a number of selective kinase ligands with compounds in the lead optimization discovery phase.²⁶⁰ Besides, an other kinase fragment library containing 357 fragments was developed by InFarmatik company²⁶³ and GSK.²⁶⁴

2.3.2. Central nervous system.

Central nervous system (CNS) is a challenging field for drug discovery. In fact, drugs that target on CNS tend to be smaller, more rigid, to have fewer hydrogen bond donors and lower TPSA than other drugs. Therefore, FBDD is a suitable approach for CNS drug discovery. Key Organics has designed the BIONET CNS fragment library in which the section criteria is stricter than rule of 3. These criteria include $MW \leq 240$, rotatable bonds ≤ 2 , $TPSA \leq 50 \text{ \AA}^2$ and $HBD \leq 2$. This library consists of 700 fragments which are carefully selected with high purity ($\geq 95\%$), experimentally assured aqueous solubility (1mM) and excellent diversity.²⁵⁷

2.3.3. Metallo-proteins

It have been noted that one-third of functional protein drug targets that contain a key catalytic or structural metal ion. They comprised of dehydrogenases, oxidoreductases, hydrolases, deacetylases and so on. These targets were suggested to require more specific interaction with fragments. Thus, AnCoreX therapeutics has created MetaKelTM library. This library comprises 500 fragments and each compound containing a metal chelating group. Despite the small size, MetaKelTM fragments demonstrated high hit rate after screening and provided ample functionality for maturation into hits and leads.²⁶⁵

2.3.4. Protein-protein interactions

Protein-protein interactions (PPI) are integral part of the majority of biological functions. PPI interfaces are usually large, up to thousands of square angstroms. Therefore, it has been demonstrated that due to low ligand efficiency of the compounds screened in PPI assays, the minimum detectable molecular weight of active PPI fragments is typically more than 300 Da. This value is contrast to FBDD strategies. Furthermore, PPI fragments often contain multiple hydrophobic moieties because hydrophobic interactions play a very important role in this target. These properties may therefore retain high aqueous solubility which is important both to enable screening at the high concentrations required for fragment-based approaches.^{266,267} Asinex has therefore designed and synthesized a wide range of poly-substituted, saturated and aromatic fragments for PPI application. A library was produced with highly soluble, hydrophobic PPI fragments taking advantage of the carboxylic acid moiety as the solubilizing group, potential point of attachment and effective mimic of Glu or Asp sidechains in protein-protein interactions.²⁶⁸

2.4. Fragment library designed for a specific screening method

As described in section 1.2.7, screening methods also influence on fragment library design. In fact, some techniques require the fragments to have specific properties in order to reduce the false prediction in hit identification. We presented herein several fragment libraries which were designed for specific screening methods.

Firstly, there are many fragment library which are designed for NMR screening. We can present notably here APGNMR07, a diverse fragment library at AstraZeneca, designed primarily for protein-detected NMR screening. This library consisted of 1,200 compounds and was stored as 200 mM stock solutions in deuterated DMSO. This library was divided into 200 cocktail groups. Each group contains six compounds in which have at least one anionic, one cationic, and four neutral compounds. This allows the library to be screened as mixtures of 6 or 12 compounds while minimizing the risk of buffering problems where too many acids or bases being combined in a single mixture.²¹⁵

Furthermore, Jordan and his coworkers²⁶⁹ have recently demonstrated that ¹⁹F-NMR fragment screening can be used as a very efficient tool for rapid and sensitive detection of fragment hits. A simple one-dimensional ¹⁹F-NMR experiment (with ¹H-decoupling) is significantly faster than traditional ¹H-NMR screening. This technique offers high throughput (potentially thousands of compounds per day) and low fragment concentration which avoid solubility challenge of fragments. However, this novel technique has been only recently introduced by targeting “fluorophilic” sites in proteins and the usefulness of ¹⁹F-NMR based methods is currently limited due to the small number of purchasable fluorinated fragments. Nowadays, the ¹⁹F-NMR focused screening library have attracted to many companies. Otava company has designed a new fluorine containing fragment library specified for ¹⁹F-NMR with more than 800 fragments. All compounds in this library have at least one mono fluoro or mono-trifluoromethyl group.²⁷⁰ In addition, Key Organics designed the BIONET fluorine fragment library which contains 1,143 mono-fluoro or mono-trifluoromethyl decorated fragments. This library allows an easier identification of the fragment bound in the active site of a target by the highly sensitive ¹⁹F-NMR technique.²⁵⁷ Maybridge has also designed a set of over 5,300 fluorine containing fragments which is a convenient source for ¹⁹F-NMR based applications²⁶² while Life Chemicals has developed a 3,900 fluorinated fragments library.²⁶¹ Novartis has recently developed their in-house library, named Local Environment of Fluorine (LEF), combined with ¹⁹F-NMR ligand-based screen fragments.²⁷¹

In X-ray crystallography screening, it has been noted that fragments are weak binders with partial occupancy, resulting in weak, difficult-to-fit electron density. Therefore, the use of a brominated fragment library would interestingly help to overcome this challenge, as bromine can be located unequivocally via anomalous scattering. Many brominated containing fragments was constructed to facilitate X-ray-based fragment screening. Moreover, brominated fragments also allow for rapid hit elaboration. There are some brominated-library such as a 1630 brominated fragments library named as BIONET Bromine Fragment Library (Key Organics company)²⁵⁷ and a 1500 ready-made bromine containing fragment library supplied by Maybridge company.²⁶² On the other hand, there is a fragment library focused on crystallography-based screening at Johnson & Johnson. The relatively low throughput of this screening method requires a balance between screening coverage and screening time. The resulting library consists of 900 compounds with a sufficient coverage of chemical space and allows screening in reasonable time. This fragment library is used as a primary screen for all targets at Johnson & Johnson company. It is typically screened using 180 crystals that have been soaked with a cocktail of approximately five fragments which are similar in structure shape. This is interesting because most groupings performed in other fragment libraries have

tended to be done to maximize the shape difference between the compounds in order to simplify the identification of the bound compound from the electron density. On the contrary, the researchers from Johnson & Johnson suggest that grouping by shape-similar criteria instead has a number of advantages.¹⁰⁴

2.5. Limitations of the actual fragment libraries

Most fragment libraries have been designed to contain a good equilibrium in properties and represent efficiently the chemical space. However, there always exist an imbalance in fragment libraries regarding success rates across all target classes. According to a recent review, actual fragment libraries are predominantly populated with heterocyclic and aromatic-derived chemotypes. This ‘flatness’ property could explain why they are less successful in identifying hits for certain targets that might require pharmacophores having alternative substitution vectors to interact with these proteins structures.²⁴⁵

On the other hand, many analysis studies on the structure shape of actual marketed drugs and bioactive compounds have concluded the positive effect of 3D-likeness property in success rate of drug development. As an example, researchers from GSK company suggested that too many aromatic rings in a molecule has a detrimental effect on human bioavailability parameters, correlates with poorer druggable developability and lead to an increased risk of attrition in development.^{272,273} In contrast, Lovering and his colleagues analyzed the effect of saturation and complexity on molecule solubility and compound progression through the drug development stages. These authors demonstrated that both complexity (as measured by a higher proportion of sp^3 -hybridized carbons) and the presence of chiral centers correlate with success when compounds transition from discovery, through clinical testing, to drugs.²⁷⁴ The similar results have recently observed by a computational analysis on the Drug Bank database.²⁷⁵ Moreover, other studies on protein binding behaviors have demonstrated that increasing the content of sp^3 -hybridized and stereogenic atoms improved binding selectivity and frequency.^{276,277} In the same manner, several authors suggested that actual fragment libraries should be expanded with more sp^3 -hybridized scaffolds in order to improve the success rate in hit identification for more demanding biological targets.^{105,245} In fact, several studies concerning 3-D fragments development have been published in literature. In 2011, a research group from Broad Institute has developed several sphere-like fragments based on diversity-oriented synthesis. This method gave access to diverse bicyclic and spirocyclic fragments while still keeping the size of the compounds down (<300 Da).²⁷⁸ Morgan and his colleagues have synthesized a series of 2-(aryl-sulfonyl)-oxetanes as 3-dimensional fragments for fragment screening.²⁷⁹ The 3D-fragments were also designed from fragmentation of natural products.²²⁷ In addition, 3D Fragment Library consortium was recently established in United Kingdom. Its goal is to develop fragment-screening libraries with enhanced 3D characteristics and evaluate their effect on the quality of fragment-based hit identification projects.²⁴⁵

The second limitation is a low ratio of halogen fragments in actual libraries. Many recent reviews have recognized a possible role of halogen bonds in medicinal chemistry.^{280,281} A large number of drugs and drug candidates in clinical development contain halogen

substituents.²⁸² Therefore, halogen-enriched fragment libraries have become an interesting topic in recent years.^{105,283}

3. Analysis of some commercial fragment libraries

In order to confirm these observations, we conducted an analysis on several commercially available fragment libraries. 95267 fragments from 6 suppliers, e.i. Key Organics, Enamine, Maybridge, Chembridge, Vitas M. Labs and Life Chemicals was assumed and filtered for several properties according to the procedure in Figure 59. The results have pointed out two interesting remarks.

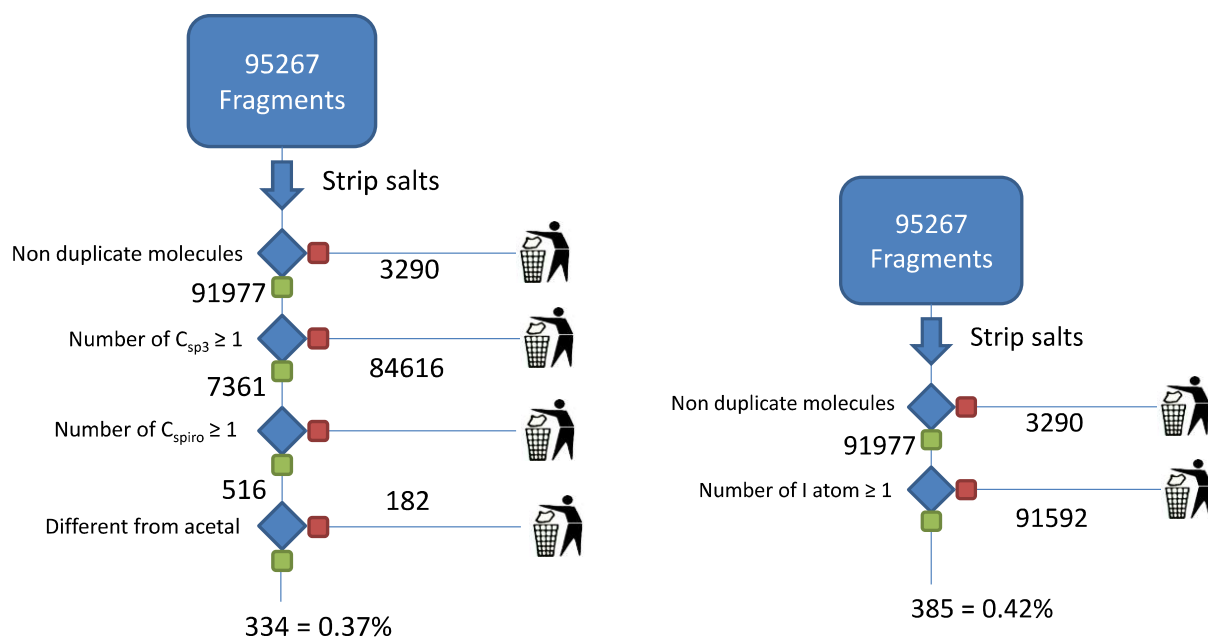


Figure 59: Proportion of C- sp^3 , spiro-carbon and iodinated fragments in commercially available libraries

First, the analysis result showed that only 8% of the whole fragment dataset have at least one carbon in the sp^3 hybridization state. Among these C- sp^3 containing fragments, only 0.56% has a spiro-carbon in structure and 0.37% are not acetals.

Second, the results also revealed that proportion of halogenated (brominated or iodinated) structures in these libraries is low, for example only 0.42% of the fragments present an iodine atom. This result is in line with a recent review.¹⁰⁵

4. Analysis of the fragment library in research group U1177

In a first step of our fragment library design, 1000 “Ro3” compliant fragments were purchased from commercial suppliers. Next, our in-house building blocks were selected to complete the primary set with 40 molecules. The physicochemical profile of our fragment library is exemplified in Figure 60.

Nowadays, the modified rule of three suggested by 3D Fragment Consortium²⁴⁵ has been used as our fragment selection criteria sets (as described in Table 14). The results showed that 93% of our fragment library validates more than five on the overall seven specification rules.

However, our library is mainly centered on sp^2 -rich aromatic compounds. The number of fragments that contain spirocyclic carbon or halogen atoms is low.

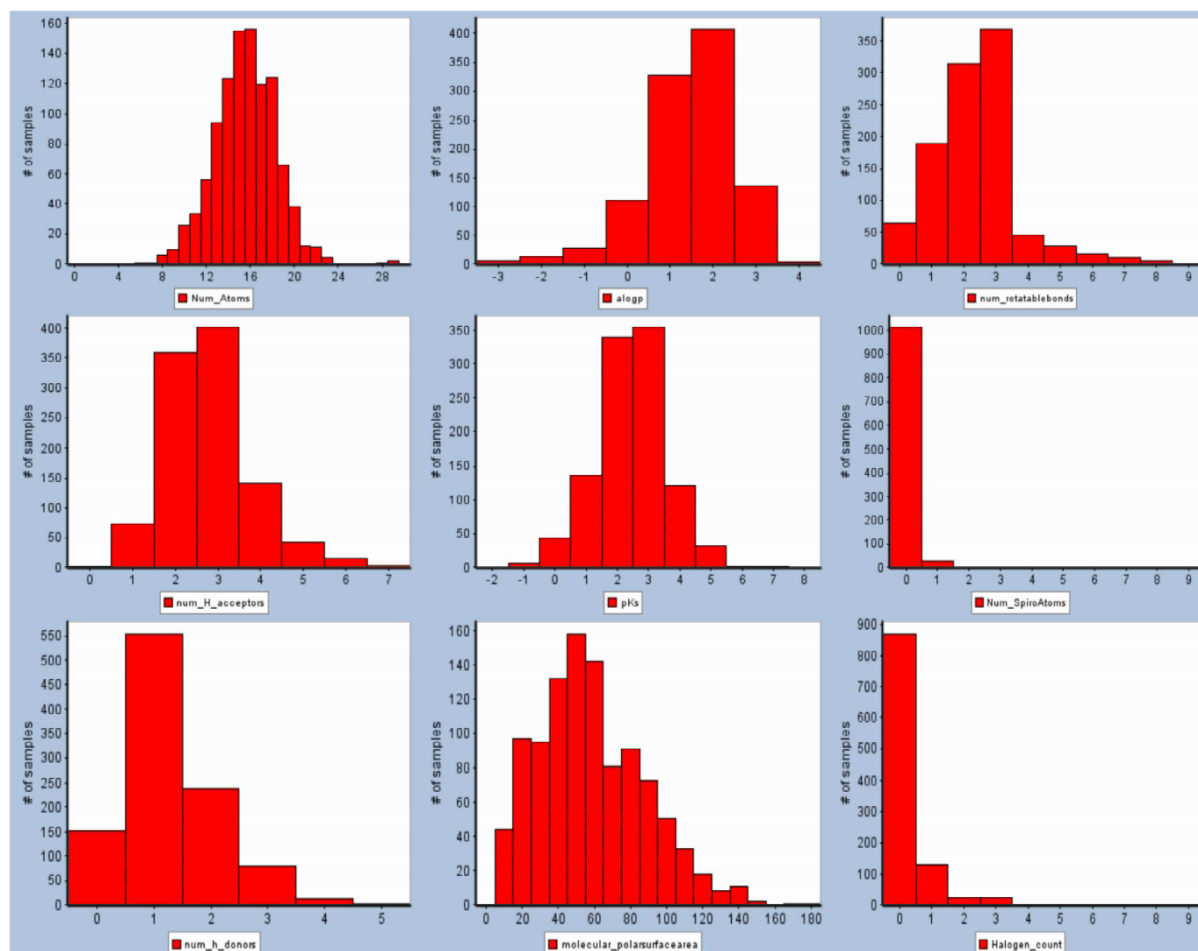


Figure 60: Physicochemical profile of U1177 fragment library

The shape of all fragments in the entire library was also analyzed. Principal moments of inertia²⁸⁴ (PMI) are simple way to calculate and evaluate the 3D diversity of a chemical structure. Molecules in their lowest-energy 3D conformer are used to calculate the three principal moments of inertia (pmi_x , pmi_y and pmi_z). These values are sorted by ascending magnitude, then normalised, dividing the two lowest values by the highest to generate normalised PMI ratios (NPR1 and NPR2). These values can be plotted in a 2D graph to provide the triangular output and used to calculate the proportion of ‘rod-like’, ‘disc-like’ and ‘sphere-like’ characteristics. The shape analysis of fragments in U1177 library is presented in Figure 61. Looking at the NPR_i plot, the compounds are clustered along the axis between rod-like and disc-like supporting the view that they have limited 3D shape.

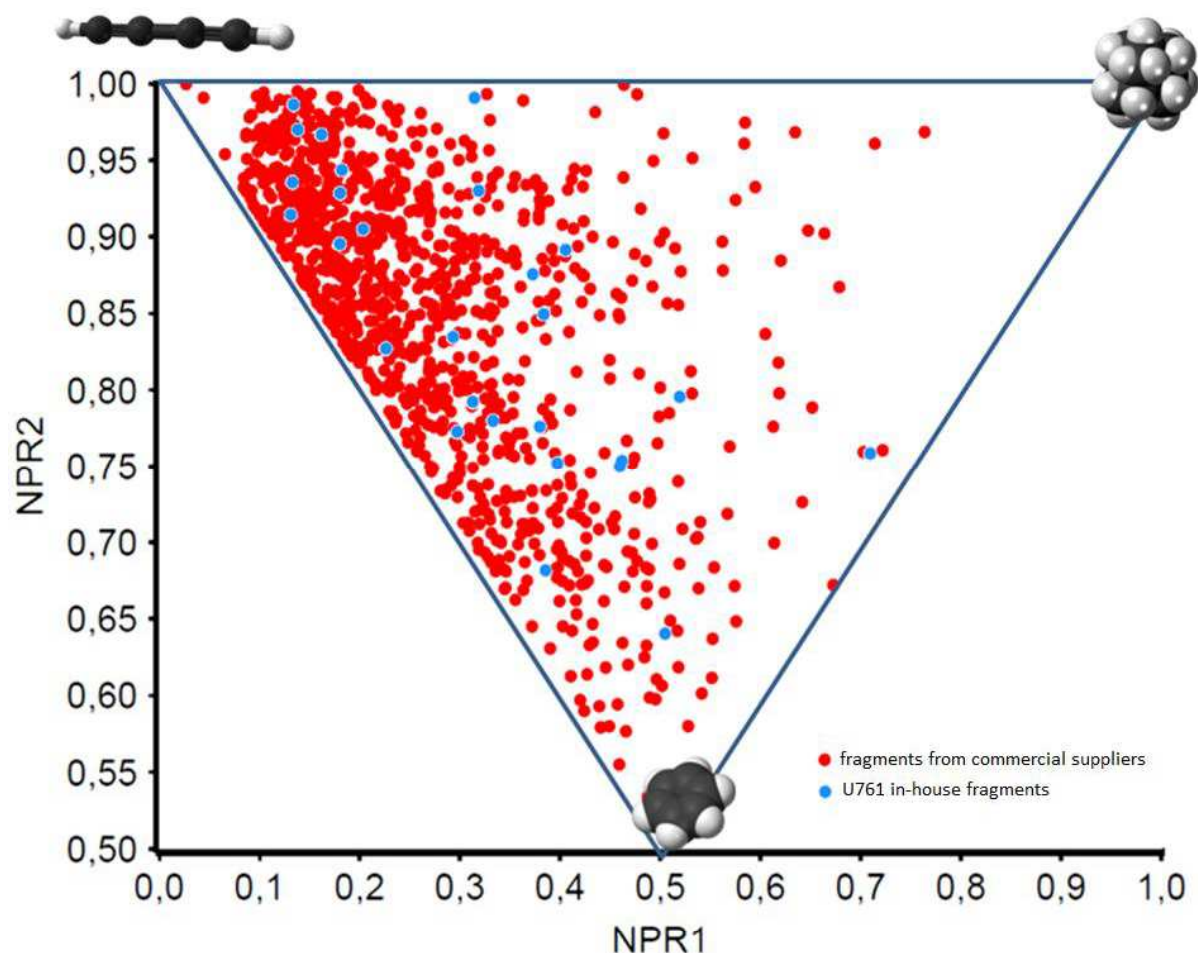


Figure 61: Molecular representation of the shapes of our fragment library using NPRi plot

5. Conclusion

In conclusion, FBDD has become a well-established approach in drug discovery. The design of fragment libraries is a pivotal element of the success in fragment screening. Many factors need to be considered in fragment library design, e.g. sources of fragments, the desired end-use of the fragment library and screening methods. Nowadays, there is an increase in fragment library design both in pharmaceutical industry and academia. However, an optimal selection of fragment library remains challenging. Analysis of several fragment libraries presented in literature, especially in our research group U1177 demonstrated that the actual fragment libraries tend to focus on sp^2 -rich compounds and did not cover well-explored areas of chemical space. In addition, the role of halogen bonds has been underestimated in actual libraries and need to be increased in the latter generations.

For these reasons mentioned above, we intend to expand the fragment library in our research group with more halogenated fragments and 3D-likeness fragments. In the first action, 80 halogen containing fragments have been selected from our available building block database and were then added to the fragment library. Next, the library will be enlarged with several original synthesized scaffolds which are enriched by $C-sp^3$ and/or spiro-carbons. These 3D-fragments should be available for screening against new biological targets to help kick-start hit discovery by fragment-based approach in our research group.

Part B. Synthesis of functionalized 2-isoxazolines as 3D fragments for fragment-based drug discovery

As a member of organic heterocyclic family, 2-isoxazoline has been studied and it has been showed that these compounds (Figure 62) are of great interest.²⁸⁵ Moreover, some natural products present 2-isoxazoline moiety in their structure. The most notable compounds are acivicin and (+)-calafianin. Acivicin²⁸⁶ is a fermentation product from *Streptomyces sviveus* which has shown promising anti-neoplastic activity and is under clinical trials. (+)-Calafianin²⁸⁷, a bromotyrosine-derived spiro-isoxazoline has been isolated from marine sponge *Aplysina gerardogreeni*. Recently, Kaur *et al.* have pointed out many 2-isoxazoline-containing natural products which exhibit a potential anticancer activity.²⁸⁸ Beside its natural occurrence, 2-isoxazoline is also an important skeleton found in many bioactive compounds of synthetic origin. Many papers have accounted in the last decade for the synthesis and occurrence of 2-isoxazoline in nature and medicinal chemistry. Isoxazoline derivatives have been reported in the literature to exhibit a broad range of biological activities, e.g. antimicrobial^{289–291}, anticancer^{292–294}, antiplatelet²⁹⁵, anti-inflammatory²⁹⁶ activities, and regular effects on central nervous system^{297–299} or sympathetic nervous system.³⁰⁰

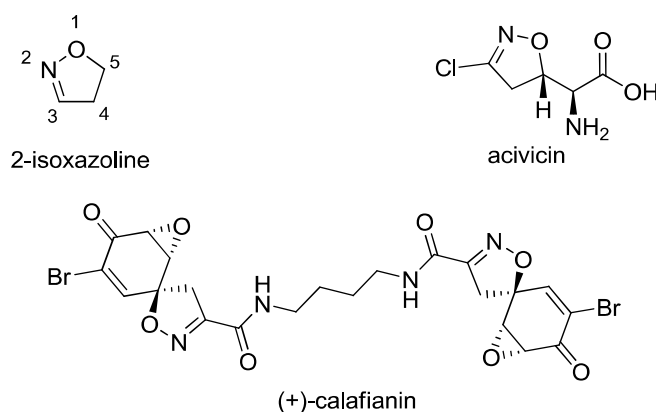


Figure 62: Structure of 2-isoxazoline and several bioactive natural products that contain this scaffold

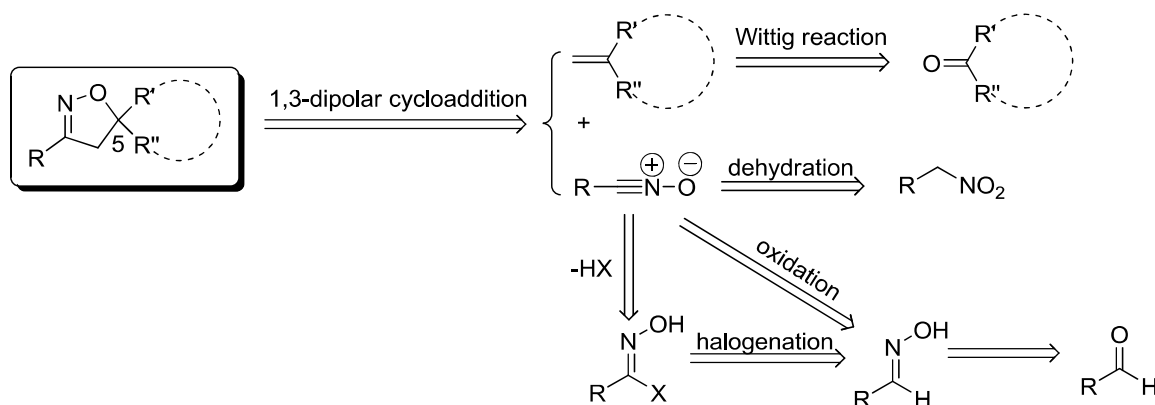
Prompted by these observations, and in order to potentially increase the chance to find hits during our screening campaigns, we focused on the design of new 2-isoxazolines as 3-dimensional fragments and we report herein their synthesis. Our objective was the optimisation of the 1,3-dipolar cycloaddition in one-pot synthesis to yield a diverse set of 3D-fragments with good physicochemical properties.

1. Synthesis of novel 2-isoxazoline fragments

1.1. Synthesis of 2-isoxazoline scaffold *via* 1,3-dipolar cycloaddition

Several synthetic methods used for the formation of 2-isoxazoline have been described in the literature.^{285,301} Among them, 1,3-dipolar cycloaddition has proved to be an excellent and general synthetic route.³⁰² The retrosynthetic analysis of 2-isoxazoline is depicted in Scheme 34. Our objective was to generate molecules bearing 2-isoxazoline scaffold *via* 1,3-dipolar cycloaddition between nitrile oxide (dipole) and 1,1-disubstitued alkene (dipolarophile). Many studies on the regioselectivity of isoxazoline synthesis by intermolecular 1,3-dipolar cycloaddition emphasized that 1,1-disubstitued alkenes react with

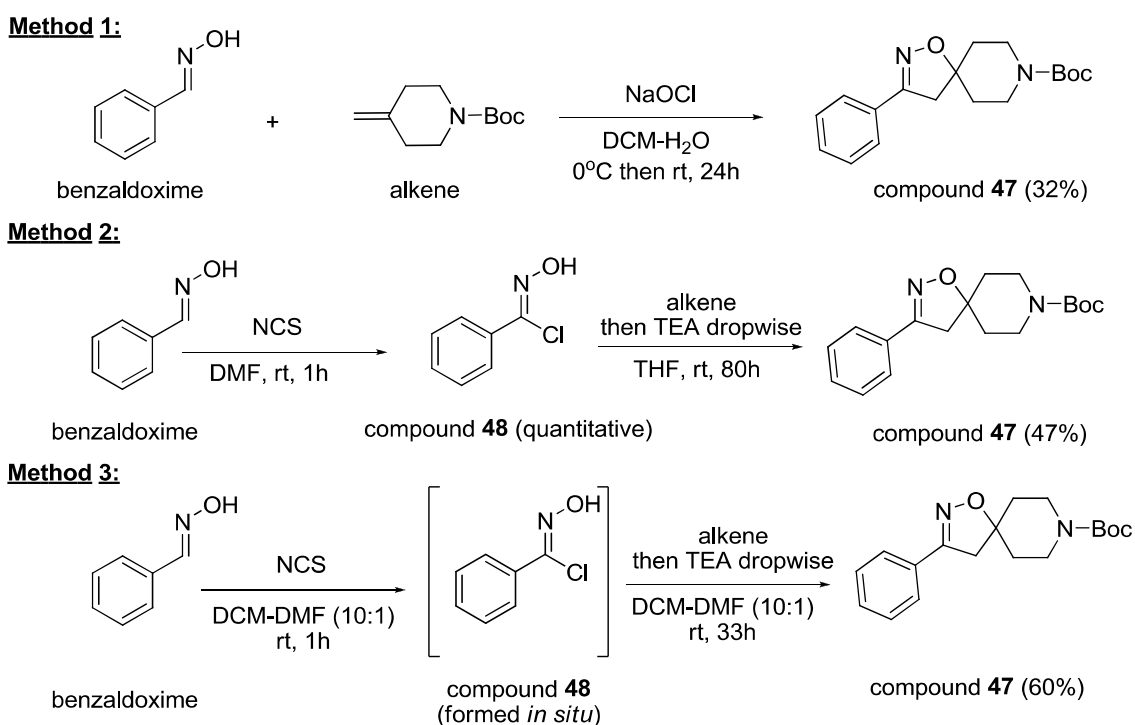
nitrile oxides to predominantly afford 5-substituted isoxazolines.^{303–305} Nitrile oxides are reactive intermediates that are usually generated *in situ* from stable precursors. They can be generated from primary nitro-alkane by dehydration or by a direct oxidation of aldoxime or halogenation of aldoxime to *N*-hydroxyiminoyl halides followed by dehydro-halogenation.²⁸⁵ The latter is the most usual method in nitrile oxide generation.³⁰⁶ In this study, aldoximes and alkenes were chosen as starting materials.



Scheme 34: Retrosynthetic analysis of 2-isoxazoline

1.2. Optimization of synthetic conditions of 1,3-dipolar cycloaddition

Benzaldoxime and *N*-Boc-4-methylene-piperidine (alkene) served as model substrates in the initial experiments (Scheme 35).



Scheme 35: Different synthetic conditions used for the synthesis of 2-isoxazoline containing compounds

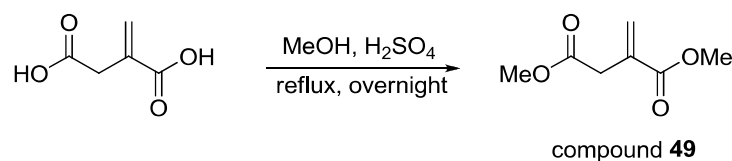
2-Isoxazoline (compound **47**) was firstly prepared using an aqueous solution sodium hypochlorite (1.6N).³⁰⁷ Unfortunately, the reaction mixture contained by-products and the targeted isoxazoline (compound **47**) was obtained in poor yield (32%). To improve yield, we considered other described conditions.^{308,309} Benzaldoxime was firstly chlorinated by *N*-chlorosuccinimide (NCS) in *N,N*-dimethylformamide (DMF). The *N*-hydroxyiminoyl

chloride (compound **48**) was isolated with quantitative yield. This intermediate was then converted to nitrile oxide followed by a 1,3-dipolar cycloaddition with *N*-Boc-4-methylene-piperidine in tetrahydrofuran (THF) to yield 47% of the desired isoxazoline (compound **47**). However, the main inconvenience of this synthetic pathway is that this process comprises two steps where the intermediate and the final product must be separately purified. This drawback becomes more challenging when a large number of isoxazoline fragments are synthesized. Furthermore, several studies in the literature have reported that some hydroxyiminoyl chloride (chloro-oxime) are unstable and must be used shortly after preparation.³¹⁰

Finally, an improvement of this synthetic method was achieved. The reaction was conducted using a one-pot procedure with a mixture of dichloromethane (DCM) and DMF (10:1) thanks to the adaptation of a published protocol.³¹¹ Benzaldoxime was converted after 1h into hydroxy-iminoyl chloride *in situ* using NCS. Addition of Boc-4-methylidene-piperidine and triethylamine allowed the formation of the targeted spiro-isoxazoline (compound **47**) in an overall yield of 60%.

1.3. Synthesis of novel 2-isoxazoline fragments from benzaldoxime

With the optimized reagents and synthetic conditions in hands (method 3, Scheme 35), the scope of the reaction was explored with benzaldoxime and a large set of gem-disubstituted alkenes in order to have at least one tetra-substituted carbon atom, or one spiranic carbon in the structure. Itaconic acid dimethyl ester **49** was successfully synthesized according to a published protocol.³¹²



Scheme 36: Synthesis of itaconic acid dimethyl ester

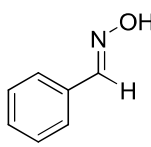
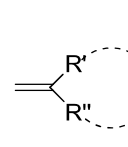
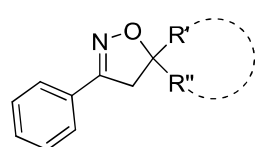
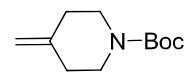
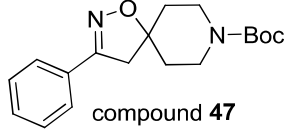
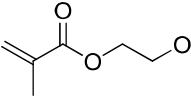
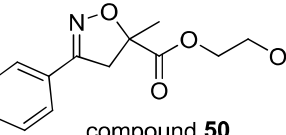
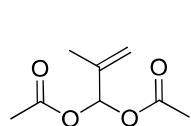
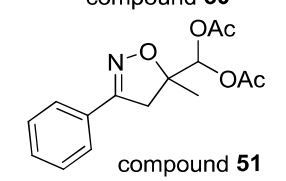
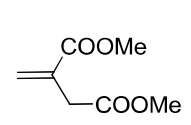
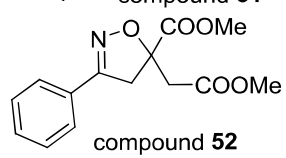
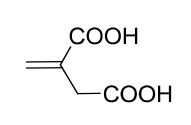
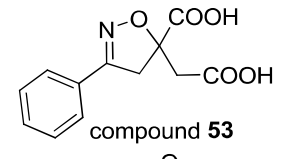
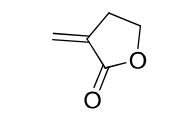
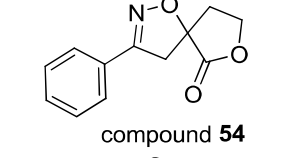
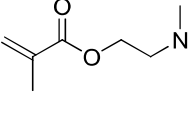
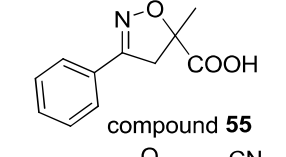
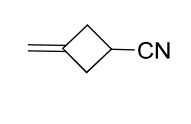
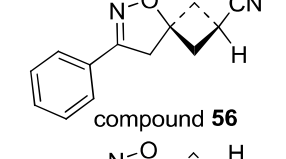
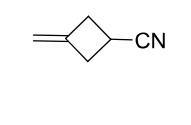
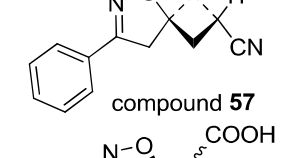
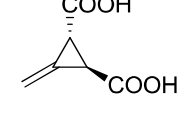
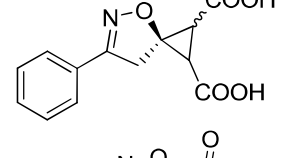
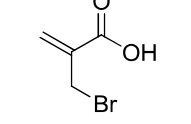
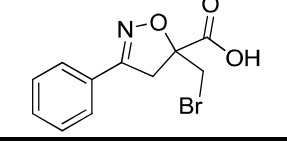
In summary, several original 2-isoxazoline containing fragments were synthesized using the optimized procedure (Table 15). As expected, 1,3-dipolar cycloaddition is controlled by the reactivity of alkenes. When alkenes are substituted with electron withdrawing groups (compound **50**, **52**, **53**, **54** and **55**), the reaction was completed after just 16 hours and isoxazolines were obtained in moderate to good yield (up to 94%). Interestingly, the presence of carboxylic function (compounds **53** or **55**) did not affect the reactivity.

On the contrary, a low reactivity was observed with alkene leading to compound **51**. Interestingly, the tert-butoxy-carbonyl (Boc) protecting group (compound **47**) was not cleaved under these mild conditions. In the case of 3-methylenecyclobutane carbonitrile used as starting alkene, reaction yielded two diastereomers (compounds **56** and **57**). After separation by flash-chromatography, the allocation of their structures was achieved using 1D-NOESY.

F_{sp^3} value is defined as the ratio of sp^3 -hybridized carbon atoms on the total carbon count. This value was calculated for these fragments.²⁷⁴ The results showed that F_{sp^3} of these fragments range from 0.25 to 0.40.

Chapter IV. Design and synthesis of novel 3D-fragments

Table 15: List of synthesized 2-isoxazoline from benzaldoxime and alkenes

Entry	Alkene	Structure	Time (h)	Yield	MW (Da)	Fsp ³	
	 benzaloxime	 alkene	1) NCS, rt, 1h 2) alkene 3) TEA, rt DCM-DMF (10:1)	 2-isoxazolines			
1		 compound 47	33	60%	316.40	-	
2		 compound 50	16	93%	249.30	0.38	
3		 compound 51	39	35%	291.30	0.40	
4		 compound 52	16	88%	277.30	0.36	
5		 compound 53	19	60%	249.20	0.25	
6		 compound 54	16	94%	217.20	0.33	
7		 compound 55	16	56%	205.20	0.27	
8		 compound 56	16	16%	212.30	0.38	
		 compound 57	16	40%	212.30	0.38	
9			16	unstable in purification	-	-	
10			16	This reaction did not work	-	-	

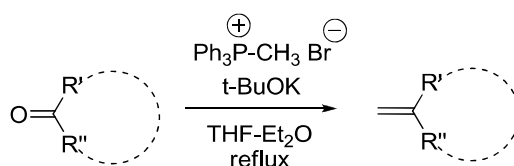
1.4. Synthesis of novel 2-isoxazoline fragments from aliphatic aldoxime

In an effort to generate more sp^3 -rich fragments with high F_{sp^3} value, benzaldoxime was then replaced by commercially available acetaldoxime or synthesized cyclopropyl-carbaldoxime. Further alkenes were prepared from commercially available ketones.

1.4.1. Preparation of starting materials for 1,3-dipolar cycloaddition

1.4.1.1. Preparation of alkenes from ketones

Several non-commercially available alkenes were obtained from the corresponding ketones using Wittig conditions as described in literature (see Scheme 37).³¹³



Scheme 37: Synthesis of alkenes using Wittig conditions

The mechanism of the Wittig's reaction is illustrated in Figure 63. The first step is the formation of ylide from phosphonium salt. The base, tert-BuOK, will deprotonate the methyl group of the phosphonium salt.

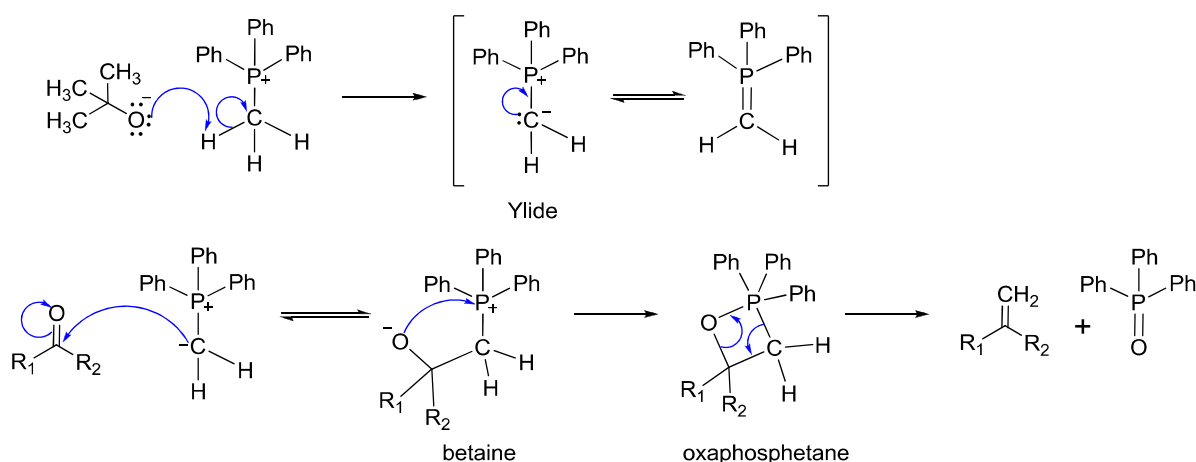
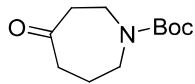
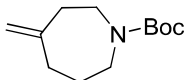
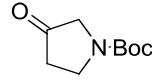
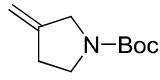
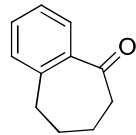
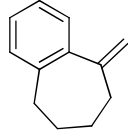
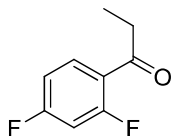
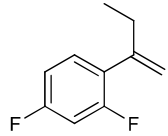
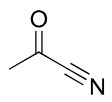
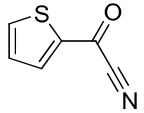
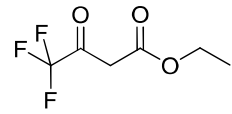
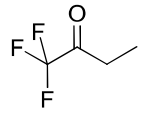


Figure 63: Mechanism of the Wittig's reaction

In a second step, addition of the ylide to the carbonyl (ketone) is postulated to lead to the zwitterionic intermediate named as betaine, which would then close to form a four-membered cyclic intermediate, an oxaphosphetane. This intermediate is then transformed to a very stable phosphine oxide and the corresponding alkene. It has been noticed that the ylide is a very strong base which can be protonated by water or alcohol. So the reaction must be conducted in anhydrous conditions. The ylide is also sensitive to oxygen. For that reason, all Wittig reactions were carried out under Argon atmosphere. As observed in the mechanism, triphenylphosphine oxide is always obtained as by-product in this reaction.

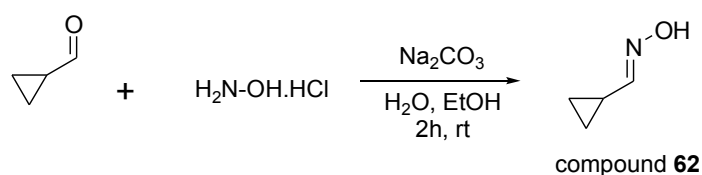
According to the Wittig conditions, four alkenes have been prepared from corresponding ketones (Table 16). However, in the case of nitrile or trifluoromethyl derivatives (entries 5 to 8), the reaction did not occur. This may be due to the poor reactivity of starting material ketones.

Table 16: List of synthesized alkene from corresponding ketones

Entry	Ketone	Alkene	Yield
1		 compound 58	59%
2		 compound 59	33%
3		 compound 60	88%
4		 compound 61	57%
5		This reaction did not work	-
6		This reaction did not work	-
7		This reaction did not work	-
8		This reaction did not work	-

1.4.1.2. Preparation of cyclopropyl aldoxime

Cyclopropylcarbaldoxime was synthesized according to a published protocol. The cyclopropyl carboxaldehyde was reacted with hydroxylamine in basic conditions to yield a isomeric mixture of *Z* and *E* cyclopropyl carbaldoxime **62** in a moderate yield (62%).



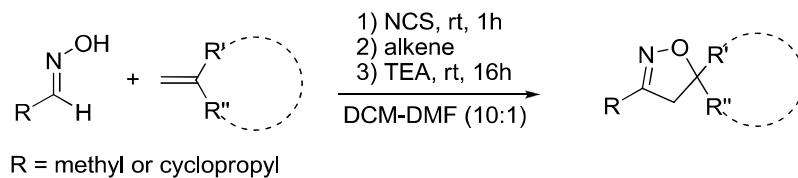
Scheme 38: Synthesis of cyclopropylcarbaldoxime

1.4.2. Synthesis of novel 2-isoxazoline fragments from aliphatic aldoxime

Starting from acetaldoxime and cyclopropylaldoxime together with several commercial or synthesized alkenes, we have obtained nine spiroisoxazoline containing compounds thanks

to 1,3-dipolar cycloaddition (Table 17). Fragments **67** and **69** were obtained in good yields thanks to the high reactivity of the starting alkene, where electron density is lowered by the lactone. The seven remaining compounds were synthesized with low to moderate yields. The F_{sp^3} was also calculated and presented in Table 17.

Table 17: List of synthesized 2-isoxazoline containing 3D-fragments

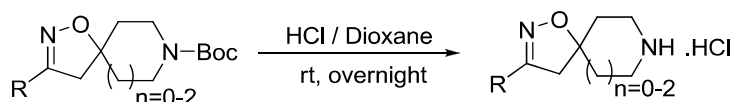


Entry	R=	Alkene	Structure	Yield	MW (Da)	F_{sp^3}
1	Me		 compound 63	42%	254.33	-
2	Me		 compound 64	37%	268.36	-
3	Me		 compound 65	55%	240.31	-
4	Cyclopropyl		 compound 66	52%	280.37	-
5	Me		 compound 67	72%	155.15	0.71
6	Me		 compound 68	10%	193.29	0.92
7	Cyclopropyl		 compound 69	87%	181.19	0.78
8	Me		 compound 70	29%	225.23	0.42
9	Me		 compound 71	32%	215.29	0.50

1.5. Cleaving of *N*-Boc protecting group

Compounds which contain a Boc protecting group were then cleaved using acidic conditions¹⁹⁸ to afford the corresponding hydrochloride salts (Table 18).

Table 18: List of synthesized 2-isoxazoline with Boc group was cleaved under acid condition



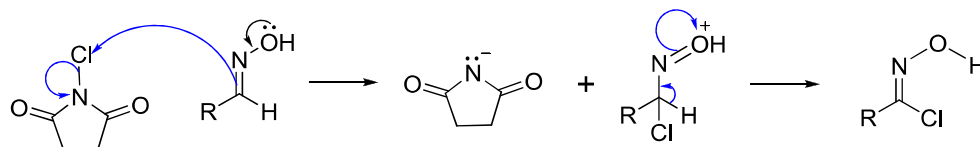
Entry	Starting material	Product	Yield (%)	MW (Da)	Fsp ³
1		 compound 72	74	252.75	0.46
2		 compound 73	70	190.68	0.88
3		 compound 74	84	204.70	0.89
4		 compound 75	90	176.65	0.86
5		 compound 76	90	216.71	0.90

1.6. Study of by-products formation during the 1,3-dipolar cycloaddition

The mechanism of this one-pot synthesis proceeds in three steps. The first step is the chlorination of the starting aldoxime by *N*-chlorosuccinimide (NCS). Next a base (TEA) is added to form the nitrile oxide *in situ* as shown in Scheme 39. In the final step, 1,3-dipolar cycloaddition between nitrile oxide (dipolar) and 1,1-disubstituted alkenes (dipolarophile) afford isoxazoline as the desired product (Scheme 39).

In some of 1,3-dipolar cycloadditions, we observed the formation of a by-product. Thanks to NMR analysis, this side-product was supposed to come from the dimerization of nitrile oxide in the absence of a reactive dipolarophile as trapping agent to yield 1,2,5-oxadiazole-2-oxide.³¹⁴ The proposal mechanism is shown in Scheme 40. To confirm this hypothesis, we conducted reactions with benzaldoxime and acetaldoxime in the absence of alkene. We observed that furoxan (compound **77**) was formed in case of acetaldoxime. In contrast, the formation of furoxan was not observed when using benzaldoxime. These results are consistent with the literature.³⁰⁶

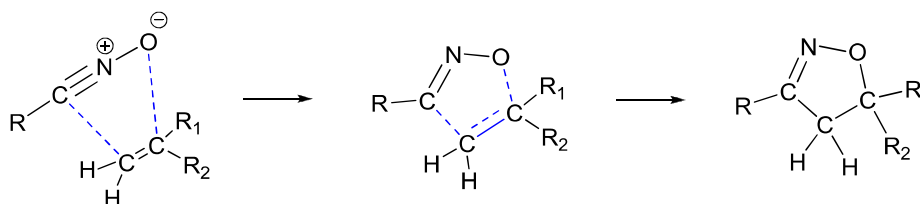
Chlorination by NCS:



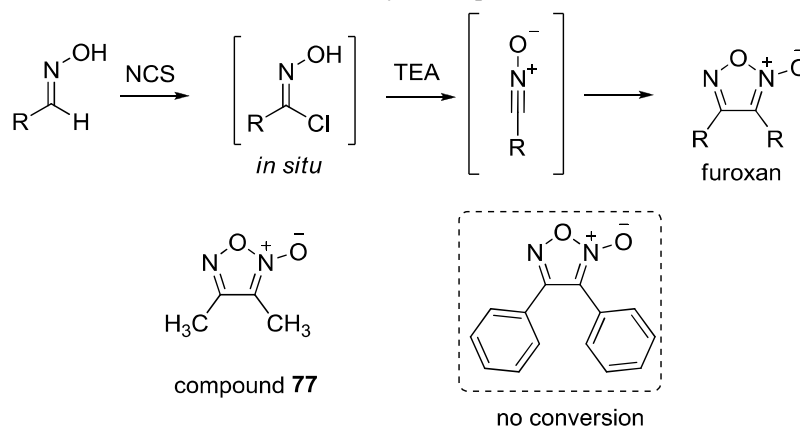
Nitrile oxide formation:



1,3-dipolar cycloaddition:



Scheme 39: Mechanism of 2-isoxazoline synthetic procedure from aldoxime and alkene

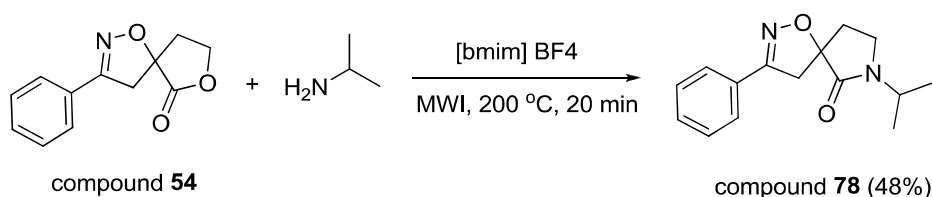


Scheme 40: By-product furoxan from dimerization of nitrile oxides

1.7. Functionalization of novel 2-isoxazoline fragments

In our collection of 2-isoxazoline fragments, compound **54** contains a lactone function. We therefore tried to increase the diversity of this fragment using nucleophiles, such as amines or alcohols.

In first attempt, we tried to convert this lactone to a lactam ring. Recently, a selective lactamization protocol of lactone in ionic liquids was developed by a research group at Uppsala university.²¹² We then applied this protocol to lactamize the lactone in compound **54** in 1-butyl-3-methylimidazolium tetrafluoroborate salt [bmim]BF₄ as ionic liquid. The lactam **78** was formed with a 48% yield (see Scheme 41).

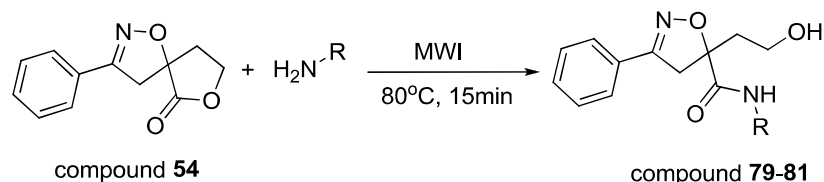


Scheme 41: Lactamization of lactone in ionic liquid

In an effort to show that ionic liquid is essential in this lactamization process, the reaction was then conducted in a solvent free condition under microwave irradiation at 200°C. In that particular condition, the desired lactam was not formed. This result confirmed that ionic liquid [bmim]BF₄ is participating in the lactamization step.

In another attempt to introduce diversity starting from compound **54**, we studied the possibility to open the lactone ring with amines, to afford amides. For that purpose, we heated compound **54** with different amines at 80°C for 15 minutes under microwave irradiations. This led to the synthesis of three new fragments in good yields (65% to 82%, Table 19).

Table 19: Synthesis of isoxazolines fragment starting from lactone **54**



Entry	Amine	product	MW	Yield	Fsp ³
1	<chem>H2NCC#C</chem>	<chem>c1ccc(cc1)C=C2NOC2C(=O)N(CC#C)CO</chem> compound 79	272.30	82%	0.33
2	<chem>H2NCCC</chem>	<chem>c1ccc(cc1)C=C2NOC2C(=O)N(CCC)CO</chem> compound 80	276.33	78%	0.47
3	<chem>H2NCCO</chem>	<chem>c1ccc(cc1)C=C2NOC2C(=O)N(CCO)CO</chem> compound 81	278.30	65%	0.43

2. Analysis of synthesized fragments

2.1. Molecular shape properties of this new set of fragments

Finally, we analyzed the overall shape coverage of our entire set of fragments by monitoring normalized PMI ratios (npr1/npr2), according to Sauer's method.²⁸⁴ This method lies on a molecular shape analysis of the fragments using three principal moments of inertia (PMI), calculated from the 3D-structure. The values were sorted by ascending magnitude I₁, I₂, and I₃. Subsequently, normalization was performed by dividing the two lower PMI-values (I₁ and I₂) by the highest value (I₃), generating two characteristic values of normalized PMI ratios (NPRs) for each compound (NPR1 and NPR2). The two values were then used to present the molecular shape in normalized PMI ratio triangle plot. This data were compared to the one obtained with 471 members of our in house library of commercially available fragments with similar molecular mass.

The graph shows that our set of substituted isoxazoline fragments (in pink) cover a large space of shapes (Figure 64) with a greater proportion of rod-like or sphere-like shapes than commercially available fragments. The calculation of the mean of NPR1+NPR2 with both sets: 1.19 ± 0.08 for 2-isoxazoline containing fragments and 1.09 ± 0.07 for the 471 commercially available fragments confirms this tendency. Interestingly, two fragments **70** and **71** which were designed from aryl alkenes (with medium F_{sp^3}) showed also sphere-like and rod-like properties. This observation suggests that the fragments with a suitable position of aromatic ring in structure could have also 3D properties. These results are conformed to a recent study in which the authors showed that a positive-correlation between F_{sp^3} and 3-dimensionality of molecule are not always observed.³¹⁵

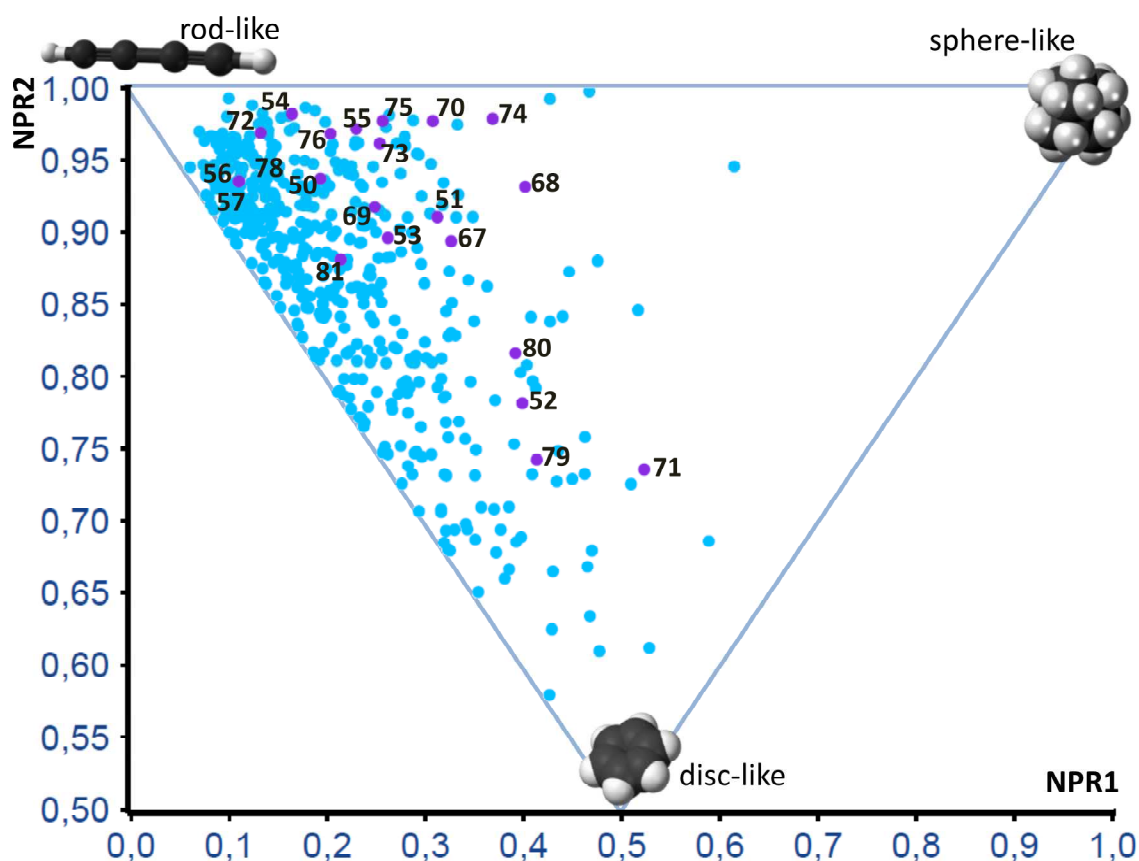


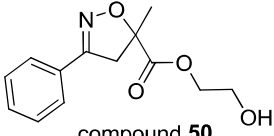
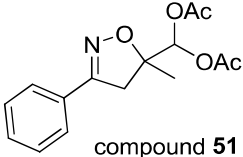
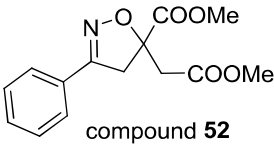
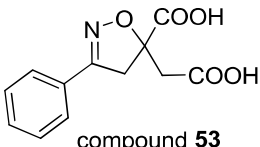
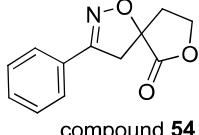
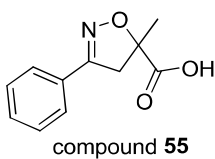
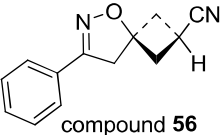
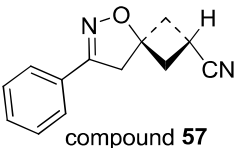
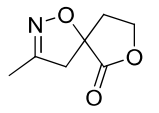
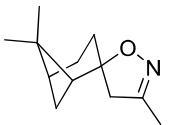
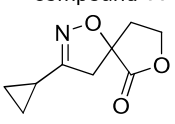
Figure 64: Molecular shape analysis of set isoxazoline containing 3D-fragments

2.2. Solubility of synthesized fragments

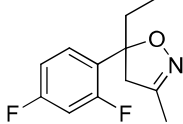
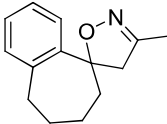
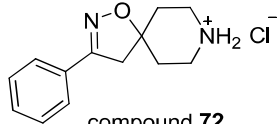
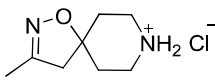
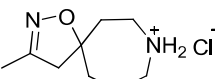
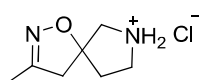
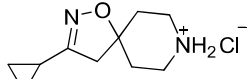
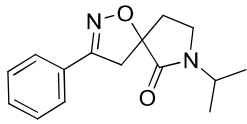
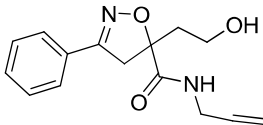
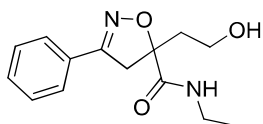
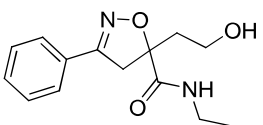
Experimental solubility of the synthesized fragments in phosphate buffer solution (PBS) at pH 7.4 was also measured using HPLC-MS method. In principle, the fragment was solubilized in DMSO at a concentration of 100 mM. This solution was then diluted in PBS to a 2 mM concentration. A reference solution in methanol at 2 mM was also prepared. However, when the fragment was confirmed insoluble in methanol, DMSO was used. In case of lactone containing fragments, methanol was replaced by acetonitrile. The solubility of these fragments is presented in Table 20.

Chapter IV. Design and synthesis of novel 3D-fragments

Table 20: Experimental solubility of synthesized fragments

Entry	Structure	Apperance	m.p. (°C)	cLogP	Solubility (mM)	Notice
1	 compound 50	liquid	-	1.53	1.0	partially unstable in PBS
2	 compound 51	liquid	-	3.02	1.0	partially unstable in PBS
3	 compound 52	solid	60-62	1.67	1.5	
4	 compound 53	solid	202-205	1.05	>2	
5	 compound 54	solid	129-131	1.96	-	unstable in PBS
6	 compound 55	solid	168-170	1.93	1.8	
7	 compound 56	solid	128-130	2.36	0.4	
8	 compound 57	solid	110-112	2.36	0.3	
9	 compound 67	solid	72-74	0.29	-	unstable in PBS
10	 compound 68	solid	47-48	3.45	1.9	
11	 compound 69	solid	52-54	0.46	-	unstable in PBS

Chapter IV. Design and synthesis of novel 3D-fragments

Entry	Structure	Appearance	m.p. (°C)	cLogP	Solubility (mM)	Notice
12	 compound 70	liquid	-	3.25	0.8	
13	 compound 71	solid	56-58	3.47	1.6	
14	 compound 72	solid	265-266	2.45	>2	
15	 compound 73	solid	238-239	0.79	>2	
16	 compound 74	solid	195-198	1.13	>2	
17	 compound 75	solid	187-190	0.45	>2	
18	 compound 76	solid	255 (dec)	0.96	>2	
19	 compound 78	solid	117-119	2.45	>2	
20	 compound 79	solid	122-124	1.18	>2	
21	 compound 80	solid	111-112	1.67	>2	
22	 compound 81	solid	114-116	0.19	1.9	

Most of the fragments containing the 2-isoxazoline motif presented a good solubility (>2mM). Only three fragments (**56**, **57** and **70**) showed a lowest solubility in PBS (0.3, 0.4 and 0.8 mM, respectively). This was not surprising as they were more hydrophobic. Moreover, the solubility of the lactones (compounds **54**, **67** and **69**) was not measured as they were unstable in the experimental conditions. Similarly, compounds **50** and **51** with an ester group in structure have been found to be also partially unstable in PBS solution.

Interestingly, compounds **68** and **71** also have a good solubility despite the lack of hydrophilic functions. This may be explained by the spiro carbon that does limit intermolecular hydrophobic interactions.

The melting points of the fragments in solid form were also measured. However, we were not able to draw any correlation between melting point and solubility value of this set of fragments. In addition, the clogP of these fragments was also calculated. But no correlation was found between clogP and experimental solubility.

3. Conclusion and outlooks

In summary, we have optimized a reliable protocol for the synthesis of a diverse set of 2-isoxazoline scaffold using 1,3-dipolar cycloaddition between chloro-oximes and alkenes. Lactone containing fragment **54** was further functionalized with amines under microwave irradiations, to show that it is possible to easily introduce diversity around these fragments. Using chemoinformatic analysis, we quantified the shapes and physical properties of the novel synthesized fragments. Experimental solubility of these the synthesized fragment were also measured. The results showed that most of these fragments have a suitable solubility to be considered for screening.

This page intentionally left blank

General conclusion

The main objective of this thesis was to develop fragment-based approaches for the discovery of biologically active molecules in the framework of TB projects.

In the first part of this thesis we report the pharmacokinetic optimization of new EthR inhibitors that were initially discovered starting from a fragment. The lead compound BDM43266 was considered as the most potent EthR inhibitors. This compound showed a high affinity for EthR ($\Delta T_m = +11.2$ °C) and a potency to boost ethionamide activity *in vitro* in the nanomolar range ($EC_{50} = 80$ nM). However, BDM43266 showed a poor *in vitro* metabolic stability in mouse liver microsomes with a half-life of 10 minutes and an intrinsic clearance of 144 $\mu\text{L}/\text{min}/\text{mg}$. This compound was therefore not suitable to start *in vivo* assays.

Analytical study of the metabolites predominantly formed during the metabolic process using high resolution MS-TOF and tandem MS, combined with their synthesis allowed the identification of the main metabolite which is formed *via* oxidation of the methyl group attached to the thiazole ring. (see Figure 65)

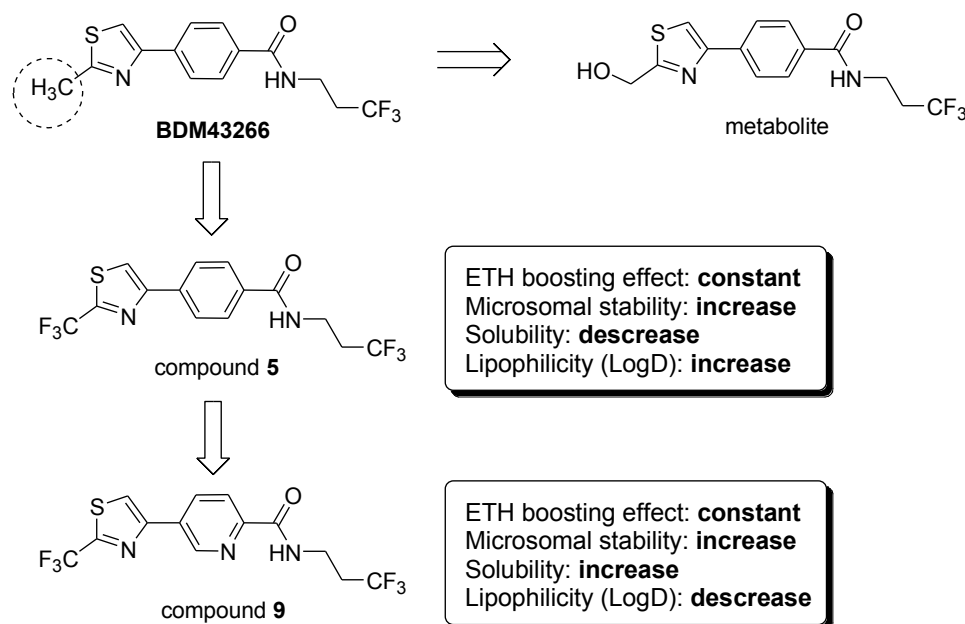


Figure 65: Metabolism study and structural modifications of BDM43266

Several key structural modifications have been carried out to increase the microsomal stability of analogues. First, a substitution of methyl group by fluorine atoms led to the improvement of the microsomal stability (compound **5**). However, this modification resulted also in a decrease of the aqueous solubility concomitant to an increase of the lipophilicity. To overcome this drawback, we replaced the benzene ring by a pyridine to yield compound **9**. These two key structural modifications allowed the identification of new potent EthR inhibitors having acceptable pharmacokinetic and physico-chemical properties for *in vivo* assays.

In the second part of this thesis, a fragment library was screened to identify MabA inhibitors. MabA is a mycobacterial β -ketoacyl-ACP reductase involved in the synthesis of long-chain fatty acids, precursors of mycolic acids, which are major constituents of the mycobacterial cell wall. This enzyme has been shown to be essential for the survival of the

bacteria. In the first stage, screening of a fragment library on MabA was performed respectively by two screening techniques: an affinity-based assay (TSA) and a high content screening (HCS) on *M. tuberculosis*. The 12 identified hits were re-synthesized and then tested using a functional assay that was developed in the course of this work. Unfortunately, none of them showed any activity at 1 mM. This result allowed us to draw two conclusions:

1. Binding of fragments to MabA, under the conditions of TSA experiment, does not seem to have any impact on the enzymatic activity of MabA. Therefore, this assay may not be predictive for the detection of true inhibitors of MabA.
2. The activity of the fragments measured in the whole cell bacteria assay may not be attributed to the inhibition of MabA and will be investigated as part of this project.

For these reasons, we decided to rescreen our set of fragments using the developed high throughput enzymatic assay. (Figure 66)

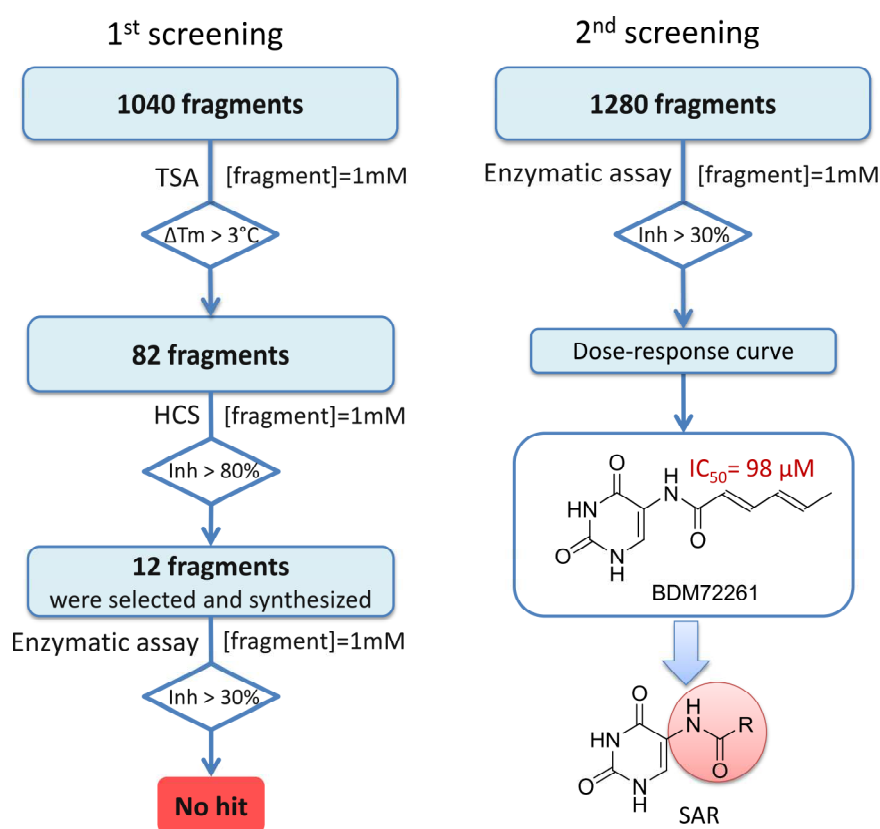


Figure 66: Identification and optimisation of MabA inhibitors by fragment-based approach

In the second screening stage, our entire library of fragments, enriched with new compounds (1280 fragments in total) has been screened on MabA using our new enzymatic assay. New family of inhibitors were discovered and especially in the 5-aminouracil series. Fragment BDM72261 was shown to inhibit MabA with an IC_{50} of $98\ \mu\text{M}$. Furthermore, a structure-activity relationship study was initiated with the synthesis of analogues. These compounds are being tested.

In the third part of this thesis, a design and synthesis of new fragments was described. The aim of this project is to build a collection of original fragments showing a 3D-structure scaffold amenable for rapid derivatization. We focused our attention on the design of

isoxazoline derivatives. We rationalized that incorporating the 2-isoxazoline motif into fragments would increase the three-dimensional characteristics, while improving physico-chemical parameters such as solubility. In the first step, a reliable protocol for the 2-isoxazoline scaffold synthesis was optimized in a one pot sequence using 1,3-dipolar cycloaddition between chloro-oximes and alkenes. (Figure 67)

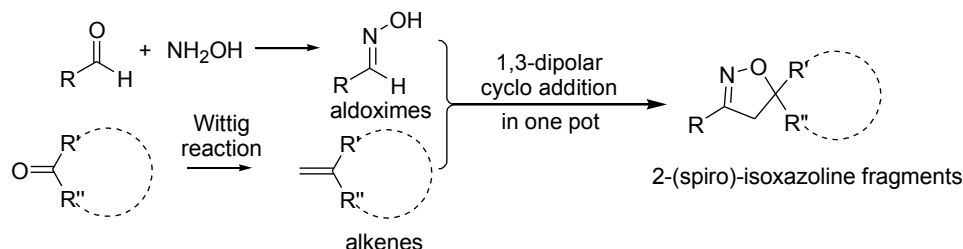


Figure 67: Synthesis of 2-isoxazoline containing fragments

With the optimized synthetic conditions in hands, the scope of the reaction was explored using three different aldoximes (benzaloxime, acetaldoxime and cyclopropyl aldoxime) and different alkenes. Non-commercial available alkenes were synthesized from corresponding ketones using Wittig conditions. In addition, the lactone containing fragment (compound **54**) was further functionalized with amines under microwave irradiations, to show that it is possible to easily introduce diversity starting from these building blocks.

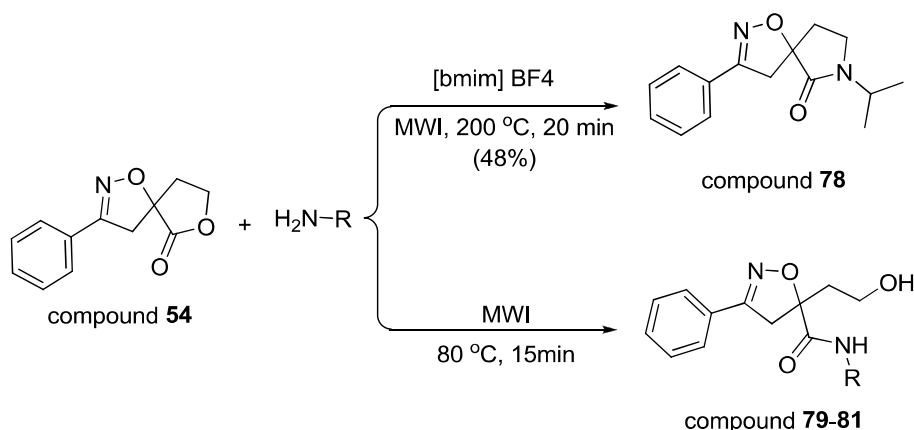


Figure 68: Diversity introduced starting from lactone **54**

The shapes and physical properties of the novel synthesized fragments were defined using cheminformatics. The results showed that the conformations of our 22 synthesized fragments were able to deploy substituents in the 3D space. The experimental solubility of these fragments was also measured and the results demonstrated that these molecules are suitable for the screening against new biological targets to help kick-start hit discovery program.

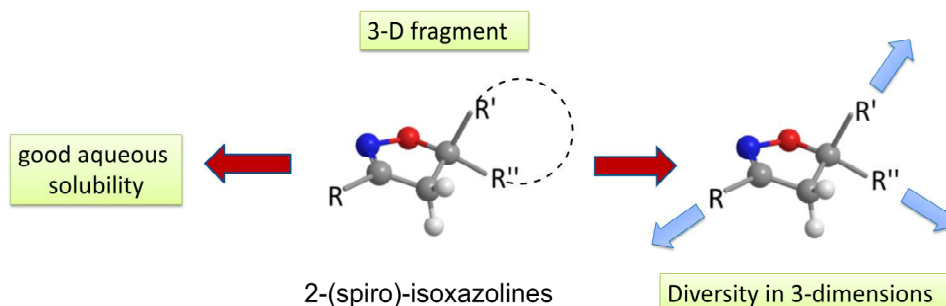


Figure 69: New isoxazoline containing 3D-fragments with good solubility

This page intentionally left blank

Experimental section

This page intentionally left blank

TABLE OF CONTENT

1.	General methods for chemical synthesis	151
1.1.	Solvent and reagents:.....	151
1.2.	Reaction procedure:.....	151
1.3.	Purification:	151
1.4.	Analysis:.....	152
2.	Chapter II: Development of novel EthR inhibitors with improved pharmacokinetic properties	153
2.1.	Synthesis of two hypothetic metabolites of compound BDM43266	153
2.2.	Metabolism study of BDM43266 in liver microsomes	157
2.3.	Development of novel EthR inhibitors with improved pharmacokinetic and physicochemical properties.....	162
2.4.	Biological assays	172
2.4.1.	Affinity of test compounds to EthR by Thermal Shift Assay:.....	172
2.4.2.	Potency assay of test compounds on <i>M. tuberculosis</i>	172
2.5.	Measurement of physico-chemical properties	173
2.5.1.	Solubility:.....	173
2.5.2.	LogD.....	173
2.6.	Metabolic Stability.....	174
2.7.	Molecular docking modelling of novel inhibitors in EthR protein.....	175
3.	Chapter III: Development of MabA inhibitors	176
3.1.	Chemical synthesis	176
3.1.1.	Synthesis of 2 hits from <i>in silico</i> screening.....	176
3.1.2.	Synthesis of hits from the primary screening.....	178
3.1.3.	Synthesis of 5-amino uracil analogs	196
3.2.	Biochemical assays	204
3.2.1.	Screening by Thermal Shift Assay (TSA)	204
3.2.2.	Screening on macrophage.....	205
3.2.3.	Screening by enzymatic assay	205
4.	Chapter IV: Synthesis of isoxazoline 3-D fragments.....	206
4.1.	Synthesis of isoxazoline by 1,3-dipolar cycloaddition.....	206
4.1.1.	Optimisation of synthetic conditions of 1,3-dipolar cycloaddition.....	206

4.1.2.	Synthesis of isoxazoline from benzaldoxime and alkenes	208
4.1.3.	Synthesis of isoxazoline from aliphatic carbaldoxime and alkenes	215
4.1.4.	General procedure for removing <i>N</i> -Boc group:	224
4.1.5.	Study on the dimerization of nitrile oxide as by product.....	227
4.2.	Functionalization of lactone containing isoxazoline fragments.....	228
4.3.	Molecular shape analysis and properties of synthesized fragments	232
4.4.	Protocol for solubility determination.....	232

1. General methods for chemical synthesis

1.1. Solvent and reagents:

Solvents for synthesis were purchased from Acros Organics as AeroSeal[®] extra dry grade. All other solvents for analysis and purification were purchased as analytical grade from commercial suppliers (Acros, Sigma-Aldrich, VWR, etc.) and used directly without further purification. Other chemical reagents were purchased from Acros, Aldrich, Fluka, Merck, Maybridge, Fluorochem, TCI, Lancaster, Matrix or Alfa Aesar as reagent grade and used without further purification unless stated otherwise.

1.2. Reaction procedure:

All reactions were carried out in dried glassware. Microwave-assisted chemical reactions were conducted on a CEM Discover[™] synthesis system or a Biotage[®] Initiator+ microwave synthesizer. Progress of all reactions was routinely monitored by thin layer chromatography (TLC) and/or by High Performance Liquid Chromatography-Mass Spectrum (HPLC-MS). TLC was performed using Merck commercial aluminum sheets coated with silica gel 60 F₂₅₄. Visualization was achieved by fluorescence quenching under UV light at 254 nm, and stained by one of the following reagents: solution of CuCl₂ in MeOH, ninhydrin solution, KMnO₄ solution or iodine.

1.3. Purification:

Purification was conducted by several following methods: (1) recrystallization, (2) flash chromatography or (3) preparative HPLC.

Flash column chromatography was performed on prepacked columns: AIT Chromato (40–60 μm) or puriFlash[®] Dry Load Silica columns (Interchim[®]) or Reveleris[®] flash cartridges (20–40 μm, Grace[®]) under pressure by a Flashmart[™] pump. Preparative HPLC were performed using one of two following systems. The first is a Varian ProStar system using an Omnisphere 10 C₁₈ column (250 mm x 41.4 mm) Dynamax from Varian, Inc. A gradient starting from 20% CH₃CN - 80% H₂O - 0.1% formic acid and reaching 100% CH₃CN - 0.1% formic acid at a flow rate of 80 mL/minutes (min) was used. Products were detected by UV absorption at 215 nm and/or 254 nm. The second is Waters-2 system using a XBridge[™] Prep C18 5 μm OBD[™], dimensions 50 mm x 250 mm column. Mobile phase is a gradient mixture of CH₃CN and water in ammonium formate buffer at pH 9.2 or pH 3.8. Flow rate at 80 mL/min was used. Products were detected by UV absorption and/or by MS.

1.4. Analysis:

HPLC-MS analysis was performed on one of two different HPLC-MS systems:

- (1) LC-MS Waters Alliance Micromass ZQ 2000 (**Waters-1**) system was equipped with a Waters 2747 sample manager, a Waters 2695 separations module, a Waters 2996 photodiode array detector (200-800nm) and a Waters Micromass ZQ2000 detector.
- (2) LC-MS Waters 3100 Mass Detectors (**Waters-2**) system was equipped with a Waters 2767 sample manager, a Waters 515 HPLC pump, a Waters Systems Fluidics Organizer, a Waters 2545 Binary Gradient Module, a Waters 2487 Dual λ Absorbance (215nm and 254nm) detector and a Waters 3100 Mass detectors.

XBridge C18 column (3.5 μ m particle size, dimensions 50mm x 4.6mm) was used for HPLC analysis. The injection volume is 20 μ L. A mixture of water and acetonitrile was used as mobile phase in gradient-elution. pH of mobile phase was adjusted with HCOOH and NH₄OH to form a buffer solution at pH 3.8 or pH 9.2 depend on the ratio of these components. The analysis time is 5 minutes (at a flow rate at 2 mL/min) or 10 minutes (at a flow rate at 1 mL/min). Purity (%) was determined by reversed phase HPLC, using UV detection (215 nm).

Infrared (IR) spectra were recorded on a Alpha FT-IR spectrometer (Bruker) with an integrated diamond ATR accessory and result was reported as wavenumber (cm⁻¹) with only major peaks reported.

NMR spectra were recorded on a Bruker DRX-300 spectrometer. The results were calibrated to signals from the solvent as an internal reference [e.g. 7.26 (residual CHCl₃) and 77.00 (CDCl₃) ppm for ¹H and ¹³C NMR spectra, respectively]. Chemical shifts (δ) are in parts per million (ppm) downfield from tetramethylsilane (TMS). The assignments were made using one-dimensional (1D) ¹H and ¹³C spectra and two-dimensional (2D) HSQC-DEPT and/or COSY and/or HMBC spectra. NMR coupling constants (*J*) are reported in Hertz (Hz), and splitting patterns are indicated as follows: broad (br), singlet (s), doublet (d), doublet of doublet (dd); double of doublet of doublet (ddd), doublet of triplet (dt); triplet (t), quartet (q), quartet of triplet (qt), quintet (quint), sextet (sext), and multiplet (m).

Also, when fluorine is present in the structure, ¹⁹F-NMR spectra was also measured.

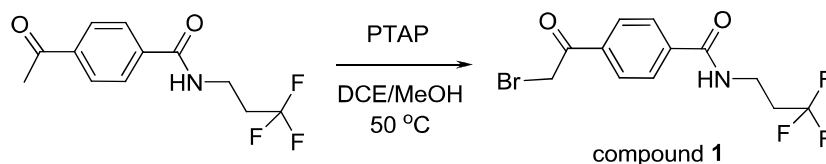
Melting points were determined on a Büchi B-540 apparatus and are uncorrected.

High-resolution mass spectrometric measurements (HRMS) were performed by HPLC-MS-ESI-TOF (Waters).

2. Chapter II: Development of novel EthR inhibitors with improved pharmacokinetic properties

2.1. Synthesis of two hypothetic metabolites of compound BDM43266

2.1.1. Synthesis of 4-(2-bromoacetyl)-N-(3,3,3-trifluoropropyl)benzamide (compound 1)



Protocol:

To a solution of 4-acetyl-N-(3,3,3-trifluoropropyl)benzamide (500 mg, 1.93 mmol, 1.0 equiv.) in mixture of 1,2-dichloroethane (DCE) and MeOH (5/2, 35 mL) at 50 °C, trimethylphenylammonium tribromide (PTAP, 725 mg, 1.1 equiv.) was added portionwise. The reaction mixture was then stirred at 50 °C overnight. After completion, solvent was evaporated under reduced pressure. The residue was dissolved in EtOAc, washed with water (x3), brine (x1), dried over anhydrous MgSO₄ and then concentrated to afford the brominated compound **1** (665 mg, quantitative yield) as pale brownish solid.

Chemical formula: C₁₂H₁₁BrF₃NO₂

MW: 338.12 g/mol

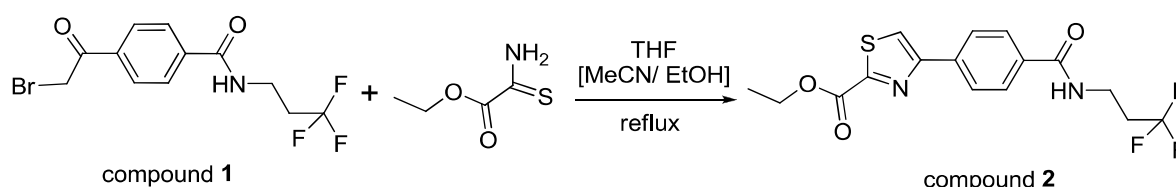
HPLC-MS (gradient method in 5 min at pH 3.8): t_R = 2.50 min

MS-(ES+) m/z 338 ([M+H]⁺ for ⁷⁹Br, 75%) ; 340 ([M+H]⁺ for ⁸¹Br, base peak)

MS-(ES-) m/z 336 ([M-H]⁻ for ⁷⁹Br, base peak) ; 338 ([M-H]⁻ for ⁸¹Br, 98%)

The MS spectral characteristics was identical to that previously reported in literature.³¹⁶

2.1.2. Synthesis of ethyl 4-[4-[3,3,3-tris(fluoryl)propylcarbamoyl]phenyl]-1,3-thiazole-2-carboxylate (compound 2)

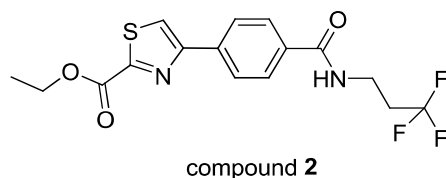


Protocol:

A solution of 4-(2-bromoacetyl)-N-(3,3,3-trifluoropropyl)benzamide **1** (169 mg, 0.5 mmol, 1 equiv.) and ethyl thiooxamate (1.5 equiv.) in THF (9 mL) was refluxed overnight. Analysis of reaction mixture by LC-MS showed that the starting material **1** was completely reacted. The desired product was formed together with a by-product resulting from the debromination of

³¹⁶ Villemagne *et al.*, *J. Med. Chem.*, 2014, vol.57, # 11, pp.4876–4888 (compound 20b)

compound **1**. THF was then evaporated under reduced pressure. The residue was dissolved in EtOAc, washed by saturated K_2CO_3 solution (x2), water (x1) and brine. The organic phase was dried over anhydrous $MgSO_4$ and concentrated under reduced pressure to give yellow solid. This crude product was purified by flash chromatography (*column*: silica gel pre-packed Puriflash 12g-30 μ m, Interchime; *eluents*: cyclohexane-*i*-PrOH (95-5), *loading technique*: dry load ; *flow-rate*: 10 mL/min; tube collection by time: 0.70-1.0 min/tube) to yield the desired compound **2** (96 mg, 52% yield) as white solid.



Chemical formula: $C_{16}H_{15}F_3N_2O_3S$

MW: 372.36 g/mol

HPLC-MS (gradient in 5 min at pH 3.8): $t_R = 3.09$ min

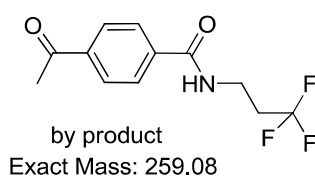
MS-(ES+) m/z 373 ($[M+H]^+$, base peak)

MS-(ES-) m/z 371 ($[M-H]^-$, base peak)

1H -NMR (300 MHz, $CDCl_3$, ppm) δ 1.47 (t, $J = 7.1$ Hz, 3H), 2.50 (qt, $J = 10.8$ Hz and $J = 6.6$ Hz, 2H), 3.75 (q, $J = 6.3$ Hz, 2H), 4.53 (q, $J = 7.1$ Hz, 2H), 6.44 (m, 1H, NH), 7.81-7.85 (m, 3H, H-Ar and H-thiazole), 8.05 (d, $J = 8.6$ Hz, 2H, H-Ar).

These spectral characteristics were identical to those previously reported.³¹⁷

Notice: In this reaction, we also obtained a by-product (15 mg, 11%). The proposed structure of this by-product was sketched below:



HPLC-MS (gradient method in 5 min at pH 3.8): $t_R = 2.63$ min

MS-(ES-) m/z 258 ($[M-H]^-$, base peak)

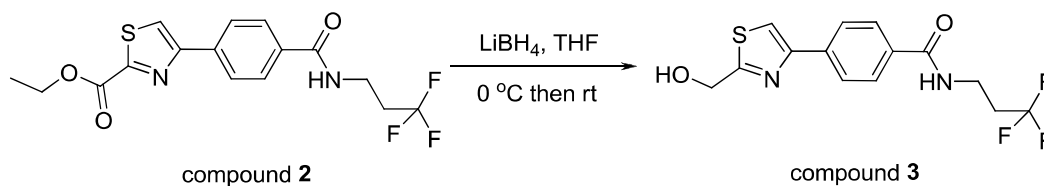
In order to limit the debromination by-process, we have also retried this synthetic procedure by using others solvents according to similar protocols in literature, e.g. CH_3CN ³¹⁸ or $EtOH$ ³¹⁹. Unfortunately, these efforts could not avoid the formation of this by-product.

³¹⁷ Willand *et al*; Patent FR/3000491 (composé 54, page 42)

³¹⁸ *J. Med. Chem.*,(1981),24,pp.1507-1510

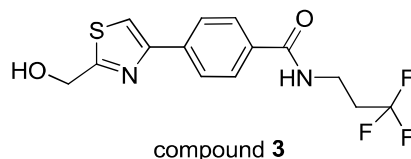
³¹⁹ *J. Molecular Structure* (2011),pp.10-23

2.1.3. Synthesis of 4-(2-hydroxymethyl-thiazol-4-yl)-N-(3,3,3-trifluoro-propyl)-benzamide (compound 3)



Protocol:³²⁰

4-[4-(3,3,3-trifluoropropylcarbamoyl)-phenyl]-thiazole-2-carboxylic acid ethyl ester **2** (35 mg, 0.09 mmol, 1.0 equiv.) was dissolved in THF (1mL) under Argon. The solution was then cooled to 0°C. Next, a LiBH₄ 2.0 M solution in THF (0.14 mL, 3.0 equiv.) was added dropwise. The reaction mixture was stirred at 0 °C in 30 min and then at room temperature for 1 hours 30 min. After completion, water (0.5 mL) was added to neutralize the excess amount of LiBH₄. The solvent was then evaporated under reduced pressure. The obtained residue was dissolved in EtOAc and washed with water (x3) to pH 7 and brine. The organic phase was dried over anhydrous MgSO₄ and concentrated under reduced pressure to afford the desired alcohol **3** (27.4 mg, 92%) as white solid.



Chemical formula: C₁₄H₁₃F₃N₂O₂S

MW: 330.33 g/mol

HPLC-MS (gradient method in 5 min at pH 3.8): t_R = 2.15 min

MS-(ES+) m/z 331 ([M+H]⁺, base peak)

MS-(ES-) m/z 329 ([M-H]⁻, base peak)

¹H-NMR (300 MHz, CD₃OD, ppm) δ 2.46-2.62 (qt, *J* = 10.6 Hz, *J* = 7.0 Hz, 2H, CH₂), 3.65 (t, *J* = 7.0 Hz, 2H, CH₂), 4.91 (s, 2H, CH₂), 7.87 (d, *J* = 8.6 Hz, 2H, H-Ar), 7.90 (s, 1H, H-thiazole), 8.01 (d, *J* = 8.6 Hz, 2H, H-Ar).

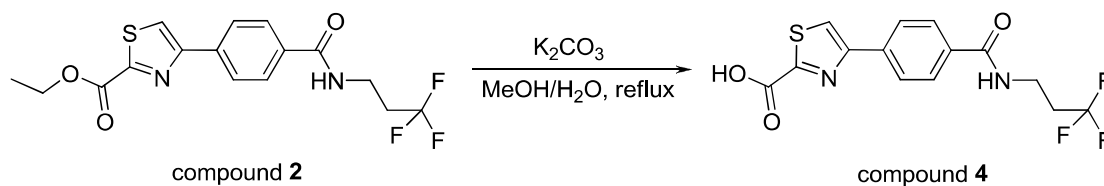
¹³C-NMR (75 MHz, CD₃OD, ppm) δ 34.1 (q, ²*J*_{CF} = 27.6 Hz), 34.5, 62.5, 116.2, 127.3, 128.0 (q, ¹*J*_{CF} = 276.2 Hz), 128.8, 134.6, 139.0, 155.3, 169.8, 175.7.

HRMS (TOF, ES+) calculated for [M+H]⁺ C₁₄H₁₄F₃N₂O₂S 331.0728, found 331.0742.

This new structure has not been reported in literature. No results were found in Reaxys, Pubchem, eMolecules and Scifinder Scholar (verified on 22/03/2015).

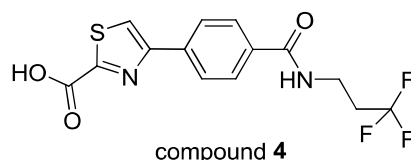
³²⁰ *J. Med. Chem.* (2006), 49(25), pp.7270-73

2.1.4. Synthesis of [4-(3,3,3-Trifluoro-propylcarbamoyl)-phenyl]-thiazole-2-carboxylic acid (compound 4)



Protocol:³²¹

4-[4-(3,3,3-trifluoropropylcarbamoyl)-phenyl]-thiazole-2-carboxylic acid ethyl ester **2** (37mg, 0.10 mmol, 1.0 equiv.) was dissolved in MeOH (4mL) at room temperature. Next, a solution of K_2CO_3 (2.0 equiv.) in water (0.5 mL) was added dropwise. The reaction mixture was refluxed for 3 hours 30 min. After completion, the solvent was then evaporated under reduced pressure. The residue was dissolved in water and pH was adjusted to 3 by a solution HCl 1N. The aqueous phase was then extracted by EtOAc ($\times 2$). The combined organic phase was washed with brine ($\times 1$), dried over anhydrous $MgSO_4$ and concentrated under reduced pressure to afford the desired compound **4** (35 mg, quantitative yield) as white solid.



Chemical Formula: $C_{14}H_{11}F_3N_2O_3S$

Molecular Weight: 344.31 g/mol

HPLC-MS (gradient method in 5 min at pH 3.8): $t_R = 1.85$ min

MS-(ES+): m/z 345 ($[M+H]^+$, base peak)

MS-(ES-): m/z 343 ($[M-H]^-$, 15%); 299 (base peak)

1H -NMR (300 MHz, CD_3OD , ppm) δ 2.46-2.62 (m, 2H, CH_2), 3.64 (t, $J = 7.0$ Hz, 2H, CH_2), 7.89 (d, $J = 8.3$ Hz, 2H, H-Ar), 8.07 (d, $J = 8.3$ Hz, 2H, H-Ar), 8.24 (s, 1H, H-thiazole).

^{13}C -NMR (75 MHz, CD_3OD , ppm) δ 31.1 (q, $^2J_{CF} = 27.8$ Hz), 34.5 (q, $^3J_{CF} = 3.7$ Hz), 119.2, 124.7, 125.0 (q, $^1J_{CF} = 276.4$ Hz), 125.9, 132.1, 135.2, 152.7, 154.2, 160.0, 166.7.

HRMS (TOF-ES+) m/z for $C_{14}H_{12}F_3N_2O_3S$ $[M+H]^+$ calculated, 345.0521; found, 345.0536.

This new structure has not been reported in literature. No results were found in Reaxys, Pubchem, eMolecules and Scifinder Scholar (verified on 22/03/2015).

Notice: we observed a rapid decarboxylation of this compound during purification by flash chromatography (eluent: DCM-MeOH, 90-10 with 1% glacial acetic acid).

³²¹ *Eur. J. Med Chem.* (2009), 44, pp.4413-4425

2.2. Metabolism study of BDM43266 in liver microsomes

Materials

All chemicals were obtained from Sigma-Aldrich (Steinheim, Germany). Solvents at LCMS grade were purchased from common sources (Sigma-Aldrich, VWR). Stock solutions of all compounds were prepared in methanol at a concentration of 0.1 mM. Pooled female mouse (CD-1) liver microsomes were purchased from BD gentest (Le Pont de Claix, France).

Microsomal incubations

All incubations were performed in a shaking water bath at 37°C. The incubation mixture were prepared in polypropylene tubes and contained 50 μ M test compound BDM43266 (1% methanol), mouse liver microsomes (1 mg of microsomal protein/mL), 5 mM MgCl₂, 1 mM NADP, 5 mM glucose-6-phosphate, 0.4 U/ml glucose-6-phosphate dehydrogenase and 50 mM potassium phosphate buffer pH 7.4 in a final volume of 0.5 mL. Sampling points were taken at 0, 60 min and 180 min and reactions were terminated by adding ice-cold acetonitrile (4 volume). The samples were centrifuged for 10 min at 10000g and 4°C to pellet precipitated microsomal protein; the supernatant was evaporated and reconstitute in water/methanol (75:25) before analysis by LC-MS/MS Control incubations were performed with denaturated microsomes with acetonitrile and sampling points were also taken at 0, 60 and 180 min.

LC-MS/MS and LC-MS analysis

The LC-MS/MS system consisted of an UHPLC Acquity I-Class connected to a Xevo TQD mass spectrometer (Waters, Les Ulis, France) equipped with an electrospray ionisation source. Analytes in incubation mixtures were separated using an Acquity BEH C18, 1.7 μ m, 50 \times 2.1mm column (Waters). The mobile phase solvents used were: (A) H₂O 0.1% HCOOH; (B) CH₃CN 0.1% HCOOH. The following mobile phase gradient was applied: 2% B during 2min, 2-98% (B) in 8min; hold at 98% (B) for 2min30s; 98%-2% B in 30s; 2% B hold for 2min. The injection volume was 2 μ L and the flow rate of 600 μ L/min. The desolvation and cone gas flow were respectively 1000 and 50 L/h; the source temperature was 600°C. The capillary and the cone voltage were optimized for each compound.

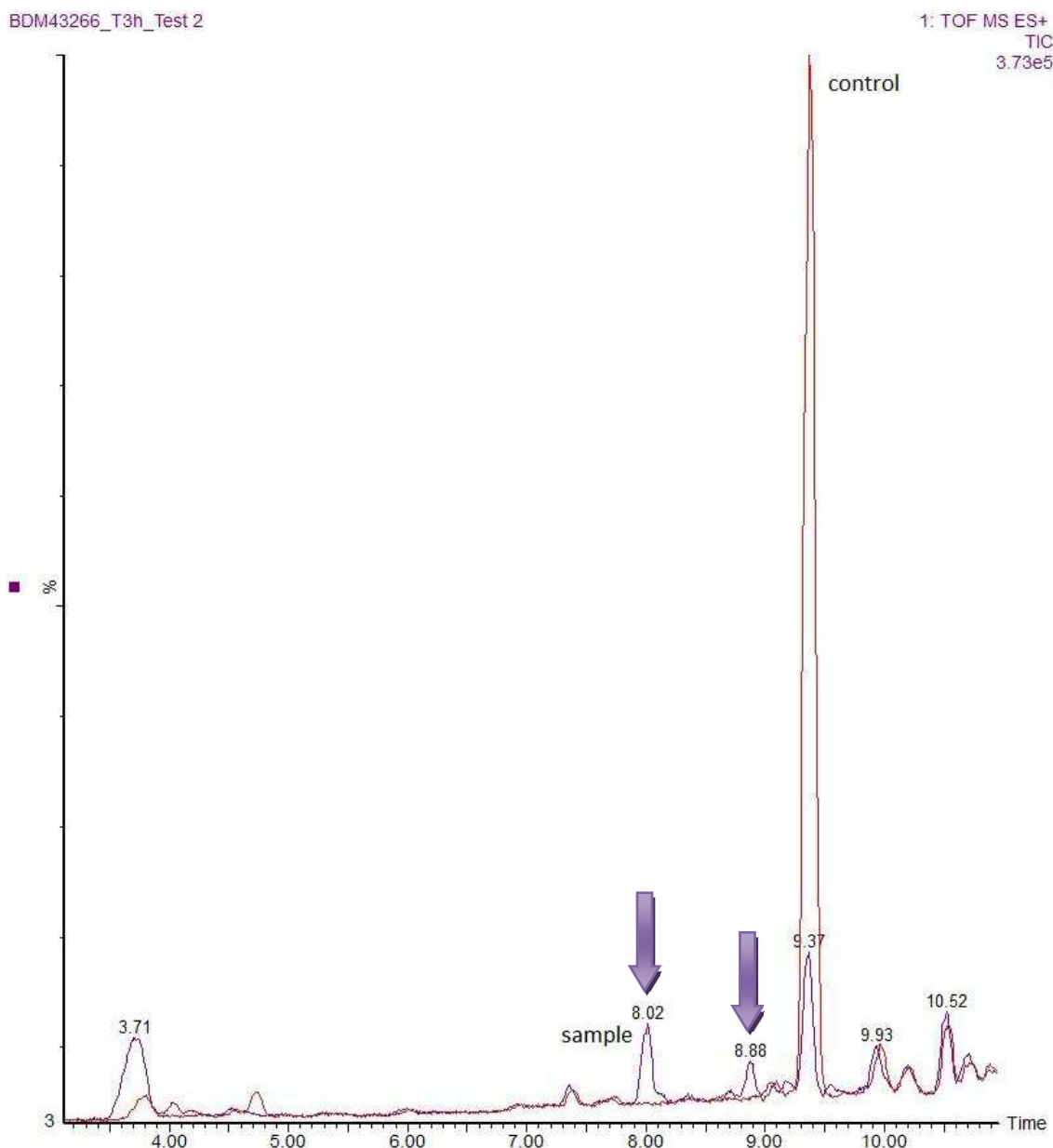
The LC-MS TOF system consisted of an HPLC connected to a LCT Premier mass spectrometer (Waters) equipped with an electrospray ionisation source. Analytes in incubation mixtures were separated using a XBridge C18, 3.5 μ m, 150 \times 4.6mm column. The mobile phase solvents used were: (A) H₂O 5mM ammonium formate buffer pH 3.8; (B) CH₃CN ammonium formate buffer pH 3.8. The following mobile phase gradient was applied: 2% B during 1min, 2-100% (B) in 11min; hold at 100% (B) for 2min; 100%-2% B in 6s; 2% B hold for 6min. The injection volume was 10 μ L and the flow rate of 1mL/min. The desolvation and cone gas flow were respectively 500 and 50 L/h; the source temperature was 250°C.

Results

Analysis by LCMS TOF allowed identifying new peaks in the sample when overlaying with control by HRMass search. Then LC-MS/MS analysis was conducted in order to determine the fragmentation profile of these peaks.

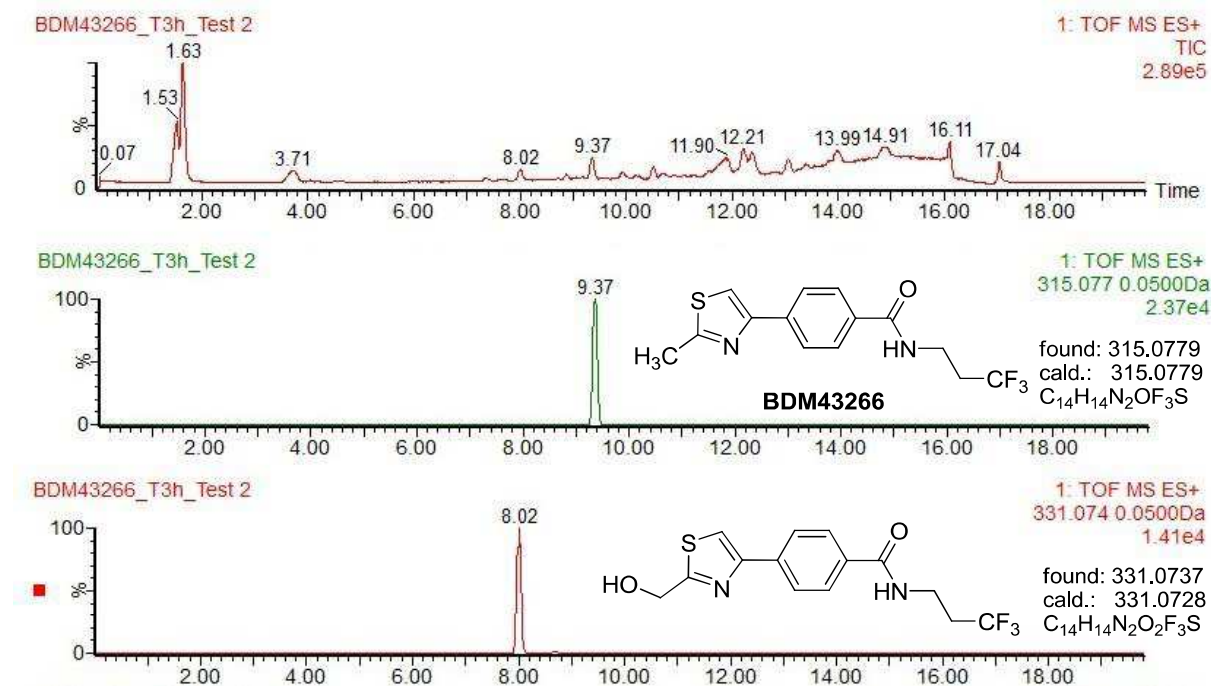
Analysis by LC-MS-TOF

Sample and control chromatogram overlay in LCMS-TOF



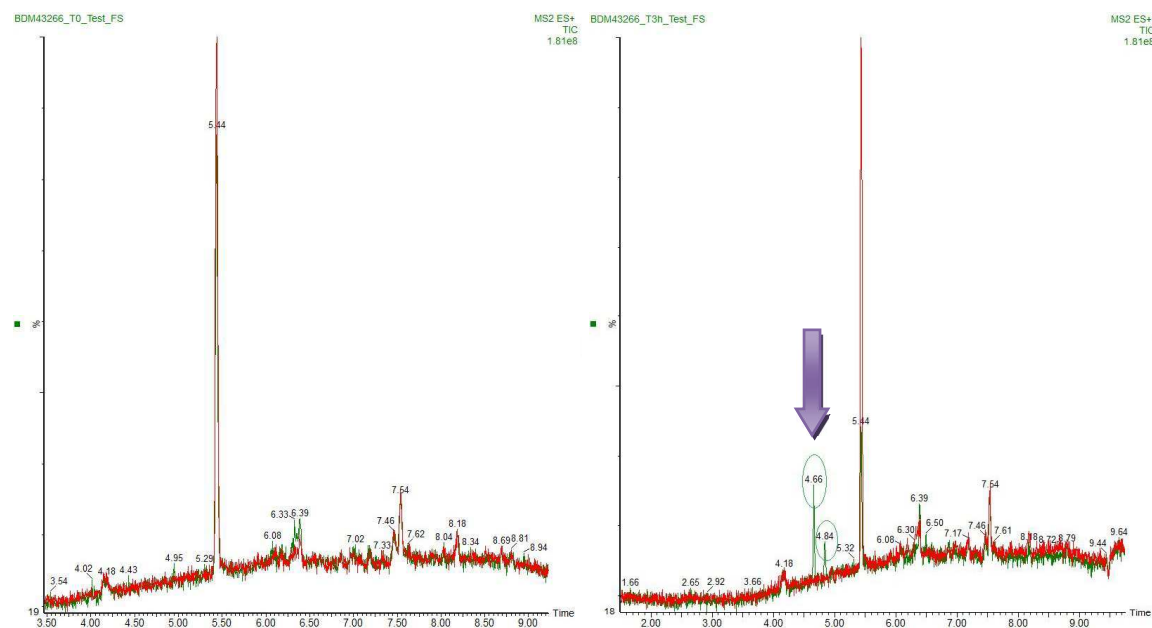
Experimental section

Mass extract analysis by LCMS-TOF

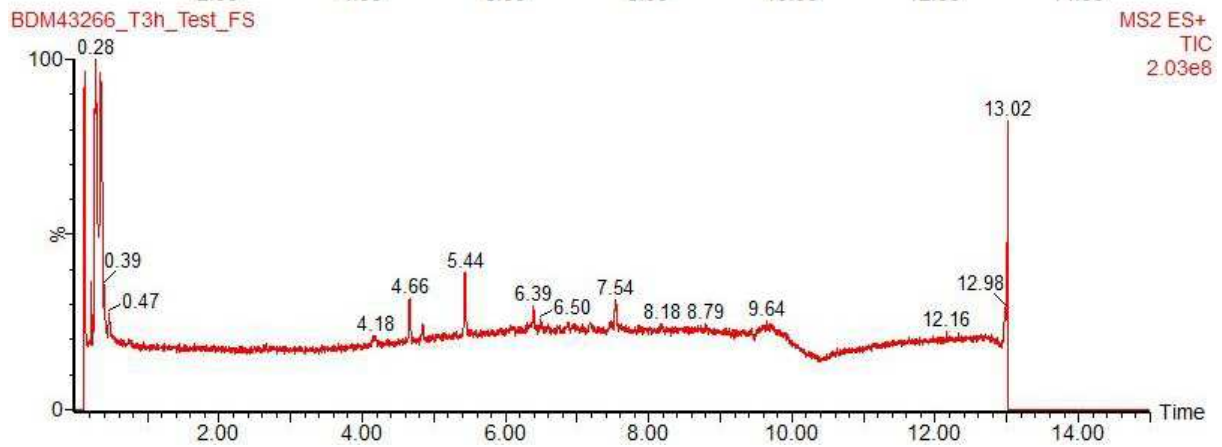
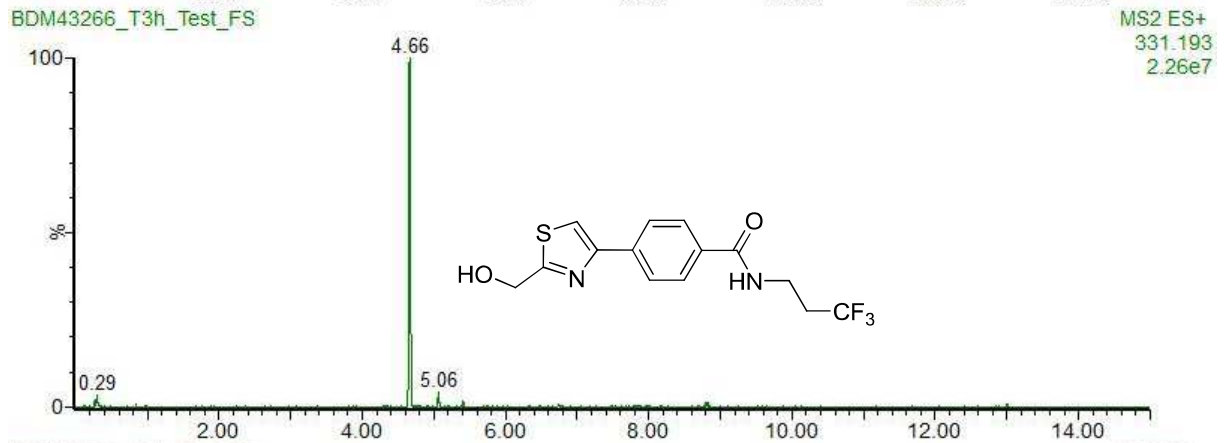
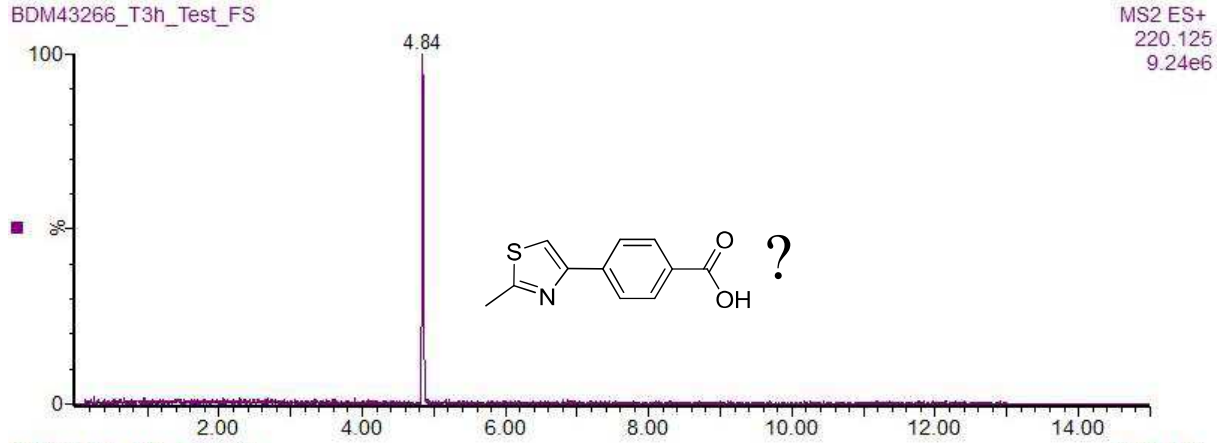


Analysis by LC-MS/MS

Overlay of sample and control chromatogram by LC-MS/MS

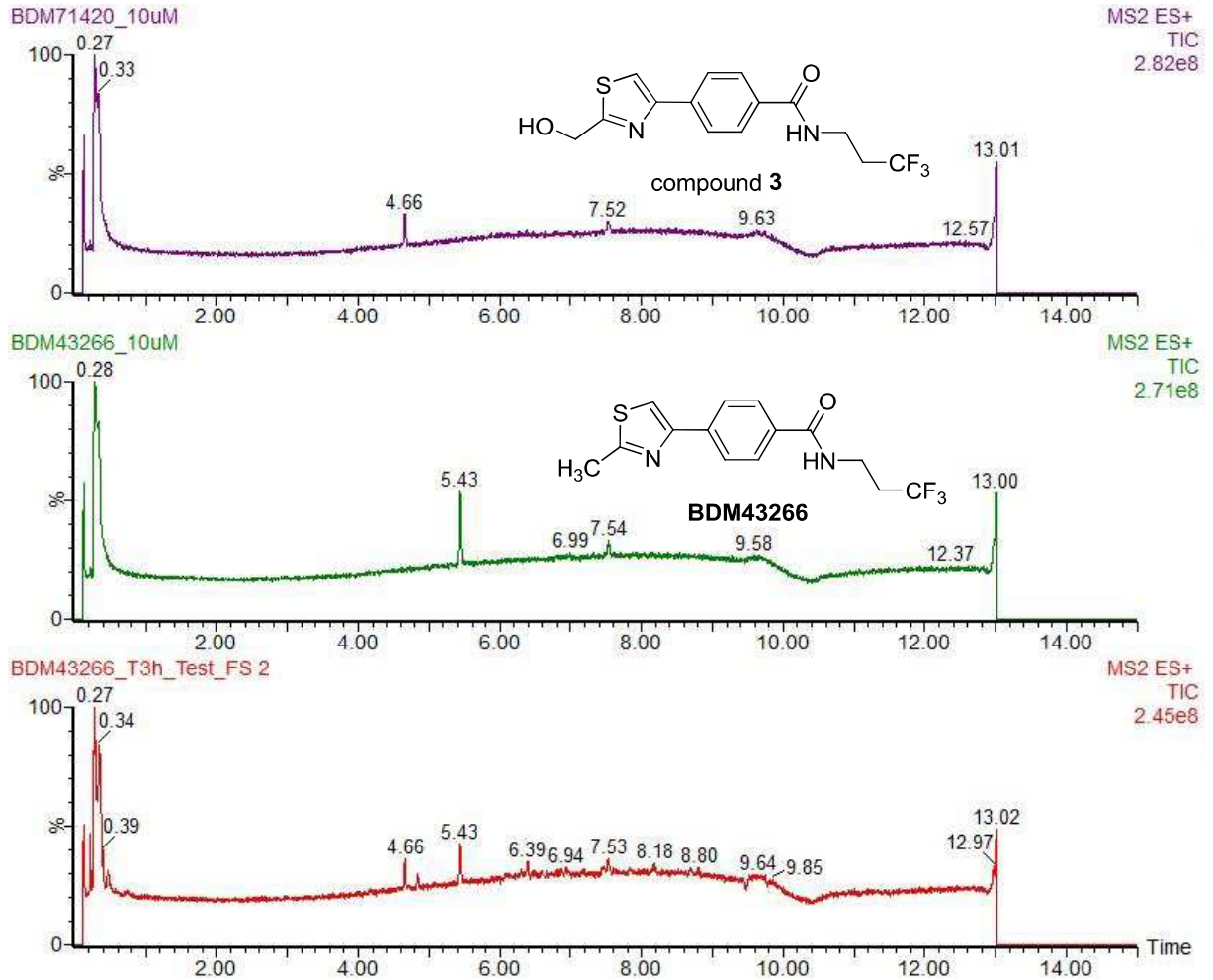


LC-MS/MS – mass extraction



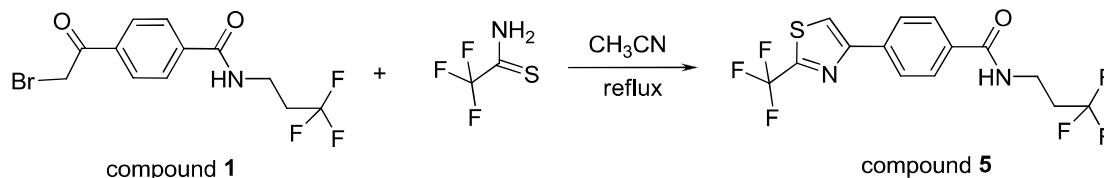
Comparison of 3 chromatograms:

- 1) The synthesized hydroxy metabolite (compound **3**)
- 2) The starting substrate (BDM43266)
- 3) The mixture of BDM43266 in microsomes after 180 min



2.3. Development of novel EthR inhibitors with improved pharmacokinetic and physicochemical properties

2.3.1. Synthesis of 4-(2-trifluoromethyl-thiazol-4-yl)-N-(3,3,3-trifluoro-propyl)-benzamide (compound 5)



A solution of 4-(2-bromoacetyl)-N-(3,3,3-trifluoropropyl)benzamide **1** (338mg, 1.0 mmol, 1 equiv.) and 2,2,2-trifluorothioacetamide (2.67 equiv.) in CH₃CN (13 mL) was refluxed for 81 hours. After completion, solvent was evaporated under reduced pressure. The residue was dissolved in EtOAc and then washed with saturated K₂CO₃ solution (x2), water (x2) and brine. The organic phase was dried over anhydrous MgSO₄ and evaporated under reduced pressure to give red solid. This crude residue was purified by flash chromatography (*column*: silica gel pre-packed Puriflash-25g-30μm, Interchime; *eluents*: cyclohexane-*i*-PrOH (95-5), *loading technique*: dry load ; *flow-rate*: 7.5 mL/min; tube collection by time: 0.70-1.0 min/tube) to yield the desired product **5** (135 mg, 37% yield) as yellowish solid. M.p.: 137.5-139.2 °C

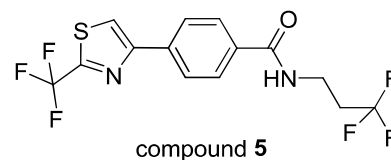
Chemical Formula: C₁₄H₁₀F₆N₂OS

MW: 368.30 g/mol

HPLC-MS (gradient in 5 min at pH 3.8): t_R = 3.49 min

MS-(ES+) *m/z* 369 ([M+H]⁺, base peak)

MS-(ES-) *m/z* 367 ([M-H]⁻, base peak)



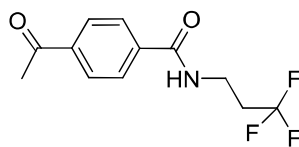
¹H-NMR (300 MHz, CD₃OD, ppm) δ 2.54 (qt, *J* = 11.0 Hz, *J* = 7.1 Hz, 2H, CH₂), 3.59 (t, *J* = 7.0 Hz, 2H, CH₂), 7.91 (d, *J* = 8.7 Hz, 2H, H-Ar), 8.08 (d, *J* = 8.7 Hz, 2H, H-Ar), 8.32 (s, 1H, H-thiazole).

¹³C-NMR (75 MHz, CD₃OD, ppm) δ 34.1 (q, ²*J*_{CF} = 27.6 Hz), 34.5, 119.9, 121.3 (q, ¹*J*_{CF} = 271.1 Hz), 127.6, 127.9 (q, ¹*J*_{CF} = 276.6 Hz), 129.0, 135.5, 137.4, 156.8 (q, ²*J*_{CF} = 40.3 Hz), 157.0, 169.6.

¹⁹F-NMR (282 MHz, CD₃OD, ppm) δ -66.96 (t, ³*J*_{HF} = 10.7 Hz, 3F), -62.87 (s, 3F).

This new structure has not been reported in literature. No results were found in Reaxys, Pubchem, eMolecules and Scifinder Scholar (verified on 22/03/2015).

Notice: In this reaction, we obtained a by-product (75 mg, 29%) as yellow solid which structure was sketched below. It could be formed by a debromination of the starting material.



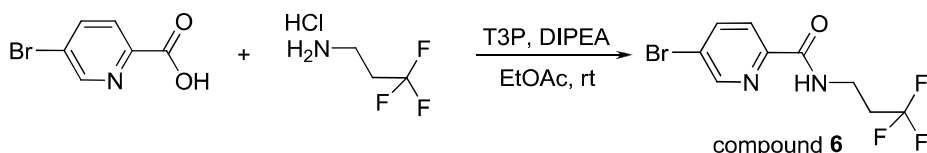
by product
Exact Mass: 259.08

HPLC-MS: $t_R = 2.62$ min (gradient method in 5 min at pH 3.8)

MS-(ES-) m/z 258 ($[M-H]^-$, base peak)

2.3.2. Synthesis of 5-(2-trifluoromethyl-thiazol-4-yl)-pyridine-2-carboxylic acid (3,3,3-trifluoro-propyl)-amide (compound 9)

Step 1 : synthesis of 5-bromo-*N*-(3,3,3-trifluoropropyl)picolinamide (compound 6)



To a solution of 5-bromopicolinic acid (400mg, 1.98 mmol, 1 equiv.) and DIPEA (1.03 mL, 3 equiv.) in EtOAc (15 mL), was added a solution of T3P 50% in EtOAc (2.1 mL, 1.8 equiv.). The reaction mixture was stirred at room temperature for 15 min and 3,3,3-trifluoropropylamine hydrochloride (1.5 equiv.) was then added. The reaction mixture was then stirred at room temperature overnight. After completion, water (15 mL) was added to the reaction mixture. The organic phase was decanted and washed with NaHCO_3 saturated solution (x1), NH_4Cl (x1), water (x2) and brine. The organic phase was then dried over anhydrous MgSO_4 and concentrated under reduced pressure to afford the desired compound **6** (552 mg, 94%) as brown solid.

Chemical Formula: $\text{C}_9\text{H}_8\text{BrF}_3\text{N}_2\text{O}$

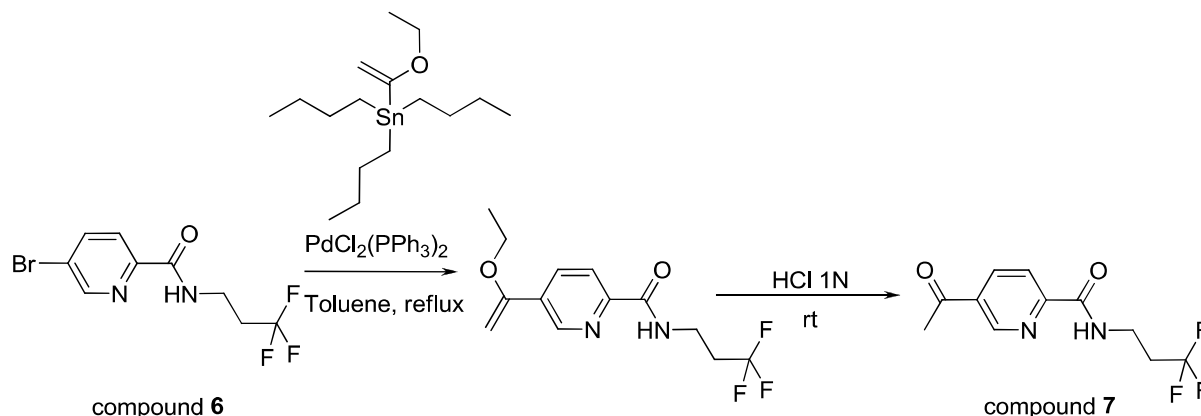
MW: 297.08 g/mol

HPLC-MS (gradient method in 5 min at pH 3.8): $t_R = 3.00$ min

MS-(ES+) m/z 297 ($[M+H]^+$ for ^{79}Br , 87%) ; 299 ($[M+H]^+$ for ^{81}Br , base peak).

These spectral characteristics were identical to those previously reported in literature.³²²

³²² Willand *et al*; Patent FR/3000491 (composé 65, page 48)

Step 2: synthesis of 5-acetyl-N-(3,3,3-trifluoropropyl)picolinamide (compound 7)

A toluene (3.5 mL) solution of $\text{PdCl}_2(\text{PPh}_3)_2$ (95 mg, 0.1 equiv.) and 5-bromo-N-(3,3,3-trifluoropropyl)-picolinamide **6** (400 mg, 1.35 mmol, 1.0 equiv.) was stirred at room temperature in a Schlenk flask under argon for 15 min. Then (1-ethoxyvinyl)tri(*n*-butyl)stannane (545 μL , 1.2 equiv.) was added and the resulting reaction mixture was refluxed at 110°C for 2 hours. Next, the reaction mixture was cooled to room temperature, then 4 mL of 1.0 N HCl were added. After stirring for 24 hours, the reaction mixture was filtered through a Celite plug. The filtrate was neutralized with saturated NaHCO_3 solution and extracted with EtOAc (3×10 mL). The combined organic phases were washed with water, brine, dried over anhydrous MgSO_4 and concentrated under reduced pressure. The crude residue was purified by flash chromatography (*column*: silica gel pre-packed Puriflash-25g-30 μm , Interchim; *diluant*: cyclohexane-EtOAc (80-20 \rightarrow 70-30) ; *loading technique*: dry load ; *flow-rate*: 9-10 mL/min; tube collection by time: 0.70-1.0 min/tube) to give the desired compound **7** (323 mg, 92%) as white solid.

Chemical Formula: $\text{C}_{11}\text{H}_{11}\text{F}_3\text{N}_2\text{O}_2$

MW: 260.21 g/mol

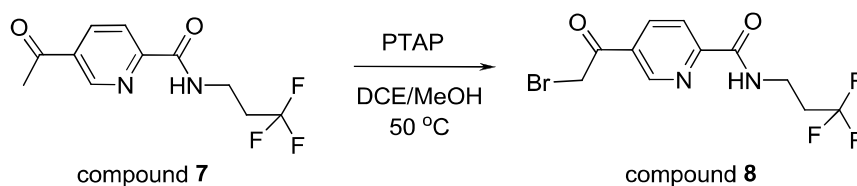
HPLC-MS (gradient in 5 min at pH 3.8): $t_{\text{R}} = 2.65$ min

MS (ES+) m/z 261 ($[\text{M}+\text{H}]^+$, base peak)

$^1\text{H-NMR}$ (300 MHz, CDCl_3 , ppm) δ 2.50 (qt, $J = 10.7$ Hz, $J = 6.6$ Hz, 2H, CH_2), 2.68 (s, 3H, CH_3), 3.78 (q, $J = 6.5$ Hz, 2H, CH_2), 8.29-8.40 (m, 3H, NH & 2H-pyridine), 9.10 (d, $J = 2.2$ Hz, 1H, H-pyridine).

These spectral characteristics were identical to those previously reported in literature.³²³

³²³ Willand *et al*; Patent FR/3000491 (composé 66, page 48)

Step 3: synthesis of 4-(2-bromoacetyl)-N-(3,3,3-trifluoropropyl)picolinamide (compound 8)

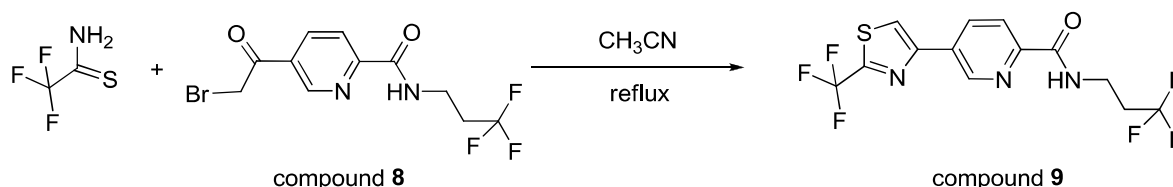
To a solution of 4-acetyl-*N*-(3,3,3-trifluoropropyl)picolinamide **7** (260 mg, 1.0 mmol, 1 equiv.) in mixture of DCE and MeOH (5-2, 17.5 mL) at 50°C, trimethylphenylammonium tribromide (413 mg, 1.1 equiv.) was added portionwise. The reaction mixture was then stirred at 50 °C overnight. After completion, solvent was evaporated under reduced pressure. The solid residue was dissolved in EtOAc and washed with NaHCO₃ saturated solution (x1), water (x3) and brine. The organic phase was then dried over anhydrous MgSO₄ and evaporated under reduced pressure to afford the desired product **8** (388 mg, quantitative yield) as yellow solid. This product was then used in the next synthetic step without further purification.

Chemical Formula: C₁₁H₁₀BrF₃N₂O₂

MW: 339.11 g/mol

HPLC-MS (gradient method in 5 min at pH 3.8): t_R= 3.22 min

MS (ES+) *m/z* 385 (95%) ; 387 (base peak) [*the desired product in acetal form*]

Step 4: synthesis of 5-(2-trifluoromethyl-thiazol-4-yl)-pyridine-2-carboxylic acid (3,3,3-trifluoro-propyl)-amide (compound 9)

A solution of 4-(2-bromoacetyl)-*N*-(3,3,3-trifluoropropyl)picolinamide **8** (339 mg, 1.0 mmol, 1.0 equiv.) and 2,2,2-trifluorothioacetamide (2.5 equiv.) in CH₃CN (13 mL) was refluxed for 96 hours. After completion, solvent was evaporated under reduced pressure. The residue was dissolved in EtOAc and then washed with saturated K₂CO₃ solution (x2), water (x3) and brine. The organic phase was dried over anhydrous MgSO₄ and evaporated under reduced pressure to give red solid. This crude product was purified by flash chromatography (*column*: silica gel pre-packed Puriflash-25g-30μm, Interchime; *eluents*: cyclohexane-*i*-PrOH (95-5), *loading technique*: dry load ; *flow-rate*: 6.5 mL/min; tube collection by time: 1.0 min/tube) to yield the desired product **9** (117 mg, 32% yield) as yellowish solid. Mp: 101.4-102.3 °C

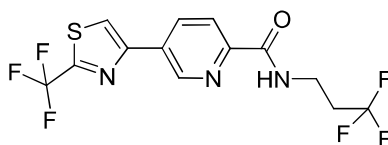
Chemical Formula: C₁₃H₉F₆N₃OS

MW: 369.29 g/mol

HPLC-MS (method gradient in 5 min at pH 3.8): $t_R = 3.43$ min

MS (ES+) m/z 370 ($[M+H]^+$, base peak)

MS (ES-) m/z 368 ($[M-H]^-$, base peak)



compound 9

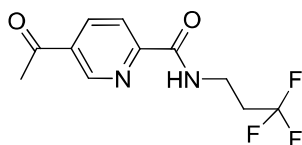
$^1\text{H-NMR}$ (300 MHz, CD_3OD , ppm) δ 2.56 (qt, $J = 11.0$ Hz, $J = 7.1$ Hz, 2H, CH_2), 3.70 (t, $J = 7.1$ Hz, 2H, CH_2), 8.17 (dd, $J = 8.2$ Hz ; $J = 0.6$ Hz, 1H, H-pyridine), 8.49 (dd, $J = 8.2$ Hz ; $J = 2.1$ Hz, 1H, H-pyridine), 8.50 (s, 1H, H-thiazole), 9.23 (dd, $J = 2.1$ Hz ; $J = 0.6$ Hz, 1H, H-pyridine).

$^{13}\text{C-NMR}$ (75 MHz, CD_3OD , ppm) δ 34.0, 34.2 (q, $^2J_{\text{CF}} = 28.1$ Hz), 121.4 (q, $^1J_{\text{CF}} = 271.8$ Hz), 121.5, 123.3, 127.9 (q, $^1J_{\text{CF}} = 276.8$ Hz), 132.9, 136.2, 147.8, 150.6, 154.2, 157.4 (q, $^1J_{\text{CF}} = 40.9$ Hz), 166.4.

$^{19}\text{F-NMR}$ (282 MHz, CD_3OD , ppm) δ -67.05 (t, $^3J_{\text{HF}} = 11.3$ Hz, 3F), -62.88 (s, 3F).

This new structure has not been reported in literature. No results were found in Reaxys, Pubchem, eMolecules and Scifinder Scholar (verified on 22/03/2015).

Notice: In this reaction, we also obtained a by-product (58 mg, 22%) as yellow solid which structure was sketched below. It could be formed by a debromination of starting material.



Exact Mass: 260.1
by product

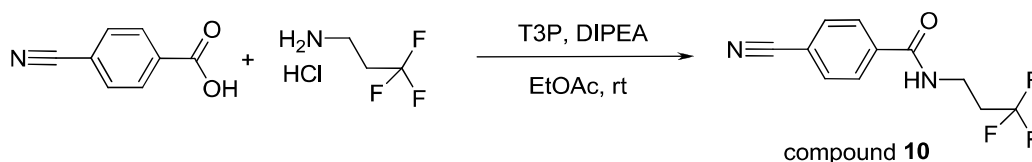
HPLC-MS (gradient method in 5 min at pH 3.8): $t_R = 2.65$ min

MS-(ES+) m/z 261 ($[M+H]^+$, base peak)

These results were identical to those previously reported in compound 7.

2.3.3. Synthesis of 4-(5-(trifluoromethyl)-1,2,4-oxadiazol-3-yl)-*N*-(3,3,3-trifluoropropyl) benzamide (compound 12)

Step 1: synthesis of 4-cyano-*N*-(3,3,3-trifluoropropyl)benzamide (compound 10)



compound 10

To a solution of 4-cyanobenzamide (1 g, 6.8 mmol, 1 equiv.) and DIPEA (3.55 mL, 3 equiv.) in EtOAc (38 mL), was added a solution of T3P 50% in EtOAc (6.02 mL, 1.5 equiv.). The reaction mixture was stirred in 15 min and then 3,3,3-trifluoropropylamine hydrochloride (1.016 g, 1.5 equiv.) was added. The reaction mixture was then stirred at room temperature overnight. After completion, the reaction mixture was added with water (15 mL) and vigorously stirred for 5 min. The organic phase was decanted and washed with NaHCO₃ saturated solution (x1), solution HCl 1N (x1), water (x2) and brine. The organic phase was then dried over anhydrous MgSO₄ and concentrated under reduced pressure to afford the desired compound **10** (338 mg, 24%) as brown solid.

Chemical Formula: C₁₁H₉F₃N₂O

MW: 242.20 g/mol

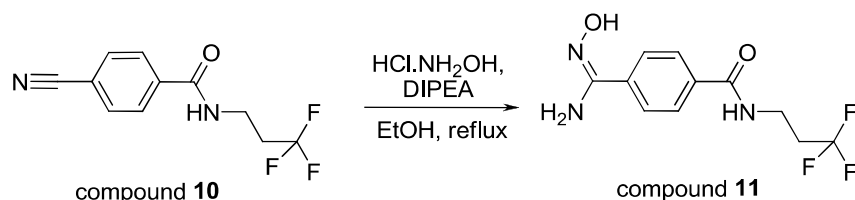
HPLC-MS (method gradient in 5 min at pH 3.8): t_R = 2.35 min

MS-(ES-) m/z 241 ([M-H]⁻, base peak)

¹H-NMR (300 MHz, CDCl₃, ppm) δ 2.49 (qt, J = 10.7 Hz, J = 6.4 Hz, 2H, CH₂), 3.74 (q, J = 6.3 Hz, 2H, CH₂), 6.50 (br s, 0.5H, NH), 7.75 (d, J = 8.5 Hz, 2H, H-Ar), 7.86 (d, J = 8.5 Hz, 2H, H-Ar).

These spectral characteristics were identical to those previously reported in literature.³²⁴

Step 2: synthesis of 4-(N-hydroxycarbaminidoyl)-N-(3,3,3-trifluoropropyl)benzamide (compound 11)



4-cyano-N-(3,3,3-trifluoropropyl)benzamide **10** (200 mg, 0.83 mmol, 1 equiv.) and hydroxylamine hydrochloride (87 mg, 1.5 equiv.) were dissolved in EtOH (4 mL). DIPEA (0.23 mL, 1.6 equiv.) was then added and the reaction mixture was refluxed for 2 hours. After completion, the solvent was evaporated under reduced pressure. The residue was then dissolved in EtOAc and washed with water (x2) and brine. The organic phase was then dried over anhydrous MgSO₄ and concentrated under reduced pressure to afford the desired compound **11** (213 mg, 93%) as white solid.

Chemical Formula: C₁₁H₁₂F₃N₃O₂

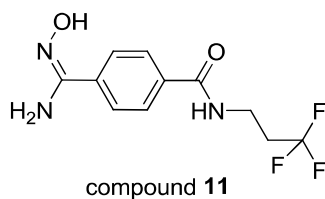
MW: 275.23 g/mol

HPLC-MS (gradient method in 5 min at pH 3.8): t_R = 1.80 min

MS-(ES+) m/z 276 ([M+H]⁺, base peak)

³²⁴ Willand *et al*; Patent FR/3000491 (composé 73, page 56)

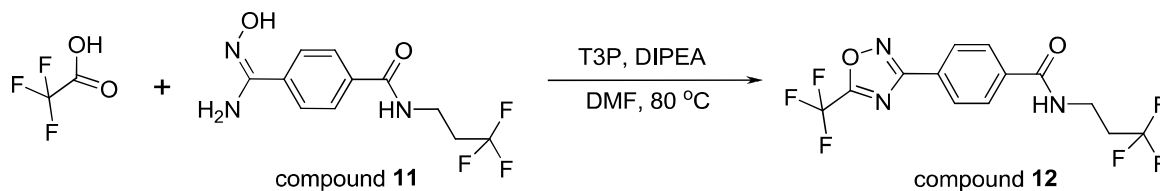
MS-(ES-) m/z 274 ($[M-H]^-$, base peak)



$^1\text{H-NMR}$ (300 MHz, DMSO- d_6 , ppm) δ 2.55 (qt, $J = 11.4$ Hz, $J = 6.9$ Hz, 2H), 3.50 (q, $J = 6.5$ Hz, 2H), 5.89 (s, 2H, NH₂), 7.77 (d, $J = 8.5$ Hz, 2H, H-Ar), 7.83 (d, $J = 8.6$ Hz, 2H, H-Ar), 8.70 (t, $J = 5.5$ Hz, 1H, NH-amide), 9.79 (s, 1H, OH).

These spectral characteristics were identical to those previously reported in literature.³²⁵

Step 3: synthesis of 4-(5-(trifluoromethyl)-1,2,4-oxadiazol-3-yl)- N -(3,3,3-trifluoropropyl)-benzamide (compound 12)



To a stirred solution of 4-(N^2 -hydroxycarbaminidoyl)- N -(3,3,3-trifluoropropyl)benzamide **11** (213 mg, 0.77 mmol, 1.0 equiv.) in DMF (5 mL), DIPEA (3.0 equiv.) was added. Then a solution of T3P 50% in DMF (2.5 equiv.) was added dropwise. Next, trifluoroacetic acid (1.1 equiv.) was added and the reaction mixture was stirred at 80 °C for 90 hours. Analysis by LC-MS showed that the reaction was not completed, a solution of T3P 50% in DMF (0.5 equiv.) was then added to the reaction mixture and heated at 80 °C for more than 24 hours. After completion, DMF was evaporated under reduced pressure and the obtained residue was dissolved in EtOAc. The organic phase was washed with water (x3), brine, dried over anhydrous MgSO₄ and concentrated under reduced pressure to give a yellow solid. This crude residue was then purified by flash chromatography (*column*: silica gel pre-packed Puriflash-12g-30 μm , Interchim; *eluent*s: cyclohexane-EtOAc (80-20); *loading technique*: dry load; *flow-rate*: 11 mL/min; tube collection by time: 0.7 min/tube) to afford the desired product **12** (88 mg, 32% yield) as white solid. Mp: 175.3-176.3 °C

Chemical Formula: C₁₃H₉F₆N₃O₂

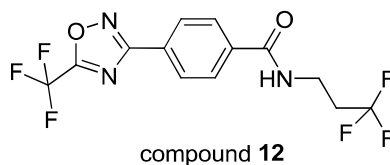
MW: 353.22 g/mol

HPLC-MS (gradient method in 5 min at pH 3.8): $t_R = 2.91$ min

MS-(ES+) m/z 354 ($[M+H]^+$, base peak)

MS-(ES-) m/z 352 ($[M-H]^-$, base peak)

³²⁵ Willand *et al*; Patent FR/3000491 (composé 74, page 57)



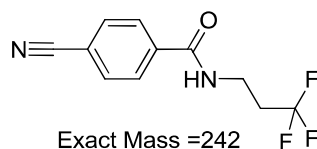
¹H-NMR (300 MHz, DMSO-d₆, ppm) δ 2.60 (qt, $J = 11.4$ Hz, $J = 7.0$ Hz, 2H, CH₂), 3.53 (q, $J = 6.7$ Hz, 2H, CH₂), 8.05 (d, $J = 8.7$ Hz, 2H, H-Ar), 8.19 (d, $J = 8.5$ Hz, 2H, H-Ar), 8.93 (t, $J = 5.6$ Hz, 1H, NH).

¹³C-NMR (75 MHz, DMSO-d₆, ppm) δ 32.8 (q, $^2J_{CF} = 26.6$ Hz), 33.3, 116.2 (q, $^1J_{CF} = 273.0$ Hz), 127.2 (q, $^1J_{CF} = 276.6$ Hz), 127.3, 127.9, 128.7, 138.0, 165.7 (q, $^2J_{CF} = 44.0$ Hz), 165.8, 168.4.

¹⁹F-NMR (282 MHz, DMSO-d₆, ppm) δ -64.72 (s, 3F), -63.85 (t, $^3J_{HF} = 11.4$ Hz, 3F).

This new structure has not been reported in literature. No results were found in Reaxys, Pubchem, eMolecules and Scifinder Scholar (verified on 22/03/2015).

Notice: In this reaction, we also obtained a by-product (69 mg, 37%) as pale yellow solid. The hypothesized structure of this by-product is sketched below:



HPLC-MS (gradient method in 5 min at pH 3.8) : $t_R = 2.29$ min

MS-(ES-) m/z 241 ([M-H]⁻, base peak)

¹⁹F-NMR (282 MHz, DMSO-d₆, ppm) δ -63.87 (t, $^3J_{HF} = 11.2$ Hz)

These results were identical to those previously reported for compound 10.

2.3.4. Synthesis of 4-(5-(trifluoromethyl)-1,2,4-oxadiazol-3-yl)-N-(3,3,3-trifluoropropyl) picolinamide (compound 15)

Step 1: synthesis of 5-cyano-N-(3,3,3-trifluoropropyl)picolinamide (compound 13)



To a solution of 5-cyanopyridine-2-carboxylic acid (1 g, 6.75 mmol, 1 equiv.) and DIPEA (4.7 mL, 4 equiv.) in EtOAc (40 mL), was slowly added a solution of T3P 50% in EtOAc (6.0 mL, 1.5 equiv.). The reaction mixture was stirred in 5 min and then 3,3,3-trifluoropropylamine hydrochloride (1.016 g, 1.5 equiv.) was added. The reaction mixture was then stirred at room temperature overnight. After completion, the reaction mixture was added with water (15 mL) and vigorously stirred for 15 minutes. The aqueous phase was extracted

by EtOAc (x2) The combined organic phase were washed with NaHCO₃ saturated solution (x1), water (x2), brine. The organic phase was then dried over anhydrous MgSO₄ and concentrated under reduced pressure to afford the desired compound **13** (780 mg, 48%) as yellow solid.

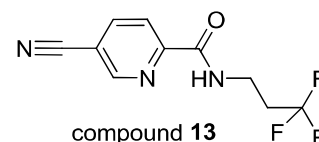
Chemical Formula: C₁₀H₈F₃N₃O

MW: 243.19 g/mol

TLC: R_f = 0.6 (cyclohexane-EtOAc, 5-5)

HPLC-MS (gradient in 5 min at pH 3.8): t_R = 2.30 min

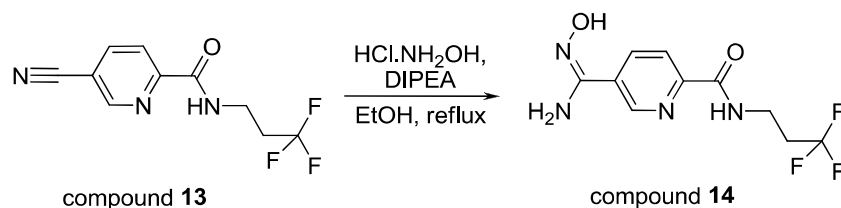
MS-(ES-) m/z 242 ([M-H]⁻, base peak)



¹H-NMR (300 MHz, CD₂Cl₂, ppm) δ 2.49 (qt, *J* = 10.8 Hz, *J* = 6.7 Hz, 2H, CH₂), 3.73 (q, *J* = 6.5 Hz, 2H, CH₂), 8.16 (dd, *J* = 8.1 Hz, *J* = 2.0 Hz, 1H, H-pyridine), 8.18 (br s, 1H, NH), 8.28 (dd, *J* = 8.1 Hz, *J* = 0.9 Hz, 1H, H-pyridine), 8.84 (dd, *J* = 2.0 Hz, *J* = 0.9 Hz, 1H, H-pyridine).

This structure has an PubChem ID number CID 63770177. But no spectral and physical data has been reported in the literature (verified in Reaxys and SciFinder Scholar on 21/03/2015)

Step 2: synthesis of 5-(*N*³-hydroxycarbaminidoyl)-*N*-(3,3,3-trifluoropropyl)picolinamide (compound **14)**



5-cyano-*N*-(3,3,3-trifluoropropyl)picolinamide **13** (365 mg, 1.5 mmol, 1.0 equiv.) and hydroxylamine hydrochloride (156.4 mg, 1.5 equiv.) were dissolved in EtOH (10 mL). DIPEA (0.42 mL, 1.6 equiv.) was then added and the reaction mixture was refluxed for 2h. After completion, the solvent was evaporated under reduced pressure. The residue was then dissolved in EtOAc and washed with water (x2) and brine. The organic phase was then dried over anhydrous MgSO₄ and concentrated under reduced pressure to afford the desired compound **14** (460 mg, quantitative yield) as light yellow solid.

Chemical Formula: C₁₀H₁₁F₃N₄O₂

MW: 276.22 g/mol

HPLC-MS (gradient method in 5 min at pH 3.8) : t_R = 1.81 min

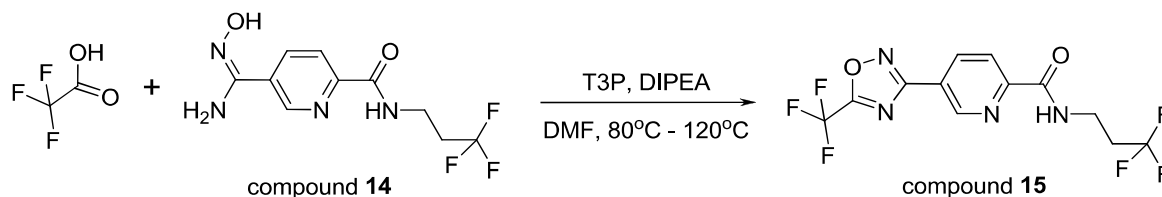
MS-(ES+) m/z 277 ([M+H]⁺, base peak)

MS-(ES-) m/z 275 ([M-H]⁻, base peak)

¹H-NMR (300 MHz, DMSO-*d*₆, ppm) δ 2.58 (qt, $J = 11.4$ Hz and $J = 7.0$ Hz, 2H, CH₂), 3.55 (q, $J = 6.5$ Hz, 2H, CH₂), 6.10 (s, 2H, NH₂), 8.03 (dd, $J = 8.2$ Hz and $J = 0.6$ Hz, 1H, H-pyridine), 8.22 (dd, $J = 8.1$ Hz and $J = 2.1$ Hz, 1H, H-pyridine), 8.92 (d, $J = 1.5$ Hz, 1H, H-pyridine), 9.04 (t, $J = 6.1$ Hz, 1H, NH-amide), 10.03 (s, 1H, OH).

This structure has an PubChem ID number CID 77005076. But no spectral and physical data has been reported in the literature (on Reaxys and SciFinder Scholar, accessed on 21/03/2015)

Step 3: synthesis of 5-(5-trifluoromethyl)-1,2,4-oxadiazol-3-yl-*N*-(3,3,3-trifluoropropyl)-picolinamide (compound 15)



To a stirred solution of 5-(*N*²-hydroxycarbaminidoyl)-*N*-(3,3,3-trifluoropropyl)picolinamide **14** (345 mg, 1.25 mmol, 1.0 equiv.) in DMF (4 mL), DIPEA (3.0 equiv.) was added. Then a solution of T3P 50% in DMF (3.0 equiv.) was added dropwise. Next, trifluoroacetic acid (1.1 equiv.) was added and the reaction mixture was stirred at 80 °C for 1 hour and then at 120 °C overnight. After completion, DMF was evaporated under reduced pressure and the obtained residue was dissolved in EtOAc, washed with water (x3) and brine. The organic phase was then dried over anhydrous MgSO₄ and concentrated under reduced pressure to give a yellow solid. This crude product was purified by flash chromatography (*column*: silica gel pre-packed Puriflash-12g-30 μ m, Interchime; *eluent*s: cyclohexane-EtOAc (80-20) ; *loading technique*: dry load ; *flow-rate*: 10 mL/min; tube collection by time: 0.7-1.0 min/tube) to afford the desired product **15** (182 mg, 41% yield) as white solid. M.p.: 104.4-105.2 °C

Chemical Formula: C₁₂H₈F₆N₄O₂

MW: 354.21 g/mol

HPLC-MS (gradient method in 5 min at pH 3.8) : $t_R = 2.93$ min

MS-(ES+) m/z 355 ([M+H]⁺, base peak)

MS-(ES-) m/z 353 ([M-H]⁻, base peak).

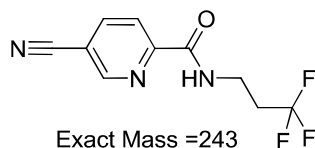
¹H-NMR (300 MHz, DMSO-*d*₆, ppm) δ 2.61 (qt, $J = 11.4$ Hz and $J = 7.0$ Hz, 2H, CH₂), 3.59 (q, $J = 6.5$ Hz, 2H, CH₂), 8.27 (dd, $J = 8.2$ Hz and $J = 0.8$ Hz, 1H, H-pyridine), 8.65 (dd, $J = 8.2$ Hz and $J = 2.1$ Hz, 1H, H-pyridine), 9.22 (t, $J = 6.0$ Hz, 1H, NH), 9.26 (dd, $J = 2.1$ Hz and $J = 0.8$ Hz, 1H, H-pyridine).

¹³C-NMR (75 MHz, DMSO-*d*₆, ppm) δ 32.8 (q, $^2J_{CF} = 27.2$ Hz), 33.0, 116.1 (q, $^1J_{CF} = 274.0$ Hz), 123.1, 123.7, 127.2 (q, $^1J_{CF} = 277.8$ Hz), 137.4, 147.3, 152.8, 163.5, 165.9 (q, $^1J_{CF} = 44.2$ Hz), 166.8.

¹⁹F-NMR (282 MHz, DMSO-*d*₆, ppm) δ - 64.74 (s, 3F), - 64.02 (t, $^3J_{HF} = 11.4$ Hz, 3F).

This new structure has not been reported in literature. No results were found in Reaxys, Pubchem, eMolecules and Scifinder Scholar (verified on 22/03/2015).

Notice: In this reaction, we also obtained a by-product (83 mg, 27%) as pale yellow solid. The hypothesized structure of this by product was sketched below:



HPLC-MS (gradient method in 5 min at pH 3.8): $t_R = 2.28$ min

MS-(ES-) m/z 242 ($[M-H]^-$, base peak)

^{19}F -NMR (282 MHz, DMSO- d_6 , ppm) $\delta - 64.03$ (t, $^3J_{HF} = 11.3\text{Hz}$)

These results were identical to those previously reported in compound **13**

2.4. Biological assays

2.4.1. Affinity of test compounds to EthR by Thermal Shift Assay:

The fluorescent dye SYPRO Orange (Invitrogen) was used to monitor protein unfolding. The thermal shift assay was conducted in a Lightcycler 480 (Roche). The system contained a heating/cooling device for temperature control and a charge-coupled device (CCD) detector for real-time imaging of the fluorescence changes in the wells of the microplate. The final sample concentrations were 10 μM EthR, 2.5 \times SYPRO Orange, 1% DMSO, and 20 μM ligand in the EthR buffer (10 mM Tris/HCl, 300 mM NaCl, pH 7.5, 0.1 mM EDTA). The samples were heated from 37 to 85 $^\circ\text{C}$ with a heating rate of 0.04 $^\circ\text{C}/\text{s}$. The fluorescence intensity was measured at Ex/Em: 465/510 nm. The data were obtained using the algorithmic program Wavemetrics Igor by applying the following designed procedure: the fluorescence intensity of each well/sample is plotted as a function of the temperature. Then, the 1D-numerical derivative of these curves is calculated. At last, the maximum data values, corresponding to the inflection points (T_m), is extracted to give T_m in a table and in a graph.

2.4.2. Potency assay of test compounds on *M. tuberculosis*

2.4.2.1. Bacteria preparation

From a 200 mL bacterial culture, prepare series of 10 fold dilutions of *M. tuberculosis* GFP in PBS using a 384-well plate (dilutions from 1 to 10-10 fold). Record fluorescence levels (RFU) and OD600 of each dilution using a microplate reader. Plate dilutions on 7H11 agar plates and grow for 2-3 weeks at 37 $^\circ\text{C}$. Count CFU on plates from the different dilutions. Plot CFU as a function of RFU and fit the curve using a linear regression to obtain parameters for the CFU = f(RFU) relationship. Same parameters can be reused for all aliquots of the same stock, but a new regression should be established for each stocks of bacteria.

2.4.2.2. Microplates preparation

Chemical compound distribution

Prepare compounds stock solutions at 10 mM by diluting pure compounds in DMSO. Store stock solutions at -20°C. Design the source and assay plate layout. Transfer stock solutions in the 384-well source plates. Prepare assay plates by transferring compounds, either directly from the source plate, or using intermediate dilution plates, to reach the final concentration needed. Concentrations used for the dose response curve (DRC) of booster compounds usually ranges from 30 to 4.5×10^{-3} μM (10 points, 3x dilutions). ETH is added to all points of the DRC at a final concentration of 0.1 $\mu\text{g/ml}$. The final amount of DMSO in the assay plate should be <1% v/v for each well.

Controls in the assay plate include DMSO at 1% (negative control) and INH at 1 $\mu\text{g/ml}$ (positive control). A reference plate should be prepared, including rifampicin, INH and ETH ranging from 30 to 1.8×10^{-3} $\mu\text{g/ml}$ (15 points, 2x dilutions). Store assay and source plates at -20°C, sealed with an adhesive aluminum sealing film. Dispense 50 μL of bacteria per well for each assay plate. If needed, fill empty wells with complete medium to limit evaporation and border-effects. Incubate the plates for 5 days at 37°C, 5% CO_2 .

Read assay plate with a microplate fluorescence reader Victor 3 (Perkin Elmer), emission and excitation filters at 488 and 520 nm, respectively.

2.5. Measurement of physico-chemical properties

These experiments were analyzed using a LC-MS/MS triple-quadrupole system (Varian 1200ws) under MRM detection with the following mass parameters: mode of ionization, electrospray; declustering potential, 50 V; collision gas pressure, 1.5 mTorr; collision energy, 20 eV.

2.5.1. Solubility:

The 10mM solution (40 μL) in DMSO of the sample was added to 1.960mL of MeOH or PBS at pH 7.4. The samples were gently shaken for 24 h at room temperature, then centrifuged for 5 min, and filtered over 0.45 μm filters. An amount equal to 20 μL of each solution was added to 180 μL of MeOH and analyzed by LC-MS/MS. The solubility was determined by the ratio of mass signal areas PBS/MeOH.

2.5.2. LogD

40 μL of the 10 mM solution in DMSO of the sample were added to 1.960 mL of mixture of octanol and PBS at pH 7.4 (1/1). The mixture was gently shaken for 2h at room temperature, then the two phases were separated. 20 μL of each solution was added to 180 μL of MeOH and analyzed by LC-MS/MS. LogD was determined as the logarithm of the ratio of concentrations of product in octanol and PBS, determined by mass signals.

2.6. Metabolic Stability

Materials

All chemicals were obtained from Sigma-Aldrich (Steinheim, Germany). Solvents were from common sources and of LCMS grade. Stock solutions of all compounds were prepared in methanol at a concentration of 0.1 mM. Pooled female mouse (CD-1) liver microsomes were purchased from BD gentest (Le Pont de Claix, France).

Microsomal incubations

All incubations were performed in duplicate in a shaking water bath at 37°C. The incubation mixture were prepared in polypropylene tubes and contained 1µM test compound (1% methanol), mouse liver microsomes (0.6 mg of microsomal protein/mL), 5 mM MgCl₂, 1 mM NADPH, 5 mM glucose-6-phosphate, 0.4 U/mL glucose-6-phosphate dehydrogenase and 50 mM potassium phosphate buffer pH 7.4 in a final volume of 0.5 mL. Sampling points were taken at 5, 10, 20, 30 and 40 min and reactions were terminated by adding ice-cold acetonitrile with internal standard (4 vol). The samples were centrifuged for 10 min at 10000g and 4°C to pellet precipitated microsomal protein. The supernatant was then subjected to LC-MS/MS analysis. Control incubations were performed in triplicate with denatured microsomes with acetonitrile containing internal standard and sampling points were taken at 0 min and 40 min (to evaluate the compound chemical stability in the experimental conditions).

LC-MS/MS analysis

The LC-MS/MS system consisted of an UHPLC Acquity connected to a Xevo TQD mass spectrometer (Waters, Les Ulis, France) equipped with an electrospray ionisation source. Analytes in incubation mixtures were separated by UHPLC using a Acquity BEH C18, 1,7µm, 50 x 2.1mm column (Waters). The mobile phase solvents used were: (A) H₂O 0.1% HCOOH; (B) CH₃CN 0.1% HCOOH. The following mobile phase gradient was applied: 2% B during 10s, 2-98% (B) in 1min 50s; hold at 98% (B) for 30s; 98%-2% B in 5s; 2% B hold for 1min 30s. The injection volume was 2µL and the flow rate of 600µL/min. The desolvation and cone gas flow were respectively 1000 and 50 L/h; the source temperature was 600°C. The capillary and the cone voltage, the collision energy and the observed transitions were optimized for each compound.

Calculations

Quantitation of each compound was achieved by conversion of the corresponding analyte/internal standard peak area ratios to percentage drug remaining, using the T₀ ratio values as 100%. *In vitro* intrinsic clearance (CL_{int} expressed as µl/min/mg) was calculated according to the following formula:

$$CL_{int} = \frac{\text{dose}}{AUC_{\infty}}$$

where **dose** is the initial amount of drug in the incubation mixture (1 μ M) and **AUC** is the area under the concentration versus time curve extrapolated to infinity.

The slope of the linear regression from log percentage remaining versus incubation time relationships (-k) was used in the conversion to *in vitro* $t_{1/2}$ values by :

$$\textit{in vitro } t_{1/2} = \frac{-0.693}{k}$$

2.7. Molecular docking modelling of novel inhibitors in EthR protein

Protein preparation: protein structure was obtained from PDB (ID: 4M3B). Then, the macromolecule was cleaned from solvents (water) and co-crystallized ligand by using Chimera (version 1.9). The hydrogens were then added. This structure was optimized by AutoDockTools in MGLTools 1.5.4 and Gasteiger partial charges and AutoDock force field were then added to each atom.

Ligand preparation: 2D structure of compounds were sketched by ISIS-Draw, converted in 3D-structure by Chimera (version 1.9). Then, these structures were optimized by AutoDockTools in MGLTools 1.5.4; Gasteiger partial charges and AutoDock force field were applied.

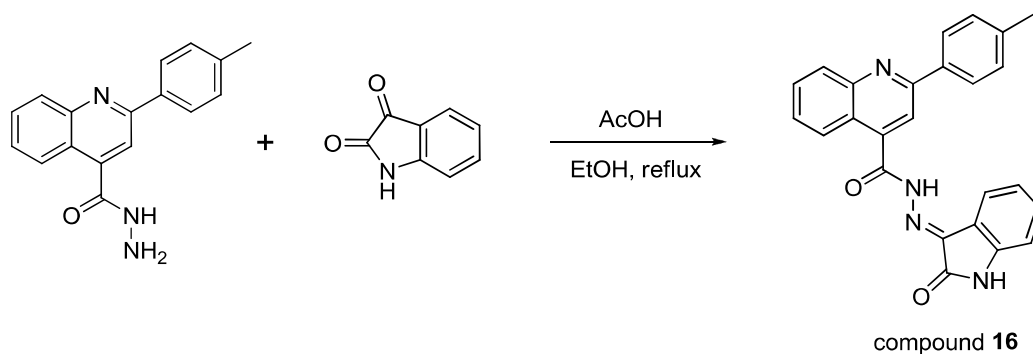
Docking: Docking study was realized in Autodock vina. Grid parameter used was centered at this position: center_x = 28.403, center_y = -11.091, center_z = -4.890 with size_x = 18.0 Å, size_y = 18.0 Å, size_z = 18.0 Å. This grid box is centered by the position of co-crystallized ligand BDM43266. Visualizing docking results was performed in Pymol (DeLano Scientific LLC).

3. Chapter III: Development of MabA inhibitors

3.1. Chemical synthesis

3.1.1. Synthesis of 2 hits from *in silico* screening

Synthesis of in silico hit ZINC05601203 (compound 16)



A solution of 2-(p-tolyl)quinoline-4-carbohydrazide (95%, 291.93 mg, 1.0 mmol, 1.0 equiv.) in EtOH (50 mL) was added to a solution of indoline-2,3-dione (99%, 148.62 mg, 1 mmol, 1.0 equiv.) in EtOH (50 mL). Then glacial acetic acid (0.1 mL) was added. The mixture was refluxed overnight. The reaction mixture was obtained as a yellow solution. Analysis of the reaction mixture by LCMS showed a peak with mass correspond to the desired structure. The solvent was evaporated in to 50 mL, there was a yellow precipitate. The mixture was then recrystallized in EtOH to yield the desired compound **16** (208 mg, 51%) as yellow solid. M.p.: 223-225 °C

Chemical formula: C₂₅H₁₈N₄O₂

MW: 406.45 g/mol

TLC: R_f = 0.5 (cyclohexan-EtOAc; 60-40)

HPLC-MS (method in 10 min at pH 3.8): t_R = 6.60 min

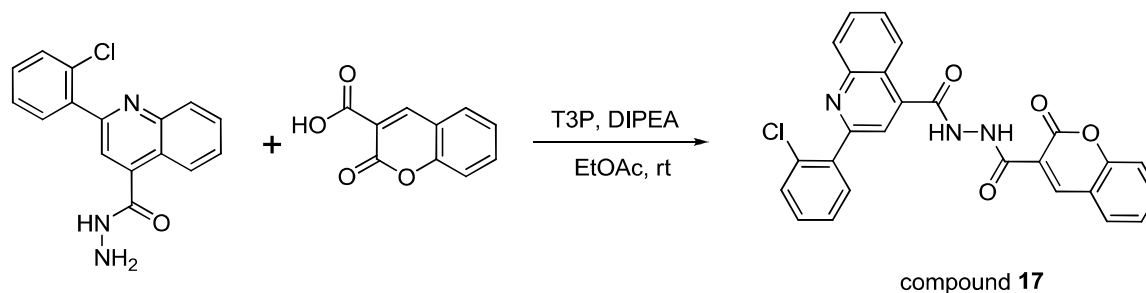
MS-(ES+) m/z 407 ([M+H]⁺, base peak)

MS-(ES-) m/z 405 ([M-H]⁻, base peak)

¹H-NMR (300 MHz, DMSO-*d*₆, ppm) δ 2.40 (s, 3H), 6.85-7.50 (m, 5H), 7.50-8.00 (m, 3H), 8.15-8.47 (m, 5H), 11.33 (s, 1H, NH), 13.27 (br s, 0.26H, NH), 13.68 (br s, 0.7H, NH)

¹³C-NMR (75 MHz, DMSO-*d*₆, ppm) δ 21.4, 111.7, 117.2, 120.0, 121.7, 123.3, 123.4, 125.4, 127.6, 128.1, 131.1, 132.7, 135.6, 139.8, 140.4, 143.2, 148.6, 148.6, 156.2, 156.3, 163.2, 163.6.

This new structure has not been reported in literature. No results were found in Reaxys, Pubchem, eMolecules and Scifinder Scholar (verified on 28/03/2015).

Synthesis of in silico hit ZINC03375877 (compound 17)

To a suspension of 2-oxochromene-3-carboxylic acid (95%, 200.17 mg, 1 mmol, 1.0 equiv.) in EtOAc (10mL), DIPEA (0.692 mL, 4eq) was added. Then a solution of T3P 50% in EtOAc (0.892 mL, 1.5 equiv.) was added dropwise. The reaction mixture became a yellow solution. After 15 minutes, a suspension of 2-(2-chlorophenyl)quinoline-4-carbohydrazide (95%, 313.42 mg, 1 mmol, 1.0 equiv.) in EtOAc was slowly added. The reaction mixture was stirred at room temperature for 1 hour and turned to a yellow -orange solution. Analysis by TLC and LC-MS showed that the desired product was formed but an amount of starting material still left. So the mixture was continued stirring at room temperature overnight. A beige precipitate was formed. So the solid was filtered and the precipitate was washed with EtOAc (20 mLx1) and water (20mLx2). This solid was then dried under vacuum to yield the desired compound **17** (301 mg, 64 %) a beige solid. M.p.: 252.1-253.2 °C

Chemical formula: C₂₆H₁₆ClN₃O₄

MW: 469.89 g/mol

TLC: R_f = 0.3 (cyclohexan-EtOAc, 60/40) ; R_f = 0.7 (DCM-MeOH, 99/1)

HPLC-MS (method in 10 min at pH 3.8): t_R = 6.60 min

MS-(ES+) m/z 470 ([M+H]⁺ for ³⁵Cl, base peak) ; 472 ([M+H]⁺ for ³⁷Cl, 38%) ; 473 (10%)

MS-(ES-) m/z 468 ([M-H]⁻ for ³⁵Cl, base peak) ; 470 ([M-H]⁻ for ³⁷Cl, 38%) ; 471 (10%)

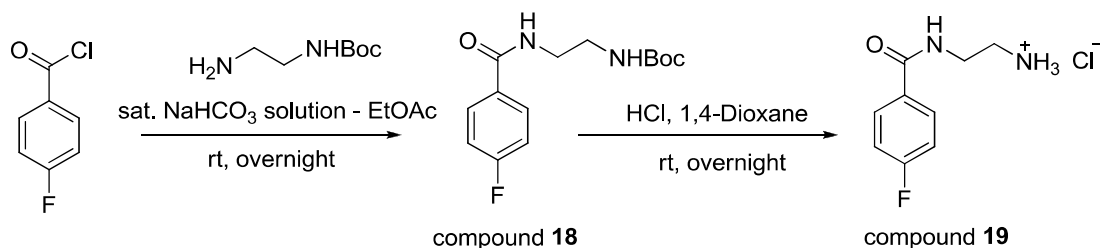
¹H-NMR (300 MHz, DMSO-*d*₆, ppm) δ 7.45 (t, *J* = 7.3 Hz, 1H), 7.54-7.58 (m, 3H), 7.65-7.68 (m, 1H), 7.72-7.82 (m 3H), 7.87-7.92 (m, 2H), 8.03 (dd, *J* = 7.8 Hz and *J* = 1.5 Hz, 1H), 8.16 (d, *J* = 8.2 Hz, 1H), 8.43 (d, *J* = 8.4 Hz, 1H), 9.0 (s, 1H), 10.69 (br s, 1H, NH, exchangeable with D₂O), 11.23 (br s, 1H, NH, exchangeable with D₂O).

¹³C-NMR (75 MHz, DMSO-*d*₆, ppm) δ 116.8, 118.7, 118.8, 121.2, 123.7, 125.7, 125.9, 128.1, 128.4, 130.0, 130.5, 130.9, 131.0, 131.2, 131.8, 132.3, 135.0, 138.9, 140.5, 148.2, 149.0, 154.5, 156.8, 160.2, 160.8, 165.3.

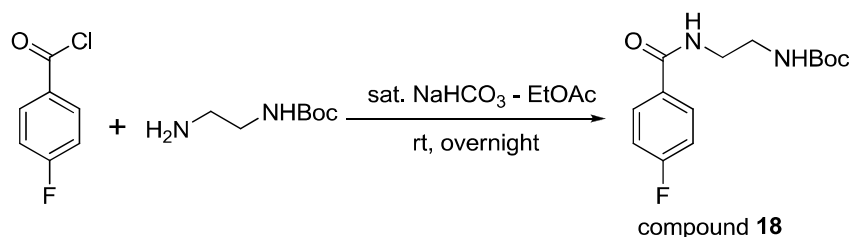
This new structure has not been reported in literature. No results were found in Reaxys, Pubchem, eMolecules and Scifinder Scholar (verified on 28/03/2015).

3.1.2. Synthesis of hits from the primary screening

3.1.2.1. Synthesis of fragment hit ID-9098328 (compound 19)



Step 1: synthesis of tert-butyl-N-{2-[(4-fluorophenyl)formamido]ethyl}carbamate



Protocol:³²⁶

t-Butyl-*N*-(2-amino-ethyl)carbamate (400 μ L, 2.54 mmol, 1.0 equiv.) was dispersed in mixture of ethyl acetate (6 mL) and saturated aqueous sodium bicarbonate solution (6 mL). To this mixture at 0°C, a solution of 4-fluorobenzoyl chloride (330 μ L, 1.1 equiv.) in ethyl acetate (2 mL) was added dropwise. The reaction mixture was warmed to room temperature and vigorously stirred overnight. After completion, the organic layer was separated and the aqueous phase was extracted with ethyl acetate (20 mL x 2). The combined organic phase were then washed with water (30 mL x 1), brine (30 mL x 1), dried over magnesium sulfate and concentrated under reduced pressure to yield the desired product **18** (741 mg, quantitative yield) as a white solid.

Chemical formula: C₁₄H₁₉FN₂O₃

MW: 282.32 g/mol

HPLC-MS (method in 5 min at pH 3.8): t_R = 2.83 min

MS-(ES+) m/z 283 ([M+H]⁺, 20%); 227 (35%); 183 ([M-Boc+H]⁺, base peak); 166 (55%).

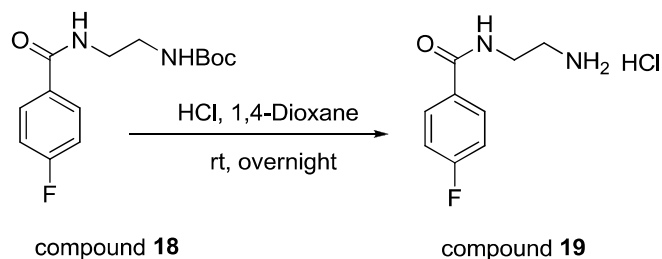
MS-(ES-) m/z 281 ([M-H]⁻, 8%); 207 (base peak).

¹H-NMR (300 MHz, CDCl₃, ppm) δ 1.43 (s, 9H, 3xCH₃), 3.41 (s, 2H, CH₂), 3.53-3.58 (m, 2H, CH₂), 5.03 (br s, 1H, NH), 7.07-7.12 (m, 2H, H-Ar), 7.82-7.87 (m, 2H, H-Ar).

These spectral characteristics were identical to those previously reported in literature.³²⁷

³²⁶ Patent US 6200989, column 10 & 11

³²⁷ Patent WO2012/4549 A1, 2012, column 30, compound 21h and 22h

Step 2: synthesis of *N*-(2-aminoethyl)-4-fluorobenzamide hydrochloride**Protocol:**³²⁸

A solution of tert-butyl-*N*-(2-[(4-fluorophenyl)formamido]ethyl)carbamate **18** (340.44 mg, 1.206 mmol, 1.0 equiv.) in 1,4-dioxane (2 mL) was cooled to 0°C. Then solution HCl 4N in dioxane (3.015 mL, 10 equiv.) was added dropwise. The mixture was stirred at room temperature overnight. A white precipitate was formed. After completion, the solid was filtered, washed with anhydrous diethyl ether and then dried under vacuum to give the desired compound **19** (209.45 mg, 79%) as white solid.

Chemical formula: C₉H₁₁FN₂O (free base)+HCl

MW: 218.66 g/mol

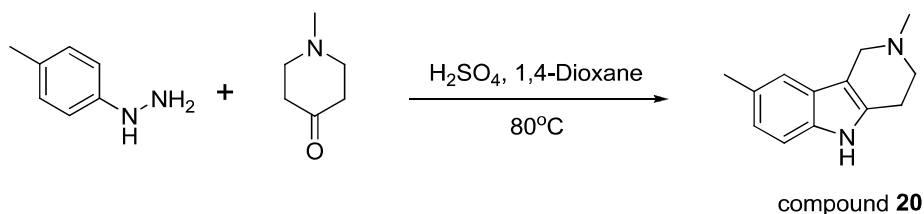
HPLC-MS (method in 5 min at pH 3.8): t_R = 2.05 min

MS-(ES+) *m/z* 183 ([M-HCl+H]⁺, 20%); 166 (base peak)

¹H-NMR (300 MHz, DMSO-*d*₆, ppm) δ 2.97-2.99 (m, 2H, CH₂), 3.52 (q, *J* = 5.9 Hz, 2H, CH₂), 7.30 (t, *J* = 8.8 Hz, 2H, H-Ar), 8.01 (dd, *J* = 5.5 Hz and *J* = 8.8 Hz, 2H, H-Ar), 8.82 (br s, 3H, NH₃⁺), 8.86 (t, *J* = 5.4 Hz, NH).

¹³C-NMR (75 MHz, DMSO-*d*₆, ppm) δ 37.6, 39.0, 115.6 (d, ¹*J*_{CF} = 21.7 Hz), 130.6 (d, ²*J*_{CF} = 8.9 Hz), 130.9 (d, ³*J*_{CF} = 3.0 Hz), 162.8, 166.1.

The ¹H-NMR spectral was identical to that previously reported in literature.³²⁷ However, the ¹³C-NMR of this structure has not been reported in literature (verified on Reaxys and Scifinder scholar on 25/03/2015)

3.1.2.2. Synthesis of fragment hit ID-5161544 (compound 20)**Protocol:**³²⁹

³²⁸ *J. Pept. Res.* 2001(58), pp. 338–341.

³²⁹ *Tetrahedron Letters*, 45(2004), pp. 4781-83

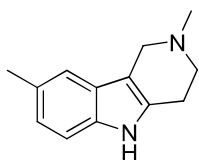
To a solution of 4-methylphenyl hydrazine (0.254 mL, 2 mmol, 1.0 equiv.) in 1,4-dioxane (10 mL), 1-methyl-4-piperidone (242.5 mg, 1.05 eq) was added. The mixture was cooled to 0 °C. Then concentrated sulfuric acid (0.7 mL,) was added dropwise. The mixture was then stirred at 80 °C in 1 hour. After completion, the reaction mixture was cooled to room temperature and then was concentrated under reduced pressure. The obtained residue was then dissolved in EtOAc and washed with NaHCO₃ saturated solution (x1), water (x1), brine (x1), dried over MgSO₄ and evaporated under reduced pressure to give the crude product as brown solid. The crude residue was then purified by flash chromatography (column: prepacked column 40g, diluant: DCM-MeOH-TEA (9-1-0.2), collection in tube Vmax=10 mm, flow rate 10 mL/min) to isolate the pure compound **20** (176 mg, 44%) as beige solid.

Chemical formula: C₁₃H₁₆N₂

MW: 200.29 g/mol

HPLC-MS (method in 5 min at pH 3.8): t_R= 2.38 min

MS-(ES+): m/z 201 ([M+H]⁺, 25%) ; 158 (base peak)



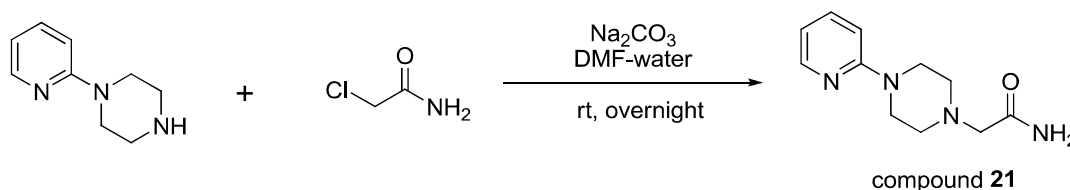
compound **20**

¹H-NMR (300 MHz, CDCl₃, ppm) δ 2.44 (s, 3H, CH₃), 2.58 (s, 3H, CH₃), 2.82 (s, 4H, 2 x CH₂), 3.68 (s, 2H, CH₂), 6.94 (d, *J* = 8.4 Hz, 1H, H-Ar), 7.13 (d, *J* = 8.4 Hz, 1H, H-Ar), 7.20 (s, 1H, H-Ar), 8.05 (s, 1H, NH).

¹³C-NMR (75 MHz, CDCl₃, ppm) δ 21.5, 23.6, 45.7, 51.8, 52.5, 107.7, 110.4, 117.3, 122.5, 126.3, 128.2, 132.0, 134.5.

These spectral characteristics were identical to those previously reported in literature.³³⁰

3.1.2.3. Synthesis of fragment hit ID-9055294 (compound 21)



Protocol:³³¹

1-(pyridin-2-yl)piperazine (666.22 mg, 4.0 mmol, 1.0 equiv.) and 2-chloroacetamide (496.19 mg, 5.2 mmol, 1.3 equiv.) were dissolved in mixture of *N,N*-dimethylformamide and water (2/1, 30mL). Sodium carbonate (1.272g, 12 mmol, 3.0 equiv.) was added in portion and the

³³⁰ Gore, Sangram *et al.*, *Org Lett.*, Vol 14, No 17, 2012, pp 4568-4571 (supporting information)

³³¹ Patent US2003/0229094 A1 page 95

mixture was stirred at room temperature overnight. After completion, the reaction mixture was then quenched in dichloromethane. The organic phase was separated, washed with water (x1), brine (x1), dried over magnesium sulfate and concentrated under reduced pressure to furnish the crude product as a almost white solid. The crude was purified by column chromatography (column: pre-packed column AIT 40g; eluents: DCM:MeOH (98:2); flow-rate: 17 mL/min; tube No22; collection by time: 0.75 min/tube) to yield one fraction (tube 24 - tube 55) which was then evaporated under reduced pressure to give compound **21** (407 mg, 46%) as white solid.

Chemical formula: C₁₁H₁₆N₄O

MW: 220.28 g/mol

HPLC-MS (method in 5 min at pH 3.8): t_R = 1.93 min

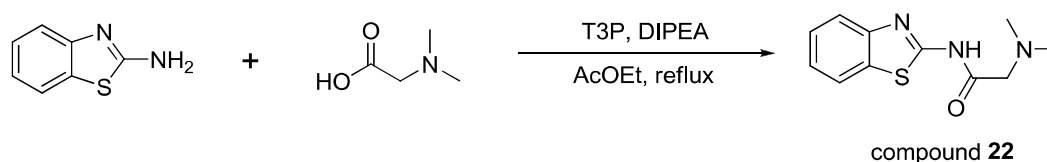
MS-(ES+): m/z 221 ([M+H]⁺, base peak); 121 (95%)

¹H-NMR (300 MHz, CDCl₃, ppm) δ 2.67 (t, *J* = 5.0 Hz, 4H, H-piperazine), 3.07 (s, 2H, CH₂), 3.57 (t, *J* = 5.0 Hz, 4H, H-piperazine), 6.03 (br s, 1H, NH₂), 6.62-6.67 (m, 2H, H-pyridine), 7.06 (br s, 1H, NH₂), 7.48 (td, *J* = 7.9 Hz and *J* = 1.9 Hz, 1H, H-pyridine), 8.18-8.20 (m, 1H, H-pyridine).

¹³C-NMR (75 MHz, CDCl₃, ppm) δ 45.3, 53.4, 61.6, 107.2, 113.6, 137.5, 147.9, 159.3, 173.3.

This structure has an PubChem ID number 6470742. But no spectral and physical data has been reported in the literature (on Reaxys and SciFinder Scholar, accessed on 21/03/2015).

3.1.2.4. Synthesis of fragment hit ID-9052337 (compound 22)



Protocol:

To a solution of 2-(dimethylamino)acetic acid (318.93 mg, 3 mmol, 1.0 equiv.) and DIPEA (2.054 mL, 4 equiv.) in EtOAc (15 mL), was added dropwise a solution of T3P 50% in EtOAc (3.568 mL, 6 mmol, 2.0 equiv.). The mixture was stirred at room temperature for 15 minutes. Then solution of 1,3-benzothiazol-2-amine (464.55 mg, 1.0 equiv.) in EtOAc (5 mL) was added dropwise. The reaction mixture was stirred at reflux overnight. After completion, the resulting mixture was quenched in water (30 mL). The aqueous phase was extracted with ethyl acetate (10mLx2). The combined organic layer was washed with a saturated solution NH₄Cl, saturated solution NaHCO₃ (x2), water (until pH 7) and brine (x1). The organic phase was dried over anhydrous magnesium sulfate and evaporated under reduced pressure to give the crude product as brown solid. Purification by column chromatography (column: pre-packed column AIT 40g ; eluents: DCM:MeOH (99:1) ; flow-rate: 10 mL/min; tube 10cm;

collection by time: 0.75 min/tube) give one fraction (tube 41 - tube 50) which then evaporated under reduced pressure to yield the desired compound **22** (390 mg, 55%) as beige solid.

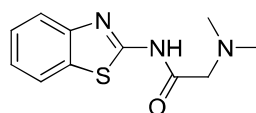
Chemical formula: C₁₁H₁₃N₃OS

MW: 235.31 g/mol

HPLC-MS (method in 5 min at pH 3.8): t_R = 2.28 min

MS-(ES+) m/z 236 ([M+H]⁺, base peak); 258 ([M+Na]⁺, 95%).

MS-(ES-) m/z 234 ([M-H]⁻, base peak).



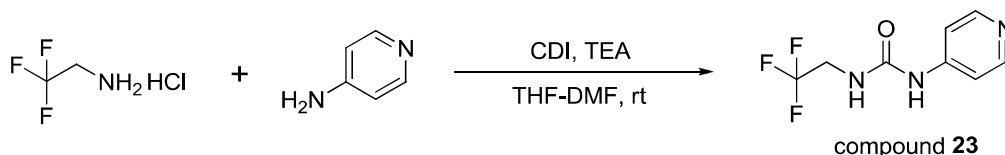
compound **22**

¹H-NMR (300 MHz, DMSO-*d*₆, ppm) δ 2.29 (s, 6H, 2xCH₃), 3.29 (s, 2H, CH₂), 7.30 (t, *J* = 7.8 Hz, 1H, H-benzothiazol), 7.43 (t, *J* = 7.8 Hz, 1H, H-benzothiazol), 7.73 (d, *J* = 7.8 Hz, 1H, H-benzothiazol), 7.97 (d, *J* = 7.8 Hz, 1H, H-benzothiazol), 12.05 (br s, 1H, NH).

¹³C-NMR (75 MHz, DMSO-*d*₆, ppm) δ 45.5, 61.8, 121.0, 122.2, 124.0, 126.6, 131.9, 149.0, 158.0, 170.2.

This compound was described in Reaxys with ID number 1078206, but no spectral and physical data have been published (verified on 21/03/2015).

3.1.2.5. Synthesis of fragment hit ID-7930121 (compound **23**)



Protocol:

Carbonyldiimidazole CDI (178.37 mg, 1.1 mmol, 1.1 equiv.) was dispersed in 5 mL of anhydrous THF. To this suspension, a solution of 4-amino pyridin (94.12 mg, 1.0 mmol, 1.0 equiv.) in DMF (5 mL) was added and the mixture was continued to stir at room temperature for 1 hour 30 min. In the next step, a solution of 2,2,2-trifluoroethan-1-amine hydrochloride (135.52 mg, 1.0 mmol, 1 eq) was separately prepared in DMF (5 mL), TEA (0.560 mL, 4 eq) was added to neutralize the HCl, the pH the solution was verified at pH 8-9. The fresh prepared solution was then slowly added to the reaction mixture. The mixture was stirred at room temperature overnight. After completion, the reaction was then concentrated in vacuum to give a light yellow solid. The crude was dissolved in ethyl acetate and then washed with water (x1), brine (x1). The organic phase was separated, dried over magnesium sulfate and evaporated under reduced pressure to give the crude as white solid. The crude residue was purified by flash chromatography (column: pre-packed column Interchim PF30SIHP-4g; diluant: DCM:MeOH (95:5); flow-rate: 12.5 mL/min; tube 10cm; collection by time: 0.55

min/tube). We obtained one fraction (tube 6 - tube 20) which was then evaporated under reduced pressure to give the desired structure **23** (56 mg, 26%) as white solid.

Chemical formula: C₈H₈F₃N₃O

MW: 219.17 g/mol

HPLC-MS (method in 5 min at pH 3.8): t_R = 2.16 min

MS-(ES+) m/z 220 ([M+H]⁺, base peak)

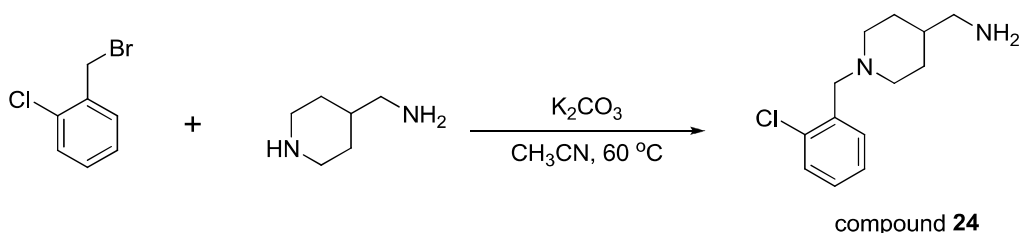
MS-(ES-) m/z 218 ([M-H]⁻, base peak)

¹H-NMR (300 MHz, DMSO-*d*₆, ppm) δ 3.93 (dq, *J* = 6.5 Hz, *J* = 9.8 Hz, 2H, CH₂), 6.99 (t, *J* = 6.5 Hz, 1H, NH), 7.38 (d, *J* = 6.5 Hz, 2H, H-pyridine), 8.31 (d, *J* = 5.5 Hz, 2H, H-pyridine), 9.21 (s, 1H, NH).

¹³C-NMR (75 MHz, DMSO-*d*₆, ppm) δ 40.9 (q, ²*J*_{CF} = 34.3 Hz), 112.6, 125.4 (q, ¹*J*_{CF} = 280.0 Hz), 147.0, 150.6, 154.8.

This structure has an PubChem ID number CID 934792. But no spectral and physical data has been reported in the literature (on Reaxys and SciFinder Scholar, accessed on 21/03/2015).

3.1.2.6. Synthesis of fragment hit ID-7976697 (compound **24**)



Protocol:³³²

K₂CO₃ (569.95 mg, 4.0 mmol, 1.0 equiv.) and 2-chlorobenzyl bromide (847.35 mg, 4.0 mmol, 1.0 equiv.) were successively added to a solution of 4-(aminomethyl)piperidine (466.09 mg, 4.0 mmol, 1.0 equiv.) in acetonitrile (25 mL). The reaction mixture was stirred at 60 °C overnight. After completion, the solvent was evaporated under reduced pressure to yield an colorless oil. This crude residue was then purified by column chromatography (column: pre-packed column 25g; eluents: dichloromethane- methanol- triethylamine / 95-4-1, flow-rate: 15 mL/min; tube No22; collection by time: 1.10 min/tube). We obtained one fraction (tube 11 - tube 18) which was evaporated under reduced pressure to afford the desired product **24** (323 mg, 34%) as colorless oil.

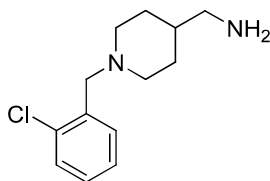
Chemical formula: C₁₃H₁₉ClN₂

MW: 238.76 g/mol

HPLC-MS (method in 5 min at pH 9.2): t_R = 2.53 min

³³² *Eur. J. Med Chem.*, 2009, 44(1), pp. 124-130

MS-(ES+) m/z 239 ($[M+H]^+$, base peak)



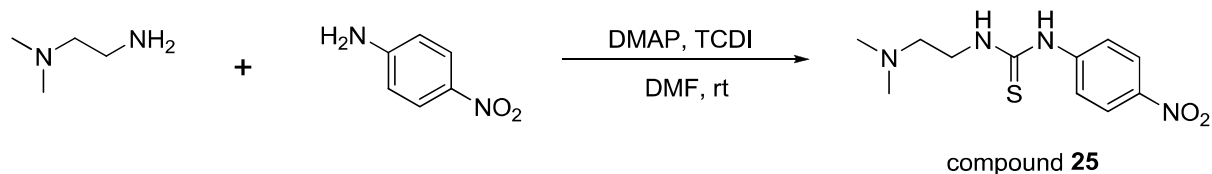
compound **24**

$^1\text{H-NMR}$ (300 MHz, CDCl_3 , ppm) δ 1.20-1.31 (m, 3H), 1.72 (d, $J = 11.5$ Hz, 2H), 1.78 (s, 2H), 2.08 (td, $J = 11.5$ Hz, $J = 2$ Hz, 2H), 2.60 (d, $J = 5.8$ Hz, 2H), 2.93 (d, $J = 11.5$ Hz, 2H), 3.60 (s, 2H), 7.17 (td, $J = 7.6$ Hz, $J = 1.7$ Hz, 1H, H-Ar), 7.23 (td, $J = 7.4$ Hz, $J = 1.6$ Hz, 1H, H-Ar), 7.34 (dd, $J = 7.6$ Hz, $J = 1.5$ Hz, 1H, H-Ar), 7.48 (dd, $J = 7.6$ Hz, $J = 1.7$ Hz, 1H, H-Ar).

$^{13}\text{C-NMR}$ (75 MHz, CDCl_3 , ppm) δ 30.0, 39.0, 48.0, 53.7, 59.5, 126.5, 127.9, 129.3, 130.6, 134.2, 136.4.

This structure has an PubChem ID number CID 2236109. But no spectral and physical data has been reported in the literature (on Reaxys and SciFinder Scholar, accessed on 21/03/2015).

3.1.2.7. Synthesis of fragment hit ID-7805186 (compound **25**)



compound **25**

Protocol:³³³

Thiocarbonyldiimidazole TCDI (1188.1 mg, 6.0 mmol, 1.5 equiv.) and 4-dimethylaminopyridine DMAP (73.3 mg, 0.6 mmol, 0.15 equiv.) were added to a stirred solution of 4-nitroaniline (569.6 mg, 4 mmol, 1.0 equiv.) in DMF (10 mL). The reaction was stirred for 2 hours at room temperature. In the next step, a solution of dimethylethylenediamine (359.81 mg, 4 mmol, 1 eq) in DMF was added dropwise. The reaction mixture was stirred for 1 hour. On the LC-MS chromatogram, there was a peak with mass corresponds to the desired compound. After completion, the solvent was evaporated under reduced pressure. The obtained residue was then dissolved in EtOAc, washed with water (30 mL x 2) and brine (30 mL x1), dried over MgSO_4 and evaporated to yield a yellow solid. This crude residue was then purified by column chromatography (column: pre-packed column 40g; eluents: dichloromethane-methanol (97-3), flow-rate: 25 mL/min; tube No22; collection by time: 1.50 min/tube) to yield the desired compound **25** (572 mg, 53%) as yellow solid.

Chemical formula: $\text{C}_{11}\text{H}_{16}\text{N}_4\text{O}_2\text{S}$

³³³ *Bioorg. Med. Chem. Letters*, 2011 (21), pp. 6782-6787

MW: 268.34 g/mol

HPLC-MS (method in 5 min at pH 3.8): $t_R = 2.48$ min

MS-(ES+) m/z 269 ($[M+H]^+$, base peak)

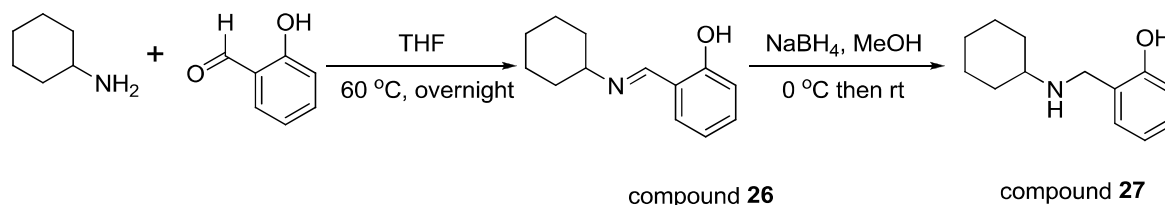
MS-(ES-) m/z 267 ($[M-H]^-$, base peak)

$^1\text{H-NMR}$ (300 MHz, DMSO- d_6 , ppm) δ 2.21 (s, 6H, 2 x CH₃), 2.46-2.49 (m, 2H, CH₂), 3.58 (s, 2H, CH₂), 7.88-7.91 (d, $J = 8.8$ Hz, 2H, H-Ar), 8.14-8.19 (m, 3H, 2H-Ar & NH), 10.38 (s, 0.7H, NH).

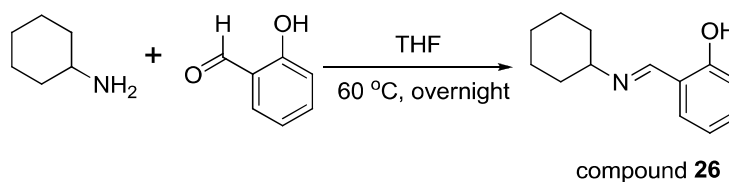
$^{13}\text{C-NMR}$ (75 MHz, DMSO- d_6 , ppm) δ 42.0, 45.3, 57.2, 120.6, 124.9, 142.2, 147.0, 180.2.

This structure has an PubChem ID number CID 2956062. But no spectral and physical data has been reported in the literature (on Reaxys and SciFinder Scholar, verified on 21/03/2015).

3.1.2.8. Synthesis of fragment hit ID-5487719 (compound 27)



Step 1: synthesis of *N*-2-hydroxybenzylidenecyclohexylamine (compound 26)



Protocol:

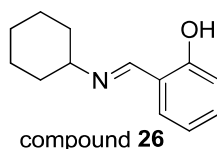
Cyclohexylamine (817.96 mg, 8.0 mmol, 1.0 equiv.) and salicylaldehyde (996.94 mg, 8.0 mmol, 1.0 equiv.) were dissolved in THF (40 mL). The mixture color immediately changed to yellow. The solution was stirred at 60 °C overnight. After completion, the mixture was dried over MgSO₄ and then evaporated under reduced pressure to give the crude product as a yellow oil (1.7 g, quantitative). This crude product was then reduced by NaBH₄ in the next reaction without further purification.

Chemical formula: C₁₃H₁₇NO

MW: 203.29 g/mol

HPLC-MS (method in 5 min at pH 3.8): $t_R = 3.47$ min

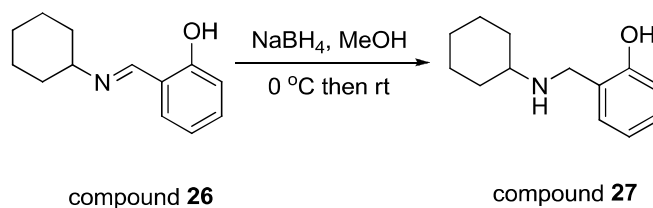
MS-(ES+) m/z 204 ($[M+H]^+$, base peak)



¹H-NMR (300 MHz, CDCl₃, ppm) δ 1.27-1.46 (m, 3H, H-cyclohexyl), 1.51-1.68 (m, 3H, H-cyclohexyl), 1.82-1.85 (m, 4H, H-cyclohexyl), 3.26 (tt, $J = 9.7$ Hz, $J = 3.4$ Hz, 1H, H-cyclohexyl), 6.87 (t, $J = 7.6$ Hz, 1H, H-Ar), 6.97 (d, $J = 8.5$ Hz, 1H, H-Ar), 7.23-7.33 (m, 2H, H-Ar), 8.37 (s, 1H, H-imine), 13.77 (br s, 1H, OH).

These spectral characteristics were identical to those previously reported in literature.³³⁴

Step 2: synthesis of 2-((cyclohexylamino)-methyl)phenol (compound 27)



Protocol:

The Schiff base *N*-2-hydroxybenzylidene-cyclohexylamine **26** (1.7 g, 8.0 mmol, 1.0 equiv.) was dissolved in MeOH (24 mL). The solution was cooled to 0°C, then NaBH₄ (605.32 mg, 2.0 equiv.) was added in portion. After 5 min, the solution color changed from yellow to colorless. The mixture was stirred for 2 hours. After completion, the solvent was evaporated under reduced pressure to give a white solid. This crude product was then washed by water (3x20 mL). Recrystallization in water afforded compound **27** (1.33 g, 81% in 2 steps) as slightly yellow crystals (m.p = 62-63 °C, lit. 62 °C³³⁵)

Chemical formula: C₁₃H₁₉NO

MW: 205.3 g/mol

HPLC-MS (method in 5 min at pH 3.8): $t_R = 2.32$ min

MS-(ES⁺) m/z 206 ([M+H]⁺, base peak)

¹H-NMR (300 MHz, CDCl₃, ppm) δ 1.34-1.08 (m, 5H), 1.65-1.58 (m, 1H), 1.78-1.73 (m, 2H), 1.98 (d, $J = 12.0$ Hz, 2H), 2.60-2.51 (m, 1H), 4.03 (s, 2H), 5.9 (br s, 1H), 6.76 (td, $J = 7.4$ Hz, $J = 1.0$ Hz, 1H), 6.84 (d, $J = 8.2$ Hz, 1H), 6.99 (d, $J = 7.3$ Hz, 1H), 7.16 (td, $J = 7.6$ Hz, $J = 1.6$ Hz, 1H).

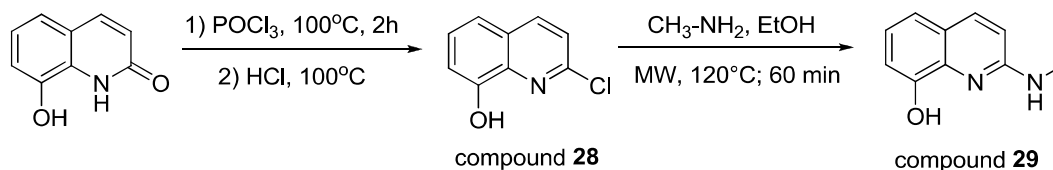
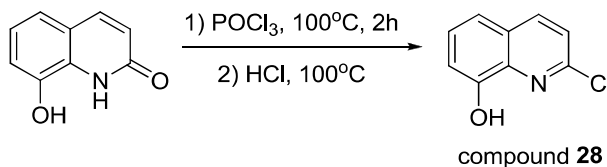
¹³C-NMR (75 MHz, CDCl₃, ppm) δ 24.8, 25.9, 33.0, 49.7, 55.6, 116.4, 118.8, 123.1, 128.0, 128.5, 158.5.

These spectral characteristics were identical to those previously reported in literature.³³⁶

³³⁴ Mierde, Hans Vander *et al.*, *European Journal of Organic Chemistry*, 2008, # 9 p. 1625 - 1631

³³⁵ *Pharmaceutical Chemistry Journal*, 1987, vol. 21, # 2 p. 110 - 114

³³⁶ Kainz, Quirin M. *et al. Chemistry - A European Journal*, 2013, vol. 19 (30), p.10038-45 (compound 8g)

3.1.2.9. Synthesis of fragment hit ID-5175081 (compound 29)**Step 1: synthesis of 2-chloro-8-hydroxy-quinolin (compound 28)****Protocol:**³³⁷

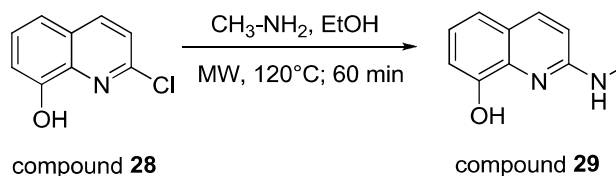
A mixture of 2,8-dihydroxyquinoline (966.97 mg, 6 mmol, 1.0 equiv.) and phosphorous oxychloride (4.835 mL, 8.8 equiv.) was stirred at 100 °C for 1h. The clear solution was cooled to room temperature and poured slowly with stirring into a mixture of NH₄OH (100 mL) and crushed ice. The off-white solid that precipitated was filtered, dissolved in concentrated HCl (10 mL), stirred at reflux for 1h and then at room temperature overnight. The mixture was then neutralized with NH₄OH at 0°C to afford a gray precipitate which then was filtered, washed with water and dried under reduced pressure to yield a gray solid (300 mg). The structure was confirmed by LC-MS. This crude product **28** was used to carry out next reaction without further purification.

Chemical formula: C₉H₆ClNO

MW: 179.61 g/mol

HPLC-MS (method in 5 min at pH 3.8): t_R = 2.99 min

MS-(ES+) m/z 180 ([M+H]⁺ for ³⁵Cl, base peak) ; 182 ([M+H]⁺ for ³⁷Cl, 30%)

Step 2: synthesis 2-methylamino-8-hydroxy-quinolin (compound 29)

2-chloro-8-hydroxy quinoline (179.61 mg, 1.0 mmol, 1 equiv.) was dispersed in a solution of methyl amine 2M in ethanol (6 mL, 12 equiv.). The reaction mixture was carried out under microwave irradiation at 120°C for 60 min. After completion, the solvent was then evaporated in reduced pressure to yield a crude product as green oil. This crude residue was then purified by column chromatography (column: pre-packed column 12g ; diluent: dichloromethane-

³³⁷ Patent WO 2004/035549, page 71

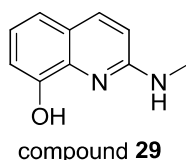
methanol (97-3), flow-rate: 12 mL/min; collection by time: 0.60 min/tube) to give the final product **29** (114 mg, 18% in 2 steps) as gray solid.

Chemical formula: C₁₀H₁₀N₂O

MW: 174.20 g/mol

HPLC-MS (method in 5 min at pH 3.8): t_R = 2.12 min

MS-(ES+) m/z 175 ([M+H]⁺, base peak)

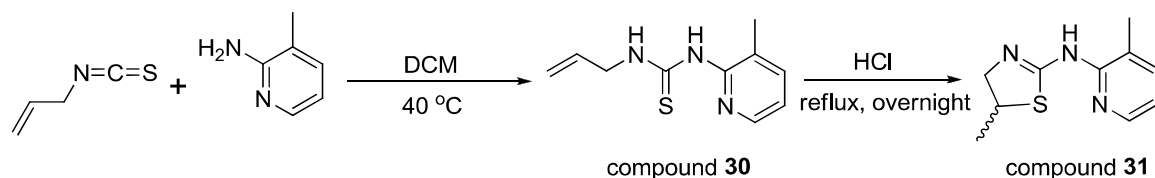


¹H-NMR (300 MHz, MeOH-*d*₄, ppm) δ 3.02 (s, 3H, CH₃), 6.72 (d, *J* = 8.8 Hz, 1H, H-quinoline), 6.92 (dd, *J* = 7.6 Hz and *J* = 1.6 Hz, 1H, H-quinoline), 7.02 (t, *J* = 7.6 Hz, 1H, H-quinoline), 7.08 (dd, *J* = 7.9 Hz and *J* = 1.6 Hz, 1H, H-quinoline), 7.76 (d, *J* = 8.8 Hz, 1H, H-quinoline).

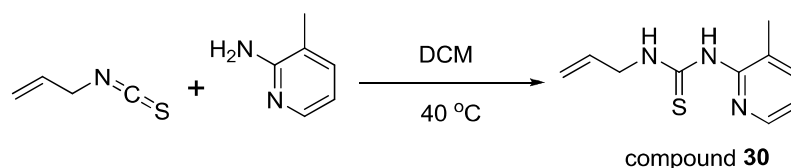
¹³C-NMR (75 MHz, MeOH-*d*₄, ppm) δ 26.8, 109.9, 112.7, 117.4, 121.4, 122.9, 136.3, 137.2, 150.1, 156.9.

This compound was described in Reaxys with an ID number 389157, but only MS spectra was described.³³⁸

3.1.2.10. Synthesis of fragment hit ID-7937388 (compound 31)



Step 1: synthesis of N-prop-2-en-1-yl-N'-(3-methylpyridin-2-yl)thiourea (compound 30)



Protocol:³³⁹

3-methyl-2-amino pyridine (0.202 mL, 1.94 mmol, 1.0 equiv.) was dissolved in 2 mL of dichloromethane, then allyl isothiocyanate (0.206 mL, 1.02 eq) was added. The reaction mixture was refluxed overnight. On the LC-MS, there was a peak with mass correspond to the desired product but there was also the starting material (3-methyl-2-amino pyridine). So we added more isothiocyanate (0.6 mL, 3.0 equiv.) to the reaction mixture and continued the

³³⁸ Patent US 6465467 B1, 2002

³³⁹ *Russian Journal of Organic Chemistry*, 2007, vol 43, No7, pp. 1030-1034

reaction at reflux for 2h. On the LC-MS, there was still amine, so we added more isothiocyanate (0.4 mL, 2.0 equiv.) and stirred at room temperature for 2 days. After completion, the reaction mixture diluted in DCM (20 mL) and washed with water, then with brine. The organic phase was separated, dried over MgSO₄ and evaporated under reduced pressure to give an yellow oil. This residue was then purified by column chromatography (column: pre-packed column 25g; eluents: cyclohexane-EtOAc (80-20), flow-rate: 12 mL/min; small tube; collection by time: 0.50 min/tube) to afford one fraction (tube 12 - tube 16) which was evaporated under reduced pressure to give the desired compound **30** (400 mg, quantitative) as light yellow oil.

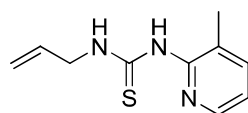
Chemical formula: C₁₀H₁₃N₃S

MW: 207.30 g/mol

HPLC-MS (method in 5 min at pH 3.8): t_R = 3.03 min

MS-(ES+) m/z 208 ([M+H]⁺, base peak)

MS-(ES-) m/z 206 ([M-H]⁻, base peak)



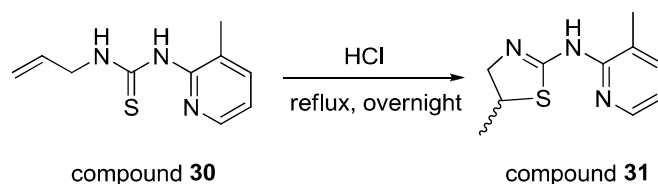
compound **30**

¹H-NMR (300 MHz, CDCl₃, ppm) δ 2.29 (s, 3H, CH₃), 4.41 (tt, *J* = 5.4 Hz and *J* = 1.7 Hz, 2H), 5.19-5.24 (dq, *J* = 10.2 Hz and *J* = 1.5 Hz, 1H), 5.29-5.36 (dq, *J* = 17.0 Hz and *J* = 1.5 Hz, 1H), 5.95-6.08 (doublet of quintet, *J* = 17.0 Hz and *J* = 5.2 Hz, 1H), 6.89-6.93 (dd, *J* = 7.4 Hz and *J* = 5.0 Hz, 1H), 7.49 (d, *J* = 7.4 Hz, 1H), 7.92 (s, 1H, NH), 8.05 (d, *J* = 5.0 Hz, 1H), 12.0 (s, 1H, NH).

¹³C-NMR (75 MHz, CDCl₃, ppm) δ 16.9, 48.2, 116.4, 118.0, 119.1, 133.2, 139.4, 143.5, 151.8, 180.1.

This structure has an PubChem number CID-4102684. But no spectral and physical data has been reported in the literature (in Reaxys and SciFinder Scholar, verified on 21/03/2015).

Step 2: synthesis of (5R/S)-5-methyl-N-(3-methylpyridin-2-yl)-4,5-dihydro-1,3-thiazol-2-amine (compound **31)**



compound **30**

compound **31**

Protocol:³⁴⁰

³⁴⁰ *Russian Journal of Organic Chemistry*, 2007, vol 43, No7, pp. 1030-1034

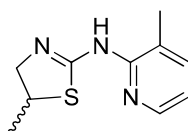
Compound **30** (400 mg, 1.93 mmol) was added to a mixture of concentrated HCl (4.8 mL) and 5 mL water. The mixture was refluxed overnight. After completion, the reaction mixture was neutralized by a solution of NaOH 40% and then extracted by EtOAc (3x 30 mL). The combined organic phase were washed with water (x1), brine (x1), dried over anhydrous MgSO₄ and evaporated under reduced pressure to give pale yellowish solid. This crude residue was then purified by column chromatography (column: pre-packed column 25g; eluents: DCM-MeOH (99-1), flow-rate: 12 mL/min; small tube; collection by time: 0.50 min/tube) to afford the desired compound **31** (156 mg, 39%) as white solid.

Chemical formula: C₁₀H₁₃N₃S

MW: 207.30 g/mol

HPLC-MS (method in 5 min at pH 3.8): t_R = 3.19 min

MS-(ES+) m/z 208 ([M+H]⁺, base peak)



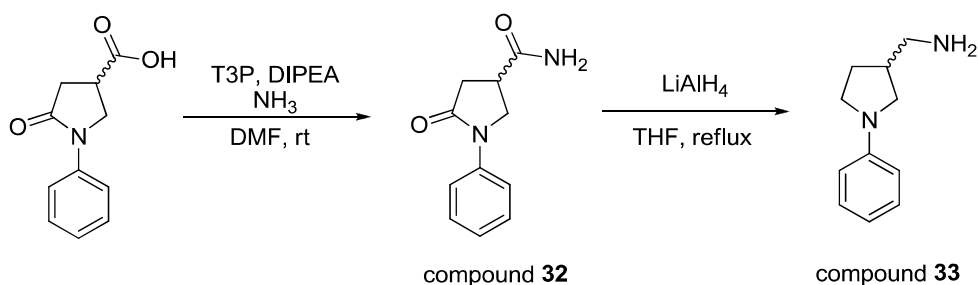
compound **31**

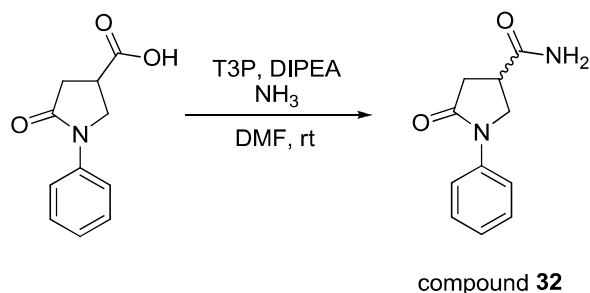
¹H-NMR (300 MHz, DMSO-*d*₆, ppm) δ 1.31 (d, *J* = 6.3 Hz, 3H, CH₃), 2.17 (s, 3H, CH₃), 3.13 (s, 1H), 3.62 (s, 2H), 6.78 (dd, *J* = 7.5 Hz and *J* = 5.1 Hz, 1H, H-pyridine), 7.42 (dd, *J* = 7.5 Hz and *J* = 1.0 Hz, 1H, H-pyridine), 8.00 (br s, 0.5 H, NH), 8.04 (dd, *J* = 5.1 Hz, *J* = 1.3 Hz, 1H, H-pyridine).

¹³C-NMR (75 MHz, DMSO-*d*₆, ppm) δ 18.1, 20.3, 39.9, 50.9, 117.4, 126.3, 138.0, 144.2, 158.9, 164.0 (the peak at 39.9 ppm which has superimposed on the peak of ¹H-DMSO residue was confirmed by HSQC_DEPT spectra)

This is a mixture of two R and S isomers which PubChem number CID-935301 (R isomer) and CID-935302 (S isomer). But no spectroscopic and physical data has been reported in the literature (in Reaxys and SciFinder Scholar, verified on 21/03/2015).

3.1.2.11. Synthesis of fragment hit ID-4003805 (compound **33**)



Step 1: synthesis of (3R/S)-5-oxidanylidene-1-phenyl-pyrrolidine-3-carboxamide (32)**Protocol:**

To a solution of 5-oxo-1-phenylpyrrolidine-3-carboxylic acid (634.69 mg, 3 mmol, 1.0 equiv.) and DIPEA (2.054 mL, 4 eq) in DMF (20 mL), was slowly added solution of T3P in DMF 50% (3.568 mL, 2 eq) and stirred the reaction mixture at room temperature in 15 min. Then solution of ammoniac 25 % (0.227 mL, 1.0 equiv.) was added dropwise to the reaction mixture. The reaction mixture was stirred at room temperature overnight. After completion, the solvent was evaporated under reduced pressure. The residue was dissolved in EtOAc and washed with solution HCl 1N (x2), water (x2), brine (x1), dried over anhydrous MgSO₄ and evaporated under reduced pressure to give a brown solid. This crude residue was purified by column chromatography (column: pre-packed column AIT 25g; eluents: DCM:MeOH (95:5); flow-rate: 12 mL/min; tube 10cm; collection by time: 0.65 min/tube) to give one fraction (tube 45 - tube 74) which was then evaporated under reduced to yield the target compound **32** (326 mg, 53%) as beige solid.

Chemical formula: C₁₁H₁₂N₂O₂

MW: 204.23 g/mol

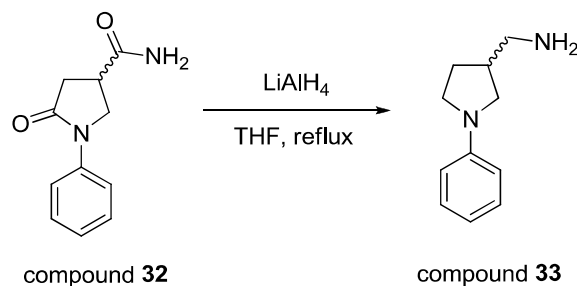
HPLC-MS (method in 5 min at pH 3.8): t_R = 2.23 min

MS-(ES+) m/z 205 ([M+H]⁺, base peak)

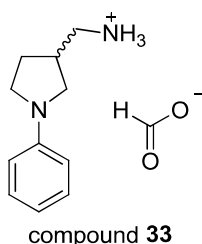
¹H-NMR (300 MHz, DMSO-*d*₆, ppm) δ 2.59-2.76 (m, 2H, CH₂), 3.15-3.25 (m, 1H), 3.84-4.00 (m, 2H, CH₂), 7.10-7.15 (tt, *J* = 7.4 Hz and *J* = 1.1 Hz, 2H, H-Ar), 7.33-7.39 (m, 2H, H-Ar), 7.57 (br s, 2H, NH₂), 7.61-7.65 (m, 1H, H-Ar).

¹³C-NMR (75 MHz, DMSO-*d*₆, ppm) δ 36.0, 36.3, 51.1, 119.9, 124.5, 129.2, 139.7, 172.7, 174.5.

This is a mixture of two R and S isomers which PubChem number CID-7376411 (R isomer) and CID-7376412 (S isomer). But no spectral and physical data has been reported in the literature (in Reaxys and SciFinder Scholar, verified on 21/03/2015).

Step 2: synthesis of [(3R/S)-1-phenylpyrrolidin-3-yl]methanamine (compound 33)**Protocol:**³⁴¹

To a stirred solution of (3R/S)-5-oxidanylidene-1-phenyl-pyrrolidine-3-carboxamide **32** (204.23 mg, 1.0 mmol, 1.0 equiv.) in anhydrous THF (50 mL) at 0°C, a solution LiAlH₄ 1M in THF (8mL, 8.0 equiv.) was added dropwise. The reaction mixture was then warmed to room temperature and refluxed for 23h. After completion, the reaction mixture was then hydrolyzed by water and a solution NaOH 2M under ice cooling. The inorganic precipitate was filtered and washed with THF. The filtrate was evaporated under reduced pressure to give a yellow oil. The crude was then dissolved in HCl 1N solution (pH 1) and washed with Et₂O and EtOAc. The aqueous phase was separated and then lyophilized to give a red gum. Analysis by LC-MS showed that this residue was not pure. So the crude residue was purified by preparative HPLC-MS system at pH 9.2 to afford the desired compound **33** (35 mg, 16%) as light yellow solid.



Chemical formula: C₁₁H₁₇N₂ (free base) + HCOOH

MW: 176.26 g/mol (free base)

HPLC-MS (method in 10 min at pH 9.2): t_R = 4.30 min

MS-(ES+) m/z 177 ([M (free base)+H]⁺, base peak)

¹H-NMR (300 MHz, D₂O, ppm) δ 1.64-1.76 (dq, *J* = 12.5 Hz and *J* = 8.1 Hz, 1H), 2.14-2.24 (dq, *J* = 12.5 Hz and *J* = 8.1 Hz, 1H), 2.50-2.66 (septet, *J* = 7.5 Hz, 1H), 2.92-3.09 (m, 3H), 3.19-3.34 (m, 2H), 3.41 (dd, *J* = 9.7 Hz and *J* = 7.5 Hz, 1H), 6.69-6.73 (d, *J* = 8.8 Hz, 2H, H-Ar) 6.73-6.78 (t, *J* = 7.3 Hz, 1H, H-Ar), 7.22-7.28 (m, 2H, H-Ar), 8.36 (s, 1H, HCOO⁻).

¹H-NMR (300 MHz, DMSO-*d*₆, ppm) δ 1.69-1.81 (m, 1H), 2.09-2.15 (m, 1H), 2.45-2.55 (m, 1H), 2.84 (d, *J* = 6.5 Hz, 2H), 2.98-3.04 (m, 1H), 3.17-3.51 (m, 3H), 6.11 (br s, 2.4H, NH₃⁺),

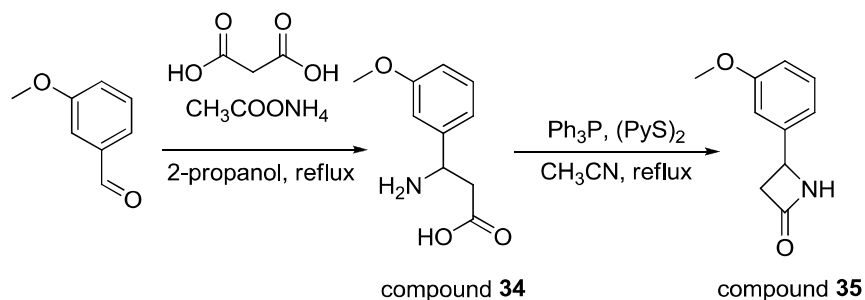
³⁴¹ *J. Med. Chem.*, 1996, Vol.39, No.17, pp. 3307-3318

6.50 (d, $J = 8.0$ Hz, 2H), 6.59 (t, $J = 7.4$ Hz, 1H), 7.15 (t, $J = 7.9$ Hz, 2H), 8.43 (br s, 1H, HCOO⁻).

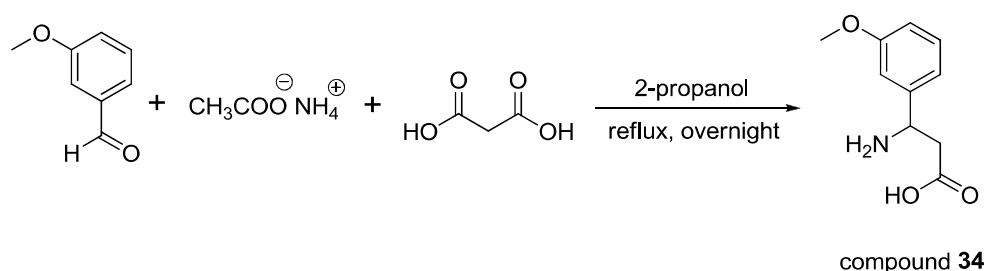
¹³C-NMR (75 MHz, DMSO-*d*₆, ppm) δ 29.1, 37.9, 42.4, 47.1, 51.4, 112.0, 115.7, 129.4, 148.0.

This is a mixture of two R and S isomers which PubChem number CID-42257598 (R isomer) and CID-42257599 (S isomer). But no spectroscopic and physical data has been reported in the literature (in Reaxys and SciFinder Scholar, verified on 21/03/2015).

3.1.2.12. Synthesis of fragment hit ID-4019055



Step 1: synthesis of 3-amino-3-(3-methoxy-phenyl)-propionic acid (compound 34)



Protocol:³⁴²

A solution of 3-methoxy benzaldehyde (3.064 ml, 25 mmol, 1.0 equiv.), ammonium acetate (2.279 g, 1.2 equiv.) and malonic acid (2.978 g, 28.3 mmol, 1.15 equiv.) in 2-propanol (25 mL) were stirred under reflux. After 30 minutes, a precipitate appeared. Analysis by LC-MS showed that there were a peak of desired product and a peak with t_R near to t_R of 3-methoxy benzaldehyde. Ammonium acetate (2.279 g, 1.2 eq) was added and the reaction mixture was continued to stir under reflux overnight. After completion, the reaction mixture was cooled to room temperature and then was filtered, the white solid was washed with 2-propanol, then dried under vacuum to yield the desired compound **34** (2.05 g, 42%) as white solid.

Chemical formula: C₁₀H₁₃NO₃

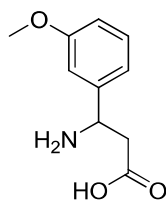
MW: 195.22 g/mol

HPLC-MS (method in 5 min at pH 3.8): $t_R = 2.03$ min

MS-(ES+) m/z 196 ([M+H]⁺, base peak)

³⁴² Patent US 6,291,503 B1 ; column 51 (compound 8a)

MS-(ES-) m/z 194 ($[M-H]^-$, base peak)

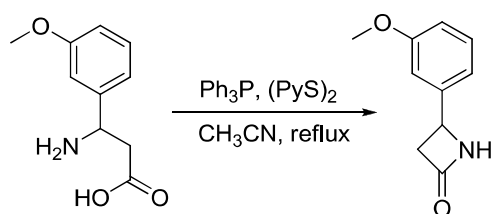


compound **34**

$^1\text{H-NMR}$ (300 MHz, trifluoroacetic acid- d_1 , ppm) δ 3.31 (dd, $J = 4.4$ Hz and $J = 18.5$ Hz, 1H), 3.54 (dd, $J = 9.9$ Hz and $J = 18.5$ Hz, 1H), 4.03 (s, 3H, OCH₃), 5.00 (dd, $J = 4.4$ Hz and $J = 9.9$ Hz, 1H), 7.18-7.22 (m, 3H, H-Ar), 7.51-7.56 (m, 1H, H-Ar).

These spectral characteristics were identical to those previously reported in literature.³⁴²

Step 2: synthesis of 4-(3-methoxy-phenyl)-azetidin-2-one (compound 35)



compound **34**

compound **35**

Protocol:³⁴³

3-Amino-3-(3-methoxy-phenyl)-propionic acid **34** (780.88 mg, 4.0 mmol, 1.0 equiv.) was suspended in acetonitrile (400 mL, 0.01 M solution). Then Ph₃P (1.259 g, 1.2 equiv.) and (PyS)₂ (1.79 g, 1.2 equiv) was added. The white suspension and was stirred at reflux for 4 hours. After completion, the reaction mixture was evaporated under reduced pressure to yield a yellow solid. We then tried to purified this crude product by flash column chromatography (column: pre-packed column 40g; eluents: DCM-Et₂O (80-20), flow-rate: 17 mL/min; tube 22; collection by time: 0.50 min/tube). Unfortunately, we obtained a yellow solid (2g) which is the mixture of the desired product and other impurities (triphenylphosphine oxide and thione). So, this crude product was tried to disperse in Et₂O, the precipitate was filtered and washed with Et₂O. The filtrate was then evaporated under reduced pressure to give a yellow gum (1.6g). The crude residue was then purified by preparative HPLC, diluent (ACN 0.1% HCOOH and H₂O 0.1% HCOOH in gradient to yield the desired compound **35** (392 mg, 55 %) as white solid.

Chemical formula: C₁₀H₁₁NO₂

MW: 177.21 g/mol

HPLC-MS (method in 5 min at pH 3.8): $t_R = 2.49$ min

³⁴³ *J. Am. Chem. Soc.*, Vol. 103, No. 9, 1981, pp 2406-2408

MS-(ES+) m/z 178 ($[M+H]^+$, base peak)

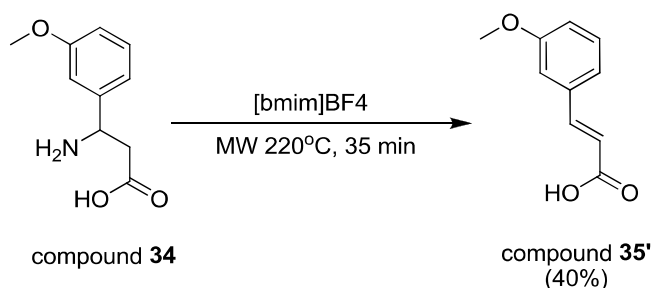
$^1\text{H-NMR}$ (300 MHz, CD_2Cl_2 , ppm) δ 2.81-2.87 (ddd, $J = 14.8$ Hz and $J = 2.6$ Hz and $J = 0.9$ Hz, 1H), 3.38-3.46 (ddd, $J = 14.8$ Hz and $J = 5.4$ Hz and $J = 2.6$ Hz, 1H), 3.83 (s, 3H, OCH_3), 4.70-4.73 (dd, $J = 5.4$ Hz and $J = 2.6$ Hz, 1H, CH-phenyl), 6.24 (br s, 1H, NH), 6.85-6.89 (m, 1H, H-Ar), 6.94-7.00 (m, 2H, H-Ar), 7.28-7.34 (t, $J = 7.8$ Hz, 1H, H-Ar).

$^1\text{H-NMR}$ (300 MHz, CDCl_3 , ppm) δ 2.82-2.88 (ddd, $J = 14.8$ Hz and $J = 2.6$ Hz and $J = 0.9$ Hz, 1H), 3.38-3.46 (ddd, $J = 14.8$ Hz and $J = 5.4$ Hz and $J = 2.6$ Hz, 1H), 3.83 (s, 3H, OCH_3), 4.70-4.73 (dd, $J = 5.4$ Hz and $J = 2.6$ Hz, 1H), 6.24 (br s, 1H, NH), 6.82-6.86 (m, 1H, H-Ar), 6.89-6.95 (m, 2H, H-Ar), 7.28 (t, $J = 7.8$ Hz, 1H, H-Ar).

$^{13}\text{C-NMR}$ (75 MHz, CDCl_3 , ppm) δ 47.9, 50.3, 55.3, 111.1, 113.6, 117.9, 129.9, 142.0, 160.0, 168.3.

The H-NMR spectral was identical to that previously reported in literature.³⁴⁴ But the $^{13}\text{C-NMR}$ spectra has not been published in literature (in Reaxys and SciFinder Scholar, verified on 21/03/2015).

By-product (compound 35') was obtained from an elimination in ionic liquid



Protocol:

Compound **34** (78.09 mg, 0.145 mmol, 1.0 equiv.) and ionic liquid [bmim]BF₄ (74.86 μL , 1 eq) was vortexed in a sealed tube. The reaction was performed under microwave irradiation at 220°C for 35 minutes. After completion, the reaction mixture was diluted with 20 mL of ethyl acetate and washed with saturated aqueous solution of NH_4Cl (x3). The organic phase was then washed with brine, dried over magnesium sulfate and evaporated under reduced pressure to give a crude product as dark brown solid. Purification by column chromatography (column: pre-packed column 12g; eluents: cyclohexan-EtOAc (50-50), flow-rate: 12 mL/min; collection in small tube; time: 0.60 min/tube) afforded compound **35'** (29.7 mg, 40%) as brown solid.

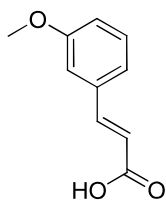
Chemical formula: $\text{C}_{10}\text{H}_{10}\text{O}_3$

MW: 178.06 g/mol

HPLC-MS (method in 5 min at pH 3.8): $t_{\text{R}} = 2.74$ min

MS-(ES-) m/z 177 ($[M-H]^-$, base peak)

³⁴⁴ Wang, Li; Shen, Chun; Xu, Ming-Hua, *Science China Chemistry*, 2011, vol.54, # 1 p.61 - 65



compound **35'**

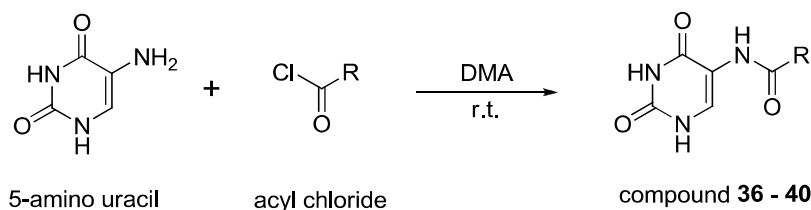
¹H-NMR (300 MHz, DMSO-*d*₆, ppm) δ 3.78 (s, 3H, OCH₃), 6.52-6.57 (d, *J* = 15.9 Hz, 1H, =CH), 6.95-6.99 (m, 1H, H-Ar), 7.22-7.25 (m, 2H, H-Ar), 7.32 (t, *J* = 7.7 Hz, 1H, H-Ar), 7.52-7.58 (d, *J* = 15.9 Hz, 1H, =CH), 12.38 (br s, 1H, COOH).

¹³C-NMR (75 MHz, DMSO-*d*₆, ppm) δ 55.7, 113.4, 116.7, 120.1, 121.2, 130.4, 136.1, 144.3, 160.1, 168.0

These spectral characteristics were identical to those previously reported in literature.³⁴⁵

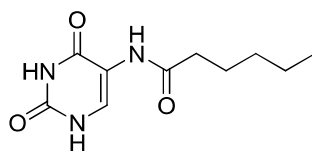
3.1.3. Synthesis of 5-amino uracil analogs

3.1.3.1. General procedure for synthesis of amide analogs from acyl chloride



5-amino uracil (1.0 equiv.) was dispersed in anhydrous *N,N*-dimethylacetamide (1.5 ml). The mixture was then cooled in an ice bath. Then the corresponding acyl chloride (1.0 equiv.) was added dropwise to the mixture. The reaction was stirred for 2 hours. We observed that the mixture was changed from yellow suspension to light yellow solution. After completion, water (5 mL) was added to the reaction mixture and a precipitate was formed. The solid was filtered and washed with a solution HCl 1N and water until pH of the filtrate to 7, dried under vacuum to yield the desired product.

Synthesis of N-(2,4-dioxo-1H-pyrimidin-5-yl)hexanamide (compound 36)



compound **36**

The reaction was conducted at a scale of 1.0 mmol. The desired compound **36** was obtained (190 mg, 84%) as white solid.

Chemical formula: C₁₀H₁₅N₃O₃

MW: 225.24 g/mol

³⁴⁵ Green Chemistry, 2011, vol. 13, # 8, p. 2130 - 2134 (supporting information)

HPLC-MS (method in 5 min at pH 3.8): t_{R} = 1.89 min

MS-(ES+) m/z 226 ($[M+H]^+$, base peak)

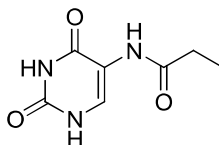
MS-(ES-) m/z 224 ($[M-H]^-$, base peak)

$^1\text{H-NMR}$ (300 MHz, DMSO- d_6 , ppm) δ 0.85 (t, J = 6.9 Hz, 3H, CH₃), 1.20-1.30 (m, 4H, 2 \times CH₂), 1.50 (quint, J = 7.2 Hz, 2H, CH₂), 2.31 (t, J = 7.4 Hz, 2H, CH₂), 8.04 (d, J = 6.0 Hz, 1H, C=CH-uracil), 9.00 (s, 1H, NH), 10.59 (d, J = 4.9 Hz, 1H, NH), 11.39 (s, 1H, NH).

$^{13}\text{C-NMR}$ (75 MHz, DMSO- d_6 , ppm) δ 14.3, 22.3, 25.3, 31.3, 35.8, 113.7 (C=CH, uracil), 129.8 (C=CH, uracil), 150.1 (C=O, uracil), 161.2 (C=O, uracil), 172.3 (C=O, amide).

This new structure has not been reported in literature. No results were found in Reaxys, Pubchem, eMolecules and Scifinder Scholar (verified on 28/03/2015).

Synthesis of *N*-(2,4-dioxo-1H-pyrimidin-5-yl)propanamide (compound 37)



compound 37

The reaction was conducted at a scale of 1.0 mmol. The desired compound 37 was obtained (131 mg, 72%) as white solid.

Chemical formula: C₇H₉N₃O₃

MW: 183.16 g/mol

HPLC-MS (method in 5 min at pH 3.8): t_{R} = 1.20 min

MS-(ES+) m/z 184 ($[M+H]^+$, base peak)

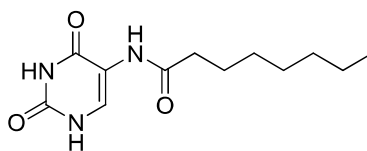
MS-(ES-) m/z 182 ($[M-H]^-$, base peak)

$^1\text{H-NMR}$ (300 MHz, DMSO- d_6 , ppm) δ 1.00 (t, J = 6.9 Hz, 3H, CH₃), 2.34 (q, J = 7.4 Hz, 2H, CH₂), 8.04 (d, J = 6.0 Hz, 1H, C=CH-uracil), 9.00 (s, 1H, NH), 10.59 (d, J = 4.9 Hz, 1H, NH), 11.40 (s, 1H, NH).

$^{13}\text{C-NMR}$ (75 MHz, DMSO- d_6 , ppm) δ 10.1, 29.1, 113.8 (C=CH, uracil), 129.7 (C=CH, uracil), 150.1 (C=O, uracil), 161.2 (C=O, uracil), 172.9 (C=O, amide).

This structure has an PubChem number CID-3572432. But no spectral and physical data has been reported in the literature (Reaxys and SciFinder Scholar, verified on 21/03/2015).

Synthesis of *N*-(2,4-dioxo-1H-pyrimidin-5-yl)octanamide (compound 38)



compound **38**

The reaction was conducted at a scale of 1.0 mmol. The desired compound **38** was obtained (219 mg, 86%) as white solid.

Chemical formula: C₁₂H₁₉N₃O₃

MW: 253.30 g/mol

HPLC-MS (method in 5 min at pH 3.8): t_R = 2.37 min

MS-(ES+) m/z 254 ([M+H]⁺, base peak)

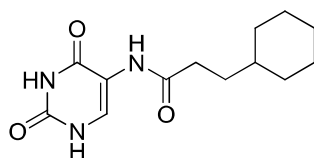
MS-(ES-) m/z 252 ([M-H]⁻, base peak)

¹H-NMR (300 MHz, DMSO-*d*₆, ppm) δ 0.85 (t, *J* = 6.9 Hz, 3H, CH₃), 1.20-1.30 (m, 8H, 4 × CH₂), 1.49 (quint, *J* = 7.2 Hz, 2H, CH₂), 2.31 (t, *J* = 7.5 Hz, 2H, CH₂), 8.04 (d, *J* = 6.2 Hz, 1H, C=CH-uracil), 9.00 (s, 1H, NH), 10.59 (d, *J* = 4.9 Hz, 1H, NH), 11.40 (s, 1H, NH).

¹³C-NMR (75 MHz, DMSO-*d*₆, ppm) δ 14.4, 22.5, 25.6, 28.9, 29.0, 31.6, 35.9, 113.7 (C=CH, uracil), 129.7 (C=CH, uracil), 150.1 (C=O, uracil), 161.2 (C=O, uracil), 172.3 (C=O, amide).

This new structure has not been reported in literature. No results were found in Reaxys, Pubchem, eMolecules and Scifinder Scholar (verified on 28/03/2015).

Synthesis of 3-cyclohexyl-N-(2,4-dioxo-1H-pyrimidin-5-yl)propanamide (compound 39)



compound **39**

The reaction was conducted at a scale of 1.0 mmol. The desired compound **39** was obtained (242 mg, 91%) as white solid.

Chemical formula: C₁₃H₁₉N₃O₃

MW: 265.31 g/mol

HPLC-MS (method in 5 min at pH 3.8): t_R = 2.32 min

MS-(ES+) m/z 266 ([M+H]⁺, base peak)

MS-(ES-) m/z 264 ([M-H]⁻, base peak)

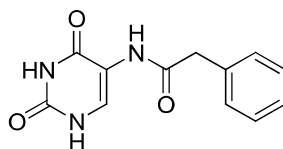
¹H-NMR (300 MHz, DMSO-*d*₆, ppm) δ 0.78-0.89 (m, 2H, H-cyclohexyl), 1.07-1.22 (m, 4H, H-cyclohexyl), 1.39 (q, *J* = 7.3 Hz, 2H, CH₂), 1.55-1.67 (m, 5H, H-cyclohexyl), 2.33 (t, *J* =

7.7 Hz, 2H, CH₂), 8.03 (d, *J* = 6.3 Hz, 1H, C=CH-uracil), 9.01 (s, 1H, NH), 10.58 (d, *J* = 4.5 Hz, 1H, NH), 11.39 (s, 1H, NH).

¹³C-NMR (75 MHz, DMSO-*d*₆, ppm) δ 26.2, 26.6, 33.0, 33.1, 33.5, 37.2, 113.8 (C=CH, uracil), 129.7 (C=CH, uracil), 150.1 (C=O, uracil), 161.2 (C=O, uracil), 172.5 (C=O, amide).

This structure has an PubChem number CID-647264. But no spectral and physical data has been reported in the literature (Reaxys and SciFinder Scholar, verified on 21/03/2015).

Synthesis of *N*-(2,4-dioxo-1H-pyrimidin-5-yl)-2-phenyl-acetamide (compound 40)



compound 40

The reaction was conducted at a scale of 0.5 mmol. The desired compound 40 was obtained (84 mg, 69%) as white solid.

Chemical formula: C₁₂H₁₁N₃O₃

MW: 245.23 g/mol

HPLC-MS (method in 5 min at pH 3.8): t_R = 1.75 min

MS-(ES+) *m/z* 246 ([M+H]⁺, base peak)

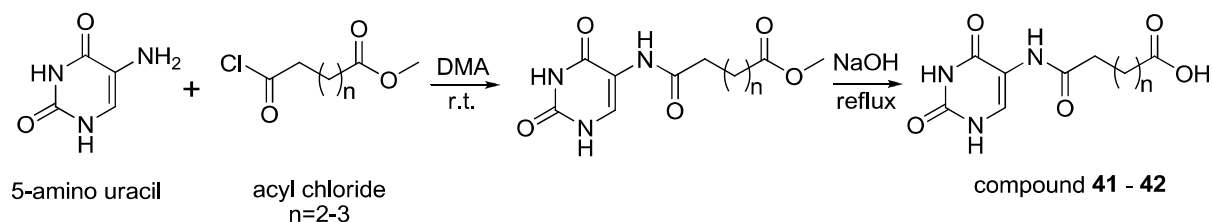
MS-(ES-) *m/z* 244 ([M-H]⁻, base peak)

¹H-NMR (300 MHz, DMSO-*d*₆, ppm) δ 3.69 (s, 2H, CH₂), 7.22-7.30 (m, 5H, H-Ar), 8.06 (d, *J* = 6.1 Hz, 1H, C=CH-uracil), 9.31 (s, 1H, NH), 10.60 (br s, 1H, NH), 11.44 (br s, 1H, NH).

¹³C-NMR (75 MHz, DMSO-*d*₆, ppm) δ 42.7, 113.8 (C=CH, uracil), 126.9 (C-Ar), 128.7 (C-Ar), 129.6 (C=CH, uracil), 136.5 (C-Ar), 150.0 (C=O, uracil), 161.1 (C=O, uracil), 170.1 (C=O, amide).

This structure has been found in literature. But only melting point and UV-Vis spectroscopy were described.³⁴⁶

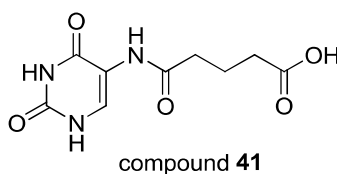
3.1.3.2. General procedure for synthesis of amide analogs from acyl chloride with methyl ester group



³⁴⁶ Du Vigneaud; Melville Chem. Penicillin, <Princeton 1949>, S. 269,298

5-amino uracil (1.0 equiv.) was dispersed in anhydrous *N,N*-dimethylacetamide (1.5 ml). The mixture was then cooled in an ice bath. Then the corresponding acyl chloride (1.0 equiv.) was added dropwise to the mixture. The reaction was stirred for 2 hours. We observed that the mixture was changed from yellow suspension to light yellow solution. After completion, water (5 mL) was added to the reaction mixture and a precipitate was formed. The solid was filtered and washed with a solution HCl 1N and water until pH of the filtrate to 7, dried under vacuum to yield a solid. However, analysis by LC-MS showed that crude solid was a mixture of ester and corresponding carboxylic acid. This crude residue could not be purified by many methods (e.g. organic solvent-aqueous phase dispersion, recrystallization, flash chromatography). Therefore, we decided to saponify this crude with NaOH aqueous solution (2.0 equiv.) in reflux. After completion, the reaction mixture was then acidified by a solution HCl 1N to pH 2. A precipitate was formed. This solid was then filtered, washed with water and dried under vacuum to yield the desired product **41-42**.

Synthesis of 4-[[2,4-bis(oxidanylidene)-1H-pyrimidin-5-yl]amino]-4-oxidanylidene-butanoic acid (compound 41)



The reaction was conducted at a scale of 1.0 mmol. The desired compound **41** was obtained (124 mg, 51% in 2 steps) as off-white solid.

Chemical formula: C₉H₁₁N₃O₅

MW: 241.20 g/mol

HPLC-MS (method in 5 min at pH 3.8): t_R = 1.20 min

MS-(ES+) m/z 242 ([M+H]⁺, 20%) ; 224 (25%) ; 128 (base peak)

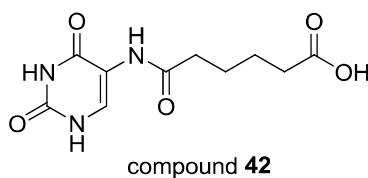
MS-(ES-) m/z 240 ([M-H]⁻, base peak) ; 126 (65%)

¹H-NMR (300 MHz, DMSO-*d*₆, ppm) δ 1.72 (quint, *J* = 7.5 Hz, 2H, CH₂), 2.21 (t, *J* = 7.4 Hz, 2H, CH₂), 2.35 (t, *J* = 7.4 Hz, 2H, CH₂), 8.01 (d, *J* = 6.1 Hz, 1H, C=CH-uracil), 9.05 (s, 1H, NH), 10.60 (d, *J* = 6.0, 1H, NH), 11.39 (br s, 1H, NH), 12.03 (s, 1H, COOH).

¹³C-NMR (75 MHz, DMSO-*d*₆, ppm) δ 21.0, 33.4, 35.0, 113.6 (C=CH, uracil), 130.2 (C=CH, uracil), 150.1 (C=O, uracil), 161.2 (C=O, uracil), 170.7 (C=O, amide), 174.6 (COOH).

This new structure has not been reported in literature. No results were found in Reaxys, Pubchem, eMolecules and Scifinder Scholar (verified on 15/04/2015).

Synthesis of 6-[(2,4-dioxo-1H-pyrimidin-5-yl)amino]-6-oxo-hexanoic acid (compound 42)



The reaction was conducted at a scale of 1.0 mmol. The desired compound **42** was obtained (136 mg, 53% in 2 steps) as light yellow solid.

Chemical formula: C₁₀H₁₃N₃O₅

MW: 255.23 g/mol

HPLC-MS (method in 5 min at pH 3.8): t_R = 1.28 min

MS-(ES+) *m/z* 256 ([M+H]⁺, 40%) ; 238 (35%) ; 128 (base peak)

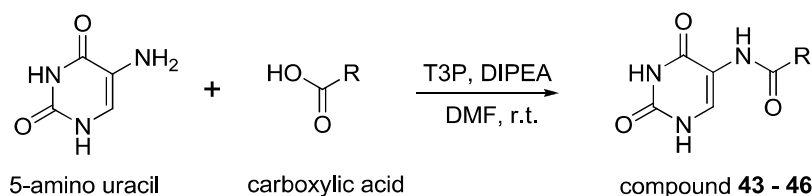
MS-(ES-) *m/z* 254 ([M-H]⁻, base peak) ; 126 (15%)

¹H-NMR (300 MHz, DMSO-*d*₆, ppm) δ 1.45-1.53 (m, 4H, 2×CH₂), 2.20 (t, *J* = 6.8 Hz, 2H, CH₂), 2.33 (t, *J* = 6.8 Hz, 2H, CH₂), 8.04 (d, *J* = 5.7 Hz, 1H, C=CH-uracil), 9.04 (s, 1H, NH), 10.60 (d, *J* = 5.7 Hz, 1H, NH), 11.40 (br s, 1H, NH), 11.98 (s, 1H, COOH).

¹³C-NMR (75 MHz, DMSO-*d*₆, ppm) δ 24.5, 25.2, 33.8, 35.5, 113.7 (C=CH, uracil), 129.8 (C=CH, uracil), 150.1 (C=O, uracil), 161.2 (C=O, uracil), 172.1 (C=O, amide), 174.9 (COOH).

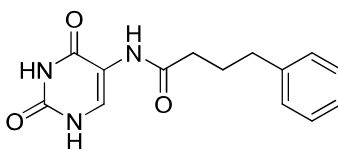
This new structure has not been reported in literature. No results were found in Reaxys, Pubchem, eMolecules and Scifinder Scholar (verified on 15/04/2015).

3.1.3.3. General procedure for amide synthesis from carboxylic acid (compound 43-46)



To a solution of the corresponding carboxylic acid (1.0 mmol, 1.0 equiv.) and DIPEA (0.68 ml, 4 mmol, 4 equiv.) in *N,N*-Dimethylformamide (2 ml), was added dropwise a solution of T3P in DMF 50% (0.876 ml, 1.5 mmol, 1.5 equiv). The mixture (as orange solution) was stirred at room temperature in 15 min. Then 5-aminouracil (129.70 mg, 1.0 mmol, 1.0 equiv.) was added in portion. The reaction mixture became a orange suspension. (because 5-amino uracil is not soluble in DMF). The reaction mixture was stirred at room temperature overnight (15-16 hours) and then converted to a red solution. After completion, purification of the reaction mixture by a suitable technique to yield the desired compound.

Synthesis of *N*-(2,4-dioxo-1*H*-pyrimidin-5-yl)-4-phenyl-butanamide (compound 43)



compound **43**

After completion, the reaction mixture was quenched in water 30 mL. A precipitate was formed. The solid was filtered, washed with solution HCl 1N, water and dried under vacuum to yield the desired compound **43** (171mg, 63%) as pale yellow solid.

Chemical formula: C₁₄H₁₅N₃O₃

MW: 273.29 g/mol

HPLC-MS (method in 5 min at pH 3.8): t_R = 2.09 min

MS-(ES+) m/z 274 ([M+H]⁺, base peak)

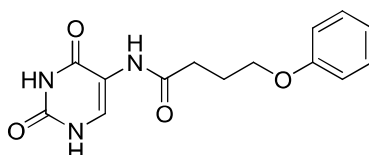
MS-(ES-) m/z 272 ([M-H]⁻, base peak)

¹H-NMR (300 MHz, DMSO-*d*₆, ppm) δ 1.80 (quint, *J* = 7.6 Hz, 2H, CH₂), 2.35 (t, *J* = 7.4 Hz, 2H, CH₂), 2.56 (t, *J* = 7.6 Hz, 2H, CH₂), 7.16-7.29 (m, 5H, H-Ar), 8.02 (s, 1H), 9.05 (s, 1H), 10.60 (br s, 1H), 11.39 (br s, 1H).

¹³C-NMR (75 MHz, DMSO-*d*₆, ppm) δ 27.5, 35.1, 35.5, 113.7(C=CH, uracil), 126.2(C-Ar), 128.7(C-Ar), 128.8 (C-Ar), 130.1 (C=CH, uracil), 142.2 (C-Ar), 150.1 (C=O, uracil), 161.2 (C=O, uracil), 172.0 (C=O, amide).

This structure has an PubChem number CID-6472724. But no spectral and physical data has been reported in the literature (Reaxys and SciFinder Scholar, verified on 28/03/2015).

Synthesis of *N*-(2,4-dioxo-1*H*-pyrimidin-5-yl)-4-phenoxybutanamide (compound **44)**



compound **44**

After completion, the reaction mixture was quenched in water 30 mL. A precipitate was formed. The solid was filtered, washed with solution HCl 1N, water and dried under vacuum to yield the desired compound **44** (205 mg, 71%) as beige solid.

Chemical formula: C₁₄H₁₅N₃O₄

MW: 289.29 g/mol

HPLC-MS (method in 5 min at pH 3.8): t_R = 2.05 min

MS-(ES+) m/z 290 ([M+H]⁺, base peak)

MS-(ES-) m/z 288 ([M-H]⁻, base peak)

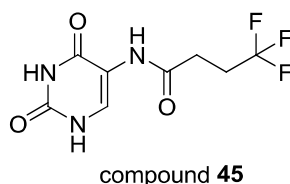
¹H-NMR (300 MHz, DMSO-*d*₆, ppm) δ 1.95 (quint, $J = 6.7$ Hz, 2H, CH₂), 2.50 (m, 2H, CH₂), 3.95 (t, $J = 6.0$ Hz, 2H, CH₂), 6.89-6.91 (m, 3H, H-Ar), 7.26 (t, $J = 7.5$ Hz, 2H, H-Ar), 8.05 (s, 1H), 9.12 (s, 1H), 10.62 (br s, 1H), 11.41 (br s, 1H).

¹³C-NMR (75 MHz, DMSO-*d*₆, ppm) δ 25.2, 32.4, 67.1, 113.7 (C=CH, uracil), 114.9 (C-Ar), 120.9 (C-Ar), 129.9 (C=CH, uracil), 130.2 (C-Ar), 150.1 (C=O, uracil), 159.0 (C-Ar), 161.2 (C=O, uracil), 171.7 (C=O, amide).

COSY spectra was also measured to confirm a CH₂ at position of ¹H-DMSO residue solvent (2.5 ppm) in ¹H-NMR.

This new structure has not been reported in literature. No results were found in Reaxys, Pubchem, eMolecules and Scifinder Scholar (verified on 28/03/2015).

Synthesis of N-(2,4-dioxo-1H-pyrimidin-5-yl)-4,4,4-trifluoro-butanamide (compound 45)



After completion, the reaction mixture was quenched in water 20 mL. The aqueous phase was then extracted by EtOAc (x3). The combined organic phase were then washed with solution of HCl 1N, water, brine and dried over anhydrous MgSO₄. The organic phase was dried under reduced pressure to give a yellow solid. Purification by flash chromatography (diluant DCM-MeOH 100%-0 then 90%-10% in 30 min) to yield the desired compound **45** (119 mg, 47%) as pale yellow solid

Chemical formula: C₈H₈F₃N₃O₃

MW: 251.16 g/mol

HPLC-MS (method in 5 min at pH 3.8): $t_R = 1.60$ min

MS-(ES+) m/z 252 ([M+H]⁺, 70%) ; 158 (base peak)

MS-(ES-) m/z 250 ([M-H]⁻, base peak)

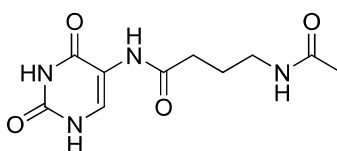
¹H-NMR (300 MHz, DMSO-*d*₆, ppm) δ 2.42-2.58 (m, 2H, CH₂), 2.62-2.67 (m, 2H, CH₂), 8.04 (s, 1H), 9.36 (s, 1H), 10.63 (s, 1H), 11.44 (s, 1H).

¹³C-NMR (75 MHz, DMSO-*d*₆, ppm) δ 28.3 (q, $^3J_{CF} = 3.3$ Hz), 28.8 (q, $^2J_{CF} = 28.6$ Hz), 113.6 (C=CH, uracil), 128.1 (q, $^1J_{CF} = 276.8$ Hz), 130.0 (C=CH, uracil), 149.9 (C=O, uracil), 161.0 (C=O, uracil), 169.3 (C=O, amide).

⁹F-NMR (75 MHz, DMSO-*d*₆, ppm): δ -65.60.

This new structure has not been reported in literature. No results were found in Reaxys, Pubchem, eMolecules and Scifinder Scholar (verified on 28/03/2015).

Synthesis of 4-acetamido-N-(2,4-dioxo-1H-pyrimidin-5-yl)butanamide (compound 46)



compound **46**

After completion, the reaction mixture was quenched in water 20 mL. When acidification by solution HCl 1N, a precipitate was formed. The solid was filtered, washed with water and dried under vacuum to yield the desired compound **46** (85 mg, 33%) as beige solid.

Chemical formula: C₁₀H₁₄N₄O₄

MW: 254.24 g/mol

HPLC-MS (method in 5 min at pH 3.8): t_R = 1.18 min

MS-(ES+) m/z 255 ([M+H]⁺, 32%), 128 (base peak)

MS-(ES-) m/z 253 ([M-H]⁻, base peak), 126 (10%)

¹H-NMR (300 MHz, DMSO-*d*₆, ppm) δ 1.61 (quint, *J* = 7.2 Hz, 2H, CH₂), 2.32 (t, *J* = 7.2 Hz, 2H, CH₂), 3.00 (q, *J* = 6.8 Hz, 2H, CH₂), 7.80 (t, *J* = 5.7 Hz, 1H), 8.02 (d, *J* = 6.0 Hz, 1H), 9.00 (s, 1H), 10.60 (d, *J* = 5.0 Hz, 1H), 11.40 (s, 1H).

¹³C-NMR (75 MHz, DMSO-*d*₆, ppm) δ 23.1, 25.8, 33.5, 38.5, 113.7 (C=CH, uracil), 130.0 (C=CH, uracil), 150.1 (C=O, uracil), 161.2 (C=O, uracil), 169.5 (C=O, amide), 171.9 (C=O, amide).

This new structure has not been reported in literature. No results were found in Reaxys, Pubchem, eMolecules and Scifinder Scholar (verified on 28/03/2015).

3.2. Biochemical assays

Purification of MabA protein: MabA protein was overproduced in a recombinant *E. coli* C41 (DE3). This strain was transformed with the *mabA* (fabG1, Rv1483) gene of *M. tuberculosis* H37Rv full length in addition with 6xHis in N-terminal. Purification of protein was conducted by FPLC (Column Ni-NTA + gel filtration).

3.2.1. Screening by Thermal Shift Assay (TSA)

The fluorescent dye SYPRO Orange (NanoOrange[®], Invitrogen) was used to monitor protein unfolding. The thermal shift assay was conducted in a LightCycler 480 (Roche). The system contained a heating/cooling device for temperature control and a charge-coupled device (CCD) detector for real-time imaging of the fluorescence changes in the wells of the microplate.

The final sample concentrations were 12 μM (0.33 mg/mL) for MabA enzyme, 3× NanoOrange, 1 % DMSO, and 1 mM fragment in the HEPES buffer (100 mM HEPES, 150 mM NaCl, pH 5). NADPH (3.33 mM) with 1% DMSO was used as positive control and

HEPES buffer was used as negative control. The samples were heated from 37 to 85 °C with a heating rate of 0.04 °C/s. The fluorescence intensity was measured at Ex/Em: 465/510 nm.

The data were obtained using the LightCycler 480 Protein Melting algorithmic program by applying the following designed procedure: the fluorescence intensity of each well/sample is plotted as a function of the temperature. Then, the 1D-numerical derivative of these curves is calculated. Finally, the maximum data values, corresponding to the inflection points (T_m), is extracted to give T_m in a table and in a graph.

3.2.2. Screening on macrophage

Raw264.7 macrophages (10^8 cells) were infected with *M. tuberculosis* H37Rv-GFP suspension at a MOI of 1:1 in 300mL for 2 h at 37 °C with shaking (100 rpm). After two washes by centrifugation at 1100 rpm for 5 min, the remaining extracellular bacilli from the infected cells suspension were killed by treatment with amikacin (20 μ M, Sigma, A2324-5G) in 1 hour. After a final centrifugation step, 40 μ L of *M. tuberculosis* H37Rv-GFP colonized macrophages were dispensed with the Wellmate (Matrix) into 384-well Evotec plates preplated with fragment solution diluted in cell medium at concentration of 1mM and incubated for 5 days at 37 °C, 5% CO₂. Macrophages were then stained with SYTO 60 (Invitrogen, S11342) for 1 h followed by plate sealing. Confocal images were recorded on an automated fluorescent ultrahigh-throughput microscope Opera (Evotec). This microscope is based on an inverted microscope architecture that allows imaging of cells cultivated in 96- or 384-well microplates (Evotec). Images were acquired with a 20 \times water immersion objective (NA 0.70). Double laser excitation (488 and 635 nm) and dedicated dichroic mirrors were used to record green fluorescence of mycobacteria and red fluorescence of the macrophages on two different cameras, respectively. A series of four pictures at the center of each well were taken, and each image was then processed using dedicated image analysis. The percent of infected cells and the number of cells are the two parameters extracted from images analysis as previously reported.³⁴⁷ Data of two replicates are average.

3.2.3. Screening by enzymatic assay

The final sample concentrations were 400 nM for MabA enzyme, 1 mM fragment in the HEPES buffer (100 mM HEPES, 150 mM NaCl, pH 7), with 1% DMSO, 50 μ M NADPH. Aceto-acetyl-CoA was used as substrate at concentration 50 μ M. HEPES buffer was used as negative control. Positive control is the mixture without MabA enzyme. Assay was conducted on a 384 wells plate. Quantification of hydroxy-butyryl-CoA product was carried out by LC-MS/MS. Result were presented as percentage of inhibition which was calculated by the following formula:

³⁴⁷ *Future Med. Chem.* 2010, 2, 1283–1293 and *Curr. Opin. Chem. Biol.* 2011, 15, 534–539

$$\% \text{ inhibition} = 100 - \left[\frac{(AUC_{\text{test}} - AUC_{\text{negative}}) \times 100}{AUC_{\text{positive}} - AUC_{\text{negative}}} \right]$$

AUC_{test} : AUC of hydroxybutyryl CoA in case of test compound

AUC_{negative} : AUC of hydroxybutyryl CoA in control sans MabA (AUCminimum)

AUC_{positive} : AUC of hydroxybutyryl CoA in control sans inhibitor (AUCmaximum)

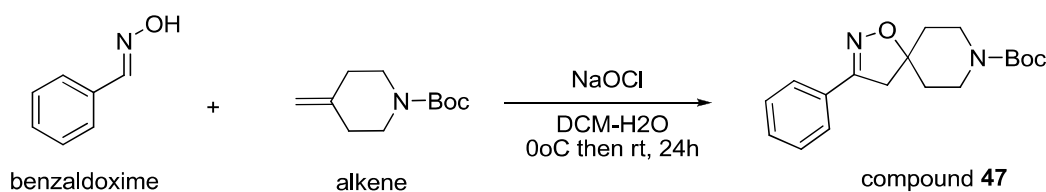
4. Chapter IV: Synthesis of isoxazoline 3-D fragments

4.1. Synthesis of isoxazoline by 1,3-dipolar cycloaddition

4.1.1. Optimisation of synthetic conditions of 1,3-dipolar cycloaddition

4.1.1.1. Synthesis of 3-phenyl-8-*N*-Boc-1-oxa-2,8-diaza-spiro[4.5]dec-2-en (47)

NaOCl as reagent (method 1)³⁴⁸



To a solution of benzaldoxime (4.12 mmol, 1 equiv.) and *N*-Boc-4-methylene piperidine (2.89 mmol, 0.7 equiv) in DCM (13mL) at 0°C, a solution of NaOCl 13% (1.6N) active chlorine (13.75 mL, 7.3 equiv.) was added dropwise. The mixture color changed from yellow to green. After 2h30, LC-MS and TLC analysis showed that the reaction have not completed. So the mixture was vigorously stirred at room temperature for 24 hours. After completion, the reaction mixture was separated. The aqueous phase was extracted by dichloromethane (10mL x 1). The combined organic phase were washed with HCl 1N solution (20 mL x1), brine (20 mL x1) and dried over anhydrous MgSO₄. The solvent was evaporated under reduced pressure to yield a white solid. This crude product was then recrystallized in EtOH to give compound 47 (291 mg, 32%) as white crystals. M.p.: 135.8-137.5 °C.

Chemical formula: C₁₈H₂₄N₂O₃

MW: 316.40 g/mol

HPLC-MS (method in 5 min at pH 3.8): t_R= 3.44 min

MS-(ES⁺): *m/z* 317 ([M+H]⁺, 30%), 261 ([M-tBu+H]⁺, base peak).

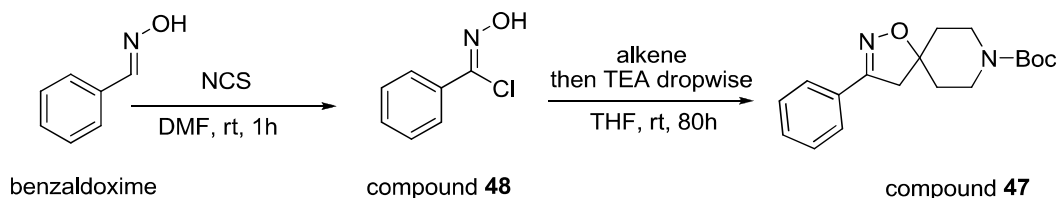
¹H-NMR (300 MHz, CD₂Cl₂, ppm) δ 1.49 (s, 9H, 3 x CH₃ of Boc), 1.70-1.94 (m, 4H, H-piperidine), 3.14 (s, 2H, 2H-isoxazoline), 3.43-3.74 (m, 4H, H-piperidine), 7.42-7.47 (m, 3H, H-Ar), 7.71-7.72 (m, 2H, H-Ar).

³⁴⁸ Milinkevich, K. A.; Ye, L.; Kurth, M. J. *J. Comb. Chem.* **2008**, *10*, 521–5.

$^{13}\text{C-NMR}$ (75 MHz, CD_2Cl_2 , ppm) δ 28.1, 35.8, 41.0, 45.1 (CH_2 -isoxazoline), 79.3, 84.5 (C-O-isoxazoline), 126.4, 128.6, 129.9, 130.1, 154.4, 156.2 (C=N-isoxazoline).

This compound was described in literature Patent WO2006/122770 (c73) but no spectroscopic and physical data was published.

NCS and TEA as reagents (method 2)



Synthesis of hydroxyiminoyl chloride (compound 48)³⁴⁹

To a solution of benzaldoxime (4.05 mmol, 1.0 equiv.) in DMF (8mL), NCS (551 mg, 1.0 equiv) was added in portion. After 10 minutes, the mixture color changed from bright yellow to yellow. The reaction mixture was stirred for 1 hour, color changed from yellow to colorless. After completion, the reaction mixture was quenched in the mixture of dichloromethane and water. The organic phase was decanted and the aqueous phase was extracted by dichloromethane (20 mLx1). The combined organic phases were washed with brine, dried over anhydrous MgSO_4 and evaporated under reduced pressure to yield compound 48 (630 mg, quantitative) as yellow liquid.

HPLC-MS (method in 5 min at pH 3.8, detected by PDA): $t_{\text{R}} = 2.70$ min

$^1\text{H-NMR}$ (300 MHz, CDCl_3 , ppm) δ 7.35-7.50 (m, 3H, H-Ar), 7.85 (dd, $J = 8.0$ Hz and $J = 1.6$ Hz, 2H, H-Ar), 8.43 (s, 1H, OH).

This spectral characteristic was identical to those previously reported.³⁵⁰

Synthesis of isoxazoline (compound 47) by 1,3-dipolar cycloaddition³⁵¹

To a 250 mL round bottom flask, (*E*)-*N*-hydroxybenzene-1-carbonimidoyl chloride 48 (311 mg, 2 mmol) and *N*-Boc-4-methylidene piperidine (0.395 mL, 1.0 equiv.) was dissolved in anhydrous THF (60 mL). The mixture was stirred in 15 minutes then the solution of TEA (0.56 mL) in THF (70 mL) was slowly added over 2 hours. A white precipitate was formed. The resulting reaction mixture was stirred at room temperature. The reaction completed after 80 hours. The mixture was filtered to eliminate the white solid. The filtrate was then evaporated under reduced pressure to give a white solid. This solid was then dissolved in dichloromethane (30 mL); the organic phase was washed with HCl 1N solution (30 mLx1) and brine (30 mLx1) and was then dried over anhydrous MgSO_4 and concentrated under reduced pressure to yield a white solid. The crude product was recrystallized in EtOH to yield 47 (295 mg, 47%) as white crystals.

³⁴⁹ Dondoni, A.; Fantin, G.; Fogagnolo, M.; Medici, A.; Pedrini, P. *Synthesis (Stuttg)*. **1987**, *1987*, 998–1001.

³⁵⁰ Vo, Quan V. et al. *Bioorganic and Medicinal Chemistry*, **2013**, vol. 21, # 19 p.5945 - 5954

³⁵¹ Iwakura, Y.; Uno, K.; Shiraiishi, S.; Hongu, T. *Bull. Chem. Soc. Jpn.* **1968**, *41*, 2954–2959.

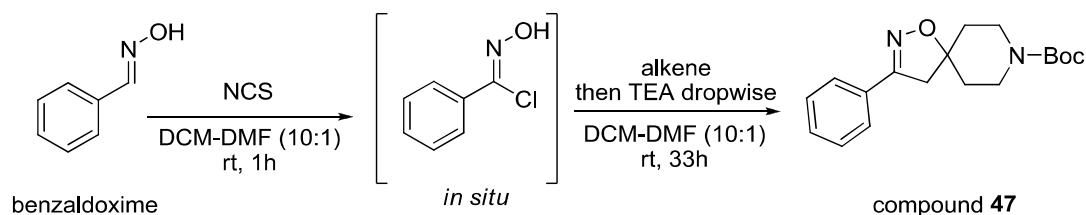
HPLC-MS (method in 5 min at pH 3.8): $t_R = 3.43$ min

MS-(ES+): m/z 317 ($[M+H]^+$, 30%); 261 ($[M-tBu+H]^+$, base peak).

$^1\text{H-NMR}$ (300 MHz, CD_2Cl_2 , ppm) δ 1.48 (s, 9H, CH_3 of Boc), 1.65-1.93 (m, 4H, H-piperidine), 3.13 (s, 2H, H-isoxazoline), 3.42-3.72 (m, 4H, H-piperidine), 7.42-7.45 (m, 3H, H-Ar), 7.66-7.67 (m, 2H, H-Ar).

The spectral data was consistent with a previous report of compound **47** in method 1.

One-pot synthesis of 2-isoxazoline (method 3)³⁵²



To a 100 mL round bottom flask, (*E*)-*N*-(phenylmethylidene) hydroxylamine (0.45 mL, 4.0 mmol), DCM (30 mL) and DMF (3 mL) were added. NCS (1.1 equiv.) was added in portions to the stirred mixture at room temperature. The progress of the chlorination was completed after 1 hour (monitored by LC-MS and TLC). Boc-4-methylidene piperidine (0.798 mL, 1.0 equiv.) was then added to the mixture followed by the slow addition of TEA solution (3.0 equiv. in 30 mL DCM) over 2 hours. The resulting reaction mixture was stirred at room temperature in 33 hours. After completion, the mixture was quenched in water. The organic phase was washed sequentially with HCl 1N, water, brine and was then dried over anhydrous MgSO_4 . Concentration under reduced pressure afforded a white solid. The crude product was purified by recrystallization in EtOH to yield compound **47** (622 mg, 49%) as white crystals.

HPLC-MS (method in 5 min at pH 3.8): $t_R = 3.43$ min

MS-(ES+): m/z 317 ($[M+H]^+$, 30%), 261 ($[M-tBu+H]^+$, 100%)

$^1\text{H-NMR}$ (300 MHz, CD_2Cl_2 , ppm) δ 1.45 (s, 9H, CH_3 of Boc), 1.68-1.90 (m, 4H, H-piperidine), 3.10 (s, 2H, H-isoxazoline), 3.39-3.70 (m, 4H, H-piperidine), 7.40-7.42 (m, 3H, H-Ar), 7.63-7.64 (m, 2H, H-Ar).

The spectral data of this compound was consistent with a previous data in method 1 and 2. This synthetic procedure was then applied in a larger scale (24 mmol) and afforded compound **47** (4.5 g, 60%) as white crystals.

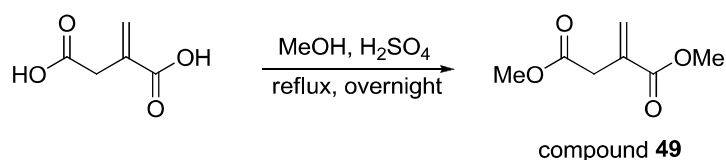
4.1.2. Synthesis of isoxazoline from benzaldoxime and alkenes

Preparation of dimethyl itaconate ester (compound **49**)³⁵³

³⁵² Patent WO 2011/146324 A1 (page 64)

³⁵³ Enoki, M.; Honda, Y.; Kuwahara, M.; Watanabe, T. *Chem. Phys. Lipids*, **2002**, 120, 9–20.

Experimental section



Dimethyl itaconate was prepared by refluxing 80 mL of MeOH containing 26.02 g (0.2 mol, 1.0 equiv.) of itaconic acid and 5.885 g (3.533 mL, ratio 0.331) of sulfuric acid overnight. After the reaction, the mixture was cooled to room temperature, concentrated under reduced pressure and then was dispersed in a solution saturated of sodium carbonate at pH 12. Dimethyl itaconate ester was extracted by ethyl acetate (x3). The organic phase was washed with water (50 mLx1) and brine (50 mLx1), and was then dried over anhydrous MgSO₄, filtered and concentrated in vacuum to yield the product dimethyl itaconate **49** (22.7g, 72%) as yellow liquid.

Chemical formula: C₇H₁₀O₄

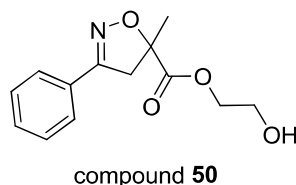
MW: 158.16 g/mol

HPLC (method in 5 min at pH 3.8, detected by PDA): t_R= 2.29 min

¹H-NMR (300 MHz, CDCl₃, ppm) δ 3.33 (s, 2H, CH₂), 3.68 (s, 3H, CH₃), 3.75 (s, 3H, CH₃), 5.71 (d, *J* = 1.2 Hz, 1H, H of =CH₂), 6.31 (s, 1H, H of =CH₂).

These spectral characteristics were identical to those previously reported.³⁵³

The following isoxazoline were synthesized by method 3 described in section 4.1.1



5-Methyl-3-phenyl-4,5-dihydro-isoxazole-5-carboxylic acid 2-hydroxy-ethyl ester (**50**): The reaction was conducted at a scale of 2.0 mmol according to method 3 (section 4.1.1). Reaction completed after 16 hours. The final product **50** was obtained (463mg, 93%) as pale yellow liquid.

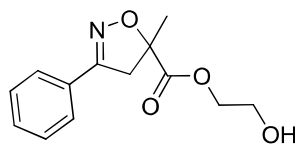
Chemical formula: C₁₃H₁₅NO₄

MW: 249.27 g/mol

HPLC-MS (method in 5 min at pH 3.8): t_R= 2.69 min

MS-(ES⁺) *m/z* 250 ([M+H]⁺, base peak).

IR (cm⁻¹): 3413 (band, O-H stretch), 1733 (C=O stretch), 1181 (C-O stretch), 1074 (C-O stretch).



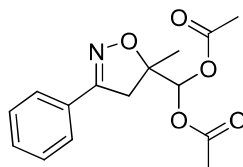
compound **50**

¹H-NMR (300 MHz, CDCl₃, ppm) δ 1.75 (s, 3H, CH₃), 2.09 (s, 1H, OH), 3.24 (d, J = 17.0 Hz, 1H, H-isoxazoline), 3.88 (t, J = 4.7 Hz, 2H, CH₂), 3.93 (d, J = 17.0 Hz, 1H, H-isoxazoline), 4.33 (t, J = 4.7 Hz, 2H, CH₂), 7.41-7.44 (m, 3H, H-Ar), 7.64-7.68 (m, 2H, H-Ar).

¹³C-NMR (75 MHz, CDCl₃, ppm) δ 23.7, 44.8 (CH₂-isoxazoline), 60.6, 67.5, 86.3 (C-O-isoxazoline), 126.8, 128.8, 128.9, 130.5, 156.6 (C=N-isoxazoline), 172.4.

HRMS (TOF, ES⁺) m/z [M+H]⁺ calculated for C₁₃H₁₆NO₄ 250.1079, found 250.1099.

This new structure has not been reported in literature. No results were found in Reaxys, Pubchem, eMolecules and Scifinder Scholar (verified on 28/03/2015).



compound **51**

Acetic acid acetoxy-(5-methyl-3-phenyl-4,5-dihydro-isoxazol-5-yl)-methyl ester (**51**): The reaction was conducted at a scale of 2.0 mmol according to method 3 (section 4.1.1). Reaction completed after 39 hours. The crude residue was purified by flash chromatography [silica gel pre-packed column AIT 25g; eluents: cyclohexane-EtOAc (9-1); flow-rate: 13 mL/min; tube 10cm; collection by time: 0.65 min/tube] to afford the pure compound **51** (203 mg, 35%) as colorless liquid.

Chemical formula: C₁₅H₁₇NO₅

MW: 291.31 g/mol

HPLC-MS (method in 5 min at pH 3.8): t_R = 3.06 min

MS-(ES⁺): m/z 292 ([M+H]⁺, 18%), 190 (base peak).

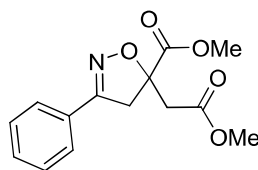
IR (cm⁻¹): 1761 (C=O stretch), 1231 (C-O stretch), 1193 (C-O stretch), 1007 (C-O stretch).

¹H-NMR (300 MHz, CDCl₃, ppm) δ 1.55 (s, 3H, CH₃), 2.07 (s, 3H, CH₃), 2.12 (s, 3H, CH₃), 3.08 (d, J = 17.0 Hz, 1H, H-isoxazoline), 3.56 (d, J = 17.0 Hz, 1H, H-isoxazoline), 6.93 (s, 1H, CH), 7.39-7.43 (m, 3H, H-Ar), 7.64-7.68 (m, 2H, H-Ar).

¹³C-NMR (75 MHz, CDCl₃, ppm) δ 20.7, 21.4, 42.1 (CH₂-isoxazoline), 86.0 (C-O-isoxazoline), 89.0, 126.6, 128.8, 129.3, 130.3, 156.3 (C=N-isoxazoline), 168.6.

HRMS (TOF, ES⁺) m/z [M+H]⁺ calculated for C₁₅H₁₈NO₅ 292.1185, found 292.1158.

This new structure has not been reported in literature. No results were found in Reaxys, Pubchem, eMolecules and Scifinder Scholar (verified on 28/03/2015).



compound **52**

5-Methoxycarbonylmethyl-3-phenyl-4,5-dihydro-isoxazole-5-carboxylic acid methyl ester (52). The reaction was conducted at a scale of 2.0 mmol according to method 3 (section 4.1.1). Reaction completed after 16 hours. The compound **52** was obtained (489 mg, 88%) as a light yellow solid. M.p.: 60-62°C [lit. 63-64°C]³⁵⁴

Chemical formula: C₁₄H₁₅NO₅

MW: 277.28 g/mol

HPLC-MS (method in 5 min at pH 3.8): t_R = 2.95 min

MS-(ES+): m/z 278 ([M+H]⁺, 85%), 260 (base peak), 218 (32%).

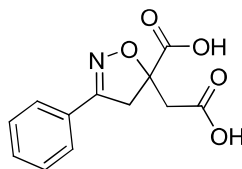
IR (cm⁻¹): 1735 (C=O stretch), 1732 (C=O stretch), 1255 (C-O stretch), 1200 (C-O stretch), 1008 (C-O).

¹H-NMR (300 MHz, CDCl₃, ppm) δ 3.00 (d, *J* = 16.5 Hz, 1H, H of CH₂), 3.28 (d, *J* = 16.5 Hz, 1H, H of CH₂), 3.52 (d, *J* = 17.3 Hz, 1H, H-isoxazoline), 3.72 (s, 3H, OCH₃), 3.83 (s, 3H, OCH₃), 4.04 (d, *J* = 17.3 Hz, 1H, H-isoxazoline), 7.41-7.44 (m, 3H, H-Ar), 7.66-7.70 (m, 2H, H-Ar).

¹³C-NMR (75 MHz, CDCl₃, ppm) δ 40.8, 43.7 (CH₂-isoxazoline), 52.1, 53.3, 85.7 (C-O-isoxazoline), 126.9, 128.6, 128.8, 130.3, 156.6 (C=N-isoxazoline), 169.8, 170.3.

HRMS (TOF, ES+) m/z [M+H]⁺ calculated for C₁₄H₁₆NO₅ 278.1028, found 278.1033.

This structure has been described in Reaxys but no spectroscopic data were published.³⁵⁵



compound **53**

5-Carboxymethyl-3-phenyl-4,5-dihydro-isoxazole-5-carboxylic acid (53). The reaction was conducted at a scale of 2.0 mmol according to method 3 (section 4.1.1). Reaction completed after 19 hours. Purification of crude product by Varian ProStar preparative HPLC system afforded compound **53** (301 mg, 60%) as white solid. M.p.: 202-205 °C [lit. 197 °C]³⁵⁴

Chemical formula: C₁₂H₁₁NO₅

³⁵⁴ Quilico; Gruenanger *Gazzetta Chimica Italiana*, **1952**, vol. 82, p. 140,1472

³⁵⁵ Quilico; Gruenanger *Gazzetta Chimica Italiana*, **1952**, vol. 82, p. 140,1472

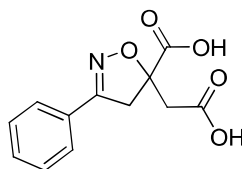
MW: 249.23 g/mol

HPLC-MS (method in 5 min at pH 3.8): $t_R = 2.23$ min

MS-(ES+) m/z 272 ($[M+Na]^+$, 30%), 250 ($[M+H]^+$, base peak), 232 (50%), 214 (35%)

MS-(ES-) m/z 248 ($[M-H]^-$, base peak).

IR (cm^{-1}): 2960 (band, O-H stretch), 1699 (C=O stretch), 1296 (C-O), 1219 (C-O).



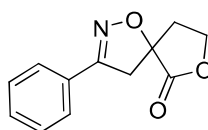
compound **53**

1H -NMR (300 MHz, DMSO- d_6 , ppm) δ 3.00 (s, 2H, CH₂), 3.57 (d, $J = 17.5$ Hz, 1H, H-isoxazoline), 3.87 (d, $J = 17.5$ Hz, 1H, H-isoxazoline), 7.43-7.47 (m, 3H, H-Ar), 7.66-7.69 (m, 2H, H-Ar), 12.92 (br s, 2H, COOH).

^{13}C -NMR (75 MHz, DMSO- d_6 , ppm) δ 41.1, 43.5 (CH₂-isoxazoline), 86.1 (C-Oisoxazoline), 127.2, 129.2, 129.3, 130.8, 157.1 (C=N-isoxazoline), 171.4, 171.6.

HRMS (TOF, ES+) m/z $[M+H]^+$ calculated for C₁₂H₁₂NO₅ 250.0715, found 250.0728.

This structure has been described in Reaxys but no spectroscopic data were published.³⁵⁵



compound **54**

3-Phenyl-1,7-dioxo-2-aza-spiro[4.4]non-2-en-6-one (54). The reaction was conducted at a scale of 0.5 mmol according to method 3 (section 4.1.1). Reaction completed after 16 hours. The crude residue was purified by flash chromatography (prepacked column silica 12g, diluent: cyclohexane-EtOAc [7-3], loading technique: dry load, flow rate 14mL/min; tube 10cm; collection by time: 0.5 min/tube] to afforded compound **54** (102 mg, 94%) as white solid. M.p.: 129-131 °C [lit. 132-133 °C]³⁵⁶

Chemical formula: C₁₂H₁₁NO₃

MW: 217.23 g/mol

HPLC-MS (method in 5 min at pH 3.8) : $t_R = 2.88$ min

MS-(ES+) m/z 218 ($[M+H]^+$, base peak), 200 (60%).

IR (cm^{-1}): 1780 (C=O), 1228 (C-O), 1199 (C-O), 1143 (C-O), 1016 (C-O).

1H -NMR (300 MHz, CDCl₃, ppm) δ 2.40 (dt, $J = 13.8$ Hz and $J = 8.8$ Hz, 1H), 2.72 (ddd, $J = 13.9$ Hz and $J = 6.4$ Hz and $J = 3.0$ Hz, 1H), 3.40 (d, $J = 17.0$ Hz, 1H, H-isoxazoline), 3.90

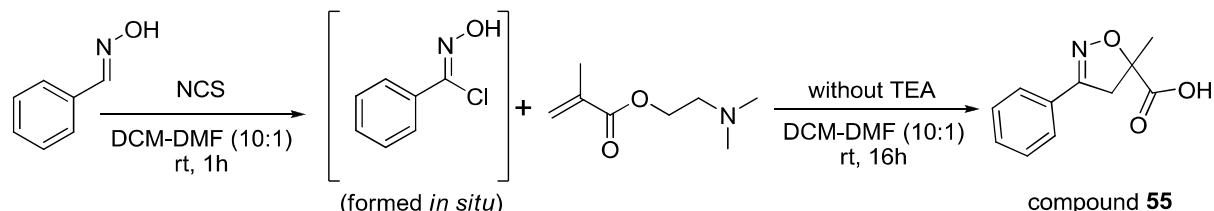
³⁵⁶ Stverkova, Slavka et al. *Liebigs Annalen*, **1995**, # 3 p. 477–480 (compound **4a**)

(d, $J = 17.0$ Hz, 1H, H-isoxazoline), 4.41-4.57 (m, 2H), 7.41-7.46 (m, 3H, H-Ar), 7.66-7.68 (m, 2H, H-Ar).

$^{13}\text{C-NMR}$ (75 MHz, CDCl_3 , ppm) δ 35.9, 42.7 (CH_2 -isoxazoline), 66.6, 84.9 (C-O-isoxazoline), 127.5, 128.9, 129.4, 131.3, 156.7 (C=N-isoxazoline), 174.6.

HRMS (TOF, ES+) m/z $[\text{M}+\text{H}]^+$ calculated for $\text{C}_{12}\text{H}_{12}\text{NO}_3$ 218.0817, found 218.0816.

These spectral characteristics were identical to those previously reported.³⁵⁶



5-methyl-3-phenyl- Δ^2 -isoxazoline-5-carboxylic acid (55): The reaction was conducted at a scale of 2.5 mmol. 2-(Dimethylamino)ethyl-2-methylprop-2-enoate was used as starting alkene. TEA was not necessary in the second step because the alkene played also role of TEA. Reaction completed after 16 hours. Interestingly, purification by flash column chromatography [prepacked 24g silica gel column, diluent: DCM- NH_3 in MeOH 90-10] afforded the saponified product **55** (284 mg, 56%) as white solid. M.p: 168-170 °C [lit.109-110 °C]³⁵⁷

Chemical formula: $\text{C}_{11}\text{H}_{11}\text{NO}_3$

MW: 205.22 g/mol

HPLC-MS (method in 5 min at pH 3.8): $t_R = 2.40$ min

MS-(ES+) m/z 206 ($[\text{M}+\text{H}]^+$, base peak)

MS-(ES-) m/z 204 ($[\text{M}-\text{H}]^-$, base peak)

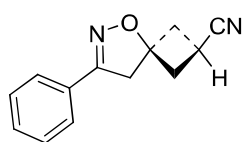
IR (cm^{-1}): 2987 (band, O-H stretch, carboxylic acid), 1576 (C=O stretch), 1223 (C-O), 1073 (C-O).

$^1\text{H-NMR}$ (300 MHz, $\text{DMSO-}d_6$, ppm) δ 1.44 (s, 3H, CH_3), 3.08 (d, $J = 17.0$ Hz, 1H, H-isoxazoline), 3.73 (d, $J = 17.0$ Hz, 1H, H-isoxazoline), 7.41-7.44 (m, 3H, H-Ar), 7.50 (br s, 1H, COOH), 7.62-7.65 (m, 2H, H-Ar).

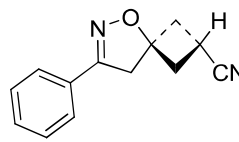
$^{13}\text{C-NMR}$ (75 MHz, $\text{DMSO-}d_6$, ppm) δ 24.8 (CH_3), 44.7 (CH_2 -isoxazoline), 88.3 (C-O-isoxazoline), 126.7, 129.2, 130.1, 130.5, 156.0 (C=N-isoxazoline), 174.9 (COOH).

These spectral characteristics were identical to those previously reported.³⁵⁷

³⁵⁷ *Synlett* 2005, No19, pp 2899-2904 (compound **30**)



compound **56**



compound **57**

7-Phenyl-5-oxa-6-aza-spiro[3.4]oct-6-ene-2-carbonitrile (56 and 57). The reaction was conducted at a scale of 1.0 mmol according to method 3 (section 3.1.3). The crude product is a mixture of 2 diastereomers. Purification of this crude residue by flash chromatography (prepacked silica GraceReveleris[®] 12g column, diluent: cyclohexane-EtOAc (80-20), dry loading method, flow-rate: 12 mL/min, tube 10 cm) afforded two separate diastereomers:

Chemical formula: C₁₃H₁₂N₂O

MW: 212.25 g/mol

Cis diastereomer (56): (33 mg, 16%) as off-white solid. M.p.: 128-130 °C

TLC R_f = 0.4 [cyclohexane-EtOAc (60-40), UV 254nm]

HPLC-MS (method in 5 min at pH 3.8): t_R = 2.94 min.

MS-(ES+) m/z 213 ([M+H]⁺, base peak)

MS (ES-) m/z 211 ([M-H]⁻, base peak)

IR (cm⁻¹): 2237 (C≡N), 1363

¹H-NMR (300 MHz, CDCl₃, ppm) δ 2.68-2.88 (m, 3H, CH₂ and CH), 2.96-3.04 (m, 2H, CH₂), 3.45 (s, 2H, CH₂-isoxazoline), 7.41-7.43 (m, 3H, H-Ar), 7.62-7.65 (m, 2H, H-Ar).

¹³C-NMR (75 MHz, CDCl₃, ppm) δ 13.6, 41.6, 45.4 (CH₂-isoxazoline), 82.2 (C-O-isoxazoline), 120.8, 126.6, 128.9, 129.0, 130.5, 156.6 (C=N-isoxazoline).

HRMS (TOF, ES+) m/z [M+H]⁺ calculated for C₁₃H₁₃N₂O 213.1028, found 213.1037.

This new structure has not been reported in literature. No results were found in Reaxys, Pubchem, eMolecules and Scifinder Scholar (verified on 28/03/2015).

Trans diastereomer (57): (85 mg, 40%) as off-white solid. M.p.: 110-112 °C

TLC R_f = 0.5 [cyclohexane-EtOAc (60-40), UV 254nm]

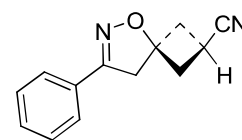
HPLC-MS (method in 5 min at pH 3.8): t_R = 2.95 min

MS-(ES+) m/z 213 [M+H]⁺, base peak)

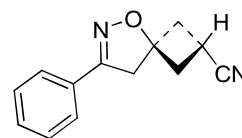
MS-(ES-) m/z 211 ([M-H]⁻, base peak)

IR (cm⁻¹): 2235 (C≡N), 1360

¹H-NMR (300 MHz, CDCl₃, ppm) δ 2.65-2.71 (m, 2H, CH₂), 2.96-3.03 (m, 2H, CH₂), 3.14-3.24 (m, 1H, CH), 3.57 (s, 2H, H-isoxazoline), 7.41-7.44 (m, 3H, H-Ar), 7.64-7.68 (m, 2H, H-Ar).



compound **56**



compound **57**

$^{13}\text{C-NMR}$ (75 MHz, CDCl_3 , ppm) δ 15.3, 40.8, 46.1 (CH_2 -isoxazoline), 84.3 (C-O-isoxazoline), 122.2, 126.7, 128.8, 129.0, 130.5, 156.9 (C=N-isoxazoline).

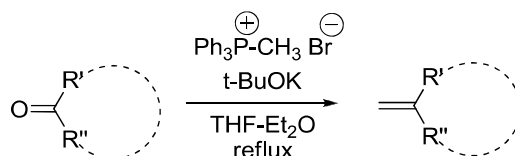
HRMS (TOF, ES+) m/z $[\text{M}+\text{H}]^+$ calculated for $\text{C}_{13}\text{H}_{13}\text{N}_2\text{O}$ 213.1028, found 213.1035.

This new structure has not been reported in literature. No results were found in Reaxys, Pubchem, eMolecules and Scifinder Scholar (verified on 28/03/2015).

The structures of these two diastereomers were distinguished by 1D-NOESY.

4.1.3. Synthesis of isoxazoline from aliphatic carbaldoxime and alkenes

4.1.3.1. Preparation of alkenes from ketones by Wittig conditions



General procedure of Wittig reaction³⁵⁸: To a stirred suspension of methyltriphenylphosphonium bromide (1.5 equiv.) in diethylether (25-45 mL) under argon was added dropwise a solution of potassium-tert-butoxide 1M in THF (1.5 equiv.). The reaction mixture was immediately turned to yellow. After refluxing for 1 hour, the corresponding ketone (1.0 equiv.) was added in portions. The mixture was stirred at room temperature overnight. After completion, the reaction mixture was then hydrolyzed by water (5-8mL). The organic phase was separated and aqueous phase was extracted by diethyl ether (2 x 10mL). The combined organic phases were washed with water (20mLx2), brine (20mLx1), dried over anhydrous MgSO_4 and concentrated under reduced pressure to yield crude product. Purification of this crude product by a suitable method afforded the corresponding alkene.

According to the described procedure, the following alkenes were synthesized:

4-Methylene-azepane-1-carboxylic acid tert-butyl ester (58): Reaction was conducted at a scale of 4.0 mmol. The crude product obtained according above procedure was then purified by flash chromatography (column: silica gel pre-packed GraceReveleris[®]12g; eluents: cyclohexane-EtOAc (95-5), flow-rate: 15 mL/min; tube collection by time: 0.45 min/tube). The final product alkene **58** was obtained (497 mg, 59% yield) as colorless liquid.

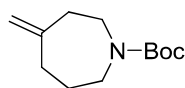
Chemical formula: $\text{C}_{12}\text{H}_{21}\text{NO}_2$

MW: 211.31 g/mol

HPLC-MS (method in 5 min at pH 3.8): $t_{\text{R}} = 3.38$ min

MS-(ES+) m/z 156 ($[\text{M}-\text{tBu}+\text{H}]^+$, base peak)

³⁵⁸Meyer-Wilmes et al. *Tetrahedron* **2009**, 65,1689–1696.



compound **58**

¹H-NMR (300 MHz, CDCl₃, ppm) δ 1.45 (s, 9H, 3xCH₃), 1.69-1.71 (m, 2H, CH₂), 2.21-2.25 (m, 2H, CH₂), 2.39-2.43 (t, J = 6.2 Hz, 2H, CH₂), 3.37-3.39 (m, 4H, 2xCH₂), 4.75 (s, 1H, H of =CH₂), 4.79 (s, 1H, H of =CH₂).

These spectral characteristics were identical to those previously reported in literature.³⁵⁹

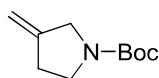
3-Methylene-pyrrolidine-1-Boc (59): Reaction was conducted at a scale of 5.0 mmol. The crude product obtained according the above procedure was then purified by flash column chromatography (*column*: silica gel pre-packed Grace Reveleris[®] 12g; *eluents*: cyclohexane-EtOAc (100-0 then 95-5), *flow-rate*: 15 mL/min; tube collection by time: 0.45 min/tube). We obtained one fraction which was evaporated under reduced pressure to give **59** (300 mg, 33%) as light yellow liquid.

Chemical formula: C₁₀H₁₇NO₂

MW: 183.25 g/mol

HPLC-MS (method in 5 min at pH 3.8): t_R = 3.21 min

MS-(ES⁺): m/z 128 ([M-tBu+H]⁺, base peak).



compound **59**

¹H-NMR (300 MHz, CDCl₃, ppm) δ 1.48 (s, 9H, 3xCH₃), 2.56 (t, J = 7.2 Hz, 2H, CH₂), 3.47 (t, J = 7.3 Hz, 2H, CH₂), 3.93 (s, 2H, CH₂), 4.96-4.99 (m, 2H, H of =CH₂).

These spectral characteristics were identical to those previously reported in literature.³⁶⁰

5-Methylene-6,7,8,9-tetrahydro-5H-benzocycloheptene (60): Reaction was conducted at a scale of 10 mmol. The crude product obtained according the above procedure was then purified by washing with mixture *n*-petane-Et₂O (95-5) and filtered over a silica gel plug (h=4 cm). The filtrate was evaporated under reduced pressure to give the desired alkene **60** (1.39 g, 88%) as colorless liquid.

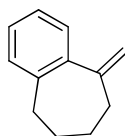
Chemical formula: C₁₂H₁₄

MW: 158.25 g/mol

HPLC-MS (method in 5 min at pH 3.8, detected by PDA): t_R = 3.97 min

³⁵⁹ Patent: US2011/269737 A1, 2011; column 49, compound 2e

³⁶⁰ Patent: WO2005/58858 A1,2005



compound **60**

¹H-NMR (300 MHz, CDCl₃, ppm) δ 1.72-1.80 (m, 2H, CH₂), 1.83-1.91 (m, 2H, CH₂), 2.40-2.44 (m, 2H, CH₂), 2.77-2.81 (m, 2H, CH₂), 5.00-5.01 (d, $J = 2.2$ Hz, 1H, H of =CH₂), 5.12-5.13 (m, 1H, H of =CH₂), 7.10-7.25 (m, 4H, H_{Ar}).

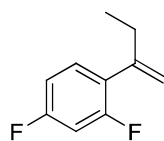
These spectral characteristics were identical to those previously reported in literature.³⁶¹

2,4-Difluoro-1-(1-methylene-propyl)-benzene (61). Reaction was conducted at a scale of 6.0 mmol. The crude product obtained according the above procedure was then purified by flash column chromatography (*column*: silica gel pre-packed GraceReveleris[®] 12g; *eluents*: cyclohexane-EtOAc (95-5), *flow-rate*: 15 mL/min; tube collection by time: 0.45 min/tube). The final product alkene **61** was obtained as light yellow liquid (576 mg, 57%).

Chemical formula: C₁₀H₁₀F₂

MW: 168.19 g/mol

HPLC-MS (method in 5 min at pH 3.8, detected by PDA): $t_R = 3.57$ min

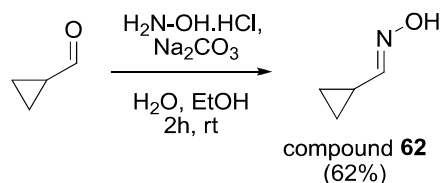


compound **61**

¹H-NMR (300 MHz, CDCl₃, ppm) δ 1.04 (t, $J = 7.4$ Hz, 3H), 2.41-2.50 (m, 2H), 5.11-5.12 (m, 1H, H of =CH₂), 5.21-5.23 (m, 1H, H of CH₂), 6.76-6.87 (m, 2H, H_{Ar}), 7.18-7.26 (m, 1H, H_{Ar}).

This structure has been published in Reaxys but no physical and spectroscopic data were found (verified on 28/03/2015)

³⁶¹ Macromolecules, 2013, vol. 46, # 9 p. 3314 - 3323

4.1.3.2. Preparation of cyclopropylcarbaldoxime (62):


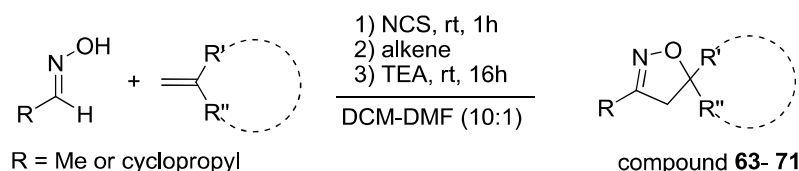
Sodium carbonate (0.8g, 7.5 mmol) was added to a solution of hydroxylamine hydrochloride (1.04 g, 15 mmol) in 5 mL of water. The cyclopropane carboxaldehyde (0.76 mL, 10 mmol) in 3 mL ethanol was added to the aqueous solution and stirred at room temperature for 2h. The reaction was monitored by TLC (UV: negative, $\text{CuCl}_2/\text{MeOH}$: positive). After 2 hours, the reaction mixture was extracted with EtOAc (20 mLx3). The combined extracts were washed with brine, dried over anhydrous MgSO_4 and evaporated under reduced pressure to give a white solid. This crude product was recrystallized from cyclohexane to afford compound **62** (530 mg, 62%) as white crystals.

Chemical formula: $\text{C}_4\text{H}_7\text{NO}$. **MW:** 85.11 g/mol

TLC $R_f = 0.50$ (cyclohexane-EtOAc 60/40), stained by CuCl_2 in MeOH).

$^1\text{H-NMR}$ (300 MHz, CDCl_3 , ppm) δ 0.60-0.67 (m, 4H, $2 \times \text{CH}_2$), 0.84-0.99 (m, 4H, $2 \times \text{CH}_2$), 1.57-1.68 (m, 1H, CH-cyclopropyl), 2.24-2.35 (m, 1H, CH-cyclopropyl), 6.03-6.06 (d, $J = 8.8$ Hz, 1H, CH=N), 6.92-6.95 (d, $J = 8.4$ Hz, 1H, CH=N), 8.54 (br s, 2H, $2 \times \text{N-OH}$). This is a isomeric mixture of syn and anti oxime.

These spectral characteristics were identical to those previously reported in literature.³⁶²

4.1.3.3. Synthesis of isoxazoline from aliphatic carbaldoxime and alkenes


The following isoxazoline were synthesized according to method 3 described in section 4.1.1.

3-Methyl-8-N-Boc-1-oxa-2,8-diazaspiro[4.5]dec-2-ene (63). Reaction was conducted at a scale of 2 mmol. The crude was purified by flash chromatography (*column*: pre-packed column 12g; *eluents*: cyclohexane- EtOAc (gradient 90-10 then 0-100), *flow-rate*: 12 mL/min; tube V_{max} 10 mL; collection by time: 0.55 min/tube) to yield **63** (212 mg, 42%) as colorless liquid.

Chemical formula: $\text{C}_{13}\text{H}_{22}\text{N}_2\text{O}_3$

MW: 254.33 g/mol

³⁶² *J. Org. Chem.* Vol.59, No.3, **1994**, pp. 622-627

TLC: $R_f = 0.3$ [diluant: cyclohexane-EtOAc (70-30); detected by ninhydrin]

HPLC-MS (method in 5 min at pH 3.8): $t_R = 2.86$ min

MS-(ES+) m/z 155 ($[M-Boc]^+$, 38%) ; 181 ($[M-tBuO]^+$, base peak); 199 ($[M-tBu+2H]^+$, 92%); 255 ($[M+H]^+$, 7%).



compound **63**

1H -NMR (300 MHz, $CDCl_3$, ppm) δ 1.46 (s, 9H, $3 \times CH_3$), 1.58-1.67 (m, 2H), 1.78-1.85 (m, 2H), 1.98 (s, 3H, CH_3), 2.67 (s, 2H, H-isoxazoline), 3.33-3.41 (m, 2H), 3.65-3.70 (m, 2H).

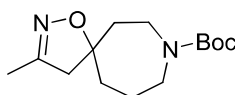
3-Methyl--8-N-Boc-1-oxa-2,8-diaza-spiro[4.6]undec-2-ene (64). Reaction was conducted with scale at 2.35 mmol. This crude product was then purified by flash chromatography (*column*: pre-packed column 12g; *eluents*: cyclohexane-EtOAc (gradient 90-10 then 60-40), *flow-rate*: 13 mL/min; tube with Vmax 10 mL; collection by time: 0.45 min/tube) to afford compound **64** (232 mg, 37%) as colorless liquid.

Chemical formula: $C_{14}H_{24}N_2O_3$

MW: 268.36 g/mol

HPLC-MS (method in 5 min at pH 3.8): $t_R = 2.92$ min

MS-(ES+) m/z 169 ($[M-Boc]^+$, 2%) ; 195 ($[M-tBuO]^+$, 95%) ; 213 ($[M-tBu+H]^+$, base peak), 269 ($[M+H]^+$, 9%).



compound **64**

1H -NMR (300 MHz, $CDCl_3$, ppm) δ 1.47 (s, 9H, $3 \times CH_3$), 1.66-2.05 (m, 9H, CH_3 and $3 \times CH_2$), 2.67 (s, 2H, H-isoxazoline), 3.21-3.29 (m, 2H, CH_2), 3.60-3.64 (m, 2H, CH_2).

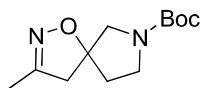
3-Methyl-7-N-Boc-1-oxa-2,7-diaza-spiro[4.4]non-2-ene (65). Reaction was conducted at a scale of 1.5 mmol. This crude was purified by flash chromatography (*column*: pre-packed column 12g; *eluents*: cyclohexane-EtOAc (gradient 90-10 --> 60-40), *flow-rate*: 12.5 mL/min; tube with Vmax 10 mL; collection by time: 0.50 min/tube) to yield compound **65** (200 mg, 55%) as white solid.

Chemical formula: $C_{12}H_{20}N_2O_3$

MW: 240.31 g/mol

HPLC-MS (method in 5 min at pH 9.2): $t_R = 2.71$ min

MS-(ES+) m/z 141 ($[M-Boc]^+$, 18%) 167 ($[M-tBuO]^+$, base peak) ; 241 ($[M+H]^+$, 50%).



compound **65**

1H -NMR (300 MHz, $CDCl_3$, ppm) δ 1.43 (s, 9H, 3 \times CH₃), 1.88-1.98 (m, 1H), 2.01 (s, 3H, CH₃), 2.18-2.26 (m, 1H), 2.91 (s, 2H, H-isoxazoline), 3.33-3.68 (m, 4H).

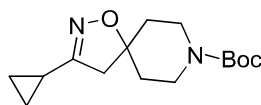
3-Cyclopropyl-8-*N*-Boc-1-oxa-2,8-diaza-spiro[4.5]dec-2-ene (66). Reaction was conducted at a scale of 2.0 mmol. This crude was purified by flash chromatography (*column*: pre-packed column 12g; *eluents*: cyclohexane-EtOAc (gradient 90-10 then 0-100), *flow-rate*: 12 mL/min; *petit tube*; collection by time: 0.55 min/tube) to afford compound **66** (294 mg, 52%) as light yellow solid.

Chemical formula: C₁₅H₂₄N₂O₃

MW: 280.37 g/mol

HPLC-MS (method in 5 min at pH 3.8): t_R =3.06 min

MS-(ES+) m/z 181 ($[M-Boc]^+$, 15%) ; 207 ($[M-tBuO]^+$, 66%) ; 225 ($[M-tBu+2H]^+$, base peak); 281 ($[M+H]^+$, 10%).



compound **66**

1H -NMR (300 MHz, $CDCl_3$, ppm) δ 0.71-0.92 (m, 4H, 2 \times CH₂-isopropyl), 1.46 (s, 9H, 3 \times CH₃-Boc), 1.55-1.83 (m, 5H, 2 \times CH₂-piperidine and CH-isopropyl), 2.53 (s, 2H, H-isoxazoline), 3.30-3.39 (m, 2H, CH₂-piperidine), 3.63-3.71 (m, 2H, CH₂-piperidine).

3-Methyl-1,7-dioxo-2-aza-spiro[4.4]non-2-en-6-one (67). Reaction was conducted at a scale of 4.0 mmol. Work up of the reaction mixture yielded the desired product **67** (447 mg, 72%) as light yellow solid. Mp: 72-74 °C.

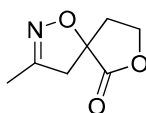
Chemical formula: C₇H₉NO₃

MW: 155.16 g/mol

HPLC-MS (method in 5 min at pH 3.8): t_R = 1.92 min

MS-(ES+) m/z 156 ($[M+H]^+$, base peak).

IR (cm⁻¹): 1767 (C=O stretch), 1221 (C-O stretch), 1015 (C-O stretch).



compound **67**

¹H-NMR (300 MHz, CDCl₃, ppm) δ 2.05 (s, 3H, CH₃), 2.26-2.37 (dt, J = 8.8 Hz and 13.8 Hz, 1H), 2.58-2.66 (ddd, J = 3.0 Hz and J = 6.4 Hz and J = 13.8 Hz, 1H), 2.97 (d, J = 17.3 Hz, 1H, H-isoxazoline), 3.48 (d, J = 17.3 Hz, 1H, H-isoxazoline), 4.35-4.50 (m, 2H).

¹³C-NMR (75 MHz, CDCl₃, ppm) δ 12.8, 35.0, 45.6 (CH₂-isoxazoline), 66.0, 83.3 (C-O-isoxazoline), 155.0 (C=N-isoxazoline), 174.4.

HRMS (TOF, ES+) m/z [M+H]⁺ calculated for C₇H₁₀NO₃ 156.0661, found 156.0659.

This new structure has not been reported in literature. No results were found in Reaxys, Pubchem, eMolecules and Scifinder Scholar (verified on 28/03/2015).

(1R,2S,5S)-3',6,6-trimethyl-4'H-spiro[bicyclo[3.1.1]heptane-2,5'-isoxazole] (**68**). Reaction was conducted at a scale of 6.0 mmol. Crude product was purified by preparative HPLC Waters (MS detector) at pH 9.2 (gradient mobile phase) to afford compound **68** (112 mg, 10%) as white cream solid. M.p.: 47-48 °C

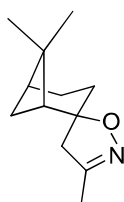
Chemical formula: C₁₂H₁₉NO

MW: 193.29 g/mol

HPLC-MS (method in 5 min at pH 9.2): t_R = 3.21 min

MS-(ES+) m/z 194 ([M+H]⁺, base peak)

IR (cm⁻¹): 2915 (C-H stretch), 1384 (C-H rock), 1325 (C-H rock), 907.



compound **68**

¹H-NMR (300 MHz, CDCl₃, ppm) δ 0.90 (s, 3H), 1.25 (s, 3H), 1.56 (d, J = 10.6 Hz, 1H), 1.73-1.99 (m, 4H), 1.95 (s, 3H), 2.04 (t, J = 5.5 Hz, 1H), 2.19-2.39 (m, 2H), 2.74 (s, 2H).

¹³C-NMR (75 MHz, CDCl₃, ppm) δ 13.6, 22.9, 23.9, 26.4, 26.8, 31.0, 38.1, 39.9, 50.9, 51.6 (CH₂-isoxazoline), 90.3 (C-O-isoxazoline), 154.9 (C=N-isoxazoline).

HRMS (TOF, ES+) m/z [M+H]⁺ calculated for C₁₂H₂₀NO 194.1545, found 194.1548.

This new structure has not been reported in literature. No results were found in Reaxys, Pubchem, eMolecules and Scifinder Scholar (verified on 28/03/2015).

3-cyclopropyl-1,7-dioxo-2-azaspiro[4.4]non-2-en-6-one (69). Reaction was conducted at a scale of 2.0 mmol. Crude product was purified by flash chromatography [column: Interchim 12g, diluant: cyclohexane-EtOAc (40-60); collection by time: 0.50min/tube; pump: 12,5ml/min] afforded product **69** (316 mg, 87%) as white solid. M.p.: 52-54 °C.

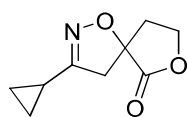
Chemical formula: C₉H₁₁NO₃

MW: 181.19 g/mol

HPLC-MS (method in 5 min at pH 3.8): t_R = 2.32 min

MS-(ES+) m/z 182 ([M+H]⁺, base peak)

IR (cm⁻¹): 1764 (C=O stretch), 1198 (C-O stretch), 1138 (C-O stretch), 1014 (stretch).



compound **69**

¹H-NMR (300 MHz, CDCl₃, ppm) δ 0.80-0.97 (m, 4H, 2×CH₂-cyclopropyl), 1.76-1.80 (m, 1H, CH-cyclopropyl), 2.23-2.33 (m, 1H, -CH₂-lactone), 2.57-2.64 (m, 1H, -CH₂-lactone), 2.81 (d, *J* = 17.0 Hz, 1H, H-isoxazoline), 3.34 (d, *J* = 17.0 Hz, 1H, H-isoxazoline), 4.33-4.48 (m, 2H, -CH₂-O-lactone).

¹³C-NMR (75 MHz, CDCl₃, ppm) δ 6.4 (CH₂-cyclopropyl), 6.6 (CH₂-cyclopropyl), 8.7 (CH-cyclopropyl), 35.0 (-CH₂-lactone), 42.5 (CH₂-isoxazoline), 65.93 (-CH₂-O-lactone), 83.1 (C-O-isoxazoline), 160.57 (C=N-isoxazoline), 174.22 (-COO-lactone).

HRMS (TOF, ES+) m/z [M+H]⁺ calculated for C₉H₁₂NO₃ 182.0817, found 182.0819.

This new structure has not been reported in literature. No results were found in Reaxys, Pubchem, eMolecules and Scifinder Scholar (verified on 28/03/2015).

5-(2,4-Difluoro-phenyl)-5-ethyl-3-methyl-2-isoxazoline (70). Reaction was conducted at a scale of 3.4 mmol. Crude product was purified by flash chromatography (*column*: pre-packed column 12g of silica; *eluents*: cyclohexane- EtOAc (gradient 80-20), *flow-rate*: 13 mL/min; collection by time: 0.60 min/tube) to afford compound **70** (224 mg, 29%) as colorless liquid.

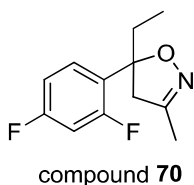
Chemical formula: C₁₂H₁₃F₂NO

MW: 225.24 g/mol

HPLC-MS (method in 5 min at pH 3.8): t_R = 3.21 min

MS-(ES+) m/z 226 ([M+H]⁺, base peak).

IR (cm⁻¹): 2971 (C-H stretch, aromatic), 2882 (C-H stretch, alkane), 1616 (C-C stretch, aromatic), 1598 (C-C stretch, aromatic), 1497 (C-H bend).



¹H-NMR (300 MHz, CDCl₃, ppm) δ 0.84 (t, $J = 7.4$ Hz, 3H), 1.96-2.03 (m, 5H), 3.07 (d, $J = 17.5$ Hz, 1H, H-isoxazoline), 3.20 (d, $J = 17.5$ Hz, 1H, H-isoxazoline), 6.76-6.90 (m, 2H, H-aromatic), 7.58-7.66 (m, 1H, H-aromatic).

¹³C-NMR (75 MHz, CDCl₃, ppm) δ 8.4, 13.3, 32.6, 49.8 (CH₂-isoxazoline), 86.9 (d, $^3J_{CF} = 3.2$ Hz, C-O-isoxazoline), 104.1 (t, $^2J_{CF} = 25.8$ Hz), 110.8 (dd, $^2J_{CF} = 20.2$ Hz, $^4J_{CF} = 2.6$ Hz), 127.5 (dd, $^2J_{CF} = 12.3$ Hz, $^4J_{CF} = 3.3$ Hz), 128.8 (dd, $^3J_{CF} = 9.4$ Hz, $^3J_{CF} = 6.1$ Hz), 156.0 (C=N-isoxazoline), 160.7 (dd, $^1J_{CF} = 247.5$ Hz, $^3J_{CF} = 12.2$ Hz), 162.2 (dd, $^1J_{CF} = 246.8$ Hz, $^3J_{CF} = 12.2$ Hz).

⁹F-NMR (282 MHz, CDCl₃, ppm) δ -112.54 (d, $J_{FF} = 7.5$ Hz), -111.65 (d, $J_{FF} = 6.9$ Hz).

HRMS (TOF, ES+) m/z [M+H]⁺ calculated for C₁₂H₁₄F₂NO 226.1043, found 226.1051.

This new structure has not been reported in literature. No results were found in Reaxys, Pubchem, eMolecules and Scifinder Scholar (verified on 28/03/2015).

3-methylspiro-[4H-1,2-oxazole-5,5'-6,7,8,9-tetrahydrobenzo-[7]-annulene] (71). Reaction was conducted at a scale of 4.0 mmol. Crude product was purified by flash chromatography (*column*: pre-packed column 40g; *eluents*: cyclohexane- EtOAc (gradient 100-0 then 80-20), *flow-rate*: 12 mL/min; tube with Vmax= 10 mL ; collection by time: 0.55 min/tube) to yield compound 71 (274 mg, 32%) as white solid. Mp: 56-58 °C

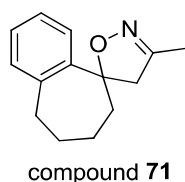
Chemical formula: C₁₄H₁₇NO

MW: 215.30 g/mol

HPLC-MS (method in 5 min at pH 3.8): $t_R = 3.27$ min

MS-(ES+) m/z 216 ([M+H]⁺, base peak)

IR (cm⁻¹): 2920 (C-H stretch, aromatic), 2851 (C-H stretch, alkane), 764, 746.



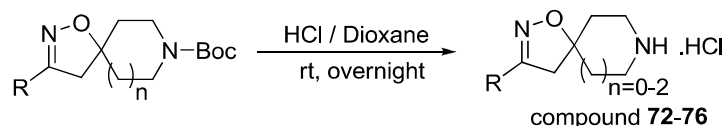
¹H-NMR (300 MHz, CDCl₃, ppm) δ 1.35-1.50 (m, 1H), 1.73-1.90 (m, 1H), 1.95-2.16 (m, 7H), 2.72-2.89 (m, 3H, 1H-isoxazoline and 2H of cycloheptane), 3.37 (d, $J = 18.0$ Hz, 1H, H-isoxazoline), 7.09-7.24 (m, 3H, H-Ar), 7.66-7.69 (m, 1H, H-Ar).

¹³C-NMR (75 MHz, CDCl₃, ppm) δ 13.5, 27.2, 27.8, 36.9, 37.8, 48.1 (CH₂-isoxazoline), 90.7 (C-O-isoxazoline), 125.3, 126.3, 127.4, 130.7, 139.0, 144.7, 155.0 (C=N-isoxazoline).

HRMS (TOF, ES+) m/z $[M+H]^+$ calculated for $C_{14}H_{18}NO$ 216.1388, found 216.1395.

This new structure has not been reported in literature. No results were found in Reaxys, Pubchem, eMolecules and Scifinder Scholar (verified on 28/03/2015).

4.1.4. General procedure for removing *N*-Boc group:



Compound with Boc protecting group (1.0 equiv.) was dissolved in 1,4-dioxane. The mixture was cooled to 0°C and a solution of HCl 4N in 1,4-dioxane (10 equiv.) was added dropwise. The reaction mixture was stirred at room temperature overnight. A white precipitate appeared. After completion, dioxane was evaporated under reduced pressure and the resulting white solid was washed by diethyl ether and dried under reduced pressure to yield the final product in form hydrochloride salt. This protocol was applied to synthesize of the following compounds:

3-phenyl-1-oxa-2,8-diaza-spiro[4.5]dec-2-en hydrochloride (72). The reaction was conducted at a scale of 0.932 mmol. The desired product **72** was obtained (175 mg, 74%) as white solid³⁶³. M.p.: 265-266 °C (dec.)

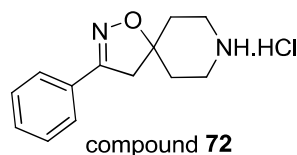
Chemical formula: $C_{13}H_{17}N_2OCl$

MW: 252.75 g/mol

HPLC-MS (method in 5 min at pH 9.2): $t_R = 2.18$ min

MS-(ES+): m/z 217 ($[M-HCl+H]^+$, base peak)

IR (cm^{-1}): 2923 (piperidine)



¹H-NMR (300 MHz, D₂O, ppm) δ 2.03-2.16 (m, 4H, H-piperidine), 3.29-3.43 (m, 6H, 2H-isoxazoline and 4H-piperidine), 7.44-7.52 (m, 3H, H-Ar), 7.60-7.63 (m, 2H, H-Ar).

¹³C-NMR (75 MHz, D₂O, ppm) δ 31.5, 41.2, 44.7 (CH₂-isoxazoline), 82.2 (C-O-isoxazoline), 126.7, 128.2, 129.0, 131.0, 159.4 (C=N-isoxazoline).

HRMS (TOF, ES+) m/z $[M-HCl+H]^+$ calculated for $C_{13}H_{17}N_2O$ 217.1341, found 217.1350.

³⁶³ This compound was described in Patent WO2006/122770 (c73) as white solid but no characterization data was published.

This structure has been described in Reaxys but no spectroscopic and physical data were published.³⁶³

3-Methyl-8-BOC-1-oxa-2,8-diazaspiro[4.5]dec-2-ene hydrochloride (73). The reaction was conducted at a scale of 0.790 mmol. The final product **73** obtained (106 mg, 70%) as white solid. M.p.: 238-239 °C (dec.)

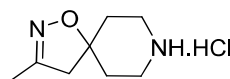
Chemical formula: C₈H₁₄N₂O. HCl

MW: 190.68 g/mol

HPLC-MS (method in 5 min at pH 9.2): t_R = 1.57 min

MS-(ES+): *m/z* 155 ([M-HCl+H]⁺, base peak).

IR (cm⁻¹): 2954 (piperidine)



compound **73**

¹H-NMR (300 MHz, D₂O, ppm) δ 1.88-2.05 (m, 7H, CH₃ and 4H-piperidine), 2.92 (s, 2H, H-isoxazoline), 3.16-3.31 (m, 4H, H-piperidine).

¹³C-NMR (75 MHz, D₂O, ppm) δ 12.4, 31.4, 41.3, 48.2 (CH₂-isoxazoline), 81.1 (C-O-isoxazoline), 160.2 (C=N-isoxazoline).

HRMS (TOF, ES+) *m/z* [M-HCl+H]⁺ calculated for C₈H₁₅N₂O 155.1184, found 155.1182.

This new structure has not been reported in literature. No results were found in Reaxys, Pubchem, eMolecules and Scifinder Scholar (verified on 28/03/2015).

3-Methyl-1-oxa-2,8-diaza-spiro[4.6]undec-2-ene hydrochloride (74). The reaction was conducted at a scale of 0.865 mmol. The final product **74** obtained (148 mg, 84%) as white solid. M.p.: 195-198 °C

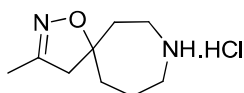
Chemical formula: C₉H₁₆N₂O. HCl

MW: 204.70 g/mol

HPLC-MS (method in 5 min at pH 9.2): t_R = 1.66 min

MS-(ES+): *m/z* 169 ([M-HCl+H]⁺, base peak).

IR (cm⁻¹): 2933 (azepane)



compound **74**

¹H-NMR (300 MHz, D₂O, ppm) δ 1.62-2.02 (m, 6H, CH₃ and 3H-azepane), 2.04-2.16 (m, 3H, 2H-azepane), 2.90 (s, 2H, 2H-isoxazoline), 3.13-3.21 (m, 2H, 2H-azepane), 3.25-3.35 (m, 2H, 2H-azepane).

¹³C-NMR (75 MHz, D₂O, ppm) δ 12.5, 19.4, 34.5, 37.4, 40.0, 45.9, 50.1 (CH₂-isoxazoline), 86.8 (C-O-isoxazoline), 160.3 (C=N-isoxazoline).

HRMS (TOF, ES⁺) m/z [M-HCl+H]⁺ calculated for C₉H₁₇N₂O 169.1341, found 169.1335.

This new structure has not been reported in literature. No results were found in Reaxys, Pubchem, eMolecules and Scifinder Scholar (verified on 28/03/2015).

3-Methyl-7-BOC-1-oxa-2,7-diaza-spiro[4.4]non-2-ene hydrochloride (**75**). The reaction was conducted at a scale of 0.832 mmol. The final product **75** was obtained (133 mg, 90%) as white solid. M.p.: 187-190 °C

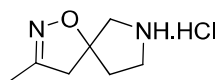
Chemical formula: C₇H₁₂N₂O. HCl

MW: 176.65 g/mol

HPLC-MS (method in 5 min at pH 9.2): t_R = 1.59

MS-(ES⁺): m/z 141 [M-HCl+H]⁺

IR (cm⁻¹): 2901 (pyrrolidine)



compound **75**

¹H-NMR (300MHz, D₂O, ppm) δ 1.91 (s, 3H, CH₃), 2.10-2.21 (m, 1H), 2.25-2.34 (m, 1H), 3.17 (s, 2H, H-isoxazoline), 3.28-3.53 (m, 4H).

¹³C-NMR (75MHz, D₂O, ppm) δ 12.2, 34.9, 43.5 (CH₂-isoxazoline), 44.8, 53.6, 90.1 (C-O-isoxazoline), 160.3 (C=N-isoxazoline).

HRMS (TOF, ES⁺) m/z [M-HCl+H]⁺ calculated for C₇H₁₃N₂O 141.1028, found 141.1034.

This new structure has not been reported in literature. No results were found in Reaxys, Pubchem, eMolecules and Scifinder Scholar (verified on 28/03/2015).

3-Cyclopropyl-1-oxa-2,8-diaza-spiro[4.5]dec-2-ene hydrochloride (76). The reaction was conducted at a scale of 1.009 mmol. The final product **76** was obtained (196 mg, 90%) as white solid. M.p.: 255°C (dec.).

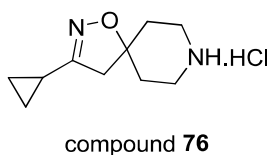
Chemical formula: C₁₀H₁₇N₂OCl

MW: 216.71 g/mol

HPLC-MS (method in 5 min at pH 9.2): t_R = 1.89 min

MS-(ES+): m/z 181 ([M-HCl+H]⁺, base peak)

IR (cm⁻¹): 2925 (piperidine)



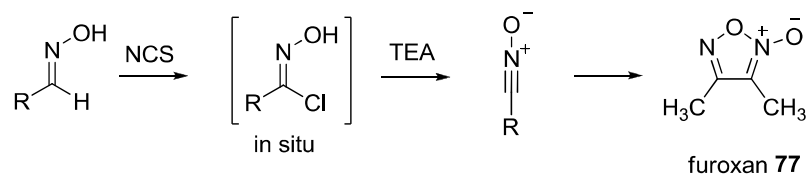
¹H-NMR (300 MHz, D₂O, ppm) δ 0.68-0.74 (m, 2H, CH₂-isopropyl), 0.86-0.92 (m, 2H, CH₂-isopropyl), 1.68-1.76 (m, 1H, CH-isopropyl), 1.86-2.03 (m, 4H, 2 x CH₂-piperidine), 2.77 (s, 2H, H-isoxazoline), 3.15-3.30 (m, 4H, 2 x CH₂-piperidine).

¹³C-NMR (75 MHz, D₂O, ppm) δ 5.7, 8.6, 31.2, 41.3, 44.5 (CH₂-isoxazoline), 80.9 (C-O-isoxazoline), 165.9 (C=N-isoxazoline).

HRMS (TOF, ES+) m/z [M-HCl+H]⁺ calculated for C₁₀H₁₇N₂O 181.1341, found 181.1339.

This new structure has not been reported in literature. No results were found in Reaxys, Pubchem, eMolecules and Scifinder Scholar (verified on 28/03/2015).

4.1.5. Study on the dimerization of nitrile oxide as by product



Acetaldoxime (0.62 mL, 10.0 mmol, 1.0 equiv.) was dissolved in a mixture of DCM (20 mL) and DMF (2 mL). NCS (1.635 g, 1.2 eq) was then added in portions to the stirred mixture at 0°C. 1 hour after addition of NCS, the reaction mixture change to blue color and then to colorless. The mixture was then warmed to room temperature and continued to stirred for 3 hours.

TEA (4.2 mL in 20 mL DCM) was then added slowly over 1 hour. The resulting reaction mixture was stirred at room temperature overnight (16 hours). A white precipitate appeared. So, the reaction mixture was filtered and the filtrate was then washed with HCl 1N (30 mL) to neutralize to pH 7 then with water (30 mL) and brine (30 mL). The organic phase was dried over anhydrous MgSO₄ and evaporated under reduced pressure to yield a light yellow liquid.

This crude was purified by a flashed chromatography to yield the final product 3,4-dimethyl furoxan **77** (912 mg, 80%) as colorless liquid.

This product **77** was analyzed by LC-MS and ¹H-NMR.

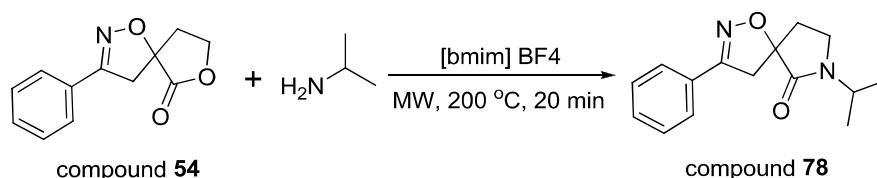
HPLC (method in 5 min at pH 3.8, detected by PDA): t_R = 2.12 min

¹H-NMR (300 MHz, CDCl₃, ppm) δ 2.14 (s, 3H), 2.33 (s, 3H)

The result confirmed that the structure formed by a dimerization of two nitrile oxides. These spectral characteristics were identical to those previously reported in literature.³⁶⁴

This assay was also conducted with benzaldoxime (0.445 mL, 4.0 mmol) as starting material. But after 16 hours, no furoxan was formed.

4.2. Functionalization of lactone containing isoxazoline fragments



7-isopropyl-3-phenyl-1-oxa-2,7-diaza-spiro[4.4]non-2-en-6-one (**78**): compound **54** (173.78 mg, 0.8 mmol, 1.0 equiv.), ionic liquid [bmim]BF₄ (1.048 mL, 7.0 eq) and 2-amino propane (0.206 mL, 3 eq) was vortexed in a sealed tube. The reaction was performed under microwave irradiation at 200°C for 20 minutes.³⁶⁵ After completion, the reaction mixture was diluted with ethyl acetate and washed with saturated aqueous NH₄Cl (30 mL x 3) and brine (30 mL). The organic phase was dried over anhydrous magnesium sulfate and concentrated under reduced pressure to give brown slurry. The crude residue was then purified by flash chromatography (prepacked column silica 12g, diluent: cyclohexane-EtOAc (7-3), loading technique: dry load, flow rate 14mL/min) to afford the desired product **78** (101 mg, 48%) as brown solid. M.p: 117-119 °C

Chemical formula: C₁₅H₁₈N₂O₂

MW: 258.32 g/mol

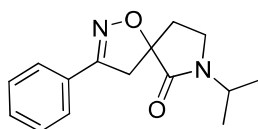
TLC: R_f = 0.4 (cyclohexan-EtOAc 50/50, detected under UV 254nm)

HPLC-MS (method in 5 min at pH 3.8): t_R = 2.80 min.

MS-(ES⁺): m/z 259 [M+H]⁺

³⁶⁴ *Tetrahedron Letters*, **2008**, 49, pp 5924-5927 (compound **3a**)

³⁶⁵ According to the protocol described in : *J.Org.Chem.* **2008**, 73, pp. 8627-30.



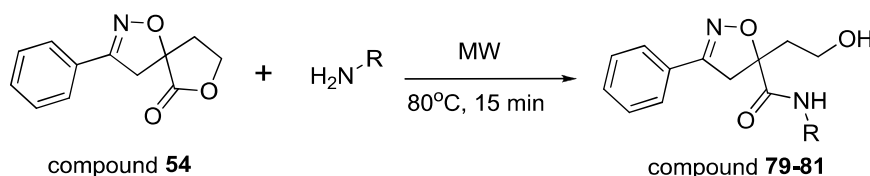
compound **78**

¹H-NMR (300 MHz, CDCl₃): δ 1.18 (d, J = 6.8 Hz, 3H, CH₃-isopropyl), 1.22 (d, J = 6.8 Hz, 3H, CH₃-isopropyl), 2.10 (dt, J = 8.0 Hz, J = 13.7 Hz, 1H), 2.51 (ddd, J = 2.4 Hz, J = 7.0 Hz, J = 13.7 Hz, 1H), 3.18 (d, J = 16.8 Hz, 1H, H-isoxazoline), 3.27-3.34 (m, 1H), 3.49 (dt, J = 10.0 Hz, J = 7.3 Hz, 1H), 3.92 (d, J = 16.8 Hz, 1H, H-isoxazoline), 4.41 (sept, J = 6.8 Hz, 1H, CH- isopropyl), 7.37-7.42 (m, 3H, H-Ar), 7.63-7.69 (m, 2H, H-Ar).

¹³C-NMR (75 MHz, CDCl₃): δ 19.7, 19.9, 33.0, 38.7, 42.0 (CH₂-isoxazoline), 43.7, 88.4 (C-O-isoxazoline), 126.9, 128.8, 129.3, 130.3, 156.1 (C=N-isoxazoline), 170.0 (C=O lactam).

This new structure has not been reported in literature. No results were found in Reaxys, Pubchem, eMolecules and Scifinder Scholar (verified on 28/03/2015).

General procedure for opening of lactone to form linear hydroxyl amide derivatives **79-81**



Compound **54** (100 mg, 0.46 mmol, 1 eq), and corresponding amine (3 eq) was vortexed in a sealed tube. The reaction was performed under microwave irradiation at 80°C for 15 minutes. After completion, the reaction mixture was diluted with dichloromethane and washed with aqueous solution saturated NH₄Cl (x3) and brine. The organic phase was dried over anhydrous magnesium sulfate and concentrated under reduced pressure to afford the desired compounds **79-81**.

5-(2-Hydroxy-ethyl)-3-phenyl-4,5-dihydro-isoxazole-N-prop-2-ynyl-5-carboxamide (**79**): according to the above procedure, desired compound **79** was obtained (102 mg, 82%) as beige solid. M.p.: 122-124 °C

Chemical formula: C₁₅H₁₆N₂O₃

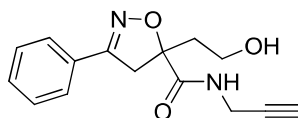
MW: 272.31 g/mol

HPLC-MS (method in 5 min at pH 3.8): t_R = 2.53 min

MS-(ES+) m/z 255 (base peak) ; 273 ([M+H]⁺, 60%)

MS-(ES-) m/z 271 ([M-H]⁻, base peak)

IR (cm⁻¹): 3361 (broad, O-H), 3223 (sharp, N-H), 3220 (narrow, -C≡C-H), 1665 (C=O stretch), 1510 (N-H bending), 1052 (C-N).



compound **79**

¹H-NMR (300 MHz, CDCl₃, ppm) δ 2.20-2.27 (m, 2H, CH and OH), 2.35-2.44 (m, 2H, CH₂), 3.47 (d, $J = 17.5$ Hz, 1H, H-isoxazoline), 3.78-3.83 (m, 3H, H-isoxazoline and 2H of CH₂), 3.94-4.03 (m, 1H, CH₂), 4.08-4.17 (m, 1H, CH₂), 7.23 (s, 1H, NH), 7.34-7.45 (m, 3H, H-Ar), 7.62-7.65 (m, 2H, H-Ar).

¹³C-NMR (75 MHz, CDCl₃, ppm) δ 29.3, 39.6, 44.7 (CH₂-isoxazoline), 58.6, 72.1, 78.6 (-C \equiv), 89.0 (C-O-isoxazoline), 126.9 (C-Ar), 128.5 (C-Ar), 128.9 (C-Ar), 130.9 (C-Ar), 158.0 (C=N-isoxazoline), 173.1 (C- amide).

HRMS (TOF, ES+) m/z [M+H]⁺ calculated for C₁₅H₁₇N₂O₃ 273.1239, found 273.1251.

This new structure has not been reported in literature. No results were found in Reaxys, Pubchem, eMolecules and Scifinder Scholar (verified on 28/03/2015).

5-(2-hydroxyethyl)-3-phenyl-N-propyl-4,5-dihydroisoxazole-5-carboxamide (**80**): according to the above procedure, desired compound **80** was obtained (99 mg, 78%) as beige solid. M.p: 111-112 °C

Chemical formula: C₁₅H₂₀N₂O₃

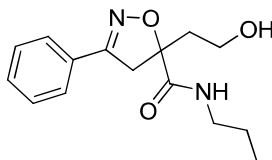
MW: 276.31 g/mol

HPLC-MS (method in 5 min at pH 3.8): $t_R = 2.63$ min

MS-(ES+): m/z 277 ([M+H]⁺, base peak)

MS-(ES-) m/z 275 ([M-H]⁻, base peak)

IR (cm⁻¹): 3320 (sharp, N-H), 3315 (broad, O-H), 1652 (C=O stretch), 1519 (N-H bending), 1051 (C-N)



compound **80**

¹H-NMR (300 MHz, CDCl₃, ppm) δ 0.91 (t, $J = 9.0$ Hz, 3H, CH₃), 1.50-1.58 (m, 2H, CH₂), 2.20-2.27 (m, 1H, CH₂), 2.32-2.39 (m, 1H, CH₂), 2.66 (br s, 1H, OH), 3.15-3.20 (m, 1H, CH₂), 3.22-3.34 (m, 1H, CH₂), 3.41-3.47 (d, $J = 18.0$ Hz, 1H, H-isoxazoline), 3.78-3.86 (m, 3H, 1H of isoxazoline and 2H of CH₂), 7.02 (br s, 1H, NH), 7.39-7.45 (m, 3H, H-Ar), 7.63- 7.65 (m, 2H, H-Ar).

$^{13}\text{C-NMR}$ (75 MHz, CDCl_3 , ppm) δ 11.4 (CH_3), 22.8 (CH_2), 39.9 (CH_2), 41.3 (CH_2), 44.8 (CH_2 -isoxazoline), 59.0 (CH_2), 89.5 (C-O-isoxazoline), 127.0 (Ar), 128.6 (Ar), 129.0 (Ar), 131.0 (Ar), 158.1 (C=N-isoxazoline), 173.3 (C-amide).

HRMS (TOF, ES+) m/z $[\text{M}+\text{H}]^+$ calculated for $\text{C}_{15}\text{H}_{21}\text{N}_2\text{O}_3$ 277.1552, found 277.1565.

This new structure has not been reported in literature. No results were found in Reaxys, Pubchem, eMolecules and Scifinder Scholar (verified on 28/03/2015).

N,5-bis(2-hydroxyethyl)-3-phenyl-4,5-dihydroisoxazole-5-carboxamide (**81**): according to the above procedure, desired compound **81** was obtained (83 mg, 65%) as white solid. M.p: 114-116 °C

Chemical formula: $\text{C}_{14}\text{H}_{18}\text{N}_2\text{O}_4$

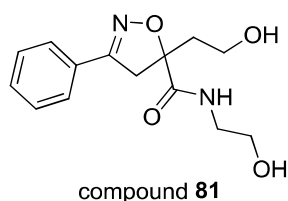
MW: 278.31 g/mol

HPLC-MS (method in 5 min at pH 3.8): $t_{\text{R}} = 2.32$ min

MS-(ES+) m/z 279 ($[\text{M}+\text{H}]^+$, base peak)

MS-(ES-) m/z 277 ($[\text{M}-\text{H}]^-$, base peak)

IR (cm^{-1}): 3392 (sharp, N-H), 3282 (broad, O-H), 3150 (broad, OH), 1656 (C=O), 1518 (N-H bending), 1065 (C-O), 1043 (C-N).



$^1\text{H-NMR}$ (300 MHz, $\text{DMSO-}d_6$, ppm) δ 2.03-2.13 (m, 2H, CH_2), 3.08-3.12 (m, 1H), 3.19-3.23 (m, 1H), 3.37-3.58 (m, 5H), 3.67 (d, $J = 17.4$ Hz, 1H, CH_2 -isoxazoline) 4.57 (t, $J = 5.1$ Hz, 1H, OH), 4.68 (t, $J = 5.4$ Hz, 1H, OH), 7.43-7.48 (m, 3H, H-Ar), 7.65-7.69 (m, 2H, H-Ar), 7.94 (t, $J = 5.7$ Hz, 1H, NH).

$^{13}\text{C-NMR}$ (75 MHz, $\text{DMSO-}d_6$, ppm) δ 40.0 (CH_2), 41.5 (CH_2), 43.4 (CH_2 -isoxazoline), 56.6 (CH_2), 59.5 (CH_2), 88.3 (C-O-isoxazoline), 126.7 (C-Ar), 128.8 (C-Ar), 128.9 (C-Ar), 130.4 (C-Ar), 157.0 (C=N-isoxazoline), 172.1 (C-amide).

HRMS (TOF, ES+) m/z $[\text{M}+\text{H}]^+$ calculated for $\text{C}_{14}\text{H}_{19}\text{N}_2\text{O}_4$ 279.1345, found 279.1353.

This new structure has not been reported in literature. No results were found in Reaxys, Pubchem, eMolecules and Scifinder Scholar (verified on 28/03/2015).

4.3. Molecular shape analysis and properties of synthesized fragments

Firstly, the 2D-structure of synthesized fragments was sketched by using MDL ISIS/Draw software. These structures were then added hydrogen and converted to 3D by CORINA software (trial version for academic, Molecular Networks Inc.). Based on these 3D-structures, ARIANA.Code software (trial version for academic, Molecular Networks Inc.) was then used to calculate the three principal moments of inertia, sorted by ascending magnitude I_1 , I_2 , and I_3 . Subsequently, normalization was performed by dividing the two lower PMI-values (I_1 and I_2) by the highest value (I_3), generating two characteristic values of normalized PMI ratios (NPRs) for each compound ($\text{NPR1} = I_1/I_3$ and $\text{NPR2} = I_2/I_3$).³⁶⁶ In addition, ARIANA.Code also calculated others 2D- molecular descriptors, e.g. molecular weight (MW), Hydrogen bond donor (HDon), Hydrogen bond acceptor (HAcc), Total polar surface area (TPSA), clogP, cLogS, number of rotatable bond (NRot). The results are presented in Table 1.

4.4. Protocol for solubility determination³⁶⁷

10 μL of a solution in DMSO (100 mM) of the synthesized fragments was added to 490 μL of MeOH or PBS at pH 7.4. The samples were gently shaken for 24 h at room temperature, then centrifuged for 5 minutes, and filtered over 0.45 μm filters. An amount equal to 10 μL of each filtrate solution was added to 990 μL of MeOH and analyzed by HPLC-MS. The solubility was determined by the ratio of mass signal areas PBS/MeOH.

³⁶⁶ Sauer, W. H. B.; Schwarz, M. K. *J. Chem. Inf. Comput. Sci.* **2003**, 43, 987-1003

³⁶⁷ This in-house method was developed from a protocol which is described in literature: Colclough, *et al. Bioorg. Med. Chem.* **2008**, 16, 6611–6616.

Experimental section

Table 1. 2D and 3D-molecular descriptors of the synthesized 2-isoxazoline fragments

Cpds	MW	HDon	HAcc	TPSA	clogP	cLogS	NRot	NPR1	NPR2
50	249.26	1	5	68.12	1.53	-2.20	5	0.10	0.96
51	291.30	0	6	74.19	3.02	-3.69	6	0.19	0.89
52	277.27	0	6	74.19	1.67	-2.63	6	0.40	0.74
53	249.22	2	6	96.19	1.05	-2.13	4	0.31	0.86
54	217.22	0	4	47.89	1.96	-2.78	1	0.16	0.98
55	205.21	1	4	58.89	1.93	-2.39	2	0.15	0.93
56	212.25	0	3	45.38	2.36	-3.05	2	0.12	0.93
57	212.25	0	3	45.38	2.36	-3.05	2	0.12	0.93
67	155.15	0	4	47.89	0.29	-1.06	0	0.32	0.91
68	193.29	0	2	21.59	3.45	-3.34	0	0.40	0.98
69	181.19	0	4	47.89	0.46	-1.30	1	0.21	0.93
70	225.23	0	2	21.59	3.25	-3.61	2	0.31	0.99
71	215.29	0	2	21.59	3.47	-3.73	0	0.41	0.82
72	216.28	1	3	33.62	2.45	-3.05	1	0.13	0.97
73	154.21	1	3	33.62	0.79	-1.33	0	0.25	0.96
74	168.24	1	3	33.62	1.13	-1.65	0	0.24	0.94
75	140.18	1	3	33.62	0.45	-0.99	0	0.25	0.97
76	180.25	1	3	33.62	0.96	-1.57	1	0.16	0.97
78	258.32	0	4	41.9	2.45	-3.30	2	0.14	0.96
79	272.30	2	5	70.92	1.18	-2.22	6	0.26	0.88
80	276.33	2	5	70.92	1.67	-2.56	6	0.27	0.85
81	278.30	3	6	91.15	0.19	-1.60	6	0.23	0.89

In 72-76 fragments, molecular weight is calculated on free base form.

This page intentionally left blank

Annexes

Annex 1 - Abbreviations

°C	degree Celsius
¹³ C NMR	carbon-13 nuclear magnetic resonance
¹ H NMR	proton nuclear magnetic resonance
3D	three dimensional
Ac	acetyl
ACP	acyl carrier protein
AFB	acid-fast bacilli
AIDS	acquired immune deficiency syndrome
aq	aqueous
ATP	adenosine triphosphate
AUC	area under the curve
AZT	azidothymidine (zidovudine)
BCG	bacillus Calmette–Guérin
Boc	<i>tert</i> -butoxycarbonyl
bp	boiling point
br	broad
calcd.	calculated
CDC	Centers for Disease Control and Prevention
CL _{int}	intrinsic clearance
cLogP	calculated logP
clogS	calculated logS
CNS	central nervous system
COSY	correlation spectroscopy
CYP 450	cytochrome P450
d	doublet
Da	dalton
DCE	1,2-dichloroethane
DCM	dichloromethane
dd	doublet of doublet
ddd	double of doublet of doublet
dec.	decomposition
DEPT	distortionless enhancement by polarization transfer
DHFR	dihydrofolate reductase
DHPS	dihydropteroate synthase
DIPEA	N,N-diisopropylethylamine
DMA	dimethylacetamide
DMAP	4-(N,N-dimethylamino) pyridine
DMF	N,N-dimethylformamide
DMSO	dimethyl sulfoxide
DNA	deoxyribonucleic acid
DOTS	Directly Observed Treatment Short course
DR-TB	drug-resistant tuberculosis
DS-TB	drug-susceptible tuberculosis
dt	doublet of triplet
<i>E. coli</i>	<i>Escherichia coli</i>

Annex 1 - Abbreviations

e.g.	exempli gratia (exemple given)
EC ₅₀	effective concentration at 50%
EMA	European Medicines Agency
EMB	ethambutol
equiv	equivalent(s)
ES-	negative electrospray
ES+	positive electrospray
ESI	electrospray ionization
Et	ethyl
ETH	ethionamide
EtOAc	ethyl acetate
EtOH	ethanol
FAD	flavin adenine dinucleotide
FAS	fatty acid synthase
FBDD	fragment-based drug discovery
FDA	food and drug agency
FT-IR	Fourier transform infrared spectroscopy
g	gram
h	hour(s)
HA	heavy atom
HAC	heavy atom count
HBA	Hydrogen bond acceptor
HBD	Hydrogen bond donor
H-bond	hydrogen bond
HCS	high content screening
HEPES	2-[4-(2-hydroxyethyl)piperazin-1-yl]ethanesulfonic acid
HIV	human immunodeficiency virus
H-MabA	histidine-tagged MabA protein
HMBC	heteronuclear multiple-bond correlation
HPLC	high performance liquid chromatography
HRMS	high-resolution mass spectrometry
HSQC	heteronuclear single quantum coherence
HTH	helix-turn-helix
HTS	high-throughput screening
Hz	Hertz
IC ₅₀	inhibitory concentration at 50%
IGRA	interferon-g release assays
INH	isoniazid
<i>i</i> -PrOH	isopropanol
IR	infrared
ITC	isothermal calorimetry
<i>J</i>	coupling constants
KARs	β-ketoacyl-ACP reductases
K _d	dissociation constant
kDa	kilodalton
K _i	inhibitor constant
L	liter
LC-MS	liquid chromatography-mass spectrometry

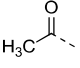
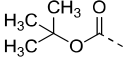
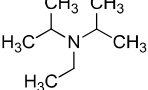
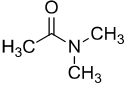
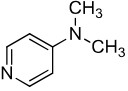
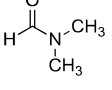
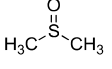
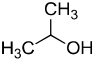
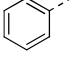
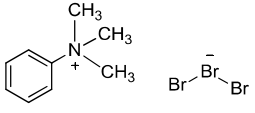
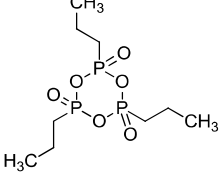
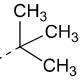
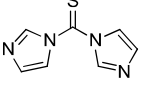
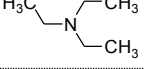

Annex 1 - Abbreviations

LC-MS/MS	liquid chromatography-tandem mass spectrometry
LE	ligand efficiency
LTBI	latent tuberculosis infection
m	multiplet
<i>m</i> -	meta-
M	molar or molarity
<i>m/z</i>	mass/charge
mabA	mycolic acid biosynthesis A
MALDI	Matrix-assisted laser desorption/ionization
MDR-TB	multidrug- resistant tuberculosis
Me	methyl
MeCN/CH ₃ CN	acetonitrile
MeOH	methanol
mg	milligram
MHz	megahertz
MIC	minimum inhibitory concentration
min	minute(s)
mL	milliliter
μL	microliter
mmol	millimole(s)
mol	mole(s)
m.p.	melting point
mpk	miligrams per kilograms (mg/kg)
MRM	multiple reaction monitoring
MTBC	<i>Mycobacterium tuberculosis</i> complex
MW	molecular weight
MWI	microwave irradiation
NAAT	Nucleic Acid Amplification Techniques
NAD ⁺	nicotinamide adenine dinucleotide (oxidized form)
NADH	nicotinamide adenine dinucleotide (reduced form)
NADP ⁺	nicotinamide adenine dinucleotide phosphate (oxidized form)
NADPH	nicotinamide adenine dinucleotide phosphate (reduced form)
NCS	<i>N</i> -chlorosuccinimide
nM	nanomolar
NMR	nuclear magnetic resonance
NOESY	nuclear overhauser effect spectroscopy
NRot	number of rotatable bonds
NTP	National Tuberculosis Control Programme
<i>o</i> -	ortho-
ORF	open reading frame
<i>p</i> -	para-
PBS	phosphate buffer saline
PDA	photo diode array
PDB	Protein Data Bank
Ph	phenyl
polyHis	poly histidines
PPD	purified protein derivatives
ppm	parts per million

Annex 1 - Abbreviations

PTAP	phenyl trimethyl ammonium perbromide (tribromide)
PZA	pyrazinamide
q	quartet
qt	quartet of triplet
quint	quintet
Rf	retardation factor
RMP/RIF	rifampicin
RNA	ribonucleic acid
Ro3	rule of three
rt	room temperature
s	singlet
s	second
SAR	structure and activity relationship
sat.	saturated
SDS-PAGE	sodium dodecyl sulfate-polyacrylamide gel electrophoresis
sext	sextet
SM	streptomycin
SPR	surface plasmon resonance
STD	saturation transfer difference
t	triplet
$t_{1/2}$	half-life
T3P [®]	propylphosphonic anhydride
TB	tuberculosis
TBDB	Tuberculosis Database
<i>t</i> -Bu	tert-butyl
TCDI	1,1'-thiocarbonyldiimidazole
TDM	trehalose-dimycolate
TDR-TB	totally drug resistant tuberculosis
TEA	triethylamine
temp	temperature
TFA	trifluoroacetic acid
THF	tetrahydrofuran
TLC	thin layer chromatography
Tm	melting temperature
TOF	Time of Flight
TPSA	total polar surface area
t_R	retention time
TSA	thermal-shift assay
TST	tuberculin skin test
UHPLC	ultra high-performance liquid chromatography
UV	ultraviolet
WaterLOGSY	Water-Ligand Observed Gradient Spectroscopy
WHO	World Health Organization
XDR-TB	extensively drug-resistant tuberculosis
XXDR-TB	extremely drug-resistant tuberculosis
δ	chemical shifts

Annex 2 – Chemical Abbreviations and Structure

Abbreviation	Chemical name	Structure
Ac	acetyl	
Boc	<i>tert</i> -butoxycarbonyl	
DCE	1,2-dichloroethane	$\text{ClH}_2\text{C}-\text{CH}_2\text{Cl}$
DIPEA	<i>N,N</i> -diisopropylethylamine	
DMA	dimethylacetamide	
DMAP	4-(<i>N,N</i> -dimethylamino) pyridine	
DMF	<i>N,N</i> -dimethylformamide	
DMSO	dimethyl sulfoxide	
Et	ethyl	$\text{H}_3\text{C}-\text{CH}_2-$
<i>i</i> -PrOH	isopropanol	
Me	methyl	$\text{H}_3\text{C}-$
MeOH	methanol	CH_3OH
Ph	phenyl	
PTAP	phenyltrimethyl ammonium perbromide	
T3P	propylphosphonic anhydride	
<i>t</i> -Bu	<i>tert</i> -butyl	
TCDI	1,1'-thiocarbonyldiimidazole	
TEA	triethylamine	
TFA	trifluoroacetic acid	$\text{F}_3\text{C}-\text{COOH}$
THF	tetrahydrofuran	

Annex 3: List of amino acids and their abbreviations

Complete name	Code 3 letters	Code 1 letter
Alanine	Ala	A
Arginine	Arg	R
Asparagine	Asn	N
Aspartic acid	Asp	D
Cysteine	Cys	C
Glutamic acid	Glu	E
Glutamine	Gln	Q
Glycine	Gly	G
Histidine	His	H
Isoleucine	Ile	I
Leucine	Leu	L
Lysine	Lys	K
Methionine	Met	M
Phenylalanine	Phe	P
Proline	Pro	P
Serine	Ser	S
Threonine	Thr	T
Tryptophane	Trp	W
Tyrosine	Tyr	Y
Valine	Val	V

Bibliography

1. Andersen, P.; Woodworth, J. S. Tuberculosis Vaccines - Rethinking the Current Paradigm. *Trends Immunol.* **2014**, *35*, 387–395.
2. Sarkar, S.; Suresh, M. R. An Overview of Tuberculosis Chemotherapy - a Literature Review. *J. Pharm. Pharm. Sci.* **2011**, *14*, 148–161.
3. Lienhardt, C.; Glaziou, P.; Uplekar, M.; Lönnroth, K.; Getahun, H.; Raviglione, M. Global Tuberculosis Control: Lessons Learnt and Future Prospects. *Nat. Rev. Microbiol.* **2012**, *10*, 407–416.
4. Sharma, S. K.; Mohanan, S.; Sharma, A. Relevance of Latent TB Infection in Areas of High TB Prevalence. *Chest* **2012**, *142*, 761–773.
5. World Health Organization. Global Tuberculosis Report 2014 (WHO/HTM/TB/2014.08). **2014**.
6. Mahajan, R. Bedaquiline: First FDA-Approved Tuberculosis Drug in 40 Years. *Int. J. Appl. basic Med. Res.* **2013**, *3*, 1–2.
7. Ryan, N. J.; Lo, J. H. Delamanid: First Global Approval. *Drugs* **2014**, *74*, 1041–1045.
8. Baker, M. Fragment-Based Lead Discovery Grows Up. *Nat. Rev. Drug Discov.* **2013**, *12*, 5–7.
9. Villemagne, B. Conception, Synthèse et Développement D'inhibiteurs Du Represseur Transcriptionnel Mycobactérien EthR Selon Une Approche Par Fragments, Université Lille 2 Droit et Santé, Thèse de doctorat, **2012**.
10. Marrakchi, H.; Ducasse, S.; Labesse, G.; Montrozier, H.; Margeat, E.; Emorine, L.; Charpentier, X.; Daffé, M.; Quémard, A. MabA (FabG1), a Mycobacterium Tuberculosis Protein Involved in the Long-Chain Fatty Acid Elongation System FAS-II. *Microbiology* **2002**, *148*, 951–960.
11. Daniel, T. M. The History of Tuberculosis. *Respir. Med.* **2006**, *100*, 1862–1870.
12. Raviglione, M. C.; Snider, D. E.; Kochi, A. Global Epidemiology of Tuberculosis. Morbidity and Mortality of a Worldwide Epidemic. *JAMA* **1995**, *273*, 220–226.
13. Glaziou, P.; Falzon, D.; Floyd, K.; Raviglione, M. Global Epidemiology of Tuberculosis. *Semin. Respir. Crit. Care Med.* **2013**, *34*, 3–16.
14. Diseases, L.; Maugeri, F. S. First Tuberculosis Cases in Italy Resistant to All Tested Drugs. *Eurosurveillance* **2012**, *12*, 17–18.
15. Rowland, K. Totally Drug-Resistant TB Emerges in India. *Nature* **2012**, 1–8.
16. Klopper, M.; Warren, R. M.; Hayes, C.; van Pittius, N. C. G.; Streicher, E. M.; Müller, B.; Sirgel, F. A.; Chabula-Nxiweni, M.; Hoosain, E.; Coetzee, G.; van Helden, P. D.; Victor, T. C.; Trollip, A. P. Emergence and Spread of Extensively and Totally Drug-Resistant Tuberculosis, South Africa. *Emerg. Infect. Dis.* **2013**, *19*, 449–455.
17. Velayati, A. A.; Masjedi, M. R.; Farnia, P.; Tabarsi, P.; Ghanavi, J.; Ziazarifi, A. H.; Hoffner, S. E. Emergence of New Forms of Totally Drug-Resistant Tuberculosis Bacilli: Super Extensively Drug-Resistant Tuberculosis or Totally Drug-Resistant Strains in Iran. *Chest* **2009**, *136*, 420–425.
18. Velayati, A. A.; Farnia, P.; Masjedi, M. R. Letter to Editor The Totally Drug Resistant Tuberculosis (TDR-TB). *Int J Clin Exp Med* **2013**, *6*, 307–309.

Bibliography

19. "Institute de la Vielle Sanitaire - Department of infectious Diseases." *Epidemiology of Tuberculosis in France*; **2014**.
20. Girard, D.; Antoine, D.; Che, D. Epidemiology of Pulmonary Tuberculosis in France. Can the Hospital Discharge Database Be a Reliable Source of Information? *Médecine Mal. Infect.* **2014**, *44*, 509–514.
21. Bernard, C.; Brossier, F.; Sougakoff, W.; Veziris, N.; Frechet-Jachym, M.; Metivier, N.; Renvoisé, A.; Robert, J.; Jarlier, V.; MDR-TB Management group of the NRC. A Surge of MDR and XDR Tuberculosis in France among Patients Born in the Former Soviet Union. *Euro Surveill.* **2013**, *18*, 20555.
22. Khuê, P. M.; Truffot-Pernot, C.; Texier-Maugein, J.; Jarlier, V.; Robert, J. A 10-Year Prospective Surveillance of Mycobacterium Tuberculosis Drug Resistance in France 1995-2004. *Eur. Respir. J.* **2007**, *30*, 937–944.
23. Huong, N. T.; Duong, B. D.; Co, N. V.; Quy, H. T.; Tung, L. B.; Bosman, M.; Gebhardt, A.; Velema, J. P.; Broekmans, J. F.; Borgdorff, M. W. Establishment and Development of the National Tuberculosis Control Programme in Vietnam. *Int. J. Tuberc. Lung Dis.* **2005**, *9*, 151–156.
24. Vietnam StopTB <http://vstp.org/> (accessed Apr 13, 2015).
25. Brosch, R.; Gordon, S. V.; Marmiesse, M.; Brodin, P.; Buchrieser, C.; Eiglmeier, K.; Garnier, T.; Gutierrez, C.; Hewinson, G.; Kremer, K.; Parsons, L. M.; Pym, A. S.; Samper, S.; van Soolingen, D.; Cole, S. T. A New Evolutionary Scenario for the Mycobacterium Tuberculosis Complex. *Proc. Natl. Acad. Sci.* **2002**, *99*, 3684–3689.
26. *Mycobacteria and TB*; Kaufmann, S. H. E.; Hahn, H., Eds.; Issues in Infectious Diseases; S. Karger AG, **2002**; Vol. 2.
27. Glassroth, J. Pulmonary Disease due to Nontuberculous Mycobacteria. *Chest* **2008**, *133*, 243–251.
28. Brown-Elliott, B. A.; Griffith, D. E.; Wallace, R. J. Newly Described or Emerging Human Species of Nontuberculous Mycobacteria. *Infect. Dis. Clin. North Am.* **2002**, *16*, 187–220.
29. Hett, E. C.; Rubin, E. J. Bacterial Growth and Cell Division: A Mycobacterial Perspective. *Microbiol. Mol. Biol. Rev.* **2008**, *72*, 126–156, table of contents.
30. Abdallah, A. M.; Gey van Pittius, N. C.; Champion, P. A. D.; Cox, J.; Luirink, J.; Vandenbroucke-Grauls, C. M. J. E.; Appelmek, B. J.; Bitter, W. Type VII Secretion--Mycobacteria Show the Way. *Nat. Rev. Microbiol.* **2007**, *5*, 883–891.
31. Takayama, K.; Wang, C.; Besra, G. S. Pathway to Synthesis and Processing of Mycolic Acids in Mycobacterium Tuberculosis. *Clin. Microbiol. Rev.* **2005**, *18*, 81–101.
32. Asselineau, J.; Lederer, E. Structure of the Mycolic Acids of Mycobacteria. *Nature* **1950**, *166*, 782–783.
33. Marrakchi, H.; Lanéelle, M.-A.; Daffé, M. Mycolic Acids: Structures, Biosynthesis, and Beyond. *Chem. Biol.* **2014**, *21*, 67–85.
34. Barry, C. E.; Lee, R. E.; Mdluli, K.; Sampson, a E.; Schroeder, B. G.; Slayden, R. a; Yuan, Y. Mycolic Acids: Structure, Biosynthesis and Physiological Functions. *Prog. Lipid Res.* **1998**, *37*, 143–179.
35. Layre, E.; Collmann, A.; Bastian, M.; Mariotti, S.; Czaplicki, J.; Prandi, J.; Mori, L.; Stenger, S.; De Libero, G.; Puzo, G.; Gilleron, M. Mycolic Acids Constitute a Scaffold for Mycobacterial Lipid Antigens Stimulating CD1-Restricted T Cells. *Chem. Biol.* **2009**, *16*, 82–92.
36. Bhowruth, V.; Alderwick, L. J.; Brown, A. K.; Bhatt, A.; Besra, G. S. Tuberculosis: A Balanced Diet of Lipids and Carbohydrates. *Biochem. Soc. Trans.* **2008**, *36*, 555–565.

Bibliography

37. Schroeder, E. K.; de Souza, N.; Santos, D. S.; Blanchard, J. S.; Basso, L. A. Drugs That Inhibit Mycolic Acid Biosynthesis in Mycobacterium Tuberculosis. *Curr. Pharm. Biotechnol.* **2002**, *3*, 197–225.
38. Lew, J. M.; Kapopoulou, A.; Jones, L. M.; Cole, S. T. TubercuList--10 Years After. *Tuberculosis (Edinb).* **2011**, *91*, 1–7.
39. Cole, S. T.; Brosch, R.; Parkhill, J.; Garnier, T.; Churcher, C.; Harris, D.; Gordon, S. V.; Eiglmeier, K.; Gas, S.; Barry, C. E.; Tekaia, F.; Badcock, K.; Basham, D.; Brown, D.; Chillingworth, T.; Connor, R.; Davies, R.; Devlin, K.; Feltwell, T.; Gentles, S.; Hamlin, N.; Holroyd, S.; Hornsby, T.; Jagels, K.; Krogh, A.; McLean, J.; Moule, S.; Murphy, L.; Oliver, K.; Osborne, J.; Quail, M. A.; Rajandream, M. A.; Rogers, J.; Rutter, S.; Seeger, K.; Skelton, J.; Squares, R.; Squares, S.; Sulston, J. E.; Taylor, K.; Whitehead, S.; Barrell, B. G. Deciphering the Biology of Mycobacterium Tuberculosis from the Complete Genome Sequence. *Nature* **1998**, *393*, 537–544.
40. Reddy, T. B. K.; Riley, R.; Wymore, F.; Montgomery, P.; DeCaprio, D.; Engels, R.; Gellesch, M.; Hubble, J.; Jen, D.; Jin, H.; Koehrsen, M.; Larson, L.; Mao, M.; Nitzberg, M.; Sisk, P.; Stolte, C.; Weiner, B.; White, J.; Zachariah, Z. K.; Sherlock, G.; Galagan, J. E.; Ball, C. A.; Schoolnik, G. K. TB Database: An Integrated Platform for Tuberculosis Research. *Nucleic Acids Res.* **2009**, *37*, D499–D508.
41. Kaufmann, S. H. How Can Immunology Contribute to the Control of Tuberculosis? *Nat. Rev. Immunol.* **2001**, *1*, 20–30.
42. Van Lettow, M.; Whalen, C. Tuberculosis. In *Nutrition and Health: Nutrition and Health in Developing Countries*; Semba, R. D.; Bloem, M. W., Eds.; Humana Press: Totowa, NJ, **2008**; Vol. 1, pp. 275–306.
43. Medecins Sans Frontieres. *Tuberculosis-Practical Guide for Clinicians, Nurses, Laboratory Technicians and Medical Auxiliaries*; **2014**.
44. Esmail, H.; Barry, C. E.; Young, D. B.; Wilkinson, R. J. The Ongoing Challenge of Latent Tuberculosis. *Philos. Trans. R. Soc. Lond. B. Biol. Sci.* **2014**, *369*, 20130437.
45. Ahmad, S.; Mokaddas, E. Recent Advances in the Diagnosis and Treatment of Multidrug-Resistant Tuberculosis. *Respir. Med.* **2009**, *103*, 1777–1790.
46. Ahmad, S. New Approaches in the Diagnosis and Treatment of Latent Tuberculosis Infection. *Respir. Res.* **2010**, *11*, 169.
47. Lange, C.; Mori, T. Advances in the Diagnosis of Tuberculosis. *Respirology* **2010**, *15*, 220–240.
48. *Tuberculosis - Current Issues in Diagnosis and Management*; Mahboub, H. B.; Vats, M. G., Eds.; InTech, **2013**.
49. Martinez, V.; Castilla-Lievre, M. A.; Guillet-Caruba, C.; Grenier, G.; Fior, R.; Desarnaud, S.; Doucet-Populaire, F.; Boué, F. (18)F-FDG PET/CT in Tuberculosis: An Early Non-Invasive Marker of Therapeutic Response. *Int. J. Tuberc. Lung Dis.* **2012**, *16*, 1180–1185.
50. Nicol, M. P. New Developments in the Laboratory Diagnosis of Tuberculosis. *Contin. Med. Educ.* **2010**, *28*, 4–6.
51. Dorman, S. E. New Diagnostic Tests for Tuberculosis: Bench, Bedside, and Beyond. *Clin. Infect. Dis.* **2010**, *50 Suppl 3*, S173–S177.
52. Anochie, P. I.; Onyeneke, E. C.; Ogu, A. C.; Onyeozirila, A. C.; Aluru, S.; Onyejebu, N.; Zhang, J.; Efere, L.; Adetunji, M. A.; Gabriel, J.; Sánchez, B. Review Recent Advances in the Diagnosis of Mycobacterium Tuberculosis. *GERMS* **2012**, *2*, 110–120.

Bibliography

53. Roy, A.; Eisenhut, M.; Harris, R. J.; Rodrigues, L. C.; Sridhar, S.; Habermann, S.; Snell, L.; Mangtani, P.; Adetifa, I.; Lalvani, A.; Abubakar, I. Effect of BCG Vaccination against Mycobacterium Tuberculosis Infection in Children: Systematic Review and Meta-Analysis. *BMJ* **2014**, *349*, g4643.
54. *Understanding Tuberculosis – New Approaches to Fighting Against Drug Resistance*; Cardona, P.-J., Ed.; First.; InTech: Rijeka, **2012**.
55. Rodrigues, L. C.; Diwan, V. K.; Wheeler, J. G. Protective Effect of BCG against Tuberculous Meningitis and Miliary Tuberculosis: A Meta-Analysis. *Int. J. Epidemiol.* **1993**, *22*, 1154–1158.
56. Trunz, B. B.; Fine, P.; Dye, C. Effect of BCG Vaccination on Childhood Tuberculous Meningitis and Miliary Tuberculosis Worldwide: A Meta-Analysis and Assessment of Cost-Effectiveness. *Lancet* **2006**, *367*, 1173–1180.
57. Colditz, G. A.; Brewer, T. F.; Berkey, C. S.; Wilson, M. E.; Burdick, E.; Fineberg, H. V.; Mosteller, F. Efficacy of BCG Vaccine in the Prevention of Tuberculosis. Meta-Analysis of the Published Literature. *JAMA* **1994**, *271*, 698–702.
58. Colditz, G. A.; Berkey, C. S.; Mosteller, F.; Brewer, T. F.; Wilson, M. E.; Burdick, E.; Fineberg, H. V. The Efficacy of Bacillus Calmette-Guérin Vaccination of Newborns and Infants in the Prevention of Tuberculosis: Meta-Analyses of the Published Literature. *Pediatrics* **1995**, *96*, 29–35.
59. Brewer, T. F. Preventing Tuberculosis with Bacillus Calmette-Guérin Vaccine: A Meta-Analysis of the Literature. *Clin. Infect. Dis.* **2000**, *31 Suppl 3*, S64–S67.
60. Sterne, J. A.; Rodrigues, L. C.; Guedes, I. N. Does the Efficacy of BCG Decline with Time since Vaccination? *Int. J. Tuberc. Lung Dis.* **1998**, *2*, 200–207.
61. Abubakar, I.; Pimpin, L.; Ariti, C.; Beynon, R.; Mangtani, P.; Sterne, J. A. C.; Fine, P. E. M.; Smith, P. G.; Lipman, M.; Elliman, D.; Watson, J. M.; Drumright, L. N.; Whiting, P. F.; Vynnycky, E.; Rodrigues, L. C. Systematic Review and Meta-Analysis of the Current Evidence on the Duration of Protection by Bacillus Calmette-Guérin Vaccination against Tuberculosis. *Health Technol. Assess.* **2013**, *17*, 1–372, v – vi.
62. Kawaida, M.; Fukuda, H.; Kohno, N.; Fujii, M.; Tanaka, J.; Inuyama, Y. BCG and Vole Bacillus Vaccines in the Prevention of Tuberculosis in Adolescence and Early Adult Life. *Bull. World Health Organ.* **1972**, *46*, 371–385.
63. Aronson, N. E.; Santosham, M.; Comstock, G. W.; Howard, R. S.; Moulton, L. H.; Rhoades, E. R.; Harrison, L. H. Long-Term Efficacy of BCG Vaccine in American Indians and Alaska Natives: A 60-Year Follow-up Study. *JAMA* **2004**, *291*, 2086–2091.
64. Rodrigues, L. C.; Pereira, S. M.; Cunha, S. S.; Genser, B.; Ichihara, M. Y.; de Brito, S. C.; Hijjar, M. A.; Dourado, I.; Cruz, A. A.; Sant’Anna, C.; Bierrenbach, A. L.; Barreto, M. L. Effect of BCG Revaccination on Incidence of Tuberculosis in School-Aged Children in Brazil: The BCG-REVAC Cluster-Randomised Trial. *Lancet* **2005**, *366*, 1290–1295.
65. Barreto, M. L.; Pereira, S. M.; Ferreira, A. A. BCG Vaccine: Efficacy and Indications for Vaccination and Revaccination. *J. Pediatr. (Rio. J.)*. **2006**, *82*, S45–S54.
66. Hesselning, A. C.; Marais, B. J.; Gie, R. P.; Schaaf, H. S.; Fine, P. E. M.; Godfrey-Faussett, P.; Beyers, N. The Risk of Disseminated Bacille Calmette-Guerin (BCG) Disease in HIV-Infected Children. *Vaccine* **2007**, *25*, 14–18.
67. Ottenhoff, T. H. M.; Kaufmann, S. H. E. Vaccines against Tuberculosis: Where Are We and Where Do We Need to Go? *PLoS Pathog.* **2012**, *8*, e1002607.

Bibliography

68. Zwerling, A.; Behr, M. A.; Verma, A.; Brewer, T. F.; Menzies, D.; Pai, M. The BCG World Atlas: A Database of Global BCG Vaccination Policies and Practices. *PLoS Med.* **2011**, *8*, e1001012.
69. Montagnani, C.; Chiappini, E.; Galli, L.; de Martino, M. Vaccine against Tuberculosis: What's New? *BMC Infect. Dis.* **2014**, *14 Suppl 1*, S2.
70. Kaufmann, S. H. E. Tuberculosis Vaccine Development: Strength Lies in Tenacity. *Trends Immunol.* **2012**, *33*, 373–379.
71. The Working Group on New TB Vaccines - Stop TB Partnership <http://www.newtbvaccines.org/vaccine-candidates/> (accessed Apr 13, 2015).
72. Kaufmann, S. H. E. Tuberculosis Vaccines: Time to Think about the next Generation. *Semin. Immunol.* **2013**, *25*, 172–181.
73. Wilkie, M. E. M.; McShane, H. TB Vaccine Development: Where Are We and Why Is It so Difficult? *Thorax* **2014**, *70*, 299–301.
74. Tameris, M. D.; Hatherill, M.; Landry, B. S.; Scriba, T. J.; Snowden, M. A.; Lockhart, S.; Shea, J. E.; McClain, J. B.; Hussey, G. D.; Hanekom, W. A.; Mahomed, H.; McShane, H. Safety and Efficacy of MVA85A, a New Tuberculosis Vaccine, in Infants Previously Vaccinated with BCG: A Randomised, Placebo-Controlled Phase 2b Trial. *Lancet* **2013**, *381*, 1021–1028.
75. Zhang, A.; Lessem, E. *An Activist's Guide to Tuberculosis Drugs*; **2014**.
76. WHO. *Treatment of Tuberculosis Guidelines*; **2010**.
77. Zumla, A.; Nahid, P.; Cole, S. T. Advances in the Development of New Tuberculosis Drugs and Treatment Regimens. *Nat. Rev. Drug Discov.* **2013**, *12*, 388–404.
78. Zhang, Y.; Yew, W. W. Mechanisms of Drug Resistance in Mycobacterium Tuberculosis. *Int. J. Tuberc. Lung Dis.* **2009**, *13*, 1320–1330.
79. Lienhardt, C.; Vernon, A.; Raviglione, M. C. New Drugs and New Regimens for the Treatment of Tuberculosis: Review of the Drug Development Pipeline and Implications for National Programmes. *Curr. Opin. Pulm. Med.* **2010**, *16*, 186–193.
80. Swindells, S. New Drugs to Treat Tuberculosis. *F1000 Med. Rep.* **2012**, *4*, 12.
81. Casenghi, M. *Development of New Drugs for TB Chemotherapy: Analysis of the Current Drug Pipeline*; **2006**; Vol. 116.
82. Böttger, E. C.; Springer, B. Tuberculosis: Drug Resistance, Fitness, and Strategies for Global Control. *Eur. J. Pediatr.* **2008**, *167*, 141–148.
83. Zhang, Y. The Magic Bullets and Tuberculosis Drug Targets. *Annu. Rev. Pharmacol. Toxicol.* **2005**, *45*, 529–564.
84. The Critical Path to TB Drug Regimens <http://www.cptrinitiative.org/> (accessed Mar 8, 2015).
85. Leandro dos Santos, J.; Dutra, L. A.; Regina, T.; de Melo, T. R. F.; Chin, C. M. New Antitubercular Drugs Designed by Molecular Modification. In *Understanding Tuberculosis – New Approaches to Fighting Against Drug Resistance*; **2011**; pp. 169–186.
86. Asif, M. Rifampin and Their Analogs: A Development of Antitubercular Drugs. *World J. Org. Chem.* **2013**, *1*, 14–19.

Bibliography

87. Zhang, Y.; Post-Martens, K.; Denkin, S. New Drug Candidates and Therapeutic Targets for Tuberculosis Therapy. *Drug Discov. Today* **2006**, *11*, 21–27.
88. Dooley, K. E.; Obuku, E. a.; Durakovic, N.; Belitsky, V.; Mitnick, C.; Nuermberger, E. L. World Health Organization Group 5 Drugs for the Treatment of Drug-Resistant Tuberculosis: Unclear Efficacy or Untapped Potential? *J. Infect. Dis.* **2013**, *207*, 1352–1358.
89. Koul, A.; Arnoult, E.; Lounis, N.; Guillemont, J.; Andries, K. The Challenge of New Drug Discovery for Tuberculosis. *Nature* **2011**, *469*, 483–490.
90. Villemagne, B.; Crauste, C.; Flipo, M.; Baulard, A. R.; Déprez, B.; Willand, N. Tuberculosis: The Drug Development Pipeline at a Glance. *Eur. J. Med. Chem.* **2012**, *51*, 1–16.
91. Wolff, K. A.; Nguyen, L. Strategies for Potentiation of Ethionamide and Folate Antagonists against Mycobacterium Tuberculosis. *Expert Rev. Anti. Infect. Ther.* **2012**, *10*, 971–981.
92. Pieren, M.; Tigges, M. Adjuvant Strategies for Potentiation of Antibiotics to Overcome Antimicrobial Resistance. *Curr. Opin. Pharmacol.* **2012**, *12*, 551–555.
93. Wolff, K. A.; Sherman, M.; Nguyen, L. *Potentiation of Available Antibiotics by Targeting Resistance – An Emerging Trend in Tuberculosis Drug Development*; **2010**.
94. NCT02333799 - ClinicalTrials <https://clinicaltrials.gov> (accessed Apr 30, 2015).
95. Shuker, S. B.; Hajduk, P. J.; Meadows, R. P.; Fesik, S. W. Discovering High-Affinity Ligands for Proteins: SAR by NMR. *Science* **1996**, *274*, 1531–1534.
96. Chessari, G.; Woodhead, A. J. From Fragment to Clinical Candidate—a Historical Perspective. *Drug Discov. Today* **2009**, *14*, 668–675.
97. Bollag, G.; Tsai, J.; Zhang, J.; Zhang, C.; Ibrahim, P.; Nolop, K.; Hirth, P. Vemurafenib: The First Drug Approved for BRAF-Mutant Cancer. *Nat. Rev. Drug Discov.* **2012**, *11*, 873–886.
98. Hajduk, P. J.; Greer, J. A Decade of Fragment-Based Drug Design: Strategic Advances and Lessons Learned. *Nat. Rev. Drug Discov.* **2007**, *6*, 211–219.
99. Whittaker, M.; Law, R. J.; Ichihara, O.; Hesterkamp, T.; Hallett, D. Fragments: Past, Present and Future. *Drug Discov. Today Technol.* **2010**, *7*, e163–e171.
100. Bienstock, R. J. *Library Design, Search Methods, and Applications of Fragment-Based Drug Design*; **2011**.
101. Scott, D. E.; Coyne, A. G.; Hudson, S. a; Abell, C. Fragment-Based Approaches in Drug Discovery and Chemical Biology. *Biochemistry* **2012**, *51*, 4990–5003.
102. Schulz, M. N.; Hubbard, R. E. Recent Progress in Fragment-Based Lead Discovery. *Curr. Opin. Pharmacol.* **2009**, *9*, 615–621.
103. Congreve, M.; Carr, R.; Murray, C.; Jhoti, H. A “Rule of Three” for Fragment-Based Lead Discovery? *Drug Discov. Today* **2003**, *8*, 876–877.
104. Boyd, S. M.; Turnbull, A. P.; Walse, B. Fragment Library Design Considerations. *Wiley Interdiscip. Rev. Comput. Mol. Sci.* **2012**, *2*, 868–885.
105. Wilde, F.; Link, A. Advances in the Design of a Multipurpose Fragment Screening Library. *Expert Opin. Drug Discov.* **2013**, *8*, 597–606.

Bibliography

106. Schultes, S.; de Graaf, C.; Haaksma, E. E. J.; de Esch, I. J. P.; Leurs, R.; Krämer, O. Ligand Efficiency as a Guide in Fragment Hit Selection and Optimization. *Drug Discov. Today Technol.* **2010**, *7*, e157–e162.
107. Rees, D. C.; Congreve, M.; Murray, C. W.; Carr, R. Fragment-Based Lead Discovery. *Nat. Rev. Drug Discov.* **2004**, *3*, 660–672.
108. Manger, M.; Scheck, M.; Prinz, H.; Von Kries, J. P.; Langer, T.; Saxena, K.; Schwalbe, H.; Fürstner, A.; Rademann, J.; Waldmann, H. Discovery of Mycobacterium Tuberculosis Protein Tyrosine Phosphatase A (MptpA) Inhibitors Based on Natural Products and a Fragment-Based Approach. *ChemBioChem* **2005**, *6*, 1749–1753.
109. Rawls, K. A.; Lang, P. T.; Takeuchi, J.; Imamura, S.; Baguley, T. D.; Grundner, C.; Alber, T.; Ellman, J. A. Fragment-Based Discovery of Selective Inhibitors of the Mycobacterium Tuberculosis Protein Tyrosine Phosphatase PtpA. *Bioorg. Med. Chem. Lett.* **2009**, *19*, 6851–6854.
110. Soellner, M. B.; Rawls, K. A.; Grundner, C.; Alber, T.; Ellman, J. A. Fragment-Based Substrate Activity Screening Method for the Identification of Potent Inhibitors of the Mycobacterium Tuberculosis Phosphatase PtpB. *J. Am. Chem. Soc.* **2007**, *129*, 9613–9615.
111. Hung, A. W.; Silvestre, H. L.; Wen, S.; Ciulli, A.; Blundell, T. L.; Abell, C. Application of Fragment Growing and Fragment Linking to the Discovery of Inhibitors of Mycobacterium Tuberculosis Pantothenate Synthetase. *Angew. Chemie - Int. Ed.* **2009**, *48*, 8452–8456.
112. Scheich, C.; Puetter, V.; Schade, M. Novel Small Molecule Inhibitors of MDR Mycobacterium Tuberculosis by NMR Fragment Screening of Antigen 85C. *J. Med. Chem.* **2010**, *53*, 8362–8367.
113. Hudson, S. a.; McLean, K. J.; Surade, S.; Yang, Y.-Q.; Leys, D.; Ciulli, A.; Munro, A. W.; Abell, C. Application of Fragment Screening and Merging to the Discovery of Inhibitors of the Mycobacterium Tuberculosis Cytochrome P450 CYP121. *Angew. Chem. Int. Ed. Engl.* **2012**, *51*, 9311–9316.
114. Hudson, S. a.; Surade, S.; Coyne, A. G.; McLean, K. J.; Leys, D.; Munro, A. W.; Abell, C. Overcoming the Limitations of Fragment Merging: Rescuing a Strained Merged Fragment Series Targeting Mycobacterium Tuberculosis CYP121. *ChemMedChem* **2013**, *8*, 1451–1456.
115. Perryman, A. L.; Yu, W.; Wang, X.; Ekins, S.; Forli, S.; Li, S.-G.; Freundlich, J. S.; Tonge, P. J.; Olson, A. J. A Virtual Screen Discovers Novel, Fragment-Sized Inhibitors of Mycobacterium Tuberculosis InhA. *J. Chem. Inf. Model.* **2015**, *55*, 645–659.
116. Tran, A. T.; West, N. P.; Britton, W. J.; Payne, R. J. Elucidation of Mycobacterium Tuberculosis Type II Dehydroquinase Inhibitors Using a Fragment Elaboration Strategy. *ChemMedChem* **2012**, *7*, 1031–1043.
117. Surade, S.; Ty, N.; Hengrung, N.; Lechartier, B.; Cole, S. T.; Abell, C.; Blundell, T. L. A Structure-Guided Fragment-Based Approach for the Discovery of Allosteric Inhibitors Targeting the Lipophilic Binding Site of Transcription Factor EthR. *Biochem. J.* **2014**, *458*, 387–394.
118. Villemagne, B.; Flipo, M.; Blondiaux, N.; Crauste, C.; Malaquin, S.; Leroux, F.; Piveteau, C.; Villeret, V.; Brodin, P.; Villoutreix, B. O.; Sperandio, O.; Soror, S. H.; Wohlkönig, A.; Wintjens, R.; Deprez, B.; Baulard, A. R.; Willand, N. Ligand Efficiency Driven Design of New Inhibitors of Mycobacterium Tuberculosis Transcriptional Repressor EthR Using Fragment Growing, Merging, and Linking Approaches. *J. Med. Chem.* **2014**, *57*, 4876–4888.
119. Quemard, A.; Laneelle, G.; Lacave, C. Mycolic Acid Synthesis: A Target for Ethionamide in Mycobacteria? *Antimicrob. Agents Chemother.* **1992**, *36*, 1316–1321.
120. Timmins, G. S.; Deretic, V. Mechanisms of Action of Isoniazid. *Mol. Microbiol.* **2006**, *62*, 1220–1227.

Bibliography

121. Banerjee, A.; Dubnau, E.; Quemard, A.; Balasubramanian, V.; Um, K. S.; Wilson, T.; Collins, D.; de Lisle, G.; Jacobs, W. R. inhA, a Gene Encoding a Target for Isoniazid and Ethionamide in Mycobacterium Tuberculosis. *Science (80-.)*. **1994**, *263*, 227–230.
122. Fattorini, L.; Iona, E.; Ricci, M. L.; Thoresen, O. F.; Orrú, G.; Oggioni, M. R.; Tortoli, E.; Piersimoni, C.; Chiaradonna, P.; Tronci, M.; Pozzi, G.; Orefici, G. Activity of 16 Antimicrobial Agents Against Drug-Resistant Strains of Mycobacterium Tuberculosis. *Microb. Drug Resist.* **1999**, *5*, 265–270.
123. Baulard, A. R.; Betts, J. C.; Engohang-Ndong, J.; Quan, S.; McAdam, R. a; Brennan, P. J.; Locht, C.; Besra, G. S. Activation of the pro-Drug Ethionamide Is Regulated in Mycobacteria. *J. Biol. Chem.* **2000**, *275*, 28326–28331.
124. DeBarber, a E.; Mdluli, K.; Bosman, M.; Bekker, L. G.; Barry, C. E. Ethionamide Activation and Sensitivity in Multidrug-Resistant Mycobacterium Tuberculosis. *Proc. Natl. Acad. Sci. U. S. A.* **2000**, *97*, 9677–9682.
125. Vannelli, T. A.; Dykman, A.; Ortiz de Montellano, P. R. The Antituberculosis Drug Ethionamide Is Activated by a Flavoprotein Monooxygenase. *J. Biol. Chem.* **2002**, *277*, 12824–12829.
126. Hanouille, X.; Wieruszkeski, J.-M.; Roussetot-Pailley, P.; Landrieu, I.; Locht, C.; Lippens, G.; Baulard, A. R. Selective Intracellular Accumulation of the Major Metabolite Issued from the Activation of the Prodrug Ethionamide in Mycobacteria. *J. Antimicrob. Chemother.* **2006**, *58*, 768–772.
127. Wang, F.; Langley, R.; Gulten, G.; Dover, L. G.; Besra, G. S.; Jacobs, W. R.; Sacchettini, J. C. Mechanism of Thioamide Drug Action against Tuberculosis and Leprosy. *J. Exp. Med.* **2007**, *204*, 73–78.
128. Flipo, M.; Desroses, M.; Lecat-Guillet, N.; Dirié, B.; Carette, X.; Leroux, F.; Piveteau, C.; Demirkaya, F.; Lens, Z.; Rucktooa, P.; Villeret, V.; Christophe, T.; Jeon, H. K.; Locht, C.; Brodin, P.; Déprez, B.; Baulard, A. R.; Willand, N. Ethionamide Boosters: Synthesis, Biological Activity, and Structure-Activity Relationships of a Series of 1,2,4-Oxadiazole EthR Inhibitors. *J. Med. Chem.* **2011**, *54*, 2994–3010.
129. Dover, L. G.; Corsino, P. E.; Daniels, I. R.; Cocklin, S. L.; Tatituri, V.; Besra, G. S.; Fütterer, K. Crystal Structure of the TetR/CamR Family Repressor Mycobacterium Tuberculosis EthR Implicated in Ethionamide Resistance. *J. Mol. Biol.* **2004**, *340*, 1095–1105.
130. Frénois, F.; Engohang-Ndong, J.; Locht, C.; Baulard, A. R.; Villeret, V. Structure of EthR in a Ligand Bound Conformation Reveals Therapeutic Perspectives against Tuberculosis. *Mol. Cell* **2004**, *16*, 301–307.
131. Carette, X.; Blondiaux, N.; Willery, E.; Hoos, S.; Lecat-Guillet, N.; Lens, Z.; Wohlkönig, A.; Wintjens, R.; Soror, S. H.; Frénois, F.; Dirié, B.; Villeret, V.; England, P.; Lippens, G.; Deprez, B.; Locht, C.; Willand, N.; Baulard, A. R. Structural Activation of the Transcriptional Repressor EthR from Mycobacterium Tuberculosis by Single Amino Acid Change Mimicking Natural and Synthetic Ligands. *Nucleic Acids Res.* **2012**, *40*, 3018–3030.
132. Frénois, F.; Baulard, A. R.; Villeret, V. Insights into Mechanisms of Induction and Ligands Recognition in the Transcriptional Repressor EthR from Mycobacterium Tuberculosis. *Tuberculosis (Edinb)*. **2006**, *86*, 110–114.
133. Ramos, J. L.; Martínez-Bueno, M.; Molina-Henares, A. J.; Terán, W.; Watanabe, K.; Zhang, X.; Gallegos, M. T.; Brennan, R.; Tobes, R. The TetR Family of Transcriptional Repressors. *Microbiol. Mol. Biol. Rev.* **2005**, *69*, 326–356.
134. Engohang-Ndong, J.; Baillat, D.; Aumercier, M.; Bellefontaine, F.; Besra, G. S.; Locht, C.; Baulard, A. R. EthR, a Repressor of the TetR/CamR Family Implicated in Ethionamide Resistance in Mycobacteria, Octamerizes Cooperatively on Its Operator. *Mol. Microbiol.* **2004**, *51*, 175–188.
135. Aronson, J. K. *Meyler's Side Effects of Antimicrobial Drugs*; Elsevier Science, **2009**.

Bibliography

136. Weber, W.; Schoenmakers, R.; Keller, B.; Gitzinger, M.; Grau, T.; Daoud-El Baba, M.; Sander, P.; Fussenegger, M. A Synthetic Mammalian Gene Circuit Reveals Antituberculosis Compounds. *Proc. Natl. Acad. Sci. U. S. A.* **2008**, *105*, 9994–9998.
137. Jacob, F.; Monod, J. Genetic Regulatory Mechanisms in the Synthesis of Proteins. *J. Mol. Biol.* **1961**, *3*, 318–356.
138. Grau, T.; Selchow, P.; Tigges, M.; Burri, R.; Gitzinger, M.; Böttger, E. C.; Fussenegger, M.; Sander, P. Phenylethyl Butyrate Enhances the Potency of Second-Line Drugs against Clinical Isolates of Mycobacterium Tuberculosis. *Antimicrob. Agents Chemother.* **2012**, *56*, 1142–1145.
139. Fussenegger, M.; Weber, W.; Schoenmakers, R. Composition for Treatment of Tuberculosis. Patent WO2009/080432, February 18, 2009.
140. Schoenmakers, R.; Weber, W.; Gitzinger, M.; Fussenegger, M.; Tigges, M.; Schneider, P. Composition for Treatment of Tuberculosis. Patent WO 2010/149761, 2010.
141. Willand, N.; Dirié, B.; Carette, X.; Bifani, P.; Singhal, A.; Desroses, M.; Leroux, F.; Willery, E.; Mathys, V.; Déprez-Poulain, R.; Delcroix, G.; Frénois, F.; Aumercier, M.; Loch, C.; Villeret, V.; Déprez, B.; Baulard, A. R. Synthetic EthR Inhibitors Boost Antituberculous Activity of Ethionamide. *Nat. Med.* **2009**, *15*, 537–544.
142. Deprez, B.; Willand, N.; Dirié, B.; Toto, P.; Villeret, V.; Loch, C.; Baulard, A. Compounds Having a Potentiating Effect on the Activity of Ethionamide and Uses Thereof. Patent WO 2008/003861, 2008.
143. Bonnel, D.; Legouffe, R.; Willand, N.; Baulard, A.; Hamm, G.; Deprez, B.; Stauber, J. MALDI Imaging Techniques Dedicated to Drug-Distribution Studies. *Bioanalysis* **2011**, *3*, 1399–1406.
144. Willand, N.; Desroses, M.; Toto, P.; Dirié, B.; Lens, Z.; Villeret, V.; Rucktooa, P.; Loch, C.; Baulard, A.; Deprez, B. Exploring Drug Target Flexibility Using in Situ Click Chemistry: Application to a Mycobacterial Transcriptional Regulator. *ACS Chem. Biol.* **2010**, *5*, 1007–1013.
145. Flipo, M.; Desroses, M.; Lecat-Guillet, N.; Villemagne, B.; Blondiaux, N.; Leroux, F.; Piveteau, C.; Mathys, V.; Flament, M.-P.; Siepmann, J.; Villeret, V.; Wohlkönig, A.; Wintjens, R.; Soror, S. H.; Christophe, T.; Jeon, H. K.; Loch, C.; Brodin, P.; Déprez, B.; Baulard, A. R.; Willand, N. Ethionamide Boosters. 2. Combining Bioisosteric Replacement and Structure-Based Drug Design to Solve Pharmacokinetic Issues in a Series of Potent 1,2,4-Oxadiazole EthR Inhibitors. *J. Med. Chem.* **2012**, *55*, 68–83.
146. Deprez, B.; Willand, N.; Flipo, M.; Desroses, M.; Baulard, A.; Leroux, F. Compound Having an EthR Inhibiting Activity - Use of Said Compounds as Drugs - Pharmaceutical Composition and Product Containing Said Compounds. Patent WO 2013/060744, 2013.
147. Bernard, C.; Willand, N.; Déprez, B.; Jarlier, V.; Baulard, A.; Veziris, N. EthR Inhibitor BDM41906 Boosts the in Vivo Antituberculous Activity of Ethionamide in a Murine Model. In *22nd European Congress of Clinical Microbiology and Infectious Diseases (31/03/2012 - 03/04/2012)*.
148. Flipo, M.; Willand, N.; Lecat-Guillet, N.; Hounsou, C.; Desroses, M.; Leroux, F.; Lens, Z.; Villeret, V.; Wohlkönig, A.; Wintjens, R.; Christophe, T.; Kyoung Jeon, H.; Loch, C.; Brodin, P.; Baulard, A. R.; Déprez, B. Discovery of Novel N-Phenylphenoxyacetamide Derivatives as EthR Inhibitors and Ethionamide Boosters by Combining High-Throughput Screening and Synthesis. *J. Med. Chem.* **2012**, *55*, 6391–6402.
149. Obach, R. S. Pharmacologically Active Drug Metabolites: Impact on Drug Discovery and Pharmacotherapy. *Pharmacol. Rev.* **2013**, *65*, 578–640.
150. Böhm, H. J.; Banner, D.; Bendels, S.; Kansy, M.; Kuhn, B.; Müller, K.; Obst-Sander, U.; Stahl, M. Fluorine in Medicinal Chemistry. *ChemBioChem* **2004**, *5*, 637–643.

Bibliography

151. Barnes-Seeman, D.; Jain, M.; Bell, L.; Ferreira, S.; Cohen, S.; Chen, X.-H.; Amin, J.; Snodgrass, B.; Hatsis, P. Metabolically Stable Tert -Butyl Replacement. *ACS Med. Chem. Lett.* **2013**, *4*, 514–516.
152. Augustine, J. K.; Vairaperumal, V.; Narasimhan, S.; Alagarsamy, P.; Radhakrishnan, A. Propylphosphonic Anhydride (T3P®): An Efficient Reagent for the One-Pot Synthesis of 1,2,4-Oxadiazoles, 1,3,4-Oxadiazoles, and 1,3,4-Thiadiazoles. *Tetrahedron* **2009**, *65*, 9989–9996.
153. Legros, J.-Y.; Primault, G.; Fiaud, J.-C. Syntheses of Acetylquinolines and Acetylisquinolines via Palladium-Catalyzed Coupling Reactions. *Tetrahedron* **2001**, *57*, 2507–2514.
154. Mdluli, K.; Spigelman, M. Novel Targets for Tuberculosis Drug Discovery. *Curr. Opin. Pharmacol.* **2006**, *6*, 459–467.
155. Lechartier, B.; Rybniker, J.; Zumla, A.; Cole, S. T. Tuberculosis Drug Discovery in the Post-Post-Genomic Era. *EMBO Mol. Med.* **2014**, *6*, 158–168.
156. Chopra, P.; Meena, L. S.; Singh, Y. New Drug Targets for Mycobacterium Tuberculosis. *Indian J. Med. Res.* **2003**, *117*, 1–9.
157. Bocanegra-garcía, V.; García, A.; Palma-nicolás, J. P.; Tamaulipas, A. De. Antitubercular Drugs Development : Recent Advances in Selected Therapeutic Targets and Rational Drug Design. **2007**.
158. Ioerger, T. R.; O'Malley, T.; Liao, R.; Guinn, K. M.; Hickey, M. J.; Mohaideen, N.; Murphy, K. C.; Boshoff, H. I. M.; Mizrahi, V.; Rubin, E. J.; Sasseti, C. M.; Barry, C. E.; Sherman, D. R.; Parish, T.; Sacchettini, J. C. Identification of New Drug Targets and Resistance Mechanisms in Mycobacterium Tuberculosis. *PLoS One* **2013**, *8*, e75245.
159. Lamichhane, G. Novel Targets in M. Tuberculosis: Search for New Drugs. *Trends Mol. Med.* **2010**, *17*, 25–33.
160. Williams, K. J.; Duncan, K. Current Strategies for Identifying and Validating Targets for New Treatment-Shortening Drugs for TB. *Curr. Mol. Med.* **2007**, *7*, 297–307.
161. Bhatt, A.; Molle, V.; Besra, G. S.; Jacobs, W. R.; Kremer, L. The Mycobacterium Tuberculosis FAS-II Condensing Enzymes: Their Role in Mycolic Acid Biosynthesis, Acid-Fastness, Pathogenesis and in Future Drug Development. *Mol. Microbiol.* **2007**, *64*, 1442–1454.
162. Ducasse-Cabanot, S.; Cohen-Gonsaud, M.; Marrakchi, H.; Nguyen, M.; Zerbib, D.; Bernadou, J.; Daffe, M.; Labesse, G.; Quemard, A. In Vitro Inhibition of the Mycobacterium Tuberculosis -Ketoacyl-Acyl Carrier Protein Reductase MabA by Isoniazid. *Antimicrob. Agents Chemother.* **2004**, *48*, 242–249.
163. Heath, R. J.; White, S. W.; Rock, C. O. Inhibitors of Fatty Acid Synthesis as Antimicrobial Chemotherapeutics. *Appl. Microbiol. Biotechnol.* **2002**, *58*, 695–703.
164. Musser, J. M.; Kapur, V.; Williams, D. L.; Kreiswirth, B. N.; van Soolingen, D.; van Embden, J. D. A. Characterization of the Catalase-Peroxidase Gene (katG) and inhA Locus in Isoniazid-Resistant and -Susceptible Strains of Mycobacterium Tuberculosis by Automated DNA Sequencing: Restricted Array of Mutations Associated with Drug Resistance. *J. Infect. Dis.* **1996**, *173*, 196–202.
165. Banerjee, A.; Sugantino, M.; Sacchettini, J. C.; Jacobs, W. R. The mabA Gene from the inhA Operon of Mycobacterium Tuberculosis Encodes a 3-Ketoacyl Reductase That Fails to Confer Isoniazid Resistance. *Microbiology* **1998**, *144*, 2697–2704.
166. Benson, D. A.; Cavanaugh, M.; Clark, K.; Karsch-Mizrachi, I.; Lipman, D. J.; Ostell, J.; Sayers, E. W. GenBank. *Nucleic Acids Res.* **2013**, *41*, D36–D42.

Bibliography

167. Gurvitz, A. The Essential Mycobacterial Genes, *fabG1* and *fabG4*, Encode 3-Oxoacyl-Thioester Reductases That Are Functional in Yeast Mitochondrial Fatty Acid Synthase Type 2. *Mol. Genet. genomics* **2009**, *282*, 407–416.
168. Dutta, D.; Bhattacharyya, S.; Roychowdhury, A.; Biswas, R.; Das, A. K. Crystal Structure of Hexanoyl-CoA Bound to B-Ketoacyl Reductase *FabG4* of Mycobacterium Tuberculosis. *Biochem. J.* **2013**, *450*, 127–139.
169. Banerjee, D. R.; Dutta, D.; Saha, B.; Bhattacharyya, S.; Senapati, K.; Das, A. K.; Basak, A. Design, Synthesis and Characterization of Novel Inhibitors against Mycobacterial B-Ketoacyl CoA Reductase *FabG4*. *Org. Biomol. Chem.* **2013**.
170. Silva, R. G.; de Carvalho, L. P. S.; Blanchard, J. S.; Santos, D. S.; Basso, L. a. Mycobacterium Tuberculosis Beta-Ketoacyl-Acyl Carrier Protein (ACP) Reductase: Kinetic and Chemical Mechanisms. *Biochemistry* **2006**, *45*, 13064–13073.
171. Silva, R. G.; Rosado, L. a; Santos, D. S.; Basso, L. a. Mycobacterium Tuberculosis Beta-Ketoacyl-ACP Reductase: Alpha-Secondary Kinetic Isotope Effects and Kinetic and Equilibrium Mechanisms of Substrate Binding. *Arch. Biochem. Biophys.* **2008**, *471*, 1–10.
172. Quemard, A.; Labesse, G.; Daffe, M.; Marrakchi, H.; Douguet, D.; Cohen-Gonsaud, M.; Ducasse, S. Use of the Protein *MabA* (*FabG1*) of Mycobacterium Tuberculosis for Designing and Screening Antibiotics. *WO/2003/082911*, October 9, 2006.
173. Cohen-Gonsaud, M.; Ducasse, S.; Hoh, F.; Zerbib, D.; Labesse, G.; Quemard, A. Crystal Structure of *MabA* from Mycobacterium Tuberculosis, a Reductase Involved in Long-Chain Fatty Acid Biosynthesis. *J. Mol. Biol.* **2002**, *320*, 249–261.
174. Cohen-Gonsaud, M.; Ducasse-Cabanot, S.; Quemard, A.; Labesse, G. Ligand-Induced Fit in Mycobacterial *MabA*: The Sequence-Specific C-Terminus Locks the Conformational Change. *Proteins* **2005**, *60*, 392–400.
175. Oppermann, U.; Filling, C.; Hult, M.; Shafqat, N.; Wu, X.; Lindh, M.; Shafqat, J.; Nordling, E.; Kallberg, Y.; Persson, B.; Jörnvall, H. Short-Chain Dehydrogenases/reductases (SDR): The 2002 Update. *Chem. Biol. Interact.* **2003**, *143-144*, 247–253.
176. Labesse, G.; Quemard, A.; Cohen-Gonsaud, M.; Ducasse-Cabanot, S.; Daffe, M. Complexes of NADP with the Protein *MabA* of Mycobacterium Tuberculosis or with Mutants Thereof, and Their Uses for Designing and Screening Antibiotics. *Pat. WO/2007/107335 A1* **2007**.
177. Rosado, L. a; Caceres, R. A.; de Azevedo, W. F.; Basso, L. A.; Santos, D. S. Role of Serine140 in the Mode of Action of Mycobacterium Tuberculosis B-Ketoacyl-ACP Reductase (*MabA*). *BMC Res. Notes* **2012**, *5*, 526.
178. Poncet-Montange, G.; Ducasse-Cabanot, S.; Quemard, A.; Labesse, G.; Cohen-Gonsaud, M. Lack of Dynamics in the *MabA* Active Site Kills the Enzyme Activity: Practical Consequences for Drug-Design Studies. *Acta Crystallogr. D. Biol. Crystallogr.* **2007**, *63*, 923–925.
179. Veyron-Churlet, R.; Zanella-Cléon, I.; Cohen-Gonsaud, M.; Molle, V.; Kremer, L. Phosphorylation of the Mycobacterium Tuberculosis Beta-Ketoacyl-Acyl Carrier Protein Reductase *MabA* Regulates Mycolic Acid Biosynthesis. *J. Biol. Chem.* **2010**, *285*, 12714–12725.
180. Parish, T.; Roberts, G.; Laval, F.; Schaeffer, M.; Daffé, M.; Duncan, K. Functional Complementation of the Essential Gene *fabG1* of Mycobacterium Tuberculosis by Mycobacterium Smegmatis *fabG* but Not Escherichia Coli *fabG*. *J. Bacteriol.* **2007**, *189*, 3721–3728.

Bibliography

181. Zhang, Y.; Cronan, J. E. Polar Allele Duplication for Transcriptional Analysis of Consecutive Essential Genes: Application to a Cluster of Escherichia Coli Fatty Acid Biosynthetic Genes. *J. Bacteriol.* **1996**, *178*, 3614–3620.
182. Reddy, A. S.; Pati, S. P.; Kumar, P. P.; Pradeep, H. N.; Sastry, G. N. Virtual Screening in Drug Discovery -- a Computational Perspective. *Curr. Protein Pept. Sci.* **2007**, *8*, 329–351.
183. Irwin, J. J.; Sterling, T.; Mysinger, M. M.; Bolstad, E. S.; Coleman, R. G. ZINC: A Free Tool to Discover Chemistry for Biology. *J. Chem. Inf. Model.* **2012**, *52*, 1757–1768.
184. The Protein Data Bank (RCSB-PDB) <http://www.rcsb.org/pdb> (accessed May 22, 2014).
185. Korb, O.; Stützle, T.; Exner, T. E. Empirical Scoring Functions for Advanced Protein-Ligand Docking with PLANTS. *J. Chem. Inf. Model.* **2009**, *49*, 84–96.
186. Pettersen, E. F.; Goddard, T. D.; Huang, C. C.; Couch, G. S.; Greenblatt, D. M.; Meng, E. C.; Ferrin, T. E. UCSF Chimera--a Visualization System for Exploratory Research and Analysis. *J. Comput. Chem.* **2004**, *25*, 1605–1612.
187. Lo, M.-C.; Aulabaugh, A.; Jin, G.; Cowling, R.; Bard, J.; Malamas, M.; Ellestad, G. Evaluation of Fluorescence-Based Thermal Shift Assays for Hit Identification in Drug Discovery. *Anal. Biochem.* **2004**, *332*, 153–159.
188. Mashalidis, E. H.; Śledź, P.; Lang, S.; Abell, C. A Three-Stage Biophysical Screening Cascade for Fragment-Based Drug Discovery. *Nat. Protoc.* **2013**, *8*, 2309–2324.
189. Davis, B. J.; Erlanson, D. A. Learning from Our Mistakes: The “Unknown Knowns” in Fragment Screening. *Bioorg. Med. Chem. Lett.* **2013**, *23*, 2844–2852.
190. Siegal, G.; Ab, E.; Schultz, J. Integration of Fragment Screening and Library Design. *Drug Discov. Today* **2007**, *12*, 1032–1039.
191. Campos-Olivas, R. NMR Screening and Hit Validation in Fragment Based Drug Discovery. *Curr. Top. Med. Chem.* **2011**, *11*, 43–67.
192. Lepre, C. A. Practical Aspects of NMR-Based Fragment Screening. *Methods Enzymol.* **2011**, *493*, 219–239.
193. Vivat Hannah, V.; Atmanene, C.; Zeyer, D.; Van Dorsselaer, A.; Sanglier-Cianférani, S. Native MS: An “ESI” Way to Support Structure- and Fragment-Based Drug Discovery. *Future Med. Chem.* **2010**, *2*, 35–50.
194. Poulsen, S.-A. Fragment Screening by Native State Mass Spectrometry. *Aust. J. Chem.* **2013**, *66*, 1495.
195. Meiby, E.; Simmonite, H.; le Strat, L.; Davis, B.; Matassova, N.; Moore, J. D.; Mrosek, M.; Murray, J.; Hubbard, R. E.; Ohlson, S. Fragment Screening by Weak Affinity Chromatography: Comparison with Established Techniques for Screening against HSP90. *Anal. Chem.* **2013**, *85*, 6756–6766.
196. Shibata, S.; Zhang, Z.; Korotkov, K. V.; Delarosa, J.; Napuli, A.; Kelley, A. M.; Mueller, N.; Ross, J.; Zucker, F. H.; Buckner, F. S.; Merritt, E. A.; Verlinde, C. L. M. J.; Van Voorhis, W. C.; Hol, W. G. J.; Fan, E. Screening a Fragment Cocktail Library Using Ultrafiltration. *Anal. Bioanal. Chem.* **2011**, *401*, 1585–1591.
197. De Cillis, G.; Di Domenico, R.; Könic, B.; Oliva, A. Administering as Urokinase Plasminogen Activator Antagonists, Antitumor and Antimetastasis Agents. Patent US 6200989 B1, March 13, 2001.
198. Han, G.; Tamaki, M.; Hruby, V. J. Fast, Efficient and Selective Deprotection of the Tert-Butoxycarbonyl (Boc) Group Using HCl/dioxane (4 M). *J. Pept. Res.* **2001**, *58*, 338–341.

Bibliography

199. Lizarzaburu, M. E.; Shuttleworth, S. J. 1,2,3,4-Tetrahydro- Γ -Carbolinium Salts: Novel Reactions with Thiols, Mediated by Polymer-Supported Reagents. *Tetrahedron Lett.* **2004**, *45*, 4781–4783.
200. Bhatia, P.; Daanen, J.; Hakeem, A.; Kolasa, T.; Matulenko, M.; Mortell, K.; Patel, M.; Stewart, A.; Wang, X.; Xia, Z. Acetamides and Benzamides That Are Useful in Treating Sexual Dysfunction. US Patent 20030229094 A1, December 11, 2003.
201. Willand, N.; Deprez, B.; Baulard, A.; Brodin, P.; Sperandio, O.; Villeret, V.; Villemagne, B. Composés Utilisables Dans Le Traitement Des Infections Mycobacteriennes. Brevet FR/3000491, 2014.
202. Zampieri, D.; Grazia Mamolo, M.; Laurini, E.; Zanette, C.; Florio, C.; Collina, S.; Rossi, D.; Azzolina, O.; Vio, L. Substituted Benzo[d]oxazol-2(3H)-One Derivatives with Preference for the sigma1 Binding Site. *Eur. J. Med. Chem.* **2009**, *44*, 124–130.
203. Szabo, M.; Agostino, M.; Malone, D. T.; Yuriev, E.; Capuano, B. The Design, Synthesis and Biological Evaluation of Novel URB602 Analogues as Potential Monoacylglycerol Lipase Inhibitors. *Bioorg. Med. Chem. Lett.* **2011**, *21*, 6782–6787.
204. Vander Mierde, H.; Van Der Voort, P.; De Vos, D.; Verpoort, F. A Ruthenium-Catalyzed Approach to the Friedländer Quinoline Synthesis. *European J. Org. Chem.* **2008**, *2008*, 1625–1631.
205. Kainz, Q. M.; Zeltner, M.; Rossier, M.; Stark, W. J.; Reiser, O. Synthesis of Trisubstituted Ureas by a Multistep Sequence Utilizing Recyclable Magnetic Reagents and Scavengers. *Chemistry* **2013**, *19*, 10038–10045.
206. Benzimidazole Derivatives and Their Use as Vanilloid Receptor Ligands. Patent WIPO WO/2004/035549.
207. Doherty, E. M.; Fotsch, C.; Bannon, A. W.; Bo, Y.; Chen, N.; Dominguez, C.; Falsey, J.; Gavva, N. R.; Katon, J.; Nixey, T.; Ognyanov, V. I.; Pettus, L.; Rzasz, R. M.; Stec, M.; Surapaneni, S.; Tamir, R.; Zhu, J.; Treanor, J. J. S.; Norman, M. H. Novel Vanilloid Receptor-1 Antagonists: 2. Structure-Activity Relationships of 4-Oxopyrimidines Leading to the Selection of a Clinical Candidate. *J. Med. Chem.* **2007**, *50*, 3515–3527.
208. Zborovskii, Y. L.; Orysyk, V. V.; Staninets, V. I.; Rusanov, E. B.; Chernega, a. N. Heterocyclization of N-Hetaryl-N'-(prop-2-En-1-Yl)thioureas by the Action of Sulfuryl Chloride. *Russ. J. Org. Chem.* **2007**, *43*, 1030–1034.
209. Nurkenov, O. a.; Gazaliev, a. M.; Ainabaev, a. a.; Kulakov, I. V. Synthesis and Intramolecular Heterocyclization of N-Allylcytisine-12-Carbothioamide. *Russ. J. Gen. Chem.* **2006**, *76*, 1181–1182.
210. Kolocouris, N.; Kolocouris, A.; Foscolos, G. B.; Fytas, G.; Neyts, J.; Padalko, E.; Balzarini, J.; Snoeck, R.; Andrei, G.; De Clercq, E. Synthesis and Antiviral Activity Evaluation of Some New Aminoadamantane Derivatives. 2. *J. Med. Chem.* **1996**, *39*, 3307–3318.
211. Schoop, A.; Mueller, G.; Brueggemeier, U.; Schmidt, D.; Stelte-Ludwig, B.; Keldenich, J. B-Phenylalanine Derivatives as Integrin Antagonists. Patent US 6291503 B1, September 18, 2001.
212. Orrling, K. M.; Wu, X.; Russo, F.; Larhed, M. Fast, Acid-Free, and Selective Lactamization of Lactones in Ionic Liquids. *J. Org. Chem.* **2008**, *73*, 8627–8630.
213. Kobayashi, S.; Iimori, T.; Izawa, T.; Ohno, M. Ph3P-(PyS)2-CH3CN as an Excellent Condensing System for .beta.-Lactam Formation from .beta.-Amino Acids. *J. Am. Chem. Soc.* **1981**, *103*, 2406–2408.
214. Ho, T.-L. *Tandem Organic Reactions*; John Wiley & Sons, Inc., **1992**.
215. Boyd, S. M.; de Kloe, G. E.; Kloe, G. E. De. Fragment Library Design: Efficiently Hunting Drugs in Chemical Space. *Drug Discov. Today. Technol.* **2010**, *7*, e147–e202.

Bibliography

216. Raju, T. N. The Nobel Chronicles. 1988: James Whyte Black, (b 1924), Gertrude Elion (1918-99), and George H Hitchings (1905-98). *Lancet* **2000**, *355*, 1022.
217. Siegel, M. G.; Vieth, M. Drugs in Other Drugs: A New Look at Drugs as Fragments. *Drug Discov. Today* **2007**, *12*, 71–79.
218. Fejzo, J.; Lepre, C. A.; Peng, J. W.; Bemis, G. W.; Murcko, M. A.; Moore, J. M. The SHAPES Strategy: An NMR-Based Approach for Lead Generation in Drug Discovery. *Chem. Biol.* **1999**, *6*, 755–769.
219. Lewell, X. Q.; Judd, D. B.; Watson, S. P.; Hann, M. M. RECAP--Retrosynthetic Combinatorial Analysis Procedure: A Powerful New Technique for Identifying Privileged Molecular Fragments with Useful Applications in Combinatorial Chemistry. *J. Chem. Inf. Comput. Sci.* **38**, 511–522.
220. Drug Bank www.drugbank.ca (accessed Apr 22, 2015).
221. NCI Drug Dictionary <http://www.cancer.gov/drugdictionary> (accessed Apr 22, 2015).
222. Supper Drug DataBase <http://bioinf.charite.de/superdrug> (accessed Apr 22, 2015).
223. The PubChem Project <http://pubchem.ncbi.nlm.nih.gov/> (accessed Apr 22, 2015).
224. ChEMBL database <https://www.ebi.ac.uk/chembl/db/> (accessed Apr 22, 2015).
225. Molinari, G. Natural Products in Drug Discovery: Present Status and Perspectives. *Adv. Exp. Med. Biol.* **2009**, *655*, 13–27.
226. Genis, D.; Kirpichenok, M.; Kombarov, R. A Minimalist Fragment Approach for the Design of Natural-Product-like Synthetic Scaffolds. *Drug Discov. Today* **2012**, *17*, 1170–1174.
227. Over, B.; Wetzel, S.; Grütter, C.; Nakai, Y.; Renner, S.; Rauh, D.; Waldmann, H. Natural-Product-Derived Fragments for Fragment-Based Ligand Discovery. *Nat. Chem.* **2012**, *5*, 21–28.
228. Füllbeck, M.; Michalsky, E.; Dunkel, M.; Preissner, R. Natural Products: Sources and Databases. *Nat. Prod. Rep.* **2006**, *23*, 347–356.
229. Davies, D. R.; Mamat, B.; Magnusson, O. T.; Christensen, J.; Haraldsson, M. H.; Mishra, R.; Pease, B.; Hansen, E.; Singh, J.; Zembower, D.; Kim, H.; Kiselyov, A. S.; Burgin, A. B.; Gurney, M. E.; Stewart, L. J. Discovery of Leukotriene A4 Hydrolase Inhibitors Using Metabolomics Biased Fragment Crystallography. *J. Med. Chem.* **2009**, *52*, 4694–4715.
230. Kirkpatrick, P.; Ellis, C. Chemical Space. *Nature* **2004**, *432*, 823–823.
231. Ertl, P. Cheminformatics Analysis of Organic Substituents: Identification of the Most Common Substituents, Calculation of Substituent Properties, and Automatic Identification of Drug-like Bioisosteric Groups. *J. Chem. Inf. Comput. Sci.* **43**, 374–380.
232. Fink, T.; Reymond, J.-L. Virtual Exploration of the Chemical Universe up to 11 Atoms of C, N, O, F: Assembly of 26.4 Million Structures (110.9 Million Stereoisomers) and Analysis for New Ring Systems, Stereochemistry, Physicochemical Properties, Compound Classes, and Drug Discove. *J. Chem. Inf. Model.* **47**, 342–353.
233. Blum, L. C.; Reymond, J.-L. 970 Million Druglike Small Molecules for Virtual Screening in the Chemical Universe Database GDB-13. *J. Am. Chem. Soc.* **2009**, *131*, 8732–8733.
234. Ruddigkeit, L.; van Deursen, R.; Blum, L. C.; Reymond, J.-L. Enumeration of 166 Billion Organic Small Molecules in the Chemical Universe Database GDB-17. *J. Chem. Inf. Model.* **2012**, *52*, 2864–2875.

Bibliography

235. Venhorst, J.; Núñez, S.; Kruse, C. G. Design of a High Fragment Efficiency Library by Molecular Graph Theory. *ACS Med. Chem. Lett.* **2010**, *1*, 499–503.
236. Chen, Y.; Shoichet, B. K. Molecular Docking and Ligand Specificity in Fragment-Based Inhibitor Discovery. *Nat. Chem. Biol.* **2009**, *5*, 358–364.
237. Ludington, J. L. Virtual Fragment Preparation for Computational Fragment-Based Drug Design. *Methods Mol. Biol.* **2015**, *1289*, 31–41.
238. Feyfant, E.; Cross, J. B.; Paris, K.; Tsao, D. H. H. *Chemical Library Design*; Zhou, J. Z., Ed.; Methods in Molecular Biology; Humana Press: Totowa, NJ, **2011**; Vol. 685.
239. Lipinski, C. a. Lead- and Drug-like Compounds: The Rule-of-Five Revolution. *Drug Discov. Today Technol.* **2004**, *1*, 337–341.
240. Köster, H.; Craan, T.; Brass, S.; Herhaus, C.; Zentgraf, M.; Neumann, L.; Heine, A.; Klebe, G. A Small Nonrule of 3 Compatible Fragment Library Provides High Hit Rate of Endothiapepsin Crystal Structures with Various Fragment Chemotypes. *J. Med. Chem.* **2011**, *54*, 7784–7796.
241. Craan, T. F. Fragment Based Drug Discovery ; Design and Validation of a Fragment Library ; Computer-Based Fragment Screening and Fragment-to-Lead Expansion Dissertation Zur, Philipps-Universität Marburg, **2011**.
242. Jhoti, H.; Williams, G.; Rees, D. C.; Murray, C. W. The “Rule of Three” for Fragment-Based Drug Discovery: Where Are We Now? *Nat. Rev. Drug Discov.* **2013**, *12*, 644–645.
243. Law, R.; Barker, O.; Barker, J. J.; Hestekamp, T.; Godemann, R.; Andersen, O.; Fryatt, T.; Courtney, S.; Hallett, D.; Whittaker, M. The Multiple Roles of Computational Chemistry in Fragment-Based Drug Design. *J. Comput. Aided. Mol. Des.* **2009**, *23*, 459–473.
244. Blomberg, N.; Cosgrove, D. a; Kenny, P. W.; Kolmodin, K. Design of Compound Libraries for Fragment Screening. *J. Comput. Aided. Mol. Des.* **2009**, *23*, 513–525.
245. Morley, A. D.; Pugliese, A.; Birchall, K.; Bower, J.; Brennan, P.; Brown, N.; Chapman, T.; Drysdale, M.; Gilbert, I. H.; Hoelder, S.; Jordan, A.; Ley, S. V; Merritt, A.; Miller, D.; Swarbrick, M. E.; Wyatt, P. G. Fragment-Based Hit Identification: Thinking in 3D. *Drug Discov. Today* **2013**, *18*, 1221–1227.
246. Murray, C. W.; Verdonk, M. L.; Rees, D. C. Experiences in Fragment-Based Drug Discovery. *Trends Pharmacol. Sci.* **2012**, *33*, 224–232.
247. Murray, C. W.; Carr, M. G.; Callaghan, O.; Chessari, G.; Congreve, M.; Cowan, S.; Coyle, J. E.; Downham, R.; Figueroa, E.; Frederickson, M.; Graham, B.; McMenemy, R.; O'Brien, M. A.; Patel, S.; Phillips, T. R.; Williams, G.; Woodhead, A. J.; Woolford, A. J.-A. Fragment-Based Drug Discovery Applied to Hsp90. Discovery of Two Lead Series with High Ligand Efficiency. *J. Med. Chem.* **2010**, *53*, 5942–5955.
248. Zartler, E.; Swain, C.; Pearce, S. Fragment Library Design: The Evolution of Fragment-Based Lead Discovery. *Drug Discov. World Winter* **2012**, *2012/2013*.
249. Hopkins, A. L.; Groom, C. R.; Alex, A. Ligand Efficiency: A Useful Metric for Lead Selection. *Drug Discov. Today* **2004**, *9*, 430–431.
250. Schuffenhauer, A.; Ruedisser, S.; Marzinzik, A. L.; Jahnke, W.; Blommers, M.; Selzer, P.; Jacoby, E. Library Design for Fragment Based Screening. *Curr. Top. Med. Chem.* **2005**, *5*, 751–762.
251. Matter, H. Selecting Optimally Diverse Compounds from Structure Databases: A Validation Study of Two-Dimensional and Three-Dimensional Molecular Descriptors. *J. Med. Chem.* **1997**, *40*, 1219–1229.

Bibliography

252. Krier, M.; Bret, G.; Rognan, D. Assessing the Scaffold Diversity of Screening Libraries. *J. Chem. Inf. Model.* **2006**, *46*, 512–524.
253. Hartshorn, M. J.; Murray, C. W.; Cleasby, A.; Frederickson, M.; Tickle, I. J.; Jhoti, H. Fragment-Based Lead Discovery Using X-Ray Crystallography. *J. Med. Chem.* **2005**, *48*, 403–413.
254. Card, G. L.; Blasdel, L.; England, B. P.; Zhang, C.; Suzuki, Y.; Gillette, S.; Fong, D.; Ibrahim, P. N.; Artis, D. R.; Bollag, G.; Milburn, M. V.; Kim, S.-H.; Schlessinger, J.; Zhang, K. Y. J. A Family of Phosphodiesterase Inhibitors Discovered by Cocrystallography and Scaffold-Based Drug Design. *Nat. Biotechnol.* **2005**, *23*, 201–207.
255. Danielson, U. H. Fragment Library Screening and Lead Characterization Using SPR Biosensors. *Curr. Top. Med. Chem.* **2009**, *9*, 1725–1735.
256. Wang, Y.-S.; Strickland, C.; Voigt, J. H.; Kennedy, M. E.; Beyer, B. M.; Senior, M. M.; Smith, E. M.; Nechuta, T. L.; Madison, V. S.; Czarniecki, M.; McKittrick, B. A.; Stamford, A. W.; Parker, E. M.; Hunter, J. C.; Greenlee, W. J.; Wyss, D. F. Application of Fragment-Based NMR Screening, X-Ray Crystallography, Structure-Based Design, and Focused Chemical Library Design to Identify Novel microM Leads for the Development of nM BACE-1 (beta-Site APP Cleaving Enzyme 1) Inhibitors. *J. Med. Chem.* **2010**, *53*, 942–950.
257. Key Organics <http://www.keyorganics.net/> (accessed Apr 22, 2015).
258. Enamine <http://www.enamine.net/> (accessed Apr 22, 2015).
259. Vitas M. Labs <http://www.vitasmlab.com/> (accessed Apr 22, 2015).
260. Chembridge <http://www.chembridge.com/> (accessed Apr 22, 2015).
261. Life Chemicals <http://www.lifechemicals.com/> (accessed Apr 22, 2015).
262. Maybridge <http://www.maybridge.com/> (accessed Apr 22, 2015).
263. Zhang, J.; Yang, P. L.; Gray, N. S. Targeting Cancer with Small Molecule Kinase Inhibitors. *Nat. Rev. Cancer* **2009**, *9*, 28–39.
264. Bamborough, P.; Brown, M. J.; Christopher, J. A.; Chung, C.; Mellor, G. W. Selectivity of Kinase Inhibitor Fragments. *J. Med. Chem.* **2011**, *54*, 5131–5143.
265. Johnson, S.; Barile, E.; Farina, B.; Purves, A.; Wei, J.; Chen, L.-H.; Shiryaev, S.; Zhang, Z.; Rodionova, I.; Agrawal, A.; Cohen, S. M.; Osterman, A.; Strongin, A.; Pellecchia, M. Targeting Metalloproteins by Fragment-Based Lead Discovery. *Chem. Biol. Drug Des.* **2011**, *78*, 211–223.
266. Fry, D. C. Protein-Protein Interactions as Targets for Small Molecule Drug Discovery. *Biopolymers* **2006**, *84*, 535–552.
267. Valkov, E.; Sharpe, T.; Marsh, M.; Greive, S.; Hyvönen, M. Targeting Protein-Protein Interactions and Fragment-Based Drug Discovery. *Top. Curr. Chem.* **2012**, *317*, 145–179.
268. Asinex <http://www.asinex.com/> (accessed Apr 22, 2015).
269. Jordan, J. B.; Poppe, L.; Xia, X.; Cheng, A. C.; Sun, Y.; Michelsen, K.; Eastwood, H.; Schnier, P. D.; Nixey, T.; Zhong, W. Fragment Based Drug Discovery: Practical Implementation Based on ¹⁹F NMR Spectroscopy. *J. Med. Chem.* **2012**, *55*, 678–687.
270. Otava Chemicals <http://www.otavachemicals.com/> (accessed Apr 22, 2015).

Bibliography

271. Vulpetti, A.; Dalvit, C. Design and Generation of Highly Diverse Fluorinated Fragment Libraries and Their Efficient Screening with Improved (19) F NMR Methodology. *ChemMedChem* **2013**, *8*, 2057–2069.
272. Ritchie, T. J.; Macdonald, S. J. F. The Impact of Aromatic Ring Count on Compound Developability--Are Too Many Aromatic Rings a Liability in Drug Design? *Drug Discov. Today* **2009**, *14*, 1011–1020.
273. Ritchie, T. J.; Macdonald, S. J. F.; Young, R. J.; Pickett, S. D. The Impact of Aromatic Ring Count on Compound Developability: Further Insights by Examining Carbo- and Hetero-Aromatic and -Aliphatic Ring Types. *Drug Discov. Today* **2011**, *16*, 164–171.
274. Lovering, F.; Bikker, J.; Humblet, C. Escape from Flatland: Increasing Saturation as an Approach to Improving Clinical Success. *J. Med. Chem.* **2009**, *52*, 6752–6756.
275. Aldeghi, M.; Malhotra, S.; Selwood, D. L.; Chan, A. W. E. Two- and Three-Dimensional Rings in Drugs. *Chem. Biol. Drug Des.* **2014**, *83*, 450–461.
276. Clemons, P. A.; Bodycombe, N. E.; Carrinski, H. A.; Wilson, J. A.; Shamji, A. F.; Wagner, B. K.; Koehler, A. N.; Schreiber, S. L. Small Molecules of Different Origins Have Distinct Distributions of Structural Complexity That Correlate with Protein-Binding Profiles. *Proc. Natl. Acad. Sci. U. S. A.* **2010**, *107*, 18787–18792.
277. Clemons, P. A.; Wilson, J. A.; Dančík, V.; Muller, S.; Carrinski, H. A.; Wagner, B. K.; Koehler, A. N.; Schreiber, S. L. Quantifying Structure and Performance Diversity for Sets of Small Molecules Comprising Small-Molecule Screening Collections. *Proc. Natl. Acad. Sci. U. S. A.* **2011**, *108*, 6817–6822.
278. Hung, A. W.; Ramek, A.; Wang, Y.; Kaya, T.; Wilson, J. A.; Clemons, P. a; Young, D. W. Route to Three-Dimensional Fragments Using Diversity-Oriented Synthesis. *Proc. Natl. Acad. Sci. U. S. A.* **2011**, *108*, 6799–6804.
279. Morgan, K. F.; Hollingsworth, I. A.; Bull, J. A. 2-(Aryl-Sulfonyl)oxetanes as Designer 3-Dimensional Fragments for Fragment Screening: Synthesis and Strategies for Functionalisation. *Chem. Commun. (Camb).* **2014**, *50*, 5203–5205.
280. Scholfield, M. R.; Zanden, C. M. Vander; Carter, M.; Ho, P. S. Halogen Bonding (X-Bonding): A Biological Perspective. *Protein Sci.* **2013**, *22*, 139–152.
281. Wilcken, R.; Zimmermann, M. O.; Lange, A.; Joerger, A. C.; Boeckler, F. M. Principles and Applications of Halogen Bonding in Medicinal Chemistry and Chemical Biology. *J. Med. Chem.* **2013**, *56*, 1363–1388.
282. Lu, Y.; Liu, Y.; Xu, Z.; Li, H.; Liu, H.; Zhu, W. Halogen Bonding for Rational Drug Design and New Drug Discovery. *Expert Opin. Drug Discov.* **2012**, *7*, 375–383.
283. Zimmermann, M. O.; Lange, A.; Wilcken, R.; Cieslik, M. B.; Exner, T. E.; Joerger, A. C.; Koch, P.; Boeckler, F. M. Halogen-Enriched Fragment Libraries as Chemical Probes for Harnessing Halogen Bonding in Fragment-Based Lead Discovery. *Future Med. Chem.* **2014**, *6*, 617–639.
284. Sauer, W. H. B.; Schwarz, M. K. Molecular Shape Diversity of Combinatorial Libraries: A Prerequisite for Broad Bioactivity. *J. Chem. Inf. Comput. Sci.* **2003**, *43*, 987–1003.
285. Namboothiri, I. N. N.; Rastogi, N. *Isoxazoline from Nitro Compounds: Synthesis and Applications*; Hassner, A., Ed.; Topics in Heterocyclic Chemistry; Springer Berlin Heidelberg, **2008**; Vol. 12.
286. O'Dwyer, P. J.; Alonso, M. T.; Leyland-Jones, B. Acivicin: A New Glutamine Antagonist in Clinical Trials. *J. Clin. Oncol.* **1984**, *2*, 1064–1071.
287. Encarnación, R. D.; Sandoval, E.; Malmstrøm, J.; Christophersen, C. Calafianin, a Bromotyrosine Derivative from the Marine Sponge *Aplysina G Erardogreeni*. *J. Nat. Prod.* **2000**, *63*, 874–875.

Bibliography

288. Kaur, K.; Kumar, V.; Sharma, A. K.; Gupta, G. K. Isoxazoline Containing Natural Products as Anticancer Agents: A Review. *Eur. J. Med. Chem.* **2014**, *77*, 121–133.
289. Aggarwal, R.; Bansal, A.; Mittal, A. Synthesis and Antimicrobial Activity of 3-(2-Thienyl)-4-Arylazo-5-Hydroxy-5-Trifluoromethyl- Δ^2 -Isoxazolines and 3-(2-Thienyl)-4-Arylazo-5-Trifluoromethylisoxazoles. *J. Fluor. Chem.* **2013**, *145*, 95–101.
290. Tangallapally, R. P.; Sun, D.; Rakesh; Budha, N.; Lee, R. E. B.; Lenaerts, A. J. M.; Meibohm, B.; Lee, R. E. Discovery of Novel Isoxazolines as Anti-Tuberculosis Agents. *Bioorg. Med. Chem. Lett.* **2007**, *17*, 6638–6642.
291. Mandawad, G. G.; Kamble, R. D.; Hese, S. V.; More, R. A.; Gacche, R. N.; Kodam, K. M.; Dawane, B. S. An Efficient Synthesis of Isoxazoline Libraries of Thiophene Analogs and Its Antimycobacterial Investigation. *Med. Chem. Res.* **2014**, *23*, 4455–4463.
292. Castellano, S.; Kuck, D.; Viviano, M.; Yoo, J.; López-Vallejo, F.; Conti, P.; Tamborini, L.; Pinto, A.; Medina-Franco, J. L.; Sbardella, G. Synthesis and Biochemical Evaluation of $\delta(2)$ -Isoxazoline Derivatives as DNA Methyltransferase 1 Inhibitors. *J. Med. Chem.* **2011**, *54*, 7663–7677.
293. Najim, N.; Bathich, Y.; Zain, M. M.; Hamzah, A. S.; Shaameri, Z. Evaluation of the Bioactivity of Novel Spiroisoxazoline Typecompounds against Normal and Cancer Cell Lines. *Molecules* **2010**, *15*, 9340–9353.
294. Reddy, D. M.; Qazi, N. a; Sawant, S. D.; Bandey, A. H.; Srinivas, J.; Shankar, M.; Singh, S. K.; Verma, M.; Chashoo, G.; Saxena, A.; Mondhe, D.; Saxena, A. K.; Sethi, V. K.; Taneja, S. C.; Qazi, G. N.; Sampath Kumar, H. M. Design and Synthesis of Spiro Derivatives of Parthenin as Novel Anti-Cancer Agents. *Eur. J. Med. Chem.* **2011**, *46*, 3210–3217.
295. Mousa, S. a.; Wityak, J. Orally Active Isoxazoline GPIIb/IIIa Antagonists. *Cardiovasc. Drug Rev.* **1998**, *16*, 48–61.
296. Habeeb, A. G.; Praveen Rao, P. N.; Knaus, E. E. Design and Synthesis of 4,5-Diphenyl-4-Isoxazolines: Novel Inhibitors of Cyclooxygenase-2 with Analgesic and Antiinflammatory Activity. *J. Med. Chem.* **2001**, *44*, 2921–2927.
297. Dallanoce, C.; Frigerio, F.; Martelli, G.; Grazioso, G.; Matera, C.; Pomè, D. Y.; Pucci, L.; Clementi, F.; Gotti, C.; De Amici, M. Novel Tricyclic Delta(2)-Isoxazoline and 3-Oxo-2-Methyl-Isoxazolidine Derivatives: Synthesis and Binding Affinity at Neuronal Nicotinic Acetylcholine Receptor Subtypes. *Bioorg. Med. Chem.* **2010**, *18*, 4498–4508.
298. Dallanoce, C.; Magrone, P.; Matera, C.; Frigerio, F.; Grazioso, G.; De Amici, M.; Fucile, S.; Piccari, V.; Frydenvang, K.; Pucci, L.; Gotti, C.; Clementi, F.; De Micheli, C. Design, Synthesis, and Pharmacological Characterization of Novel Spirocyclic Quinuclidinyl- Δ^2 -Isoxazoline Derivatives as Potent and Selective Agonists of $\alpha 7$ Nicotinic Acetylcholine Receptors. *ChemMedChem* **2011**, *6*, 889–903.
299. Dallanoce, C.; Canovi, M.; Matera, C.; Mennini, T.; De Amici, M.; Gobbi, M.; De Micheli, C. A Novel Spirocyclic Tropanyl- Δ^2 -Isoxazoline Derivative Enhances Citalopram and Paroxetine Binding to Serotonin Transporters as Well as Serotonin Uptake. *Bioorg. Med. Chem.* **2012**, *20*, 6344–6355.
300. Conti, P.; Dallanoce, C.; De Amici, M.; De Micheli, C.; Klotz, K.-N. Synthesis of New Δ^2 -Isoxazoline Derivatives and Their Pharmacological Characterization as B-Adrenergic Receptor Antagonists. *Bioorg. Med. Chem.* **1998**, *6*, 401–408.
301. Paul Savage, G. Spiro Isoxazolines via Nitrile Oxide 1,3-Dipolar Cycloaddition Reactions. *Curr. Org. Chem.* **2010**, *14*, 1478–1499.

Bibliography

302. Zhao, H.; Li, X.; Ran, X.; Zhang, W. Theoretical Study of Reaction Mechanism and Regioselectivity of Spiro-Isoxazoline Derivatives Synthesized by Intermolecular 1,3-Dipolar Cycloaddition. *J. Mol. Struct. THEOCHEM* **2004**, *683*, 207–213.
303. Oravec, P.; Fiserá, L.; Ertl, P.; Vegh, D. Regioselectivity in the 1,3-Dipolar Cycloaddition of Nitrile Oxides to 3,3-Methylene-5,5-Dimethyl-2-Pyrrolidinone. *Monatshefte für Chemie / Chem. Mon.* **1991**, *122*, 821–828.
304. Fiserá, L.; Sauter, F.; J., F.; Feng, Y.; Ertp, P.; Mereiter, K. Cycloadditions of Nitrile Oxides and Nitrones to Studies in Regio- and Stereoselectivity Scheme. *Monatshefte für Chemie / Chem. Mon.* **1994**, *125*, 553–563.
305. Frohlich, J.; Fiserá, L.; Sauter, F.; Feng, Y.; Ert, P. Regioselectivity of Cycloadditions of Nitrile Oxides and Nitrones to 4-Methylene- Tetrahydrothiopyrane. *Monatshefte für Chemie / Chem. Mon.* **1995**, *126*, 75–84.
306. Kumar, K. A.; Govindaraju, M.; Jayaroopa, P.; Kumar, G. V. Nitrile Oxides: A Key Intermediate in Organic Synthesis. *Int. J. Pharm. , Chem. Biol. Sci.* **2012**, *3*, 91–101.
307. Milinkevich, K. A.; Ye, L.; Kurth, M. J. Synthesis of 5-(thiazol-5-Yl)-4,5-Dihydroisoxazoles from 3-Chloropentane-2,4-Dione. *J. Comb. Chem.* **2008**, *10*, 521–525.
308. Dondoni, A.; Fantin, G.; Fogagnolo, M.; Medici, A.; Pedrini, P. A New Convenient Preparation of 2-, 4-, and 5- Thiazolecarboxaldehydes and Their Conversion into the Corresponding Carbonitrile N -Oxides: Synthesis of 3-Thiazolylisoxazoles and 3-Thiazolylisoxazolines. *Synthesis (Stuttg).* **1987**, *1987*, 998–1001.
309. Iwakura, Y.; Uno, K.; Shiraishi, S.; Hongu, T. 1,3-Dipolar Cycloaddition Reaction of Thiophenecarbonitrile N-Oxides with Various Dipolarophiles. *Bull. Chem. Soc. Jpn.* **1968**, *41*, 2954–2959.
310. Zhang, J.; Curran, D. P. Stereoselective Synthesis of 1,2-Diols by the Cycloadditive Strategy: Total Synthesis of (±)-Exo-Brevicomín and (±)-and (-)-Pestalotin. *J. Chem. Soc. Perkin Trans. 1* **1991**, *3*, 2627.
311. Duffy, J. L.; Bao, J.; Ondeyka, D. L.; Tyagarajan, S.; Shao, P.; Ye, F.; Katipally, R.; Finke, P. E.; Zang, Y.; Plotkin, M. A. Spiro Isoxazoline Compounds as SSTR5 Antagonists. Patent WO 2011/146324, November 24, 2011.
312. Enoki, M.; Honda, Y.; Kuwahara, M.; Watanabe, T. Chemical Synthesis, Iron Redox Interactions and Charge Transfer Complex Formation of Alkylitaconic Acids from Ceriporiopsis Subvermispora. *Chem. Phys. Lipids* **2002**, *120*, 9–20.
313. Meyer-Wilmes, I.; Gerke, R.; Fitjer, L. Helical Primary Structures of 1,3-Spiroannelated Five-Membered Rings: (±)-trisp[4.1.1.4.2.2]heptadecane and (±)-tetraspiro[4.1.1.1.4.2.2.2]heneicosane. *Tetrahedron* **2009**, *65*, 1689–1696.
314. Gonçalves, R. S. B.; Dos Santos, M.; Bernadat, G.; Bonnet-Delpon, D.; Crousse, B. A One-Pot Synthesis of 3-Trifluoromethyl-2-Isoxazolines from Trifluoromethyl Aldoxime. *Beilstein J. Org. Chem.* **2013**, *9*, 2387–2394.
315. Firth, N. C.; Brown, N.; Blagg, J. Plane of Best Fit: A Novel Method to Characterize the Three-Dimensionality of Molecules. *J. Chem. Inf. Model.* **2012**, *52*, 2516–2525.



COLLEGE DOCTORAL

École Doctorale
BIOLOGIE SANTÉ



UNIVERSITÉ LILLE 2 DROIT ET SANTÉ (FRANCE)

en cotutelle avec

UNIVERSITÉ DES SCIENCES MÉDICALES DE HỒ CHI MINH VILLE (VIET NAM)

Résumé

Thèse de doctorat

Spécialité: Sciences du médicament

Conception, synthèse et développement de nouveaux composés antituberculeux selon une approche par fragments

présentée et soutenue publiquement le 26 juin 2015 à Lille

par **TRẦN Ngọc Châu**

devant le jury composé de:

M. Benoît DÉPREZ

Professeur à l'Université Lille 2 Droit et Santé

Membre invité

Mme. Line BOUREL-BONNET

Professeur à l'Université de Strasbourg

Rapporteur

M. Pierre VERHAEGHE

Professeur à l'Université Toulouse III Paul Sabatier

Rapporteur

M. Nicolas WILLAND

Professeur à l'Université Lille 2 Droit et Santé

Directeur de thèse

M. LÊ Minh Trí

Professeur à l'Université des Sciences Médicales de Ho Chi Minh-ville

Co-directeur de thèse

Unité mixte de recherche INSERM U1177 (ancien nom U761)
Médicaments et Molécules pour Agir sur les Systèmes Vivants (M2SV)
Institut Pasteur de Lille – Université Lille 2 – Université Lille Nord de France
3, rue du Professeur Laguesse B.P. 83 59006 LILLE cedex

[Cette page a été intentionnellement laissée blanche]

1. Introduction générale

La tuberculose (TB) est une des plus anciennes maladies affectant l'homme, mais ce n'est pas encore une maladie du passé.

La tuberculose a toujours été présente dans l'histoire humaine et elle a peut-être tué plus de personnes que tous les autres pathogènes microbiens. A partir du 19^{ème} siècle, la compréhension de la pathogenèse de cette maladie a commencé avec la contribution de nombreux chercheurs. Ces études, notamment réalisées par Robert Koch en 1882, ont permis d'aboutir à l'identification du bacille responsable de cette infection comme étant *Mycobacterium tuberculosis*, appelé par la suite bacille de Koch.

La découverte de cette bactérie comme agent étiologique de la tuberculose a accéléré la recherche et le développement des outils nécessaires au traitement et à la prévention de cette maladie. En 1921, c'est la première fois que le vaccin produit par Calmette et Guérin (vaccin BCG) a été utilisé en clinique. Par la suite, de nombreux médicaments antituberculeux ont ensuite été développés, par exemple la streptomycine, l'isoniazide, la rifampicine, l'éthambutol et le pyrazinamide. A partir de 1967 et jusqu'à aujourd'hui, la quadrithérapie antituberculeuse est utilisée pour traiter la tuberculose. Toutes ces avancées ont conduit à une diminution remarquablement rapide des cas de tuberculose dans le monde. A partir de ce moment, beaucoup de gens ont cru que cette maladie avait quasiment été éradiquée. Cependant, au milieu des années 80, avec l'apparition du SIDA, la tuberculose a rapidement refait son apparition.

En 1993, l'Organisation Mondiale de la Santé (OMS) a déclaré que la tuberculose était «une urgence de santé publique mondiale». Plus de 20 ans après, cette maladie infectieuse causée par *Mycobacterium tuberculosis*, reste toujours un problème à l'échelle de la planète. Malgré des progrès très importants enregistrés dans la lutte contre la tuberculose dans le monde, l'OMS estime que 9 millions de personnes ont contracté cette maladie en 2013 et que 1,5 million sont morts durant cette même année. Aujourd'hui, la tuberculose reste l'une des principales causes de mortalité due à une infection bactérienne. De plus, l'émergence de la tuberculose multirésistante nécessite le développement de nouveaux outils et de nouvelles stratégies thérapeutiques.

Les traitements actuels de la tuberculose présentent encore des inconvénients majeurs et l'émergence de souches résistantes aux médicaments antituberculeux imposent la découverte de nouvelles alternatives thérapeutiques. L'augmentation du nombre de composés dans le pipeline des candidats aux phases cliniques est une réponse positive à cette situation. Toutefois, il faudra un certain temps avant que certains de ces composés soient approuvés. L'espoir a récemment pris forme avec l'approbation conditionnelle par la FDA et l'EMA de deux nouveaux médicaments: Sirturo™ (bedaquiline) et Deltyba™ (delamanid). Cependant nous sommes encore loin d'une solution globale pour le traitement de tous les patients étant donné que ces deux médicaments ont été accordés exclusivement pour le traitement des infections pulmonaires dues aux souches multirésistantes lorsque les traitements alternatifs ne peuvent pas être utilisés en raison de la résistance ou de l'intolérance. De plus, il existe toujours la possibilité que la bactérie puisse rapidement développer des résistances liées au mécanisme d'action de ces nouveaux médicaments. En conclusion, l'identification de composés actifs qui peuvent être utilisés en toute

sécurité, dans les combinaisons avec les médicaments de première et seconde ligne est encore fortement requise.

C'est pour toutes ces raisons que l'arsenal thérapeutique doit être renforcé. Ce travail de thèse repose sur la découverte et l'optimisation de nouveaux composés antituberculeux selon des approches dont le point de départ commun est le criblage de petites molécules appelées fragments.

2. Amélioration de propriétés pharmacocinétiques et physico-chimiques d'inhibiteurs potentiels d'EthR

La première partie de ce manuscrit présente la continuité d'un travail démarré au cours de la thèse de Baptiste Villemagne et qui a pour but de potentialiser l'activité de l'éthionamide, un médicament antituberculeux utilisé pour le traitement de seconde intention. Le répresseur transcriptionnel EthR a été validé comme étant un élément clé dans la bioactivation de l'éthionamide (ETH).

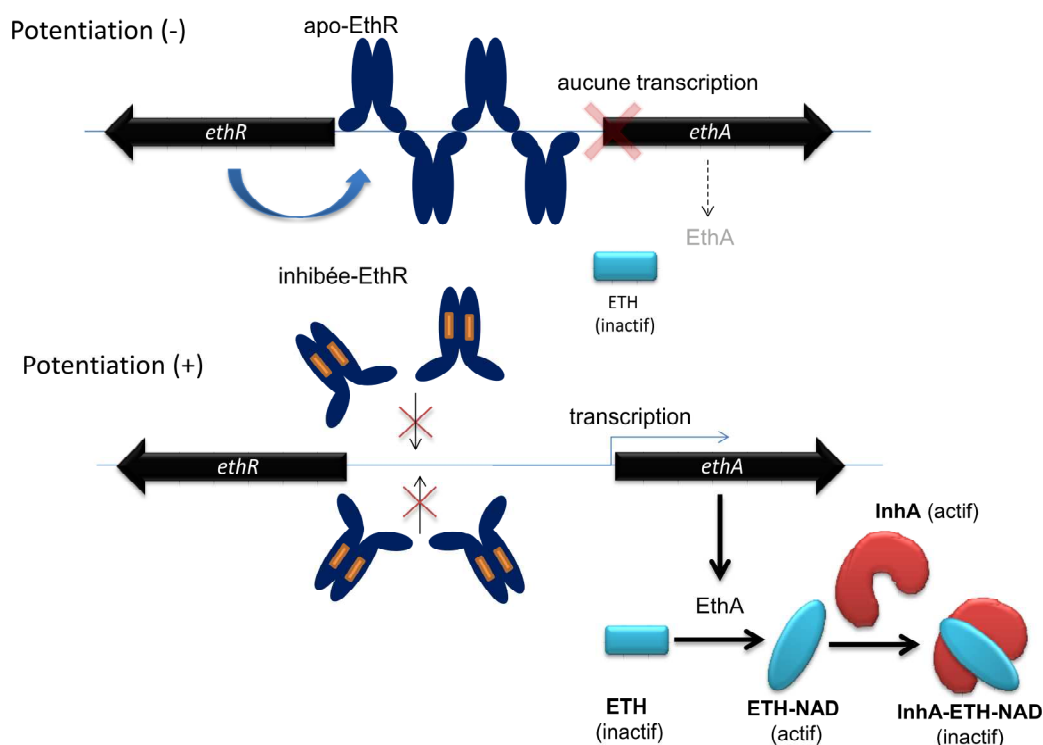


Figure 1: Inhibition du répresseur transcriptionnel EthR pour potentialiser l'activité de l'éthionamide

La structure du répresseur transcriptionnel EthR se présente sous forme d'un homodimère. Chaque monomère possède neuf hélices- α . Les trois hélices α_1 à α_3 forment le domaine HTH (Helix-Turn-Helix) qui est responsable de la fixation à l'ADN. Les six hélices α_4 à α_9 forment la partie centrale de la protéine. Le domaine de régulation de cette protéine consiste en un tunnel long formé majoritairement de résidus hydrophobes. Les inhibiteurs d'EthR qui peuvent se lier dans ce tunnel vont induire un changement de la conformation de la protéine. En conséquence, les distances entre les deux domaines HTH de chaque monomère va augmenter. Avec cette configuration, ce répresseur transcriptionnel n'est plus capable de venir se fixer sur l'opérateur d'*ethA*.

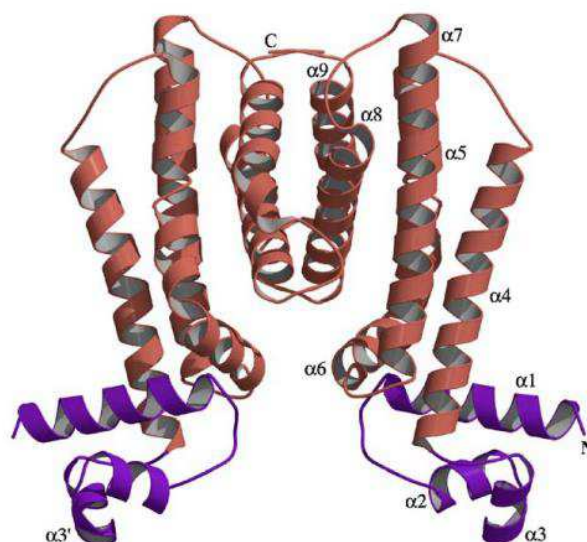


Figure 2: La structure du répresseur transcriptionnel EthR représentée sous la forme d'un homodimère

Les inhibiteurs de cette cible, développés selon une approche par fragments ont permis de potentialiser l'activité de l'éthionamide *in vitro*. Cependant, la faible stabilité microsomale de ces composés a été un frein à leur utilisation *in vivo*.

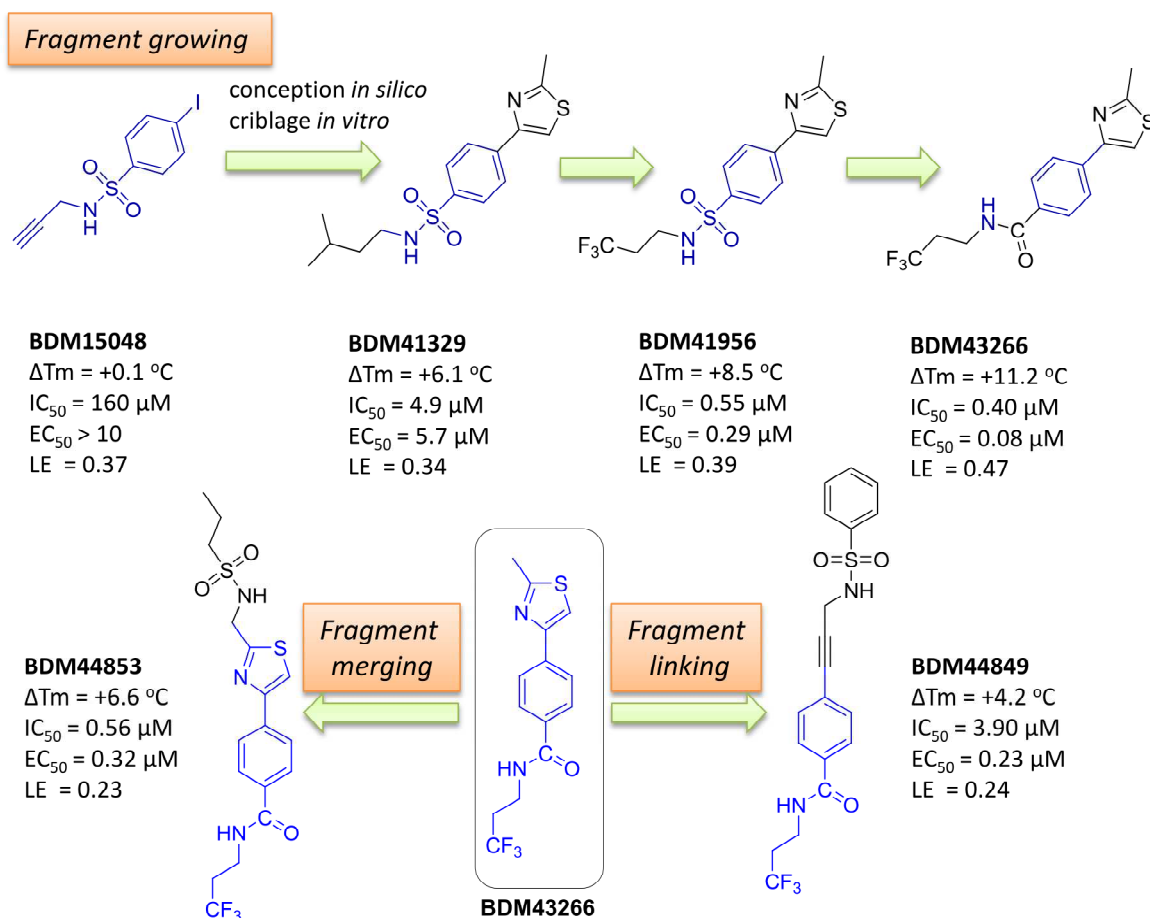
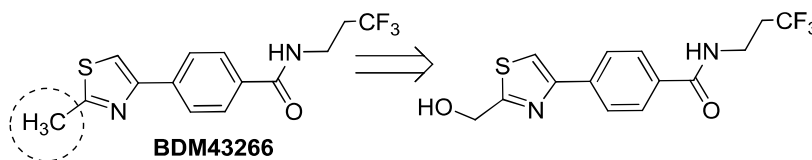


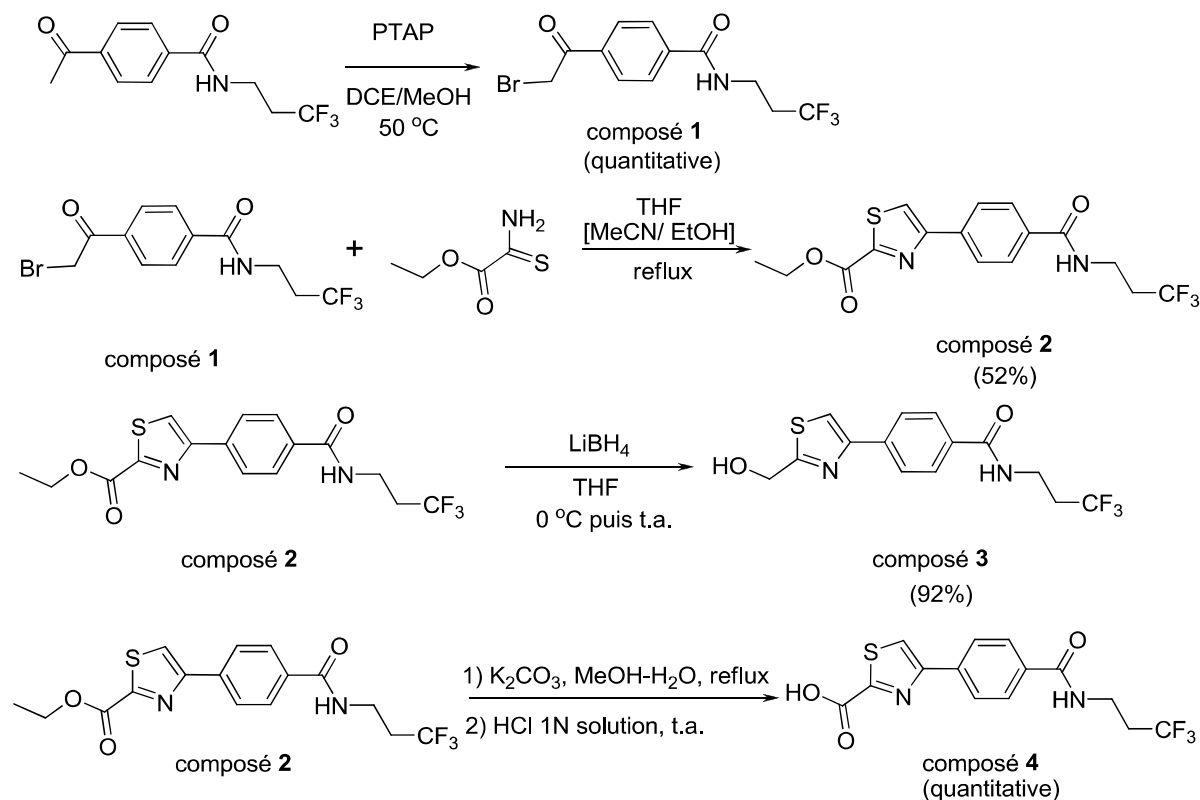
Figure 3: Les inhibiteur d'EthR développés selon une approche par fragment

Dans la première partie de cette thèse, une étude de la métabolisation du composé tête de série (BDM43266) sur microsomes murins a été réalisée. Cette étude a montré que le métabolite

majoritaire semblait être le dérivé hydroxylé provenant de l'oxydation du groupement méthyle branché sur le cycle thiazole (Scheme 1). Nous avons également pensé que l'alcool correspondant pouvait ensuite être oxydé en acide carboxylique, mais sans que nous puissions l'identifier clairement. Les deux métabolites hypothétiques du composé BM43266 ont donc été synthétisés et utilisés pour confirmer les analyses réalisées par spectrométrie de masse (Scheme 2).

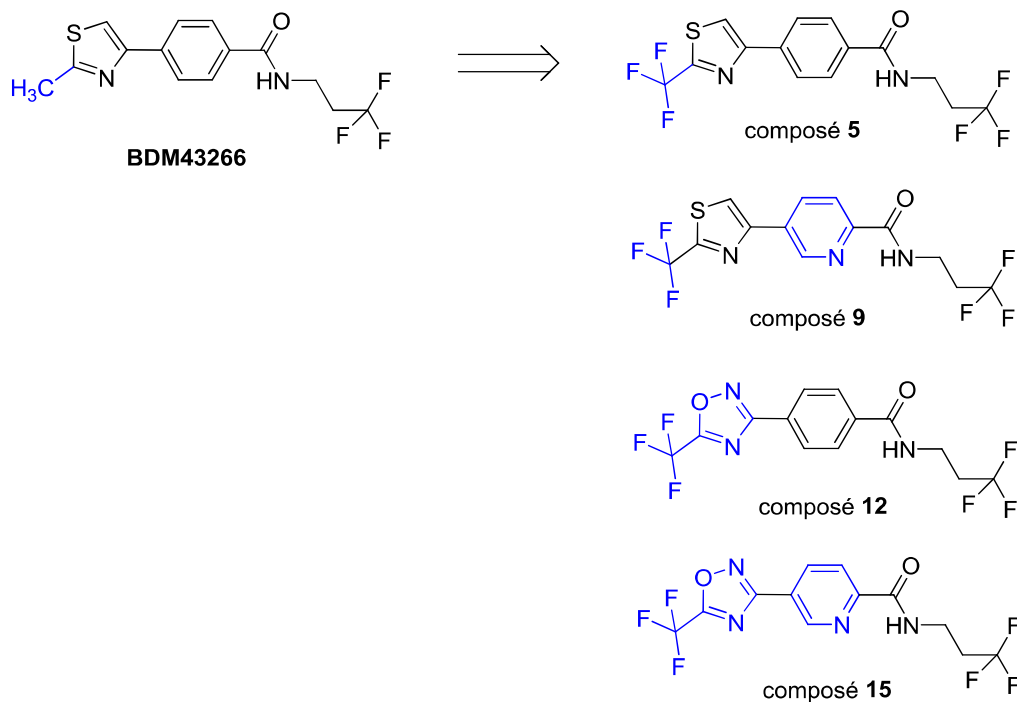


Scheme 1: Oxidation de la group methyle sur thiazole



Scheme 2: Synthèse des deux métabolites hypothétiques du BDM43266

L'utilisation de ces composés a permis de confirmer l'identité du métabolite majoritairement observé. Ceci nous a également permis de voir que ce métabolite était beaucoup moins actif que la molécule parente. Afin d'augmenter la stabilité microsomale du composé 'lead', nous avons donc introduit des atomes de fluor sur le groupement méthyle, point clé du métabolisme. Nous avons également essayé de diminuer le caractère lipophile des dérivés synthétisés en remplaçant le cycle phényle central par cycle pyridinique, ou en remplaçant le cycle thiazole par un cycle 1,2,4-oxadiazole.



Scheme 3: Liste des composés étudiés afin d'augmenter la stabilité métabolique du composé lead BDM43266 tout en conservant des propriétés pharmacodynamiques optimales.

Les composés présentés dans le Scheme 3 ont été synthétisés avec succès et nous avons mesuré leur activité dans les différents tests d'affinité et fonctionnels développés dans le cadre de ce projet. La plupart des modifications réalisées n'ont pas eu d'impact négatif sur l'activité de ces analogues. Seul le composé **15**, s'est révélé moins afin pour EthR et moins efficace dans le test de potentialisation de l'éthionamide réalisé sur bactéries.

L'étude de la stabilité métabolique de ces dérivés a permis de confirmer nos hypothèses. Les composés présentant ce groupement trifluorométhyle se sont tous avérés plus stables. De plus le remplacement du benzène par une pyridine a permis de compenser l'augmentation du caractère lipophile en conservant une solubilité équivalente au composé de référence (ex : composé **9**, solubilité = 17.2 µg/mL vs composé **5**, solubilité = 8.2 µg/mL, Table 1).

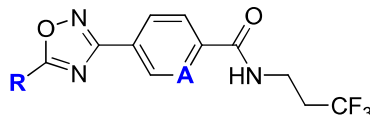
Table 1: Les activités biologiques, les propriétés pharmacocinétiques et physico-chimiques des dérivés thiazole 5 et 9

	R	A	ΔTm (°C)	EC ₅₀ (µM)	HA	MW (Da)	LE	t _{1/2} (min)	CL _{int} (µL/min/mg)	Solubilité (µg/mL)	logD
BDM43266	CH ₃	C	10.6	0.10	21	314.33	0.46	10	144	14.7	2.8
composé 5	CF ₃	C	9.9	0.10	24	368.30	0.40	19	62	8.2	3.6
composé 9	CF ₃	N	9.5	0.098	24	369.29	0.40	16	79	17.2	3.3

ΔTm = Tm(holo-protéine)-Tm(apo-protéine) en test TSA ; EC₅₀ est la concentration du ligand qui permet de retrouver 50% de l'activité de l'éthionamide à la CMI/10 ; HA = nombre des atomes autres que des hydrogènes ; MW = masse moléculaire LE = -1.37log(EC₅₀) ; t_{1/2} = la demi-vie en présence de microsomes ; CL_{int} = Clairance intrinsèque.

Dans le cas du remplacement du cycle thiazole par un cycle 1,2,4-oxadiazole, soit le composé est plus stable mais beaucoup moins soluble (composé **12**, Table 2), soit le composé est stable, aussi soluble que le produit de référence mais moins actif (composé **15**, Table 2).

Table 2: Les activités biologiques, les propriétés pharmacocinétiques et physico-chimiques des dérivés 1,2,4-oxadiazole



	R	A	ΔT_m (°C)	EC_{50} (μM)	HA	MW (Da)	LE	$t_{1/2}$ (min)	CL_{int} ($\mu L/min/mg$)	Solubilité ($\mu g/mL$)	logD
BDM71159	CH ₃	C	9.3	0.082	21	299.25	0.46	7	172	21.8	2.3
composé 12	CF ₃	C	10.2	0.073	24	353.22	0.41	22	34	2.4	3.5
composé 15	CF ₃	N	7.3	0.39	24	354.21	0.37	17	73	16.8	3.0

Par conséquent, les composés **5** et **9**, qui ont montré le meilleur compromis en terme, d'activités, de solubilité et de stabilité microsomale seront caractérisés dans le modèle animal pour envisager un éventuel test d'activité.

En outre, une étude de la modélisation moléculaire a été réalisée afin d'illustrer les interactions possibles entre ces dérivés et les résidus présents dans le site de liaison d'EthR. Une corrélation entre l'affinité de liaison et l'activité biologique a été étudiée.

3. Synthèse et développement d'inhibiteurs de MabA

La deuxième partie de cette thèse s'est concentrée sur la synthèse d'inhibiteurs de MabA, une β -cétolactone synthase mycobactérienne participant à la synthèse des acides gras à longue chaîne, précurseurs des acides mycoliques qui sont les constituants majeurs de la paroi mycobactérienne.

L'isoniazide et plusieurs autres médicaments (éthionamide, isoxyl, thiocétazone et thiolactomycine) ciblent la biosynthèse des acides mycoliques via le système FAS-II. Cette voie de biosynthèse est essentielle et spécifique à mycobactéries et a prouvé être une riche source de cibles pour les antibiotiques déjà développés. La protéine MabA, également nommé FabG1, est une enzyme clé impliquée dans ce processus. Elle catalyse la réduction des dérivés β -cétolactone à longue chaîne en présence de NADPH. Cette enzyme a été démontrée génétiquement comme étant essentielle pour la survie de la bactérie et à ce jour aucun inhibiteur 'drug-like' de cette enzyme n'a encore été identifié. Elle représente donc une cible de choix pour démarrer un programme de découverte de médicaments.

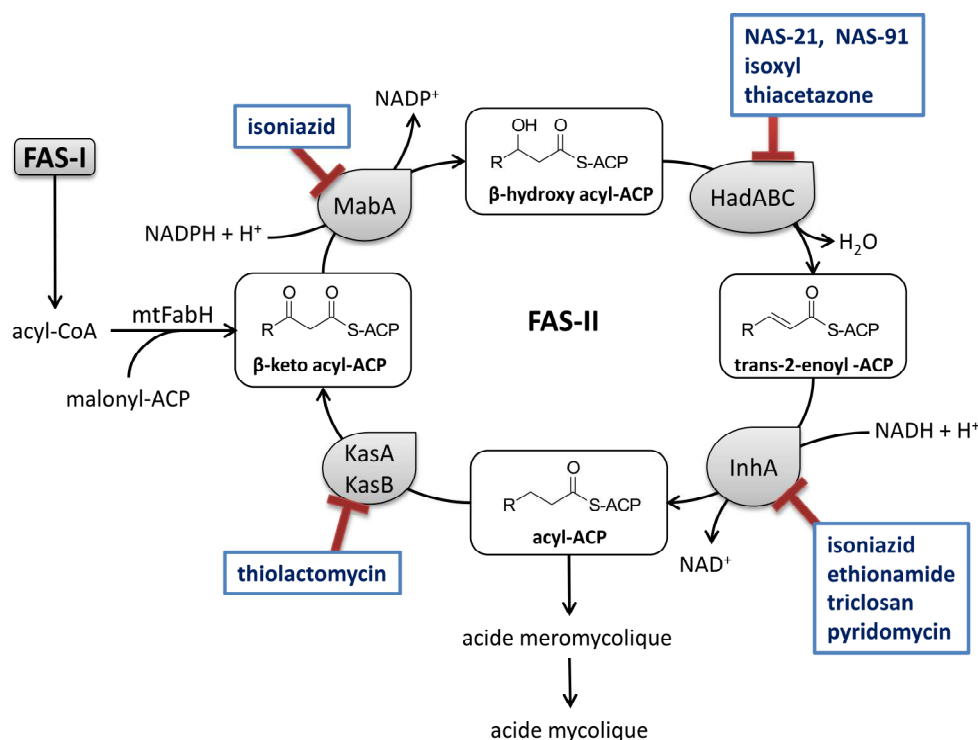


Figure 4: Les enzymes dans le système FAS-II et leur inhibiteurs

Un premier criblage *in silico* réalisé sur une chimiothèque de composés 'drug-like' sélectionnés dans la base de données ZINC, à partir des données cristallographiques de l'enzyme disponibles dans la littérature, ne nous a pas permis d'identifier des inhibiteurs fonctionnels.

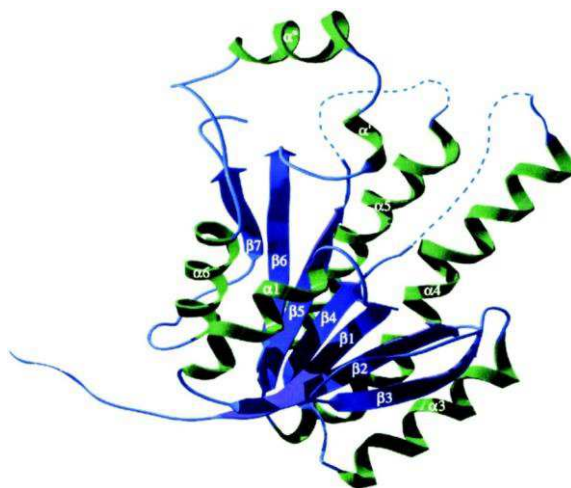
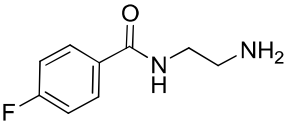
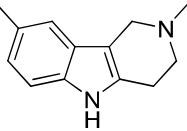
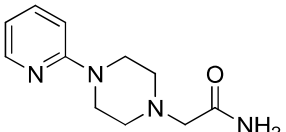
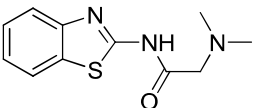
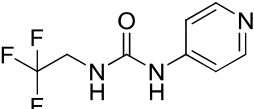
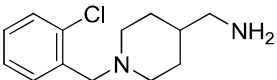
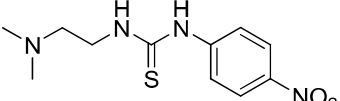
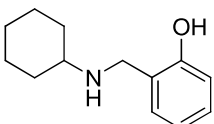
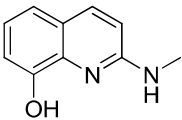
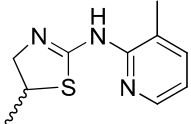
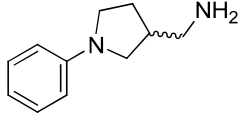
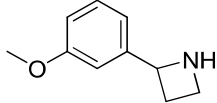


Figure 5: Structure 3D de l'enzyme MabA

Pour améliorer nos chances de trouver des inhibiteurs de faible poids moléculaire, avec des propriétés physico-chimiques adéquates pour pénétrer dans les mycobactéries et atteindre leur cible, nous nous sommes de nouveau tournés vers une approche de conception d'inhibiteurs de MabA basée sur l'identification et l'optimisation de fragments. Pour cela, une première chimiothèque de 1040 fragments a été criblée en utilisant un test d'affinité de ces composés à l'enzyme. Ce criblage nous a permis d'identifier 82 hits qui ont été confirmés dans une étude dose-réponse. De ces 82 hits, 12 molécules ont été sélectionnées sur la base de leur capacité à inhiber la croissance mycobactérienne *in vitro* (Table 3). Ces 12 composés ont alors été

synthétisés pour être testés dans un test secondaire. De façon étonnante, aucun de ces composés n'a alors montré d'activité inhibitrice de MabA bien que présentant une affinité pour la forme apo de l'enzyme et une activité sur l'inhibition de la croissance de la bactérie.

Table 3: Structures des hits obtenus par le premier criblage TSA et sélectionnés sur la base de leur activité sur bactéries

Fragment ID	Structure	ΔT_m	% inhibition
1		3.1	> 95
2		3.7	> 95
3		3.7	> 95
4		3.8	> 95
5		4.1	> 95
6		5.4	80
7		3.1	> 95
8		3.3	82
9		4.8	> 95
10		3.7	> 95
11		3.9	> 95
12		3.8	> 95

Nous avons donc émis l'hypothèse que le test TSA n'était pas le meilleur outil pour l'identification d'inhibiteurs fonctionnels de MabA. Un nouveau criblage utilisant le test développé au sein du laboratoire, reposant sur la détection par spectrométrie de masse du produit de la réaction enzymatique, a été conduit cette fois-ci sur 1280 composés (Figure 6).

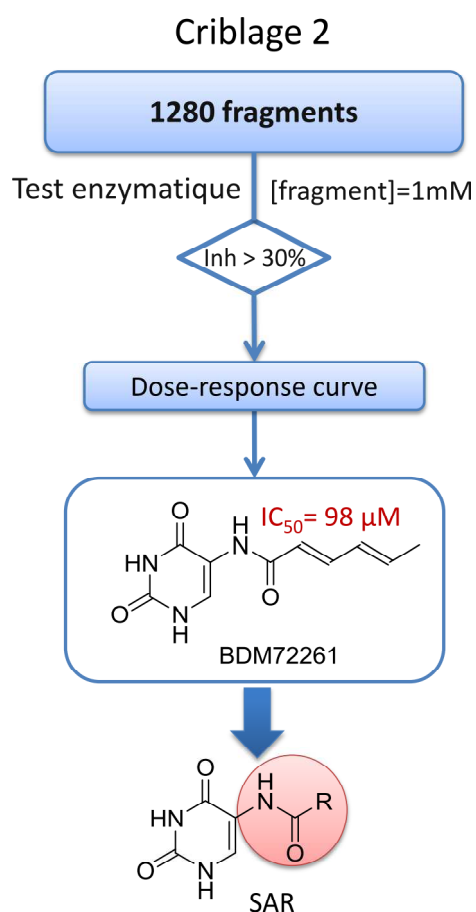
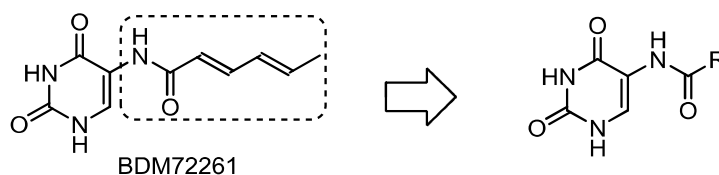


Figure 6: Le deuxième criblage des fragments sur l'enzyme MabA

Le criblage de cette chimiothèque a été mené à une concentration de 1 mM pour chaque fragment. 50 fragments ayant montré un pourcentage d'inhibition supérieur à 30% ont été testés dans une expérience de dose-réponse à huit concentrations différentes. Les résultats ont conduit à l'identification de 12 hits appartenant à neuf familles chimiques différentes avec des IC_{50} allant de 30 à 300 μ M. Le composé le plus actif dans cette série a montré une IC_{50} égale à 98 μ M (Figure 7). Dans le cadre de la sélection, la famille de composés contenant un motif 5-amino-uracile a été choisie pour être optimisée dans le cadre de ma thèse.



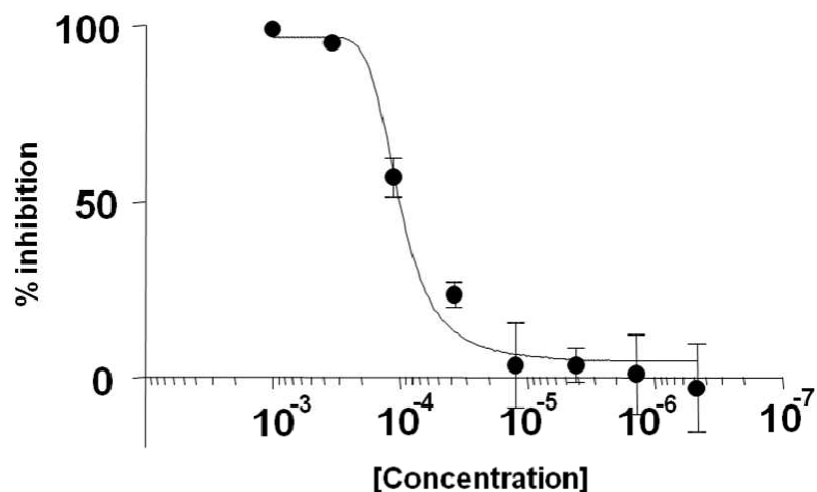
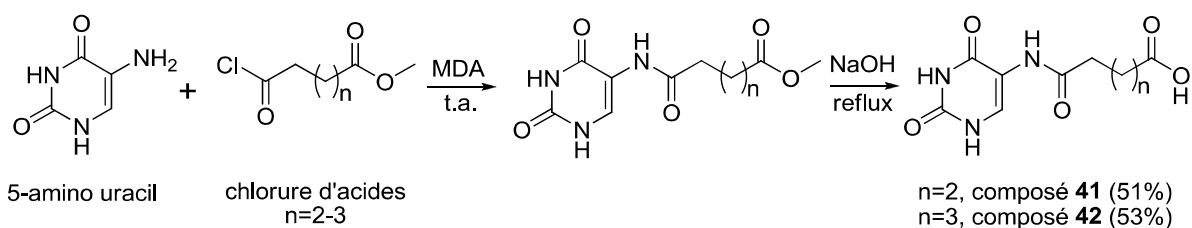
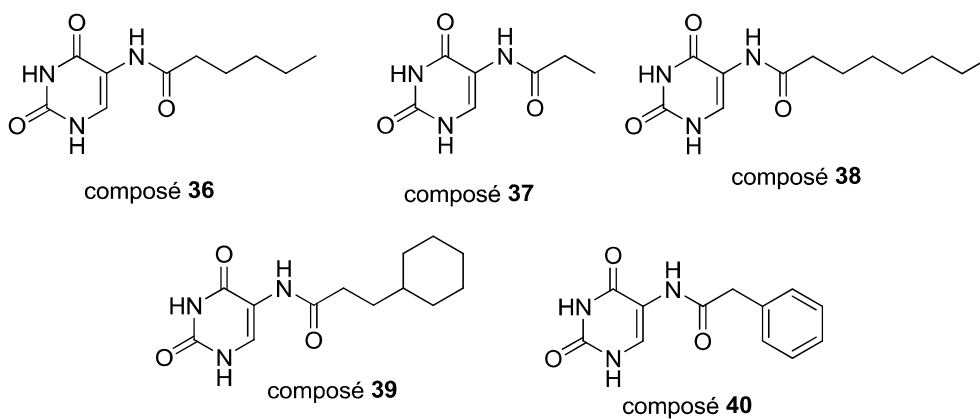
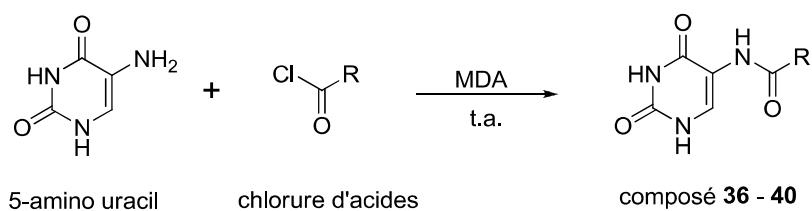


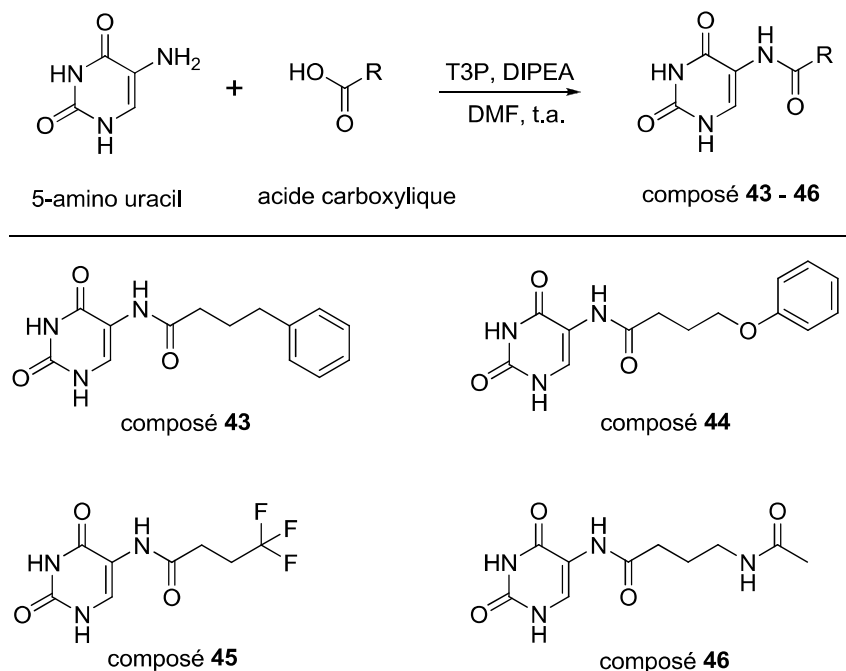
Figure 7: Inhibiteur de MabA BDM72261 identifié après criblage.

11 analogues ont ainsi pu être synthétisés selon les schémas de synthèse suivants:

- Acylation du 5-amino-uracile en présence de chlorures d'acides:



- Acylation du 5-amino-uracile en présence d'acides carboxyliques préalablement activés :



Ces différents composés sont en cours de test et les résultats obtenus permettront d'établir les premières relations structure-activité avec ces composés.

4. Développement de fragments 3-D

Dans la troisième partie, un travail de conception et de synthèse de nouveaux fragments, visant à compléter la chimiothèque actuelle a été effectué.

Une étude sur notre chimiothèque de fragments a montré que le nombre de fragments présentant des caractéristiques 3D était limité. Notamment le nombre de molécules présentant des atomes de carbones spiraniques ou des atomes de carbones tétrasubstitués était faible.

Nous avons donc choisi de développer une méthode de synthèse rapide de fragments originaux comportant un motif 2-isoxazoline permettant d'introduire un atome de carbone de type spiranique ou hautement substitué (Figure 8).

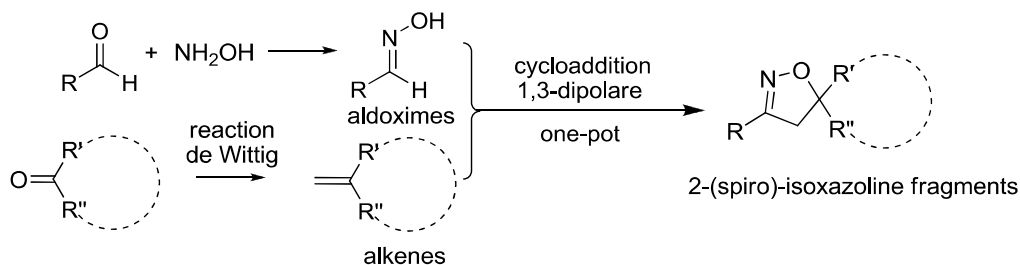


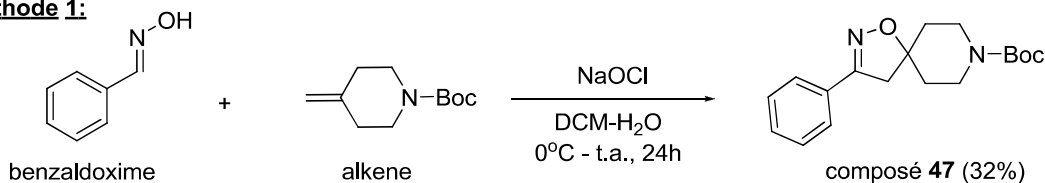
Figure 8: Réactions utilisés pour la synthèse de fragments contenant un motif 2-isoxazoline

Plusieurs procédés de synthèse utilisés pour la formation de 2-isoxazoline ont été décrits dans la littérature. Parmi eux, les cycloadditions 1,3-dipolaires se sont avérées être les plus robustes. Notre objectif était de générer des fragments comportant ce motif 2-isoxazoline via la

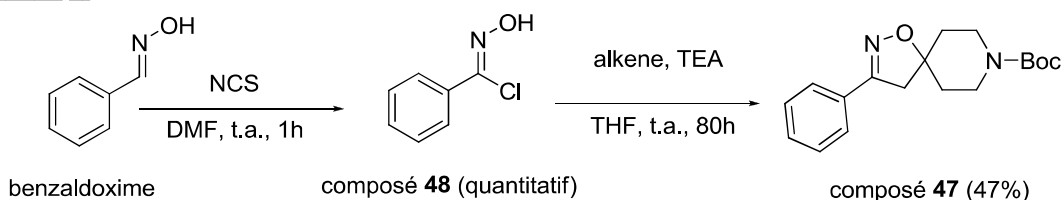
cycloaddition 1,3-dipolaire entre un oxyde de nitrile (dipole) et un alcène 1,1-disubstitué (dipolarophile).

Le benzaldoxime et la N-Boc-4-méthylèneépiperidine ont servi de substrats modèles dans la mise au point des conditions expérimentales. Le procédé de synthèse finalement optimisé est réalisé en un seul pot en présence d'un mélange de dichlorométhane (DCM) et de diméthylformamide (DMF) (10: 1). Dans une première étape, le benzaldoxime est transformé au bout d'une heure en chloroxime *in situ* par la réaction avec le N-chlorosuccinimide (NCS). L'addition ensuite de Boc-4-méthylidèneépiperidine et de la triéthylamine permet la formation de la BOC spiro-isoxazoline **47** avec un rendement global de 60% (Figure 9).

Méthode 1:



Méthode 2:



Méthode 3:

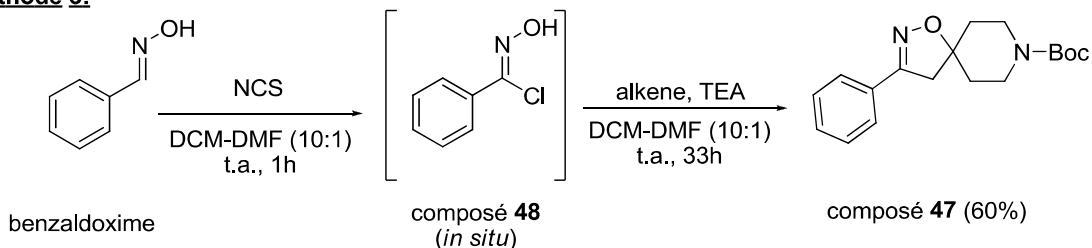
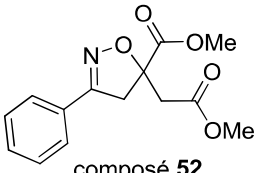
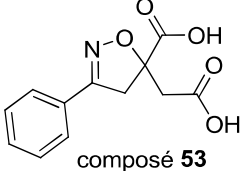
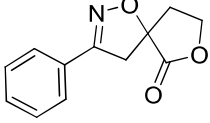
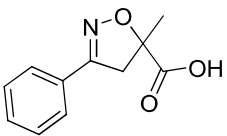
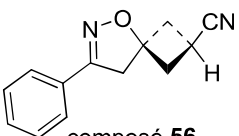
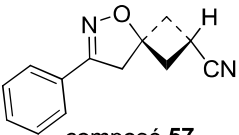
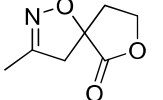
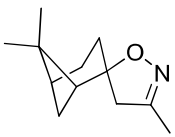
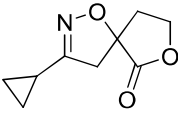
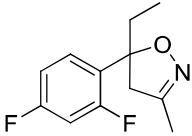


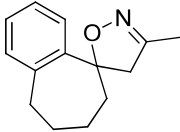
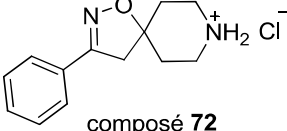
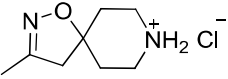
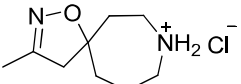
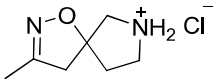
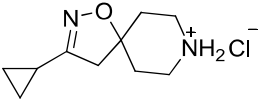
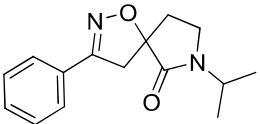
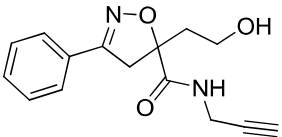
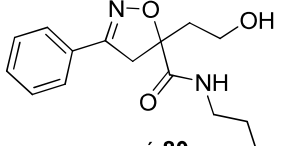
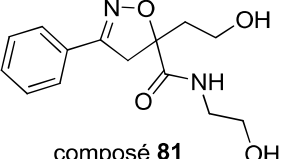
Figure 9: Méthodes utilisées pour l'optimisation de la synthèse du composé 47.

Le scope de cette réaction a été exploré avec le benzaldoxime, l'acétaldoxime et le cyclopropylaldoxime et des alcènes gem-disubstitués. 22 fragments ont ainsi pu être synthétisés avec des rendements compris entre 10 et 94% (Table 4).

Table 4: Liste des fragments synthétisés et leur propriétés

Entry	Structure	Rdt.(%)	MW (Da)	Fsp ³	Solubilité (mM)
1	 composé 50	93	249.3	0.38	1.0
2	 composé 51	35	291.3	0.40	1.0

Entry	Structure	Rdt.(%)	MW (Da)	Fsp ³	Solubilité (mM)
3	 composé 52	88	277.3	0.36	1.5
4	 composé 53	60	249.2	0.25	>2
5	 composé 54	94	217.2	0.33	-
6	 composé 55	56	205.2	0.27	1.8
7	 composé 56	16	212.3	0.38	0.4
8	 composé 57	40	212.3	0.38	0.3
9	 composé 67	72	155.1	0.71	-
10	 composé 68	10	193.3	0.92	1.9
11	 composé 69	87	181.2	0.78	-
12	 composé 70	57	225.2	0.42	0.8

Entry	Structure	Rdt.(%)	MW (Da)	Fsp ³	Solubilité (mM)
13	 composé 71	32	215.3	0.50	1.6
14	 composé 72	44*	216.3 [#]	0.46	>2
15	 composé 73	30*	154.2 [#]	0.88	>2
16	 composé 74	31*	168.2 [#]	0.89	>2
17	 composé 75	50*	140.2 [#]	0.86	>2
18	 composé 76	47*	180.3 [#]	0.90	>2
19	 composé 78	48	258.3	0.47	>2
20	 composé 79	82	272.3	0.33	>2
21	 composé 80	78	276.3	0.47	>2
22	 composé 81	65	278.3	0.43	1.9

*le rendement (Rdt.) est calculé après deux étapes

[#]la masse moléculaire est calculée pour la forme non chlorhydratée

La lactone **54** a en outre été fonctionnalisée avec des amines dans différentes réactions conduites sous irradiations micro-ondes. Ceci a permis l'introduction rapide de diversité à partir de ce fragment (Figure 10).

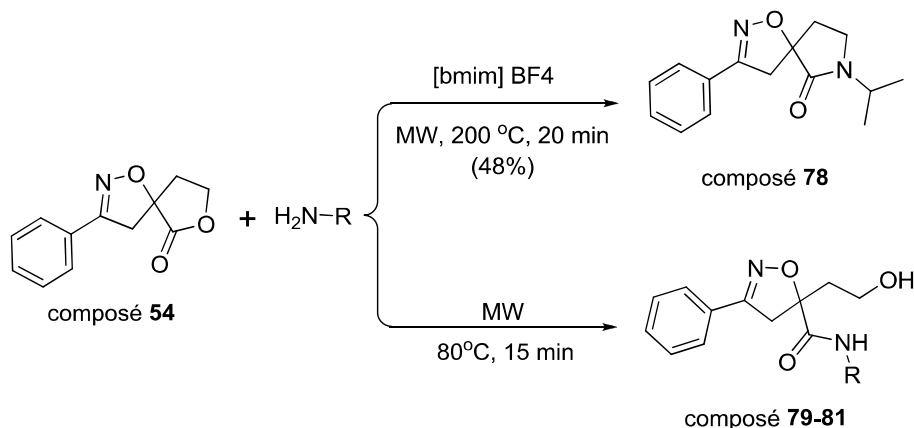


Figure 10: Diversité introduite à partir de la lactone **54**

La solubilité de ces fragments a été également mesurée expérimentalement et les résultats ont montré que la plupart de ces composés présente une solubilité supérieure à 2 mM, ce qui est particulièrement intéressant dans le cadre de leur utilisation en criblage.

Finalement, une analyse conformationnelle a permis de montrer que ces fragments incorporant le motif 2-isoxazoline avait une tendance plus élevée à adopter une structure tridimensionnelle que des fragments commerciaux de même masse moléculaire (Figure 11). De plus, ils sont davantage capables de venir déployer des substituants dans les trois dimensions de l'espace autour du motif 2-isoxazoline.

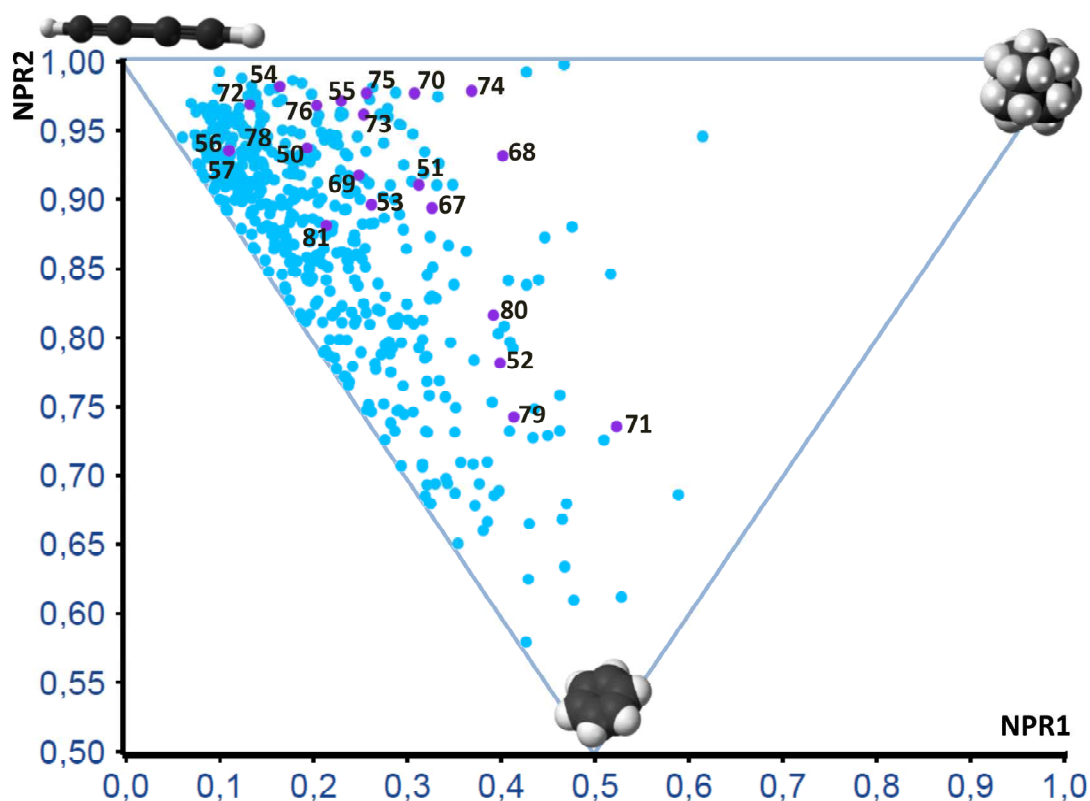


Figure 11: Comparaison entre les fragments 2-isoxazoline avec fragments commerciaux

Ce travail a permis de valider la synthèse de fragments originaux, comportant un motif 2-isoxazoline et a été récemment accepté pour publication dans le journal *Tetrahedron Letters*. L'incorporation de ces composés dans les prochains criblages effectués au laboratoire permettra très certainement d'identifier de nouveaux synthons permettant le développement de nouvelles molécules biologiquement actives.

Thesis title:

DESIGN, SYNTHESIS AND DEVELOPMENT OF NOVEL ANTITUBERCULOSIS AGENTS BY FRAGMENT BASED APPROACH

Abstract:

In 1993, the World Health Organization (WHO) declared Tuberculosis (TB) as a global public health emergency. Over 20 years later, this infectious disease caused by *Mycobacterium tuberculosis*, remains a major public health problem. Despite the significant progress in the fight against TB worldwide, WHO estimates that 9 million people contracted the disease in 2013 and 1.5 million died in that year. In addition, the emergence of multidrug-resistant tuberculosis (MDR-TB) requires the development of new tools and new therapeutic strategies. Recently, two new compounds, bedaquiline and delamanid were approved in MDR-TB treatment in order to strengthen the actual MDR-TB chemotherapy. Nevertheless, there is always the possibility that the tubercle bacillus can quickly develop resistance related to the mechanism of action of these new drugs. Therefore, the actual therapeutic arsenal must be strengthened. This thesis is based on the discovery and optimization of new anti-TB compounds starting from the screening of small molecules called fragments.

The first part of this thesis is the continuation of the research project which was started during the thesis of Baptiste Villemagne. This work aims to develop compounds that can boost the activity of ethionamide, a second-line drug used to treat MDR-TB. The transcriptional repressor EthR has been validated as a key element in the bioactivation of ethionamide. EthR inhibitors were developed by using a fragment-based approach and were optimized to potentiate the activity of ethionamide *in vitro*. However, the low microsomal stability of the lead compound has limited its use *in vivo*. The metabolism study of the lead compound and key structural modifications allowed a development of new potent EthR inhibitors having acceptable pharmacokinetic and physico-chemical properties for *in vivo* testing.

The second part of this thesis focused on the synthesis of MabA inhibitors. MabA is a mycobacterial β -ketoacyl-ACP reductase involved in the synthesis of long-chain fatty acids, precursors of mycolic acids, which are major constituents of the mycobacterial cell wall. This enzyme has been shown to be essential for the survival of the bacteria but until now no inhibitor has been identified. Screening of a library of fragment molecules on MabA was performed *via* two different assays (affinity assay using TSA and an enzymatic assay). The identified hits were re-synthesized and tested in a functional assay. The optimization steps to improve the activity of the hits are also described. Compounds with activity in the micromolar range were discovered.

In the third part, a design and synthesis of new fragments is described. The aim of this project is to build a collection of original fragments showing a 3D-structure scaffold amenable for rapid derivatization. The fragments that contains an original isoxazoline motif were synthesized from alkenes and aldoxime as starting building-blocks by using 1,3-dipolar cycloaddition. The conformational analysis of these structures has shown that they were, as expected, able to deploy substituents in the 3D space. The experimental solubility of these fragments was also measured and the results demonstrated that these molecules are suitable for the screening against new biological targets to help kick-start hit discovery program.

Key-words: anti-tuberculosis, EthR inhibitors, MabA inhibitors, ethionamide booster, 3D-fragments

CONCEPTION, SYNTHÈSE ET DÉVELOPPEMENT DE NOUVEAUX COMPOSÉS ANTITUBERCULEUX SELON UNE APPROCHE PAR FRAGMENTS

Résumé:

En 1993, l'Organisation Mondiale de la Santé déclarait que la tuberculose était « une urgence de santé publique mondiale ». Plus de 20 ans après, cette maladie infectieuse causée par *Mycobacterium tuberculosis*, reste toujours un problème à l'échelle de la planète. Malgré des progrès très importants enregistrés dans la lutte contre la tuberculose dans le monde, l'OMS estime que 9 millions de personnes ont contracté cette maladie en 2013 et que 1,5 million sont morts durant cette même année. De plus, l'émergence de la tuberculose multirésistante nécessite le développement de nouveaux outils et de nouvelles stratégies thérapeutiques. Récemment, deux nouveaux composés, bedaquiline et delamanid ont reçu une autorisation temporaire d'utilisation dans le but de renforcer l'arsenal thérapeutique. Néanmoins, il existe toujours la possibilité que la bactérie puisse rapidement développer des résistances liées au mécanisme d'action de ces nouveaux médicaments. C'est pour toutes ces raisons que l'arsenal thérapeutique doit être renforcé. Ce travail de thèse repose sur la découverte et l'optimisation de nouveaux composés antituberculeux selon des approches dont le point de départ commun est le criblage de petites molécules appelées fragments.

La première partie de ce manuscrit présente la continuité d'un travail démarré au cours de la thèse de Baptiste Villemagne et qui a pour but de potentialiser l'activité de l'éthionamide, un médicament antituberculeux utilisé pour le traitement de seconde intention. Le répresseur transcriptionnel EthR a été validé comme élément clé dans la bioactivation de l'éthionamide. Les inhibiteurs de cette cible, développés selon une approche par fragments ont permis de potentialiser l'activité de l'éthionamide *in vitro*. Cependant, la faible stabilité microsomale de ces composés a limité leur utilisation *in vivo*. L'étude de la métabolisation du composé tête de série et la modification structurale de ce dernier a permis le développement des nouveaux inhibiteurs d'EthR présentant des propriétés pharmacocinétiques et physico-chimiques désormais acceptables pour la réalisation de tests *in vivo*.

La deuxième partie de cette thèse s'est concentrée sur la synthèse d'inhibiteurs de MabA, une β -cétosynthase mycobactérienne participant à la synthèse des acides gras à longue chaîne, précurseurs des acides mycoliques qui sont les constituants majeurs de la paroi mycobactérienne. Cette enzyme a été montrée comme étant indispensable à la survie de la bactérie mais aucun inhibiteur à ce jour n'a été identifié. Le criblage d'une chimiothèque de fragments sur MabA a été réalisé *via* deux tests différents (un test d'affinité pour la cible TSA et un test enzymatique). Les hits ainsi identifiés ont été resynthétisés et testés dans un test fonctionnel. Les étapes d'optimisation de l'activité des hits reconfirmés sont ainsi décrites. Ces résultats ont permis de développer des composés présentant des activités de l'ordre du micromolaire.

Dans la troisième partie, un travail de conception et de synthèse de nouveaux fragments, visant à compléter la chimiothèque actuelle a été effectué. Les fragments originaux contenant un motif isoxazoline ont été synthétisés à partir d'alcènes et d'aldoximes utilisés en tant que synthons de départ, selon une réaction de cycloaddition 1,3-dipolaire. L'analyse conformationnelle de ces fragments a permis de montrer que ces structures venaient enrichir l'espace de la diversité, notamment par l'introduction de structures permettant le déploiement des substituants dans les 3 dimensions de l'espace. La solubilité expérimentale de ces fragments a été également mesurée et nous avons pu montrer que ces molécules étaient adaptées au criblage.

Mots-clés: antituberculeux, inhibiteur d'EthR, inhibiteur de MabA, activation d'éthionamide, fragment 3D

Unité de recherche INSERM U1177 (ancien nom U761)

Médicaments et Molécules pour Agir sur les Systèmes Vivants (M2SV)

Institut Pasteur de Lille - Faculté de Pharmacie de Lille – Université Lille 2 – Université Lille Nord de France

3 rue du professeur Laguesse - 59006 Lille cedex - FRANCE